FATIGUE CRACK GROWTH MEASUREMENT AND DATA ANALYSIS

Hudak/Bucci, *editors*

ASTM STP 738

AMERICAN SOCIETY FOR TESTING AND MATERIALS

FATIGUE CRACK GROWTH MEASUREMENT AND DATA ANALYSIS

A symposium
sponsored by ASTM
Committees E-9 on Fatigue
and E-24 on
Fracture Testing
AMERICAN SOCIETY FOR
TESTING AND MATERIALS
Pittsburgh, Pa., 29–30 Oct. 1979

ASTM SPECIAL TECHNICAL PUBLICATION 738
S. J. Hudak, Jr., Southwest Research Institute,
and R. J. Bucci, Alcoa Laboratories, editors

ASTM Publication Code Number (PCN)
04-738000-30

AMERICAN SOCIETY FOR TESTING AND MATERIALS
1916 Race Street, Philadelphia, Pa. 19103

Library of Congress Catalog Card Number: 80-70650

NOTE

The Society is not responsible, as a body,
for the statements and opinions
advanced in this publication.

Printed in Baltimore, Md.
July 1981

Foreword

The Symposium on Fatigue Crack Growth Measurement and Data Analysis, sponsored by ASTM Committees E-9 on Fatigue and E-24 on Fracture Testing, was held in Pittsburgh, Pa., on 29–30 Oct. 1979. S. J. Hudak, Jr., Southwest Research Institute, and R. J. Bucci, Alcoa Laboratories, served as symposium chairmen and also edited this publication.

Related ASTM Publications

Part-Through Crack Fatigue Life Prediction, STP 687 (1979), $26.25, 04-687000-30

Fatigue Mechanisms, STP 675 (1979), $65.00, 04-675000-30

Service Fatigue Loads Monitoring, Simulation, and Analysis, STP 671 (1979), $29.50, 04-671000-30

Cyclic Stress-Strain and Plastic Deformation Aspects of Fatigue Crack Growth, STP 637 (1977), $25.00, 04-637000-30

Fatigue Crack Growth Under Spectrum Loads, STP 595 (1976), $34.50, 04-595000-30

Effect of Load Spectrum Variables on Fatigue Crack Initiation and Propagation, STP 714 (1980), $27.00, 04-714000-30

Crack Arrest Methodology and Applications, STP 711 (1980), $44.75, 04-711000-30

Fracture Mechanics, STP 700 (1980), $53.25, 04-700000-30

Flaw Growth and Fracture, STP 631 (1977), $49.75, 04-631000-30

Commercial Opportunities for Advanced Composites, STP 704 (1980), $13.50, 04-704000-33

Nondestructive Evaluation and Flaw Criticality for Composite Materials, STP 696 (1979), $34.50, 04-696000-33

Evaluations of the Elevated Temperature Tensile and Creep Rupture Properties of 12 to 27 Percent Chromium Steels, DS 59 (1980), $24.00, 05-059000-40

A Note of Appreciation to Reviewers

This publication is made possible by the authors and, also, the unheralded efforts of the reviewers. This is a body of technical experts whose dedication, sacrifice of time and effort, and collective wisdom in reviewing the papers must be acknowledged. The quality level of ASTM publications is a direct function of their respected opinions. On behalf of ASTM we acknowledge with appreciation their contribution.

ASTM Committee on Publications

Editorial Staff

Contents

STATISTICAL ANALYSIS AND REPRESENTATION OF DATA

ENGINEERING APPLICATIONS

APPENDIXES

SUMMARY

Introduction

The application of fracture mechanics concepts to fatigue crack growth has made substantial progress since its inception nearly two decades ago. Much of this progress is recorded in previous ASTM Special Technical Publications (STPs). The current STP presents the proceedings of the ASTM Symposium on Fatigue Crack Growth Measurement and Data Analysis which was held in Pittsburgh, Pa., on October 29 and 30, 1979. This symposium, sponsored jointly by ASTM Committees E-9 on Fatigue and E-24 on Fracture Testing, summarized the 1979 state of the art of fatigue crack growth rate testing. The planning of the symposium was linked to the establishment in 1978 of the first industry-wide, consensus standard for fatigue crack growth rate testing—ASTM Method E 647-78 T on Constant-Load-Amplitude Fatigue Crack Growth Rates Above 10^{-8} m/Cycle. The symposium objectives were to (*1*) document background information which formed the basis for ASTM E 647, (*2*) provide a forum for exchanging experiences with ASTM E 647, (*3*) assess new developments in fatigue crack growth rate testing, and (*4*) exchange ideas and define problems in the use of fatigue crack growth rate information in materials' evaluation, design, and reliability assessment.

The success of the symposium is evidenced by the quality of the papers in this publication. They provide information on specimen size requirements, optimum procedures for fatigue threshold and low growth rate measurements, remote crack monitoring systems, data processing procedures, statistical characterization of primary and processed data, mathematical models for data representation and interpolation, and use of fatigue crack growth information in fracture control plans. Information presented in this STP should be useful to engineers involved in measuring and applying fatigue crack growth rate information to structural design. Researchers engaged in the study of materials' behavior and in elucidating fatigue mechanisms will also find this information useful in designing experiments which are free of confounding effects arising from improper specimen design or testing procedures.

Since many of the papers in this publication cite and discuss sections of ASTM E 647, this test method is conveniently reprinted as Appendix I of this STP. Appendix II is a document, developed within ASTM Committee E-24, which expands ASTM E 647 to include procedures for near-threshold fatigue crack growth rate measurements. The latter document represents one stage in the evolutionary process toward ASTM standardization. Although changes are likely to occur before final adoption of the near-threshold fatigue crack growth rate test method, it serves as a useful testing guideline in the interim.

S. J. Hudak, Jr.

Southwest Research Institute, San Antonio, Tex., symposium co-chairman and co-editor

R. J. Bucci

Alcoa Laboratories, Alcoa Center, Pa., symposium co-chairman and co-editor

General Test Procedures

R. J. Bucci[1]

Development of a Proposed ASTM Standard Test Method for Near-Threshold Fatigue Crack Growth Rate Measurement

REFERENCE: Bucci, R. J., **"Development of a Proposed ASTM Standard Test Method for Near-Threshold Fatigue Crack Growth Rate Measurement,"** *Fatigue Crack Growth Measurement and Data Analysis, ASTM STP 738,* S. J. Hudak, Jr., and R. J. Bucci, Eds., American Society for Testing and Materials, 1981, pp. 5-28.

ABSTRACT: Results are summarized which provide the basis for development of the proposed ASTM standard test method for measuring and presenting very slow cyclic rates of fatigue crack propagation. The technique for obtaining very slow rate data as K decreases with crack extension is described. Data are reviewed that show the individual and combined effects of various precracking and testing procedures, loading rates, and other testing parameters. The data are used to demonstrate the utility of the method and its limitations. Guidelines are given for the minimization of transient growth rate processes which can confound interpretation of the data. Analytical procedures for fitting near-threshold data are also discussed.

KEY WORDS: fatigue (materials), crack propagation, fracture, stress intensity, threshold, test method, aluminum alloy

Background

Practical limitations in manufacture, inspection, and use of many structural components prohibit complete elimination of flaws. It is therefore pertinent to question whether cracks may emanate and grow from these flaws, and, if so, at what rate. To evaluate the possibility of crack growth under the influence of cyclic stress, it is useful in some structures to employ the concept of threshold stress-intensity factor range (ΔK_{TH}) below which fatigue crack growth (FCG) will not occur. In other structural members where flaws prevail, slowly propagating fatigue cracks occupy a significant portion of the usable component lifetime. Designers are therefore interested in near-

[1] Staff engineer, Alcoa Laboratories, Alcoa Center, Pa. 15069.

threshold FCG rates ($da/dN < 10^{-8}$ m/cycle), since these rates correspond to early stages of crack growth where remedial measures can be instituted. The knowledge of ΔK_{TH} and very slow propagation rates are also important for the study of stress interaction effects, particularly those where FCG retardation occurs after an overload in a spectrum loading sequence [*1,2*].[2]

Proper characterization of a materials' FCG-rate relationship, da/dN versus ΔK, is of first-order importance in assembling fracture-mechanics analysis of crack growth [*3*]. In most cases the value of ΔK_{TH} cannot be directly established, but is extrapolated from available data. The task of defining a "true" threshold is difficult and obviously a function of measurement sensitivity, length of observation, and technique. Until better methods to quantify the value of ΔK_{TH} are needed and available, the concept of ΔK_{TH} has been provisionally accepted in certain applications (for example, Ref *4*). It should be recognized, however, that for some material-environment combinations the slope of the da/dN versus ΔK relationship has been found to be finite, at least down to FCG rates on the order of 10^{-10} m/cycle [*3,5*]. Standardization of testing practice to provide an accurate description of near-threshold FCG rates and a more precise method of defining ΔK_{TH} is therefore warranted.

Progress on Standardization of FCG Testing

Efforts to standardize FCG test methodology within ASTM Subcommittee E24.04 on Subcritical Crack Growth have been an ongoing process since 1970. Some of the testing guidelines have evolved from efforts to standardize fracture toughness measurement [*6,7*], while other contributions were derived from specific FCG programs (for example, Refs *5* and *8*). There presently exists a tentative method for measurement of steady-state FCG rates above 10^{-8} m/cycle (ASTM E 647-78 T).[3] Under ASTM Task Group E24.04.03 on Low ΔK Testing, standardization of low ΔK-FCG rate testing has progressed on a separate timetable because of the added complexity and more limited experience at acquiring data within this regime. Low FCG rate test practice has advanced to the state that a proposed standard test method, which consolidates procedures for both high-rate and low-rate testing, has been prepared as an ASTM E24.04 working document.[4] ASTM Task Group E24.04.03 is undertaking an experimental round-robin program to assess the proposed low ΔK test practice.

Object

It is the purpose of this report to provide background and supporting data for the procedures given in the proposed low ΔK test method. The utility of

[2]The italic numbers in brackets refer to the list of references appended to this paper.
[3]ASTM E 647-78 T is reprinted in this volume as Appendix I, pp. 321-339.
[4]This proposed test method is reprinted in this volume as Appendix II, pp. 340-356.

data formulated under the method, its limitations, and potential problem areas are also discussed.

Specialized Procedures for Near-Threshold FCG Rate Testing

Many of the low ΔK-FCG rate test guidelines parallel those of ASTM E 647. These include requirements on grips, fixtures, specimen design, measurement of crack length versus cycles data, data processing, and reporting. As illustrated by the data in Fig. 1, near-threshold rates are more sensitive to small variations in ΔK and to stress ratio R, where $R = K_{min}/K_{max}$, than are intermediate rates. Variability of low-rate measurement may also be amplified by increased sensitivity to alloy microstructure, environment, crack geometry, and loading precision. Screening low-rate measurements for anomalous effects is more difficult because of the long duration between measurements and the general lack of testing experience within this regime.

The proposed test method was constructed by modifying ASTM E 647 with additional provisions for better control of variability associated with low-rate measurement. The modifications aim to ensure that results are representative of the materials' "steady-state" FCG response, and that effects of confounding transient processes on collected data are minimized. The most notable modifications to ASTM E 647 include additional precracking requirements and a specialized procedure for testing such that K decreases with crack extension. An operational definition of the FCG threshold is also suggested as that value of ΔK corresponding to $da/dN = 10^{-10}$ m/cycle. The latter suggestion is useful for comparing materials, but caution is recommended if employing this definition to design.

K-*Increasing versus* K-*Decreasing Test Procedure*

Low FCG rate data can be established by a loading program which results in either increasing or decreasing ΔK as the test progresses. When load amplitude is constant, ΔK-values increase with crack extension in most specimen geometries. The constant-load-amplitude, K-increasing technique is a simple and satisfactory method of data acquisition for $da/dN > 10^{-8}$ m/cycle as described in ASTM E 647. This method requires a precrack that has been growing at or below the test load. When near-threshold rates are sought, such precracking becomes very time consuming and practically impossible. To expedite precracking, loads are often shed in decrements as large as possible until the targeted da/dN or ΔK value is approached [*9*]. The load amplitude is then maintained constant, and da/dN data acquired as K increases with crack extension [*4,9–11*]. Efficient use of this technique requires considerable test experience with the material of interest so that crack arrest and transient effects are avoided.

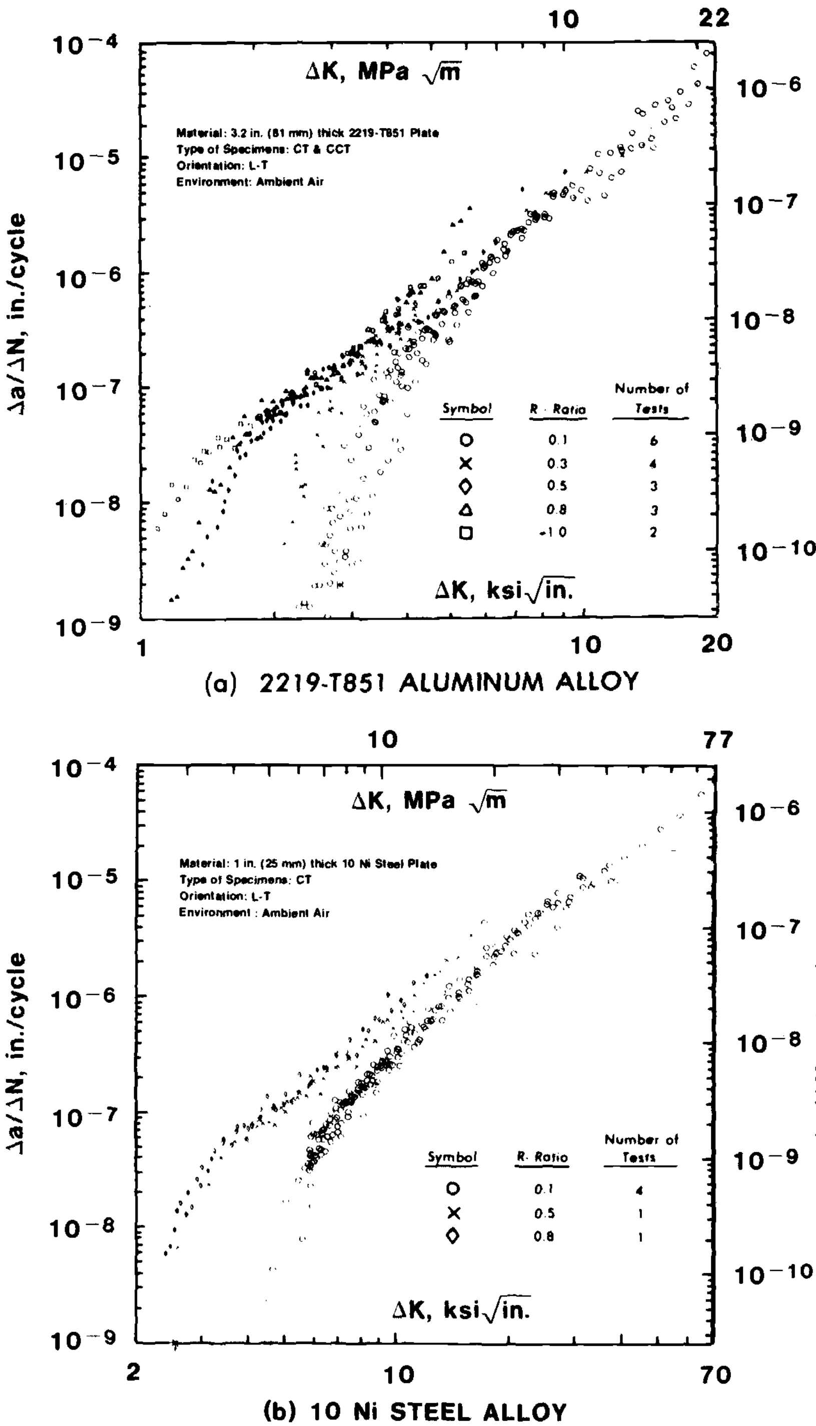

FIG. 1—*Effect of stress ratio* (R) *on low fatigue crack propagation rates of 2219-T851 aluminum and 10Ni steel alloys.*

Use of the K-decreasing approach allows the precracking step to be accomplished more efficiently. Crack-propagation data can then be obtained as load, and ΔK gradually decreases according to a predetermined schedule. This approach is attractive since valid FCG rate information can be established while working down to the targeted *da/dN.* Moreover, the K-decreasing process may be halted at any crack length, the load range fixed, and the test resumed as a K-increasing test in accordance with ASTM E 647. Conducting a K-decreasing test followed by a K-increasing test within a single experiment provides an excellent tool for assessing repeatability and/or sorting out transient FCG processes which might confound interpretation of the test results. A K-decreasing test is somewhat more complex than the K-increasing test, but the advantages of the K-decreasing approach seem to far outweigh the added complexity.

Reference *5* and Fig. 2 indicate that equivalent low-rate data are obtained from the standard compact-type (CT) and center-crack-tension (CCT) specimen configurations. For either the CT or CCT specimen, the K-decrease with crack extension can be provided by programmed shedding of load (or displacement) amplitude, or by constant deflection amplitude. Programmed shedding of load or displacement can be accomplished either by discrete steps, as illustrated in Fig. 7 of the proposed method, or in continuous fashion by computer control [*12*]. Experience [*5*] has shown that it is generally easier and more precise to control and monitor K by load cell measurement remote from the specimen rather than by specimen deflection measurement. Programmed load shedding offers the advantage of selection and control of a gradual rate of K-reduction such that the fractional change in estimated plastic-zone size with crack extension remains bounded. The programmed load-shed technique also offers a greater range of K-traversal over the usable portion of specimen crack length than does the constant deflection technique [*5,12*].

Good agreement of low and intermediate FCG rate data obtained by the K-increasing (constant-load-amplitude) and the proposed K-decreasing (programmed load shedding) method at various R-values is shown in Figs. 3 and 4 for 2219-T851 aluminum alloy, and in Fig. 5 for 10Ni steel. Also shown in Fig. 3 are limited data at intermediate FCG rates where K-decrease with crack extension was obtained by the constant-amplitude-deflection technique. For many of the individual tests shown in Figs. 3 to 5, data were initially obtained by the K-decreasing approach, and later in the same test by the K-increasing approach. Thus, the K-increasing data provides a check on validity of the K-decreasing data from the same test specimen. Transient and anomalous data, when present, were readily detected and eliminated by this process.

Comparable good agreement of K-increasing and K-decreasing test results has been demonstrated for other materials [*12,13*] where test procedures were in accordance with the proposed test method guidelines.

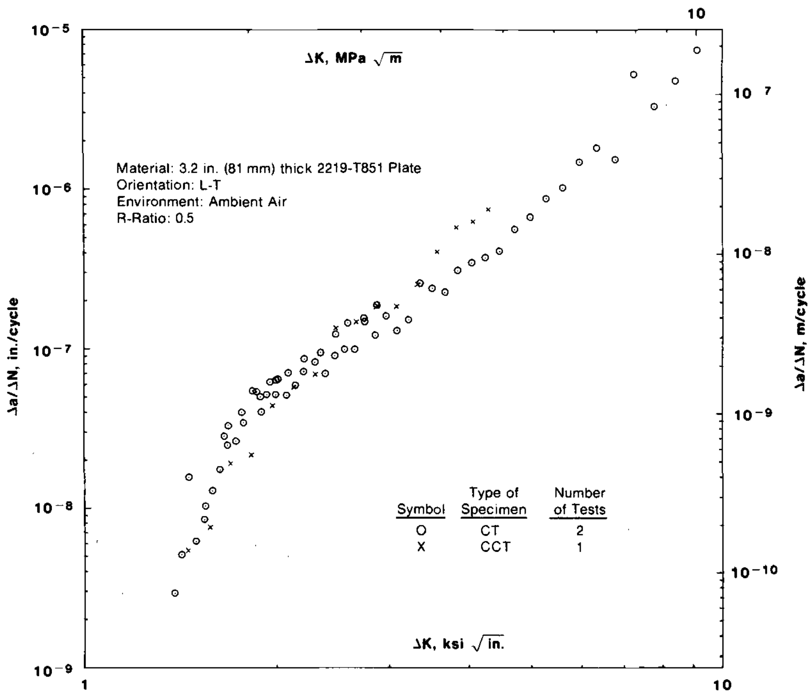

FIG. 2—*Effect of specimen plane geometry on low fatigue crack growth rates.*

Basis for Proposed K*-Decreasing Test Procedure*

The steady-state FCG response may be obtained only by minimizing the occurrence of transient processes which may confound interpretation of the test results. Transient FCG processes occur, particularly, when test variables are changed or when crack configuration or fracture mechanism changes as the test progresses. Accordingly, ASTM E 647 notes several means of minimizing the influence of transient effects for FCG rates above 10^{-8} m/cycle obtained by the K-increasing approach. Correct interpretation of low-rate data requires added controls because of greater sensitivity to small load (K) changes and the long test times involved. For example, because low rates show high sensitivity to stress ratio R, it is recommended that R be kept constant during both final stages of precracking and the actual test. The bases for several additional requirements of the proposed low-rate test method are next described.

Load-Shed Magnitude—The interaction effect where growth of a crack is slowed by previous application of an overload has been well documented in the literature (for example, Ref *14*). It was observed during K-decreasing low

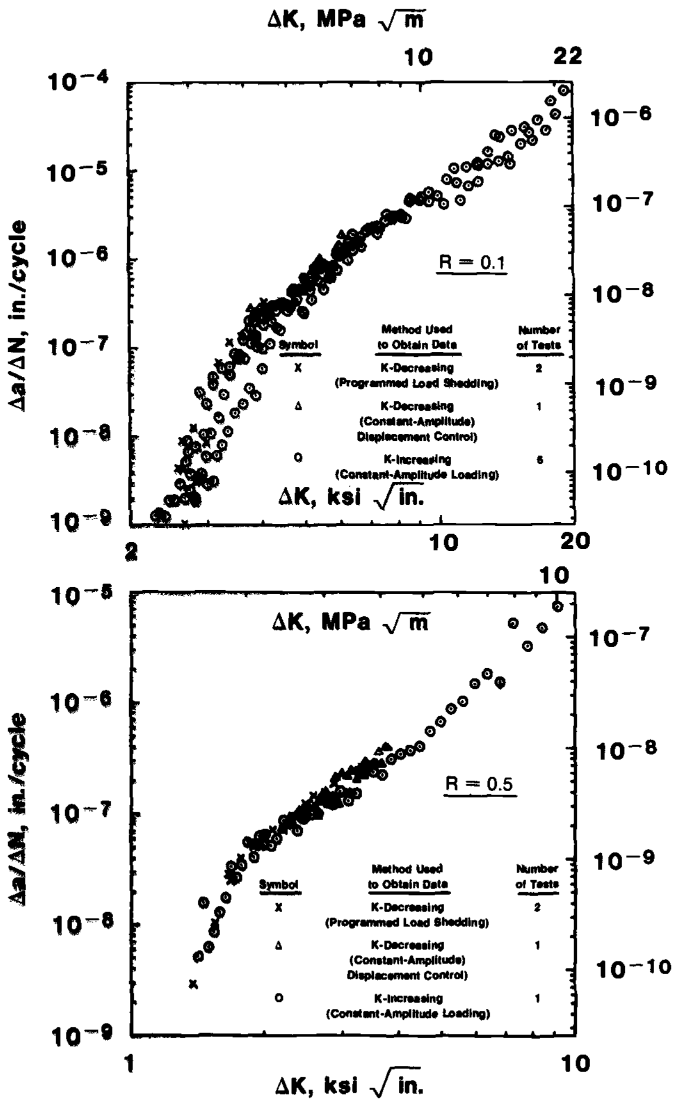

Material: 2219-T851 Aluminum Plate, 3.2 in. (81 mm) Thickness
Specimens: CT, B = 0.25 in. (6.4 mm), W = 2 in. (51 mm)
Orientation: L-T
Environment: Ambient Air

FIG. 3—*Comparison of* K-*increasing and* K-*decreasing test methods on aluminum alloy 2219-T851 at* R = *0.1 and 0.5* [5].

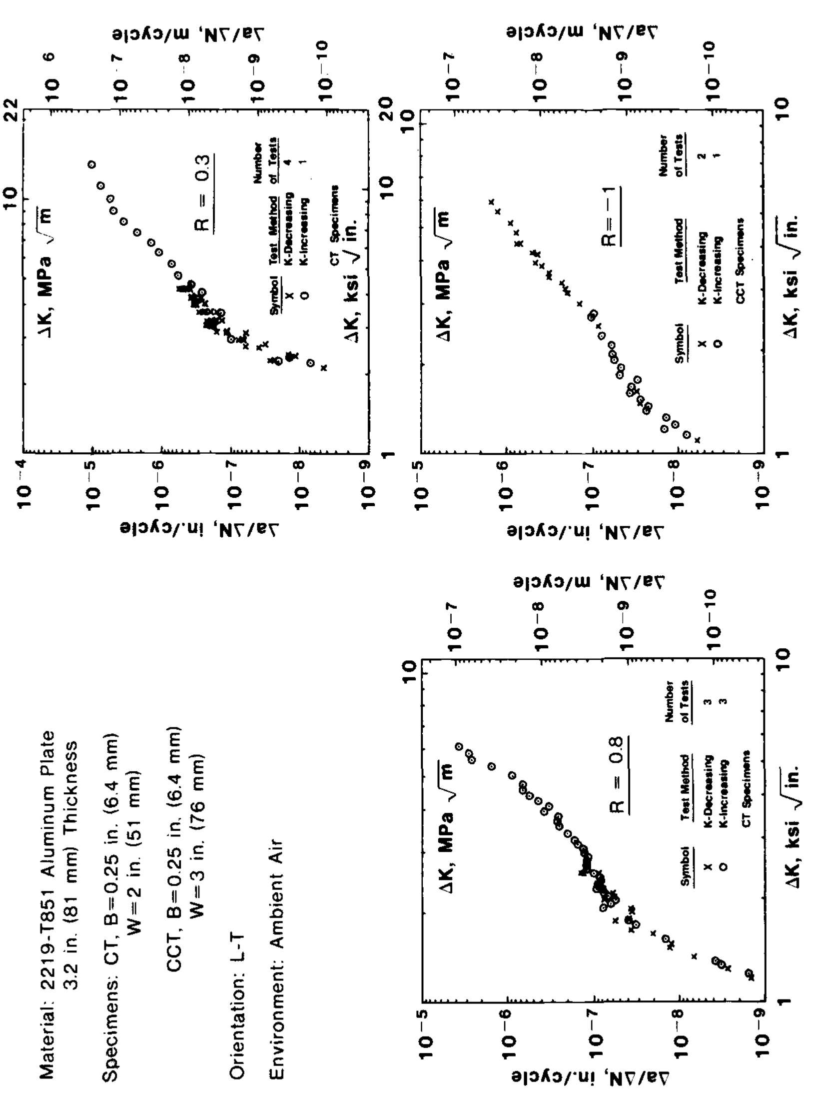

FIG. 4—*Comparison of* K-*increasing and* K-*decreasing test methods on aluminum alloy 2219-T851 at* R = *0.3, 0.8, and −1* [5].

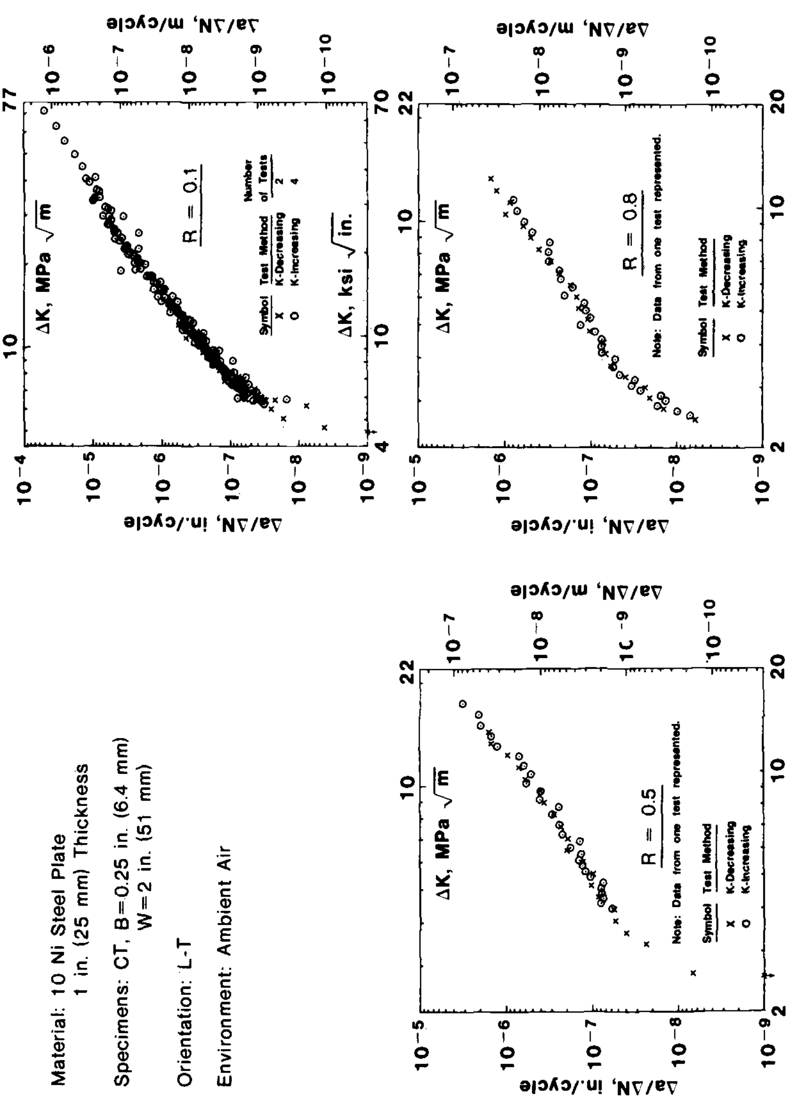

FIG. 5—*Comparison of K-increasing and K-decreasing test methods on 10Ni steel alloy at R = 0.1, 0.5, and 0.8* [5].

ΔK experiments on aluminum alloy 2219-T851 [*5*] that stepped load reductions of about 20 percent or greater were followed by a period of growth-rate stabilization extending over several estimated monotonic plastic-zone diameters.[5] However, where the monotonic plastic zone was small relative to the crack increment (Δa) between crack-length observations, the effect of the overload transient was negligible. Other work performed on several materials [*15*] has shown that FCG delay associated with block overloading occurs over a crack increment of less than three times the monotonic plastic-zone size of the last overload cycle.

(a) Precracking—The aforementioned observations provide a basis for the precracking requirements stated in Section 8.3.2 of the proposed method. Specifically, these are (*1*) no step reduction in K_{max} shall be greater than 20 percent, and (*2*) the final precrack length, (a_o) shall be greater than $(3/\pi) \cdot (K_{max_i}/\sigma_{ys})^2 + a_i$, where K_{max_i} is the terminal value of K_{max} at any prior load step, and a_i is the corresponding crack length. The latter requirement ensures that the final precrack length is separated from the largest overload plastic-zone boundary by at least three plastic-zone diameters.

(b) Cyclic crack growth rate measurement—Section 8.6.6 of the proposed test method places tighter requirements on the load shedding process when acquiring data by the K-decreasing approach. These requirements may be summarized as follows: (*1*) a 10 percent maximum is placed on the magnitude of the load shed, (*2*) a minimum increment of crack growth per data point is given, and (*3*) a bound is placed on the normalized rate of K-decrease (discussed next section). Justification for these requirements is based on equivalency of results from K-increasing and K-decreasing tests [*5*], as in Figs. 3 to 5. Restricting the magnitude of the load shed to 10 percent limits the change in the plastic-zone size to approximately $(0.01/2\pi)(K_{max}/\sigma_{ys})^2$. At near-threshold ΔK for most materials this change in plastic-zone size is many times smaller than the minimum 0.50-mm crack-length increment suggested in the proposed method. Data of Fig. 6 [*16*] indicate that there is no detectable effect on the apparent threshold stress-intensity factor when the magnitude of an overload is within 10 percent of the load during the baseline cycles. As a step down in load has a similar effect on the subsequent FCG behavior as an overload, the aforementioned requirement is consistent with the data of Fig. 6.

Bound on Normalized Rate of K-*Decrease*—It has been shown [*12*] that a constant rate of change in monotonic plastic-zone size with increasing crack extension can be approximated mathematically as

$$K_{max} = K_{max_o} \exp[C(a - a_o)] \tag{1}$$

where K_{max_o} is the initial stress-intensity corresponding to the initial length a_o, a is the instantaneous crack length, and C is a constant with dimensions

[5] The monotonic plastic-zone diameter can be estimated as $(1/2\pi) \cdot (K_{max}/\sigma_{ys})^2$ for plane stress.

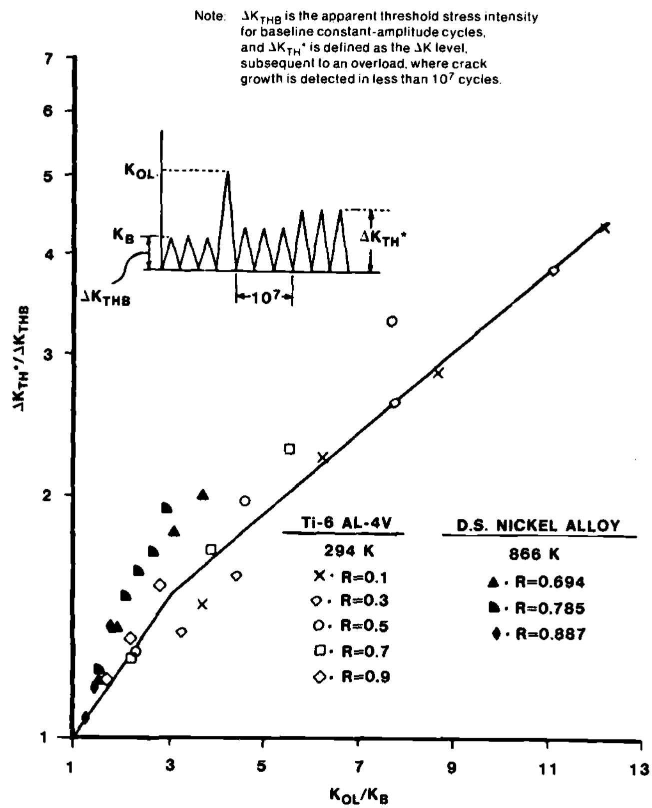

FIG. 6—*Relative change in fatigue crack growth threshold after single-cycle overloads as a function of the relative overload for two alloys and various stress ratios* [16].

of 1/length. For a test at constant R, the stress-intensity factors K_{min} and ΔK follow the same relationship; namely

$$K_{min} = K_{min_o} \exp[C(a - a_o)] \tag{2}$$

$$\Delta K = \Delta K_o \exp[C(a - a_o)] \tag{3}$$

From these the normalized K-gradient for the K-decreasing test at constant R-value may be expressed as

$$(1/K) \cdot (dK/da) = C \tag{4}$$

in which K may be any of K max, K min, or ΔK. Note that a constant value of C implies that the percent change in K is constant for equal increments in crack length.

Section 8.6.2 of the proposed test method recommends that C be controlled within prescribed limits. This requirement was found to be necessary to minimize growth-rate transients in the K-decreasing test [5, 12]. According to Eqs 1 to 4, a limit on C assures a gradual rate of K-decrease such that the fractional change of estimated plastic-zone size is bounded. The limit on C also assures that a reasonable number of da/dN versus ΔK data points (about five or more) are obtained per decade of growth rate.

The schedule of loading for a K-decreasing test can be accomplished by first specifying values of K_{max} and C for use in Eq 1. Load steps can then be selected such that the change in K remains bounded within the requirements of the method. The optimum value of C must be chosen with consideration given to alloy type, load ratio, and environment. Usable values of C should be established by demonstrating agreement between K-decreasing and valid K-increasing test results. Experience [5, 12] has shown that C-values between zero and -0.08 mm^{-1} (-2.0 in.$^{-1}$) (that is, $C > -0.08$ mm^{-1}) are acceptable at positive R-values for a variety of alloys. This is demonstrated by the summary of K-decreasing results shown respectively for 2219-T851 aluminum alloy and 10Ni steel [5] in Figs. 7 and 8. These plots compare at various values of C, the ratio of ΔK at a given low da/dN value in each test to the mean ΔK at the same da/dN corresponding to all valid results at the same R-value, K-increasing as well as K-decreasing.[6] In all cases, when the value of C was algebraically greater than -0.08 mm^{-1}, agreement between the K-decreasing and K-increasing result was good. However, as the value of C algebraically decreased below this value, there were instances where K-decreasing and K-increasing results disagreed. The disagreement, when it occurred, was confined to low positive R-values, in particular $R = 0.1$.

The abundance of points shown in Figs. 7 and 8 with values of $C < -0.08$ mm^{-1} suggests that perhaps the bound on C can be relaxed to further optimize testing. Any modification, however, must await further experience with additional materials, environments, and loading variables. Thus, when the recommended bounds on C are not met, the proposed method suggests that crack-growth-rate data be validated by demonstrating equivalance between K-decreasing and K-increasing data.

The bias below unity for the ratio of ΔK-decreasing to ΔK mean at the same FCG rate, as indicated in Fig. 7 for the aluminum alloy, suggests that K-decreasing FCG rates were generally faster than K-increasing FCG rates. This surprisingly consistent trend is opposite to expectations based on consideration of overload-retardation phenomena. Nonvalid K-decreasing data observed at high negative C-values and at $R = 0.1$ for 2219-T851 aluminum alloy (Fig. 9) show radical acceleration over valid results obtained by both K-increasing and K-decreasing approaches. Similar, though less extensive, observations were made with the 10Ni steel, also at $R = 0.1$ [5]. Maintaining the nominal value of C within the limits recommended in the proposed

[6] The mean ΔK-values were established by fitting the Weibull four-parameter equation to all of the valid FCG rate data obtained at a given R-value. This curve-fitting procedure is described in a later section.

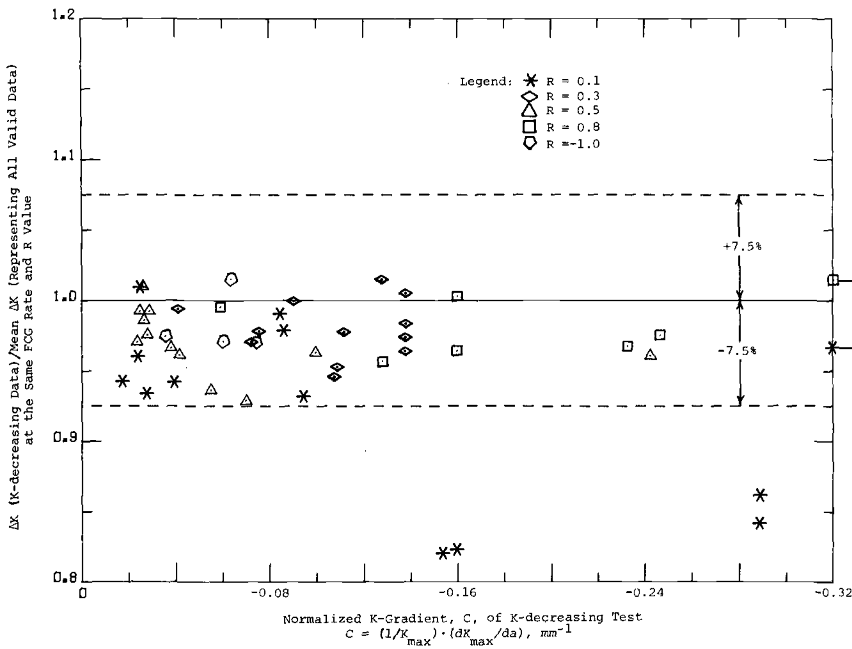

FIG. 7—*Effect of normalized* K*-gradient on near-threshold FCG rates established by* K*-decreasing method in aluminum alloy 2219-T851.*

method appears to be an effective means of limiting this anomalous behavior. Some plausible explanations for the growth-rate acceleration observed under rapid rates of K-decrease and at low positive R are suggested in the following discussion dealing with transient effects.

Minimizing Effect of FCG Transients

Though the proposed test method provides some guidance for minimizing the effect of FCG transients, it is not always possible to eliminate these effects, particularly at low ΔK. For example, transient FCG characteristics associated with test interruptions have been reported in the literature (for example, Ref *17*). The proposed method recommends that interruptions be kept to a minimum; however, certain interruptions may be unavoidable (for instance, holidays, weekends, electrical power failures, etc.). The user of the proposed method must, therefore, accept responsibility for judging acquired data to minimize bias introduced by transient behavior. The following sections discuss and provide recommendations for dealing with possible transient effects which might confound low-rate measurement and interpretation.

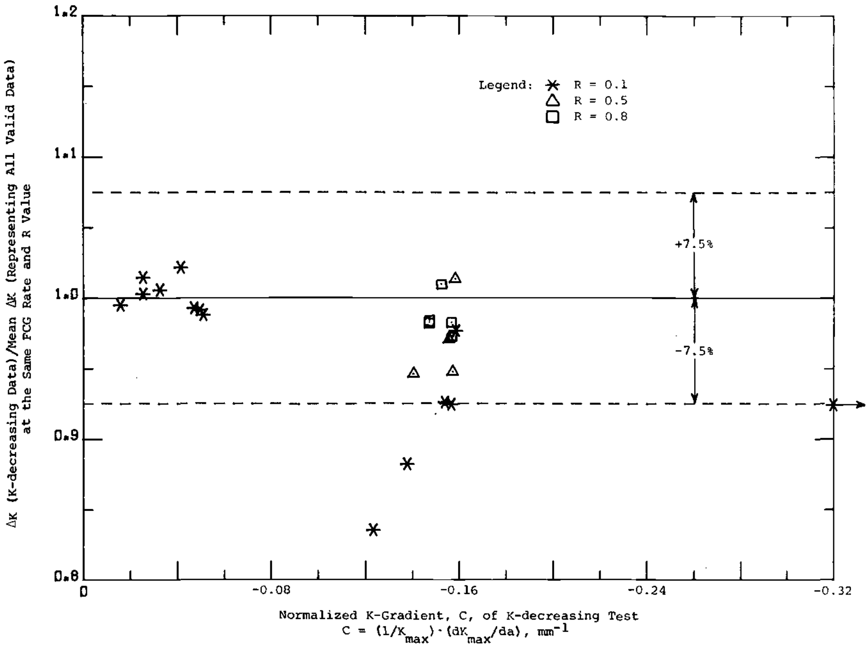

FIG. 8—*Effect of normalized K-gradient on near-threshold FCG rates established by K-decreasing method in 10Ni steel.*

Transients Dependent upon Crack Size and Geometry

Predicting growth of very small cracks (say ~0.1 mm) using near-threshold FCG rates established with standard fracture-mechanics-type specimens requires some caution because of unresolved questions of similitude between short and long crack behaviors [*18-21*].[7] Until the similitude question is resolved near-threshold data established according to the proposed method should be considered as representing the materials' steady-state FCG response emanating from a "reasonably long" propagating crack. A "reasonably long" crack implies that the crack is of sufficient length that transition from the initiation to propagation stage of fatigue is complete. The crack-length increment over which this transition occurs depends on the material, environment, and geometry (such as notches) of the component being tested.

To explore anomalous crack-length effects reference can be made to experimental observations of crack closure stresses in various materials. Closure stresses develop from interference of contacting fracture surfaces left

[7] The similitude question of long-crack versus short-crack behavior is currently being addressed by joint ASTM Committee E-9/E-24 Task Group on Small Cracks.

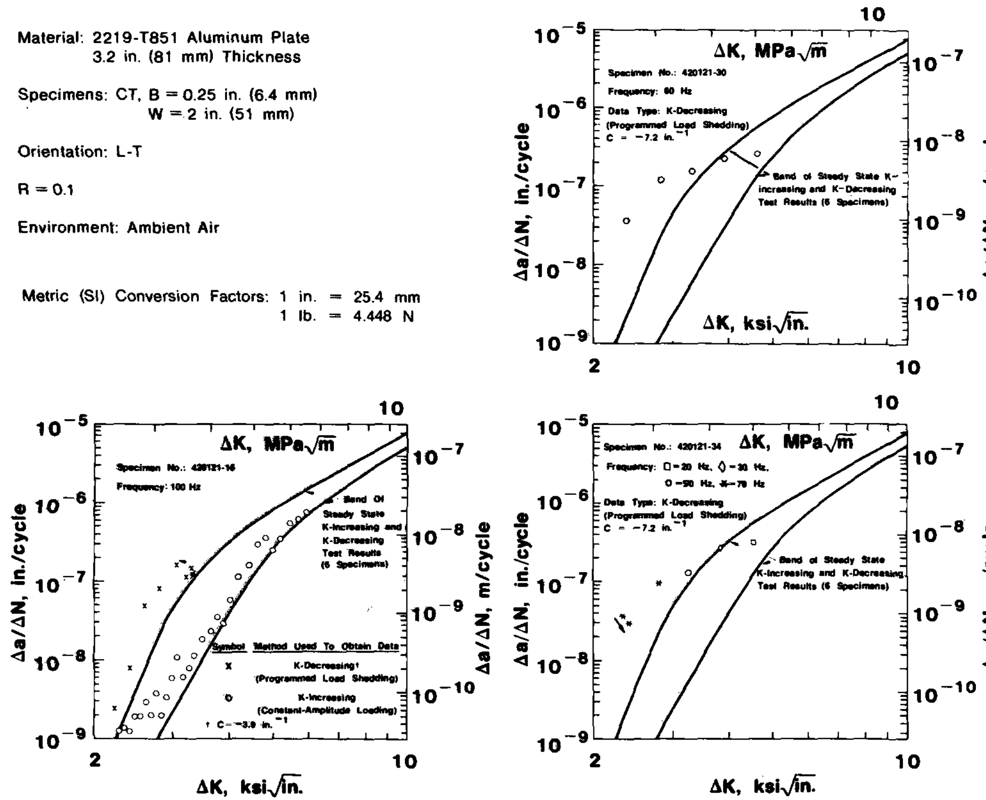

FIG. 9—*Typical examples of non-steady-state fatigue crack growth rates at* R = *0.1 obtained when rate of K-decrease with crack extension is high* [5].

in the wake of a propagating crack. These internal stresses provide a force system which tends to clamp the crack shut. When closure stresses are present a positive crack-opening load (P_{op}) is required to fully open the crack [*22*]. It has also been established that the value of P_{op} increases from a value near zero at the initiation of a microcrack to a finite positive value with the evolution of a macrocrack [*23*]. It is hypothesized here that the elevation in P_{op} and resulting decrease in effective stress-intensity factor (ΔK_{EFF})[8] with crack extension accounts at least in part for the observations in Refs *20* and *21*, and perhaps those of Fig. 9, where growth rates of short cracks were faster than rates predicted by long-crack data.

Upon bypass of the initiation stage and accepting the assumption of Refs *22*, *24*, and *25*, long-crack specimens subjected to constant-amplitude loading eventually attain a stable value of P_{op} with increase in crack extension [*22,24,25*]. This steady-state value of P_{op} is material and R-ratio dependent, as indicated by the results of Fig. 10. For aluminum alloy 2024-T3 the ratio of P_{op} to maximum applied load (P_{max}) is large, so that the length of crack extension from the specimen starter notch to attainment of the steady-state value of P_{op} would be different than that for aluminum alloy 7075-T651 where the ratio P_{op}/P_{max} is appreciably lower. For the fine-grained aluminum powder metallurgy alloy CT91, closure stresses were not detectable at any crack length [*26*], so that the crack length, to attainment of a stable P_{op} for CT91, would be much smaller than that of either alloys 7075 or 2024.

Minimum Crack Length Requirement for Precracking

The importance of precracking is to provide a sharp, straight, and symmetrical fatigue crack of adequate length so that (*1*) the fracture mechanism has stabilized with respect to conditions of the material and environment under test, (*2*) any effect of the machined starter notch is removed and (*3*) any permanent or transient behavior caused by crack-shape irregularities or precrack load history or both are minimized. Safeguards from these transient effects are provided by the minimum precrack length and crack-straightness requirements in Section 8.3 of ASTM E 647.

The aluminum alloy 2024-T351 test results of Fig. 11 [*27*] further illustrate the need for a minimum precrack length requirement. These data were developed from tests on identical specimens tested at various constant-load amplitudes. It was found that regardless of initial load, a crack length on the order of 3.8 mm (0.15 in.) from the notch tip was required for data to fit the general trend line shown. The possibility of a "false" interpretation of threshold is rather obvious from these results.

The minimum precrack length requirement of the proposed test method

[8] ΔK_{EFF} is defined by the difference between $K_{max} - K_{op}$ where K_{max} and K_{op} are the values associated respectively with maximum applied load and opening load [*22*].

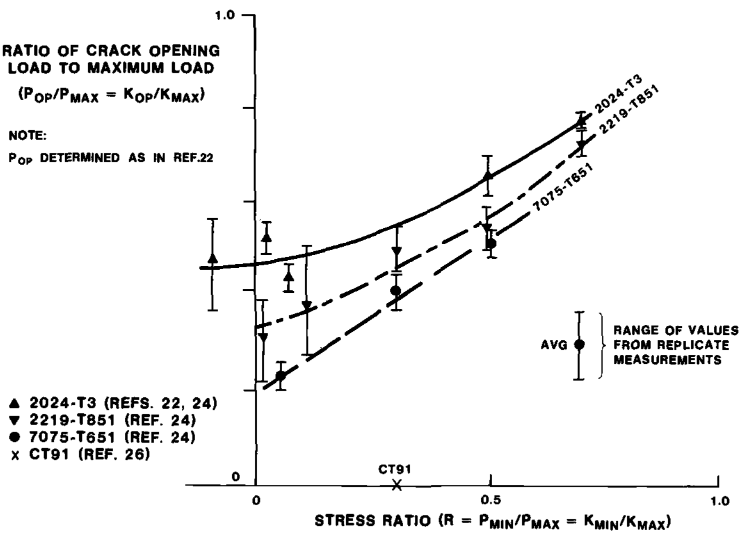

FIG. 10—*Relationship between ratio of crack-opening load to maximum load* (P_{op}/P_{max}) *and stress ratio* (R) *established from fatigue crack growth experiments on high strength aluminum alloys.*

was taken from ASTM E 647, which states that the final precrack length shall not be shorter than 0.10 *B* or *h*, whichever is greater (see Fig. 5 of ASTM E 647; this figure is reprinted as Fig. 5 in the proposed method). This requirement was based largely on experience obtained from intermediate and high FCG rate testing. However, the author's experience [*4,5,10,11*] from precracking and low-rate testing of CT specimens of approximately 6.4 mm (0.25 in.) thickness indicates that a minimum precrack extension of 2.5 mm (0.10 in.) beyond the starter notch is generally required to eliminate transient behavior due to insufficient crack length. Based on this experience and on Ref *27*, it is recommended that the minimum precrack length requirement of ASTM E 647 be increased to 2.5 mm, 0.10 *B*, or *h*, whichever is greater. This increase seems justified by uncertainty on dependence of transition crack size on material. Though arbitrary, the 2.5-mm minimum length requirement appears sufficient until greater experience is acquired for different materials. Meanwhile, additional assurance against anomalous low-rate results due to insufficient precrack size can be obtained by comparison of *K*-decreasing and *K*-increasing data generated from a single specimen, as recommended in Section 8.6 of the proposed method.

Transients Due to Competing Effects of Environment

Transient growth rate behavior may also arise as a result of environmental effects. For example, when a crack is propagated in an innocuous environ-

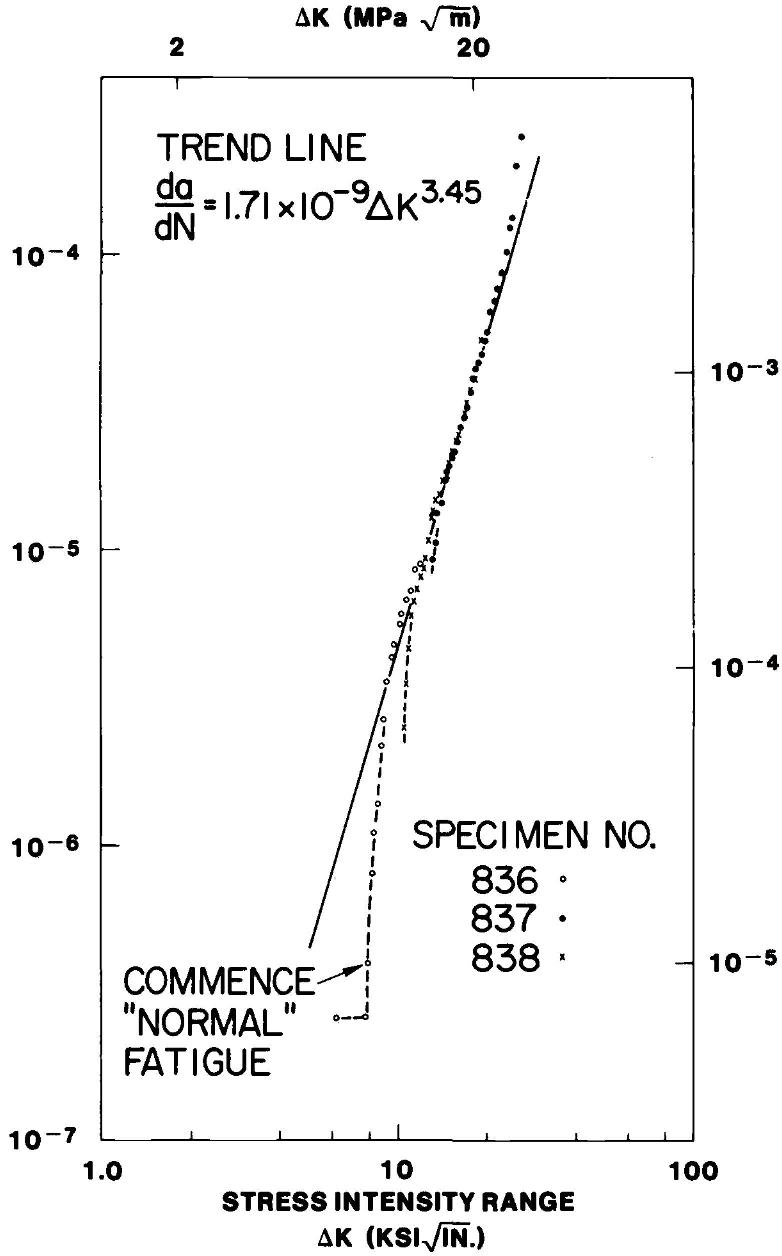

FIG. 11—*Anomalous fatigue crack growth rate data for 2024-T351 aluminum alloy* [27].

ment and then immediately thrust into contact with an aggressive environment, it is generally observed that growth rate accelerates above the rate previously achieved in the innocuous environment. However, if the propagation rate is very slow, retardation or arrest may result with continued exposure to the environment. Nordmark and Fricke [*28*], for example, showed that crack arrest in 7475-T7351 aluminum alloy tested in sump water was attributed to reduction in ΔK_{EFF} caused by gradual buildup of corrosion product on the crack surface (Fig. 12). Insufficient exposure time to permit buildup of closure forces due to corrosion products affords a possible explanation for the accelerated rate of growth observed when the crack length is very short, as in Refs *20* and *21*. The same cause may also explain the higher than expected rates where the rate of K-decrease with crack extension is high, as in Fig. 9. The former case represents further justification for incorporating 2.5 mm as a minimum precrack length requirement. In the latter case, the rapid rate of K-decrease may be postulated as sufficient to outpace buildup of corrosion products during early stages of the K-decreasing test.

Using the single-specimen K-decreasing followed by K-increasing technique represents to this author the best way of recognizing transient behavior of the types described. It has been the author's experience that agreement between K-increasing and K-decreasing results is generally more difficult to obtain in alloy-environment combinations that show greater susceptibility to stress-corrosion cracking.

Operational Definition of FCG Rate Threshold Stress Intensity

Section 9.4 of the proposed method offers an "operational" definition of ΔK_{TH} given as that ΔK corresponding to a FCG rate of 10^{-10} m/cycle. This definition affords a practical means of characterizing a material's FCG resistance, but caution is required in extending this concept to design. To determine the value of ΔK at 10^{-10} m/cycle, the proposed method suggests regressing a straight line through a minimum of five log da/dn versus log ΔK data points within the regime of 10^{-9} to 10^{-10} m/cycle.

Several criticisms of this procedure have been stated as follows [*29,30*]: (*1*) if the actual log da/dN versus log ΔK relationship is nonlinear, the straight-line fit has a problem defining the asymptote as da/dN approaches zero; (*2*) in a restricted data range the linear fit will be sensitive to the number of data points; and (*3*) a different fit to the data is obtained depending upon whether the sum of the squared residuals is minimized in either the X (log ΔK) or Y (log da/dN) direction. Because of the apparently asymptotic behavior of the da/dN versus ΔK relationship in the near-threshold regime, the sum of the squared residuals can better be minimized in linear analyses by selecting log

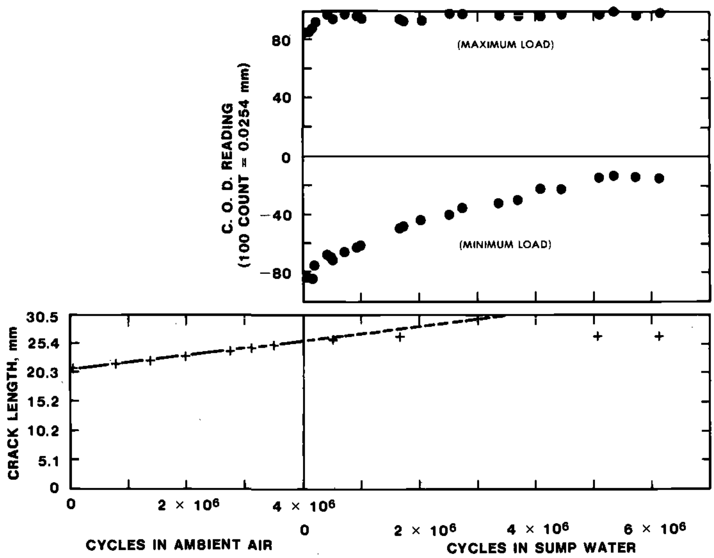

FIG. 12—*Crack-opening displacement measurements showing that crack arrest occurs in 7475-T7351 CT specimens tested in sump water because of gradual buildup of closure forces caused by corrosion products on the crack surfaces* [28].

ΔK as the dependent variable. However, Objection (3) can be removed by a fitting method which utilizes nonlinear optimization to minimize the sum of the squared normalized distances (that is, the perpendicular residuals) [*31*].

Objection (1) can be removed by using a nonlinear equation such as the four-parameter Weibull function[9] which is better able to accommodate the asymptotic behavior of the FCG rate relationship. Mueller [*31*] applied the improved nonlinear optimization procedure to fit the four-parameter Weibull function to data from Ref *5*, and obtained excellent correlation over the total range of FCG rates (Fig. 13). Figure 14 shows expansion of Mueller's four parameter Weibull fit in the near-threshold regime compared with linear fits of the indicated data where either log ΔK or log da/dN were considered as the dependent variable in the regression analysis.

Each of these curve-fitting approaches has its own particular advantage. The improved optimization technique for minimizing residuals perpendicular to the fitted curve combined with a descriptive growth-rate equation, such as the four-parameter Weibull, is better able to accommodate nonlinear da/dN versus ΔK response and reduces problems associated with the ap-

[9] Application of the four-parameter Weibull function to FCG rate description is given by [*32*]

$$da/dN = B_1 + (B_1 - B_1) - \ln[1 - (\Delta K/B_4)]^{1/B_3}$$

where B_1, B_2, B_3, and B_4 are constants.

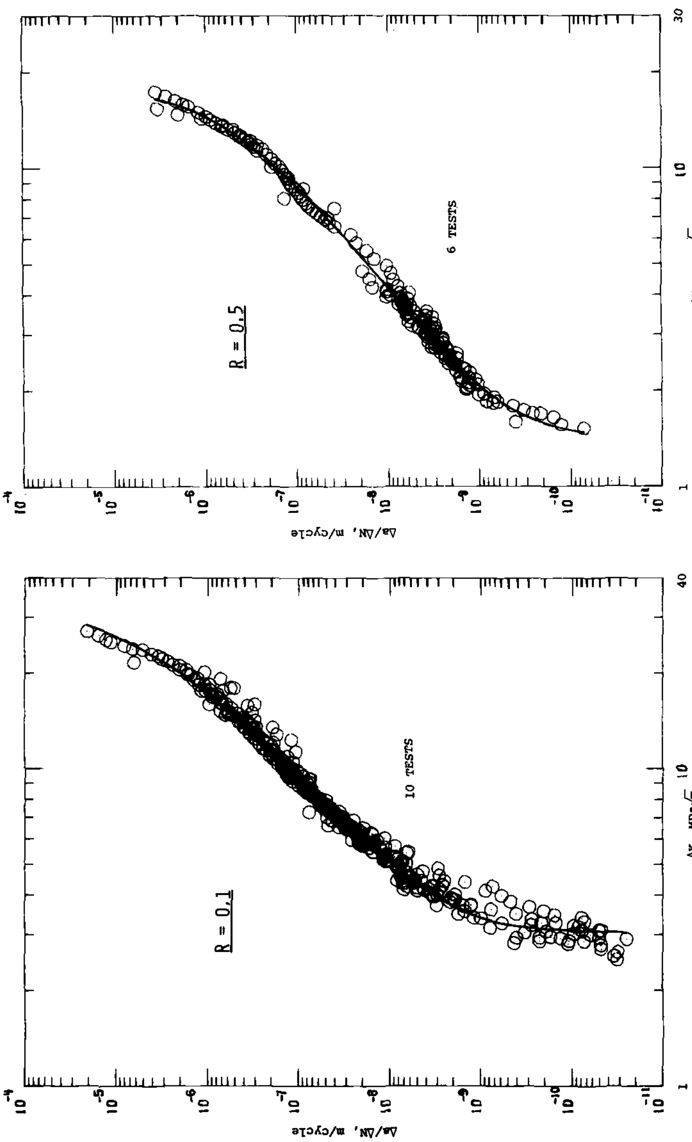

FIG. 13—*Four-parameter Weibull fit to fatigue crack growth data of aluminum alloy 2219-T851 at* R = *0.1 and 0.5.*

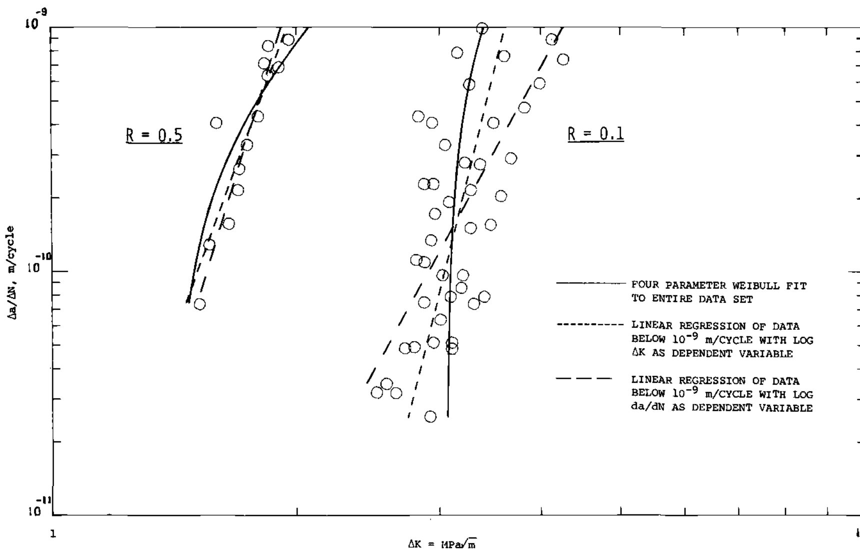

FIG. 14—*Fits to near-threshold data for aluminum alloy 2219-T851 by various approaches.*

parent asymptotes. This approach is also advantageous for fitting a broad range of growth rates. However, when sufficient near-threshold data points are available, linear regression with log ΔK as the dependent variable is simpler to use and does a good job at representing this more restricted regime. On the other hand, when the number of near-threshold data points is small, the nonlinear approach takes advantage of a larger data set to describe low ΔK behavior, as in Fig. 13. In this case, fitting near-threshold data by the nonlinear approach would be less sensitive to the number of low ΔK data points than the linear approach, which is restricted to a narrower range of data (about one decade of da/dN). Further experience is warranted before specific recommendations can be adopted as standard procedure.

Summary

A proposed test method for measurement of FCG rates below 10^{-8} m/cycle has been established. (It is reprinted in this volume as Appendix II.) The method was constructed by modifying ASTM E 647 to include special procedures for low growth-rate measurement as K decreases with crack extension. Test results supporting the recommended procedures have been described.

Provisions of the test method aim to ensure that the low ΔK-rate measurements obtained are representative of "steady-state" material response. Guidelines are given for minimizing transient FCG processes which may confound interpretation of the data. These transient processes are material dependent and are affected by interactions with load history, crack size, and environment. Arguments are presented which suggest that the ASTM E 647 precrack length requirement be increased to ensure a minimum 2.5-mm crack extension from the starter notch. This reduces the risk of encountering transient FCG processes associated with growth of short cracks and exposure to environment.

Limitations of the proposed linear curve-fitting approach for defining an operational value of stress-intensity threshold were described. Alternative curve-fitting approaches and their relative advantages were discussed.

Acknowledgments

The Air Force Materials Laboratory is gratefully acknowledged for its support which expedited development of the proposed test method under discussion. The author also gratefully acknowledges the members of the ASTM E24.04.03 steering committee (J. K. Donald, N. E. Dowling, A. W. Gunderson, S. J. Hudak, Jr., S. R. Novak, A. Saxena, and R. P. Wei) who contributed to the preparation and review of the proposed method. Finally, the author acknowledges R. C. Malcolm and L. N. Mueller of Alcoa Laboratories for many fruitful discussions on the subject and for their valued contributions to the experimental work and critique of the manuscript.

References

[1] Willenborg, J., Engle, R. M., and Wood, H. A., "A Crack Growth Retardation Model Using an Effective Stress Intensity Concept," AFFDL-TM-71-1-FBR, Air Force Flight Dynamics Laboratory, Jan. 1971.

[2] Wood, H. A., Gallagher, J. P., Engle, R. M., and Potter, J. M., "Current Practice on Estimating Crack Growth Damage Accumulation with Specific Application to Structural Safety, Durability, and Reliability," AFFDL-TR-75-32, Air Force Flight Dynamics Laboratory, Jan. 1976.

[3] Bucci, R. J. in *Part-Through Crack Fatigue Life Prediction, ASTM STP 687,* American Society for Testing and Materials, 1979, pp. 47–73.

[4] Paris, P. C., Bucci, R. J., Wessel, E. T., Clark, W. G., Jr., and Mager, T. J. in *Stress Analysis and Growth of Cracks, ASTM STP 513,* American Society for Testing and Materials, 1972, pp. 141–176.

[5] Hudak, S. J., Jr., Saxena, A., Bucci, R. J., and Malcolm, R. C., "Development of Standardized Methods of Testing and Analyzing Fatigue Crack Growth Rate Data," AFML TR-78-40, Air Force Materials Laboratory, May 1978.

[6] ASTM Standard Test Method for Plane-Strain Fracture Toughness of Metallic Materials (E 399-78a), *1980 Annual Book of ASTM Standards,* Part 10.

[7] Brown, W. F., Jr., and Srawley, J. E., *Plane Strain Crack Toughness Testing of High Strength Metallic Materials, ASTM STP 410,* American Society for Testing and Materials, 1967.

[8] Clark, W. G., Jr., and Hudak, S. J., Jr., *Journal of Testing and Evaluation,* Vol. 3, No. 6, 1975, p. 454.

[9] Paris, P. C., "Testing for Very Slow Growth of Fatigue Cracks," *Closed Loop Magazine,* MTS Systems Corporation, Vol. 2, No. 5, 1970.

[*10*] Bucci, R. J., Paris, P. C., Hertzberg, R. W., Schmidt, R. A., and Anderson, A. F. in *Stress Analysis and Growth of Cracks, ASTM STP 513*, American Society for Testing and Materials, 1972, pp. 125-140.
[*11*] Bucci, R. J., Clark, W. G., Jr., and Paris, P. C. in *Stress Analysis and Growth of Cracks, ASTM STP 513*, American Society for Testing and Materials, 1972, pp. 177-195.
[*12*] Saxena, A., Hudak, S. J., Jr., Donald, J. K., and Schmidt, D. W., *Journal of Testing and Evaluation*, Vol. 6, No. 3, May 1978, pp. 167-174.
[*13*] Bucci, R. J., unpublished data, Alcoa Laboratories, Alcoa Center, Pa., 1979.
[*14*] *Fatigue Crack Growth Under Spectrum Loads, ASTM STP 595*, American Society for Testing and Materials, 1976.
[*15*] Mills, W. J., "Load Interaction Effects on Fatigue Crack Growth in 2024-T3 Aluminum and A514F Steel Alloys," Ph.D. dissertation, Lehigh University, 1975.
[*16*] Hopkins, S. W., Rau, C. A., Leverent, G. R., and Yeun, A. in *Fatigue Crack Growth Under Spectrum Loads, ASTM STP 595*, American Society for Testing and Materials, 1976, pp. 125-141.
[*17*] Miller, G. A., Hudak, S. J., Jr., and Wei, R. P., *Journal of Testing and Evaluation*, Vol. 1, No. 6, 1973, pp. 524-530.
[*18*] Schijve, J., and Jacobs, F. A., "Fatigue Crack Propagation in Unnotched and Notched Aluminum Alloy Specimens," NLR-TR-M2128, National Aerospace Laboratories, Amsterdam, Netherlands, May 1964.
[*19*] Schijve, J. in *Fatigue Crack Propagation, ASTM STP 415*, American Society for Testing and Materials, 1967, pp. 415-459.
[*20*] Pearson, S., *Engineering Fracture Mechanics*, Vol. 7, 1975, pp. 235-247.
[*21*] Dowling, N. E., "Crack Growth During Low Cyclic Fatigue of Smooth Axial Specimens," Scientific Paper 76-1E7-PALFA-P2, Westinghouse Research Laboratories, Pittsburgh, Pa.; also in *Cyclic Stress-Strain and Plastic Deformation Aspects of Fatigue Crack Growth, ASTM STP 637*, American Society for Testing and Materials, 1977, pp. 97-121.
[*22*] Elber, W. in *Damage Tolerance in Aircraft Structures, ASTM STP 486*, American Society for Testing and Materials, 1971, pp. 230-242.
[*23*] Morris, W. L., *Metallurgical Transactions A*, Vol. 10A, Jan. 1979, pp. 5-11.
[*24*] Bucci, R. J. and Paris, P. C., unpublished data of Del Research Corporation, Hellertown, Pa., 1972.
[*25*] Bell, P. D. and Wolfman, A. in *Fatigue Crack Growth Under Spectrum Loads, ASTM STP 595*, American Society for Testing and Materials, 1976, pp. 157-171.
[*26*] Sanders, R. E., Otto, W. L., and Bucci, R. J., "Fatigue-Resistant Aluminum P/M Alloy Development," AFML-TR-79-4131, Air Force Materials Laboratory, Sept. 1979.
[*27*] Sullivan, A. M. and Crooker, T. W., "Evaluation of Fatigue Crack Growth Rate Determination Using a Crack Opening Displacement Technique for Crack Length Measurement," NRL Report 7912, Naval Research Laboratories, Washington, D.C., Sept. 1975.
[*28*] Nordmark, G. E. and Fricke, W. G., *Journal of Testing and Evaluation*, Vol. 6, No. 5, Sept. 1978, pp. 301-303.
[*29*] Donald, J. K. and Schmidt, D. W., "Methods of Determining ΔK-Threshold from Low-Rate Fatigue Crack Growth Data," minutes of ASTM Task Group E24.04.03 meeting, Philadelphia, Pa., 8 Nov. 1978.
[*30*] Mueller, L. N., "Using Nonlinear Regression Statistics to Fit the Four-Parameter Weibull Function to Fatigue Crack Growth Rate Data," presented at ASTM Task Group E24.04.03 meeting, Philadelphia, Pa., 8 Nov. 1978.
[*31*] Mueller, L. N., presentation before ASTM Task Group E24.04.03, Pittsburgh, Pa., 30 Oct. 1979.
[*32*] Bowie, G. E. and Hoeppner, D. W., *Nuclear Metallurgy*, Vol. 20, Part 2, 1976, pp. 1171-1178.

C. Amzallag,[1] *P. Rabbe,*[1] *C. Bathias,*[2] *D. Benoit,*[3] *and M. Truchon*[3]

Influence of Various Parameters on the Determination of the Fatigue Crack Arrest Threshold

REFERENCE: Amzallag, C., Rabbe, P., Bathias, C., Benoit, D., and Truchon, M., **"Influence of Various Parameters on the Determination of the Fatigue Crack Arrest Threshold,"** *Fatigue Crack Growth Measurement and Data Analysis, ASTM STP 738,* S. J. Hudak, Jr., and R. J. Bucci, Eds., American Society for Testing and Materials, 1981, pp. 29-44.

ABSTRACT: This report presents the results of a round-robin work on the fatigue crack arrest threshold (ΔK_{th}) of 2618 aluminium alloy and AISI 316 steel. The main purpose was to develop a method for the determination of ΔK_{th}, and to examine the influence of various test parameters on this threshold. Among the parameters considered, only the load ratio (R) and the environment (vacuum) appear to have a significant influence on very slow fatigue crack growth rates (FCGR). Moreover, while the results obtained with the 316 steel show a great scatter, the importance of the adopted procedure is pointed out.

KEY WORDS: fatigue testing, fatigue crack growth, crack arrest threshold, test procedure

The determination of the resistance of a material to fatigue crack propagation and the calculations of defect tolerance rely on the relationship between crack growth rate per cycle (da/dN) and the amplitude of the stress intensity factor ΔK.

In a range of rates between 10^{-3} and 10^{-5} mm/cycle, the propagation law for many materials has the form

$$da/dN = C \cdot \Delta K^m$$

C and m are constants depending on the material.

[1] Research engineer and Head of Department of Mechanics, respectively, Creusot-Loire, Centre de Recherches, Firminy, France.

[2] Professor, Université de Technologie de Compiègne, Compiègne, France.

[3] Research engineer, Institut de Recherches de la Sidérurgie Française, Saint Germain-en-Laye, France.

At lower values of the crack growth rate, it is generally found that there is a characteristic value of ΔK, called the threshold ΔK_{th}, for which the rates rapidly become very small [*1–15*].[4] This threshold ΔK_{th} constitutes, as it were, a hinge between the notion of crack initiation and the notion of crack growth. It has often been thought that, like the endurance limit, it could be an intrinsic criterion of the material.

For a given material several factors may have an influence on ΔK_{th}. Among them, the R-ratio ($R = K_{min}/K_{max}$) and the environment are known to be the most important. Other factors, such as frequency, may also affect the threshold behavior. In order to offer a firmly established experimental basis for the influence of various parameters on crack growth rate at low ΔK, an extensive program has been undertaken by the French Metallurgical Society (see Note at end of this paper). Ten laboratories were involved in this study. The main object of this program was to determine low fatigue crack growth rates (FCGR) using a series of systematic tests in which the most significant parameters were studied.

Presentation of the Study

Materials

The study was conducted on a 316 stainless steel (water-quenched from 1100°C) used in the nuclear power industry and on a 2618 (T651) aluminium alloy used in the aircraft industry for supersonic applications.

The chemical composition and the mechanical properties of the alloys are listed in Table 1.

Parameters

The various parameters investigated were the specimen type, the specimen thickness (B), the crack length (a), the test frequency, the waveform, and the environment (air or vacuum). Tests under vacuum were carried out in an hermetically sealed chamber, providing of 10^{-5} torr [*16*]. They are detailed in Table 2 with their range of variation.

General Features of the Procedures

The reference specimen was a compact-tension specimen, with a thickness $B = 20$ mm and a width $W = 2B$. The low FCGR values were obtained by using a load-shedding technique.

[4] The italic numbers in brackets refer to the list of references appended to this paper.

TABLE 1—*Chemical composition and mechanical properties of the materials.*

	Chemical Composition								
Aluminum Alloy 2618 (T651)	Fe	Si	Cu	Ni	Mg	Ti	Mn	Cr	Zn
	1.15	0.20	2.55	1.13	1.64	0.15	0.065	0.01	0.1
	Mechanical Properties								
	σ_y = 402 MPa		σ_u = 447 MPa		ϵ_f = 7 %		K_{Ic} = 20 MPa$\sqrt{m}$		
	Chemical Composition								
AISI 316 Stainless Steel	C	Mn	Si	S	P	Ni	Cr	Mo	Co
	0.055	1.85	0.52	0.03	0.03	10.7	16.8	2.1	0.17
	Mechanical Properties								
	σ_y = 220 MPa		σ_u = 580 MPa						

The standard procedures supplied to all participants were:

1. *2618 Aluminum Alloy:*
   Initial $\Delta K \sim 11$ MPa$\sqrt{m}$ $(\sim K_{Ic}/2)$
   $R = P_{min}/P_{max} = 0.1$
   10 percent load steps when $da/dN < 2 \times 10^{-5}$ mm/cycle, 20 percent when $da/dN > 10^{-5}$ mm/cycle
   Crack increments between successive load sheds $\Delta a \geq \frac{1}{2\pi}(K_{max}/\sigma_y)^2$
   End of test when $10^{-7} < da/dN < 10^{-6}$ mm/cycle and $0.45 < a/W < 0.55$
2. *AISI 316:*
   Initial $\Delta K \sim 16$ MPa$\sqrt{m}$
   $R = P_{min}/P_{max} = 0.15$
   10 percent load steps
   Crack increments $\sim$ 0.3 mm
   End of test when $da/dN \sim 10^{-7}$ mm/cycle and $a/W \geq 0.5$

These procedures give a decrease in ΔK with crack extension of about 0.7 MPa$\sqrt{m}$/mm for the aluminum alloy and -2.2 MPa$\sqrt{m}$/mm for the stainless steel. These values may vary when parameters such as *W, R,* and *a/W* are changed in order to study their influence on low FCGR.

During all the experiments, the crack was monitored on the faces of the specimen with a travelling microscope (magnification of 20 to 40).

The *a* versus *N* data were reduced by the secant method in accordance with ASTM Method E 647-78 T (reprinted in this volume as Appendix I, pp.

TABLE 2—*Parameters investigated.*

Parameter	Material	
	2618 aluminum alloy	AISI 316
Specimen type	Compact Tension ($W = 2B$)	
	CCT with $B = 20$, $W = 120$ mm	CCT with $B = 20$, $W = 90$ mm
Specimen thickness, (B)	5 to 40 mm	5 to 25 mm
Crack length	$0.4 < \frac{a}{W} < 0.6$	$0.5 < \frac{a}{W} < 0.6$ (CT) $0.2 < \frac{2a}{W} < 0.6$ (CCT)
Frequency	0.5 to 130 Hz	
Waveform	sine, square, and triangle	
Environment	air argon vacuum 10^{-5} torr	air vacuum 10^{-5} torr

321-339). At each step of the test, the value of ΔK was calculated at the middle of the crack length increment, and the value of da/dN was taken as the average one over the crack increment.

The tests were conducted until no detectable crack propagation occurred within 10^6 cycles. The threshold value was then calculated with the load and crack length corresponding to the previous step. In these conditions, the lowest crack growth rates obtained were close to 10^{-7} mm/cycle. A limited amount of experiments were carried out below 10^{-7} mm/cycle.

Results

2618 Aluminum Alloy

This alloy exhibits a typical threshold effect (Fig. 1) in the range of the crack growth rates which were determined; that is, below approximately $da/dN = 10^{-6}$ mm/cycle, the slope of the da/dN versus ΔK curve is almost vertical.

The threshold value was determined for a rate da/dN of 10^{-7} mm/cycle. In the standard testing procedure which was used [that is, a sine wave form, a frequency of 30 to 50 Hz, a load ratio $R = 0.1$, compact type (CT) specimen] the crack arrest threshold is 3 MPa$\sqrt{\text{m}}$($\pm$0.5 MPa$\sqrt{\text{m}}$).

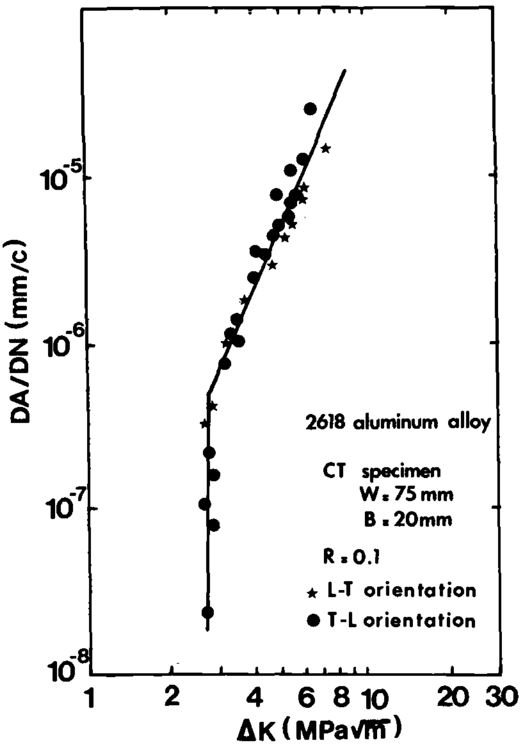

FIG. 1—*Typical crack growth rate behavior of the 2618 aluminum alloy below 10^{-5} mm/cycle observed by using the load-shedding procedure.*

The values of ΔK as a function of the various parameters studied are listed in Table 3. These values are average ones between at least three tests.

Parameters Which Have Little Effect on the Crack Arrest Threshold—The 2618 aluminium alloy results of Table 3 show that the threshold is independent of the specimen crack length over the range of $a/W = 0.4$ to 0.6, the wave form. Figure 1 shows that it is also independent of the specimen orientation with respect to the rolling direction.

For specimen thicknesses ranging from 5 to 50 mm, the ΔK-value corresponding to the rate 4×10^{-6} mm/cycle varies from 3.6 to 4.5 MPa$\sqrt{\text{m}}$. Since these differences cannot be separated from the data scatter, we must conclude that there is no effect of the thickness on the value of the threshold.

Between 0.5 and 130 Hz, frequency had very little effect on the results. Notice that the threshold corresponding to 0.5 Hz was obtained by frequency reduction after the rate decreased below 10^{-6} mm/cycle.

Specimen configuration also showed little effect on the crack arrest thresh-

TABLE 3—*Effect of various parameters on low FCGR of 2618 aluminum alloy.*

Parameter Studied	Variation of the Parameter Studied	Crack Growth Rate, mm/cycle	Corresponding Values of ΔK, MPa$\sqrt{m}$
	5		4.5
	10		3.8
Specimen thickness (B)	20	4×10^{-6}	3.9
	30		4.2
	40		3.6
Specimen type	CCT	10^{-6}	3.7
	CT		3.2
	0.1		2.9
Load ratio (R)	0.5	10^{-7}	1.8
	0.7		1.2
	0.4	10^{-7}	3.0
Crack length (a/W)	0.5	2×10^{-7}	3.2
	0.6	10^{-6}	3.1
Frequency	40	10^{-6}	3.2
	130		3.8
	sine		3.5
Waveform	square	10^{-6}	3.2
	triangle		3.6
	vacuum 10^{-5} torr		3.9
Environment ($R = 0.1$)	argon	10^{-7}	3.2
	air		2.9

old. The results obtained for center notched and compact specimens are very similar.

Parameters Which Strongly Affect the Crack Arrest Threshold—The stress ratio, $R = \sigma_{min}/\sigma_{max}$, has a strong influence on the low crack growth rates of this alloy. The transition between Stage I and Stage II of FCGR tends to appear at lower rates when the R-ratio is larger. Also, the crack arrest threshold decreases when the R-ratio increases (Fig. 2). It can be shown that ΔK_{th} depends on R according to the following relationship:

$$\Delta K_{th} = 3\,(1 - R)^{0.61} \text{ at } 10^{-7} \text{ mm/cycle}$$

These results are in agreement with those of Klesnil and Lukas [3].

The environment appears to have an influence on the threshold, but less than in the region where $da/dN > 10^{-5}$ mm/cycle.

In dry argon, one finds that, for a given value of R, the crack arrest threshold is slightly larger than in air. For $R = 0.1$, ΔK_{th} is equal to 3.25 MPa$\sqrt{m}$, and for $R = 0.5$ it reaches a value of 2.15 MPa$\sqrt{m}$ in argon.

In vacuum the difference becomes larger. Figure 3 shows that the FCGR curve obtained in vacuum does not show a well-defined knee. When the stress intensity factor decreases, the crack growth rate decreases uniformly and, because of this, the principle of threshold is not as well defined as in air.

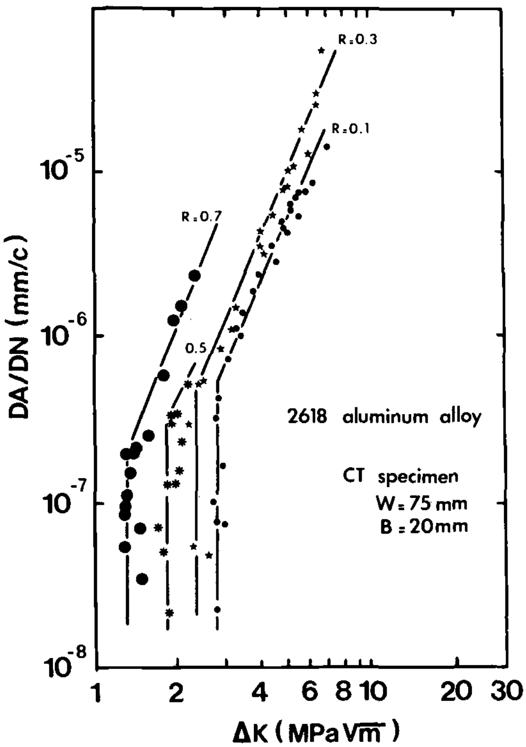

FIG. 2—*Effect of the* R-*ratio on the low FCGR of the 2618 aluminum alloy (two tests per value of* R).

Results on 316 Stainless Steel

The stainless steel exhibits a different behavior from that found in the aluminium alloy. The da/dN versus ΔK curve does not present a well-defined knee down to 10^{-7} mm/cycle. The curve exhibits a continuous slope for crack growth rates between 10^{-7} and 10^{-3} mm/cycle (Fig. 4).

Some experiments carried out below 10^{-7} mm/cycle have shown the existence of a knee, in the da/dN versus ΔK curve, around 10^{-7} mm/cycle.

The results are presented in Table 4. These data cannot be considered as threshold values, but only as values of ΔK corresponding to a given crack growth rate.

The results obtained exhibited larger scatter in the data. For example, Fig. 5 reports the results obtained under the same experimental conditions: $R = 0.15$ and specimens with $B = 20$ mm and $W = 2B$. For a given value of ΔK in the range $5 < \Delta K < 10$ MPa$\sqrt{\text{m}}$, the crack growth rate scatter is 1 to 4 within a given laboratory and 1 to 6 for all laboratories.

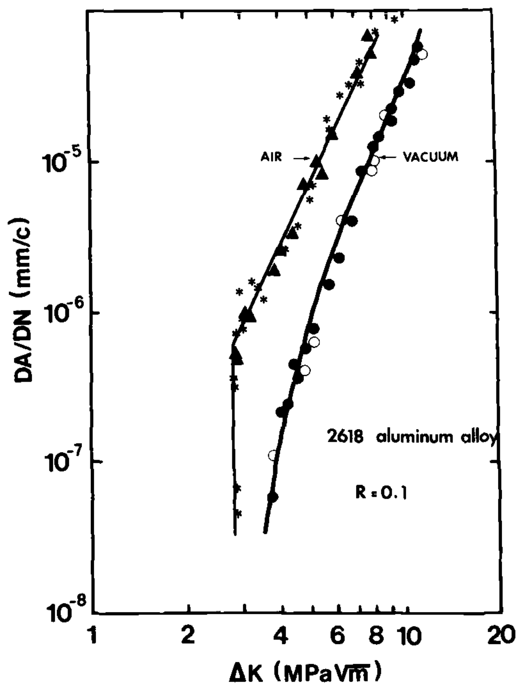

FIG. 3—*Effect of the environment on the low FCGR of the 2618 aluminum alloy.*

The test parameters such as specimen type, thickness, crack length, and wave form have no influence on the low FCGR region (Table 4).

The effect of the environment (air or vacuum) was found negligible in this material. Only the R-ratio affects the low FCGR of the 316 steel (Table 4). In this domain the value of ΔK at a given rate decreases as R increases.

Discussion

2618 Aluminum Alloy Results

The establishment of the crack arrest threshold of the 2618 aluminum alloy does not present any difficulty, and the scatter of the data among the laboratories is only ± 10 percent on ΔK, which is acceptable. The difficulties experienced for the second alloy studied are not evident here, probably because the crack front remains almost straight in every case. Therefore the proposed method is convenient.

The fact that the specimen geometry does not affect the results is signifi-

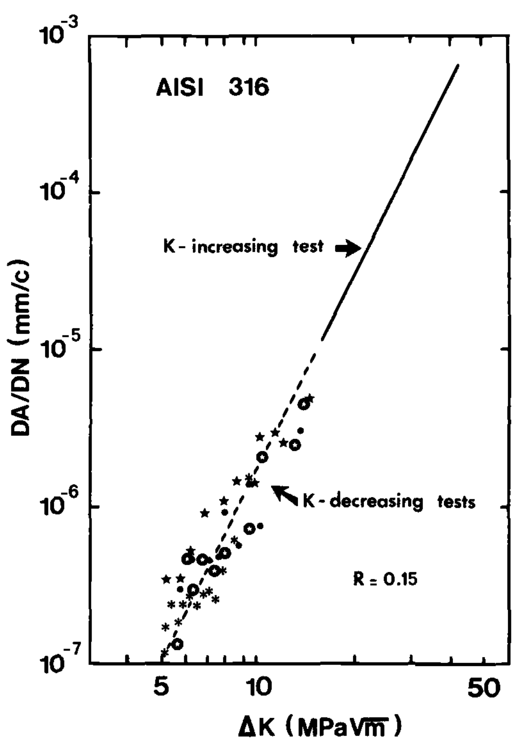

FIG. 4—*Typical behavior of the AISI 316 steel in the low FCGR range.*

cant because, if the threshold criterion is to be used in design, one must ascertain that this parameter does not change with geometry.

No effect of the sampling direction was observed. This observation confirms that some metallurgical parameters which are known to affect the endurance limit do not play the same role for the threshold.

AISI 316 Results

Scatter of the Results—It was noticed previously that the FCGR variability in the investigated range could be 1 to 6 for a given value of ΔK. This is much more than the 1 to 2 variability in FCGR within the range $10^{-5} < da/dN < 10^{-3}$ mm/cycle [*17*]. In our opinion there are several reasons for this:

1. *Difficulty in Following the Fixed Procedure When Load Shedding is Manually Applied to the Specimen*—As several days are needed to finish this type of test, it is often necessary to reduce frequency during nights in order to allow the operator to monitor crack growth. Doing so, transient phenomena may occur during the cracking process, which may influence the final result.

TABLE 4—*Effect of various parameters on low FCGR of 316 steel.*

Parameter Studied	Variation of the Parameter Studied	Crack Growth Rate, mm/cycle	Corresponding Values of ΔK, MPa$\sqrt{m}$
	5		8.0
	10		7.0
Specimen thickness (B)	20	3×10^{-6}	6.5
	25		7.0
Specimen type	CCT	10^{-6}	7.2
	CT		9.0
	0.1		5.8
Load ratio (R)	0.6	10^{-7}	4.2
	0.8		3.5
	0.4		6.6
Crack length (a/W)	0.5	10^{-7}	5.9
	0.6		5.7
	triangle		8.5
Waveform	square	10^{-6}	9.6
	air		9.0
Environment	vacuum 10^{-5} torr	10^{-6}	8.6

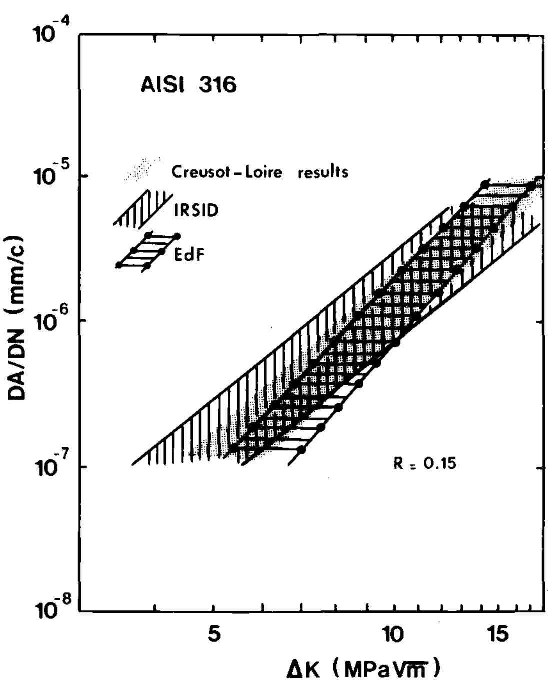

FIG. 5—*Scatterbands of the low FCGR results obtained in three different laboratories.*

These troubles are absolutely unforeseeable and are not reproducible. An optimum approach would be to carry out the load shedding with an automatically controlled testing machine.

2. *Small Crack Increment Used at Each Load Step*—This increment was insufficient to minimize the delay observed after each load shed. It was chosen equal to 0.3 mm because of the small value of the specimen width W.

3. *Crack Tunnelling Effect.*

Figures 4 and 5 refer to surface crack length measurements. However, an examination of the fracture surfaces of cracked specimens made in 316 steel shows that the crack curvature varies enormously from one specimen to another in this material. In particular, it is much more accentuated in the case of tests carried out with large values of dK/da.

Moreover, for a given specimen, crack curvature varies from one step to another, becoming accentuated as ΔK decreases (Fig. 6). We have thus calculated that the correction factor γ defined by

$$\gamma = (\Delta K_{\text{midthickness}} - \Delta K_{\text{surface}})/\Delta K_{\text{surface}}$$

was on the order of 22 percent for $\Delta K_{\text{surface}} \simeq 5$ MPa$\sqrt{\text{m}}$, and 15 percent for $\Delta K_{\text{surface}} \simeq 10$ MPa$\sqrt{\text{m}}$. As all the steps are not always well marked, it seems difficult in these precise cases to apply a proper correction.

If the crack front takes on a new curvature whenever the load amplitude varies, the midthickness crack growth rate of the specimen is not equal to that measured on the surface. Logically, to the ΔK-correction which displaces the test points along a horizontal line must be added a (da/dN) correction which displaces these same points along a vertical line. This remark regarding the crack front curvature greatly penalizes the results of these fatigue tests at low propagation rates. They are not all representative of the real values of the threshold ΔK_{th} and of the low growth rates.

As a consequence, it seems necessary to get data about the susceptibility of a given material to crack tunnelling prior to any threshold test. In this condition, it is possible to choose the correct specimen size which minimizes the effect of crack tunnelling on ΔK-values. In particular, the choice of a greater value of ratio W/B is a good way to achieve this point.

ΔK *Decreasing Rate*

Generally, the load shedding rate applied to the great majority of the specimens tested in this work violated ASTM recommendations when it was expressed in terms of dK/da [*18*]. Most of the tests were carried out under the conditions described in Table 5.

From Fig. 7 where center-cracked-tension (CCT) and compact type (CT) results are compared, different FCGR curves can be drawn. It happens that the tests carried out with the lower ΔK decrease rates give results at the upper

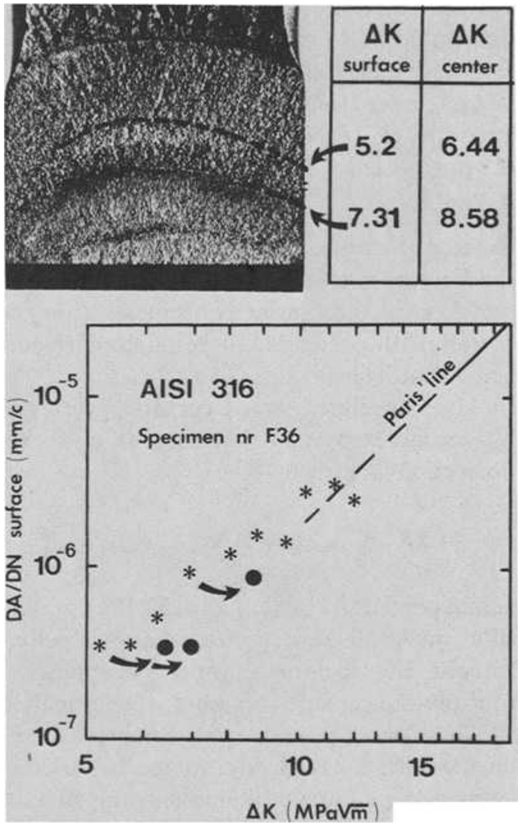

FIG. 6—*Influence of the crack tunnelling on the ΔK-values at the center and at the surface of the specimen.*

TABLE 5—ΔK *decreasing rates observed for various test conditions.*

Material	Test Condition	dK/da	$\frac{1}{K} \times \frac{dK}{da}$
2618 aluminum alloy	standard	-0.7	$-0.17\ \text{mm}^{-1}$
AISI 316	standard	-2.20	$-0.33\ \text{mm}^{-1}$
	CCT $\frac{2a}{W} = 0.23$	-1.38	...
	0.42	-1.29	...
	0.62	-0.67	...
	Ref *18*	-0.3	...

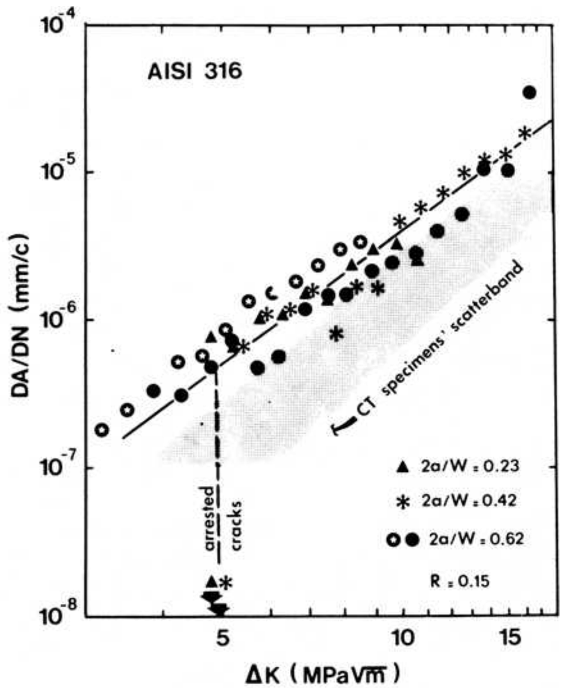

FIG. 7—*Comparison between the results obtained with CT 20 specimens and CCT specimens.*

bound of the scatterband. So, for a given value of ΔK, measured FCGR are decreasing with respect to the procedure used, according to the following order: (*1*) CCT with $2a/W = 0.62$, (*2*) CCT with $2a/W = 0.42$ and 0.23, and (*3*) the standard procedure with CT 20 specimens. The main conclusion that can be drawn from these results is that the rate of ΔK decrease is a parameter that has an influence on low FCGR. No effect on low FCGR can be attributed to specimen type, as it is possible to observe comparative behaviors with large enough CT or CCT specimens.

General Conclusions

This investigation has shown that different materials may exhibit different behaviors in the low FCGR range:

1. For 2618 aluminum alloy, the existence of a crack arrest threshold has been demonstrated with no ambiguity, because of the presence of a knee in the curve representing the low FCGR.
2. For AISI 316 steel, it has not been possible to establish a vertical asymp-

tote on this line, and it appeared useful to define the value of the threshold ΔK_{th} at a prescribed crack growth rate.

The principal observations made during this investigation are:

1. The data scatter obtained at low crack growth rates ($< 10^{-5}$ mm/cycle) is small for the 2618 aluminum alloy, but it is wider for the 316 steel because of the standard specimen geometry which causes crack tunnelling and allows only small crack increments at each load step.
2. With the load-shedding procedure used in this work, the test parameters (such as the specimen geometry, its thickness, the crack length, the test frequency, and the wave form) do not have any effect on the low FCGR.
3. When the R-ratio increases, the threshold ΔK_{th} decreases. Among all the parameters studied, the R-ratio has the largest influence on ΔK_{th}.

A Note on the Fatigue Commission of the French Metallurgical Society

This work is a part of the activities of the Fatigue Commission of the French Metallurgical Society whose president is M. G. Pomey, head of the Centre des Matériaux, Corbeil.

This program has been initiated and coordinated by C. Bathias, professor at Université de Technologie de Compiègne and consultant at Société Nationale Industrielle Aerospatiale.

The primary participants are:

Mm. Petrequin and Gauthier	CEA—Saclay
Mm. Rabbe and Amzallag	Creusot-Loire—Firminy
Mm. Valibus and Grattier	EdF—Renardières
M. Petit	ENSMA—Poitiers
M. Pineau	ENSMP—Corbeil
Mme. Benoit; Mm. Lieurade and Truchon	IRSID—Saint Germain-en-Laye
M. Ferton	PECHINEY—Voreppe
M. Bathias	SNIAS—Suresnes/U.T.C.
M. Pluvinage	Université de Metz

References

[1] Ritchie, R. O., *Metal Science Journal*, Aug.-Sept. 1977, p. 368.
[2] Frost, N. E., Pook, L. P., and Denton, K., *Engineering Fracture Mechanics*, Vol. 3, 1971, p. 109.
[3] Klesnil, M. and Lukas, P., *Engineering Fracture Mechanics*, Vol. 4, 1972, p. 77.
[4] Klesnil, M. and Lukas, P., *Materials Science and Engineering*, Vol. 9, 1972, p. 231.
[5] Pook, L. P., *Stress Analysis and Growth of Cracks, ASTM STP 513*, American Society for Testing and Materials, 1972, p. 106.
[6] Bucci, R. J., Paris, P. C., Hertzberg, R. W., Schmidt, R. A., and Anderson, A. F. in *Stress Analysis and Growth of Cracks, ASTM STP 513*, American Society for Testing and Materials, 1972, p. 125.
[7] Paris, P. C., Bucci, R. J., Wessel, E. T., Clark, W. G., and Mager, T. R. in *Stress*

Analysis and Growth of Cracks, ASTM STP 513, American Society for Testing and Materials, 1972, p. 141.

[8] Bucci, R. J., Clark, W. G., and Paris, P. C. in *Stress Analysis and Growth of Cracks, ASTM STP 513,* American Society for Testing and Materials, 1972, p. 177.

[9] Kitagawa, H., Nishitani, H., and Matsumoto, J. in *Proceedings,* Third International Congress on Fracture, Paper V 444/A, Munich, 1973.

[10] Schmidt, R. A. and Paris, P. C., *Progress in Flaw Growth and Fracture Toughness Testing, ASTM STP 536,* American Society for Testing and Materials, 1973, p. 79.

[11] Robinson, J. I. and Beevers, C. J., *Metal Science Journal,* Vol. 7, 1973, p. 153.

[12] Irving, P. E. and Beevers, C. J., *Metallurgical Transactions,* Vol. 5, 1974, p. 391.

[13] Cooke, R. J., Irving, P. E., Booth, G. S., and Beevers, C. J., *Engineering Fracture Mechanics,* Vol. 7, 1975, p. 69.

[14] Masounave, J. and Bailon, J. P., *Scripta Metallurgica,* Vol. 10, 1976, p. 165.

[15] McEvily, A. J. and Groeger, J. in *Fracture 1977, Proceedings,* Fourth International Conference on Fracture, Vol. 2, Waterloo, Canada, June 1977.

[16] Bouchet, B., Boisson, P., Chaunet, H., Nadeau, A., and Petit, J., *Mechanique Materiaux Electricite,* Vol. 327, 1977, p. 29.

[17] Clark, W. G. and Hudak, S. J., *Journal of Testing and Evaluation,* Vol. 3, No. 6, 1975, pp. 454–476.

[18] Hudak, S. J., Saxena, A., Bucci, R. J., and Malcolm, R. C., "Development of Standard Methods of Testing and Analyzing Fatigue Crack Growth Rate Data," Westinghouse Research Report No. 77-9E7-AFCGR-R1, March 1977.

DISCUSSION

Jacques Masounave[1] *and Jean-Paul Bailon*[1] *(written comment)*—Our comments concern the microstructural aspect of the nonpropagation threshold. Your results show that the nonpropagation threshold ΔK_T for 2618 alloy is not affected by the relative orientation of the crack with respect to the rolling direction. This means that ΔK_T is the same whether the effective grain size is large or small. For aluminum alloy we also found no influence of grain size on ΔK_T. We propose the following explanation.

We found that grain size has a large influence in low-carbon steel,[2] which can be described by the relationship

$$\Delta K_{TF} = K_o + K_f d^{1/2} \tag{1}$$

where F refers to ferrite, and K_o and K_f are materials constants (see Fig. 8). For a biphased steels (ferritic-pearlitic) we obtained the relation

$$\Delta K_{TF \cdot p} = f_F \Delta K_{TF} + (1 - f_F) \Delta K_{TP} \tag{2}$$

[1] Département de Génie Métallurgique, Ecole Polytechnique de Montréal, Montréal, Quebec, Canada.

[2] Masounave, J. and Bailon, J.-P., *Scripta Metallurgica,* Vol. 10, 1976, pp. 165–170.

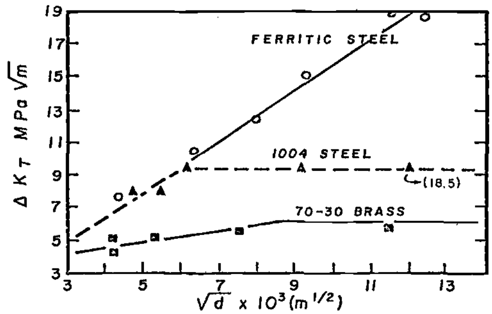

FIG. 8—*Illustration referred to in Discussion.*

where f_F is the volume fraction of ferrite, and P refers to pearlite. For pearlite we obtained, experimentally, a constant value of 10.8 MPa$\sqrt{m}$. This value is not affected by variation of size of pearlite lamelle or by variation of size of pearlite colonies.

On the other hand, more recent work[3] shows that, at least for certain metals (aluminum alloys, 70-30 brass, 316 L stainless steels), ΔK_T does not increase indefinitely with grain size. This work shows that ΔK_T attains a constant value, above a constant grain size. This value of grain size is related to the value of the size of the cyclic plastic zone.

The well-known Hall-Petch relation is, for monotonic strength,

$$\sigma_y = \sigma_o + k_y d^{-1/2} \tag{3}$$

where σ_o describes the effect of matrix on the yield stress, and k_y describes the effect of grain boundaries. In Eq 1 the parameter K_f should describe the effect of grain boundaries on ΔK_T. Based on data in the literature, the following correlation between the parameters was obtained:[4]

$$K_f = 2780\, k_y^{\,2} \tag{4}$$

This correlation indicates that the threshold in ferritic steel is affected by grain size (k_y is large). On the other hand, Eq 4 indicates that aluminum alloys should be almost insensitive to variations of grain size (k_y is small).

[3] Lanteigne, J., Ph.D. thesis, Ecole Polytechnique de Montréal, Montréal, Quebec, Canada.
[4] Bailon, J.-P., Masounave, J., and Lanteigne, J., *Scripta Metallurgica*, Vol. 12, 1978, pp. 607-611.

L. A. James[1]

Specimen Size Considerations in Fatigue Crack Growth Rate Testing

REFERENCE: James, L. A., "**Specimen Size Considerations in Fatigue Crack Growth Rate Testing,**" *Fatigue Crack Growth Measurement and Data Analysis, ASTM STP 738,* S. J. Hudak, Jr., and R. J. Bucci, Eds., American Society for Testing and Materials, 1981, pp. 45–57.

ABSTRACT: The effect of specimen size upon the fatigue crack growth rate behavior of annealed AISI Type 304 stainless steel was studied at two stress ratios at an elevated temperature. The resulting data were examined in the light of the present ASTM size criterion (based upon monotonic yield strength) and a proposed criterion based upon the material flow strength. The flow stress criterion is considerably less restrictive than the present ASTM criterion. The results of this study indicate that the flow stress criterion is entirely appropriate for strain-hardening materials such as austenitic stainless steels.

KEY WORDS: crack propagation, plastic deformation, fatigue testing, flow stress, strain hardening, specimen size criterion

Linear-elastic fracture mechanics (LEFM) techniques presently offer the most generally applicable method for estimating the in-service extension of cracks and flaws in structural components. As the name implies, LEFM methods are valid only as long as there is a linear and elastic relationship between the loads applied to a cracked structure (or specimen) and the resulting displacements. There is, of course, a zone of plastically deformed material in the immediate vicinity of the crack tip, but this is allowable as long as the plastic zone is relatively small compared with the other dimensions of the structure (or specimen). Hence, the small plastic zone is surrounded by a much larger region of elastically loaded material, and the linear-elastic response is essentially preserved.

LEFM analyses of crack extension in structural components can only be as valid as the data that is input into them. Such crack growth rate data are usually obtained on specimens in the laboratory, and for reasons of economy (material, testing machine size, etc.) it is often desirable to have such

[1]Fellow engineer, Westinghouse Hanford Company, Richland, Wash. 99352.

specimens as small as possible. If, however, the specimens become too small, then there is the possibility that the crack tip plastic zone size will approach the other dimensions of the specimen, thereby invalidating the use of LEFM methods on that specimen.

In order to minimize the possibility of this occurring and to standardize the other aspects of crack growth rate testing, the American Society for Testing and Materials (ASTM) has developed a Tentative Test Method for Constant-Load-Amplitude Fatigue Crack Growth Rates Above 10^{-8} m/Cycle (E 647-78 T).[2] Much of the background information and rationale leading to the development of ASTM E 647 may be found in Ref *1*.

ASTM E 647 limits the relative size of the plastic zone in a compact specimen, and hence the specimen size, by limiting the minimum size of the remaining uncracked ligament ($W - a$), where W = the specimen width, and a = the crack length (see ASTM E 647 for symbols and nomenclature pertaining to the ASTM compact specimen). It is essentially equivalent to restricting the plane stress monotonic plastic zone size ($2r_y$)

$$2r_y = \frac{1}{\pi}\left[\frac{K_{\max}}{\sigma_y}\right]^2 \tag{1}$$

to a fixed percentage of the remaining ligament ($K_{\max}$ = the maximum stress intensity factor, and σ_y = the monotonic yield strength). This is accomplished through the relationship

$$(W - a) \geq \frac{4}{\pi}\left[\frac{K_{\max}}{\sigma_y}\right]^2 \tag{2}$$

Combining Eqs 1 and 2 shows that the ASTM E 647 size requirement limits the monotonic plastic zone to about 25 percent of the uncracked ligament.

While the size criterion of Eq 2 is probably appropriate for relatively high-strength materials which undergo little or no strain-hardening, there is evidence [*1*-*5*][3] that it is unnecessarily restrictive (that is, requires specimen sizes larger than necessary) for relatively low-strength materials that exhibit considerable strain-hardening (for example, annealed austenitic stainless steels). It was suggested [*2*] that a more appropriate size criterion for these strain-hardening materials would be to replace the monotonic yield strength (σ_y) in Eq 2 with the flow stress (σ_f)

$$\sigma_f = \frac{\sigma_y + \sigma_u}{2} \tag{3}$$

[2]ASTM E 647-78 T is reprinted in this volume as Appendix I, pp. 321-339.

[3]The italic numbers in brackets refer to the list of references appended to this paper.

where σ_u = the ultimate strength. References *1* to *5* present data which support the concept of a flow stress criterion for such materials.

It was, however, considered desirable to conduct additional tests to verify the validity of a remaining ligament criterion based upon the flow stress, particularily at elevated temperatures and at stress ratios ($R = K_{min}/K_{max}$) considerably higher than zero. Therefore the object of the present study was to conduct tests upon relatively large specimens of a strain-hardening material (which generally satisfied the criterion based upon monotonic yield strength) and to compare the results with similar data from relatively small specimens of the same material (which generally violated the monotonic yield criterion).

Experimental Procedure

The specimens used in this study were of the ASTM compact specimen design (see ASTM E 647), and were constructed of annealed AISI Type 304 stainless steel. The material was furnished by the Westinghouse R&D Center, and was the same heat of Type 304 utilized in Ref *3*.

Tensile tests were not conducted on this material at 288°C (550°F). They were conducted at room temperature and reported in Ref *3*.

$$\left.\begin{aligned}\sigma_y &= 269\text{ MPa (39.0 ksi)}\\ \sigma_u &= 579\text{ MPa (84.0 ksi)}\\ \sigma_f &= 424\text{ MPa (61.5 ksi)}\end{aligned}\right\}\text{monotonic}$$

$$\sigma_y = 421\text{ MPa (61.0 ksi)—cyclic}$$

Note the approximate equivalence of the flow stress and the cyclic yield for this material. The present crack growth tests were conducted at 288°C (550°F), and the percentage reductions in room temperature properties at this temperature give [*6*]

$$\sigma_y = (0.617)(39.0) = 165\text{ MPa (24.0 ksi)}$$

$$\sigma_u = (0.767)(84.0) = 444\text{ MPa (64.4 ksi)}$$

Therefore, using Eq 3, a flow stress of 305 MPa (44.2 ksi) is calculated for 288°C (550°F).

Two specimen sizes were employed in the testing: 1T specimens with width W = 50.8 mm (2.0 in.) and thickness B = 6.35 mm (0.25 in.), and 4T specimens with W = 203 mm (8.0 in.) and B = 25.4 mm (1.0 in.). The 4T specimens were tested so as to maximize the amount of data taken under conditions satisfying the monotonic yield strength criterion. The 1T specimens, on the other hand, were tested so that they essentially violated the monotonic criterion from the start of the test, while the data overlap with the 4T specimens was maximized. Two stress ratios were studied: R = 0.05 and R = 0.5.

The specimens were tested on MTS feedback-controlled testing machines using load as the control parameter. A sinusoidal waveform at a cyclic frequency of 150 cpm (2.5 Hz) was used for all tests. Testing was conducted in air-circulating furnaces at 288°C (550°F). Temperatures were controlled to within 1°C (2°F) for 1T specimens, and to within 2.2°C (4°F) for 4T specimens. Crack lengths were determined periodically throughout each test on both sides of each specimen using a travelling microscope. (See Ref *7* for detailed crack length versus cycles data for each specimen.) In general, all of the testing and data analysis procedures for ASTM E 647 were adhered to.

The crack growth rates (da/dN) were calculated using the "secant method" [*8*]. The stress intensity factor was obtained using the relationship

$$K = \frac{P}{B\sqrt{w}}\left[\frac{2+\alpha}{(1-\alpha)^{1.5}}\right][0.886 + 4.64(\alpha) - 13.32(\alpha)^2 + 14.72(\alpha)^3 - 5.6(\alpha)^4] \quad (4)$$

where P = the applied load, and α = the relative crack length ($\alpha = a/W$). Although the stress intensity factor range (ΔK) is usually employed as the crack-driving parameter, it is felt [*1*] that the maximum stress intensity factor (K_{max}) is of greater importance in establishing size criteria than is ΔK. Therefore the results of this study were displayed as logarithmic plots of da/dN as a function of K_{max}.

Results and Discussion

Tests were conducted at stress ratios of 0.05 and 0.5, and these results are plotted in Figs. 1 and 2, respectively. Also plotted in these figures are the K-levels where each specimen size (either 1T or 4T) fails either the criterion based upon the monotonic yield strength (Eq 2) or the criterion based upon the flow stress.

A number of observations may be made regarding the data shown in Figs. 1 and 2. Firstly, it is apparent that there is excellent agreement at both stress ratios between the data for the 1T and 4T specimens, regardless of whether the monotonic yield strength criterion is satisfied or not. In general, the data scatter is within the factor of two considered "normal" for intralaboratory tests on the same heat of material [*8*]. Data at both stress ratios are easily fitted by linear relationships between log (da/dN) and log (K_{max}). Linear regression lines through all data shown in Figs. 1 and 2 are plotted in the respective figures. In addition, linear regression analyses were performed for each specimen individually, excluding data that violated the flow stress criterion. These regression constants are given in Table 1. It will be noted that the slopes (n) for the two different specimen sizes tested at R = 0.5 are practically identical. On the other hand, the slope for the 1T specimen tested at R = 0.05 is somewhat

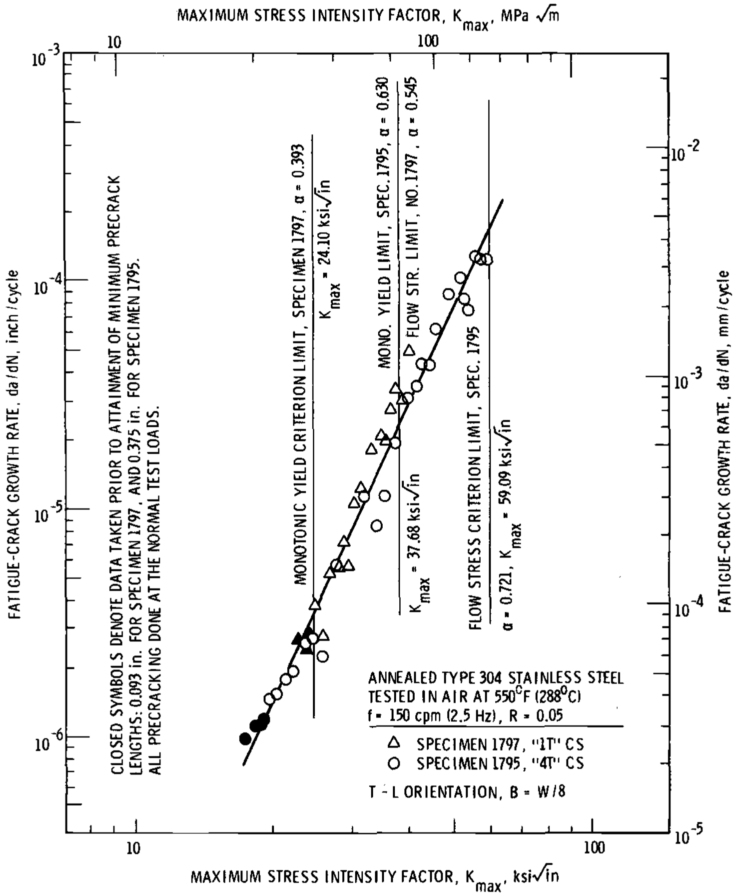

FIG. 1—*Fatigue crack growth behavior of 1T and 4T specimens of annealed Type 304 stainless steel tested in air at 288°C (550°F) at a stress ratio* R = *0.05.*

higher than that for the 4T specimen tested under similar conditions. This difference is partially compensated for by differences in the constants C such that the curve for the 1T specimen is approximately a factor of 1.03 lower than that for the 4T specimen at the lower end of the data overlap, and approximately a factor of 1.56 higher at the upper end of the data overlap. It is not known if these differences are statistically significant or not. However, there is considerable overlap of the scatter bands, and the differences certainly lie within the range where it is difficult to separate actual behavioral differences from normal experimental scatter. Hence, the author is inclined to regard such differences as minimal or nonexistant. Similar observations regarding the equivalence of results between specimens of different sizes (the smaller of which did not meet the monotonic yield criterion) may be found in Refs *1* to *5*.

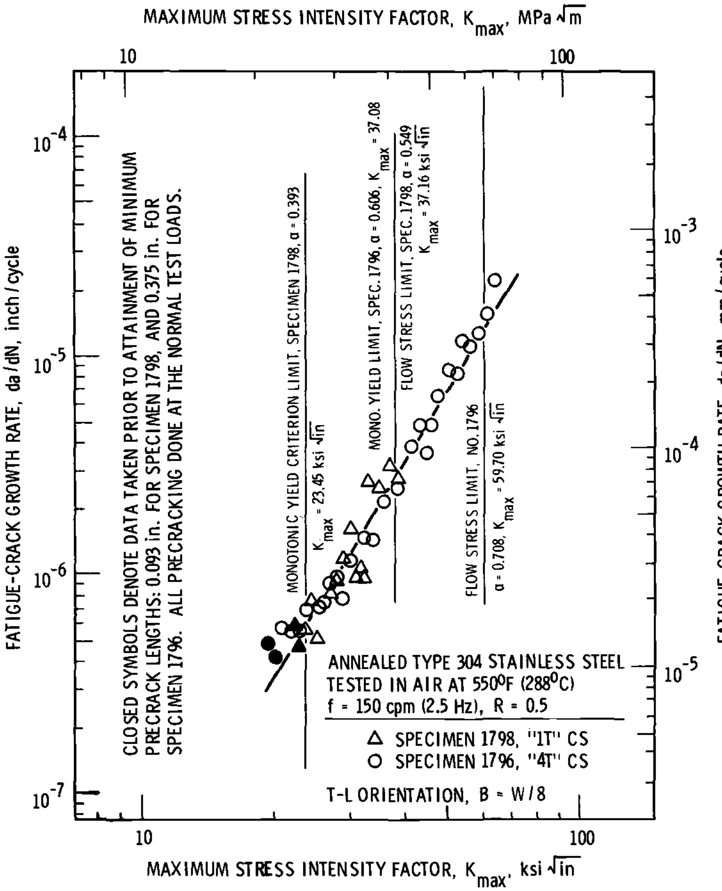

FIG. 2—*Fatigue crack growth behavior of 1T and 4T specimens of annealed Type 304 stainless steel tested in air at 288°C (550°F) at a stress ratio of* R = *0.5.*

TABLE 1—*Regression constants*[a] *for the crack growth law* $da/dN = C(K_{max})^n$.

Specimen No.	Specimen Size	C	n	Correlation Coefficient[b]
1795	4T	3.130×10^{-12}	4.338	0.9925
1797	1T	7.502×10^{-14}	5.493	0.9829
1795, 1797	1T, 4T	2.567×10^{-12}	4.416	0.9865
1796	4T	2.318×10^{-11}	3.235	0.9877
1798	1T	1.849×10^{-11}	3.274	0.8995
1796, 1798	1T, 4T	1.494×10^{-11}	3.354	0.9813

[a]Units: da/dN = inch/cycle, K_{max} = ksi$\sqrt{\text{inch}}$.
[b]Unity indicates a "perfect" linear fit.

One of the questions raised in Ref *1* was that a criterion such as the proposed flow stress criterion (which implicitly depends upon strain-hardening) might be appropriate for stress ratios close to zero (where stress reversals are large) and yet not be appropriate at higher stress ratios (where stress reversals are much smaller). This is because there are actually two plastic zones at the tip of a fatigue crack: a relatively large "monotonic yield zone" created during the tensile loading portion of each fatigue cycle, and a smaller "cyclic yield zone" created during the stress reversals occurring on the unloading portion of each cycle. As discussed in Ref *1*, the cyclic zone can be considerably smaller than the monotonic zone in strain-hardening materials tested at relatively high stress ratios. Reference *1* also pointed up that the validity of the flow stress criterion at high stress ratios was uncertain due to the lack of data for different specimen sizes in strain-hardening materials under these conditions. The results shown in Fig. 2 certainly lend support to the validity of the flow stress criterion, at least for annealed Type 304 stainless steel at stress ratios up to $R = 0.05$.

The 4T specimens were instrumented with a clip gage that allowed measurement of the load-line displacements at the test temperature. The original intention was to measure the total load-line displacements in the manner suggested in Appendix X2 of ASTM E 647, thereby determining the crack length at which the total actual displacement (elastic plus plastic) exceeded some given percentage of the theoretical elastic displacement. However, it was found that the vibration during testing of the heavy braided metal clip gage leads (necessary for elevated temperature testing) caused the clip gage to constantly shift and reseat on the load-line knife edges. However, although it was not possible to obtain total deflection versus crack length information (as suggested in ASTM E 647), it was possible to obtain load versus load-line displacement information (at elevated temperature) at the completion of a given block of cycles. This was done for both 4T specimens; a typical load-displacement curve is shown in Fig. 3.

Theoretical load-line displacements were calculated using the relationship [*9*]

$$\frac{BEV}{P} = \left(\frac{1 + \alpha}{1 - \alpha}\right)^2 [2.16299 + 12.219(\alpha) - 20.065(\alpha)^2 - 0.9925(\alpha)^3 + 20.609(\alpha)^4 - 9.9314(\alpha)^5] \quad (5)$$

where

B = thickness,
E = Young's modulus,
V = load-line displacement,
P = load, and
$\alpha = a/W$.

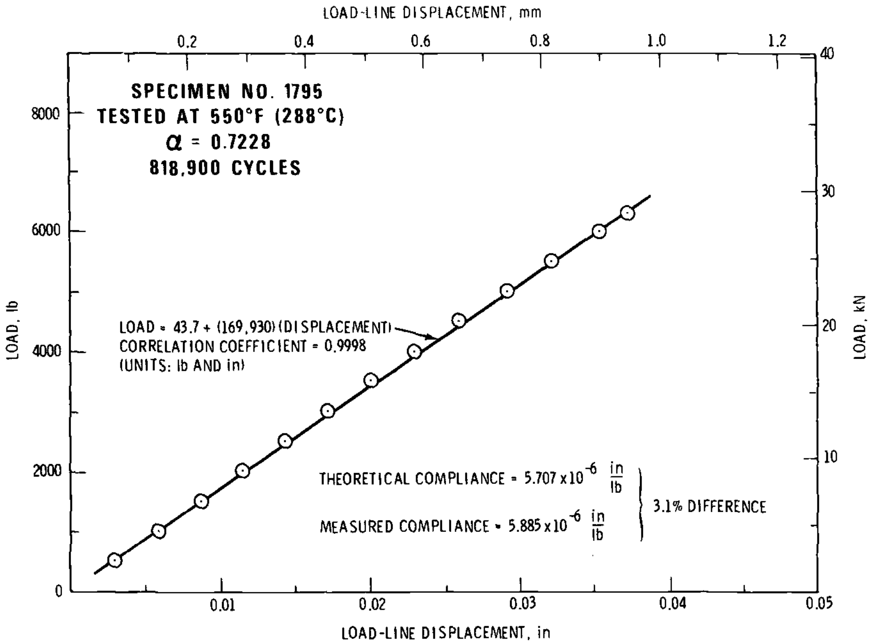

FIG. 3—*Load-displacement behavior of Specimen 1795 at* $\alpha = 0.7228$.

A value of $E = 177.5$ GPa (25.75×10^6 psi) for Type 304 at 288°C (550°F) was obtained from the Nuclear Systems Materials Handbook.

Load-displacement readings were made on a point-to-point basis, and the series of readings fitted with a linear regression analysis; the inverse of the slope being the measured compliance at that value of α. The results are listed in Table 2. In general, the linearity between loads and displacements is excellent, as indicated by the values of the correlation coefficients very close to unity. Comparisons are made with the theoretical compliances calculated using Eq 5. In general, the agreement between theoretical and measured compliances is good, although there is a tendency for the differences to increase with decreasing values of α. Differences between theoretical and measured compliances may be due, in part, to one or more of the following reasons: (*1*) Since the original intent was to measure total load-line displacements, the clip gage was calibrated for much larger displacements than shown in Fig. 3. Hence accuracy might be slightly reduced at lower values of α. (*2*) The assumed value of E could be slightly different, which would affect compliance calculations at all values of α. (*3*) Theoretical compliances were based on crack lengths measured on the surfaces of the specimens, and crack "tunnelling" (which would increase with increasing α) is therefore not ac-

TABLE 2—*Comparison of theoretical and measured compliances.*

Specimen No.	Load Cycles	$\alpha = a/W$	Theoretical Compliance[a]	Measured Compliance[a]	Correlation Coefficient on Measured Compliance
1795	796 400	0.6061	2.549×10^{-6}	2.910×10^{-6}	0.9999
1795	816 900	0.6961	4.631×10^{-6}	4.905×10^{-6}	0.9997
1795	818 900	0.7228	5.707×10^{-6}	5.885×10^{-6}	0.9998
1796	2 319 000	0.6830	4.206×10^{-6}	4.715×10^{-6}	0.9996
1796	2 342 000	0.7228	5.704×10^{-6}	5.894×10^{-6}	0.9992

[a]Units: inch/pound.

counted for in the theoretical calculations. Nevertheless, the agreement between measured and theoretical compliances is reasonable, and linear relationships between load and displacement are observed throughout each test.

Unloading from, and reloading to, a plastic state generally produces a linear relationship between load and displacement (on a macroscale). In an elastic—perfectly plastic material (that is, no strain-hardening) the unloading and reloading would be linear, and one would arrive back at the same yield point after each unloading cycle. In a strain-hardening material (for example, Type 304 stainless steel) the unloading and reloading would also be linear on a macroscale (see Fig. 3), but a slightly higher yield level would be reached after each such cycle, thereby extending the range of linearity for the next cycle. Hence the basic thesis advanced in this paper is that employing the flow stress is a convenient way of accounting for such strain-hardening.

"Before-and-after" photographs of 1T and 4T specimens tested at $R = 0.05$ are shown in Figs. 4 and 5. Although not shown, the specimens tested at $R = 0.5$ are quite similar in appearance. The most striking features of these photographs are the extensive crack-tip plasticity and the permanent opening displacement along the crack line. These photographs were taken at the completion of testing, and it must be remembered that by this time both specimens had failed to satisfy the flow stress criterion.

A person viewing specimens in such a condition would justifiably suggest that they could not be analyzed with LEFM methods. Yet at crack lengths only slightly less than those pictured (see Ref *7* for tabular data), these specimens still satisfied the flow stress criterion and (in the case of the 1T specimens) were producing results in excellent agreement with "valid" data satisfying the monotonic yield criterion. In addition, the crack-tip plasticity and permanent opening displacements were not visibly different from those pictured in Figs. 4 and 5.

We are thus faced with an apparent paradox. LEFM methods continue to

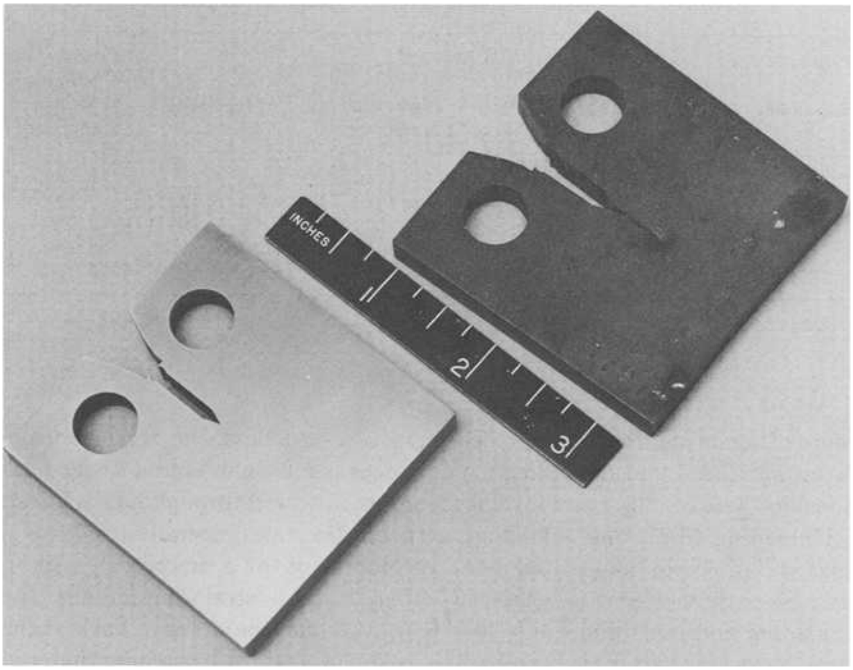

FIG. 4—*"Before-and-after" photographs of 1T specimens (Specimen 1797 at α = 0.5658).*

empirically describe cracking behavior (witness the excellent agreement in da/dN versus K_{max} curves and the agreement between theoretical and measured compliances) on specimens where visual observation (and some analytical treatments) indicates they should not. The basic concepts of LEFM (for example, the calculation of K) can be rigorously derived from the theory of elasticity, but it should be remembered that no rigorous derivation exists for predicting the relationship between da/dN and K; it remains an empirical observation. The results of this study suggest that this empirical observation perhaps has a wider range of applicability than suggested by rigid adherence to linear-elastic requirements.

Finally, it will be noted in Figs. 1 and 2 that some of the data points at the lower values of K_{max} are closed, rather than open, symbols. These represent data that were taken prior to the attainment of the minimum precrack specified by ASTM E 647. This requirement states that the minimum precrack length from the machined notch shall be one tenth the specimen thickness (B) or the height (h) of the notch, whichever is the greater. For the 1T specimens used in this study $0.1B$ = 0.635 mm (0.025 in.) and h = 2.36 mm (0.093 in.), and for the 4T specimens $0.1B$ = 2.54 mm (0.10 in.) and h = 9.53 mm (0.375 in.). Hence the h-dimension governs in both cases. The

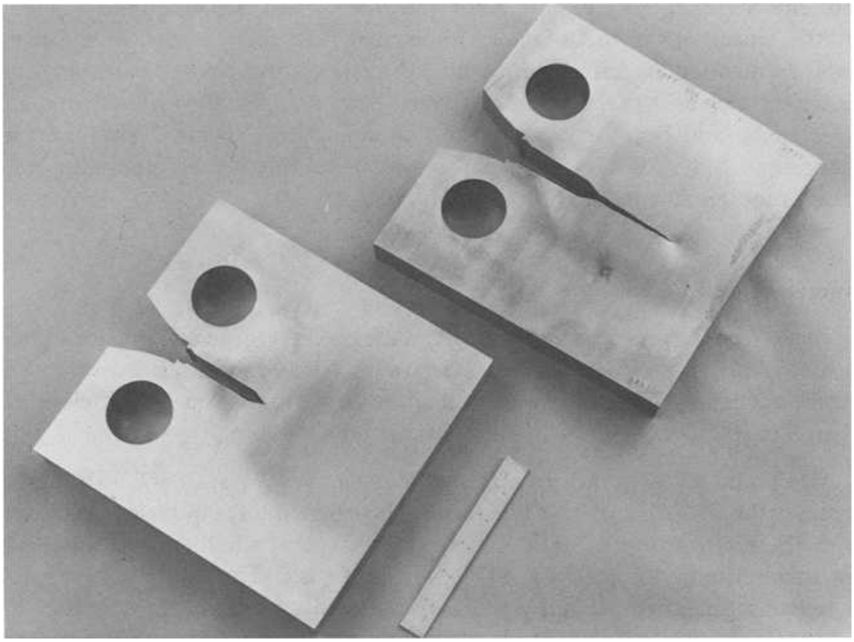

FIG. 5—*"Before-and-after" photographs of 4T specimens (Specimen 1795 at $\alpha = 0.7228$).*

closed data points in Figs. 1 and 2 suggest that this requirement on minimum precrack length might be somewhat restrictive. Little or no difference in behavior is noted between open and closed data points in the same general vicinity. Similar observations were made by James and Mills[4] concerning the minimum precrack requirements during the testing of standard ASTM compact specimens and the proposed round compact specimens at room and elevated temperatures in precipitation heat-treated Alloy 718.

The minimum precrack length requirement is, of course, intended to minimize the possibility of an influence of the machined notch, since the effect of the notch is not accounted for in Eq 4. Some guidance regarding the effect of notches on the K-solutions for cracks may be found in Ref *10*. Cracks emanating from rectangular notches (probably more severe in their interaction with the crack than the V-shaped notches used in compact specimens) in an infinite sheet were studied. Although the infinite sheet represents a different geometry than the compact specimen, Ref *10* should nevertheless allow an upper-bound estimate of the interaction. These results show that when the precrack length is greater than about $h/2$, the interaction factor is approximately 1.01, while at a length of h (corresponding to the

[4]This publication, pp. 70–82.

present ASTM E 647 requirement) the interaction factor is approximately 1.005. Since both of these factors are smaller than many of the other uncertainties involved in fatigue crack growth testing, and since the rectangular notch of Ref *8* is probably more severe than notches allowed on compact specimens, and because of the results shown in Figs. 1 and 2 and given in James and Mills,[4] it does not seem unreasonable to relax the minimum precrack requirements of ASTM E 647.

Summary and Conclusions

The effect of specimen size upon the fatigue crack growth behavior of annealed AISI Type 304 stainless steel (a material exhibiting considerable strain-hardening behavior) was studied at two stress ratios at an elevated temperature. The results may be summarized as follows:

1. 1T and 4T compact specimens have been tested at 288°C (550°F) at stress ratios of 0.05 and 0.5. The results show essentially equivalent behavior over the entire range of data overlap, regardless of whether the remaining ligament criterion of ASTM E 647 is satisfied or not. The results also support a remaining ligament based upon flow stress for strain-hardening materials such as austenitic stainless steels; the flow stress criterion is considerably less restrictive than that of ASTM E 647.
2. Load-line displacement measurements were made on the two 4T specimens at the test temperature of 288°C (550°F). Linear relationships between loads and displacements, plus good agreement between theoretical and measured compliances were obtained, even at very long crack lengths where the flow stress criterion was violated.
3. Limited results suggest that the ASTM E 647 criterion for minimum precrack length from the machined notch could be relaxed somewhat, thereby permitting slightly more data to be taken at shorter crack lengths.

Acknowledgments

This work was performed by Westinghouse Hanford Company, a subsidiary of Westinghouse Electric Corporation, under U.S. Department of Energy Contract DE-AC14-76FF02170.

References

[1] Hudak, S. J., Jr., Saxena, A., Bucci, R. J., and Malcolm, R. C., "Development of Standard Methods of Testing and Analyzing Fatigue Crack Growth Rate Data," Report AFML-TR-78-40, Air Force Materials Laboratory, May 1978.

[2] James, L. A., "Some Observations Regarding Specimen Size Criteria for Fatigue-Crack Growth Rate Testing," HEDL-TME 77-87, Westinghouse Hanford Company, Richland, Wash., August 1977.

[3] Brose, W. R. and Dowling, N. E. in *Elastic-Plastic Fracture, ASTM STP 668,* J. D. Landes, J. A. Begley, and G. A. Clarke, Eds., American Society for Testing and Materials, 1979, pp. 720-735.

[4] Dowling, N. E. and Walker, H., "Fatigue Crack Growth Rate Testing of Two Structural Steels," Scientific Paper 77-1D3-PALFA-P3, Westinghouse R&D Center, Pittsburgh, Pa., November 1977.

[5] Sullivan, A. M. and Crooker, T. W., "Specimen Size Effects in Fatigue-Crack Growth Rate Testing," *Report of NRL Progress,* Naval Research Laboratory, January 1978, pp. 17-18.

[6] Smith, G. V., *An Evaluation of the Yield, Tensile, Creep, and Rupture Strengths of Wrought 304, 316, 321, and 347 Stainless Steels at Elevated Temperatures, ASTM Data Series DS 5S2,* American Society for Testing and Materials, 1969.

[7] James, L. A., "Specimen Size Considerations in Fatigue-Crack Growth Rate Testing," HEDL-TME 78-99, Westinghouse Hanford Company, Richland, Wash., December 1978.

[8] Clark, W. G. and Hudak, S. J., Jr., *Journal of Testing and Evaluation,* Vol. 3, No. 6, 1975, pp. 454-476.

[9] Saxena, A. and Hudak, S. J., Jr., *International Journal of Fracture,* Vol. 14, No. 5, 1978, pp. 453-468.

[10] Neal, D. M., *International Journal of Fracture Mechanics,* Vol. 6, No. 4, 1970, pp. 393-400.

R. C. Brown[1] *and N. E. Dowling*[1]

Automatic Decreasing Stress-Intensity Fatigue Crack Growth Rate Testing Using Low-Cost Circuitry

REFERENCE: Brown, R. C. and Dowling, N. E., "**Automatic Decreasing Stress-Intensity Fatigue Crack Growth Rate Testing Using Low-Cost Circuitry,**" *Fatigue Crack Growth Measurement and Data Analysis, ASTM STP 738,* S. J. Hudak, Jr., and R. J. Bucci, Eds., American Society for Testing and Materials, 1981, pp. 58-69.

ABSTRACT: To run decreasing-K tests to very low growth rates, around 10^{-7} mm/cycle, it has previously been necessary to use a digital computer controlled system, or to manually shed the load at prescribed crack lengths. In this work, low-cost, off-the-shelf electronic circuitry was used to control decreasing-K tests so that very low crack growth rates were achieved. This was done automatically, using the compliance method of crack measurement for the electronic control inputs. By switching to constant load limit control, an increasing-K test may be conducted using the same specimen. This predetermined, decreasing-K technique was verified by comparing decreasing and increasing-K data at low growth rates for an alloy steel.

KEY WORDS: fatigue, testing, fracture mechanics, threshold, stresses, cracks, control, electronic, materials, intensity, growth, circuits

Manual load shedding at prescribed crack lengths and digital computer control methods have been developed and used in fracture mechanics to achieve low growth rates (10^{-7} mm/cycle) at stress intensities approaching the threshold value. Both have limitations. Manual load shedding requires many small load decreases to prevent crack arrest. The digital computer approach, using the compliance method of crack measurement,[2] is capable of automatic control of the load steps, but has the disadvantage of purchase

[1]Mechanical research technician and fellow engineer, respectively, Westinghouse R&D Center, Pittsburgh, Pa. 15235.

[2]Saxena, A. and Hudak, S. J., Jr., *International Journal of Fracture*, Vol. 14, No. 5, 1978, pp. 453-468.

and programming costs. The solution was to develop a system using inexpensive digital and analog components with some manual override.

Figure 1 shows the major component blocks of this system, which is designed for use with closed-loop electrohydraulic testing equipment. The circuit was first built in 1976 for fatigue crack growth threshold testing. Before completion of the circuit, however, the tests were run by other means. In late 1978, new fatigue crack growth threshold tests were called for, and the circuit was completed and modified for use at that time.

This paper describes the workings of the circuit and presents data from actual tests run using it. The hope is that this paper will enable laboratories desiring to do this type of work to develop similar circuits and implement them with a minimum of cost.

Decreasing Stress-Intensity Testing

For fatigue crack growth rate testing in the low-rate, threshold region, it is necessary to decrease the stress intensity (K) as crack growth proceeds. In particular, K should decrease exponentially, as explained by Saxena et al,[3] according to

$$K_{\max} = K_{\max,o} e^{C(a-a_o)} \tag{1}$$

where $K_{\max}$ is the maximum stress intensity during a loading cycle, a is crack length, and C is a constant describing the rate of change of $K_{\max}$. The quantities $K_{\max,o}$ and a_o are beginning-of-test values of $K_{\max}$ and a, respectively. Equation 1 is illustrated in Fig. 2 where the variation in $K_{\max}$ with crack length is plotted for particular values of $K_{\max,o}$ and C.

If a specimen geometry and size is chosen, Eq 1 requires that the applied load change in a specific manner with crack length. For the specimen geometry used here, which is shown in Fig. 3, and for the values of $K_{\max,o}$, a_o and C indicated, the curve of Fig. 4 results. This curve is obtained from linear elastic fracture mechanics analysis by noting that stress intensity and load (P) are related by

$$K = \frac{P}{B\sqrt{W}} f(a/W) \tag{2}$$

where specimen thickness (B), specimen width (W), and crack length (a) are specifically defined as in Fig. 3. The dimensionless function $f(a/W)$ depends on the specimen geometry. Specific values of this function for the geometry of Fig. 3 were obtained from Saxena and Hudak.[2] These were used to obtain Fig. 4 and the K/P values given in Table 1.

[3]Saxena, A., Hudak, S. J., Jr., Donald, J. K., and Schmidt, D. W., *Journal of Testing and Evaluation*, Vol. 6, No. 3, 1978, pp. 167-174.

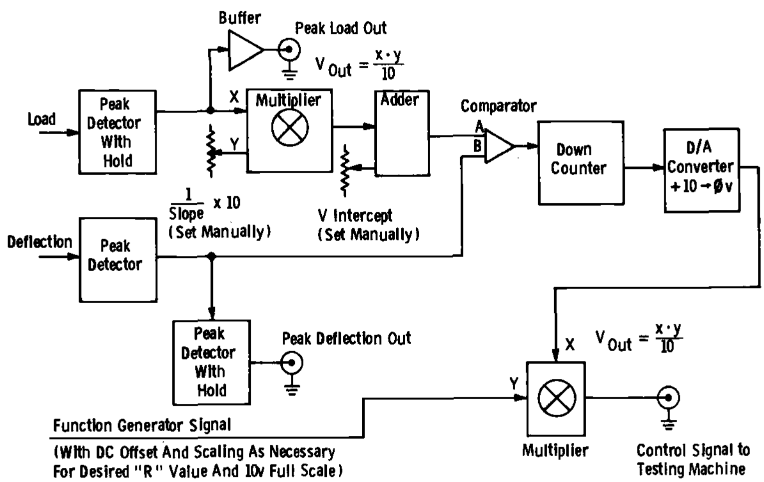

FIG. 1—*Block diagram for control system.*

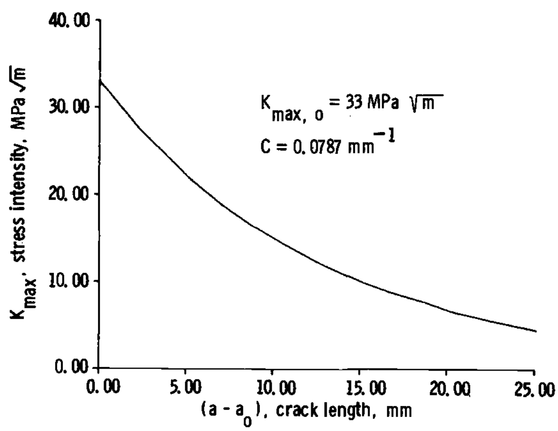

FIG. 2—*Stress intensity* (K) *versus crack length; calculated for example* K*-decreasing test.*

Specimen deflections (V) during decreasing K according to Eq 1 may also be obtained from linear elastic fracture mechanics analysis.

$$V = \frac{P}{BE} g(a/W) \tag{3}$$

where E is the elastic modulus of the material under test, and $g(a/W)$ is a second dimensionless function. The function $g(a/W)$ depends on specimen

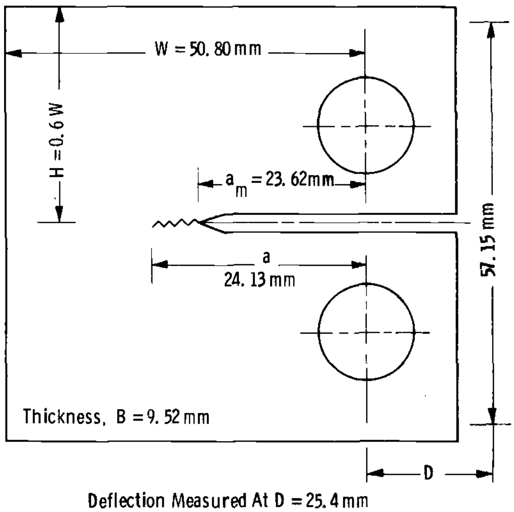

FIG. 3—*Specimen geometry (dimensions in millimetres).*

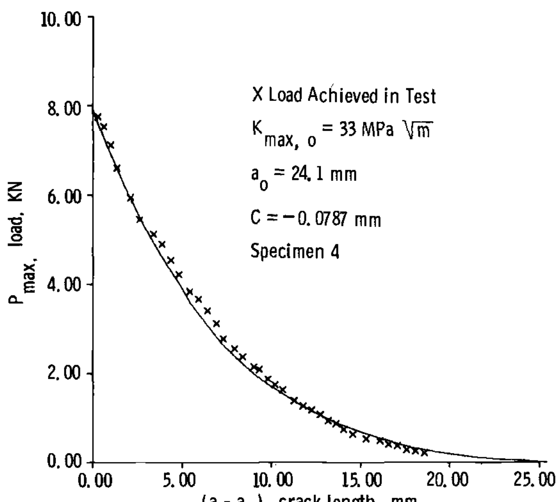

FIG. 4—*Load versus crack length calculated for a* K-*decreasing test, and the actual loads achieved.*

geometry, and also on the location of the deflection measurement, principally the distance D of Fig. 3. Values of $g(a/W)$ from Saxena and Hudak[2] were used to obtain the V/P values given in Table 1.

Equation 1 and Table 1 may be combined to calculate the locus of P_{max}

TABLE 1—*Stress intensities and deflections for specimen of Fig. 3 (a_o = 24.13 mm; E = 206 820 MPa; thickness = 9.525 mm).*

$(a - a_o)$, mm	a/W	K/P, $\frac{\text{MPa}\sqrt{\text{m}}}{\text{kN}}$	V/P, $\frac{\text{mm}}{\text{kN}}$
0	0.475	4.18	0.028
2.54	0.525	4.87	0.035
5.08	0.575	5.79	0.044
7.62	0.625	7.04	0.057
10.16	0.675	8.84	0.078
12.70	0.725	11.54	0.111
15.24	0.775	15.91	0.166
17.78	0.825	23.72	0.294
20.32	0.875	40.20	0.604
22.86	0.925	88.34	1.775
25.40	0.975	466.48	16.99

versus V_{max} during a decreasing-K test. This is illustrated by Fig. 5 for the particular geometry of Fig. 3, and for the same values of $K_{max,o}$, a_o, and C used for Figs. 2 and 4. One method of conducting a decreasing-K test is to decrease the load, either manually or automatically, as crack growth proceeds, so that the locus of P_{max} versus V_{max} follows a curve such as in Fig. 5. This is the basis of the digital computer control tests described by Saxena et al.[3] The same object is accomplished in this paper by replacing the digital computer with a specially designed electronic control circuit.

In the approach used here, the P_{max} versus V_{max} curve is approximated by straight line segments, such as the two dashed lines in Fig. 5. The circuit of Fig. 1 controls to a straight line which is specified by the settings of two variable resistors. Thus, after completion of line segment (V_1, P_1) to (V_2, P_2), these settings are changed so that the test proceeds along line (V_2, P_2) to (V_3, P_3).

Several tests were conducted at $R = 0.1$,[4] one of which followed the specific straight lines shown in Fig. 5. The a_o value used includes a short precrack beyond the machined notch length a_m of Fig. 3. A sinusoidal waveform was used, with the frequency being varied during the test between 10 and 90 Hz, with the latter value being used at the very low growth rates.

Measured loads and crack lengths from this test are shown in Fig. 4. The agreement between this data and the calculated curve indicates that the desired control was reasonably approximated. Crack length versus cycles data from this test are shown in Fig. 6 as square symbols; growth rates are plotted versus ΔK in Fig. 7 as (+) symbols.

A second test was conducted using control lines similar to those in Fig. 5,

[4]By definition $R = P_{min}/P_{max}$, and as a consequence of linear elastic behavior $K_{min}/K_{max} = R = V_{min}/V_{max}$.

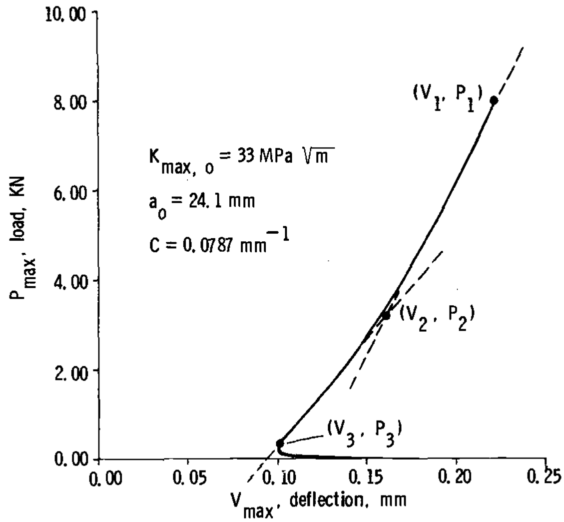

FIG. 5—*Load versus deflection locus calculated for a K-decreasing test, and the straight line approximations used.*

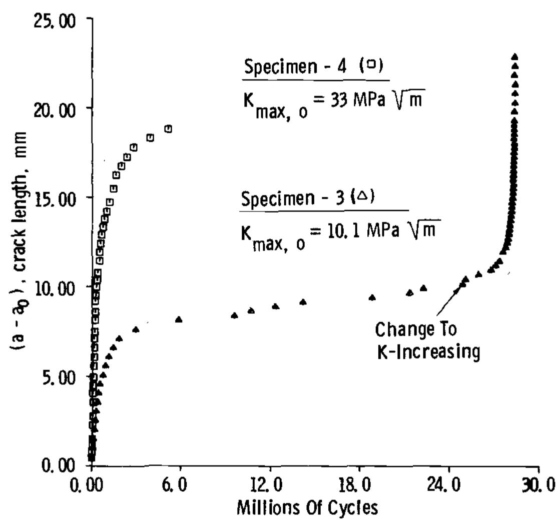

FIG. 6—*Crack length versus cycles data for two K-decreasing tests, and also for subsequent constant load (K-increasing) cycling for one of the specimens.*

the only difference being that the loads and deflections were modified as appropriate for $K_{max} = 10.1$ MPa$\sqrt{m}$. After the crack growth rate had decreased to a value near 8×10^{-8} mm/cycle, the control circuit was removed, and the test was continued in simple load control at the current value of P_{max}, resulting in a K-increasing portion of the test. Crack length versus cycles data from this test are shown in Fig. 6 as triangles; crack growth rate versus stress intensity data, da/dN versus ΔK, are shown in Fig. 7 as circles and triangles. The growth rates were obtained using the seven-point incremental polynomial procedure described in ASTM Tentative Test Method for Constant-Load-Amplitude Fatigue Crack Growth Rates Above 10^{-8} m/cycle (E 647-78 T).[5]

The following characteristics of the data in Figs. 6 and 7 indicate the success of the control circuit and the satisfactory quality of the data obtained: (*1*) Very low growth rates were achieved. (*2*) The crack length versus cycles data form a smooth curve. (*3*) The K-decreasing and K-increasing portions agree on the da/dN versus ΔK plot. (*4*) The growth rate data above 10^{-5} mm/cycle agree with other data (not presented) on the same material tested under constant load in accordance with ASTM E 647.

Electronic Control Circuit

In Fig. 1 it is shown that our input to the control circuit consists of load, deflection, and the function generator signal. The internal controls of the circuit are slope and intercept controls. These correspond to the slope and V-axis intercept of a straight line, such as the line given by (V_1, P_1) and (V_2, P_2) in Fig. 5. To set the internal controls the formula

$$\frac{V_1 - V_2}{P_1 - P_2} = 1/\text{slope} \tag{4}$$

is used. P_1 is the initial load, P_2 is the end load, V_1 is the initial deflection, and V_2 is the end deflection. These are in volts of load and deflection. To set the intercept value, the formula used is

$$V_{\text{intercept}} = V_1 - P_1\,(1/\text{slope}) \tag{5}$$

The effect of these controls is to decrease the value of P_{max} as crack growth causes the deflection to increase, so that the test follows the desired straight line of Fig. 5. At Input A to the comparator, the circuit provides a calculation of peak deflection (V_{max}) based on the measured peak load P_{max}.

$$V_{max} = \frac{P_{max}}{(\text{slope})} + V_{\text{intercept}} \tag{6}$$

[5]ASTM E 647-78 T is reprinted in this volume as Appendix I, pp. 321-339.

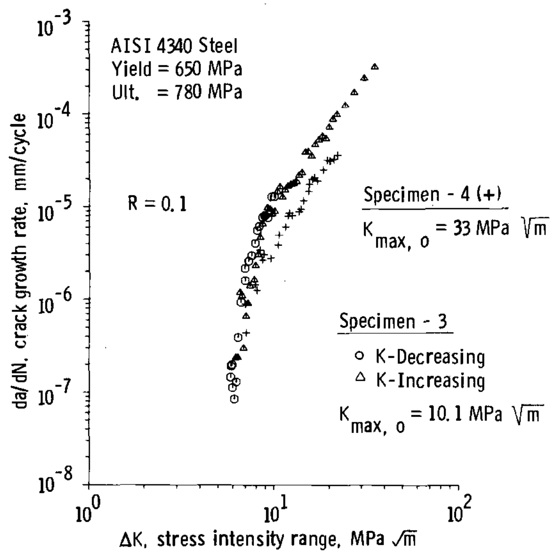

FIG. 7—*Crack growth rate versus stress intensity data for two* K*-decreasing tests, and also for subsequent load* (K*-increasing*) *cycling of one of the specimens.*

This voltage is compared, on every cycle, to the actual measured peak value of deflection, the deflection signal being Input B to the comparator in Fig. 1. When set correctly, the output of the comparator is zero and the counter remains at the full value. When the crack begins to grow, the load will remain the same but the peak deflection value will increase. This in turn causes the comparator to go high and start the counter, counting down. This reduces the function generator signal to the test machine and the load decreases. This will continue until the measured and desired values of deflection are again the same, which will only occur somewhere along the control line. When this condition is met, the comparator goes low and the counter holds its value.

The function generator input to the control circuit is assumed to previously have been d-c offset as necessary to provide a signal having a minimum-to-maximum voltage ratio corresponding to the desired R-ratio of the test, and also to have been scaled to 10 V full scale. If the function generator in use does not have this capability, the required offsetting and scaling can be performed externally by a simple circuit.

The use of digital counters and conversion to an analog signal is necessary when very slow growth rates in the 10^{-7} mm/cycle range are to be reliably achieved. To use analog techniques to hold the load value for the required long periods of time would cause the circuit to loose accuracy in the region where maximum accuracy is needed.

In addition to the circuitry needed for machine control, peak d-c outputs are available for the load and deflection, so the machine operator can plot the decrease on an x-y plotter. If, before the test is started, the control lines are drawn on the graph paper, casual observation of these peak outputs will confirm machine control and agreement with the desired P_{max} versus V_{max} control lines. In all cases it has been found that closely matching the load cell and the deflection measuring devices to the load and deflection limits provides the maximum accuracy for this control unit, mainly by limiting the electrical noise.

In the following example, it will be seen that a load range change was necessary at the start of the second slope to provide sufficient voltage for proper operation of the circuit at the low growth rates. Using the example of Fig. 5, we have

Loads	Deflections	Machine Ranges
$P_1 = 7.90$ kN	$V_1 = 0.221$ mm	Load = 11.12 kN full scale (10 V)
$P_2 = 3.17$ kN	$V_2 = 0.161$ mm	Deflections = 0.254 mm full scale (10 V)

Hence

$$P_1 = 7.10\text{ V} \qquad V_1 = 8.70\text{ V}$$

$$P_2 = 2.85\text{ V} \qquad V_2 = 6.34\text{ V}$$

Therefore

$$1/\text{slope} = \frac{V_1 - V_2}{P_1 - P_2} = 0.555;\ \text{dial setting } 5.55$$

$$V_{intercept} = V_1 - P_1\,(1/\text{slope}) = 4.76\ \text{dial setting}$$

For the second straight-line segment of Fig. 5, a load range of 4.448 kN full scale was selected for maximum voltage output. Then

Loads	Deflections	Machine Ranges
$P_2 = 3.17$ kN	$V_2 = 0.161$ mm	Load = 4.45 kN full scale
$P_3 = 0.34$ kN	$V_3 = 0.101$ mm	Deflections = 0.254 mm full scale

Hence

$$P_2 = 7.13\text{ V} \qquad V_2 = 6.34\text{ V}$$

$$P_3 = 0.76\text{ V} \qquad V_3 = 3.98\text{ V}$$

Equations 4 and 5, with the numerical subscripts appropriately modified, give new dial settings. If the load range had not been changed, P_3 would have been only 3 percent of full scale. Even $P_3 = 0.76$ V, or 8 percent of full scale, is smaller than desirable.

In actual practice, the ideally calculated and observed deflections will not be in perfect agreement, due to such causes as inaccuracy in the analysis of Eq 3, curvature of the front of the precrack, or inaccuracy in the value of the elastic modulus. This is handled at the beginning of the test as follows: With the circuit set, a manual compliance is taken to the maximum load value. The deflection value is compared with the calculated value. If the stiffness of the specimen is not exactly as expected, determine the percentage of error. Then modify all V's by this percentage, recalculate the dial settings for slope and offset, and conduct the test using these modified values.

Discussion

All of our testing with this circuit has been directed to fatigue crack growth threshold testing. But because of the ability of the circuit to control any straight line segment in the first quadrant, it is possible to use it to conduct a test where K is held constant. The load versus deflection locus corresponding to constant K is determined from Eqs 2 and 3, hence from Table 1 for the specimen of this study. Such a locus is illustrated in Fig. 8. The resulting curve may be approximated by straight line segments, and the control circuit of Fig. 1 used just as described earlier.

In this testing some problems were encountered. For one, as noted before, the load and deflection transducers must be matched to their maximum expected outputs for each stage of the test, so that no transducer is used at a

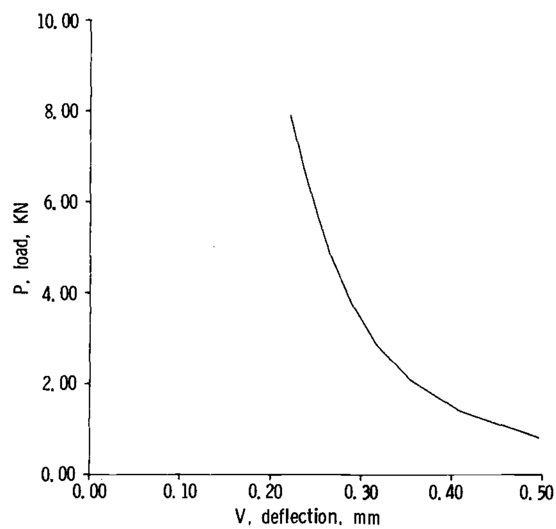

FIG. 8—*Load versus deflection locus calculated for a constant stress intensity of* K = *33 MPa* $\sqrt{m}$ *for the specimen of Fig. 3.*

small fraction of full scale. This ensures a lower noise content of the control signals, especially at the lower loads.

Another problem is one of hydraulic line surges which can cause a spike in the load and deflection signals. When this occurs, usually over only a few cycles, the counter will count down, thinking the crack has grown. The result will be that the specimen is cycled at a level which is below the control line. Such a spike can retard crack growth, and subsequent cycling below the control line is, of course, also undesirable. The best solution would be a separate hydraulic power supply for the test machine running these tests. A partial solution to this problem is for the machine operator to compare V_{max} and P_{max} with the desired control line on the x-y plotter and make manual corrections with the span control to bring the test back to proper levels. Another method is to add additional circuitry to sense the underdrive condition and cause the counter to count back up to the proper level. This could add a problem of causing the circuit to constantly hunt for the proper levels. However, either manual or automatic correction of the control following a spike only avoids cycling below the control line, any retardation effect due to the spike still being present.

The system now being used is satisfactory for use in obtaining data at low growth rates if a high-speed hydraulic system is used. The test can be started at slower rates (10 to 20 Hz) and increased in frequency after the crack rate has slowed. Having to stop the test and shut off the hydraulics to change load control ranges requires a technician be available when the changeover point occurs. A technician is also required to take readings of crack length on the specimen as the test progresses.

A full digital control system has certain advantages, automatically following the control curve (Fig. 5), and changing ranges and function generator speeds as the test dictates. The computer can also indirectly measure crack length by the compliance method and check against under-programming errors. It also has the advantage of automatically handling and processing the data, which is already stored in memory, thus producing data plots at the end of the test. With our system, all data are collected and plotted at the test's end by hand.

Note that the circuit used here and a digital control system share many of the same problems. Both require high-quality hydraulics and low-noise electronic signals.

Summary

The planned object of a low-cost fatigue crack growth threshold test system, capable of growth rates in the 10^{-8} mm/cycle range, has been met by this circuit. The results shown in Figs. 6 and 7 are a demonstration that this testing, long considered out of reach for most testing laboratories, can be achieved with a minimum of extra equipment. The method of relying on the compliance of the specimen to obtain the desired control proved to be one which can be used in a simple electronic control system. In the initial testing, we have achieved very encouraging results. These tests, along with possible further improvements to our present hydraulic control system, will allow high-quality fatigue crack growth threshold test results to be obtained using the low-cost control circuit described.

Recommendations

To receive full advantage of the present circuit, our laboratory would need the following equipment for a large-scale effort in fatigue crack growth threshold testing: (*1*) an actuator and valve assembly which would closely match our specimen size for low-load and high-frequency operation, (*2*) a separate hydraulic power supply to reduce hydraulic line surges to a minimum, (*3*) a load cell and linear variable differential transformer, the latter having been found to have the most reliable output at the higher frequencies (150 to 200 Hz), closely matched to the intended loads and deflections in the tests, and (*4*) a short, stiff, well-aligned load frame in which to run these tests.

To run these tests in a full digital control system would require a digital computer complete with necessary input/output control devices for data collection and machine control. Also, all of the items listed for use with the present system would be required for good machine stability and reliable computer operation of the tests. In addition to the equipment needed for computer control, there would be training time required to teach a technician programming, and time required to write and debug the necessary programs for machine control and data handling.

L. A. James[1] *and W. J. Mills*[1]

An Evaluation of the Round Compact Specimen for Fatigue Crack Growth Rate Testing

REFERENCE: James, L. A. and Mills, W. J., "**An Evaluation of the Round Compact Specimen for Fatigue Crack Growth Rate Testing,**" *Fatigue Crack Growth Measurement and Data Analysis, ASTM STP 738,* S. J. Hudak, Jr., and R. J. Bucci, Eds., American Society for Testing and Materials, 1981, pp. 70–82.

ABSTRACT: A proposed round compact specimen was evaluated for its suitability for fatigue crack growth rate testing. The results were compared with results from standard compact specimens [per ASTM Tentative Test Method for Constant-Load-Amplitude Fatigue Crack Growth Rates Above 10^{-8} m/Cycle (E 647-78 T)], and the two specimens were found to yield equivalent results. A number of K-solutions have also been proposed for the round compact specimens, and these are reviewed. The agreement between the various solutions was quite good, and the Newman Equation was used to evaluate the present results.

KEY WORDS: crack propagation, stress intensity, fatigue testing, specimen design, compact specimen

Nomenclature

a	Crack length
A_t	Crack length measured from specimen center to crack tip
B	Specimen thickness
C	Specimen compliance
d	See Fig. 1
da/dN	Fatigue crack growth rate
D	Specimen diameter
E	Young's Modulus
f	Cyclic frequency
G	Strain energy release rate
K	Stress intensity factor

[1]Fellow engineer and senior engineer, respectively, Westinghouse Hanford Company, Richland, Wash. 99352.

L See Fig. 1
P Applied load
r Radius of loading holes
R Stress ratio, P_{min}/P_{max}
R_o Specimen radius, $R_o = D/2$
W Specimen width
Y Dimensionless geometry factor, see Eq 8
α Relative crack length, a/W
Γ Stress intensity coefficient
δ Load-line displacement
ΔK Stress intensity factor range, $K_{max} - K_{min}$
σ_m Bending component of fictitious normal net stress
σ_p Uniform component of fictitious normal net stress

Fatigue crack growth tests commonly utilize the ASTM compact specimen that has been standardized in ASTM Tentative Test Method for Constant-Load-Amplitude Fatigue Crack Growth Rates Above 10^{-8} m/Cycle (E 647-78 T).[2] This specimen offers many desirable features. It has a well-characterized K-solution, offers a wide range of K-levels within a single specimen at a given load, is conservative of material, has a relatively high compliance, and requires relatively low loads to achieve a given K-level. Perhaps the biggest disadvantage of the standard compact specimen (CS) is its relatively high cost. Since fracture mechanics tests are sometimes required on materials with a circular cross section (for example, round bar stock, sintered products, etc.), a round version of the compact specimen would have attractive cost-saving features and, indeed, several such specimens have been proposed and utilized [*1–6*].[3] ASTM Committee E-24 on Fracture Testing is currently considering round compact specimens for standardization. Because most of the previous studies have been aimed at fracture toughness testing applications, the present study was undertaken to evaluate the round compact specimen (RCS) design for fatigue crack growth rate testing.

Stress Intensity Factor Solutions

A requirement for any specimen design to be considered as a laboratory standard is an accurate K-solution over a wide range of crack lengths. A number of K-solutions for RCS designs have been proposed [*1,2,6,7,9,10*], they will be briefly reviewed and compared herein.

Feddern and Macherauch [*1*] conducted compliance tests on round compact specimens (see Nomenclature and Fig. 1) and derived the relationship given in Eq 1. This relationship was proposed for the range $0.3 < \alpha < 0.7$.

[2] ASTM E 647-78 T is reprinted in this volume as Appendix I, pp. 321–339.
[3] The italic numbers in brackets refer to the list of references appended to this paper.

$$K = \frac{P\sqrt{a}}{BW}[29.6 - 162\alpha + 492.6\alpha^2 - 663.4\alpha^3 + 405.6\alpha^4] \quad (1)$$

Mowbray and Andrews [2] conducted compliance tests and two analytical procedures (finite element and J-integral) to derive K-solutions. The expressions from the three methods all gave similar results, but they considered the finite element results to be the most accurate. Their relationships for K and load-line displacement are given in Eqs 2 and 3, respectively, for the range $0.475 < \alpha < 0.825$.

$$K = \frac{P}{B\sqrt{W}}\exp[-8.51 + 56.67\alpha - 112.01\alpha^2 + 98.18\alpha^3 - 28.47\alpha^4] \quad (2)$$

$$\delta = \frac{P}{EB}\exp[11.77 - 65.63\alpha + 175.61\alpha^2 - 194.99\alpha^3 + 82.94\alpha^4] \quad (3)$$

Gross [6], using a boundary collocation technique, derived the relationship of Eq 4, where

$$K = \Gamma(\sigma_p + \sigma_m)\sqrt{A_t(1 - A_t/R_o)} \quad (4)$$

Γ, σ_p, σ_m, A_t, and R_o are defined in Nomenclature. Equation 4 is valid over the range $0.533 < \alpha < 0.80$. In a later paper [7] Gross extended his collocation solution for K to cover the range $0.133 < \alpha < 1.0$. Crack surface dis-

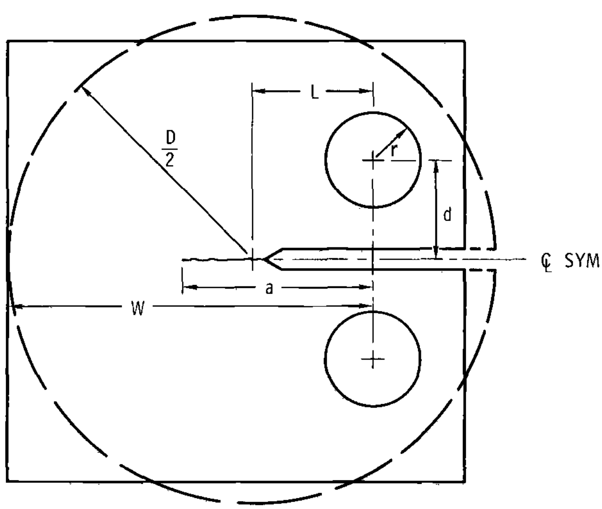

FIG. 1—*Standard compact specimen and proposed round compact specimens.*

placements have also been determined by Gross [8] over the range $0.2 < \alpha < 0.933$.

Cull and Starrett [4] conducted compliance experiments on an RCS and, although they did not derive values of K from these compliances, their plots of $2BEC$ versus a/W can be used to derive K using the expressions of Eq 5 for the range $0.3 < \alpha < 0.6$.

$$\frac{d(2BEC)}{d(a/W)} = 2BEW\left[\frac{dC}{da}\right]$$

$$G = \frac{P^2}{2B}\frac{\partial C}{\partial a} \tag{5}$$

$$K = \sqrt{GE}$$

Underwood and Kendall [9] have developed a C-shaped specimen for fracture mechanics testing. Although it differs from the RCS shown in Fig. 1, in the limit the C-specimen approaches the RCS as the inner radius shrinks to zero. Therefore the equation for the C-specimen can be used to estimate K in the RCS over the relatively narrow range $0.633 < \alpha < 0.7$, if the inner radius is taken to be zero.

Gregory [10], using an asymptotic analysis, developed the expression of Eq 6, valid over the range $0.5 < \alpha < 0.8$, where $b = W - a$.

$$K = \frac{P}{B\sqrt{W}}\left[\frac{2}{\left(\frac{D}{W}\right)\left(\frac{D}{W} - \frac{b}{W}\right)}\right]^{1/2}\left[\frac{\frac{D}{W} - \frac{b}{W}}{0.3557\left(\frac{b}{W}\right)^{1.5}} + \frac{2 - \frac{D}{W}}{0.9665\left(\frac{b}{W}\right)^{0.5}}\right] \tag{6}$$

Finally, Newman [11] has used boundary collocation methods to derive an expression for the stress intensity factor of the RCS that is valid over a wide range of α: $0.25 \leq \alpha < 1.0$. This relationship, given in Eq 7, is being recommended for standardization by ASTM Subcommittee E24.01 on Fracture Mechanics Test Methods [12], and is the equation used to calculate the present results.

$$K = \frac{P}{B\sqrt{W}}\left[\frac{2 + \alpha}{(1 - \alpha)^{1.5}}\right][0.76 + 4.8\alpha - 11.58\alpha^2 + 11.43\alpha^3 - 4.08\alpha^4] \tag{7}$$

It is interesting to compare the various relationships for K, but in order to do so they must be expressed in a common manner. (The geometries utilized by the various investigators are summarized in Table 1.) A convenient way of comparing the results is through the use of a nondimensional geometry factor, Y, defined in Eq 8. Values of Y for the various

$$K = \frac{P}{B\sqrt{W}} Y \tag{8}$$

K-solutions are plotted in Fig. 2 as a function of α. It is seen that, in general, the agreement is quite good.[4] Also plotted is the solution [13] for the standard compact specimen as given by Eq 9.

$$K = \frac{P}{B\sqrt{W}} \left[\frac{2 + \alpha}{(1 - \alpha)^{1.5}} \right] \times [0.886 + 4.64\alpha - 13.32\alpha^2 + 14.72\alpha^3 - 5.6\alpha^4] \tag{9}$$

It will be noted in Fig. 2 that Eqs 7 and 9 give reasonably similar results, and the higher values of Y associated with the RCS at large values of α are undoubtedly related to the removal of the material in the corners of the specimen.

Experimental Procedure

The material used to evaluate the RCS in this study was Alloy 718, a precipitation-hardenable nickel-base alloy. The chemical composition of this material is given in Table 2. All specimens (with the exception of Specimen 1907) were obtained from a piece of 76.2 mm (3 in.) diameter bar stock. Specimen 1907 was machined from a 50.8 mm (2 in.) diameter bar from a different heat of material. Following machining, the specimens were given a precipitation heat treatment consisting of:

> Solution anneal 1 h at 1093°C (2000°F), cool to 718°C (1325°F) at 56°C/h (100°F/h), age 4 h at 718°C (1325°F), cool to 621°C (1150°F) at 56°C/h (100°F/h), age 16 h at 721°C (1150°F), air cool.

Tensile tests were not performed on this material, but the average room temperature hardness in the heat-treated condition was $R_c = 41.7$. The results of tensile tests on another heat of Alloy 718 given the same heat-treatment (resulting in $R_c = 41.4$) and originally reported in Ref *16* are $\sigma_y =$

[4] The authors received the results of an experimental compliance analysis by D. M. Fisher and R. J. Buzzard ("Comparison Tests and Experimental Compliance Calibration of the Proposed Standard Round Compact Plane Strain Fracture Toughness Specimen," Report NASA-TM-81379, NASA Lewis Research Center, 1979) too late to incorporate in the main text of this paper. However, their results agree quite well with those of Gross [6] and Newman [11].

TABLE 1—*Comparison of specimen geometries for round compact specimens.*

Specimen	L/W	D/W	Hole Location d/W	Hole Location r/W
Feddern & Macherauch (Ref *1*)	0.333	1.333	0.266	0.133
Mowbray & Andrews (Ref *2*)	0.333	1.333	0.333	0.083
Cull & Starrett (Ref *4*)	0.333	1.333	0.250	0.083
Gross (Ref *6-8*)	0.333	1.333	...	...
Underwood & Kendall (Ref *9*)	0.333	1.333	0.266	0.133
Gregory (Ref *10*)	0.333	1.333	...	...
Newman	0.325	1.350	0.275[a]	0.125[a]
Present work[b]	0.333	1.333	0.311	0.083
Present work[c]	0.325	1.350	0.275[a]	0.125[a]

[a] Same as standard ASTM E 647-78 T compact specimen.
[b] Specimens 1519 to 1522.
[c] Specimen 1907.

1011 MPa (146.7 ksi) and 866 MPa (125.6 ksi) at 24°C and 538°C, respectively.

Two types of specimens were employed in this study: standard compact specimens (per ASTM E 647) with nominal width and thickness dimensions of 38.1 mm (1.50 in.) and 8.89 mm (0.35 in.), respectively, and round compact specimens with nominal width, diameter, and thickness dimensions of 51.2 mm (2.25 in.), 76.2 mm (3.00 in.), and 8.89 mm (0.35 in.), respectively. Specimen 1907 had W and B dimensions of 37.6 mm (1.48 in.) and 7.62 mm (0.30 in.), respectively. All specimens were in the *C-R* orientation per ASTM Test Method for Plane-Strain Fracture Toughness of Metallic Materials (E 399-78a).

The specimens were fatigue cycled on a feedback-controlled electrohydraulic testing machine using load as the control parameter. Tests were conducted in an air environment at room temperature and at 538°C (1000°F). Sinusoidal waveforms were employed at frequencies of 600 cpm and 40 cpm for the tests at room temperature and 538°C, respectively. The stress ratio ($R = P_{min}/P_{max}$) was 0.05 for all tests. The test parameters are summarized in Table 3.

Crack lengths were determined periodically throughout each test using a traveling microscope. Fatigue crack growth rates (da/dN) were calculated using the "secant method" [*17*], and the corresponding stress intensity factors (K) were calculated using Eq 7 or 9, as appropriate. The results were displayed as plots of $\log(da/dN)$ versus $\log(\Delta K)$, where ΔK is the stress intensity factor range ($K_{max} - K_{min}$).

A few of the data points were "not valid" according to ASTM E 647. These data were plotted as closed symbols. At low values of ΔK, a few data points were obtained for crack extensions less than 2.5 mm (0.10 in.) from the

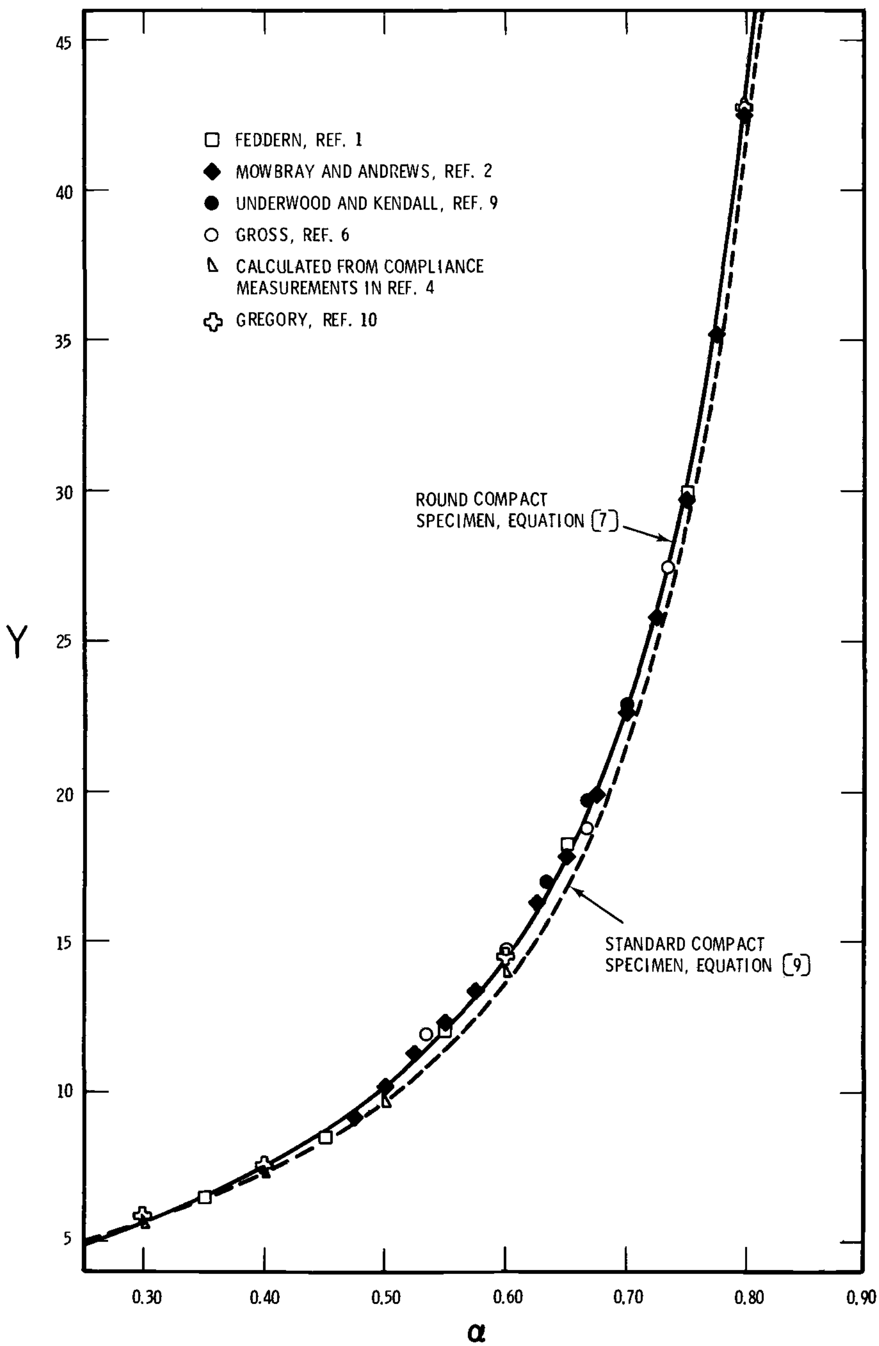

FIG. 2—*Comparison of results for various expressions for the round compact specimen.*

TABLE 2—*Chemical composition of Alloy 718 used in this study.*[a]

Element	Percent by Weight
C	0.04
Mn	0.15
Fe	17.97
S	0.005
Si	0.15
Cu	0.10
Ni	53.06
Cr	18.50
Al	0.62
Ti	0.95
Co	0.09
Mo	3.06
Cb & Ta	5.29

[a]Except Specimen 1907.

TABLE 3—*Summary of test parameters.*

Specimen Number[a]	Specimen Type	Test Temperature, °C	Maximum Load, N	Range of α Tested	Cyclic Frequency, cpm
1516	Std. CS	24	4003	$0.400 < \alpha < 0.806$	600
1517	Std. CS	24	6005	$0.405 \leq \alpha < 0.727$	600
1518	Std. CS	538	4448	$0.415 < \alpha < 0.719$	40
1519	RCS	24	3559	$0.502 < \alpha < 0.847$	600
1520	RCS	24	5338	$0.508 < \alpha < 0.807$	600
1521	RCS	538	3559	$0.493 < \alpha < 0.781$	40
1522	RCS	538	5338	$0.497 < \alpha < 0.719$	40
1907	RCS	24	4226	$0.300 < \alpha < 0.782$	600

[a]All specimens tested at stress ratio $R = 0.05$.

machined notch. At high values of ΔK, a few data points violated the criterion for remaining uncracked ligament size

$$(W - a) \geq \frac{4}{\pi}\left(\frac{K_{max}}{\sigma_y}\right)^2 \tag{10}$$

where σ_y is the 0.2 percent offset monotonic yield strength. Although these data easily satisfied a less restrictive criterion based on flow strength rather than yield strength,[5] they are nevertheless displayed herein as "invalid".

[5]This publication, pp. 45-57.

Results and Discussion

The results of the crack growth tests conducted at room temperature and 538°C (1000°F) are shown in Figs. 3 and 4, respectively. At both test temperatures the two specimen designs appear to give equivalent results. The two round compact specimens tested at each temperature had test loads differing by 50 percent, thereby producing the same value of K with different combinations of load and crack length. Again, agreement between the two specimens is excellent. Reference *17* established that a scatter factor of 2 is considered normal for intralaboratory tests on a single heat, and the present results fall within that general guideline. The slightly greater scatter at 538°C (1000°F) is attributed to the greater difficulty in measuring the crack lengths at elevated temperatures.

To further evaluate the equivalency of the results, least-squares regression analyses were performed on the data for each specimen design at both temperatures. The results (expressed in U.S. Customary Units) are given below (individual regression lines are not plotted in Figs. 3 and 4).

Standard CS at 24°C (Specimens 1516 and 1517)
$\log(da/dN) = -20.441 + 3.3159 \cdot \log(\Delta K)$
Correlation coefficient[6] = 0.9895

Round CS at 24°C (Specimens 1519 and 1520)
$\log(da/dN) = -20.246 + 3.2674 \cdot \log(\Delta K)$
Correlation coefficient = 0.9913

Standard CS at 538°C (Specimen 1518)
$\log(da/dN) = -17.181 + 2.6829 \cdot \log(\Delta K)$
Correlation coefficient = 0.9626

Round CS at 538°C (Specimens 1521 and 1522)
$\log(da/dN) = -17.023 + 2.6505 \cdot \log(\Delta K)$
Correlation coefficient = 0.9750

Only those data considered valid by ASTM E 647 (that is, the open symbols in Figs. 3 and 4) were included in the regression analyses. It is seen that the regression equations for the two specimen designs are very similar. In fact, comparison of these equations at the extreme growth rates where data for the two designs overlap indicates a maximum difference in da/dN between the two equations at room temperature of 9.9 percent, and at 538°C (1000°F) a maximum difference of 4.6 percent. Again, this is considered well within normal scatter and indicates the equivalency of the results.

It is interesting to note that, even though the "invalid" data were not included in the regression analyses, examination of Figs. 3 and 4 suggests that they continued to exhibit behavior comparable to that of the valid data.

Although there are minor differences in the quantities L/W, D/W, d/W,

[6] A correlation coefficient of unity indicates a "perfect" linear fit.

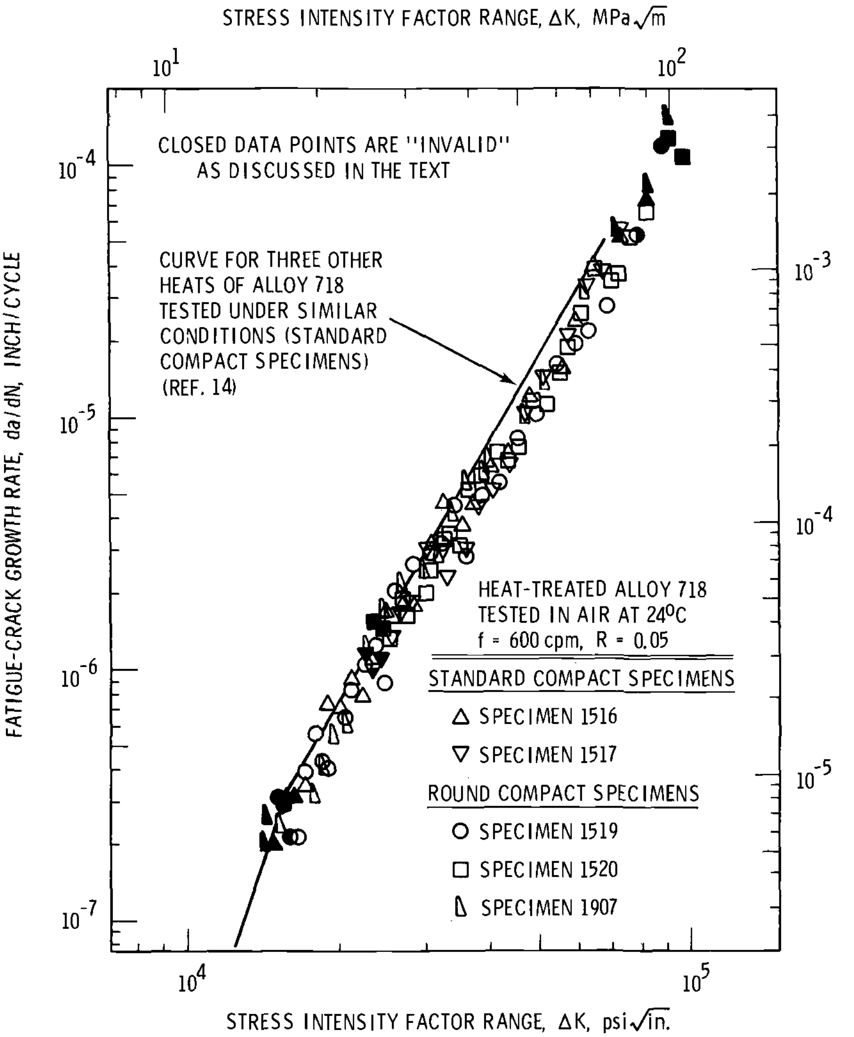

FIG. 3—*Comparison of results for standard and round compact specimens tested at room temperature.*

and r/W between the specimen analyzed by Newman and some of those used in the present work and previous studies (see Table 1), the excellent agreement between the various K-solutions (see Fig. 2) and the good agreement in the present study between standard and round specimens suggest that these minor dimensional variations are relatively unimportant.

Finally, the regression lines for other heats of similarly heat-treated Alloy

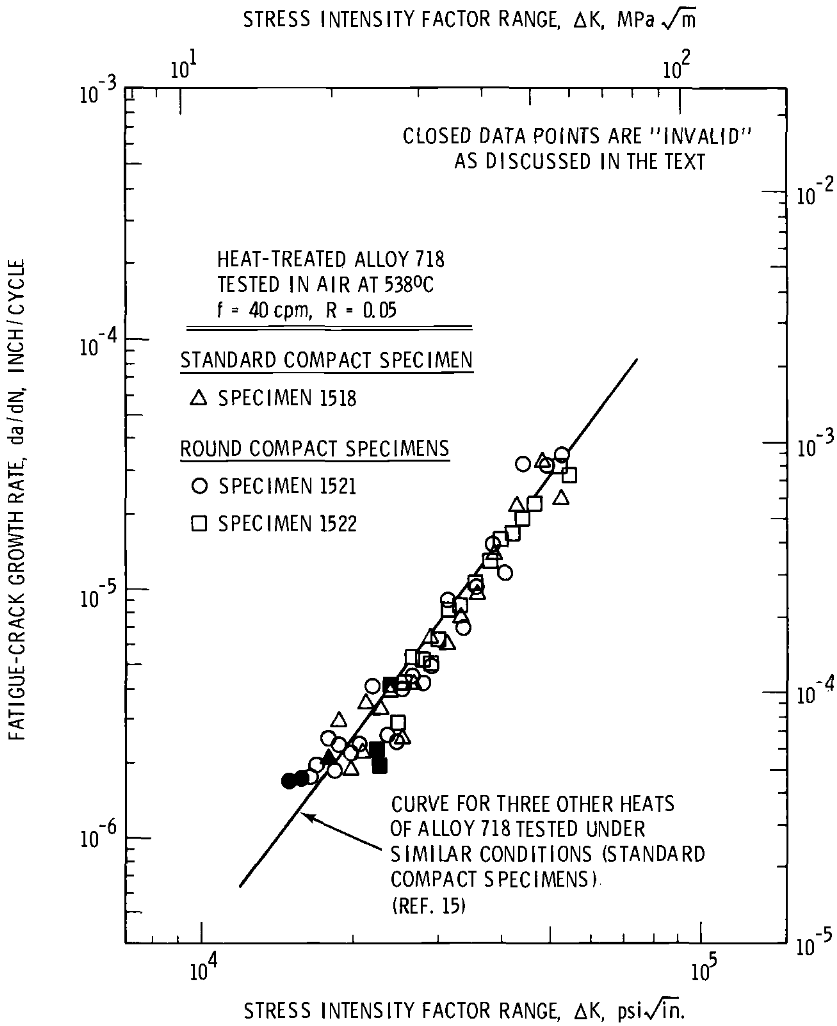

FIG. 4—*Comparison of results for standard and round compact specimens tested at 538°C (1000°F).*

718 tested under identical conditions of temperature, frequency, waveform, and stress ratio (using standard compact specimens) are shown in Figs. 3 and 4 for comparison purposes. It will be seen that the agreement between the present results and those of the previous studies is quite good, again suggesting the equivalency of the RCS.

Summary and Conclusions

The various K-solutions suggested for the RCS were reviewed, and found to be in good agreement with one another. The Newman Equation (Eq 7), considered one of the most accurate over the widest range of values of α, is recommended by ASTM Subcommittee E24.01, and hence is the expression with which the present results are evaluated.

Although a large number of specimens were not tested, the results of this study suggest that the standard compact specimens and the round compact specimen yield equivalent results for room temperature and elevated temperature fatigue crack growth rate testing. Hence, considering the economic advantage of the RCS for some product forms, it appears to be a satisfactory alternative to the standard CS in these instances.

Acknowledgments

This work was performed by Westinghouse Hanford Company, a subsidiary of Westinghouse Electric Corporation, under U.S. Department of Energy Contract EY-76-C-14-2170. The authors wish to acknowledge the assistance of D. J. Criswell in conducting the tests.

References

[*1*] Feddern, V. G. and Macherauch, E., *Zeitschrift für Metallkunde*, Vol. 63, No. 12, pp. 882-884.

[*2*] Mowbray, D. F. and Andrews, W. R., "Stress Intensity Factor Calibration for a Compact Specimen with a Round Profile," Technical Information Series, General Electric Company, Schenectady, N.Y., January 1975.

[*3*] Ingelstrom, N. and Ustimenko, V., *Power Metallurgy*, Vol. 18, No. 36, 1975, pp. 303-322.

[*4*] Cull, A. D. and Starrett, H. S., "A Study of Fracture Mechanics for Graphitic Materials," Report AFML-TR-75-125, Air Force Materials Laboratory, October 1975.

[*5*] Van Der Sluys, W. A., Palme, H. S., and Nair, P. K. *Proceedings*, Conference on Environmental Degradation of Engineering Materials, Virginia Polytechnic Institute and State University, Blacksburg, 1977, pp. 687-699.

[*6*] Gross, B., *Journal of Testing and Evaluation*, Vol. 5, No. 6, 1977, pp. 457-460.

[*7*] Gross, B. in *Developments in Theoretical and Applied Mechanics*, Vol. 9, R. M. Hackett, Ed., Plenum Press, New York, 1978, pp. 195-203.

[*8*] Gross, B., "Mode I Crack Surface Displacements for a Round Compact Specimen Subject to a Couple and Force," Technical Memorandum 79096, NASA Lewis Research Center, Cleveland, May 1979.

[*9*] Underwood, J. H. and Kendall, D. P., "*K* Results and Comparison for a Proposed Standard *C*-Specimen," Report WVT-TR-74041, Watervliet Arsenal, September 1974.

[*10*] Gregory, R. D., *Mathematical Proceedings*, Cambridge Philosophical Society, Vol. 85, Part 3, 1979, pp. 523-538.

[*11*] Newman, J. C., Jr., "Stress Intensity Factors and Crack Opening Displacements for Round Compact Specimens," Report NASA-TM-80174, NASA Langley Research Center, 1979.

[*12*] Underwood, J. H., Newman, J. C., Jr., and Seeley, R. R., *Journal of Testing and Evaluation*, Vol. 8, No. 6, November 1980, pp. 308-313.

[*13*] Srawley, J. E., *International Journal of Fracture*, Vol. 12, No. 3, 1976, pp. 475-476.

[*14*] James, L. A., "Heat-to-Heat and/or Melt Practice Variation in Crack Growth Behavior of

Inconel 718," in Report ORNL-5349, Oak Ridge National Laboratory, December 1977, pp. 196-199.

[*15*] James, L. A., "Heat-to-Heat and/or Melt Practice Variations in Crack Growth Behavior of Alloy 718," in Report ORNL-5380, Oak Ridge National Laboratory, March 1978, pp. 153-160.

[*16*] James, L. A., "Fatigue-Crack Propagation Behavior of Inconel 718," Report HEDL-TME 75-80, Westinghouse Hanford Company, September 1975.

[*17*] Clark, W. G. and Hudak, S. J., Jr., *Journal of Testing and Evaluation*, Vol. 3, No. 6, 1975, pp. 454-476.

Remote Crack Monitoring Techniques

G. R. Yoder,[1] L. A. Cooley,[1] and T. W. Crooker[1]

Procedures for Precision Measurement of Fatigue Crack Growth Rate Using Crack-Opening Displacement Techniques

REFERENCE: Yoder, G. R., Cooley, L. A., and Crooker, T. W., "**Procedures for Precision Measurement of Fatigue Crack Growth Rate Using Crack-Opening Displacement Techniques,**" *Fatigue Crack Growth Measurement and Data Analysis, ASTM STP 738,* S. J. Hudak, Jr., and R. J. Bucci, Eds., American Society for Testing and Materials, 1981, pp. 85–102.

ABSTRACT: This paper describes experimental and analytical procedures whereby the conventional commercial fracture mechanics clip-gage can be used for precision measurement of fatigue crack growth rate in compact-type specimens. Potential sources of error in measuring crack length via crack-opening displacement (COD) techniques are delineated. Comparisons are made between crack-length data obtained via specimen surface observations and COD techniques. Comparisons are also made between data analyzed by the secant and 7-point incremental polynomial methods. It is emphasized that COD techniques can enhance the accuracy of the secant method of data reduction. Step-loading procedures using COD techniques are described. Proposed amendments to ASTM Tentative Test Method for Constant-Load-Amplitude Fatigue Crack Growth Rates Above 10^{-8} m/Cycle (E 647-78 T) regarding incrementing of crack-length measurements via COD techniques are discussed.

KEY WORDS: clip gage, crack opening displacement (COD), fatigue crack growth rate, data analysis, secant method, 7 point incremental polynomial

We are presently engaged in two types of fatigue crack growth rate (FCGR) testing programs. The first program involves the influence of microstructural parameters on FCGR in high-strength titanium alloys. This program requires a high rate of FCGR data generation because of the large number of relevant microstructural parameters under investigation. The second program involves the influence of environmental parameters on FCGR

[1]Metallurgist, metallurgist, and mechanical engineer, respectively, Mechanics of Materials Branch, Material Science and Technology Division, Naval Research Laboratory, Washington D.C. 20375.

in a variety of alloys in marine environments. This program often requires crack-length measurements to be performed under adverse conditions.

In both programs, we have found crack-length measurement via crack-opening displacement (COD) techniques to be a highly valuable procedure. In this paper we will attempt to provide a detailed description of how these procedures are carried out and how our techniques have been verified per ASTM Tentative Test Method for Constant-Load-Amplitude Fatigue Crack Growth Rates Above 10^{-8} m/Cycle (E 647-78 T).[2]

Experimental Details

The data shown in this report were obtained on two high-strength $\alpha + \beta$ titanium alloys, designated Alloys 1 and 2. Alloy 1 is Ti-6Al-4V containing 0.06 weight-percent interstitial oxygen. Alloy 2 is Ti-8Al-1Mo-1V containing 0.11 weight-percent interstitial oxygen. Both alloys were tested in the beta-annealed condition with coarse-grained Widmanstätten microstructures. Tensile properties of the two alloys for the transverse (T) orientation are given in Table 1.

FCGR data were obtained from 1-T WOL-type (CT) specimens with a half-height to width (h/W) ratio of 0.486. In each case, specimen width (W) was 64.8 mm, specimen thickness (B) was 25.4 mm, and the crack path was in the TL orientation [*1*].[3] Details of the specimen geometry and the stress-intensity factor expression are given in Ref *2*.

FCGR testing was performed on an MTS 810.04 electrohydraulic closed-loop materials testing system. All FCGR tests were conducted in ambient room air under tension-tension cycling with a haversine waveform. A cyclic frequency of 5 Hz and a load ratio of $R = P_{min}/P_{max} = 0.1$ were used.

COD measurements were made on the CT specimens using an MTS 632.02B-01 clip-gage [sensitivity of 7.874 mV per millimetre of COD, excitation voltage of 7.775 volts direct current (VDC)] and a BLH Electronics Model 3564 power supply. The clip-gage was fixed to the specimen at the crack mouth via knife edges mounted on the specimen with set screws driven into drilled and tapped holes (Fig. 1). Care was taken to align the knife-edge surfaces parallel to the surfaces of the notch. Clip-gage signals were read out on the 100-mV range of a Hewlett-Packard 3440A/3443A digital voltmeter during momentary interruption of the test. Optical measurements of crack length were made on both faces of the CT specimen using Gaertner traveling optical micrometers at a magnification of approximately X15. Both the test specimen and the experimental apparatus listed are widely used conventional fracture mechanics test equipment. No special apparatus of any kind was used in this investigation.

[2]ASTM E 647-78 T is reprinted in this volume as Appendix I, pp. 321–339.
[3]The italic numbers in brackets refer to the list of references appended to this paper.

TABLE 1—*Tensile properties.*

Alloy	0.2 % Yield Strength (σ_{ys}), MPa	Tensile Strength (σ_{UTS}), MPa	Young's Modulus (E),GPa	Reduction in Area, %	Elongation, %
1	740	818	115	34	10
2	794	894	128	21	11

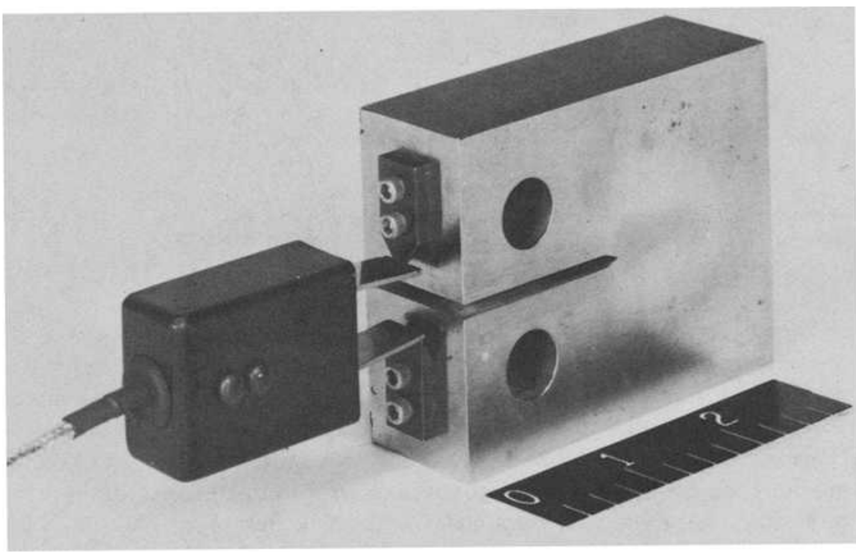

FIG. 1—*WOL-type compact-type (CT) specimen with clip-gage attached.*

Procedures for Crack-Length Measurement via COD

The basic procedures for obtaining crack length from measurements of COD in CT specimens are well documented [*3,4*]. It is our experience, however, that the success of this method for precision measurement of crack length rests upon strict adherence to certain detailed procedures now outlined.

The first step in this procedure is an accurate COD calibration for the specimen of interest. A schematic of a typical normalized calibration curve of $EB(\mathrm{COD})/P$ versus crack length-to-width ratio (a/W) is shown in Fig. 2. For the work described in this paper, we relied upon COD calibration expressions formulated in Ref *5*. It is useful to emphasize here that the term COD in this paper refers exclusively to crack-mouth-opening displacement, whereas the term compliance refers to relationships involving load-line displacement.

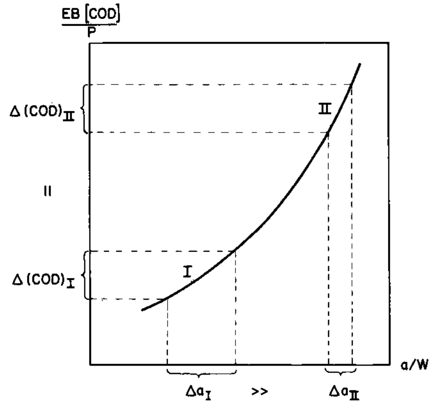

FIG. 2—*Schematic illustration of a normalized crack-opening displacement (COD) calibration curve, showing the manner in which crack length increments* (Δa) *selected on the basis of a constant COD increment Δ(COD) vary as a function of crack depth* (a/W).

The second step requires an accurate determination of the normalized parameter $EB(\mathrm{COD})/P$. Load (P) and COD are experimental measurements which are normally read from digital electronic instrumentation. B is readily obtained from ordinary micrometer measurements of specimen thickness. However, we have found that the selection of an appropriate value of Young's modulus (E) can be a significant source of error in this procedure. Satisfactory values of E can be obtained from tensile test data or from COD measurements at points where a postmortem trace of the crack front is apparent from the fracture surface. (In the case of alloy microstructures for which such traces are difficult to ascertain, it is possible to estimate E from the uncracked CT specimen. However, such values of E should be treated with caution due to the known variance between the compliance characteristics of machined notches and sharp cracks.) An unacceptable approach, in our view, is the use of a "handbook" value for E for the generic class of the alloy being tested. This is especially unsatisfactory for titanium alloys where E can vary by more than 15 percent due to heat treatment alone.

Values of COD at maximum load (P_{max}) are obtained experimentally according to the system illustrated in Fig. 3. The typical nonlinear shape of the initial portion of the P versus COD curve raises another admonition regarding the accuracy of this crack-length measurement procedure, as documented in Ref. *6*. Because of this nonlinearity, more than one digital reading of P versus COD must be taken to obtain the *true* value of the upper, linear slope of these curves. The practice we have developed is to record P and COD at two points, P_{max} and ½ P_{max}. The degree to which this nonlinearity occurs in P versus COD curves varies widely, depending upon speci-

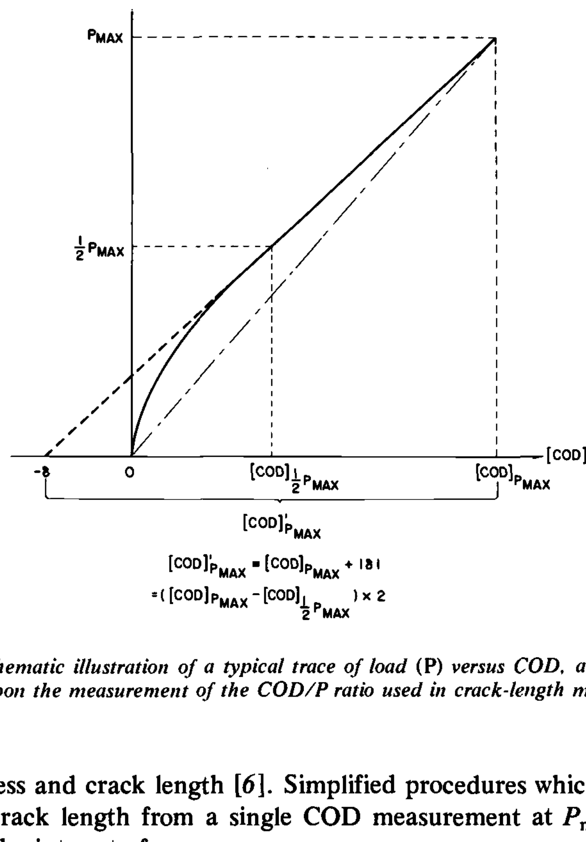

FIG. 3—*Schematic illustration of a typical trace of load* (P) *versus COD, and the effect of nonlinearity upon the measurement of the COD/P ratio used in crack-length measurement.*

men thickness and crack length [*6*]. Simplified procedures which attempt to determine crack length from a single COD measurement at P_{max} are to be avoided in the interest of accuracy.

A final consideration which is of importance on the basis of our experience is the selection of Δa-increments between crack-length readings. According to Section 8.6.2.3 of ASTM E 647, the minimum value of Δa is required to be 0.25 mm (0.01 in.) or ten (10) times the crack-length measurement precision, whichever is greater. Thus, where Δa is measured optically at the specimen surface with a traveling microscope, the minimum required value of Δa remains *constant* throughout the course of the test. *By contrast, with use of the clip-gage for crack-length measurement, it is not the minimum value of* Δa *that remains constant. Rather, in parallel with Section 8.6.2.3, it is the minimum value of the interval between measurements of clip-gage output of COD as read from the digital voltmeter,* Δ*(COD), that must remain constant throughout the course of the test* in order that the measurements will reflect a precision of at least ten (10) times the measurement precision. With the apparatus described in the preceding section, we have found replicate measurements of clip-gage output to have a precision of about ± 0.01 mV, as read from the digital electronic voltmeter. Consequently, we have found—as will be illustrated in subsequent sections—that Δ(COD) increments of approximately 0.20 mV provide excellent results. With the 7-point incremental polynomial method of data reduction, we find that Δ(COD) increments of 0.20 mV (±0.10 mV) provide results that are in close agreement with those obtained from optical measurements of crack length at the specimen surface ($\bar{a}_s$) as per ASTM E 647. With the secant method, we have found that the resultant scatter in da/dN is virtually the same as obtained with the 7-point incremental polynomial method if the intervals of Δ(COD) are somewhat more restrictive, namely, 0.20 mV (+0.10/−0.04 mV).

With either method of data reduction, it is important to note that with the COD technique for measurement of crack length, where a nominally constant value for Δ(COD) increments should be used, the *corresponding increments in actual crack growth* $\Delta(\bar{a}_{COD})$ *can vary as much as an order of magnitude, depending on* a/W. This effect, illustrated in Fig. 2, derives from the fact that $EB(\text{COD})/P$ increases exponentially as a function of a/W. For the 1-T WOL-type CT specimen (W = 64.8 mm), with increments of Δ(COD)≈0.20 mV, $\Delta(\bar{a}_{\text{COD}})$ values can be as large as 2.5 mm at low a/W values and can approach 0.25 mm at high a/W values. In comparison, ASTM E 647 specifies crack-length measurement intervals 0.25 mm ≤ Δa ≤ 1.3 mm. We wish to close this section by re-emphasizing the importance of instrumentation accuracy considerations in the successful use of COD for precision crack-length measurements.

Comparison of Crack-Length Measurement Techniques

With each of three replicate specimens of Alloy 1, which were individually cycled at overlapping ranges of ΔK, measurements of crack length were made by both the optical technique ($\bar{a}_s$) at the specimen surface as per ASTM E 647 and the COD clip-gage technique ($\bar{a}_{\text{COD}}$) as outlined previously. For the 7-point incremental polynomial method of reducing the crack length versus elapsed cycles (a versus N) data, results from the two measurement techniques can be compared in Figs. 4 and 5 for $\bar{a}_s$ and $\bar{a}_{\text{COD}}$, respectively. The dashed line in Fig. 5 traces the reference curve from Fig. 4 to facilitate comparison. It is readily apparent that both methods of crack-length measurements provide virtually identical results. Scatter amongst the data from the three specimens is minimal in both instances.

It is noted that values of surface crack length were corrected for tunneling as measured from final crack front profiles. Tunneling depths varied from 0.89 to 1.35 mm (0.035 to 0.053 in.) The value of E = 115 GPa was averaged from two 12.8-mm (0.505-in.)-diameter tensile tests. Further, as suggested earlier, approximately constant intervals of Δ(COD) ≈ 0.20 mV (±0.10 mV) were used in the $\bar{a}_{\text{COD}}$ technique relative to Fig. 5.

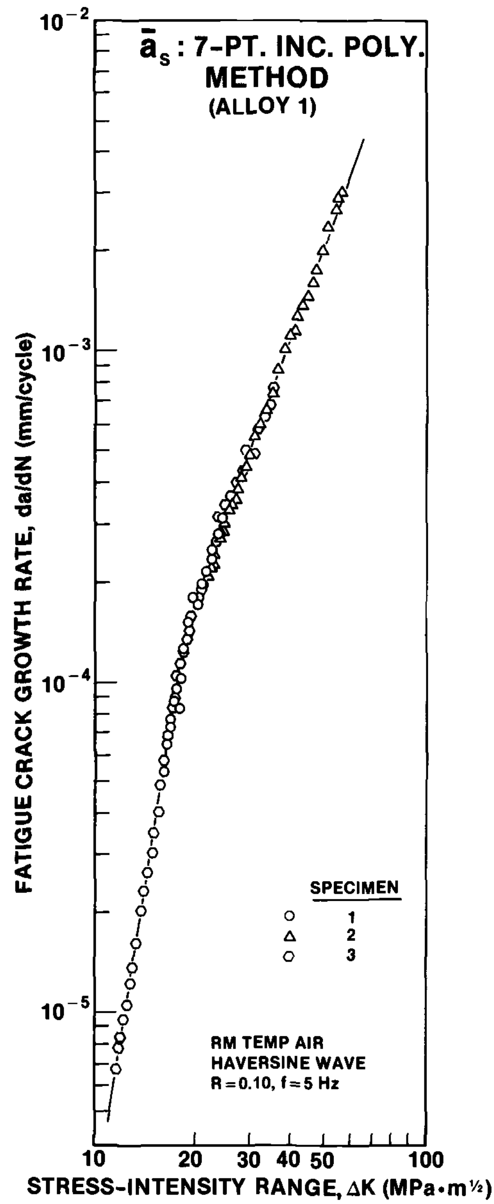

FIG. 4—da/dN *versus* ΔK *data for Alloy 1 from three replicate specimens, with crack-length measurements via optical technique and data reduction via 7-point incremental polynomial method.*

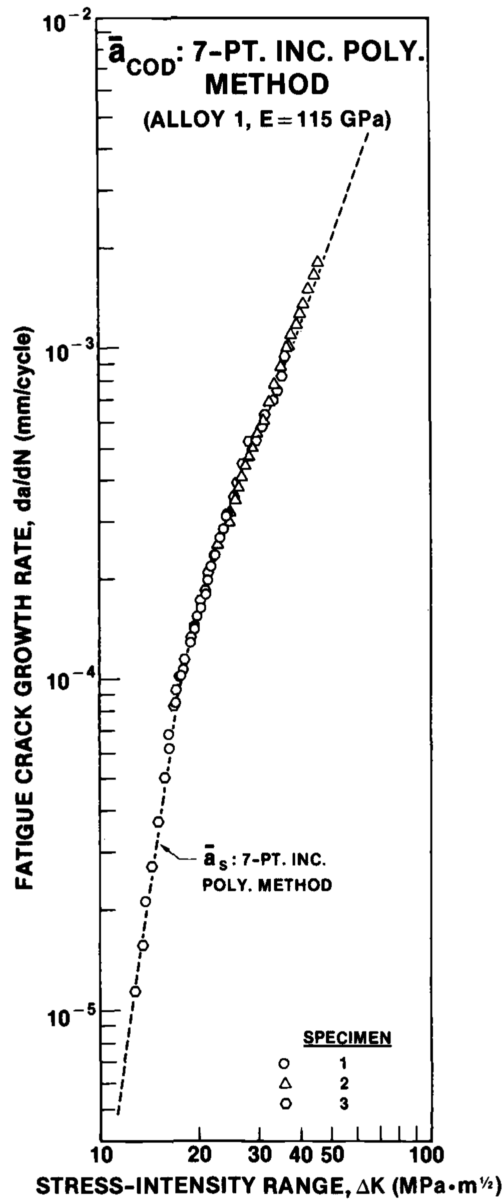

FIG. 5—da/dN *versus* ΔK *data for Alloy 1 from three replicate specimens, with crack-length measurements via COD technique and data reduction via 7-point incremental polynomial method. The dashed line is the reference curve from Fig. 4.*

Comparison of Data-Reduction Methods

In a single-specimen test of Alloy 2, crack length was measured by the COD clip-gage technique ($\overline{a}_{COD}$). As with Alloy 1, we measured E from duplicate tensile tests. Figures 6 and 7 afford comparison of the reduction of the $\overline{a}_{COD}$ versus N data by the 7-point incremental polynomial and secant methods, respectively. For the 7-point incremental polynomial method (Fig. 6), approximately constant increments of Δ(COD)$\approx$0.20 mV ($\pm$0.10 mV) were again used. The dashed line in Fig. 7 traces the reference curve from Fig. 6 to facilitate comparison with the secant method. The correspondence between the two sets of data is excellent. However, note by the separately denoted data symbols that when using the secant method of data reduction, increased scatter in the *da/dN*-ΔK data becomes apparent when the Δ(COD) interval becomes less than 0.16 mV.[4] Thus, as indicated earlier, increments of Δ(COD) should be restricted to 0.20 mV (+0.10/−0.04 mV) for optimization of the secant method. If this is done, Fig. 7 suggests that the scatter in *da/dN* generated by the secant method is virtually the same as obtained with the 7-point incremental polynomial method, as displayed in Fig. 6.

This observation might at first seem surprising, since it is well-known that the secant method generates much greater scatter in the reduction of optically measured crack-growth data ($\overline{a}_s$ versus N) obtained from the specimen surface [2]. The difference observed herein with $\overline{a}_{COD}$ versus N data is attributed to a pair of factors: Firstly, the COD clip-gage measurement inherently averages crack-growth variations through the specimen thickness (which is significant since fatigue cracks grow discontinuously at any one point along the crack front, including the surface). Secondly, measurements of crack growth from Δ(COD) increments of about 0.20 mV in size are made with relatively high precision from digital electronic voltmeter readings with an accuracy of about $\pm$0.01 mV.

Procedures for Step-Loading

Step-loading offers several advantages for FCGR testing. It offers the opportunity to generate a greater span of *da/dN*-ΔK data from a single specimen, which can be a great advantage in situations where test materials are limited. It can also substantially reduce the number of elapsed cycles necessary to generate a *da/dN*-ΔK curve, thus hastening data generation. This aspect can be of particular importance in time-consuming, low-frequency corrosion-fatigue tests. The principal benefit comes from step-loading through the early stages of the test at low *a/W* and *da/dN* values where the gradient, *dK/da*, is shallow. What follows is a brief description of how we systemati-

[4]Increments of ΔCOD as small as 0.10 mV were not considered in Fig. 7.

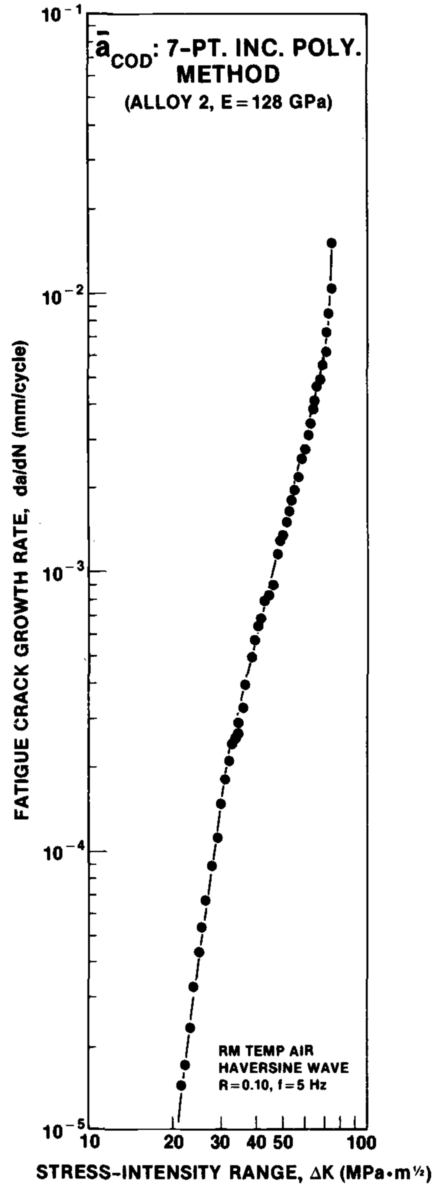

FIG. 6—da/dN *versus* ΔK *data for Alloy 2, with data reduction via 7-point incremental polynomial method and crack-length measurement via COD technique.*

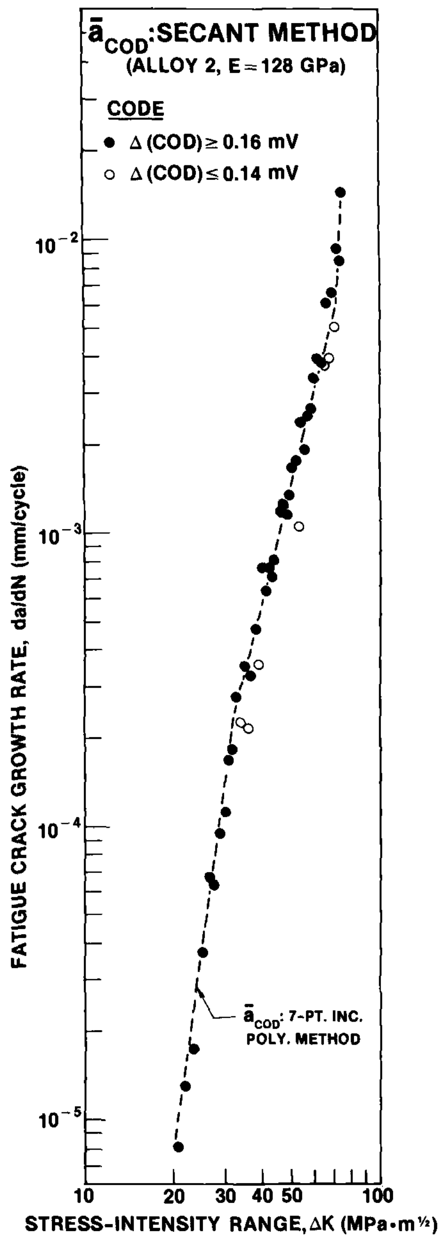

FIG. 7—da/dN *versus* ΔK *data for Alloy 2, with data reduction via secant method and crack-length measurement via COD technique. The dashed line is the reference curve from Fig. 6. Note the apparent increase in scatter when the* Δ(COD) *intervals fall below 0.16 mV.*

cally define a step-loading program based upon COD measurements of crack length and the secant method of data reduction.

The first step involves the preliminary interval selection, shown schematically in Fig. 8. A number of data points are chosen with ΔK-values spaced equidistant on the logarithmic ΔK-scale. With use of the secant data-reduction method, we allow the extent of each interval of constant-load amplitude to be governed by the criterion of a Δ(COD) increment of 0.20 mV. This criterion consequently determines the extent of each ΔK-interval, as well as the amount of load change between intervals. A specific example for a step-loading test on Alloy 2 is shown in Fig. 9. The anticipated effect of a ± 5 percent uncertainty on da/dN is illustrated. The test program, defined in terms of specific loads, is shown in Fig. 10. Note the small increments of maximum load change ($\Delta P_{max} \approx 3$ to 6 percent) and ΔK incremental change per step. The da/dN-ΔK data resulting from this program are shown in Fig.

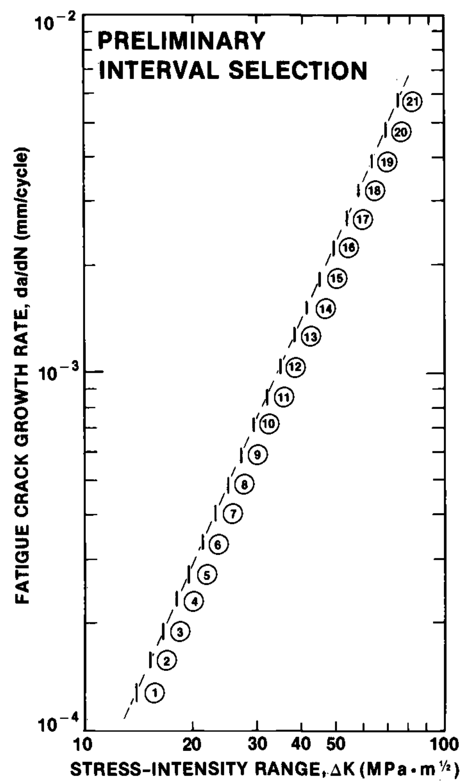

FIG. 8—*Schematic illustration of the preliminary data interval selection procedure for a step-loading program.*

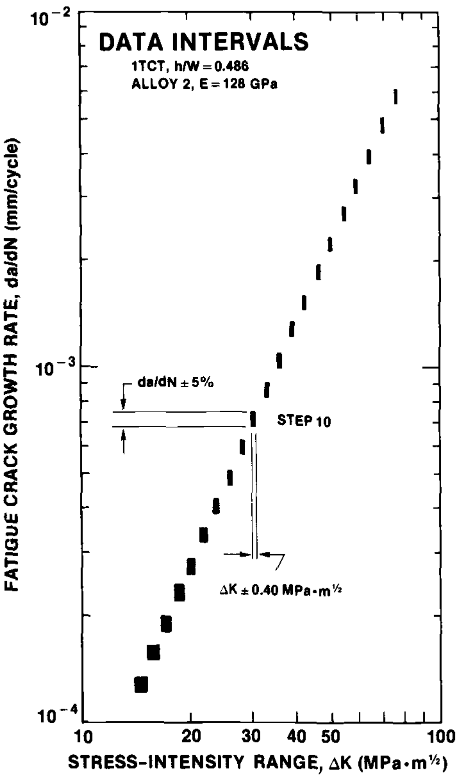

FIG. 9—*Data intervals for step-loading program for Alloy 2, based upon crack-length measurement via COD increment technique.*

11. The reference line shown comes from constant-load-amplitude data shown in Fig. 6. We have made numerous comparisons of this type and find these step-loading procedures to be perfectly satisfactory. However, these procedures do rely upon the use of the secant method of data reduction, which in our experience is greatly enhanced by clip-gage measurement of crack length.

One area of concern in step-loading is the possibility of nonsteady-state transients in da/dN introduced as a result of the periodic incremental load increases. This concern is the rationale for limiting ΔP_{max} to values of less than 10 percent in all of our tests. To date, we have seen no evidence of transient phenomena as a result of step-loading, including data from tests conducted in seawater where hydrogen embrittlement mechanisms are operative [7].

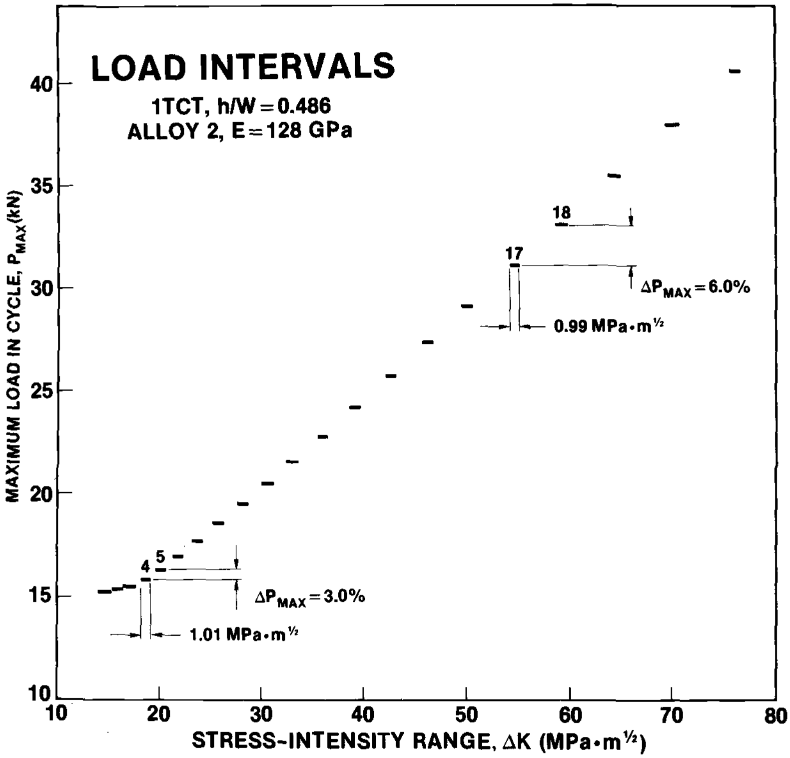

FIG. 10—*Load intervals for step-loading program outlined in Fig. 9. Note that maximum step-loading increments* (ΔP_{max}) *remain small throughout the test.*

Proposed Amendment to ASTM E 647

Section 8.6.2.1 of ASTM E 647 specifies that, for the CT specimen, crack-length measurement intervals shall be spaced according to

$$\Delta a \leq 0.02\ W \text{ for } 0.25 \leq a/W \leq 0.60$$

$$\Delta a \leq 0.01\ W \text{ for } a/W \geq 0.60$$

with the further provision that the minimum Δa shall be 0.25 mm (0.01 in.). Where crack lengths are obtained by optical measurement, these rules appear to be satisfactory. However, as we have attempted to show in this paper, an altogether different set of rules may be applicable where crack lengths are obtained by COD measurement.

Specifically, for the WOL-type CT specimen, present rules specify that the maximum Δa shall not exceed 1.25 mm (0.50 in.). For crack-length measurement at low a/W values using COD techniques, this maximum value should

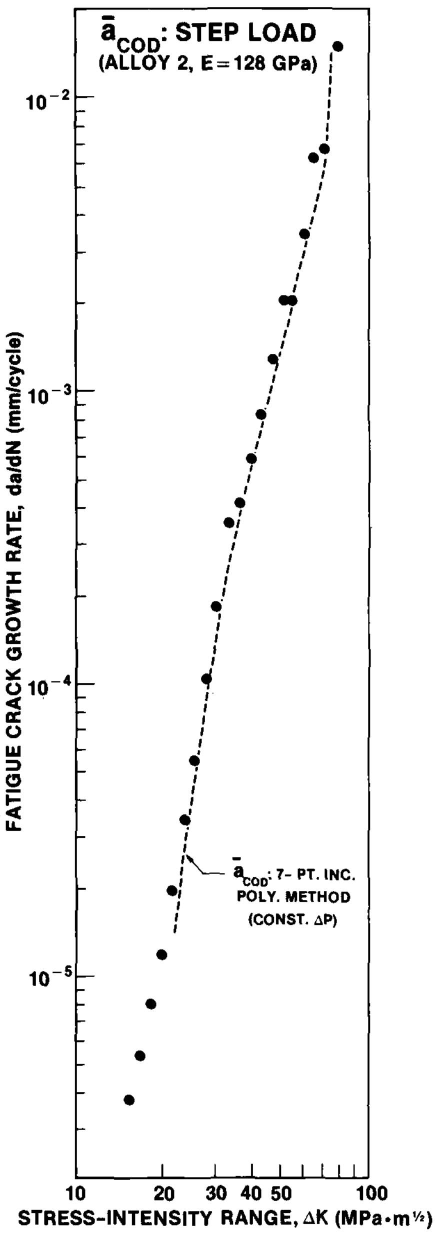

FIG. 11—da/dN *versus* ΔK *data for Alloy 2 generated via step-load procedures with secant method of data reduction. The dashed line is the reference curve from Fig. 6.*

be doubled. This is necessary to accommodate the requirements of the COD technique and, on the basis of our experience, results in no significant change in the final da/dN-ΔK curve.

Summary

In this paper we have attempted to summarize recent developments and experience in our laboratory relating to FCGR test methods:

1. When proper procedures spelled out in this paper are followed, COD measurement of crack length in FCGR testing is convenient, reliable, and accurate.
2. Using COD measurement of crack length, which inherently averages crack-length variations through the specimen thickness, the 7-point incremental polynomial and secant methods of data reduction produce virtually identical da/dN-ΔK results.
3. Using COD measurement of crack length combined with the secant method of data reduction, step-loading programs which hasten the gathering of da/dN-ΔK data can be successfully utilized.
4. Minor amendments should be made to the crack-length measurement provisions of ASTM E 647 to accommodate procedures for COD measurement of crack length.

Acknowledgments

Funding for this study was provided by the Naval Sea Systems Command and the Office of Naval Research. The authors gratefully acknowledge the experimental assistance of G. W. Jackson and M. L. Cigledy.

References

[1] Goode, R. J., *Materials Research and Standards*, Vol. 12, No. 9, September 1972, pp. 31-32.
[2] Clark, W. G., Jr., and Hudak, S. J., Jr., *Journal of Testing and Evaluation*, Vol. 3, No. 6, November 1975, pp. 454-476.
[3] McHenry, H. I., *Journal of Materials*, Vol. 6, No. 4, 1971, pp. 862-873.
[4] Sullivan, A. M. and Crooker, T. W., *Engineering Fracture Mechanics*, Vol. 9, No. 1, 1977, pp. 159-166.
[5] Saxena, Ashok and Hudak, S. J., Jr., *International Journal of Fracture*, Vol. 14, No. 5, October 1978, pp. 453-468.
[6] Sullivan, A. M. and Crooker, T. W., *Engineering Fracture Mechanics*, Vol. 9, 1977, pp. 749-750.
[7] Bogar, F. D., Yoder, G. R., Crooker, T. W., "Verification of Step-Loading Procedures for Fatigue-Crack-Growth-Rate Testing in Natural Seawater," Report of NRL Progress, Naval Research Laboratory, Washington, D.C., September 1979, pp. 19-21.

DISCUSSION

S. J. Hudak, Jr.[1] (*written discussion*)—I would like to compliment the authors on their informative paper on the utilization of elastic compliance methods in fatigue crack growth rate testing. I would also like to comment on two issues which were raised in the paper.

Firstly, it was shown that under certain conditions comparable results, both in terms of a mean response and variability about the mean, are obtainable using the secant and 7-point incremental polynomial data reduction techniques (Fig. 6 versus Fig. 7). This agreement was attributed to (*1*) natural data smoothing due to the fact that the compliance method gives a through-thickness, average crack length, and (*2*) the precision of the compliance procedures documented in the paper. I would like to emphasize the second point, for I believe it to generally be the prime factor in controlling data variability. Specifically, it has been shown through analytical studies that the ratio of the crack-length measurement interval (Δa) to measurement precision has a strong influence on the variability associated with various data-reduction techniques, particularly the secant method.[2,3] When this ratio is maintained greater than 10, the variability of the secant method approaches that of the incremental polynomial method. In fact, these results provided the basis for the requirement in Section 8.6.2.3 of ASTM E 647 that the minimum Δa should be at least ten times the measurement precision. Your results in Fig. 7 (solid data points) conform to this requirement, thus the agreement between the two data-reduction techniques is understandable.

Although the natural averaging of the compliance technique may also contribute to this agreement, it is probably of secondary importance, since it has been shown that the compliance technique is not essential to achieving similar agreement between the two data-reduction techniques. For example, the same agreement has been demonstrated using data based on visual crack-length measurements at the specimen surface when the Δa to precision ratio was favorable (see Fig. 31 in Clark and Hudak[4]).

My second comment pertains to your suggested modification to Section 8.6.2.1 of ASTM E 647 regarding the minimum crack-length measurement

[1]Senior research scientist, Southwest Research Institute, San Antonio, Tex. 78284.
[2]Clark, W. G., Jr., and Hudak, S. J., Jr., "The Analysis of Fatigue Crack Growth Rate Data," *Application of Fracture Mechanics to Design, Proceedings*, Sagamore Army Materials Research Conference, Vol. 22, Plenum, New York, 1979.
[3]Wei, R. P., Wei, W., and Miller, G. A., *Journal of Testing and Evaluation*, Vol. 7, No. 2, 1979, pp. 90–95.
[4]Clark, W. G., Jr., and Hudak, S. J., Jr., *Journal of Testing and Evaluation*, Vol. 3, No. 6, 1975, pp. 454–476.

interval. I do not believe a different set of rules are needed when compliance techniques are used in place of visual measurements of crack length. The object of Section 8.6.2 is to provide crack-length measurement intervals such that data are nearly evenly distributed with respect to ΔK; this you have satisfactorily achieved by taking data at a constant deflection interval. The Δa-values of Section 8.6.2.1 were intended as recommendations or suggestions to achieve the aforementioned condition. Thus the first few measurements during your tests do not violate any requirement of ASTM E 647. Perhaps this point needs to be clarified in ASTM E 647 to avoid further misunderstandings by other users of the method.

G. R. Yoder, L. A. Cooley, and T. W. Crooker (author's closure)—We wish to thank Mr. Hudak for his thoughtful remarks. With regard to his initial comment, we would like to make two observations: (*1*) Any suggestion that the secant and incremental polynomial methods provide virtually identical results (if the requirement section 8.6.2.3 of ASTM E 647 is met) would seem to be clearly at variance with the sentiments of Note 9, Section 9.2 of ASTM E 647, wherein it is stated that ". . . the secant method often results in increased scatter in da/dN relative to the incremental polynomial method, since the latter numerically 'smoothes' the data . . . This apparent difference in variability introduced by the two methods needs to be considered, especially in utilizing da/dN versus ΔK data in design;" and (*2*) In Clark and Hudak[4] it is stated that "Figure 31 clearly indicates that when the raw data . . . represent a relatively smooth curve with little scatter, each of the four data processing techniques yield [*sic*] essentially identical crack growth rate results. However . . . when the a versus N data do not represent a smooth curve . . . the crack growth rate data associated with the different curve fitting procedures varies [*sic*] considerably . . ." The point we wish to make here is that the latter case, relative to the former, need not arise solely or even primarily, on the basis of a difference in measurement precision, but rather on the basis of *material* effects. In fact, we are presently in the process of drafting a paper that documents the influence of alloy microstructure on the variability of a versus N data about the mean, for a given measurement precision. In those instances where a versus N data, measured optically at the specimen surface, do not represent a smooth curve (owing to microstructural effects), we feel that the inherent through-thickness averaging of the compliance related techniques can be a benefit of primary importance.

With regard to Mr. Hudak's second comment, we do not believe that the problem rests so much with a misunderstanding of Section 8.6.2 of ASTM E 647 as it does with the question of whether users of compliance related techniques should be encouraged to violate an ASTM recommended practice.

R. P. Wei[1] *and R. L. Brazill*[1]

An Assessment of A-C and D-C Potential Systems for Monitoring Fatigue Crack Growth

REFERENCE: Wei, R. P. and Brazill, R. L., "**An Assessment of A-C and D-C Potential Systems for Monitoring Fatigue Crack Growth,**" *Fatigue Crack Growth Measurement and Data Analysis, ASTM STP 738,* S. J. Hudak, Jr., and R. J. Bucci, Eds., American Society for Testing and Materials, 1981, pp. 103-119.

ABSTRACT: Electrical potential techniques for crack length measurements have been used for over 15 years to monitor subcritical crack growth. These techniques, based on the changes in electrical resistance of a specimen with crack extension, utilize either a d-c or, more recently, an a-c measurement system. The d-c and a-c systems are described, and the operating characteristics of two specific systems are discussed. A description of the empirical calibration of a specimen using these systems is included. Operating data are included for crack length measurements in a steel compact tension specimen. The d-c system, operated at a current of 10 A, had a crack length resolution of 0.013 mm. The a-c system, employing a lock-in amplifier as a tuned amplifier to provide noise rejection, can be operated at a much lower current of 0.75 A and provided a crack length resolution of 0.010 mm. By design, the a-c system would reject thermal (d-c) electromotive force introduced into the measurement circuit, whereas the d-c system had no such capability. Both systems, however, would be sensitive to changes in resistivity of the material with temperature. In materials of high magnetic permeability, alternating current is not uniformly distributed through the specimen thickness and tends to be concentrated near the specimen surface. The consequences of this "skin effect" in relation to crack length measurements are discussed. Operating procedures that assist in reducing noise and improving measurement sensitivity in both systems are described.

KEY WORDS: measurement techniques, fracture mechanics, fatigue crack growth, crack length, electrical potential, instrumentation

Electrical potential techniques have been in use for over 15 years for measuring crack lengths in metallic fatigue and fracture specimens [*1-10*].[2] The use of these techniques is based on the fact that the electrical resistance of a specimen increases with crack extension. This increase in resistance is

[1] Professor of Mechanics and research assistant, respectively, Lehigh University, Bethlehem, Pa. 18015.

[2] The italic numbers in brackets refer to the list of references appended to this paper.

reflected as, and is directly related to, a measurable increase in electrical potential across the specimen having a constant current passing through it. An alternative method for monitoring crack length is through the use of metal film deposited onto the specimen or a metal foil bonded onto the specimen. Crack lengths in nonconducting specimens can be measured by this method. Both direct-current (d-c) and alternating-current (a-c) systems can be used for measuring the changes in potential, utilizing standard measurement techniques.

Direct-current systems were the first to be used [*1–4*]. The initial systems involved measurements of electrical potential changes in the millivolt range [*1,2*]. Because of the low resistance of metallic specimens, high direct currents (on the order of tens of amperes) were needed. Measurements were typically made on a point-by-point basis because of the particular measurement (null) technique, and the need to have the current switched on only during measurements to minimize specimen heating. To avoid the use of these high direct currents, systems capable of measuring potentials in the microvolt range were later utilized [*3,4*]. Point-by-point measurements were made at first using a null technique [*3,4*]. With the availability of low-noise, high-gain d-c amplifiers, continuous recording systems are now commonly utilized [*5,7*].

The d-c systems are somewhat limited, however, because of their sensitivity to thermally induced electromotive force (emf) (associated with thermocouple effects) and the limited potential for further reduction in their sensitivity to "noise". To circumvent some of these limitations of the d-c systems, alternating-current systems have been assembled to take advantage of the noise rejection capabilities of lock-in amplifiers and the high gain associated with these amplifiers [*8,9*]. These systems, being a-c systems, would be insensitive to thermally induced d-c potentials, and are capable of sensitivity in the nanovolt range. Signal discrimination is facilitated in a-c systems by the ability to tune the measuring instrument to the excitation frequency.

Both the d-c and the a-c potential systems have gained acceptance as reliable, accurate, and cost-effective methods for measuring crack lengths in fatigue and in other fracture specimens. They can be readily integrated into a suitable data acquisition system for continuous monitoring of crack growth experiments. They can also form an integral part of automated materials testing systems for data acquisition and provide for control of simple and complex crack growth experiments.

In this paper an assessment of the a-c and d-c potential systems for monitoring fatigue crack growth is made. The measurement methods and elements of the systems are reviewed briefly. Calibration, sensitivity, and operating characteristics of these systems are discussed. The systems are compared using a specific specimen for illustration. Some suggestions for the use of these systems are given.

Potential Measurement Systems

The most elementary and standard method for measuring electrical potential involves the direct comparison of the unknown potential against a calibrated standard potential. The comparison is made with a potentiometer or a Wheatstone bridge, and the measurement is made by "nulling" a galvanometer or a suitable null detector. Because of the "slow" response of the galvanometer and the need for manual adjustments, it is necessary to make these measurements on a point-by-point basis, and often with test interruption.

To allow for continuous measurements, with no test interruptions, more sophisticated systems incorporating high-gain amplifiers are used. To improve measurement sensitivity, the change in potential with respect to some reference level (such as the potential of the uncracked specimen) is often used. Typical d-c and a-c potential systems are illustrated in Figs. 1 and 2 [*5,8,9*]. The characteristics of these systems are discussed in the following sections.

D-C System

The block diagram of a typical d-c potential system is illustrated in Fig. 1. The system is composed of a "constant" current source, with a current measurement instrument, a potentiometer to provide a reference voltage, null detector or high-gain d-c amplifier, and the appropriate recording instruments. Since the specimen resistance is very low (much less than 1 Ω), the constant current source is often replaced by a constant voltage source, with suitable current limiting resistors to establish the desired current level. In addition to or in place of the recording instruments, the output of the amplifier may be connected to a data acquisition system or to a digital computer. In more recent systems the potentiometer is eliminated and "zero suppression" is handled by internal circuits in the amplifier.

Amplification of the small d-c potentials encountered in crack length measurements is accomplished by converting the signal into alternating current and amplifying the resulting a-c signal. Rectification and filtering, following amplification, result in an amplified d-c voltage that is proportional to the incoming signal. Conversion is usually accomplished by means of a mechanical "chopper" operated at a frequency to minimize line-frequency noise, but which allows for the elimination of sideband components. An input transformer is usually used ahead of the a-c amplifier for impedance matching and for placing the input signal in the desired operating region of the amplifier. Feedback networks are often used to improve linearity.

The scheme and components used for d-c amplification are designed for

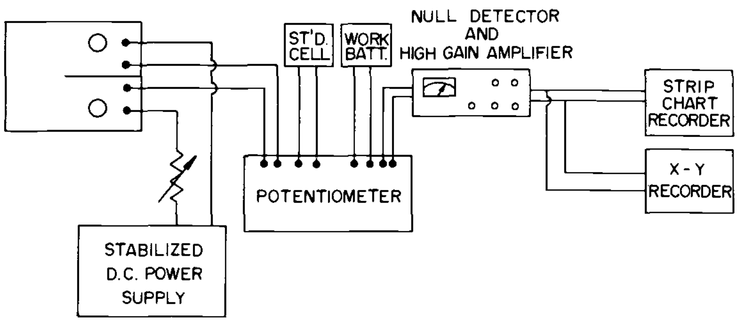

FIG. 1—*Block diagram of the d-c potential system.*

low-noise operation. The system operates, however, as a broadband amplifier. The output from the demodulator contains noise which entered the chopper with the unfiltered input signal. To improve the signal-to-noise ratio, an integrating d-c amplifier is used in the final stage of amplification.

A-C System

A typical a-c potential system is illustrated in the block diagram in Fig. 2. The system is built around a lock-in amplifier, and includes, in addition, a power amplifier (operated as a constant current operational amplifier), an isolation transformer, and appropriate recording and data acquisition systems. The power amplifier is driven by a reference signal from the lock-in amplifier to supply the specimen with a constant-current a-c excitation signal. The constant current level is determined by the wiring configuration of the power amplifier and the sampling circuit resistors. Typically, this is approximately 0.75 A.

The reference frequency is used internally by the lock-in amplifier to tune in to the frequency of the specimen potential signal in the same way that an AM radio receiver is tuned to the frequency of a transmitted carrier frequency. However, unlike an AM receiver where the carrier signal is removed and the modulating signals drive the output amplifier, the lock-in amplifier is designed to remove the modulating signals (noise) from the reference frequency component (that is, the desired potential signal). The selection of reference frequency depends on such factors as source impedance, predominant frequencies of noise, and internal transfer characteristics of the lock-in amplifier. The choice of reference frequency will be discussed later.

The specimen potential signal, mixed with broadband noise from sources of electromagnetic interference (EMI), is applied to the lock-in by way of an isolation transformer used both for isolation and to improve the source impedance seen by the lock-in amplifier. The input signal to the lock-in

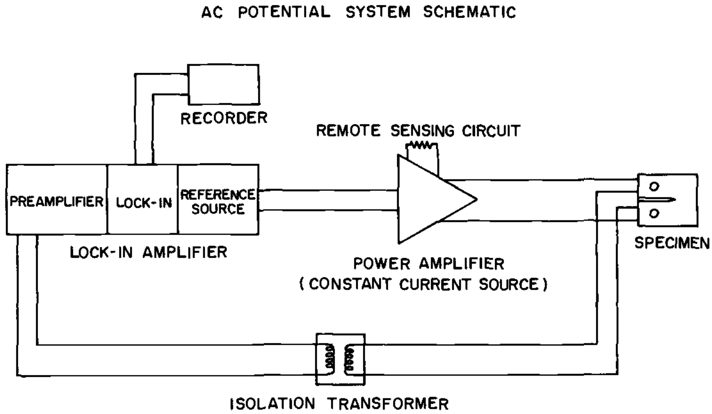

FIG. 2—*Block diagram of the a-c potential system.*

amplifier is first preamplified and passed through a bandpass filter which brackets the reference frequency. A phase-sensitive detector, driven at the reference frequency, convolutes the remaining signal into sum and difference frequency components relative to the reference frequency. Since the frequency of the desired potential signal is identical to the reference frequency, it produces the only zero frequency difference (dc) component and is proportional to the amplitude of the specimen potential signal. The d-c component is retrieved by means of a low-pass filter, amplified and displayed on a meter, and is available at the output jack for recording.

The choice of reference frequency is based primarily on two considerations. Firstly, frequencies of noise sources, such as line frequency (60 Hz), must be avoided to minimize interference. Higher harmonics of these frequencies should be also avoided as these can produce zero frequency difference components with respect to the reference frequency. The second consideration is the effect of frequency on the current density through the thickness of the specimen. The current density is nonuniform through the thickness of a conductor carrying an alternating current, with a higher current density occurring near the surfaces. This so-called "skin effect" is produced by the interaction of the alternating current or electron flow with the magnetic field it produces [*11*]. The nonuniform current density effectively reduces the conductor's flow area and increases its apparent resistance. The effect is more pronounced at high frequencies and in materials of high magnetic permeability. Therefore the reference frequency should be chosen as low as practicable to provide a more uniform current density through the specimen thickness. Skin effect, on the other hand, may be used to enhance measurement sensitivity for surface cracks. The skin effect is discussed in more detail in the Appendix.

Once the reference frequency has been selected, impedance matching may be required between the signal source (specimen) and the lock-in amplifier. This is done to improve the operating performance of the system. Noise figure contours supplied with the lock-in amplifier can be used to determine the optimum source impedance for a given reference frequency and system configuration. Partial impedance matching was provided by the isolation transformer, with a 1000:1 turn ratio, to increase the low source impedance of the specimen. The transformer also served to isolate the excitation and measurement circuits.

A reference frequency of 93 Hz was chosen empirically for the system shown in Fig. 2, principally to minimize the influence of line-frequency (60 Hz) noise. This frequency is sufficiently low so that the "skin effect" does not present a significant problem in most cases. For steel specimens of sufficient thickness, such as the 25.4-mm-thick 2.25Cr-1Mo steel specimen used for illustration here, significant skin effect may be encountered (see Appendix). Skin effect can increase the effective resistance of the specimens, and hence increase the electrical potential at a given current. In effect, it can increase the measurement sensitivity and is beneficial when the crack front curvature is not severe (for example, in the case of fatigue crack growth). With skin effect, detection of crack growth in the midthickness region is less sensitive, and its consequence needs to be assessed when significant crack tunneling is expected. For such cases, special calibrations or the use of a d-c system may be more advisable.

Calibration

To use the potential systems for measuring crack lengths, the relationship between specimen crack length and potential for a particular specimen planform must be established. This relationship can be determined experimentally, analytically [*12*], or by numerical methods [*13,14*]. Analytical techniques are suitable for simple specimen geometries (such as center-cracked tension specimens), but are difficult to use because of problems encountered in modelling the complex geometry of most specimens [*2,3,5*]. Numerical methods, unless they are quite sophisticated, tend to yeild relatively crude results. Experimental determination with a specimen, on the other hand, is the most straightforward because actual operating conditions can be exactly duplicated. This method also provides data for making statistical estimates of the uncertainty in crack length measurements.

When determining specimen crack lengths from potential measurements, it is desirable to eliminate specimen-dependent effects from these measurements. Normalization of potential readings with respect to a reference potential for each specimen is used to eliminate from these measurements any variations in potential caused by changes in specimen resistivity with temperature or by thickness differences from one specimen to another. Normalized potential, however, is only dependent on changes in specimen resistance produced by crack extension when all other variables remain constant. The normalized potential depends on the distributed electric field within the specimen, and thus each specimen planform and probe position in general requires a separate calibration to determine how crack length is related to the normalized potential. Conversely, however, geometrically similar (but dimensionally different) specimens should exhibit the same normalized potential dependence on normalized crack length (that is, the ratio between crack length and the reference crack length). The normalized potential, from which crack length can be determined after calibration, is usually taken to be the ratio of the difference between the absolute and reference potentials ($V - V_r$) to the reference potential (V_r), or

$$V^* = \frac{V - V_r}{V_r} \tag{1}$$

The reference potential, V_r, is the specimen potential corresponding to a reference crack length.

Experimental calibrations for different specimens and materials have been reported in the literature [*2-10*]. For illustration and for comparison between the a-c and d-c systems, calibration data from a 2.25Cr-1Mo (A542, Class 2) steel are given here [*10*]. Several compact tension specimens, having dimensions shown in Fig. 3, were used to determine the functional relationship between crack length and normalized potential. Calibration tests were carried out by fatigue cracking the specimens in air while monitoring the potential. Crack length measurements were correlated with the potential data to determine the calibration equation.[3] Calibration data obtained with both a d-c and an a-c potential system are shown in Fig. 4, along with a fitted polynomial curve for the data. Both systems show approximately a 50 percent increase in normalized potential occurring over the useful crack length range of the specimen, so that good crack length sensitivity is obtained. Data obtained from both systems are in agreement over the entire range of crack lengths.

The equation of the experimental calibration curve can be expressed as

$$a = 15.9 + 52.0V^* + 26.0V^{*2} - 41.4V^{*3} \quad (a \text{ in mm}) \tag{2}$$

[3]Since the crack front usually has some degree of curvature to it, and because the electrical potential is related to the uncracked ligament of the crack plane, the potential system gives a measure of some average crack length. For this reason, the crack length for the calibration was taken as the five-point average of post-test measurements, taken at the sides, quarter points, and midpoint of the crack plane. The position of the crack front at each measurement time was made visible by changing the fatigue load levels at each interval, causing a change in crack surface texture so that the position of the crack front was visible after the test.

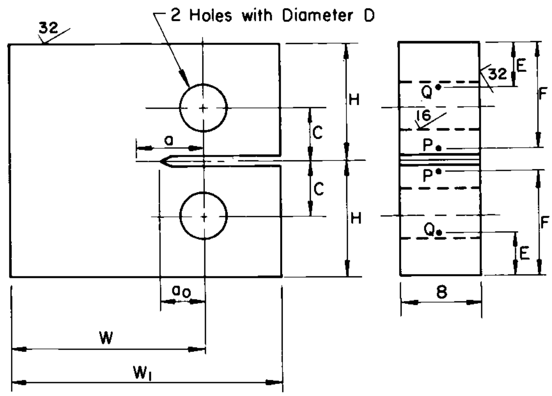

	B	a_0	W	H	W_1	C	D	E	F
cm	2.54	1.59	6.35	3.81	8.90	1.78	1.59	1.40	3.38
in.	1.00	0.625	2.50	1.50	3.50	0.70	0.625	0.55	1.33

P - potential lead connection point
Q - current lead connection point

FIG. 3—*Compact tension specimen used in comparison of the a-c and d-c potential systems.*

The coefficients were determined from the experimental data by the method of least squares, and statistics on the precision of the data were used to select the order of the polynomial for the calibration equation.

It should be noted that the measured a-c potential across the specimen includes the resistive as well as the reactive components of specimen impedance, while d-c potential measurements are only affected by the resistive portion. It is possible that these reactive components of specimen impedance (capacitance and inductance) contribute significantly to the a-c potential measurement. Based on the good agreement between the a-c and d-c calibration data, it appears that the resistive component is the major contributor to the specimen impedance in this steel.

Comparison Between A-C and D-C Systems

General Considerations

The crack length resolution of an electrical potential system is a function of the instrument sensitivity for a given specimen geometry, and is limited primarily by the level of noise in the system. The resolution of potential is on the same order of magnitude as the noise level when instrument drift can be neglected. The sensitivity, or equivalent crack growth to produce a full scale output, depends on the amplifier gain, the specimen geometry, the place-

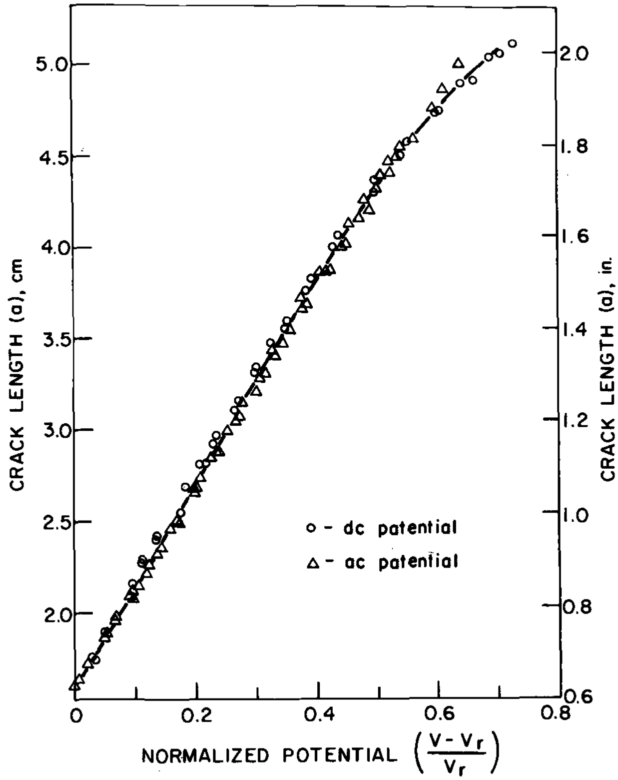

FIG. 4—*Calibration curve for a-c and d-c potential systems. Operating values given in Table 1.*

ment of the potential leadwires [*6*], and the applied current to the specimen. For a compact tension specimen (Fig. 3), an increase in crack length of approximately 30 mm (1.2 in.) caused a potential increase of about 50 percent relative to the reference potential.

The crack length resolution determines the uncertainty in the crack length measurement and is thus important in the calculation of crack growth rates (using the secant method, for example). If the uncertainty in crack length is σ_a and is constant, then the relative uncertainty in the crack growth increment Δa is

$$\frac{\sigma_{\Delta a}}{\Delta a} = \frac{\sqrt{2}\sigma_a}{\Delta a} \tag{3}$$

Thus, for a desired relative uncertainty in the crack growth increment $(\sigma_{\Delta a}/\Delta a)$,

$$\Delta a \propto \sigma_a \tag{4}$$

In other words, the increment of crack growth required to achieve a given uncertainty in that increment or in crack growth rate depends directly on σ_a and, therefore, on resolution.

A-C versus D-C System

A comparison was made between the a-c and d-c systems using data from 2.25Cr-1Mo steel specimens for illustration. Two separate bases for comparison can be used, one in which the operating sensitivities are comparable and the other in which the potential levels are equal. These comparisons are given in Tables 1 and 2.

The case of comparable operating sensitivity is considered in some detail. From Table 1, it can be seen that for the d-c potential system shown in Fig. 1, at an excitation current of 10 A, the potential ranges from about 400 to 600 μV over the normal range of specimen crack lengths. The range of measured a-c potentials (using an excitation current of 0.75 A rms) for the same specimen is from about 100 to 150 μV with a signal-to-noise ratio of about 5000:1. This is slightly improved over the 4000:1 ratio obtained with the d-c system operated at the higher current.

Using a potential offset to increase the allowable instrument sensitivity, the d-c system is operated at about 100 μV/V. This translates into an operating sensitivity of approximately 14 mm/V. The same sensitivity can be obtained in the a-c system with the lock-in amplifier operated at a gain of 4×10^4.

The instrument sensitivities, noise levels, and potential values for the two systems yield comparable calculated resolutions of 0.013 mm for the d-c system and 0.010 mm for the a-c system. These values reflect only the instrument dependent variables, but not statistical uncertainties associated with the calibration. The actual crack length resolution for the two systems is somewhat higher.

The uncertainty in the change in crack length (or in crack growth rates from the secant method) due to uncertainties in the measured potential was calculated for the third-order calibration equation given previously (Eq 2). The calculation is based on a crack interval Δa associated with a change in normalized potential $\Delta V^* = 0.01$. A maximum error of 6.5 percent was obtained for the d-c system; the a-c system had a slightly better 5.5 percent error. The signal-to-noise ratio was assumed to be constant, and the coefficients of the calibration equation were assumed to be error free.

It is seen that crack length measurements can be made with both the a-c and d-c potential systems at quite comparable levels of resolution and crack length uncertainty. These measurements can be made with commercially available instruments, with normal care required for measuring microvolt

TABLE 1—*Comparison of normal operating values for the a-c and d-c potential systems.*

	Direct Current	Alternating Current
Base potential	400 μV	100 μV
Required current	10 A	0.75 A
Noise level at output	0.1 μV	0.02 μV
Signal-to-noise ratio on absolute potential	4000:1	5000:1
Signal-to-noise ratio on potential difference for $\Delta V^* = 0.01$	40:1	50:1
Uncertainty in Δa associated with $\Delta V^* = 0.01$ for the indicated noise level	6.5 %	5.5 %
Operating sensitivity:		
Amplifier gain	10^4	4×10^4
Potential	100 μV/V	25 μV/V
Crack length	14 mm/V	14 mm/V
Operating resolution:		
Potential	0.1 μV	0.02 μV
Crack length	0.013 mm	0.010 mm
Sensitivity to thermal emf	high	none
Sensitivity to leadwire movement	none	moderate

level signals. The current required for the a-c system, however, is less than one tenth that for the d-c system. At equal potential levels (see Table 2), on the other hand, it can be seen that the a-c system provides much greater sensitivity and better precision, while still operating at a somewhat lower current level.

Some Further Considerations

One practical consideration in the choice of a system is the problem of the thermal emf which is generated when a temperature difference exists between the leadwire-to-specimen junctions in the measurement circuit. Using a d-c potential system, this thermal emf will produce an additive error in the potential measurements which must be eliminated or accounted for. The advantage of using an a-c potential system is that any d-c error, including a thermal emf, which is introduced in the potential is eliminated from the a-c measurement. On the other hand, as mentioned earlier, the reactive components of the specimen impedance must be considered in the a-c potential measurements. These considerations include the inductive and capacitive coupling between the leadwires, which is in evidence when a small potential change occurs with leadwire movement. The first of these problems can be handled by special calibration, and the latter is remedied by twisting both the current and potential measurement leadwire pairs together.

Several other aspects common to both types of potential systems which should be considered when measuring fatigue crack growth are the system

TABLE 2—*Comparison of a-c and d-c potential systems having the same base potential.*

	Direct Current	Alternating Current
Base potential	400 μV	400 μV
Required current	10 A	3 A
Noise level at output	0.1 μV	0.02 μV
Signal-to-noise ratio on absolute potential	4000:1	20000:1
Signal-to-noise ratio on potential difference for $\Delta V^* = 0.01$	40:1	200:1
Uncertainty in Δa associated with $\Delta V^* = 0.01$ for the indicated noise level	6.5 %	1.4 %
Operating sensitivity:		
Amplifier gain	10^4	5×10^4
Potential	100 μV/V	20 μV/V
Crack length	14 mm/V	3 mm/V
Operating resolution:		
Potential	0.1 μV	0.02 μV
Crack length	0.013 mm	0.003 mm
Sensitivity to thermal emf	high	none
Sensitivity to leadwire movement	none	moderate

time response, crack closure, and testing in aqueous environments. The time response of the electronics should be matched to the particular operating characteristics of the test. A certain degree of electrical and mechanical damping is usually necessary to reduce or average out random fluctuations in the measured potential. Overdamping, however, can lead to errors in crack growth rate, especially at higher crack velocities. In this case, the system response is so slow that the system output lags behind the actual specimen potential. Thus, there are upper limits to the crack growth rates which can be measured with a potential system, and system time response should be selected to match the desired damping effect.

Crack closure in fatigue can cause periodic fluctuations in measured potential due to shorting over portions of the crack face during low load portions of the loading cycle. Depending on the fatigue frequency and the system time response, these fluctuations can be masked by the damping characteristics of the measurement system, and the measurement will be an averaged reading which may vary with frequency. By obtaining readings with the use of a computer controlled data acquisition system, the potential measurement can be made at the maximum load point in each cycle, and the effect of crack closure can be reduced.

Another error in potential measurements may occur when a substantial amount of plastic deformation occurs in the material ahead of the crack tip. Changes in potential can occur, caused by a change in shape of the crack tip and changes in resistivity of the plastically deformed material ahead of the crack tip. These changes in potential are not associated with an increase in crack length, making crack length measurements inaccurate. For specimens that satisfy the linear fracture mechanics requirements of ASTM Tentative Test Method for Constant-Load-Amplitude Fatigue Crack Growth Rates Above 10^{-8} m/Cycle (E 647-78 T)[4] this is not a problem.

Potential measurements made on specimens tested in aqueous environments may contain errors due to conduction of current across intergranular crack surfaces that remain in partial physical contact. In general, a reduction in potential occurs in such cases. The errors introduced from this source should be accounted for when calculating specimen crack lengths.

Operating Hints

This section presents, as a review, several operating guidelines which will avoid problems encountered in using a-c and d-c potential systems:

1. Remove oxides from both the specimen and the leadwires, as they can introduce very large resistance into the excitation and measurement circuits. The presence of oxides at junctions can serve as a source of significant thermal emf errors in a d-c potential system.
2. Reduce susceptibility to electromagnetic interference (EMI) by using shielded or coaxial cable wherever possible. Twist leadwire pairs together.
3. Use low thermal connections (crimp connections) in the measurement circuit to avoid the introduction of thermal emf errors.
4. Avoid dissimilar metal connections.
5. Compensate for unavoidable thermal emf sources by measuring the apparent specimen potential with no excitation (d-c system).
6. For an a-c system, use a frequency which is low enough to avoid skin effect, which avoids line frequency and other EMI sources, and for which sidebands can be filtered out.
7. Be aware of changes in potential when testing in aqueous and in other aggressive environments.
8. Avoid large-scale specimen plasticity.
9. Select a time response which meets the damping requirements of the system.

By following these precautions, one can minimize most of the problems that may be encountered when using a potential technique to measure specimen crack lengths in fatigue.

Summary

Electrical potential techniques can provide reliable and accurate measurements of crack lengths, and are suitable for use in subcritical crack

[4]ASTM E 647-78 T is reprinted in this volume as Appendix I, pp. 321-339.

growth studies. These systems can be readily interfaced with data acquisition devices or automated materials test systems. Either d-c or a-c measurement systems may be employed. Both systems provide high crack length resolution and measurement sensitivity.

Two existing electrical potential systems were described, including the empirical calibrations of both systems. The calibration data for the systems were nearly identical, and a common calibration equation was found. The d-c system employed a quality high-gain d-c amplifier which had a resolution in potential of approximately 0.1 μV, and was limited by the instrument noise and the power supply stability. The a-c potential system, with a quality lock-in amplifier, had a potential resolution of better than 0.02 μV due to the noise rejection capability of the lock-in amplifier.

Compared to the d-c system, a comparable signal-to-noise ratio was achieved with the a-c system while using one tenth of the operating current. When these systems were operated at the same potential, the crack length resolution using the a-c system was about four times better than with the d-c system.

The d-c potential systems are sensitive to thermally induced emf which can introduce significant errors into the crack length measurement. The a-c measurement systems do not respond to d-c signals and are insensitive to thermally induced emf. Excellent noise rejection is provided by a-c systems that employ a lock-in amplifier as a tuned amplifier. Interpretation of data requires special attention in an a-c system when significant crack tunneling is involved because of the "skin effect" which can occur in materials of high magnetic permeability, particularly at high operating frequencies. This effect is caused by nonuniformity of current density through the specimen thickness that reduces measurement sensitivity in the midthickness region.

The reactive components of the measured potential resulting from distributed capacitance and inductance in the specimen and connecting wires must be considered in a-c potential system measurements. Temperature changes affect the measured potential in both a-c and d-c systems, which limits the measurement of low crack growth rates.

On balance, d-c systems are much easier to understand and use, and provide reasonable measurement sensitivity and precision. An a-c system, on the other hand, provides comparable sensitivity and resolution at greatly reduced operating current. Because of its narrow band operation, it is capable of better signal-to-noise ratio, and can better reject external disturbance (such as those introduced by radio-frequency induction heaters). The choice of systems depends, therefore, on many of these special considerations.

Appendix

The Skin Effect in A-C Potential System Measurements

An a-c flow in a conductor is affected by the magnetic field it induces, producing a current density that varies with depth into the conductor. In a cylindrical conductor, for example, the maximum current density occurs at the surface and decreases exponentially towards the center so that most of the current flows in a thin surface layer. This is the so-called "skin effect" in a-c flow [11]. The skin effect effectively reduces the current flow area and increases the apparent resistance per unit length. The operating data in Table 1 show evidence of the skin effect, where the apparent specimen resistance is approximately three times higher using the a-c system than with the d-c system. An estimate of this effect may be made using the following approximate analysis.

For a semi-infinite conductor, the current density is given by Ref 11 as

$$J = J_o e^{-x/\delta} \tag{5}$$

where

J = current density,
x = depth into the conductor,
J_o = surface current density ($x = o$),
δ = $\sqrt{\rho/\pi f \mu}$ = skin depth where $J = J_o/e$,
ρ = conductor resistivity,
f = cyclic operating frequency, and
μ = absolute magnetic permeability of the conductor.

To estimate skin effect, the specimen is modelled as a flat-plate conductor having the same thickness, b, as the specimen. It is assumed that the current density can be represented by the superposition of profiles of the form given by Eq 1 from each of the conductor faces. It is further assumed that the effective thickness, b_e, is proportional to the skin depth, δ. The superimposed current density profile can be then written as

$$J = J_o (e^{-x/\delta} + e^{-b/\delta} e^{x/\delta}) \tag{6}$$

In this equation, x is the distance into the conductor from one face in the thickness direction. The total current, I, passing through the height, h, of the conductor is obtained by integration of Eq 6.

$$\begin{aligned} I &= h \int_o^b J\,dx = hJ_o \int_o^b (e^{-x/\delta} + e^{-b/\delta} e^{x/\delta})\,dx \\ &= 2\delta h J_o (1 - e^{-b/\delta}) \end{aligned} \tag{7}$$

The effective thickness, b_e, is obtained by equating this current to the case where the current density is constant (equal to J_o) but the conductor thickness is b_e.

$$I = J_o b_e h = 2\delta h J_o (1 - e^{-b/\delta}) \tag{8}$$

or

$$b_e = 2\delta\,(1 - e^{-b/\delta}) \tag{9}$$

and

$$b_e \approx 2\delta \text{ if } b >> \delta \tag{10}$$

Thus the effective specimen thickness is approximately proportional to the skin depth.

The a-c potential, V, is inversely proportional to the effective thickness, b_e; thus, by Eqs 5 and 10, V is directly proportional to the square root of operating frequency.

$$V \propto \frac{1}{b_e} \propto \frac{1}{\delta} \propto \sqrt{f} \tag{11}$$

To verify the validity of Eq 11, a specimen was connected to the a-c potential system, and readings were taken at ten operating frequencies from 5 to 200 Hz and for seven different crack lengths. The readings were corrected for amplitude attenuation caused by the input (band pass) filters. At each of the crack lengths, the readings were normalized with respect to the reading at 93 Hz. These data were averaged for each frequency and are shown in Fig. 5 as a function of $\sqrt{f}$. A least squares regression equation was determined from the data to be

$$V_a = 0.104\sqrt{f}\,V_{a,93}\,\mathrm{Hz}^{-1/2} \tag{12}$$

The correlation coefficient was 0.999. It should be noted that the behavior at low frequencies would be expected to deviate from the linear behavior and to approach a finite value of $V_a/V_{a,93} = 0.3$ at $f = 0$.

As a further check on the skin effect, the magnetic permeability was calculated from Eqs 5, 11, and 12, and a typical a-c potential of 100 μV for the notch potential of an uncracked specimen. The relative magnetic permeability was calculated to be

$$\mu_r \approx 100 \tag{13}$$

This value is in the range of values typically found for steels [*15*].

Specimen crack length measurements made with a potential system which produces

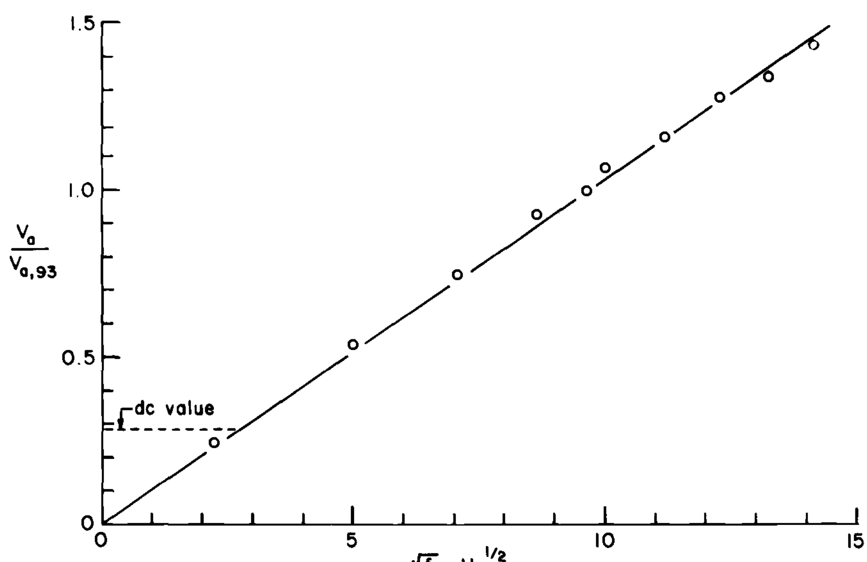

FIG. 5—*Effect of frequency on average a-c potential (normalized to the value at 93 Hz) measured on a 2.25Cr-1Mo steel compact tension specimen.*

a uniform current density in the specimen inherently result in a through-thickness average crack length, since the potential depends on the area of the uncracked ligament. The skin effect increases the sensitivity to surface crack length measurements. If the extent of tunneling is small (as in fatigue crack growth) the influence of skin effect on crack length measurement will be minimal. The use of empirical calibrations of specimens, under conditions of operating frequency and crack front curvature similar to those used in testing, avoids the need for measurement corrections.

References

[1] Steigerwald, E. A. and Hanna, G. L. in *Proceedings.* American Society for Testing and Materials, Vol. 62, 1962, p. 885.

[2] Johnson, H. H., *Materials Research and Standards*, Vol. 5, 1965, p. 442.

[3] Li, Che-Yu and Wei, R. P., *Materials Research and Standards*, Vol. 6, 1966, p. 392.

[4] Wei, R. P., Talda, P. M., and Li, Che-Yu in *Fatigue Crack Propagation, ASTM STP 415*, American Society for Testing and Materials, 1967, p. 460.

[5] Gangloff, R. P. and Wei, R. P., *Metallurgical Transactions, Annual*, Vol. 8A, 1977, p. 1043.

[6] Ritchie, R. O., Garrett, G. G., and Knott, J. F., *International Journal of Fracture Mechanics*, Vol. 7, 1971, p. 462.

[7] Shih, T. T. and Wei, R. P., "A Study of Crack Closure in Fatigue," NASA Cr-2319, National Aeronautics and Space Administration, 1973.

[8] Unangst, K. D., Shih, T. T., and Wei, R. P., *Engineering Fracture Mechanics*, Vol. 9, 1977, p. 725.

[9] Wei, R. P. and Brazill, R. L., "An A-C Potential System for Crack Length Measurement," *The Measurement of Crack Length and Shape During Fracture and Fatigue*, C. J. Beevers et al, Eds., Engineering Materials Advisory Services, Ltd., Chameleon Press, London, 1980, p. 190.

[10] Brazill, R. L., Simmons, G. W., and Wei, R. P., *Journal of Engineering Materials and Technology, Transactions of the American Society of Mechanical Engineers*, Vol. 101, No. 3, 1979, p. 199.

[11] Johnson, W. C., *Transmission Lines and Networks,* McGraw-Hill, New York, 1950, p. 58.

[12] Clark, G. and Knott, J. F., *Journal of the Mechanics and Physics of Solids,* Vol. 23, No. 4/5, 1975, p. 265.

[13] Ritchie, R. O. and Bathe, K. J., *International Journal of Fracture Mechanics*, Vol. 15, No. 1, 1979, p. 47.

[14] Aronson, G. H. and Ritchie, R. O., *Journal of Testing and Evaluation*, Vol. 7, No. 4, 1979, p. 208.

[15] Bolz, R. E. and Tuve, G. L., Eds., *Handbook of Tables for Applied Engineering Science*, CRC Press, Cleveland, 1977, pp. 304-306.

R. P. Gangloff[1]

Quantitative Measurements of the Growth Kinetics of Small Fatigue Cracks in 10Ni Steel

REFERENCE: Gangloff, R. P., "**Quantitative Measurements of the Growth Kinetics of Small Fatigue Cracks in 10Ni Steel,**" *Fatigue Crack Growth Measurement and Data Analysis, ASTM STP 738,* S. J. Hudak, Jr., and R. J. Bucci, Eds., American Society for Testing and Materials, 1981, pp. 120-138.

ABSTRACT: An experimental method, developed to monitor the formation and subcritical propagation of small surface cracks, was evaluated and confirmed by comparisons with conventional "large" crack data. Analytical procedures were developed to produce quantitative crack growth rate—stress-intensity data from measured electrical potential values. Accurate and reproducible results were obtained for surface-defected specimens of 10Ni steel, machined from the heat of material investigated in an ASTM interlaboratory exchange program. Specifically, crack growth rates between 10^{-6} and 10^{-3} mm/cycle were correlated uniquely with the stress-intensity range, independent of crack depth (0.10 to 0.80 mm) and applied stress (30 to 90 percent of σ_{ys}). Data obtained for small surface cracks were in excellent agreement with the growth rate—stress-intensity relationship developed based on conventional tests with compact tension and center crack panel specimens. Accelerated cracking, associated with "short" crack effects, was not observed. The electrical potential monitoring technique for small surface cracks was qualified for investigations of "short" crack effects, and for screening studies requiring timely data acquisition.

KEY WORDS: fatigue (materials), crack propagation, fracture mechanics, steel, defects

The structural integrity of materials may be degraded by the stable (subcritical) growth of cracks, formed from small defects under the influences of sustained or cyclic stresses and embrittling environments [*1-5*].[2] Analyses of this failure mode for life prediction and alloy development are complicated by several unique factors. Total life measurements are difficult to interpret quantitatively because of statistical variations in defect size, location, and

[1]Metallurgist, Corporate Research—Science Laboratory, Exxon Research and Engineering Company, Linden, N.J. 07036; formerly with Corporate Research and Development, General Electric Company, Schenectady, N.Y. 12345.

[2]The italic numbers in brackets refer to the list of references appended to this paper.

geometry [*6*]. For a single defect, uniform crack propagation may be preceded by a portion of life related to crack formation about the blunt flaw, analogous to crack initiation at notches [*7*]. The factors that control the importance of this component are poorly understood. Conventional fracture mechanics methods [*8*] may not adequately describe the propagation of small cracks associated with defects. The growth rates associated with small cracks can exceed those values predicted based on conventional stress intensity—crack growth rate relationships for long-through crack specimens [*9-14*]. The size scale which bounds "small" from "large" crack behavior has not been established unambiguously; however, several estimation techniques have been reported [*15,16*]. In addition to complicating mechanical effects, the growth of small cracks may be influenced by geometry-dependent variations in the chemical environment at the crack tip [*16,17*]. Additional anomalies in crack growth behavior may be encountered owing to unique microstructural interactions with small propagating cracks [*3*]. Finally, the growth of small cracks is often associated with either applied net section plastic strains [*18,19*] or with high stresses near the yield strength of the alloy [*20*]. The crack growth laws which describe such situations are only partially understood.

A technique was recently developed [*21*] to facilitate studies of the influences of metallurgical, mechanical, and environmental variables on the formation and growth of small cracks. Specifically, cracking was monitored continuously by a precision electrical potential technique. Constant direct current was passed through a specimen, and the potential differences associated with points adjacent to an artificial surface defect and subsequent crack were measured. Electrical potential values were transformed to crack depths through an analytical model. The accuracy, resolution, and long-term stability of the electrical potential technique were established experimentally for conditions of importance to elevated temperature, subcritical cracking in nickel-based superalloys [*5,21*].

Crack depth data, obtained as a function of loading time or fatigue cycles for small surface cracks, provide a basis for further analyses of crack growth kinetics. The driving force for cracking may be based on either elastic fracture mechanics or alternate stress or plastic strain parameters [*8,18,19*]. An example of the former analysis is illustrated in Fig. 1. Fatigue crack growth rate—stress intensity range data were obtained from electrical potential monitoring of a small surface crack in A286 stainless steel. Specific test conditions are summarized in this figure. The stress-intensity solution employed for the data analysis was derived by Coles et al [*20*], as discussed in an ensuing section. These data were in excellent agreement with results obtained by James [*22*] for conventional compact tension specimens of A286 steel. While the comparison contained in Fig. 1 suggested that accurate crack growth rate data were obtained for small surface cracks, agreement may have been fortuitous. Different lots of A286 were tested at markedly different loading fre-

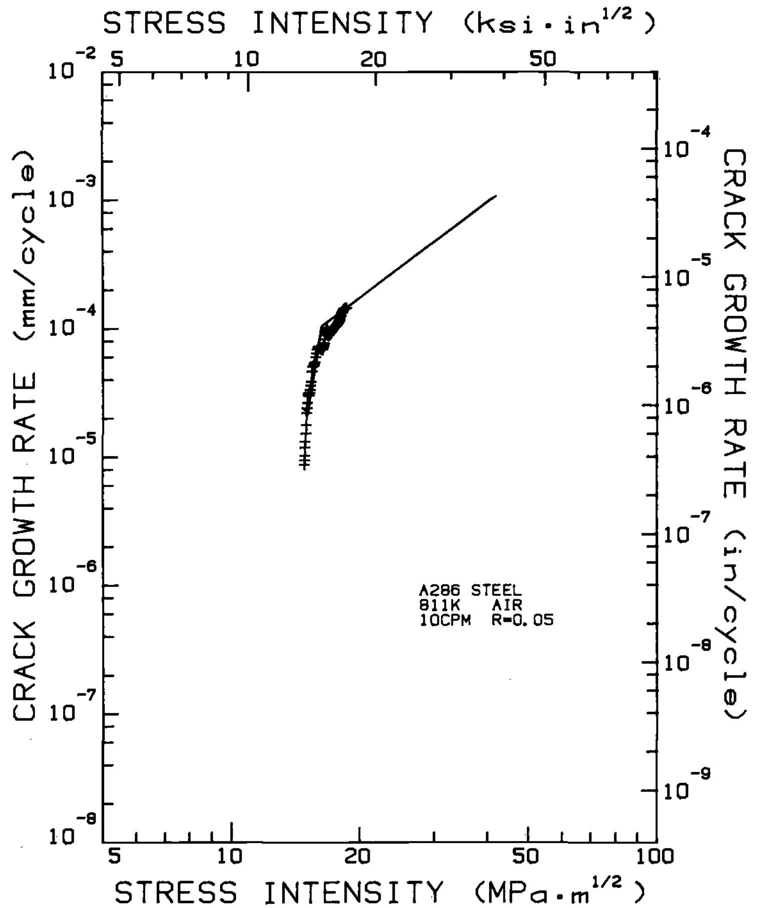

FIG. 1—*Crack growth rate stress-intensity range data based on electrical potential monitoring of a small surface crack, and compared with results reported* [22] *for compact tension specimens. A286 steel, 811 K, 10 cpm,* $\Delta\sigma$ *= 427 MPa,* R *= 0.05.*

quencies. (Elevated temperature environmental effects are operative in A286, and are responsible for a significant frequency sensitivity [*19*].) Additionally, the accuracy of the stress-intensity solution employed for the surface-flawed specimen was not established. Furthermore, the applicability of such a formulation to a "small" crack may be questioned.

The object of the current investigation was to evaluate the accuracy and reproducibility of quantitative crack growth rate—stress-intensity data obtained from electrical potential measurements of small propagating surface cracks. It was reasoned that, if qualified for well-controlled test conditions, the electrical potential-based technique could be applied to more complex problems involving the formation and growth of small cracks.

The growth of fatigue cracks in high-strength 10Ni steel specimens was studied. Extensive data were available, based on conventional compact tension tests of specimens from the same heat of material [*23*]. Additionally, the effect of test environment was minimal for this steel [*23,24*]. Anomalous growth effects related to crack size should have been minimized owing to the high strength of the alloy and the low stress-intensity levels employed [*9*]. Nonetheless, a range of applied stress levels and crack depths were investigated to evaluate the influence of crack size on the growth rate response.

Experimental Procedures

Material and Specimen Geometry

10Ni-8Co-1Mo steel specimens were obtained from the plate investigated in the ASTM sponsored round-robin tests [*25*] and follow-up studies [*23*] directed at the standardization of fatigue crack growth rate testing procedures. The 0.2 percent offset yield strength of this material equalled 1300 MPa. Additional mechanical properties and the processing schedule and chemical composition of the 10Ni steel have been reported elsewhere [*23*].

The round specimen geometry shown in Fig. 2*a* was employed for fatigue testing. Surface defects were introduced along a chord of the specimen cross section at the minimum diameter by electrospark discharge machining. The nominal dimensions of the defect illustrated in Figs. 2*b* and *c* were selected based on the results of a previous study [*21*], and included a_n = 0.10 mm, b = 0.06 mm, c_n = 0.70 mm, and a tip radius less than 0.025 mm.[3] Alumel potential probes (0.12 mm in diameter) were beaded and spot welded into small indentations located at a distance of 0.40 mm (L_p, Fig. 2*b*) above and below the defect tip along the defect center line. Copper current input leads were welded to each sample at the locations shown in Fig. 2*a*.

Mechanical Testing and Electrical Potential Instrumentation

Specimens were loaded cyclically at a frequency of 20 cpm in a closed-loop electrohydraulic test machine. All tests were conducted in moist (laboratory) air at about 300 K. Constant load conditions were employed, and the ratio (R) of the minimun to maximum applied stress equalled 0.10. The alignment of the specimen loading system was monitored periodically with a strain-

[3]For a chord defect in a round cross section

$$a_n = \frac{2R - \sqrt{4R^2 - 2C_n^2}}{2}$$

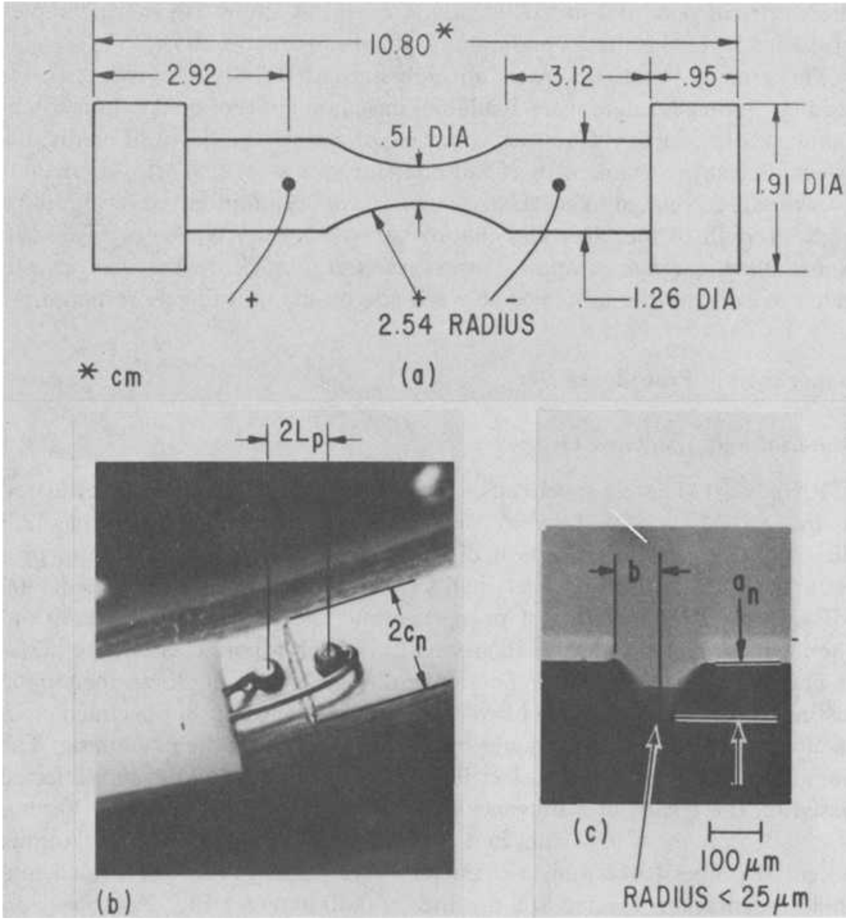

FIG. 2—*Surface defected, electrical potential monitored, specimen geometry:* (a) *schematic,* (b) *macrophotograph, and* (c) *optical comparator image.*

gauged hourglass specimen. For each case examined, less than ±3 percent difference existed between the nominal applied and surface stresses.

Fatigue cracking was monitored by the direct-current electrical potential technique described elsewhere [*21*]. A constant input current of 10.000 ± 0.005 A was employed. The electrical potential associated with the advancing surface crack was measured at the maximum load position of each fatigue cycle, and corrected for the thermal contribution to the total value [*21*]. Resultant electrical potential values were averaged over a block of 100 loading cycles. Block averages (V_T) were normalized by the value obtained for the initial surface defect (V_N). Data acquisition and all calculations were conducted in real time within a PDP-8E minicomputer, and the resultant values were recorded on magnetic tape. Maximum and minimum load values were also acquired on magnetic tape in conjunction with corresponding electrical potentials.

The resolution and long-term stability of the electrical potential measurements were considered [21]. For specimens of 10Ni steel loaded at room temperature, short-term variations in V_T/V_N were less than ± 0.2 percent. For the lead position and defect geometry employed, this uncertainty was equivalent to a crack depth resolution of between 1 and 3μm. Instrumentation was sufficiently stable to permit measurement of crack growth rates above 10^{-6} mm/cycle for low-frequency loading conditions.

Analytical Procedure

A crack depth value (a) was computed for each measured electrical potential (V_T/V_N), based on an analytical calibration procedure described elsewhere [21]. This technique was employed to account for variations in specimen geometry, including the values of L_p, a_n, c_n, and b defined in Fig. 2. For each fatigue experiment, about 100 voltage values were converted to crack depths. The crack depth increment between successive measurements varied between about 4 and 15 μm, as illustrated in an ensuing figure. Crack growth rates were computed for each crack depth value by the seven-point incremental polynomial method [23].

A variety of stress-intensity solutions exist for an elliptical surface flaw in a finite plate subjected to uniform tension [26]. The solution developed by Newman and Raju [26] is plotted in Fig. 3 for the maximum stress intensity at point N. The relationship between surface crack length (c) and crack depth (a) was established empirically for the chord-defected specimen [21]. Surface crack growth initiated after about 0.40 mm of crack penetration. The curvature of the round sample was ignored, and the plate width and length values were assumed to equal the sample diameter. LeFort [27] suggested that, for a circular arc crack in a round bar, the complete elliptical integral of the second kind (ϕ) could be replaced by

$$\Psi = \frac{\pi a}{4}\left(\frac{\text{crack perimeter}}{\text{crack area}}\right) \tag{1}$$

to account for specimen curvature. (Ψ equals Φ exactly for a semi-elliptical surface crack in a flat plate.) LeFort's modification to the Newman-Raju solution is plotted in Fig. 3 for the defected hourglass geometry. Comparisons between the stress-intensity solutions for edge cracks, in rectangular and in round specimens, supported the use of Eq 1 to account for specimen curvature. Specifically, $\Delta K/\Delta\sigma = 0.55\sqrt{\text{mm}}$ for a round specimen ($R = 5.1$

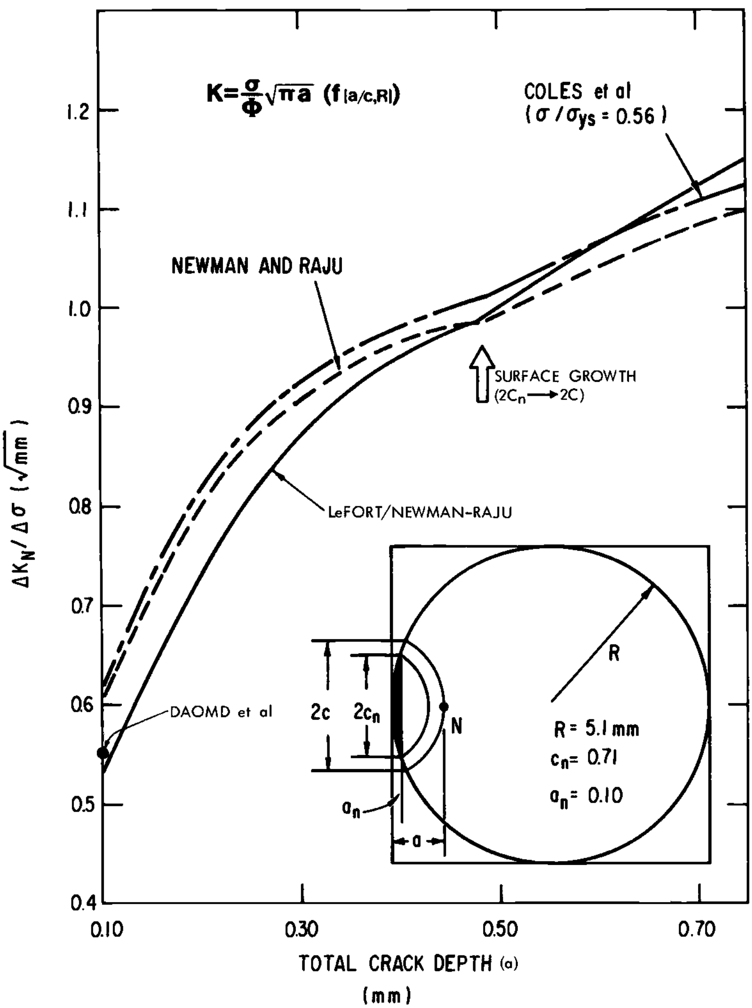

FIG. 3—*Bounding stress-intensity solutions for the chord-defected round specimen.*

mm) containing a 0.10-mm-deep edge crack [*28*]. Coles et al [*20*] employed a stress-intensity solution for the semi-elliptical surface flaw that included an effective crack length plasticity correction (Fig. 3). The three stress-intensity solutions plotted in Fig. 3 agreed within 14 percent or less. The LeFort/Newman-Raju and the Coles et al solutions were employed as bounds to compute the stress-intensity range at point N for each crack depth and growth rate value.

Presentation and Discussion of Results

Fatigue cracking, emanating from surface defects in specimens of 10Ni steel, was monitored continuously by the electrical potential technique. Each experiment was terminated after the crack grew about 0.7 mm (shown to scale in Fig. 3) because of uncertainties in the stress-intensity solutions [*26*]. Additionally, the final fatigue crack depth and surface length values were required as input parameters for crack length and stress-intensity calculations [*21*].

Crack Depth Monitoring

For each fatigue experiment with specimens of 10Ni steel, the crack advanced uniformly from the artificial defect. Surface cracking was limited and well described by an empirical correlation developed for nickel-based superalloys [*21*]. A typical fatigue crack morphology and the associated chord defect are illustrated in Fig. 4. For this specimen, initial cracking was produced by a low applied stress-intensity range, and delineated by a stress range increase from 365 to 985 MPa. The change in fracture surface roughness is evident. This experiment confirmed that near-defect crack growth was uniform, consistent with the results obtained for nickel and iron-based superalloys tested at higher temperatures and faster crack growth rates [*21*]. [Nonuniform, near-defect cracking would be favored at very low (near-threshold) crack growth rates.] The observations illustrated in Fig. 4 suggested that electrical potential values could be analyzed to produce accurate crack depth values, and that the stress-intensity model summarized in Fig. 3 was applicable.

The analytical electrical potential model provided accurate predictions of the final fatigue crack depth for each specimen of 10Ni steel (Table 1). Specifically, the difference between each predicted and optically measured crack depth was less than 13 percent, including the location of the load increase marking shown in Fig. 4. Note that, for an input current of 10 A, the initial electrical potential was about 200 μV for specimens of 10Ni steel containing the 0.10-mm-deep surface defect. Voltage increases of between 50 and 60 percent were observed for 0.7 mm of fatigue crack growth.

Cyclic crack depth data for 10Ni steel are plotted in Fig. 5. The results of five experiments, conducted at constant applied stress levels of between 30 and 85 percent of the yield strength of the steel, are shown. Several descriptive parameters for these tests are included in Table 2. Two features of these data affected the calculations of crack growth rate and stress intensity. Variations were observed in the potential measurements for the 10Ni steel specimens, as reflected by the irregularities in the crack length data contained in Fig. 5. This behavior was pronounced for low growth rate cracking at 20 cpm, and was related to the low values of V_N for 10Ni steel. The long

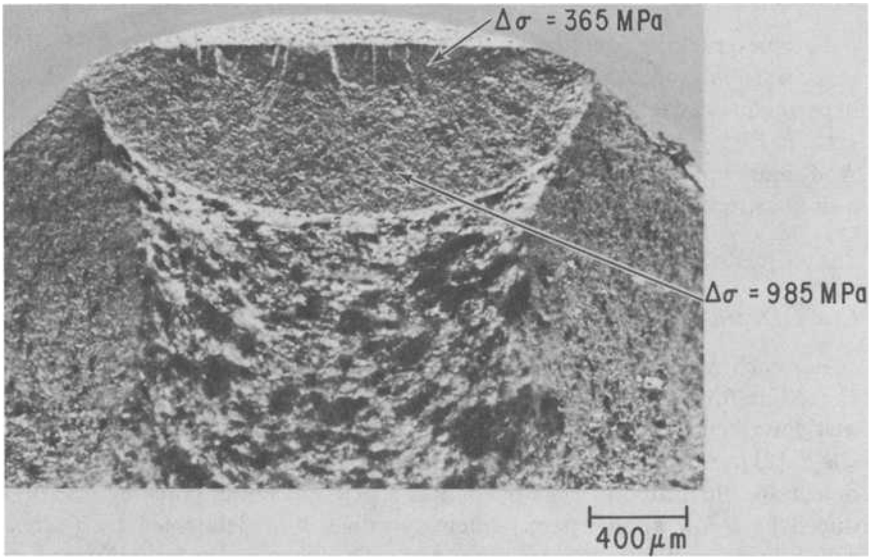

FIG. 4—*Fatigue crack growth in a chord-defected specimen of 10Ni steel. Note the change in fracture surface appearance produced by an increase in the applied stress range from 365 to 985 MPa at* R = *0.10, 297 K, 20 cpm.*

TABLE 1—*Predictions of the analytical electrical potential model.*

Test Number	Potential Increase at Fracture,[b] %	Measured Crack Depth, mm	Predicted Crack Depth, mm	Difference, %
1[a]	1.061	0.272	0.251	−7.7
2	1.495	0.759	0.749	−1.3
3	1.502	0.775	0.833	+7.5
4	1.556	0.719	0.808	+12.4
1[a]	1.562	0.780	0.787	+0.9

[a]Load increase at a = 0.272 mm.
[b]V_N = 200 μV @ 10 A.

term stability of V_T/V_N was reduced compared with that observed for nickel-based alloys [21], and low growth rate measurements were hindered. No attempt was made to improve stability, because of the limited number of steel samples available for testing. Secondly, extended crack formation components, characterized by an initial period of cyclic loading without an increase in potential, were not observed for the stress levels investigated. Cracking commenced immediately upon application of the load. This

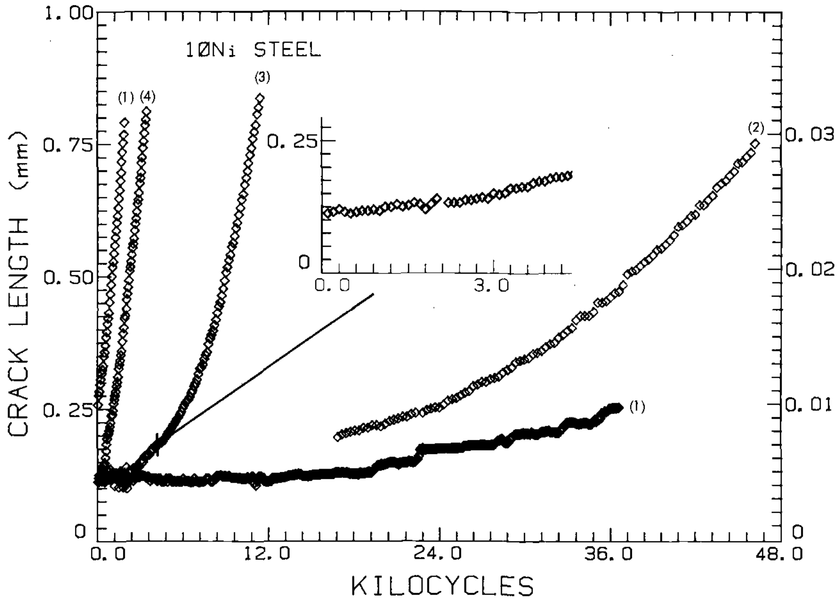

FIG. 5—*Surface crack depth data for defected specimens of 10Ni steel, loaded cyclically at five constant stress levels, 297 K, 20 cpm,* R = *0.10.*

behavior is consistent with that observed for nickel-based superalloys, and is probably related to the extreme sharpness of the artificial surface defects (Fig. 2) [*7,21*].

Crack Growth Kinetics

The cyclic crack depth results shown in Fig. 5 were further analyzed to produce quantitative crack growth rate—stress-intensity data. A unique functional relationship was obtained, independent of crack size and applied stress. Specific results are plotted in Figs. 6 and 7 for stress-intensity values computed based on the Coles et al and LeFort/Newman-Raju solutions, respectively. da/dN (ΔK) data were obtained for cracking adjacent to the surface defect and extending to the point of test termination (Table 2). The very low growth rate data points ($\Delta\sigma$ = 365 MPa) were determined by least-squares regression analyses of the cyclic crack length data contained in Fig. 5. These values were equal to those computed by local (seven-point polynomial) differentiation of crack length data calculated from 1000-cycle, block-averaged V_T/V_N values. Note that crack growth rates on the order of 2×10^{-6} mm/cycle were resolved at a very low test frequency, and in a reasonable time period of about 30 h. Extensive crack growth rate data for

TABLE 2—*Crack growth parameters.*

Test Number	Stress Range, MPa	$\frac{\sigma_{max}}{\sigma_{ys}}$	Defect Depth (a_n), mm	Crack Growth Rate Range, mm/cycle	Crack Depth Range for $da/dn - \Delta K$ $(a_o$ to $a_f)$, mm	$\frac{a_o}{r_y}$ to $\frac{a_f}{r_y}$[a]
1[b]	365	0.31	0.12	7×10^{-7} to 8×10^{-5}	0.12 to 0.25	63 to 68
2	400	0.34	0.11	5×10^{-6} to 3×10^{-5}	0.21 to 0.72	55 to 75
3	655	0.56	0.11	1.5×10^{-5} to 1.5×10^{-4}	0.14 to 0.83	16 to 28
4	923	0.78	0.11	6×10^{-5} to 2.5×10^{-4}	0.12 to 0.81	9 to 14
1[b]	985	0.84	0.12	2×10^{-4} to 4×10^{-4}	0.29 to 0.79	9 to 12

[a] $r_y = \frac{1}{6\pi}\left(\frac{K_{max}}{\sigma_{ys}}\right)^2$.

[b] Load increase at $a = 0.27$ mm.

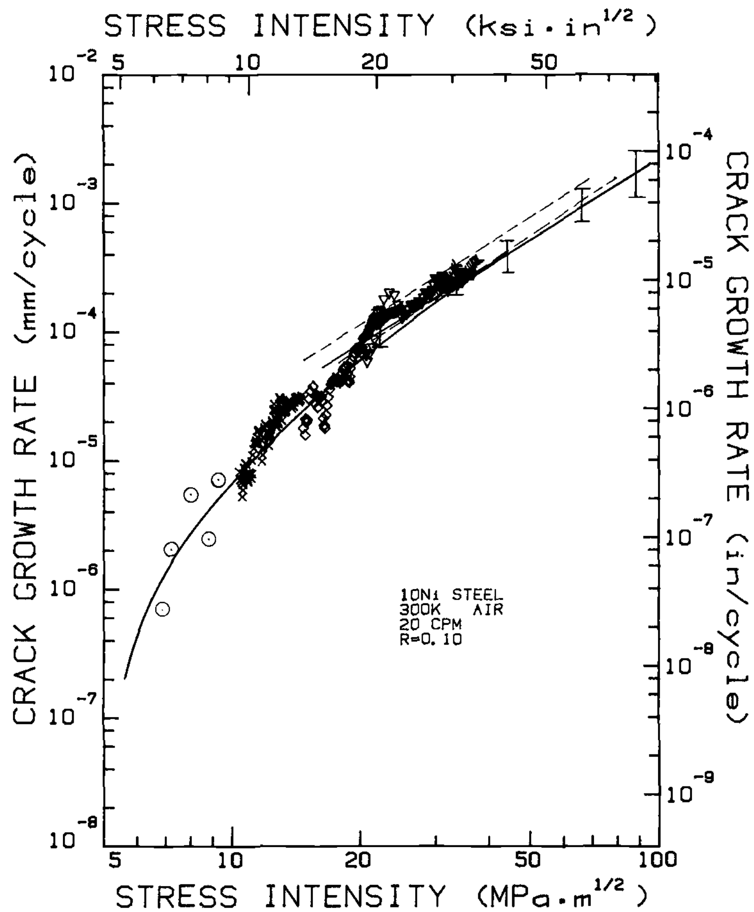

FIG. 6—*Crack growth rate—stress-intensity data established for surface-defected specimens of 10Ni steel, and compared with extensive results obtained by standard test techniques* [23]. *Stress-intensity solution reported by* Coles et al [20].

the same heat of 10Ni steel, obtained through the use of wedge opening load (WOL), compact tension, and center cracked tension samples, are summarized in Figs. 6 and 7. High ΔK-data obtained in fifteen laboratories are represented by a power law relationship, determined through regression analysis of mean growth rates and bounded by one standard deviation [*25*]. Less extensive low growth rate data are also presented [*23*]. All published crack growth rate data for 10Ni-8Co-1Mo steel were obtained at loading frequencies greater than 5 Hz. The dotted lines define a scatter band which includes growth-rate information measured for a similar high strength steel (12Ni-5Cr-3Mo) at test frequencies between 6 and 600 cpm [*24*].

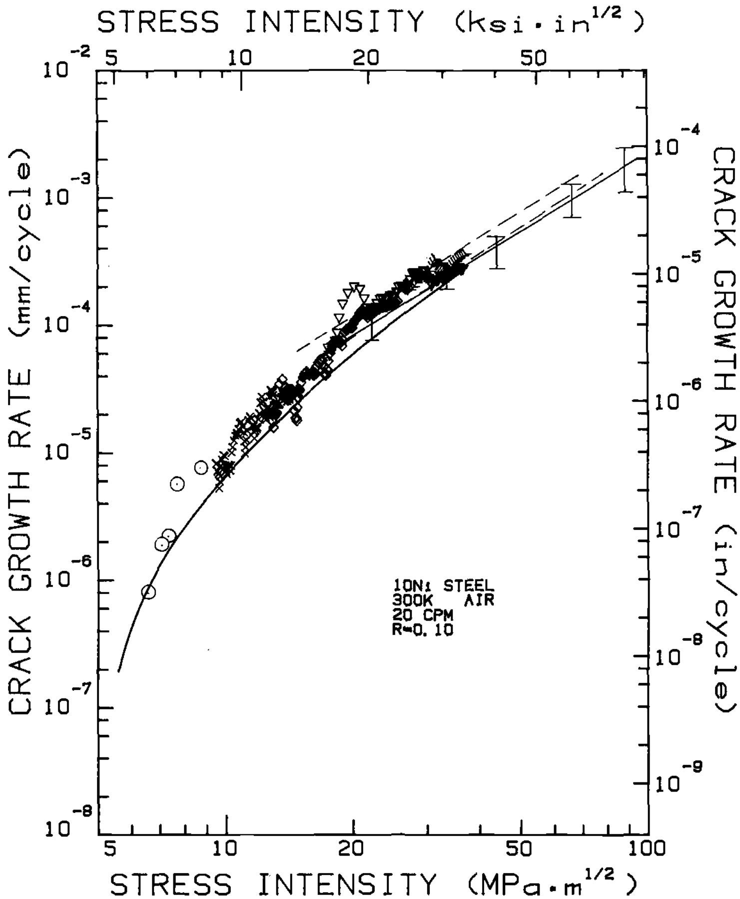

FIG. 7—*Crack growth rate—stress-intensity data established for surface-defected specimens of 10Ni steel, and compared with extensive results obtained by standard test techniques* [23]. *Stress-intensity solution due to Newman and Raju* [26], *modified by LeFort's approach* [27].

Electrical potential monitoring of small surface cracks provides a useful tool for timely evaluations of the influences of environment, material, and loading variables on fatigue defect tolerance, including the critical low growth rate regime of cracking. Quantitative crack growth rate data were obtained in reduced test times compared with conventional techniques. For example, the *da/dN* data contained in Figs. 6 and 7 between the stress intensity values of 12 and 25 MPa $\cdot$ m$^{1/2}$ were obtained for a total crack depth change of 0.6 mm, produced by 10 000 load cycles applied to a single specimen. 300 000 cycles, producing 15 mm of crack growth, would have been required to establish the same range of growth rate data for a WOL specimen loaded under constant stress conditions at an initial a/W ratio of 0.30. For loading at 20 cpm, these tests required 8.3 and (hypothetically) 250 h, respectively. If such data were generated for a loading cycle that included a 1-min tensile hold, then test times of 7 days and 208 days respectively, would have been required.

Accurate and meaningful crack growth rate data were obtained through electrical potential monitoring of small surface cracks. This conclusion was based on an analysis of the data contained in Figs. 1, 6, and 7, with emphasis placed on several critical factors: (*1*) crack length measurement accuracy, (*2*) material variables, (*3*) environmental effects, (*4*) stress-intensity solution accuracy, and (*5*) short-crack effects.

The results summarized in Table 1, when viewed in conjunction with the findings of previous experiments, established the accuracy of the electrical potential monitoring procedure [*21*]. The surface flaw and conventional da/dN (ΔK) data presented in Figs. 6 and 7 were obtained for samples machined from the same plate of 10Ni steel. The effect of material variability was minimized. Furthermore, the comparison between the groups of data presented in Figs. 6 and 7 was not influenced by test environment. While these results were obtained at different loading frequencies in moist laboratory air, Barsom demonstrated that da/dN (ΔK) was not influenced measurably by large variations in test frequency between 6 and 600 cpm for several high-strength steels [*24*]. The specific range is reproduced in Figs. 6 and 7. Hudak et al [*23*] reported that, for the heat of 10Ni steel studied, crack growth rates were *reduced* slightly for tests conducted in moist air at 6 cpm compared with 300 cpm. Frequency was investigated at an R-value of 0.8 to accentuate potential environmental effects; reduced crack growth rates were related to transient effects associated with test interruptions.

Two uncertainties in the stress-intensity solution for the chord-defected specimen could have affected the comparison summarized in Figs. 6 and 7. The stress-intensity factor for a crack growing from a surface notch is generally less than the value associated with a surface crack of equivalent length. Novak and Barsom [*29*] estimated that the effect of the notch was, however, negligible for crack depths greater than

$$0.25\sqrt{a_n \rho} \text{ for } b/a_n < 1.0 \quad (2)$$

where ρ = notch-tip radius. This critical distance equalled 0.01 mm for the specimen geometry investigated (Fig. 2). In general, the data shown in Figs. 6 and 7 were not acquired this close to the defect (Table 2). No evidence was obtained to support anomalously low crack growth rates associated with reduced stress intensities in the vicinity of chord defects. Data obtained for crack depths far from the notch agreed with the results obtained at shorter depths for higher stress tests. Additionally, crack growth rate data obtained within 0.05 mm of the defect tip were disgarded. The remaining data were described by a single relationship between *da/dN* and ΔK, analogous to that observed for the complete data set contained in Figs. 6 and 7.

It was speculated that the small and systematic differences between the surface flaw and large crack data (Figs. 6 and 7) were related to uncertainties in the stress-intensity solution for the surface-defected round specimen geometry. The good agreement observed for the results of the experiments conducted at different stress levels supported the general forms of the empirical aspect ratio formulation and the two stress-intensity solutions. The solution for K proposed by Coles et al [*20*] provided good absolute correlation between surface flaw and conventional data for both 10Ni and A286 steels (Figs. 1, 6, and 7). The slopes of the initial portions of the tests conducted at 400 and 655 MPa (X and ◇, Fig. 6) appeared abnormally steep, probably due to small inaccuracies in the stress-intensity solution. In contrast, smooth transitions between overlapping *da/dN* (ΔK) data sets were observed for results computed based on the LeFort/Newman-Raju stress intensity (Fig. 7). This solution appeared, however, to underestimate ΔK by about 5 to 10 percent for all crack depths. Based on the trends shown in Figs. 6 and 7, the plastic zone correction[4] employed by Coles et al was combined with the LeFort/Newman-Raju solution to produce the results contained in Fig. 8. The agreement between the small surface crack and more conventional growth rate data was excellent.

The growth rate results contained in Figs. 6, 7, and 8 were, in all likelihood, not influenced by anomalous effects associated with very small cracks [*9–16*]. The complete set of data was well described by a single-valued crack growth rate law (for example, Fig. 8) independent of crack size and applied stress. Clark [*9*] obtained results which suggested that subcritical crack growth was characterized uniquely by the stress-intensity factor when the crack length was at least 25 times larger than the crack-tip plastic zone.[5] The lower limit of this parameter was not established. The initial and final crack depth to monotonic plastic zone size ratios for the specimens of 10Ni steel are listed in Table 2. There was no evidence of crack growth rate acceleration or ΔK_{th} reduction (Figs. 6, 7, and 8) for the ranges of a_o/r_y investigated, including values as low as 9. Relationships developed by Usami and Shida [*16*], and El Haddad et al [*15*] were employed to further evaluate the importance of short crack effects for the conditions of the current study. The crack size dependence of the threshold cyclic stress was computed for 10Ni steel based on the former analysis, and compared with the predictions of a conventional

[4] $K = K_{\text{LeFort/Newman-Raju}} \left[1 - \dfrac{\sigma_{\text{applied}}}{\sigma_{\text{yield}}}\right]^{-0.05}$

$= K_{\text{LeFort/Newman-Raju}}\,[1.122]$ for $\sigma_a/\sigma_{ys} > 0.9$

[5] Estimated by the quantity $r_y = \dfrac{1}{6\pi}\left(\dfrac{K_{\max}}{\sigma_{ys}}\right)^2$.

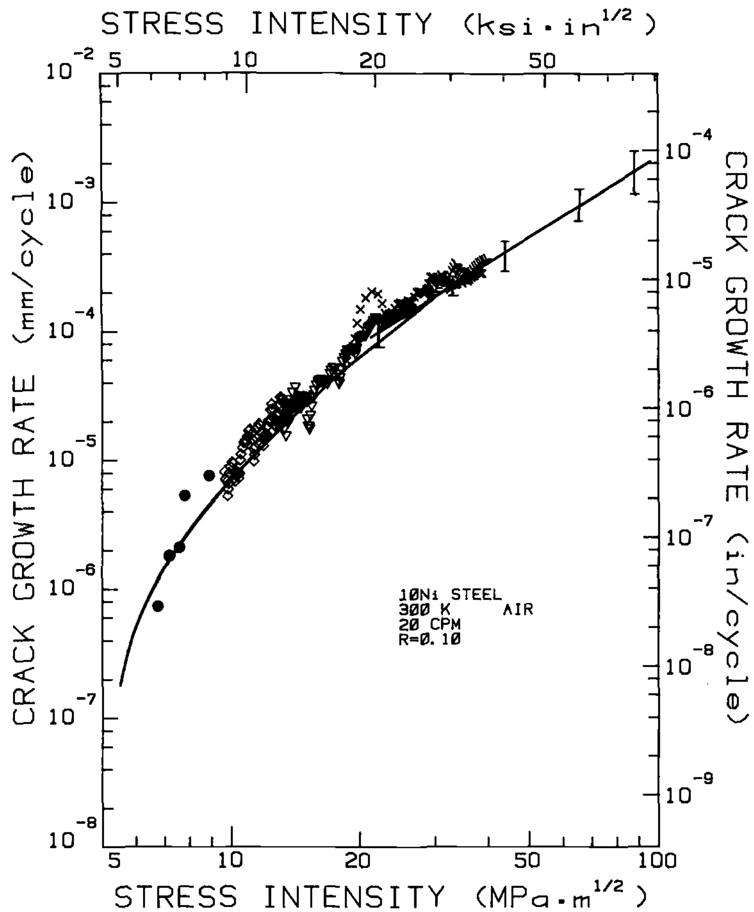

FIG. 8—*Fatigue crack growth rate data from Fig. 7, re-plotted to reflect the influence of a plastic zone size correction.*

fracture mechanics expression in Fig. 9.[6] Deviations in the predictions of the two analyses were only observed for crack depths less than 0.07 mm; a 10 percent difference in threshold stress (or stress intensity) was predicted for a crack depth of 0.02 mm. The surface crack depths employed for fatigue experimentation were significantly larger than the limiting values shown in Fig. 9. Alternatively, El Haddad et al [*15*] suggested that

$$\Delta K = \Delta\sigma\sqrt{\pi(a + \ell_o)} \tag{3}$$

[6]The cyclic yield strength (σ_{yc}) for 10Ni steel equalled 1100 MPa [*30*].

where ℓ_o is a material constant given by

$$\ell_o = \frac{1}{\pi}\left(\frac{\Delta K_{\text{th}}}{\Delta\sigma_e}\right)^2 \tag{4}$$

Equations 3 and 4 resulted in a similar crack size dependence to that suggested by Usami and Shida (Fig. 9). ℓ_o equalled 0.013 mm for 10Ni steel, based on the assumption that the smooth specimen endurance limit ($\Delta\sigma_e$) equalled σ_{yc} [*15*]. The constant length (ℓ_o) was an order of magnitude less than the smallest surface flaw depths employed during the current study. As such, revised stress-intensity values based on Eq 3 were less than 10 percent larger than the values characteristic of the beginning of a typical fatigue experiment ($a_o \geq 0.12$ mm) as plotted in Figs. 6, 7, and 8. The additive effect of ℓ_o (Eq 3) was diminished to less than 2 percent for crack growth increments in excess of a_n (or $a > 0.20$ mm). Based on these comparisons, anomalous "short crack" effects were minimized for the high-strength steel and crack size conditions investigated.

Summary and Conclusions

An electrical potential measurement technique and associated analytical procedures, developed previously to monitor the formation and subcritical

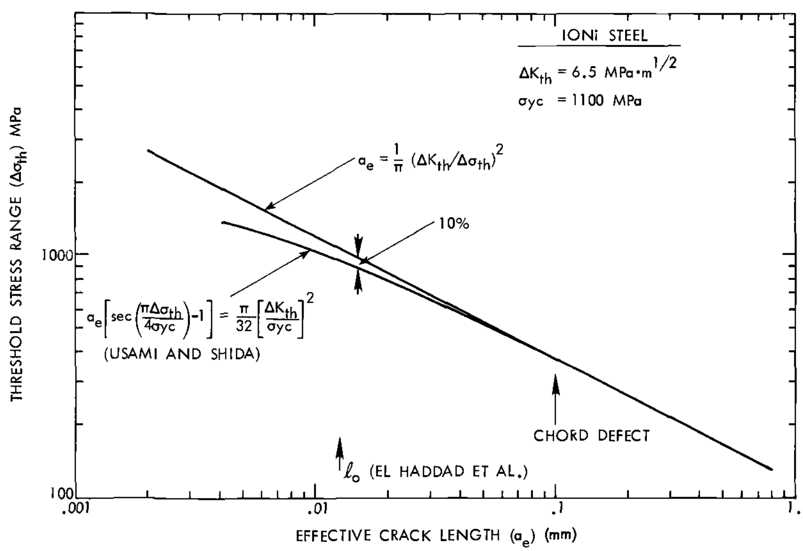

FIG. 9—*Predicted dependence of threshold stress on crack size for 10Ni steel, based on an analysis proposed by Usami and Shida* [16].

growth of small surface cracks, were extended and evaluated. Analyses were developed to compute quantitative crack growth rate—stress-intensity data from crack depth values for nominally elastic, sustained, or cyclic loading conditions.

Fatigue crack growth rate data, obtained for small surface cracks in 10Ni steel, were in excellent agreement with the results of extensive standardized crack growth rate testing of the same plate of material. The growth of small surface cracks was described by a unique da/dN (ΔK) relationship, independent of crack depth between 0.1 and 0.8 mm and applied stress between 0.3 σ_{ys} and 0.9 σ_{ys}. Accelerated growth associated with "short" cracks was not observed, consistent with the predictions of several alternative models.

It was concluded that accurate, quantitative, and reproducible crack growth kinetics were obtained by electrical potential monitoring of small surface cracks. The technique was validated to study the formation and growth of small cracks for a wide range of material, environment, and loading conditions. Results were obtained in significantly reduced test times compared with more conventional methods, facilitating screening-type evaluations of defect tolerance.

Acknowledgments

This investigation was conducted while the author was affiliated with the General Electric Corporate Research and Development Center. W. R. Catlin and R. A. Rosa assisted with the mechanical testing and data analysis procedures. Informative discussions were conducted with M. G. Benz, M. F. Henry, and R. H. Van Stone. 10Ni steel was provided by S. J. Hudak, Jr., affiliated with the Southwest Research Institute. These important contributions are gratefully acknowledged.

References

[1] Eylon, D. and Hyzak, J. M., *Metallurgical Transactions*, Vol. 9A, 1978, pp. 127-129.
[2] Gell, M. and Leverant, G. R. in *Fatigue at Elevated Temperatures, ASTM STP 520*, American Society for Testing and Materials, 1973, pp. 37-67.
[3] Cook, T. S., Lankford, J., and Sheldon, G. P., "Research on Growth of Microcracks in Nickel-Base Superalloys," Technical Report AFML-TR-78-133, Air Force Materials Laboratory, Wright-Patterson Air Force Base, Ohio, 1978.
[4] Jack, A. R. and Paterson, A. N. in *Proceedings*, Institute of Mechanical Engineers Conference on Fatigue, Paper C107/77, 1977, pp. 75-83.
[5] VanStone, R. H. and Gangloff, R. P. in *Proceedings*, 2nd International Conference on Rapid Solidification Processing, Reston, Va., in press.
[6] Baskir, S., Taupin, P., and Antolovich, S. D., *Metallurgical Transactions*, Vol. 10A, 1979, pp. 1481-1490.
[7] Barsom, J. M. and McNicol, R. C. in *Fracture Toughness and Slow-Stable Cracking, ASTM STP 559*, American Society for Testing and Materials, 1974, pp. 183-204.
[8] Collipriest, J. E., Jr. in *The Surface Crack: Physical Problems and Computational Solu-*

tions, J. L. Swedlow, Ed., American Society of Mechanical Engineers, New York, 1972, pp. 43-61.
[9] Clark, W. G., Jr. in *Cracks and Fracture, ASTM STP 601*, American Society for Testing and Materials, 1976, pp. 138-153.
[10] Talug, A. and Reifsnider, K. in *Cyclic Stress-Strain and Plastic Deformation Aspects of Fatigue Crack Growth, ASTM STP 637*, American Society for Testing and Materials, 1977, pp. 81-96.
[11] Pearson, S., *Engineering Fracture Mechanics*, Vol. 7, 1975, pp. 235-247.
[12] Smith, R. A., *International Journal of Fracture Mechanics*, Vol. 13, 1977, pp. 717-720.
[13] Ohuchida, H., Usami, S., and Nishioka, A., *Bulletin of the Japan Society of Mechanical Engineers*, Vol. 18, No. 125, 1975, pp.1185-1193.
[14] Chauhan, P. and Roberts, B. W., *Metallurgist and Materials Technologist*, March 1979, pp. 131-136.
[15] El Haddad, M. H., Smith, K. N., and Topper, T. H., *Journal of Engineering Materials and Technology, Transactions of the American Society of Mechanical Engineers*, Vol. 101, 1979, pp. 42-46.
[16] Usami, S. and Shida, S., *Fatigue of Engineering Materials and Structures*, Vol. 1., 1979, pp. 471-481.
[17] Aikire, R. and Sutari, D., *Journal of the Electrochemical Society*, Vol. 26, 1979, pp. 15-22.
[18] Tomkins, B., Sumner, G., and Wareing, G. in *Proceedings of International Symposium on Low-Cycle Fatigue Strength and Elasto-Plastic Behavior of Materials*, K. T. Rie and E. Haibach, Eds., Deutscher Verbon für Materialprufung E. V., Berlin, 1979, pp. 495-507.
[19] Solomon, H. D. and Coffin, L. F. in *Fatigue at Elevated Temperatures, ASTM STP 520*, American Society for Testing and Materials, 1973, pp. 112-122.
[20] Coles, A., Johnson, R. E., and Popp, H. G., *Journal of Engineering Materials Technology*, Vol. 98, 1976, p. 305.
[21] Gangloff, R. P., "Electrical Potential Monitoring of Fatigue Crack Formation and Growth from Small Defects," Technical Report 79CRD267, General Electric Corporate Research and Development, Schenectady, N. Y., 1979.
[22] James, L. A., "The Effect of Temperature on the Fatigue-Crack Propagation Behavior of A286 Steel," Technical Report HEDL-TME 75-82, Hanford Engineering Development Laboratory, 1976.
[23] Hudak, S. J., Jr., Saxena, A., Bucci, R. J., and Malcolm, R. C., "Development of Standard Methods of Testing and Analyzing Fatigue Crack Growth Rate Data," Technical Report AFML-TR-78-40, Air Force Materials Laboratory, Wright-Patterson Air Force Base, Ohio, 1978.
[24] Barsom, J. M. in *Corrosion Fatigue*, National Association of Corrosion Engineers, Houston, 1972, pp. 424-436.
[25] Clark, W. G., Jr., and Hudak, S. J., Jr., *Journal of Testing and Evaluation*, Vol. 3, 1975, pp. 454-476.
[26] Newman, J. C., Jr., "A Review and Assessment of the Stress-Intensity Factors for Surface Cracks," NASA Technical Memorandum 78805, National Aeronautics and Space Administration, Langley Research Center, Hampton, Va., 1978.
[27] LeFort, P. C., private communication, 1979.
[28] Daomd, O. E. K., Cartwright, D. J., and Carney, M., *Journal of Strain Analysis*, Vol. 13, 1978, pp. 83-89.
[29] Novak, S. R. and Barsom, J. M. in *Cracks and Fracture, ASTM STP 601*, American Society for Testing and Materials, 1976, pp. 409-447.
[30] Saxena, A. and Hudak, S. J., Jr., in *Fracture Mechanics, ASTM STP 677*, American Society for Testing and Materials, 1979, pp. 215-232.

H. Nakajima,[1] *T. Shoji,*[2] *M. Kikuchi,*[2] *H. Niitsuma,*[3]
and M. Shindo[1]

Detecting Acoustic Emission During Cyclic Crack Growth in Simulated BWR Environment

REFERENCE: Nakajima, H., Shoji, T., Kikuchi, M., Niitsuma, H., and Shindo, M., **"Detecting Acoustic Emission During Cyclic Crack Growth in Simulated BWR Environment,"** *Fatigue Crack Growth Measurement and Data Analysis, ASTM STP 738,* S. J. Hudak, Jr., and R. J. Bucci, Eds., American Society for Testing and Materials, 1981, pp. 139–160.

ABSTRACT: An attempt is made to detect and analyze acoustic emissions from cyclic crack growth in SA 533 Grade B steel in the simulated boiling-water reactor (BWR) water environment. Significant levels of signals caused by the environment-enhanced crack growth were obtained through appropriate noise reduction techniques. By reducing the frictional noises between the loading pins and the specimen, and by characterizing the spectrum of signals emitted from various sources, discrete signal identification was made possible. From an empirical relationship between the energy of emission and the crack growth rate, the possibility of utilizing this type of acoustic emission technique was discussed in relation to future continuous monitoring of operating nuclear plants.

KEY WORDS: acoustic emission, spectrum analysis, crack growth monitoring, SA 533 Grade B steel, corrosion fatigue, simulated BWR environment

The acoustic emission technique is considered one of the potential tools among a number of nondestructive testing methods for the monitoring of structural integrity of a plant under operating conditions. As typically recognized, it is desirable to continuously monitor the nuclear reactor pressure vessel for crack extension during operation. For this reason, the acoustic emission (AE) technique has been a subject of extensive laboratory

[1]Materials Engineering Laboratory, Division of Nuclear Fuel Research, Japan Atomic Energy Research Institute, Tokai-mura, Ibaraki-ken, Japan.
[2]Department of Engineering Science, Faculty of Engineering, Tohoku University, Sendai, Japan.
[3]Department of Electrical Engineering, Faculty of Engineering, Tohoku University, Sendai, Japan.

studies in the fields of plastic deformation, fatigue, and fracture in pressure vessel steels during the past ten years.

In the literature, however, it is noted that there are limited investigations focused on the detection of acoustic emission from the crack growth in high temperature and pressure aqueous environments, despite the fact that most probable situations are expected in such cases [*1,2*].[4] Some preliminary trials in a model vessel have also been made [*3*].

The probable technical barriers are the difficulties in performing tests under well-defined simulated conditions, and also in eliminating extraneous background noise and the confirmation of true acoustic emission signals, as is the case in most acoustic emission studies.

It has been suspected that the acoustic emission technique might be of limited utility in detecting the stable crack growth which occurs due to fatigue, but might have a greater probability of success in detecting gross cracking of large extents present in the later stages of the structural damaging process [*4*]. On the other hand, it could be pointed out that most data bases in this concern have been confirmed in the crack growth in air or noncorrosive environments.

The fatigue crack growth of the low alloy steels was found to be accelerated substantially in a high-temperature water environment when the loading frequency was low (typically below 10 cpm) [*5–7*]. Since the factor of acceleration can be as high as 10 [*8*], there is an expectation of obtaining sufficient signal levels from the fatigue crack growth process, when more realistic simulation of the practical conditions is made in terms both of the test environments and the loading conditions.

The purpose of this investigation is to explore the capability of the acoustic emission monitoring to detect cyclic crack extension in tests with a simulated boiling-water reactor (BWR) environment.

Experimental

The fatigue tests were performed with a ±10-ton electrohydraulic fatigue testing machine integrated with a high temperature and pressure recirculating autoclave system so that the water chemistry was maintained to simulate the BWR service water environment. Entire parts of the water-circulating system were made of Type 304 stainless steel so that the chemical condition of the water was similar to that expected in a BWR primary coolant. The chemical condition of the water was continuously monitored by electrical conductivity and oxygen meters at the exit of the test section. The details of the apparatus construction and specifications have been reported elsewhere [*5*].

The material used in this investigation was SA 533 Grade B steel extracted

[4]The italic numbers in brackets refer to the list of references appended to this paper.

from typically 165-mm-thick plate. In order to cross-check the obtained results, some of the specimens were heat-treated to develop different microstructures without changing the chemical composition from the original condition. The material so treated was expected to respond to the environment differently [9]. Of the two types of microstructure employed, one was the standard condition (that is, original tempered bainite), and the other was martensite obtained by oil quenching the block of material before machining. Chemical compositions, thermal histories, and mechanical properties are given in Table 1.

The geometry of the specimens used in the present study is given in Fig. 1. The specimen design aims at keeping a constant stress intensity factor range (ΔK) under a given constant load amplitude during crack growth. Testing under such a constant condition provides the statistical accuracy of the measurements on both crack growth and acoustic emission relative to the standard C-T specimens. The reproducibility of the equivalent stress cycles ensured by the use of this type of specimen is also expected to favor the analysis of the obtained acoustic emission signals.

The stress intensity factor (K) for this specimen can be calculated by the following equation [10]

$$K = \sqrt{\frac{4P^2 \times \alpha}{Bn \times B}} \tag{1}$$

where

K = stress intensity factor, MPa$\sqrt{\text{m}}$,
P = applied load, MN,
B = overall specimen thickness, m,
Bn = specimen thickness measured between roots of side grooves, m, and
$\alpha = 3.13 \times 10^2$, 1/m.

Prior to testing in water, the specimens were given cyclic loadings for the purpose of prefatigue cracking. The length of the precrack in each specimen was about 5 mm. The load cycles at which the precracking operations were made were kept below the levels that gave ΔK of 25 MPa$\sqrt{\text{m}}$. Fatigue test conditions conducted are summarized in Table 2. At each test, crack growth rates in air were measured by monitoring crack extension, before and after the tests in water, which gave better information bases to compare the results for different environments in the same single specimen.

After each set of tests, the fracture surfaces were examined to verify the crack extension during given load conditions. No tendency of crack tunneling was observed on the fracture surface of whole specimens.

The crack extension length in each loading condition was between 1.5 and 2.0 mm, which gave sufficient accuracy to obtain the crack growth rate in the

TABLE 1—*Chemical composition, heat treatment, and room temperature mechanical properties of specimen materials.*

Specimen No.	Chemical Composition (w/o)												
	C	Si	Mn	P	S	Ni	Cr	Mo	Cu	V	Sb	As	Sn
A-1	0.19	0.25	1.28	0.009	0.013	0.61	0.04	0.55	0.13	0.004	...	...	...
B-1	0.17	0.02	1.48	0.011	0.006	0.58	0.16	0.52	0.13	0.003	0.0041	0.015	0.008
B-2	0.17	0.02	1.48	0.011	0.006	0.58	0.16	0.52	0.13	0.003	0.0041	0.015	0.008

Specimen No.	Heat Treatment	Tension			
		Yield Strength, MPa	Ultimate Tensile Strength, MPa	Total Elongation, %	Reduction of Area, %
A-1	899°C × 8 h W.Q. → 671°C A.C. → 566°C × 2 h → 621°C × 50 h	452	597	27.2	65.8
B-1	890°C × 3.5 h A.C. → 660°C × 3.5 h F.C. → 600°C × 40.5 h F.C.	480	610	27.0	69.2
B-2	1000°C × 30 min O.Q.	1003	1128	19.3	73.0

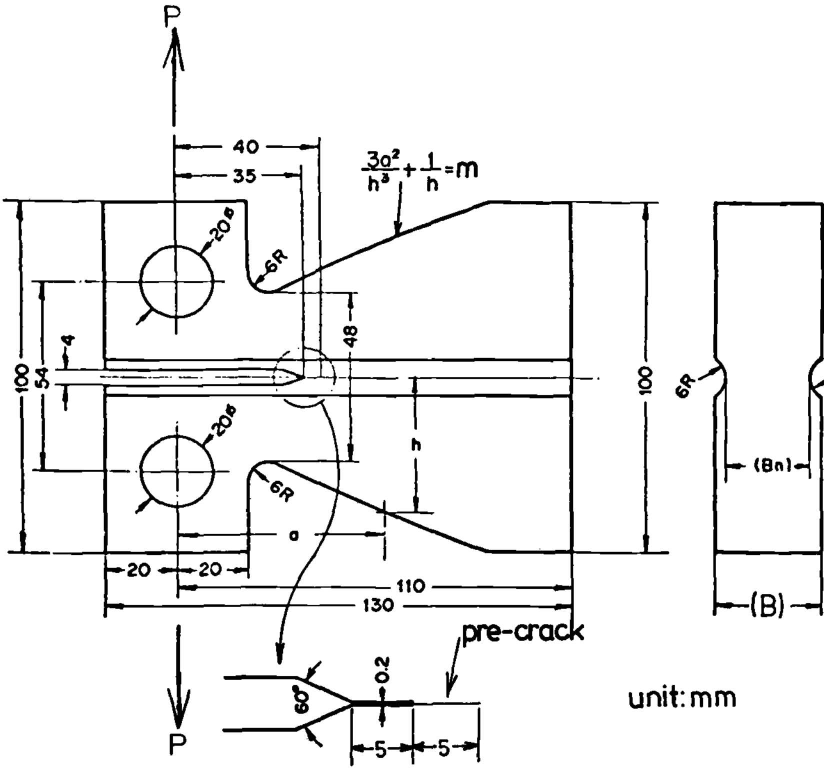

FIG. 1—*Geometry of tapered double-cantilever beam-type specimen.*

form of $\Delta a/\Delta N$. The fatigue crack growth rate was measured using two independent techniques: (*1*) compliance measurements by means of a linear variable differential transformer (LVDT) attached to the specimen shoulder, and (*2*) beach-mark observations on the fracture surfaces. In the tests with the stress intensity factor range below 46.5 $\text{MPa}\sqrt{\text{m}}$, the length of crack growth measured by the two different techniques agreed within an error of ± 0.04 mm. However, the length measured by the compliance technique was known to be somewhat less than the growth length measured by the beach-mark technique in the tests with the stress intensity factor range above 46.5 $\text{MPa}\sqrt{\text{m}}$.

The compliance technique was therefore used only to monitor qualitatively the linearity between the crack growth length and the number of loading cycles under the latter conditions. The final crack growth rates were based on the total crack extension divided by the number of cycles ($\Delta a/\Delta N$) which produced that increment in each load condition. The results of

TABLE 2—*Summary of specimen preparation and test conditions for high-temperature water environment.*

	Specimen			Fatigue Test			Demineralized Pure Water			
	Thickness		Orientation,							
Specimen No.	B, mm	Bn, mm	ASTM E 399	Ratio, P_{min}/P_{max}	Wave Form	Frequency, H_z	Temperature, °C	Pressure, MPa	Dissolved Oxygen, ppm	Conductivity, $\mu \cdot mho \cdot cm^{-1}$
A-1	25	21	T-L	0.2	Sine					
B-1	30	24	L-S	0.1	Triangular	1/60	288	8.2	< 0.2	> 1
B-2	30	24	L-S	0.1	Triangular					

measurements made in this manner were basically from the average of the large number of equivalent events, since the crack growth was a linear function of the number of cycles. The preliminary reproducibility tests in air on the stress intensity factor range versus *da/dN* relation with four independent specimens gave a correlation coefficient of 0.996, which is substantially high compared with the generally expected value in the incremental polynomial tests of the standard C-T specimens.

Figures 2 and 3 show block diagrams of the systems of acoustic emission detection and signal processing, respectively, used in the present study.

Figure 4 shows a typical experimental setup specific to the acoustic emission detection for high temperature and pressure tests. A piezoelectric transducer with a resonant frequency of 1 MHz was located outside the test vessel and connected through a stainless steel waveguide (4 mm diameter by 750 mm long) welded directly to the end surface of the specimen.

Considering the effect of waveguide on the attenuation of the acoustic emission signal emitted during cyclic crack growth, the waveguide condition was carefully reproduced in each test. Such adjustment of the setup allowed direct comparison between signals obtained from different specimens.

At first, the signals emitted during the load cycling were transmitted through the waveguide and were converted to electrical signals by a piezoelectric transducer located at the other end of the waveguide. These electrical signals were inputted to the signal processing system with a frequency band of 2 kHz to 1 MHz (Fig. 2). The level histograms of the signal peak values were printed out at intervals of 2 sec during the tests. At the same time, the signals were recorded by a VTR-type magnetic tape data recorder with a frequency range of 100 Hz to 1 MHz. After the test, the recorded signals were inputted to an energy detector through a band pass filter that had a variable cut-off frequency.

On the other hand, the waveform and frequency spectrum of the signals were analyzed by means of an oscilloscope and a spectrum analyzer, respectively (Fig. 3).

Results and Discussion

Crack Growth Rate

The crack growth data obtained under constant load amplitude in ambient air showed a linear dependence of crack length and load cycles (Fig. 5). This suggested that the expected constant ΔK condition was valid.

Figure 6 shows experimentally determined ΔK versus crack growth rate (*da/dN*) relationships in ambient air and BWR water environments. Kondo et al [5] have shown that the crack growth rate of tempered bainite microstructure is accelerated in high-temperature water; the same degree of

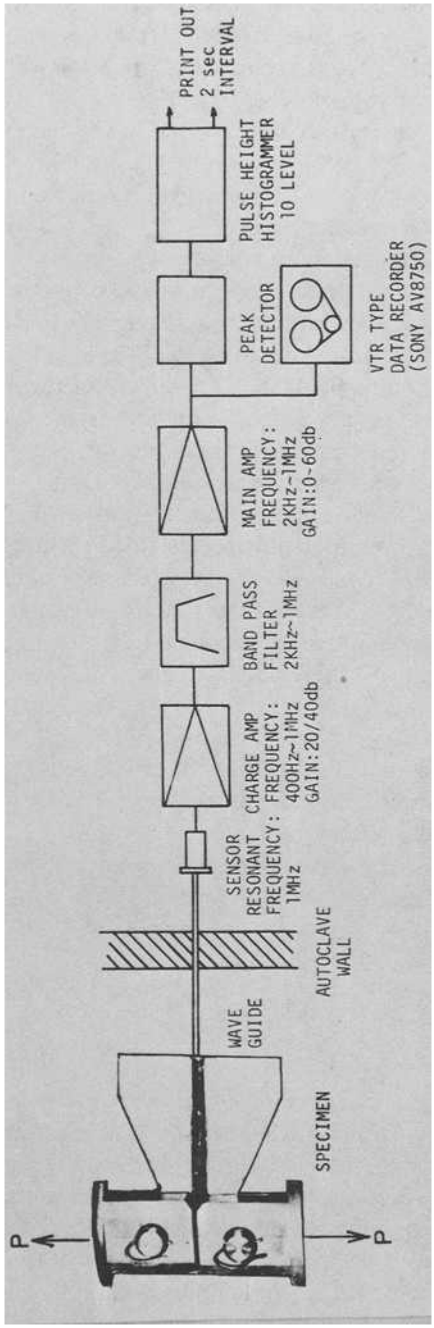

FIG. 2—*Block diagram of wide-band acoustic-emission measurement system.*

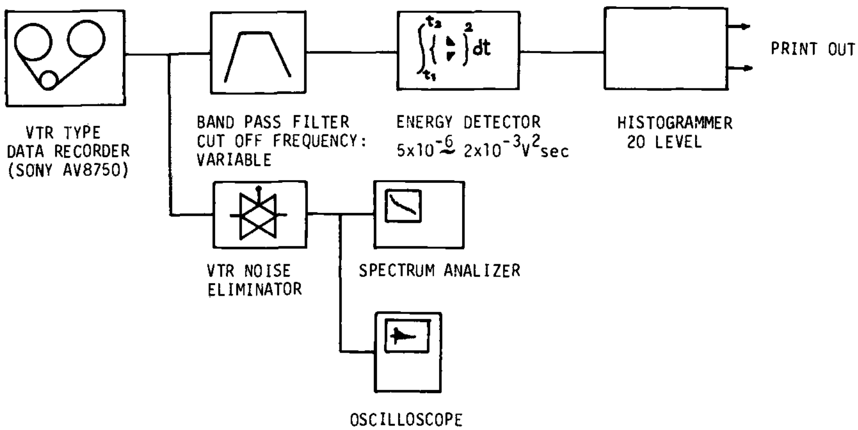

FIG. 3—*Block diagram of data processing.*

environment-enhanced crack growth is also observed in the present study. The generally recognized log-linear relationship between ΔK versus da/dN was confirmed in both the air and water environments within the range of the present tests.

$$da/dN = C_1(\Delta K)^{n_1} \tag{2}$$

where C_1 and n_1 are material constant and exponent, respectively. The values obtained empirically in both the air and high-temperature water environments are summarized in Table 3.

The fatigue crack growth rate of Specimen A-1 is larger than that of Specimen B-1 at the stress intensity factor range of 35.5 MPa$\sqrt{m}$ in the high-temperature water environment, both of which were with the typical tempered bainite microstructure. The difference would have originated from possible variability in the test conditions (such as the stress waveform, the R-ratio, and the specimen orientation).

On the other hand, the apparent difference in the crack growth rates between the two heats of base metals obtained with the stress intensity factor range above 38 MPa$\sqrt{m}$ was small irrespective of the different secondary test conditions mentioned previously.

As concerns the microstructure produced by heating and quenching to obtain a full martensite structure (Specimen B-2), the magnitude of the environmental enhancement in crack growth rate was less than that noted for the tempered bainite microstructure (Specimen B-1), with no environmental enhancement at all noted above a ΔK of 62 MPa$\sqrt{m}$.

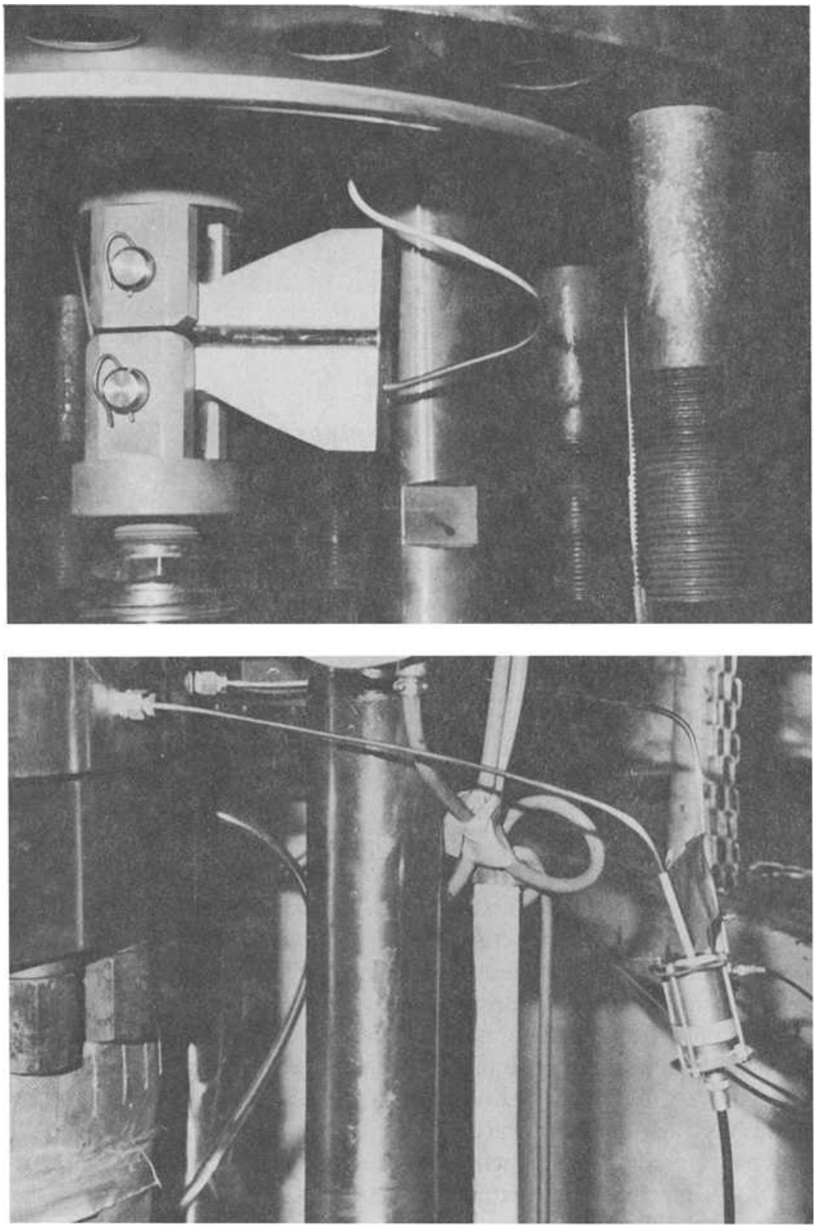

FIG. 4—*Experimental setup for signal detection.*

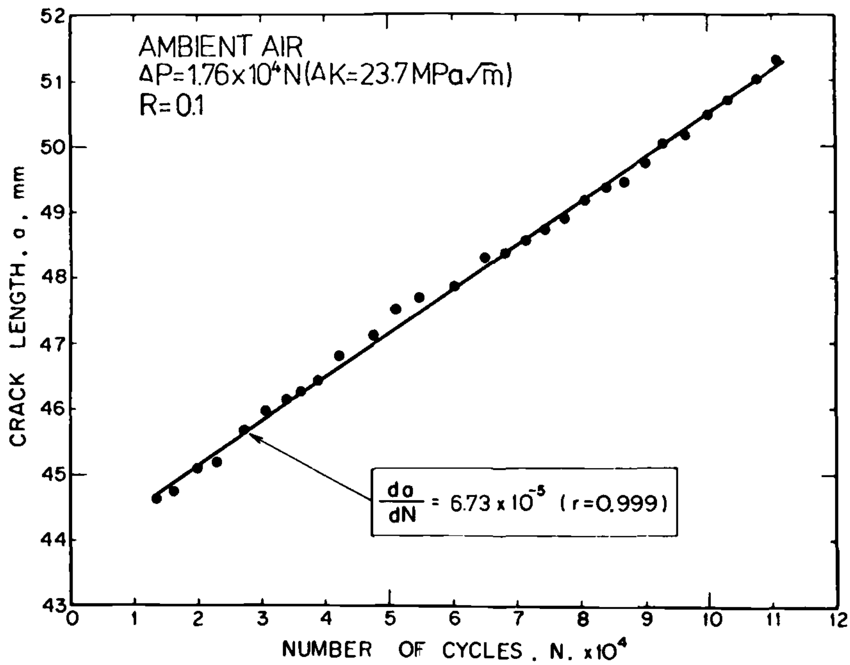

FIG. 5—*Typical crack growth curve obtained in ambient air for CDCB specimen.*

False Signals and Their Separation

A large number of intensive acoustic emission (AE) signals were detected in the high temperature and pressure aqueous environment during load cycles even below the ΔK of 30 MPa$\sqrt{m}$ at the detection sensitivity of 20 dB and above. Furthermore, considerable levels of audible sounds were also emitted during periods of increasing load. Figure 7 shows the typical intensive signal pattern and its spectrum characteristics for the latter case. Most of these waves were the signals with frequencies below 500 kHz. The log-log plots of da/dN versus wave energies per unit specimen thickness per loading cycles of signals ($d\Sigma \mathrm{E_{AE}}/\mathrm{mm}/dN$) obtained in the early analyses are shown in Fig. 8. The apparent correlations between the two quantities looked encouraging. They were interpreted as if showing the relation

$$da/dN = C_2 (d\Sigma \mathrm{E_{AE}}/\mathrm{mm}/dN)^{n_2} \tag{3}$$

where C_2 and n_2 are material constant and exponent, respectively.

The feasibility of the results was doubtful at the moment when no exact source mechanism survey had been made. However, through a few critical

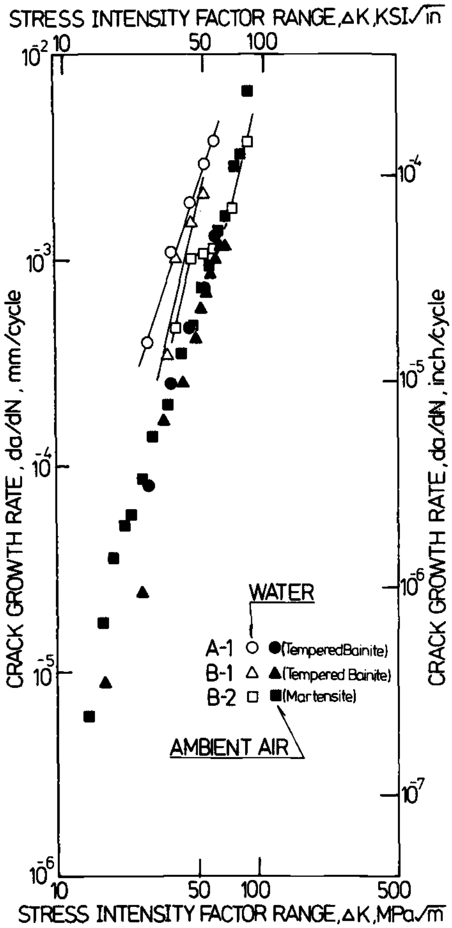

FIG. 6—*Results of fatigue crack growth rate in ambient air and simulated BWR environments.*

TABLE 3—*Values of* C_l *and* n_l *determined experimentally in Eq 2.*[a]

	In Air		In Water	
Specimen No.	C_1	n_1	C_1	n_1
A-1	1.41×10^{-9}	3.31	2.48×10^{-8}	2.90
B-1	1.16×10^{-10}	3.84	1.11×10^{-10}	4.23
B-2	2.22×10^{-9}	3.19	...	...

[a]*da/dN*, mm/cycle; ΔK, MPa$\sqrt{m}$.

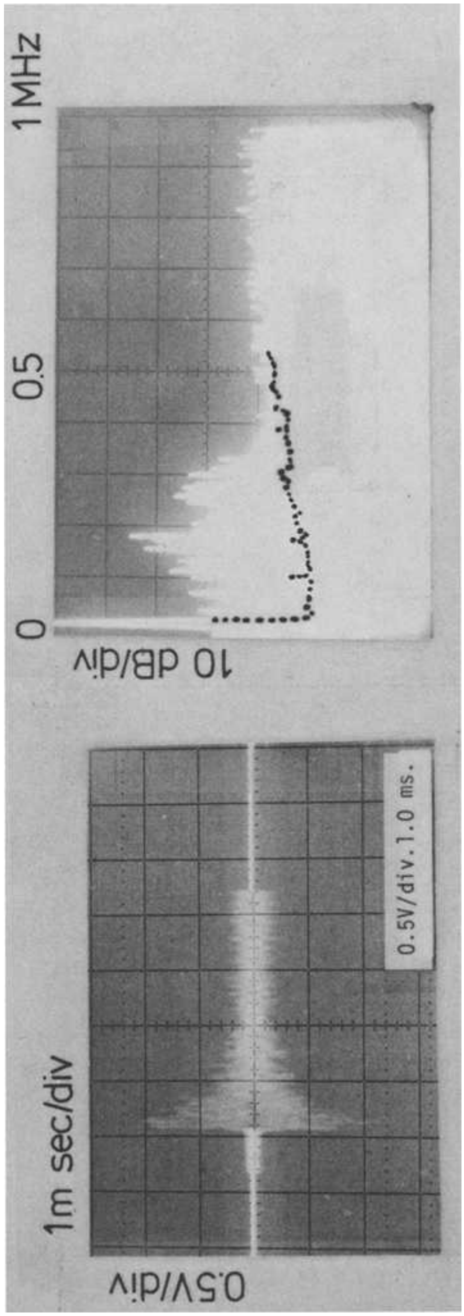

FIG. 7—*Typical waveform and its frequency spectrum of false signal originated from friction between loading pins and specimen. (The dotted curve is the noise level.)*

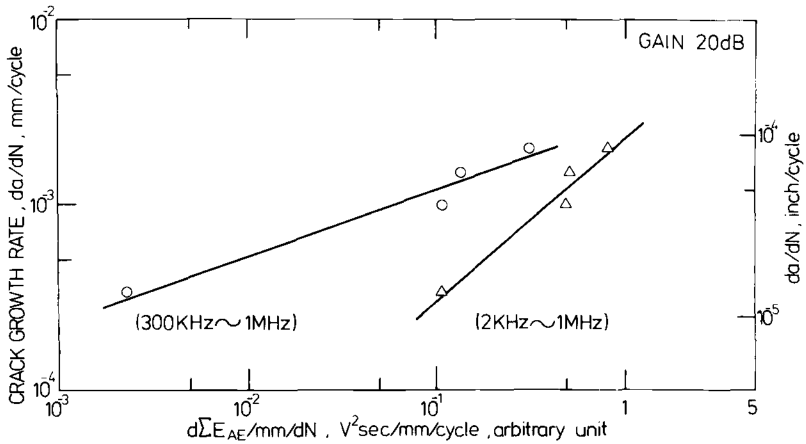

FIG. 8—*Apparent relationship between crack growth rate versus energy of false signal.*

tests using specimens with cracks blunted intentionally with a drill hole, the sources of the most detectable levels were determined to have originated in the friction between the loading pins and the specimen. The phenomenon was tricky because the sounds were emitted only in the high-temperature water; also, the use of the constant ΔK-type specimens was the essential basis of obtaining the apparent correlation line in Fig. 8 because of the simplicity among the factors (including ΔK, da/dN, load, and, perhaps, the energy expenditure due to friction).

At the next trial, loading pins coated with Teflon were provided for reducing the frictional noise between the loading pins and the blunted specimen. Through the latter trials with such a setup, no intensive signals were detected during loading cycles in high-temperature water over a wide range of loading levels. Only signals that were considered as background noise were revealed at the detection sensitivity of 70 dB (Fig. 9). The spectra of background noises were signals with frequencies below 500 kHz. They corresponded to hydraulic noises reported by other investigators [*2*].

Through these trials it was discovered that coating the contact surfaces (such as in the loading pins and the specimen with the Teflon layer) could reduce the frictional noise by about three orders of magnitude. The reduction enabled the detection sensitivity to increase up to 70 dB, which was equivalent to that employed for the detection in ambient air environments where no meaningful signal was detected at this high-detection sensitivity.

These results confirmed the inessential nature of the initially obtained signals.

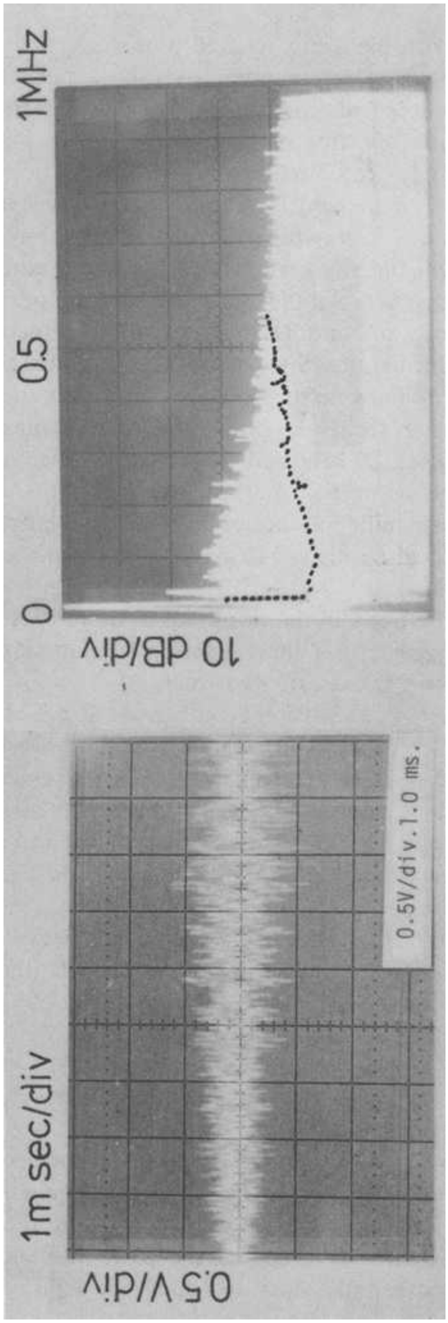

FIG. 9—*Typical waveform and its frequency spectrum of signal obtained through appropriate noise reduction techniques. (The dotted curve is the noise level.)*

True Acoustic Emission Signals Due to Cyclic Crack Growth in Water

Crack growth tests with the Teflon-coated pins were conducted. In these tests two parallel output signals were monitored. In such a setup, substantial signals, discretely separable from the background noise, were obtained from the specimens with cracks growing in water environment.

Figure 10 shows the typical burst-type wave pattern and its spectrum characteristics, which can be addressed with particular reference to the environment-enhanced crack growth in the BWR water environment. The signals were detected during the periods of rising load, and most of them were detected at the stage between 0.8 peak load and the peak load.

Figure 11 shows the da/dN and $d\Sigma\,\mathrm{E_{AE}}/\mathrm{mm}/dN$ as functions of ΔK for as-received material with bainite (Specimen A-1). Both lines show a similar linear trend. In Fig. 12 the same relations are shown for the material with martensite. In both figures the $d\Sigma\,\mathrm{E_{AE}}/\mathrm{mm}/dN$ were obtained as those with a frequency range between 20 kHz and 1 MHz, since the energy of signals with a frequency range between 2 and 20 kHz involved the noise due to machine vibration, waveguide resonance, etc. In the latter material the acoustic emission results also followed closely the observed nonlinear relation between ΔK and da/dN.

The coincidence of the trend in the two kinds of quantities in terms of the dependence on ΔK suggests that the acoustic emission signals monitored reflected the crack growth at least qualitatively.

In Fig. 12 the high acoustic emission activity peak at ΔK of 46.5 MPa$\sqrt{\mathrm{m}}$ seems not to follow the crack growth characteristics. However, this increased level of acoustic emission could be recognized to be reasonable by the fracture surface examination; namely, the high acoustic emission activity corresponds to the two large lamellar tearings on the fracture surface. These lamellar tearings might produce the additional acoustic signals caused by rubbing the crack surface.

Figure 13 confirms the resultant linear relationship between the $d\Sigma\,\mathrm{E_{AE}}/\mathrm{mm}/dN$ and da/dN on a log-log scale. From these results, the following empirical relationship was obtained

$$da/dN = C_3(d\Sigma\,\mathrm{E_{AE}}/\mathrm{mm}/dN)^{n_3} \tag{4}$$

where C_3 and n_3 are 1.48×10^{-3} and 0.21, respectively, when da/dN is in mm/cycle and $d\Sigma\mathrm{E_{AE}}$ is in $\mathrm{V^2}$ sec.

The results shown in Fig. 13 indicate that a crack advance event of $\sim 10^{-3}$ mm in one cycle may be accompanied by an acoustic emission event whose integrated energy can vary by about two orders of magnitude. This is partly because of the steepness of the slope in the plot, and suggests that the measured energy is a potentially sensitive means for determining the crack growth rate.

Practically, this scatter is allowable for making a reasonable estimation of

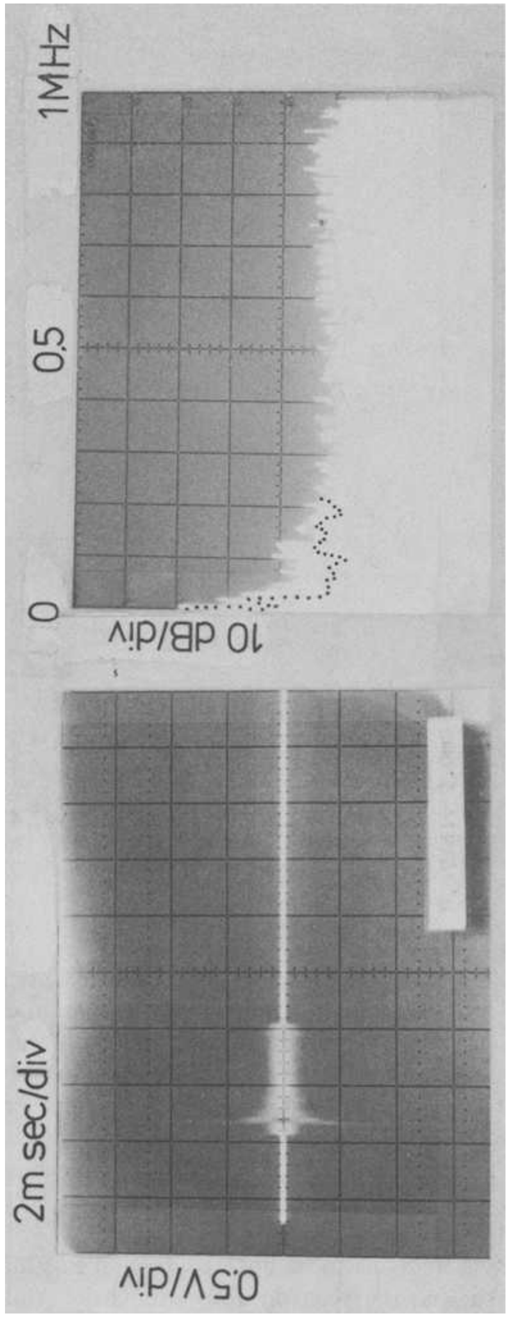

FIG. 10—*Burst-type waveform and its frequency spectrum of signal with particular reference to the environment-enhanced crack growth in high-temperature water. (The dotted curve is the noise level.)*

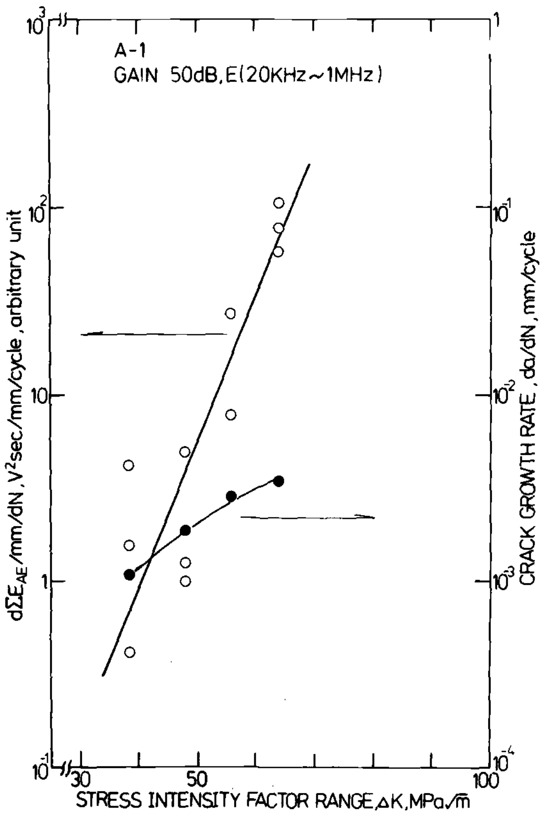

FIG. 11—*Dependence of crack growth rate and wave energy as functions of stress intensity factor range for material with bainite.*

a crack growth rate under the conditions used herein. This is because the value of exponent n_3 in Eq 4 is small enough to estimate the crack growth rate from the rate of integrated acoustic emission energy within an acceptable accuracy. The maximum scatter in crack growth data is a factor of 3 which is equivalent or even better than the present level of the reproducibility of fatigue crack growth rate tests in simulated reactor water in laboratories. The small value of n_3 implies that the acoustic emission technique is a promising basis from which to monitor the crack growth rate under cyclic loading, specifically in high-temperature water.

Though much work remains to be done to develop this methodology for plant monitoring, such as the acoustic wave attenuation and sophisticated triangulation techniques in the actual application to the reactor structures,

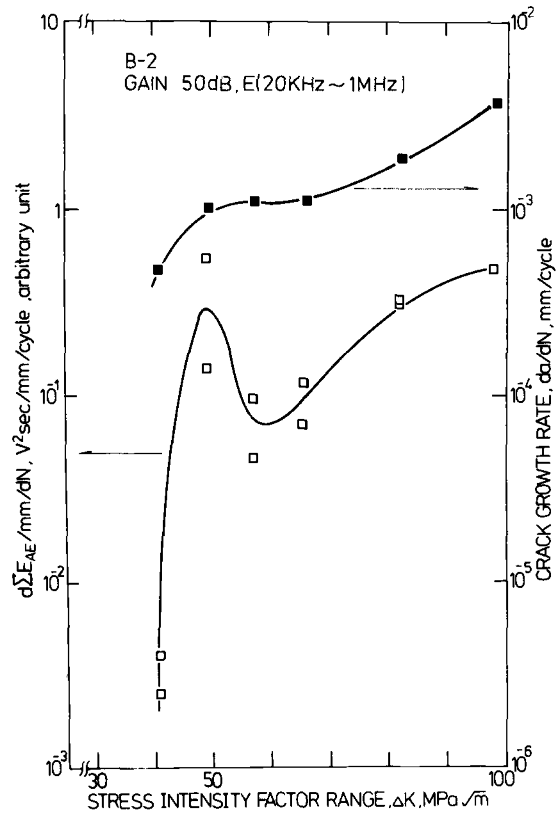

FIG. 12—*Dependence of crack growth rate and wave energy as functions of stress intensity factor range for material with martensite.*

the present results may give a basis to encourage further extensions of the technique.

It can be stated in conclusion that the acoustic emission detection achieved in the present work provides semiquantitative means of detecting and measuring the rate of cyclic crack growth specific in the simulated BWR environments.

Conclusion

Based on the laboratory study on acoustic emission detected during corrosion fatigue tests of SA 533 Grade B steel in high temperature and pressure aqueous environment, the following conclusions can be drawn:

1. The acoustic emission monitoring in detecting growing cracks under cyclic loading was shown to be feasible when the growth was made in the high-temperature water environment typical of BWR primary coolant.

2. The detection was made possible by avoiding noises specific to the test system with high-temperature water.

3. The relationship between the energy of the detected acoustic emission and the cyclic crack growth rate suggested in the present study is believed to provide a promising basis for potential future application of acoustic emission monitoring techniques to plant monitoring when other technical difficulties associated with estimating the crack growth rate are solved.

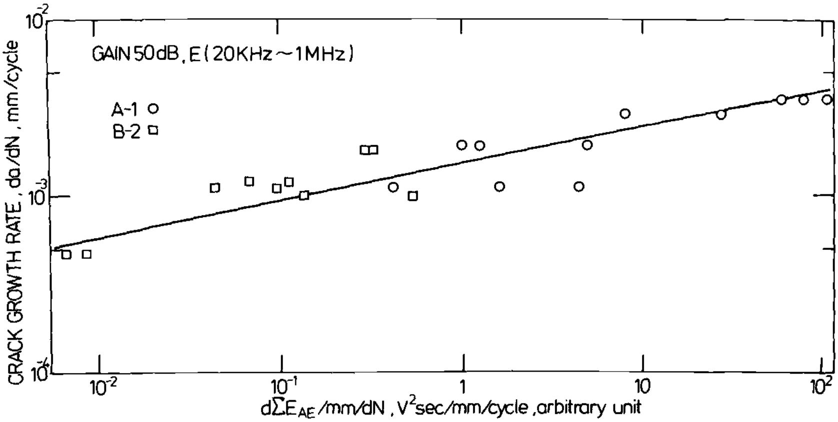

FIG. 13—*Relationship between crack growth rate versus wave energy with particular reference to the environment-enhanced crack growth in high-temperature water.*

Acknowledgments

Many useful discussions and suggestions made by Dr. T. Kondo and Professors M. Suzuki and H. Takahashi during the course of the present study are gratefully acknowledged.

The authors are also indebted to the contributions of their colleagues at JAERI and Tohoku University in performing the corrosion fatigue tests and acoustic emission monitoring.

The present work employed specimen materials supplied by the courtesy of Hitachi-Babcock Company and the International Cooperative Group for Cyclic Crack Growth Rate.

References

[1] Gopal, Raj, *Monitoring Structural Integrity by Acoustic Emission, ASTM STP 571*. American Society for Testing and Materials, 1975, pp. 200-220.
[2] Vetrano, J. B. and Jolly, W. D., *Materials Evaluation*, Vol. 30, No. 1, 1972, pp. 9-12.
[3] Suguri, S. et al, CRIEPI-74003, Central Research Institute of Electric Power Industry, June 1974 (in Japanese).
[4] Stahlkopf, K. E. and Daut, G. J., *Nuclear Safety*, Vol. 17, No. 1, Jan.-Feb. 1976, p. 33.
[5] Kondo, T., Kikuyama, T., Nakajima, H., Shindo, M., and Nagasaki, R. in *Proceedings*, 1st International Conference on Corrosion Fatigue, NACE and AIME, 1972, pp. 539-556.
[6] Mager, T. R., Landes, J. D., Moon, D. M., and McLaughlin, V. J., "The Effect of Low Frequencies on the Fatigue Crack Growth Characteristics of A533 Grade B Class 1 Plate in an Environment of High-Temperature Primary Grade Nuclear Reactor Water," WCAP-8256, Westinghouse Electric Corporation, December 1973.
[7] Gerber, T. L., Heald, J. D., and Kass, E., "Fatigue Crack Growth in SA508-Cℓ2 Steel in a High-Temperature, High-Purity Water Environment," ASME PV & P-Materials-Nuclear Conference, Miami, June 1974.
[8] Bamford, W. H. in *Proceedings*, Conference on The Influence of Environment on Fatigue, Institute of Mechanical Engineering, 1977, pp. 51-56.
[9] Suzuki, M., Takahashi, H., Shoji, T., Kondo, T., and Nakajima, H. in *Proceedings*, Conference on The Influence of Environment on Fatigue, Institute of Mechanical Engineering, 1977, pp. 161-169.
[10] Mostovoys, S., Crosley, B. P., and Ripling, E. J., *Journal of Materials*, Vol. 2, No. 3, 1967, pp. 661-681.

DISCUSSION

J. Masounave, J.-P. Bailon, and F. Hamel[1] *(written discussion)*—You show a relationship between acoustic emission and the stress intensity factor ΔK. In this plot you obtain a maximum and a minimum similar to those obtained by other authors. Different mechanisms have been invoked to explain this type of variation (transition between brittle and ductile fracture etc.).

In a recent work[2] it was shown that these maximum and minimum could be explained by constructive and destructive interference from the acoustic waves reflected from the edges of the C-T specimen. A wave emitted by crack propagation is considered to be reflected at different points of the sample surfaces. By very simple calculations,[3] it is possible to show that, measured at a given site on the specimen, the acoustic emission can be obtained as a function of the crack length (Fig. 14).

This interference pattern was simulated using a transducer-like emitting source which was moved to different positions. The acoustic emissions were detected by a second transducer positioned at the top edge of the C-T specimen. Maximum and minimum rates of emission were again measured.

[1] Département de Génie Métallurgique, Ecole Polytechnique de Montréal, Montréal, Canada.
[2] Hamel, F., M. Sc. A. thesis, Polytechnic School, Montreal, Canada, 1979.
[3] Hamel, F., Bassim, N., and Bailon, J.-P., *Ultrasonics*. Vol. 17, 1979, pp. 125-127.

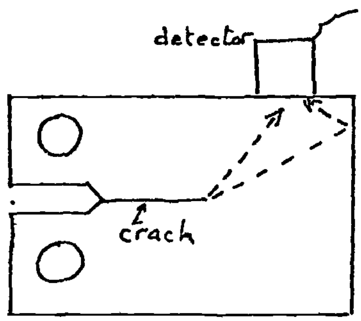

FIG. 14—*Schematic illustration of the interference from the acoustic waves deflected from the edge of the specimen.*

Thus it appears probable that the maximum and minimum observed are only the result of the interference pattern.

Two questions come to mind. Did you employ a constant load amplitude? Would you care to comment on the applicability of this explanation based on constructive and destructive interference to your constant K specimens?

H. Nakajima, T. Shoji, M. Kikuchi, M. Niitsuma, and M. Shindo (authors' closure)—Question 1: Yes. For a given stress intensity factor range, a constant load amplitude was employed. *Question 2*: There are some minor effects of constructive and destructive interference from the acoustic waves reflected from the edges of the specimen. However, these effects are not considered to be related to the maximum and minimum in Fig. 12. This is because the estimated wave length is nearly 25 mm, while the crack advance in each set of tests is between 6 and 8 mm in our specimen. No significant interference can be expected from these two values.

Statistical Analysis and Representation of Data

F. Bastenaire,[1] *H.-P. Lieurade,*[1] *L. Régnier,*[1] *and M. Truchon*[1]

Statistical Analysis of Fatigue Crack Growth

REFERENCE: Bastenaire, F., Lieurade, H.-P., Régnier, L., and Truchon, M., "**Statistical Analysis of Fatigue Crack Growth,**" *Fatigue Crack Growth Measurement and Data Analysis, ASTM STP 738,* S. J. Hudak, Jr., and R. J. Bucci, Eds., American Society for Testing and Materials, 1981, pp. 163-170.

ABSTRACT: The object of this paper, which assumes the validity of Paris's equation, is to derive satisfactory estimates of the two constants C and m in the following conditions: (*1*) numerical process leading to the estimates of C and m is based on a rationale that takes into account the physical and statistical aspects of fatigue crack growth, and (*2*) the result of the fit compares favorably with existing procedures.

KEYWORDS: fatigue crack growth, Paris's equation, statistical analysis

A few years ago little attention was given to the scatter of crack propagation data, and it was commonly stated that, as compared with that observed in conventional *S-N* data, the scatter was not much of a nuisance.

A deeper understanding of the repercussions of crack propagation rate uncertainties on life prediction seems to have brought about a different point of view. In recent times there has been widespread interest and discussion about the analysis—notably the statistical analysis—of crack propagation test data.

Despite this change in ideas, the approach to this problem has most often been very empirical as appears, for instance, from the widespread use of data-smoothing methods whose effects on data—apart from smoothing—are for a large part unknown. The major drawback of data-smoothing methods is to give the impression that after their application one is left with the true curve and to supply no information about the uncertainty that remains in the smoothed curve. The point that, in order to supplement predictions with con-

[1]Head of Statistics Department, head of Fatigue and Weldability Department, research engineer, Statistics Department, and research engineer, Fatigue Department, respectively, IRSID, Saint Germain en Laye, France.

fidence limits, the statistician needs a mathematical and probabilistic model on which to operate seems to have been completely missed.

At the present time, many statistical aspects of fatigue crack propagation needed to set up a mathematical model are obviously still unknown. It is our feeling, however, that a model allowing for a random distribution of mechanical properties in the volume of a metal should, even subject to further improvements as more information flows in, permit a reasonable analysis of crack propagation data.

Statistical Nature of Fatigue Crack Growth

In the present analysis, fatigue crack growth is regarded as a random process both on a microscopic and macroscopic scale.

Some reflection on the nature of this growth leads us to discard a straightforward application of conventional statistical methods to the couples of data a_i (crack length) and n_i (number of cycles) because the random causes acting on a_i, n_i also act on a_j, n_j for that part of the crack path that is common to a_i and a_j, that is, min $\{a_i, a_j\}$. For this reason, a_i and a_j, if the crack is observed at pre-selected values of the number of cycles n, or inversely, n_i and n_j, if the observations take place at pre-selected values of the crack length a, are not independent random variates.

On the contrary, it is to be expected from the random nature of the structural properties of metals that the highest degree of independence between, say, the number of cycles Δn_i and Δn_j needed for the crack to extend by two amounts Δa_i, Δa_j is reached when these extensions refer to *distinct* parts of a specimen, and the more so, the farther apart they are located.

It can reasonably be expected that an accurate probabilistic description of a crack growth would involve the introduction of an autocorrelation function but, on the scale where fracture mechanics theory and practice operate, the actual correlation is probably very loose and, in any case, this point can be checked by the statistical analysis of residual errors.

In view of this and considering that most available statistical methods of analysis rely on the assumption of stochastic independence between the variates under consideration, attention must be focused on the treatment of the crack length increments Δa_i rather than the lengths a_i themselves. It can be noted that since the knowledge of a_o and the Δa_i's is equivalent to that of the a_i's no loss of information can result from shifting from the a_i's to the Δa_i's.

Statistical Model of Crack Length Increments

Expected Value of Crack Length Increment

Under the steady-state condition where the stress-intensity factor ΔK would be maintained constant, the expected value of the crack length increment produced by Δn load cycles, say Δa, regarded as a random variate, would obviously be proportional to Δn.

$$E(\Delta a) = C \cdot \Delta n \tag{1}$$

where C is a constant.

Under the same conditions, the Paris law indicates that Δa, regarded as a deterministic quantity, would be

$$\Delta a = C\, \Delta K^m\, \Delta n \tag{2}$$

This can be understood, in a probabilistic framework, as expressing in effect

$$E(\Delta a) = C\, \Delta K^m\, \Delta n \tag{3}$$

that is, for constant ΔK,

$$E(\Delta a/\Delta K^m) = C \cdot \Delta n \tag{4}$$

and, for an infinitely small step,

$$E(da/\Delta K^m) = C\, dn \tag{5}$$

Then, integrating both sides,

$$\int E\,(da/\Delta K^m) = E\left[\int da/\Delta K^m\right]$$
$$= \int C dn$$

hence

$$E\left[\int_{a_i}^{a_{i+1}} \Delta K^{-m}\, da\right] = C\,(n_{i+1} - n_i) \tag{6}$$

The Error Term in the Crack Growth

Equation 6 expresses the mathematical expectancy of

$$\int_{a_i}^{a_{i+1}} \Delta K^{-m}\, da$$

but this quantity itself, as a random variate, differs from $c(n_{i+1} - n_i)$ and it is necessary to express its difference through an error term. Writing

$$\int_{a_i}^{a_{i+1}} \Delta K^{-m}\, da = C(n_{i+1} - n_i)\epsilon_i \tag{7}$$

a new random variate ϵ_i is introduced whose distribution will be assumed lognormal with median approximately equal to unity and constant variance σ^2 [$\log \epsilon_i \sim N(0, \sigma^2)$]. The assumption that σ^2 is constant is suggested by the common observation that, in the $\log(\Delta a/\Delta n)$ versus $\log \Delta K$ diagram, the data points are usually scattered over a constant width band.[2]

Equation 7 can then be written, taking the natural logarithms of both sides, as

$$\ln \int_{a_i}^{a_{i+1}} \Delta K^{-m}\, da = \ln C + \ln (n_{i+1} - n_i) + \eta_i \tag{8}$$

where $\eta_i = \ln \epsilon_i$.

In the right-hand side of Eq 8, $\ln C$ then appears in linear form, whereas m does not in the left-hand side. As long as the crack length increments $(a_{i+1} - a_i)$ are small, however, and ΔK is therefore nearly constant over a_i, a_{i+1},

$$\ln \int_{a_i}^{a_{i+1}} \Delta K^{-m}\, da$$

is approximately linear with respect to m.

Since this holds only approximately, linearity is *not* assumed in the method which we describe below and

$$\ln \int_{a_i}^{a_{i+1}} \Delta K^{-m}\, da$$

is instead differentiated with respect to m and successive increments in the value of m determined until m reaches a limit value. This allows us to cope with relatively widely spaced a_i's while the approximately linear relationship of

$$\ln \int_{a_i}^{a_{i+1}} \Delta K^{-m}\, da$$

with m ensures convergence in very few computing steps.

To estimate the two coefficients m and C in Eq 8, let us expand its left-hand side:

$$\ln \int_{a_i}^{a_{i+1}} \Delta K^{-m}\, da = f_i(m) \tag{9}$$

[2]Virkler, D. A., Hillberry, B. M., and Goel, P. K., "The Statistical Nature of Fatigue Crack Propagation," Technical Report AFFDL-TR-7843, Air Force Flight Dynamics Laboratory, Wright-Patterson Air Force Base, Ohio, 1978.

$$\ln \int_{a_i}^{a_{i+1}} \Delta K^{-m}\, da = f_i(m_o) + (m - m_o)\left[\frac{\partial f_i(m)}{\partial m}\right]_{m_o} \tag{10}$$

Introducing this expression into Eq 8, one gets

$$f_i(m_o) - \ln(n_{i+1} - n_i) = \ln C + (m_o - m)\left[\frac{\partial f_i(m)}{\partial m}\right]_{m_o} + \eta_i \tag{11}$$

For given m_o, both $f_i(m_o)$ and $[\partial f_i(m)/\partial m]_{m_o}$ can be calculated; $f_i(m_o)$ is computed using numerical integration. For the second quantity, we have

$$\begin{aligned}\frac{\partial f_i(m)}{\partial m} &= \left(\frac{\partial}{\partial m}\int_{a_i}^{a_{i+1}} \exp[-m \ln(\Delta K)]\, da\right) \\ &\quad \Bigg/ \left(\int_{a_i}^{a_{i+1}} \exp[-m \ln(\Delta K)]\, da\right) \\ &= -\left(\int_{a_i}^{a_{i+1}} \ln(\Delta K) \exp[-m \ln(\Delta K)]\, da\right) \\ &\quad \Bigg/ \left(\int_{a_i}^{a_{i+1}} \exp[-m \ln(\Delta K)]\, da\right)\end{aligned} \tag{12}$$

and therefore $[\partial f_i(m)/\partial m]_{m_o}$ can also be computed through numerical integration.

Letting

$$\begin{aligned} x_i &= -\left[\frac{\partial f_i(m)}{\partial m}\right]_{m_o} \\ y_i &= f_i(m_o) - \ln(n_{i+1} - n_i) \\ \alpha &= \ln C \\ \beta &= m - m_o \end{aligned} \tag{13}$$

Equation 11 can be written as

$$y_i = \alpha + \beta x_i + \eta_i \tag{14}$$

where η_i is normally distributed with constant variance. Starting from m_o, estimates a and b of α and β will be obtained by application of the conventional method of least squares. An estimate of m is then obtained:

$$m_1 = m_o + b \tag{15}$$

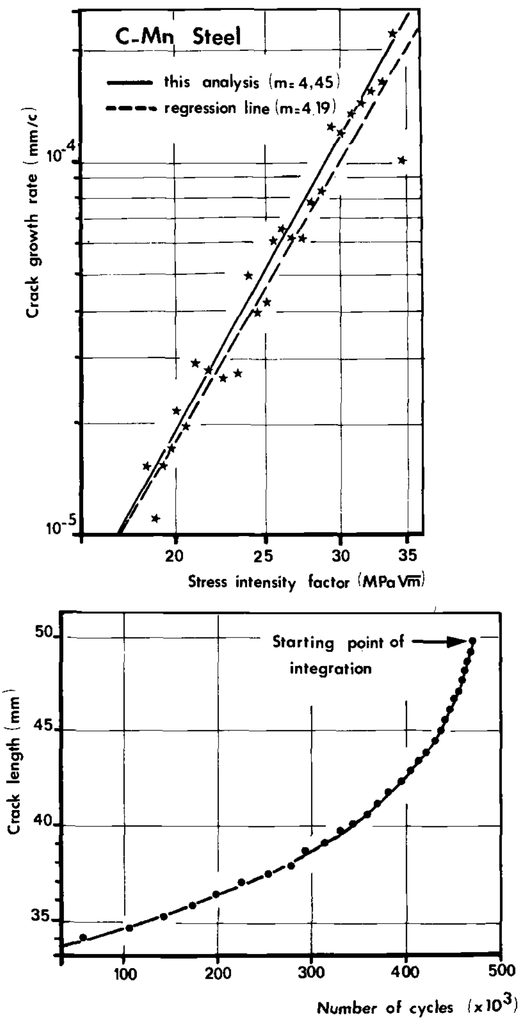

FIG. 1—*Typical result of a fatigue crack growth experiment.*

which, again, can be used as a new initial value to compute m_2 and so on. This iterative process is stopped when convergence occurs.

Application

This data-processing method has been successfully employed on a large number of fatigue crack growth data which were known to satisfy the Paris equation.

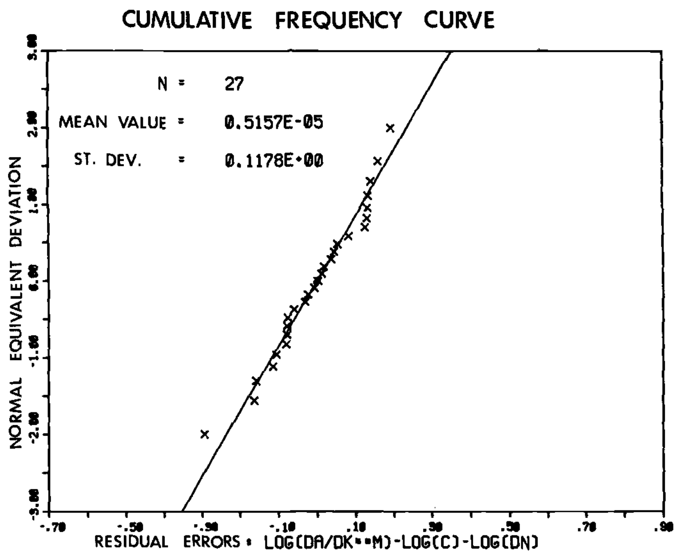

FIG. 2—*Verification of the normal distribution of the residual errors calculated by the present analysis of fatigue crack growth data.*

A typical example of application on a carbon-manganese steel is shown in Fig. 1. In the (log da/dn; log ΔK) diagram, the fitted Paris line is plotted in comparison with the data points and regression line calculated by the secant method. It can be seen that the two solutions may give different results. This can be attributed to the badly estimated da/dn extreme values (especially in the range of the high fatigue crack growth rates) which are not counterbalanced by subsequent data. In the regression analysis these values have the same weight as the other better-estimated data points, while it is not the case for the processing method developed herein.

Additionally, the fitted Paris equation is integrated to get a curve which is plotted in a (a, n) diagram in order to be compared with the raw experimental data points. The last point (a_f; N_f) has been chosen as the starting point for integration, and we get

$$N = N_f - \int_a^{a_f} \frac{da}{C\Delta K^m}$$

Doing so, the error δa on the crack length measurements and particularly on a_f has a negligible effect on n, because for the highest fatigue crack growth rate the quantity

$$\int_{a_f - \delta a}^{a_f} \frac{da}{C\Delta K^m}$$

is small compared with $N_f - N_o$.

Moreover, for each set of fatigue crack growth rate data, the normality of the errors η_i is checked, and it can be seen in Fig. 2 that this hypothesis is experimentally verified.

Conclusion

Based on the consideration that in a fatigue crack growth experiment the increments of crack length $(a_{i+1} - a_i)$ are likely to be independent random variables, a data-processing method is proposed to estimate the parameters of the Paris equation in the case of an individual test.

Further work is needed to get more information on the variance of the crack growth process.

J. T. Fong[1] *and N. E. Dowling*[2]

Analysis of Fatigue Crack Growth Rate Data from Different Laboratories

REFERENCE: Fong, J. T. and Dowling, N. E., "**Analysis of Fatigue Crack Growth Rate Data from Different Laboratories,**" *Fatigue Crack Growth Measurement and Data Analysis, ASTM STP 738*, S. J. Hudak, Jr., and R. J. Bucci, Eds., American Society for Testing and Materials, 1981, pp. 171–193.

ABSTRACT: A simple-minded yet quantitative approach to assessing interlaboratory fatigue crack growth rate data is proposed. Seven sets of da/dN versus ΔK data from six laboratories on nominally the same material and loading conditions in a cooperative test program sponsored by the Society of Automotive Engineers (SAE) are analyzed to illustrate this *ad hoc* approach. Each set of data is subjected to a standard first-order linear regression analysis based on the method of least squares. Three characteristics of the regression line [namely, the location of the "center" of the data, the slope, and the vertical half-width of the confidence band (for some specified level of confidence)] are used to define a composite measure of the closeness of one regression line to another. To illustrate the benefit of a statistically sound interlaboratory test program, the single-specimen SAE data are supplemented with fictitious replica data for the application of an interlaboratory data analysis procedure first proposed by Mandel (*ASTM Standardization News*, Vol. 5, No. 3, 1977, p. 17). "New" information based on the *ad hoc* approach of this paper and Mandel's method of interlaboratory data analysis is discussed in the context of other work on fatigue crack growth rate data analysis and the economic aspect of engineering testing.

KEY WORDS: applied regression analysis, data analysis, engineering judgment, fatigue, fatigue crack growth, fracture mechanics, interlaboratory data analysis, interlaboratory test program, linear regression analysis, mathematical modeling, statistics, steels

In 1974 the Fatigue Design and Evaluation Committee of the Society of Automotive Engineers (SAE) sponsored a cooperative program on fatigue crack growth rate testing for two steels typical of those used in the ground

[1] Physicist, Center for Applied Mathematics, National Bureau of Standards, Washington, D.C. 20234.

[2] Fellow engineer, Westinghouse Research and Development Center, Westinghouse Electric Corporation, Pittsburgh, Pa. 15235.

vehicle industry. In February 1979 Dowling and Walker [*1*][3] reported the results of this cooperative testing program, there being participation by seven laboratories with test results from a total of 54 specimens. Using an incremental polynomial procedure [*2*], Dowling and Walker first obtained the fatigue crack growth rates (da/dN) from the crack length versus cycles data (a versus N), and then plotted the calculated da/dN against the stress-intensity range (ΔK) for both steels. This was done at a variety of stress ratios (R) with and without a modification of ΔK for negative stress ratios. At the end of their report, Dowling and Walker concluded that "in control tests on two typical structural steels at $R = 0.1$, excellent agreement is obtained among the seven participating laboratories, four of which had no previous experience with this type of testing" [Ref *1*, p. 9].

The purpose of this paper is two-fold: (*1*) Using conventional techniques of data analysis, a portion of the SAE data [*1*] is analyzed to illustrate a simple-minded yet quantitative approach to assessing interlaboratory fatigue crack growth rate data; and (*2*) Using fictitious replica-specimen data to supplement the single-specimen SAE data [*1*] for the application of an interlaboratory data analysis procedure due to Mandel [*3*], "new" information is derived to illustrate the benefit of a statistically admissible interlaboratory test program.

We begin by reviewing the nomenclature and formulas for the conventional analysis of data as documented by Draper and Smith [*4*]. In particular, we adopt their viewpoint that in the absence of a prior estimate of the error variance σ^2, a fit of a set of data from a single specimen by a standard linear regression analysis cannot evaluate the specimen-to-specimen variability. We next examine a portion of the SAE data [*1*] by regression analysis to prepare for the introduction of an *ad hoc* comparison of any two sets of da/dN versus ΔK data. An "agreement matrix" is defined to formalize this *ad hoc* procedure and illustrate it with a numerical calculation based on seven sets of data from the SAE program. Then, in order to accomplish the second purpose of this paper, we introduce Mandel's interlaboratory data analysis procedure [*3*] and illustrate it with a numerical example based on a portion of the SAE data and some fictitious data where needed. Finally, our results in the context of other works on fatigue crack growth data analysis [*2,5*] and the economic aspect of engineering testing [*6*] are discussed.

To assist those readers who wish to perform the same analysis as described in this paper, we include a listing of the FORTRAN program for reducing the crack length versus cycles data to crack growth rate data as used by Dowling and Walker [*1*] (Appendix I) and a listing of the BASIC program as implemented on a Tektronix 4051 graphical system for the regression analysis of the SAE crack growth rate data (Appendix II).

[3] The italic numbers in brackets refer to the list of references appended to this paper.

Fitting a Straight Line by Least Squares

While most engineers can calculate the slope of a straight line by the method of least squares in fitting a given set of data $y(x)$, it is still not common knowledge among the engineering test community that the straight-line model should be tested *twice*, once for the significance of the regression analysis with all its usual assumptions on the error term (for example, mean $= 0$, variance $= \sigma^2$) and secondly for the goodness or the lack of fit. The first test requires an estimate s^2 from the linear fit of the variance σ^2 in order to apply the so-called F-test.[4] Implicit in the calculation of the first test is the assumption that the straight-line model is correct and s^2 is indeed an estimate of σ^2. To conduct the second test (that is, the test for the lack of fit) two possibilities occur: (*1*) A prior estimate of σ^2 is available; and (*2*) Repeat measurements of y have been made at the same value of x, and no estimate of σ^2 is available. Due to lack of time or funding, many engineering test programs for discovering new information for novel applications are still designed around the notion of a single specimen per run. This means neither (*1*) nor (*2*) applies, and the engineer is usually left with an open question on the goodness of the fit of the straight-line model.

To encourage the inclusion of at least one replica per run for all engineering test programs for which no prior estimate of σ^2 is available, we present in this section a brief summary of the nomenclature and the formulas of the standard first-order linear regression analysis of data as fully documented by Draper and Smith [*4*, Chapter 1]. A more complete discussion must necessarily include an examination of residuals [*4*, Chapter 3], which is omitted here for brevity.

We begin by denoting the set of data $y(x)$ by its primitive form $\{(x_i, y_i), i = 1, \ldots, n\}$. The goal of fitting the data by a straight line is expressed mathematically by the linear, first-order equation[5]

$$y = \beta_0 + \beta_1 x + \epsilon \tag{1}$$

that is, for a given x a corresponding observation y consists of the value $\beta_0 + \beta_1 x$ plus an amount ϵ, the error term, by which any individual y may fall off the straight line. Clearly, for every pair of (x_i, y_i) the error term ϵ_i would be different, and the usual assumptions on ϵ include the statement that the ϵ_i are independent random variables with mean zero and variance σ^2 (unknown).[6] The computational task is to calculate three quantities, b_0, b_1, and s^2, as estimates of the three unknown parameters, β_0, β_1, and σ^2,

[4] See Ref *4*, pp. 24-26.

[5] In standard statistical terminology, "linear" refers to the parameters (β's) and "order" to the highest power of an independent variable. For example, $y = \beta_0 + \beta_1 x + \beta_2 x^2 + \epsilon$ is a second-order (in x) linear (in the β's) regression model.

[6] See Ref *4*, p. 17.

respectively. If we denote $\bar{x} = (\Sigma x_i)/n$, $\bar{y} = (\Sigma y_i)/n$, and let the symbol Σ stand for the usual summation sign for $i = 1, \ldots, n$, the formulas for b_1 and b_0 are

$$b_1 = \frac{\Sigma x_i y_i - n\bar{x}\bar{y}}{\Sigma(x_i)^2 - n(\bar{x})^2} \tag{2}$$

and

$$b_0 = \bar{y} - b_1\bar{x} \tag{3}$$

The equation of the straight line with b_0 and b_1 determined from the data in accordance with Eqs 2 and 3 assumes the form

$$Y = b_0 + b_1 x \tag{4}$$

where Y denotes the predicted value of y for a given x.

To calculate s^2 we introduce the identity

$$y_i - Y_i \equiv (y_i - \bar{y}) - (Y_i - \bar{y}) \tag{5}$$

where the term on the left, $y_i - Y_i$, is known as the "residual about the regression," and the two terms on the right are known, respectively, as the "residual about the mean" and the "deviation from the mean due to regression." An identity equivalent to Eq 5, involving the sum of squares (SS) of each of the three terms in Eq 5, can be derived[7] to yield an estimate of s^2:

$$\Sigma(y_i - Y_i)^2 \equiv \Sigma(y_i - \bar{y})^2 - \Sigma(Y_i - \bar{y})^2 \tag{6}$$

and

$$s^2 = \frac{\Sigma(y_i - Y_i)^2}{n - 2} \tag{7}$$

The standard practice is to calculate the SS about the mean, $\Sigma(y_i - \bar{y})^2$, from the data, and the SS due to regression, $\Sigma(Y_i - \bar{y})^2$, from Eq 4, and to use their difference and Eqs 6 and 7 to calculate s^2. It is not difficult to see that if n is the number of points in the original set of data, then $n - 1$ is the degrees of freedom (df) of the SS about the mean, 1 is the df of the SS due to regression, and $n - 2$ is the df of the SS about the regression. A well-known concept in regression analysis, the so-called mean square term which equals SS divided by df, leads to a trivial definition of MS_R, the mean square due to regression; namely

$$MS_R = \frac{\Sigma(Y_i - \bar{y})^2}{1} = \Sigma(Y_i - \bar{y})^2 \tag{8}$$

[7] See Ref *4*, pp. 13-14.

A standard result in statistics[8] allows us to test for the significance of the regression calculation by comparing an F-ratio ($= \mathrm{MS_R}/s^2$) with a critical F-value corresponding to $F(1 - \alpha, 1, n - 2)$ of a tabulated F-distribution for a level of confidence equal to 100 $(1 - \alpha)$ percent. The regression is said to be insignificant at level α if the calculated F-ratio is less than the critical one.

To test for lack of fit under the condition that a prior estimate of the variance σ^2 of the error term ϵ is available, we compare the calculated s^2 with the estimate of σ^2 and (*1*) if s^2 is significantly greater than σ^2, we say that there is lack of fit and we would reconsider the straight-line model which would be inadequate in its present form, or (*2*) if s^2 is close to σ^2, we say that there is no lack of fit and we cannot reject the model.

If a prior estimate of σ^2 is not available, we cannot test for the lack of fit unless repeat measurements of y have been made at the same value of x to permit an estimate of σ^2. For example, if two replicas were used for each test with $2n$ pairs of data given by $\{(x_i, y_i), i = 1, \ldots, n\}$ and $\{(x_i, y_i'), i = 1, \ldots, n\}$, two quantities, s_e^2 and $\mathrm{MS_L}$, can be calculated and their ratio used to test whether there is lack of fit. The quantity s_e^2, known as the mean square for pure error, takes the following special form for two replicas:

$$s_e^2 = \left\{ \sum_{i=1}^{n} (y_i - y_i')^2 \right\} / (2n) \tag{9}$$

The quantity $\mathrm{MS_L}$, known as the mean square for lack of fit, is given by

$$\mathrm{MS_L} = \frac{\Sigma(y_i - Y_i)^2 + \Sigma(y_i' - Y_i)^2 - \{\Sigma(y_i - y_i')^2\}/2}{n - 2} \tag{10}$$

where Σ again stands for the summation of terms from $i = 1, 2, \ldots, n$. The F-ratio ($= \mathrm{MS_L}/s_e^2$) is compared with the 100 $(1 - \alpha)$ percent point of an F-distribution with $(n - 2)$ and n degrees of freedom given by $F(1 - \alpha, n - 2, n)$. The straight-line model is said to be adequate and suffer no lack of fit at level α if the calculated F-ratio is less than the critical one for the problem at hand.[9]

Regression Analysis of SAE Data

The SAE test program consisted of 54 fatigue crack growth rate tests on two structural steels (Man-Ten of U.S. Steel Corporation, and RQC-100 of Bethlehem Steel Corporation) [*1*]. Table 1 shows how 26 of those 54 tests are

[8] See Ref *4*, pp. 24-26.

[9] Formulas for more than two replicas are given in Ref *4*, pp. 26-32.

TABLE 1—*SAE fatigue crack growth test matrix for Man-Ten* [2].

$R =$	P_{max},	Frequency,	Number of Man-Ten Specimens Tested by						
P_{min}/P_{max}	10^3 lb	Hz	Lab. 1	Lab. 2	Lab. 3	Lab. 4	Lab. 5	Lab. 6	Lab. 7
0.1	1.60	5	1	1	1	1	1	...	2
	4.00	2	1	...	1	1	1	1[a]	1
		5	...	1	...	...	...	...	...
0.24	1.96	20	...	...	...	...	1	...	...
0.5	1.60	20	...	...	...	...	...	1[a]	...
	4.80	3	...	...	...	...	1	...	...
0.8	4.00	20	...	...	...	...	1	...	...
	5.60	10	...	...	...	...	1	...	...
−0.5	1.60	3	...	...	...	...	...	...	1
		12 to 15	...	...	1	...	...	...	...
−1.0	1.60	3	...	...	...	...	...	...	2
		12 to 15	...	...	1	...	...	...	...

[a] A second specimen cracked inadvertently along a direction transverse to that prescribed by the test program is excluded in this table for consistency.

distributed in a test matrix for a single material (Man-Ten, 0.2 percent yield of 360 MPa) for a variety of load ratios (R), maximum loads (P_{max}), and test frequencies.[10]

Two general observations can be made from Table 1. Firstly, only one laboratory (Laboratory 7) did two tests with replicas. Without replicas in all other cases, it is not possible to conduct without further assumptions an interlaboratory data analysis [3] to yield a defensible estimate of the within-laboratory and between-laboratory variabilities. Without a prior estimate of the variance σ^2 of the measurement error ϵ, we have shown in the previous section that we cannot even complete a regression analysis with a test for lack of fit for any individual test involving only one specimen. The test matrix shown in Table 1 is therefore not well-suited for a rigorous interlaboratory data analysis or a complete regression analysis on an individual laboratory basis.[11]

The second observation has to do with the concept of a control series of tests. The first two series of tests for $R = 0.1$ ($P_{max} = 1.60$, 5 Hz; $P_{max} = 4.00$, 2 Hz) were considered by Dowling and Walker [1] as control series. This is not very satisfying even though it is common knowledge among fatigue researchers that frequency probably plays no role in such tests. By fixing the frequency at 5 Hz for both tests, such as the first and the third rows in Table 1 ($P_{max} = 1.60$, 5 Hz; $P_{max} = 4.00$, 5 Hz), the concept of a genuine control group of tests would have been preserved.

Because of these two observations, it becomes inappropriate for us to apply conventional techniques to all the data reported in Ref 1. Instead, we choose to analyze a small portion of the SAE data [namely, the first series listed in Table 1 ($R = 0.1$, $P_{max} = 1.60$, 5 Hz)] to achieve the two purposes of this paper mentioned earlier. A total of 6 laboratories with 7 tests (Laboratories 1 to 5 have one test each; Laboratory 7 has two tests) is considered, firstly for an incomplete regression analysis in order to illustrate a quantitative approach for assessing agreement among interlaboratory data, and then for a mathematical exercise in interlaboratory data analysis in the sense of Mandel [3], using fictitious data to supplement what is available from the SAE test program.

To simplify our investigation, we take as a starting point the crack growth rate data (da/dN versus ΔK) as derived from the observed crack length versus cycles data (a versus N) by Dowling and Walker [1]. For completeness, we include a listing of the FORTRAN program for their data reduction task using the incremental polynomial method (Appendix I). A typical computer printout (Laboratory 1, Man-Ten, $R = 0.1$, $P_{max} = 1.60$, 5 Hz) as furnished

[10] For brevity, we omit a similar test matrix for the other 28 tests on RQC-100 steel.

[11] A closer examination of the two-replica data of Laboratory 7 furnished by Dowling revealed that the tests did not correspond to repeat measurements of one dependent variable on the same values of the independent variable. Thus the conclusion holds for all laboratories in this SAE test program.

TABLE 2—*Computer printout for data reduction via a FORTRAN program (UNIVAC 1100 Time/Sharing) (see Appendix I for program listing).*

CRACK GROWTH RATE AND STRESS INTENSITY DATA REDUCTION
INCREMENTAL POLYNOMIAL FOR DA/DN

SPEC M7A MAN-TEN LAB 1

COMPACT SPECIMEN H/W=0.486

DELTA P= 1.5000 KIPS PMIN= 0.1700 KIPS R= 0.1018
B= 0.3750 INCHES W= 2.5500 INCHES A0= 0.7670 INCHES
TESTING FREQUENCY= 5.0000 HERTZ

Total Cycles	Crack Length Observed	Crack Length Calculated	Stress Intensity	Growth Rate
0.	0.8670	...	...	...
19330.	0.8870	...	...	...
42920.	0.9570	...	...	...
56680.	0.9320	0.9452	19.20	1.144−06
69940.	0.9470	0.9595	19.44	1.259−06
78650.	0.9670	0.9602	19.45	1.287−06
91000.	0.9870	0.9861	19.89	1.851−06
102710.	1.0070	1.0094	20.30	2.010−06
111150.	1.0270	1.0261	20.59	2.055−06
120500.	1.0470	1.0466	20.96	2.145−06
129450.	1.0670	1.0669	21.34	2.193−06
138900.	1.0870	1.0868	21.71	2.243−06
147890.	1.1070	1.1066	22.10	2.377−06
157230.	1.1270	1.1289	22.54	2.586−06
163930.	1.1470	1.1466	22.90	2.728−06
170880.	1.1670	1.1663	23.31	2.925−06
177470.	1.1870	1.1866	23.75	3.123−06
184310.	1.2070	1.2083	24.23	3.233−06
189900.	1.2270	1.2263	24.64	3.469−06
195530.	1.2470	1.2461	25.11	3.731−06
201620.	1.2670	1.2699	25.70	3.962−06
205520.	1.2870	1.2851	26.09	4.276−06
210270.	1.3070	1.3059	26.65	4.670−06
215280.	1.3270	1.3303	27.34	5.363−06
218150.	1.3470	1.3451	27.78	5.811−06
221980.	1.3670	1.3687	28.51	6.376−06
224430.	1.3870	1.3857	29.07	6.836−06
227400.	1.4070	1.4059	29.76	7.306−06
230390.	1.4270	1.4288	30.59	7.938−06
232720.	1.4470	1.4470	31.30	8.442−06
234920.	1.4670	1.4661	32.07	9.207−06
237130.	1.4870	1.4874	33.00	1.005−05
239130.	1.5070	1.5078	33.93	1.084−05
240820.	1.5270	1.5265	34.85	1.165−05
242510.	1.5470	1.5467	35.90	1.282−05
244080.	1.5670	1.5672	37.03	1.438−05
245520.	1.5870	1.5883	38.27	1.588−05
246680.	1.6070	1.6072	39.45	1.754−05
247680.	1.6270	1.6254	40.67	1.912−05
248820.	1.6470	1.6483	42.29	2.119−05
249690.	1.6670	1.6666	43.68	2.379−05
250550.	1.6870	1.6873	45.35	2.695−05
251310.	1.7070	1.7086	47.18	3.114−05
251850.	1.7270	1.7254	48.71	3.601−05
252470.	1.7470	1.7485	50.96	5.208−05
252920.	1.7670	1.7713	53.34	6.948−05
253260.	1.7870	...	...	...
253510.	1.8270	...	...	...
253780.	1.8470	...	...	...

by Dowling via a UNIVAC 1100 Time/Sharing system is given in Table 2. The last two columns in Table 2, labelled "Stress Intensity" and "Growth Rate," correspond to the variables x and y, respectively, for the purpose of conducting a regression analysis as described in the previous section.

To facilitate the calculations of parameters b_1, s^2, MS_R, and the F-ratio for a test of significance of the regression line $Y = b_0 + b_1 x$, a computer program was written in BASIC and implemented on a Tektronix 4051 graphical system (Appendix II) with both tabular and graphical output (Table 3 and Fig. 1). The sample output in Table 3 corresponds to the crack growth rate data given in Table 2 with $n = 43$, the number of data points for the Laboratory 1 test on Man-Ten steel at $R = 0.1$, $P_{max} = 1.60$, and a frequency of 5 Hz. Since the calculated F-ratio ($= 5384.3$) exceeds the critical F (0.95, 1, 41), the regression is found to be significant at a 95 percent confidence level. The computer program also includes an estimate of the standard error of the parameter b_1 [denoted by s.e. (b_1)] defined as

$$\text{estimated s.e.}\,(b_1) = \left\{s^2/\Sigma(x_i - \bar{x})^2\right\}^{1/2} \tag{11}$$

In Fig. 1 the data from Laboratory 1 were fitted with a straight line with slope equal to b_1 and a 95 percent confidence interval for a new observation is shown. This interval, which is centered on Y_k and whose length depends on an estimate of the variance, is given by

$$Y_k \pm t(n-2, 0.975)\left\{1 + \frac{1}{n} + \frac{(x_k - \bar{x})^2}{\Sigma(x_i - \bar{x})^2}\right\}s \tag{12}$$

where $t(n-2, 0.975)$, the 97.5 percent point of a t-distribution with $(n-2)$ degrees of freedom, is appropriate for a two-sided 95 percent level of confidence.[12]

The Tektronix-BASIC program was applied to all seven sets of data; a summary of the characteristics of the regression line with its confidence band for each set of data is given in Table 4. To allow for the formulation of a quantitative approach to assess the "goodness" of agreement among several sets of crack growth data, we choose to define a domain of comparison by specifying x_{min} and x_{max} (Fig. 2). This leads to the notion of a common center of data defined by the midpoint on the x-axis between x_{min} and x_{max}, and a comparison of three characteristic values, namely, the location parameters y_i, the vertical half-width parameters h_i, and the slope intercept parameters p_i, for each set of data. The standard error of the slope of regression, though listed in Table 4 as one of the attributes from the regression analysis, is ignored because of its secondary influence on the nature of the fitted data.

[12] See Ref 4, pp. 23–24.

TABLE 3—*Typical computer printout for regression analysis via a Tektronix-BASIC program (Tektronix 4051) (see Appendix II for program listing).*

```
          *** ANALYSIS OF VARIANCE TABLE ***

N=43               a=0.05

REGRESSION IS SIGNIFICANT

SOURCE             DEGREE   SUM OF SQUARES   MEAN SQUARES       TEST FOR SIG. OF REG.

TOTAL (CORRECTED)    42     8.90282342105

REGRESSION           1      8.83554271199    8.83554271199
................................ (R2=0.992442767212) .......

RESIDUAL             41     0.0672807090621  0.00164099290395   5384.26625167
                                                                CRITICAL F1=4.08

B1 IS SLOPE OF REGRESSION LINE
E(B1)=3.53479378674
V(B1)=0.00232060721568      73.377559592
                                     s.e.(B1)=0.0481726812175   CRITICAL
................................                                T1=2.02
PARAMETERS FOR ESTIMATING AGREEMENT MATRIX
   DOMAIN OF DATA: X-MIN =1.4 X-MAX =1.6
   CENTER OF DATA: X-COORD =1.5 Y-COORD =-5.07242070673
   SLOPE OF REGRESSION LINE =3.53479378674
   VERTICAL HALF-WIDTH OF CONFIDENCE =0.0828477886069
```

Agreement Matrix for Crack Growth Rate Data

To assess whether two sets of data (for example, the ith and the jth) are in good agreement, we propose an *ad hoc* measure A_{ij}, which assigns equal weights to each of the three characteristics defined in the last section. By normalizing the characteristics of the jth set with respect to those of the ith set, the *ad hoc* measure A_{ij} may be defined as

$$A_{ij} = 1 - \sqrt{(1 - y_j/y_i)^2 + (1 - h_j/h_i)^2 + (1 - p_j/p_i)^2} \tag{13}$$

We observe that this definition implies a perfect agreement if $A_{ij} = 1.0$, and that, in general, A_{ij} lies between 1.0 and $-\infty$. By adopting a threshold for good agreement at, for example, 0.6, which is subjective and completely arbitrary, the proposed measure A_{ij} can nevertheless be interpreted to yield interesting information as is shown in the following numerical example:

$$A = [A_{ij}] = \begin{vmatrix} 1 & 0.82 & \cdots & 0.65 & 0.79 & \cdots & \cdots \\ 0.79 & 1 & 0.65 & \cdots & 0.72 & \cdots & \cdots \\ \cdots & \cdots & 1 & \cdots & \cdots & \cdots & \cdots \\ 0.73 & 0.65 & \cdots & 1 & 0.82 & \cdots & \cdots \\ 0.78 & 0.78 & \cdots & 0.80 & 1 & \cdots & \cdots \\ \cdots & \cdots & \cdots & \cdots & \cdots & 1 & 0.81 \\ \cdots & \cdots & \cdots & \cdots & \cdots & 0.80 & 1 \end{vmatrix} \tag{14}$$

The matrix A in Eq 14 corresponds to the seven sets of data from the SAE test program (Table 4). Whenever the value of an entry A_{ij} falls below the threshold value of, for example, 0.6, the entry is suppressed to show the lack of good agreement between the ith and the jth sets of data. The matrix A implies that the seven sets of data seem to fall into three classes: (*1*) Class A—Laboratories 1, 2, 4, and 5, (*2*) Class B—Laboratory 3, and (*3*) Class C—Laboratory 7, Specimens 1 and 2. The fact that Laboratory 3 is in a class by itself does not necessarily mean its measurement is inferior. As a matter of fact, when we plot the y-coordinate of the center of data versus the slope of regression line with their appropriate bands[13] for all seven sets of data in Fig. 3, we see immediately that Laboratory 3 stands out as the source of the "best" data in the sense of a "smallest" band of uncertainty in both y-coordinate and the slope of the regression line.

[13]The bands for the slope of the regression line are based on the standard error taken from Table 4 with the application of a 95 percent confidence factor. The bands for the y-coordinate of the center data are the vertical half-width taken from Table 4.

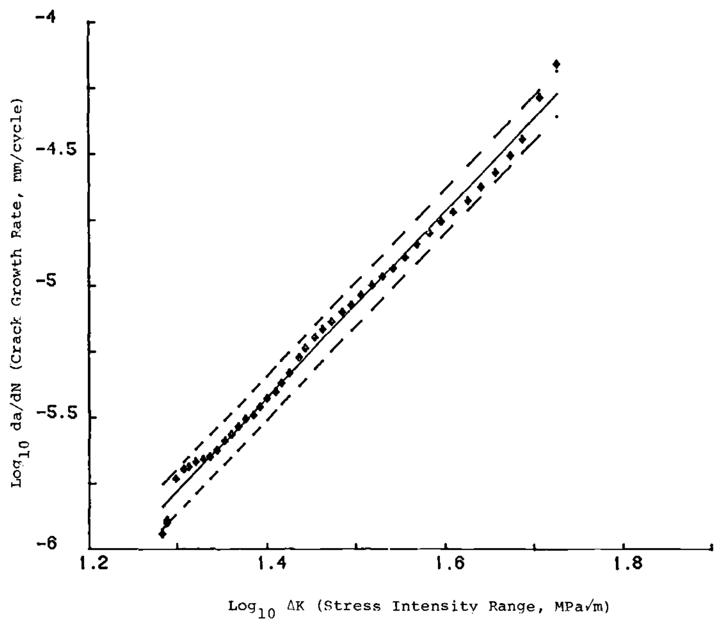

FIG. 1—*Typical computer-aided plot of* da/dN *versus* ΔK *data and the regression line with 95 percent confidence band (data from Laboratory 1, Man-Ten,* R = *0.1,* P_{max} = *1.60, 5 Hz).*

TABLE 4—*Summary of characteristics from regression analysis of seven sets of Man-Ten data (*R=*0.1,* P_{max} = *1.60, 5 Hz).*

		Location of Center of Data			Slope of Regression	
Lab.	Specimen	x-Co-ordinate $Log_{10}\Delta K$	y-Co-ordinate $Log_{10}da/dN$	Vertical Half-Width of 95% Confidence Band	Mean	Standard Error
1	1	1.50	−5.072	±0.083	3.535	0.048
	2	...	...	...	...	...
2	1	1.50	−5.131	±0.074	3.038	0.041
	2	...	...	...	...	...
3	1	1.50	−5.067	±0.049	3.218	0.027
	2	...	...	...	...	...
4	1	1.50	−4.969	±0.111	3.263	0.057
	2	...	...	...	...	...
5	1	1.50	−4.924	±0.094	3.014	0.056
	2	...	...	...	...	...
7	1	1.50	−5.143	±0.259	3.760	0.142
	2	1.50	−5.072	±0.223	4.221	0.175

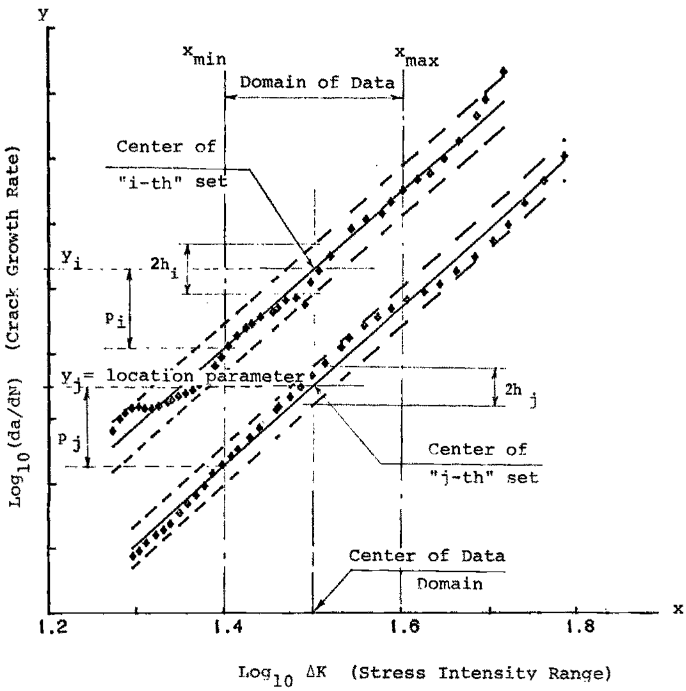

FIG. 2—*Characterization of two sets of fatigue crack growth data for evaluating an agreement index* A_{ij}.

Interlaboratory Data Analysis—An Example

As observed in the section on Regression Analysis of SAE Data, the lack of replica data in the SAE test program makes it impossible to conduct an interlaboratory data analysis in the sense of Mandel [3]. It is still instructive, however, to illustrate Mandel's analysis by introducing fictitious data to supplement the SAE data. In particular, let us consider a mathematical example of estimating the within-laboratory and between-laboratory variances of the slope of the regression line as calculated earlier for the seven sets of SAE data ($R = 0.1$, $P_{max} = 1.60$, frequency = 5 Hz; Man-Ten). Based on values of the mean slope listed in Table 4, we assemble a table of data in Table 5 by permitting Laboratories 1 to 5 to borrow data from their neighbors (1 from 2, 2 from 3, etc., through 5 from 1). If m is the number of replicas used in each laboratory ($m = 2$ in this case), Mandel's analysis for a k-laboratory data set essentially depends on the variance formula

$$\sigma_{\bar{X}}^2 = \sigma_B^2 + \sigma_W^2/m \tag{15}$$

that is,

$$\begin{matrix}\text{variance} \\ \text{of the mean}\end{matrix} = \begin{matrix}\text{between-laboratory} \\ \text{variance}\end{matrix} + (1/m) \begin{matrix}\text{within-laboratory} \\ \text{variance}\end{matrix}$$

Let $\bar{X}_i$ be the average of the data from the ith laboratory, $i = 1, \ldots, k$, and $\bar{\bar{X}}$ be the mean of the laboratory averages, then the total variance $\sigma_{\bar{X}}{}^2$ can be estimated by

$$s_{\bar{X}}{}^2 = \left\{ \sum_{i=1}^{k} (\bar{X}_i - \bar{\bar{X}})^2 \right\} / (k - 1) \tag{16}$$

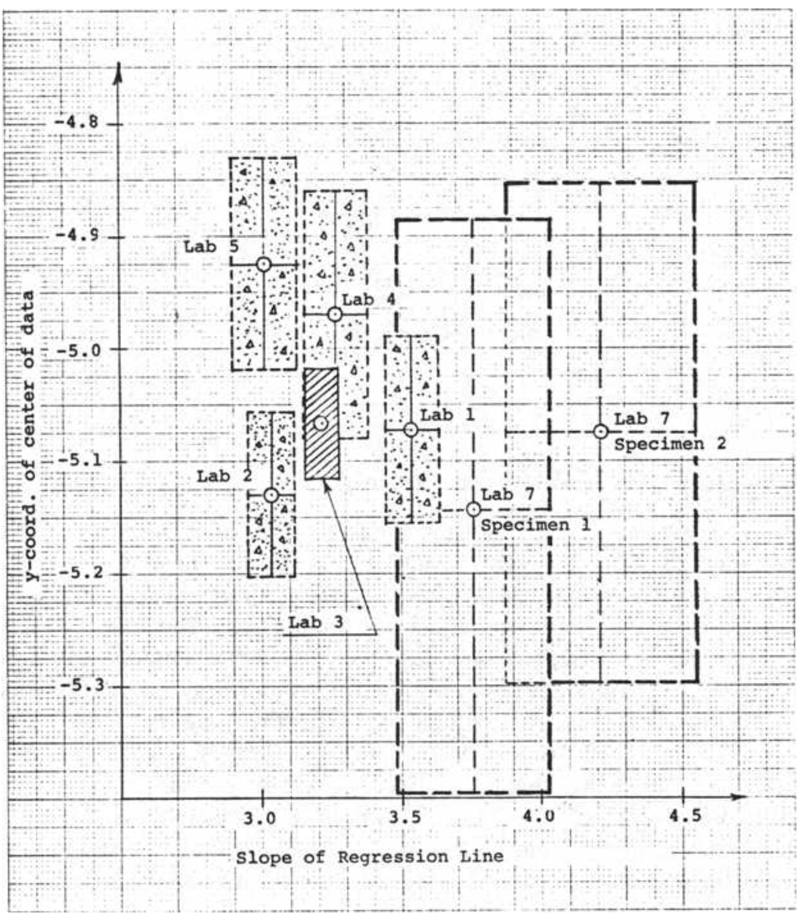

FIG. 3—*Characteristics of fatigue crack growth data from six laboratories with 95 percent confidence limits (data obtained from Man-Ten,* R = *0.1,* P_{max} = *1.60, 5 Hz).*

TABLE 5—*Example of within-laboratory and between-laboratory variance analysis for slope of regression line (borrowed data).*

Lab.	Data		Average ($\bar{X}$)	Standard Deviation	Variance
1	3.535	(3.038)[a]	3.2865	0.3514	0.12348
2	3.038	(3.218)[a]	3.1280	0.1273	0.01621
3	3.218	(3.263)[a]	3.2405	0.0318	0.00101
4	3.263	(3.014)[a]	3.1385	0.1761	0.03101
5	3.014	(3.535)[a]	3.2745	0.3684	0.13572
7	3.760	4.221	3.9905	0.3260	0.10628
			Average $= \bar{\bar{X}} = 3.3431$		$\Sigma = 0.41371$
			Standard Deviation $= s_{\bar{X}} = 0.32425$		$s^2_{\text{Rep}} = \Sigma/6 = 0.06895$
					$s_W = \sqrt{0.06895} = 0.2626$

$$s_B = \sqrt{(0.32425)^2 - \frac{0.06895}{2}} = 0.2658$$

[a] For the purpose of this exercise, laboratory without replica is permitted to "borrow" data from a neighboring laboratory to complete the data requirement of an interlaboratory analysis. For example, the data for the replica of Laboratory 1 comes from Laboratory 2, that from Laboratory 2 comes from Laboratory 3, etc., until we reach Laboratory 5 whose data comes from Laboratory 1.

Let s_i^2 be the variance of the data from the ith laboratory, $i = 1, \ldots, k$, then the within-laboratory variance σ_W^2 (sometimes known as the replication variance σ^2_{Rep}) can be estimated as

$$s_W^2 = \left\{\sum_{i=1}^{k} s_i^2\right\}/k \tag{17}$$

By Eq 15 the between-laboratory variance is found as illustrated in the numerical example of Table 5.

As explained by Mandel [3], the within-laboratory variance is a measure of the "repeatability" of the test, and the between-laboratory variance is a measure of the "reproducibility" of the measurement. Both measures are essential to the study of the "precision" of the method of measurement. More importantly, the estimates of the two variances, s_B^2 and s_W^2, can be used directly to determine in what way the precision of the test method can be improved through the running of replicate measurements. Let us rewrite Eq 15 in Mandel's notation as

$$\sigma_m^2 = (\sigma_W^2/m) + \sigma_B^2 \tag{18}$$

where σ_m^2 denotes the total variance for an average of m replicates. Let σ_1^2 be the total variance for a single measurement, then $\sigma_1^2 > \sigma_m^2$ for $m > 1$.

One can now define an improvement in the total variance, in percent, due to an increase in m as

$$100 \frac{\sigma_1{}^2 - \sigma_m{}^2}{\sigma_1{}^2} = 100 \frac{m - 1}{m} \frac{1}{1 + (\sigma_B{}^2/\sigma_W{}^2)} \tag{19}$$

Equation 19 can be used to guide the planning of a second round of interlaboratory testing after the initial round yields estimates of both $\sigma_B{}^2$ and $\sigma_W{}^2$. For example, if the goal is to improve the total variance by 30 percent for the series of measurements discussed in Table 5, the ratio $\sigma_B{}^2/\sigma_W{}^2$ can be estimated by the ratio $s_B{}^2/s_W{}^2$ or $0.07066/0.06895 = 1.025$. Equation 19 then yields $m > 2.6$, or a 3-replica series would suffice. It is also useful to know that the most one can improve, by allowing m to go to infinity, is about 49 percent, which indicates perhaps that a 3-replica series may be the most economical.

Discussion

By introducing a quantitative approach to assessing the goodness of agreement of different sets of crack growth rate data, we aim to separate the contributions from different laboratories into distinct classes, each of which is more or less uniform in the sense of the *ad hoc* measure A_{ij}. It is reasonable to speculate that the between-laboratory variance within each class should be smaller than for all classes combined. This is based on the notion that for the latter case the inhomogeneity of laboratory practice necessarily leads to a larger estimate of the between-laboratory variance.

To show that this speculation is indeed valid, it would be interesting to apply our approach to a 15-laboratory, 78-test interlaboratory crack growth rate testing program sponsored by ASTM Committee E-24 on Fracture Testing [*2*]. As noted by Clark and Hudak [*2*], two of their techniques in assessing the interlaboratory variability (namely, the graphical comparison and the standard deviation analysis) are limited to the characterization of the variability at specific ΔK-levels. Unfortunately, when they resorted to a third technique (the least-square regression analysis) they neither tested their results for lack of fit nor were they aware of the procedure subsequently advocated by Mandel [*3*] in conducting an appropriate interlaboratory level-by-level data analysis.[14] Using the concept of an agreement matrix defined in this paper, the 15-laboratory data of Ref *2* may be partitioned into classes to reveal the magnitudes of the interlaboratory variabilities for all classes as well as for the entire set of test data. This partitioning of laboratories into more homogeneous subclasses would encourage the investigators to find, within

[14] See ASTM Practice for Conducting an Interlaboratory Test Program to Determine the Precision of Test Methods (E 691-79) for a more up-to-date reference on interlaboratory data.

each subclass, commonalities which may be causes of large variabilities. The investigation is also helpful to identify data which may not be good enough to contribute usefully to an interlaboratory test program.

In attempting to illustrate a new approach in data analysis, we ignored the important fact documented by Wei et al [5] that considerable variability in fatigue crack growth rate can result from the choice of crack length measurement interval and from the associated data-processing procedures. Our goal is limited to calling to the attention of the engineering test community that two or more replicas are needed to constitute a credible test program. The study of the variability of a test program can be related to the economic aspect of the engineering decision-making process [6]. It is hoped that our results in this investigation and the call for more replicas will eventually lead to the possibility of a rational engineering safety factor based on a study of laboratory and field variabilities.

Conclusion

The fitting of fatigue crack growth rate data by a straight line can be tested both for the significance of the regression line and for a possible lack of fit if either a prior estimate of the error variance is available or there are repeat measurements based on two or more replicas per test. Comparison of crack growth rate data from different laboratories can be made on an *ad hoc* yet quantitative basis through the use of an agreement matrix. This quantitative approach can divide the different laboratories into classes, each of which is likely to have a smaller interlaboratory variability than the entire set of laboratories. Mandel's approach [3] to interlaboratory data analysis can be used to guide the planning of more replicate measurements to improve the precision of crack growth rate testing results described in Refs *1* and *2*.

Acknowledgments

We wish to thank Dr. James Lechner of the National Bureau of Standards for critical comments and Ivan Fong of the Massachusetts Institute of Technology for computer programming assistance during the course of this investigation.

References

[*1*] Dowling, N. E. and Walker, H., "Fatigue Crack Growth Rate Testing of Two Structural Steels," *SAE Transactions*, Society of Automotive Engineers, 1979, Paper No. 790459.

[*2*] Clark, W. G., Jr., and Hudak, S. J., Jr., *Journal of Testing and Evaluation*, Vol. 3, No. 6, 1975, pp. 454-476.

[*3*] Mandel, J., *ASTM Standardization News*, Vol. 5, No. 3, 1977, p. 17.

[4] Draper, N. E. and Smith, H., *Applied Regression Analysis*, John Wiley, New York, 1966.
[5] Wei, R. P., Wei, William, and Miller, G. A., *Journal of Testing and Evaluation*, Vol. 7, No. 2, 1979, pp. 90-95.
[6] Fong, J. T., *Nuclear Engineering and Design*, Vol. 51, 1978, pp. 45-54.

APPENDIX I

FORTRAN Program for Reducing Crack Length versus Cycle Data to *da/dN* versus ΔK by Incremental Polynomial Method

```
      DIMENSION A(100,3),C(7),ID(30),X(100),Y(100)
  100 FORMAT(30A1,I6)
  101 FORMAT(I3)
  102 FORMAT(5(F6.0,F9.0))
  103 FORMAT(/21X,3 0A1)
  104 FORMAT(/20X,'COMPACT SPECIMEN H/W=0.486')
  105 FORMAT(/20X,'COMPACT SPECIMEN H/W=0.6')
  109 FORMAT(/' DELTA P=',F9.4,' KIPS  PMIN=',F9.4,' KIPS  R=',F7.4)
  110 FORMAT(' B=',F8.4,' INCHES  W=',F8.4,' INCHES  A0=',F8.4,' INCHES'
     1)
  111 FORMAT(' TESTING FREQUENCY=',F8.4,' HERTZ')
  112 FORMAT(F9.0,F14.4)
  113 FORMAT(F9.0,F14.4,F11.4,F12.2,1PE15.3)
  114 FORMAT(/'   TOTAL',11X,'CRACK LENGTH',8X,'STRESS',6X,'GROWTH',/
     1'  CYCLES',7X,'OBSERVED  CALCULATED  INTENSITY',5X,'RATE')
  115 FORMAT(1H1)
  116 FORMAT(6F10.0)
  120 FORMAT(' ',9X,'CRACK GROWTH RATE AND STRESS INTENSITY DATA REDUC-
      TION',/20X,'INCREMENTAL POLYNOMIAL FOR DA/DN')
 1000 FORMAT(F8.4,E12.4)
  998 READ(5,100,END=999)ID,N
      READ(5,101)IST
      READ(5,116)PMIN,DELP,F,B,W,A0
      READ(5,102)(A(I,2),A(I,1),I=1,N)
      NN=N-3
      DO 1 I=1,N
      A(I,2)=A(I,2)+A0
    1 CONTINUE
      DO 2 I=4,NN
      C1=(A(I-3,1)+A(I+3,1))/2.
      C2=(A(I+3,1)-A(I-3,1))/2.
      DO 3 J=1,7
      C(J)=(A(I-4+J,1)-C1)/C2
    3 CONTINUE
      SX=0.
      SX2=0.
      SX3=0.
      SX4=0.
      SXY=0.
      SX2Y=0.
      SY=0.
      DO4 J=1,7
      SX=SX+C(J)
      SX2=SX2+C(J)**2
      SX3=SX3+C(J)**3
      SX4=SX4+C(J)**4
      SXY=SXY+C(J)*A(I-4+J,2)
      SX2Y=SX2Y+C(J)**2*A(I-4+J,2)
      SY=SY+A(I-4+J,2)
    4 CONTINUE
      DEN=7.*(SX2*SX4-SX3**2)-SX*(SX*SX4-SX2*SX3)+SX2*(SX*SX3-SX2**2)
      BO=(SY*(SX2*SX4-SX3**2)-SX*(SXY*SX4-SX2Y*SX3)+SX2*(SXY*SX3-SX2
```

```
      1*SX2Y))/DEN
      B1=(7.*(SXY*SX4-SX3*SX2Y)-SY*(SX*SX4-SX3*SX2)+SX2*(SX*SX2Y-SX2*SXY
      1))/DEN
      B2=(7.*(SX2*SX2Y-SX3*SXY)-SX*(SX*SX2Y-SX2*SXY)+SY*(SX*SX3-SX2**2
      1))/DEN
      A(I,3)=B0+B1*C(4)+B2*C(4)**2
      Y(I)=B1/C2+2.*B2*(A(I,1)-C1)/C2**2
      AW=A(I,3)/W
      GO TO (10,20),IST
   10 IF(AW.GT.0.7)GO TO 21
      FAW=30.96-195.8*AW+730.6*AW**2-1186.3*AW**3+754.6*AW**4
      X(I)=DELP*SQRT(A(I,3))/B/W*FAW
      GO TO 2
   20 IF(AW.GT.0.7)GO TO 21
      FAW=29.6*AW**0.5-185.5*AW**1.5+655.7*AW**2.5-1017.*AW**3.5+
     1638.9*AW**4.5
      X(I)=DELP/B/SQRT(W)*FAW
      GO TO 2
   21 X(I)=DELP*(5.*W+3.*A(I,3))/(2.*B*(W-A(I,3))**(3./2.))
      GO TO 2
    2 CONTINUE
      R=PMIN/(PMIN+DELP)
      WRITE(6,115)
      WRITE(6,120)
      WRITE(6,103)(ID(I),I=1,30)
      IF(IST.EQ.1)WRITE(6,104)
      IF(IST.EQ.2)WRITE(6,105)
      WRITE(6,109)DELP,PMIN,R
      WRITE(6,110)B,W,A0
      WRITE(6,111)F
      WRITE(6,114)
      DO 11 I=1,3
      WRITE(6,112)(A(I,J),J=1,2)
   11 CONTINUE
      DO 12 I=4,NN
      A(I,4)=A(I,4)/1000.
      WRITE(6,113 )(A(I,J),J=1,3),X(I),Y(I)
   12 CONTINUE
      NN=NN+1
      DO 13 I=NN,N
      WRITE(6,112)(A(I,J),J=1,2)
   13 CONTINUE
      GO TO 998
  999 CONTINUE
      END
```

APPENDIX II

Tektronix-BASIC Program for a Regression Analysis of da/dN versus ΔK Data with Graphical Output

```
1 GO TO 100
4 GO TO 910
8 GO TO 1600
100 INIT
110 PRINT "L  REGRESSION ANALYSIS — STEP 1_"
120 PRINT "ENTER NUMBER OF DATA POINTS:  ";
130 INPUT N1
140 PRINT "ARE THE POINTS ORDERED? [Y OR N]:  ";
150 INPUT A$
```

```
160 PRINT "_ENTER % LEVEL OF CONFIDENCE:  ";
170 INPUT L1
180 PRINT "ENTER 1 IF ONE-SIDED, 2 IF TWO-SIDED:  ";
190 INPUT L2
200 IF L2<>1 AND L2<>2 THEN 180
210 A9=2*(1-L1/100)/L2
220 PRINT "ENTER t(";N1-2;",";A9;") [FROM TABLE]:  ";
230 INPUT T1
240 PRINT "ENTER F(1-A9,";1;",";N1-2;") [FROM TABLE]:  ";
250 INPUT F1
260 PRINT "_ENTER INDEPENDENT VARIABLE SCALAR CONSTANT (1 IF NONE):  ";
270 INPUT P0
280 PRINT "ENTER DEPENDENT VARIABLE SCALAR CONSTANT (1 IF NONE):  ";
290 INPUT Q0
300 C1=0
310 E1=0
320 D1=0
330 P1=0
340 X1=0
350 X2=0
360 Y1=0
370 DIM P(N1),Q(N1),X(N1),Y(N1),Z(N1),C(N1),D(N1),E(N1),V(N1),W(N1)
380 PRINT "L INDEPENDENT VARIABLE","DEPENDENT VARIABLE"
390 FOR I=1 TO N1
400 IF INT((I-1)/30)<>(I-1)/30 OR I=1 THEN 420
410 PAGE
420 PRINT " X(";I;") = ";
430 INPUT P(I)
440 P(I)=P(I)*P0
450 X(I)=LGT(P(I))
460 X1=X1+X(I)
470 X2=X2+X(I)*2
480 PRINT "KII  Y(";I;") = ";
490 INPUT Q(I)
500 Q(I)=Q(I)*Q0
510 Y(I)=LGT(Q(I))
520 Y1=Y1+Y(I)
530 P1=P1+X(I)*Y(I)
540 NEXT I
550 X1=X1/N1
560 Y1=Y1/N1
570 B1=(P1-N1*X1*Y1)/(X2-N1*X1*X1)
580 FOR I=1 TO N1
590 C(I)=X(I)-X1
600 C1=C1+C(I)*2
610 D(I)=Y(I)-Y1
620 D1=D1+D(I)*2
630 E(I)=B1*(X(I)-X1)
640 E1=E1+E(I)*2
650 Z(I)=Y1+E(I)
660 NEXT I
670 PAGE
680 PRINT "ENTER DOMAIN OF DATA FOR ESTIMATING AGREEMENT MATRIX"
690 PRINT "DOMAIN X-MIN (A1) =";
700 INPUT A1
710 IF A1<X(1) THEN 690
720 PRINT "DOMAIN X-MAX (A2) =";
730 INPUT A2
```

```
740 IF A2)X(N1) THEN 720
750 A=(A1+A2)/2
760 R2=E1/D1
770 S2=(D1-E1)/(N1-2)
780 F2=E1/S2
790 V2=S2/C1
800 V1=SQR(V2)
810 T2=ABS(B1/V1)
820 FOR I=1 TO N1
830 V(I)=S2*(1+1/N1+(X(I)-X1)*2/C1)
840 W(I)=SQR(V(I))
850 IF X(I)(A THEN 880
860 IF X(I-1))A THEN 880
870 M=I-1
880 NEXT I
890 B=Z(M)+B1*(A-X(M))
900 S=W(M)+(W(M+1)-W(M))*(A-X(M))/(X(M+1)-X(M))
910 PRINT @41:"L              *** ANALYSIS OF VARIANCE TABLE ***"
920 PRINT @41:
930 PRINT @41:
940 PRINT @41:"N=";N1,"a=";A9
950 PRINT @41:
960 IF R2)0.5 THEN 990
970 PRINT @41:"REGRESSION IS NOT SIGNIFICANT"
980 GO TO 1000
990 PRINT @41:"REGRESSION IS SIGNIFICANT"
1000 PRINT @41:
1010 PRINT @41:
1020 PRINT @41:
1030 PRINT @41:"SOURCE","DEGREE","SUM OF SQUARES","MEAN SQUARES";
1040 PRINT @41:"              TEST FOR SIG. OF REG. "
1050 PRINT @41:
1060 PRINT @41:
1070 PRINT @41:"TOTAL (CORRECTED)",N1-1,D1
1080 PRINT @41:
1090 PRINT @41:
1100 PRINT @41:"REGRESSION",1,E1,E1
1110 PRINT @41:
1120 PRI @41:"........................ (R2=";R2;") ........................"
1130 PRINT @41:
1140 PRINT @41:
1150 PRINT @41:
1160 PRINT @41:"RESIDUAL",N1-2,D1-E1,S2;"         ";F2
1170 PRINT @41:" "," "," ","                    CRITICAL F1=";F1
1180 PRINT @41:
1190 PRINT @41:
1200 PRINT @41:"B1 IS SLOPE OF REGRESSION LINE"
1210 PRINT @41:
1220 PRINT @41:"E(B1)=";B1," "," ","V(B1)=";V2p"                    ";T2
1230 PRINT @41:" "," "," ","s.e.(B1)=";V1;"          CRITICAL T1=";T1
1240 PRINT @41:
1250 PRINT @41:"..........................................."
1260 PRINT @41:
1270 PRINT @41:
1280 PRINT @41:"PARAMETERS FOR ESTIMATING AGREEMENT MATRIX"
1290 PRINT @41:
1300 PRINT @41:"     DOMAIN OF DATA: X-MIN =";A1;"  X-MAX =";A2
1310 PRINT @41:
```

```
1320 PRINT @41:"      CENTER OF DATA: X-COORD =";A;"   Y-COORD =";B
1330 PRINT @41:
1340 PRINT @41:"      SLOPE OF REGRESSION LINE =";B1
1350 PRINT @41:
1360 PRINT @41:"      VERTICAL HALF-WIDTH OF CONFIDENCE =";T1*S
1370 FOR I=1 TO 5
1380 PRINT @41:
1390 NEXT I
1400 PRINT @41:"L                ***** INPUT DATA *****"
1410 PRINT @41:
1420 PRINT @41:
1430 PRINT @41:"INDEPENDENT VARIABLE","DEPENDENT VARIABLE"
1440 PRINT @41:
1450 FOR I=1 TO N1
1460 PRINT @41:P(I)," ",Q(I)
1470 NEXT I
1480 FOR I=1 TO 5
1490 PRINT @41:
1500 NEXT I
1510 PRINT @41:"L             *** OUTPUT INFORMATION FOR PLOTTING ***"
1520 PRINT @41:
1530 PRINT @41:
1540 PRINT @41:"LOG(INDEP. VAR.)","LOG(DEP. VAR.)","FITTED VALUE";
1550 PRINT @41:"        STAND. DEV.          ERROR BOUND"
1560 PRINT @41:
1570 FOR I=1 TO N1
1580 PRINT @41:X(I),Y(I),Z(I),W(I);"          ";T1*W(I)
1590 NEXT I
1600 PRINT "GRAPHICS PLOT PARAMETERS"
1610 PRINT "X-MIN =  ";
1620 INPUT M1
1630 PRINT "X-MAX =  ";
1640 INPUT M2
1650 PRINT "X-TIC MARK INTERVAL =  ";
1660 INPUT M3
1670 PRINT
1680 PRINT "Y-MIN =  ";
1690 INPUT M4
1700 PRINT "Y-MAX =  ";
1710 INPUT M5
1720 PRINT "Y-TIC MARK INTERVAL =  ";
1730 INPUT M6
1740 WINDOW M1,M2,M4,M5
1750 VIEWPORT 10,120,10,90
1760 AXIS @1:M3/2,M6/2
1770 FOR I=M1 TO M2 STEP M3
1780 MOVE @1:I,M4
1790 PRINT @1:"JH";I
1800 NEXT I
1810 FOR I=M4 TO M5 STEP M6
1820 MOVE @1:M1,I
1830 PRINT @1:"HHHHH";I
1840 NEXT I
1850 FOR I=1 TO N1
1860 MOVE @1:X(I),Y(I)
1870 RDRAW @1:0,0
1880 SCALE 1,1
1890 RMOVE @1:0,0.5
```

```
1900 RDRAW @1:-0.5,-0.5
1910 RDRAW @1:0.5,-0.5
1920 RDRAW @1:0.5,0.5
1930 RDRAW @1:-0.5,0.5
1940 WINDOW M1,M2,M4,M5
1950 NEXT I
1960 M7=1.0E+300
1970 FOR I=1 TO N1
1980 M7=M7 MIN X(I)
1990 NEXT I
2000 FOR J=1 TO N1
2010 IF X(J)=M7 THEN 2030
2020 NEXT J
2030 M8=Z(J)
2040 M9=-1.0E+300
2050 FOR I=1 TO N1
2060 M9=M9 MAX X(I)
2070 NEXT I
2080 FOR J=1 TO N1
2090 IF X(J)=M9 THEN 2110
2100 NEXT J
2110 M0=Z(J)
2120 MOVE @1:M7,M8
2130 DRAW @1:M9,M0
2140 FOR H=-1 TO 1 STEP 2
2150 FOR I=1 TO N1
2160 IF A$="N" THEN 2200
2170 IF INT(I/2)<>I/2 THEN 2200
2180 DRAW @1:X(I),Z(I)+T1*W(I)*H
2190 GO TO 2220
2200 MOVE @1:X(I),Z(I)+T1*W(I)*H
2210 RDRAW @1:0,0
2220 NEXT I
2230 NEXT H
2240 PRINT
2250 PRINT
2260 PRINT "DO YOU WISH TO STORE THIS DATA ON TAPE? [Y OR N]: ";
2270 INPUT B$
2280 IF B$="N" THEN 2350
2290 PRINT "ENTER TAPE FILE NUMBER: ";
2300 INPUT F0
2310 FIND F0
2320 FOR I=1 TO N1
2330 WRITE P(I),Q(I)
2340 NEXT I
2350 END
```

D. F. Ostergaard,[1] *J. R. Thomas,*[1] *and B. M. Hillberry*[1]

Effect of Δa-Increment on Calculating da/dN from a versus N Data

REFERENCE: Ostergaard, D. F., Thomas, J. R., and Hillberry, B. M., **"Effect of Δa-Increment on Calculating da/dN from a versus N Data,"** *Fatigue Crack Growth Measurement and Data Analysis, ASTM STP 738,* S. J. Hudak, Jr., and R. J. Bucci, Eds., American Society for Testing and Materials, 1981, pp. 194-204.

ABSTRACT: Data from a previously reported study were analyzed to determine the effect of the Δa-increment on the error in calculating the fatigue crack growth rate from recorded a versus N data. The data had been recorded from 68 replicate fatigue crack growth tests on center crack panels of 2024-T3 aluminum alloy using a Δa-increment of 0.2 mm. Two different differentiation methods were considered, the secant method and the quadratic seven-point incremental polynomial method. The influence of the Δa-increment was determined by evaluating da/dN using all the data, every second, every fourth, every eighth, and every sixteenth data point. The minimum error for calculating da/dN was found to be for Δa between 0.8 and 1.6 mm. An evaluation of the type of distribution for da/dN showed that of the five distributions considered no single distribution adequately represented all da/dN regardless of the Δa-increment.

KEY WORDS: fatigue, growth rate, measurement, data analysis

The fracture mechanics approach to the analysis of fatigue crack propagation has become a valuable tool in establishing design criteria and structural integrity. It also serves as a valuable tool for the selection and evaluation of materials. This approach relies on an accurate knowledge of the fatigue crack propagation behavior of the material as determined from laboratory tests. However, inherent variability in the fatigue behavior, variability of test conditions, and variability of data collection and analysis procedures result in considerable variation in the resulting crack propagation rate.

Fatigue crack propagation data are generally collected by recording the crack length and corresponding number of cycles under specified test condi-

[1]Graduate research assistant, graduate research assistant, and Professor of Mechanical Engineering, respectively, School of Mechanical Engineering, Purdue University, West Lafayette, Ind. 47907.

tions. From this the crack growth rate is determined using some differentiation scheme; the results are then presented as the growth rate (da/dN) versus the corresponding applied stress intensity [K (or ΔK)]. In the application to design and evaluation of structures the fatigue crack growth rate is integrated to obtain either crack growth or life.

To obtain valid crack growth rate data it is necessary to carefully control test conditions. Hudak et al [*1*],[2] working in cooperation with ASTM Committee E-24 on Fracture Testing and the Air Force Materials Laboratory, have recently completed the development of a tentative test method for crack growth rate testing which has been approved by ASTM. This Tentative Test Method for Constant-Load-Amplitude Fatigue Crack Growth Rates Above 10^{-8} m/Cycle is designated ASTM E 647-78 T.[3]

The variability in crack growth rate data can be due to a number of factors. In the development of the standard numerous data from several sources were analyzed [*1,2*]. The variability due to data collection and analysis can have a significant effect on the results. Clark and Hudak [*2*] and Wei et al [*3*] studied the influence of the size of the crack length measurement increment and the differentiation method on the variability and bias using a computer simulation for the measured data. It was found that the crack length measurement interval and precision can significantly influence the variability of the resulting growth rate, and that the differentiation method can introduce significant bias in the results.

Virkler et al [*4*] investigated the variability in the number of cycles (N) to grow a crack a specified distance and the crack growth rate. He conducted 68 replicate tests and examined both the distribution of N and da/dN using several differentiation methods. Several different distributions were considered to determine which distribution best represented the data. In Virkler's study the measurement increment was constant.

In the present study, Virkler's data are analyzed to determine the influence of the size of the measurement increment on the error in the crack growth rate determination. In addition, the effect of the Δa-increment on the type of distribution for da/dN is examined.

Virkler's Data

The data set collected by Virkler [*4,5*] consists of crack length versus number of cycles for 68 replicate tests run under identical conditions. The specimens were 152 mm (6 in.) wide, 2.54 mm (0.100 in.) thick, center-crack panels of 2024-T3 aluminum alloy. The specimens were cut from a single lot of material. Each specimen was numbered as it was removed from the shipping crate, then the specimens were tested in a random order as selected by a

[2]The italic numbers in parenthesis refer to the list of references appended to this paper.
[3]ASTM E 647-78 T is reprinted in this volume as Appendix I, pp. 321–339.

computer program which utilized a random number generator. The crack was initiated from an EDM slot in the center of the specimen and grown to a one-half crack length of 9.0 mm. The initial load and load reduction schedule followed to grow the crack to 9.0 mm was identical for each test specimen. Only one end of the crack was measured, with the reference being the centerline of the specimen. Also, only one side of the crack was measured. The entire expected crack path on both sides of the specimen was sealed with clear polyethylene which enclosed a silica gel dessicant to ensure a dry atmosphere at the crack tip.

The crack length was measured with a X150 zoom stereo microscope mounted on a horizontal measuring traverse. A digital resolver on the traverse provided a direct digital output. This output was also connected to a printer which permitted direct, simultaneous recording of the crack length and the number of cycles. The data were recorded by advancing the microscope traverse 0.2 mm and pressing the printer push button when the tip of the crack reached the cross hair in the microscope. The crack was illuminated by a strobe light synchronized with the load.

The tests were run under constant load amplitude condition with the load controlled to within 0.2 percent. The stress ratio was 0.2. Each test was run continously after it was started. The crack was grown from 9.0 to 49.8 mm. From 9.0 to 36.2 mm, data were recorded each 0.2 mm; from 36.2 to 44.2 mm, each 0.4 mm; and from 44.2 to 49.8 mm, each 0.8 mm because of the faster growth rates in the latter regions.

The resolution of the digital traverse was 0.001 mm. A measure of the crack length measurement precision was made by stopping the test at a predetermined crack length and then making 10 repeat measurements from a centerline scribe mark to the crack tip using the microscope and traverse system. This procedure was then repeated for 10 different crack lengths. The mean and standard deviation of each set of 10 repeat measurements was computed, and the error of the original data point was then calculated in terms of this mean and standard deviation. The mean of the errors was

$$\overline{X_e} = 0.00141 \text{ mm}$$

with a standard deviation of

$$\sigma_e = 0.000139 \text{ mm}$$

These results show that the error was less than 1 percent of the Δa-increment.

The a versus N results for the 68 tests are shown in Figure 1.

Effect of Δa-Increment on Crack Growth Rate

The crack growth rate was determined for each test using the secant and the quadratic seven-point incremental polynomial differentiation techniques.

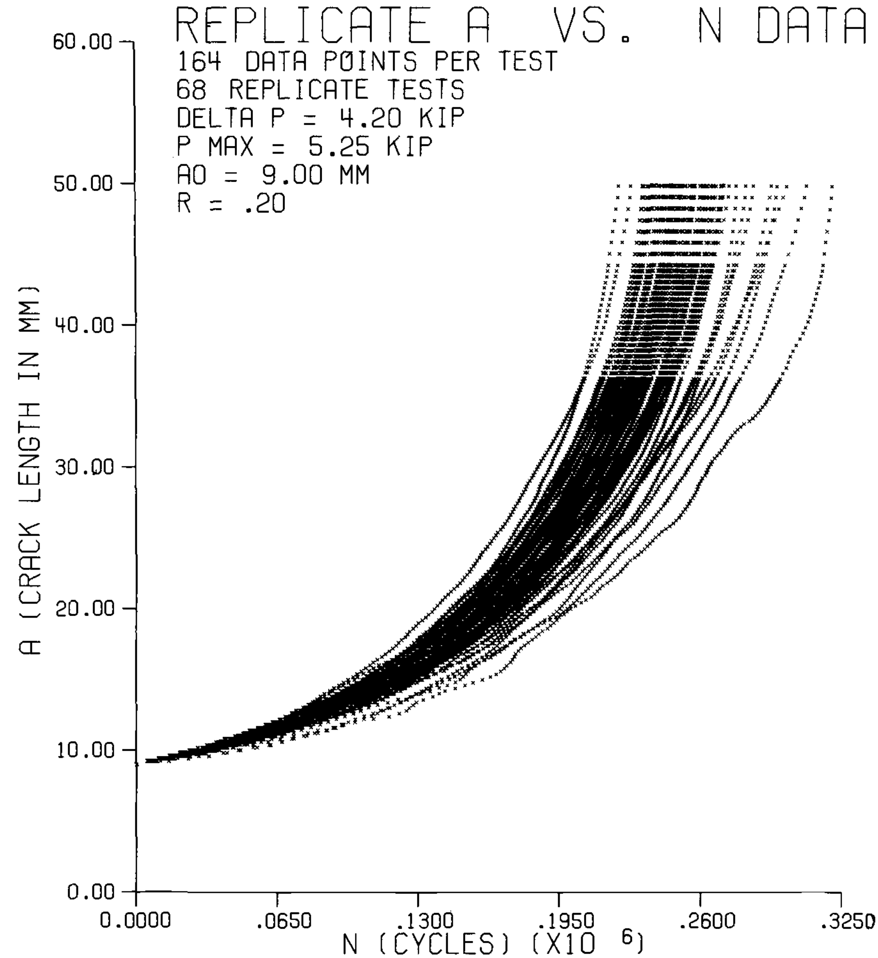

FIG. 1—*Replicate* a *versus* N *data set from Virkler's study* [4].

The resulting crack growth rate was then integrated using a combined Simpson's and trapezoidal method to calculate the number of cycles to grow the crack to the specified length. This calculated number of cycles was then compared with the observed number of cycles to define the error associated with the differentiation method.

The data were analyzed to determine the percent error for each differentiation method first using every data point, $\Delta a = 0.2$ mm; then every second data point, $\Delta a = 0.4$ mm; every fourth data point, $\Delta a = 0.8$ mm; every eighth data point, $\Delta a = 1.6$ mm; and every sixteenth data point, $\Delta a = 3.2$

mm. For each Δa-increment, all 68 tests were evaluated and an average percent error determined. Figure 2 shows typical a versus N data. Figures 3 and 4 show da/dN versus ΔK for the quadratic seven-point differentiation method with $\Delta a = 0.2$ mm and $\Delta a = 0.8$ mm, respectively. Figure 5 shows the average percent error for each differentiation method as a function of Δa. As can be seen, the error initially decreases wth increasing Δa, reaches a minimum, and then increases. This indicates that there is an optimum Δa to minimize the error. It should be mentioned that part of the bias in the results shown here is due to the integration method; however, these results are in close agreement with the results of Wei et al [3] who used a computer simulation. Their results also showed that the quadratic seven-point incremental polynomial method introduced considerably more error than the secant method. This agrees with the results of this study, as can be seen in Fig. 5. The results are also shown in Table 1, which includes the number of times a given Δa provided a minimum error.

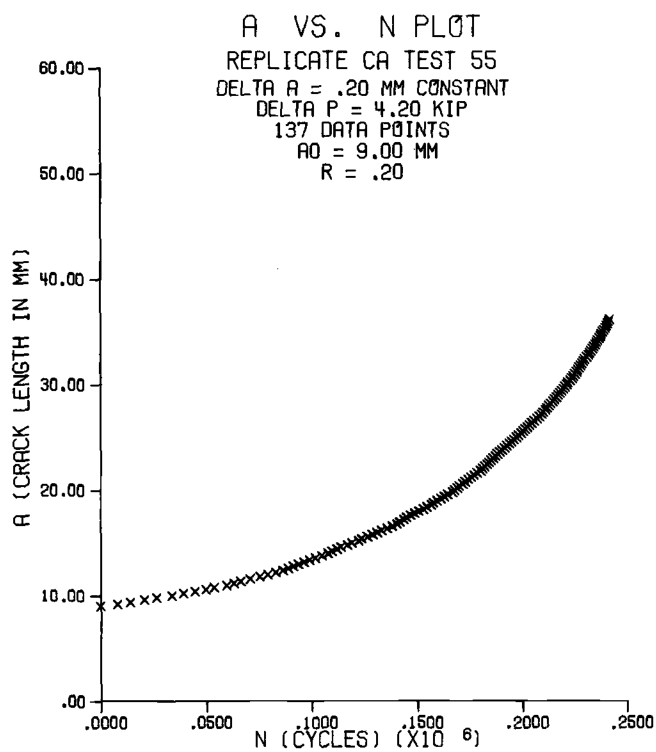

FIG. 2—*Typical* a *versus* N *data (Test No. 55).*

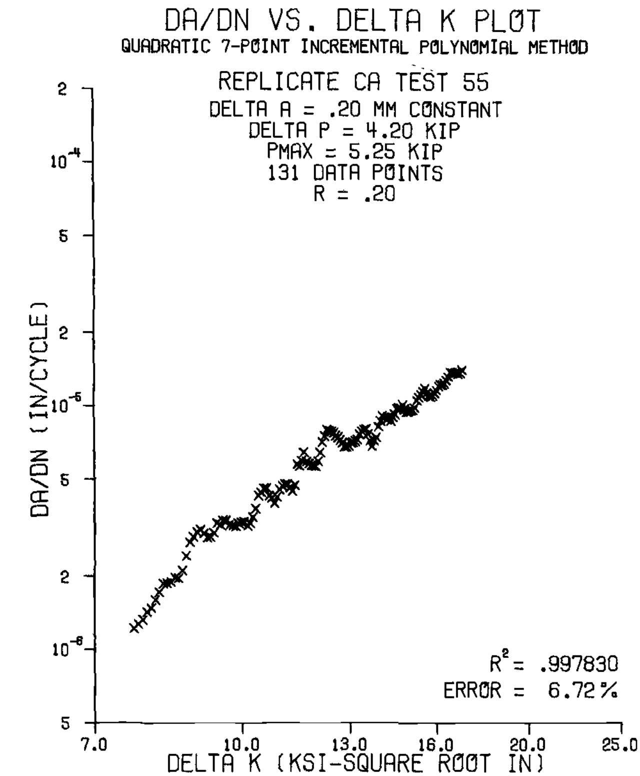

FIG. 3—da/dN *versus* ΔK *for quadratic seven-point incremental polynomial differentiation method with* Δa *equal to 0.2 mm.*

Distribution of *da/dN*

Virkler et al [*4,5*] did an extensive study to determine the type of distribution which best represented the variance in fatigue crack propagation. In his study he developed a computer program in which a set of data is evaluated to determine which of the following distributions best represent the data: 2-parameter normal, 2-parameter lognormal, 3-parameter lognormal, 3-parameter Weibull, or 3-parameter gamma. He found that the distribution which best represented the cycle count data (number of cycles to grow the crack to a given length) was the 3-parameter lognormal. Virkler also examined the *da/dN* distribution method. He found that none of the candidates' distributions could clearly be considered as the best distribution for *da/dN*.

Since the Δa-increment (0.2 mm) was small in Virkler's study, it was an-

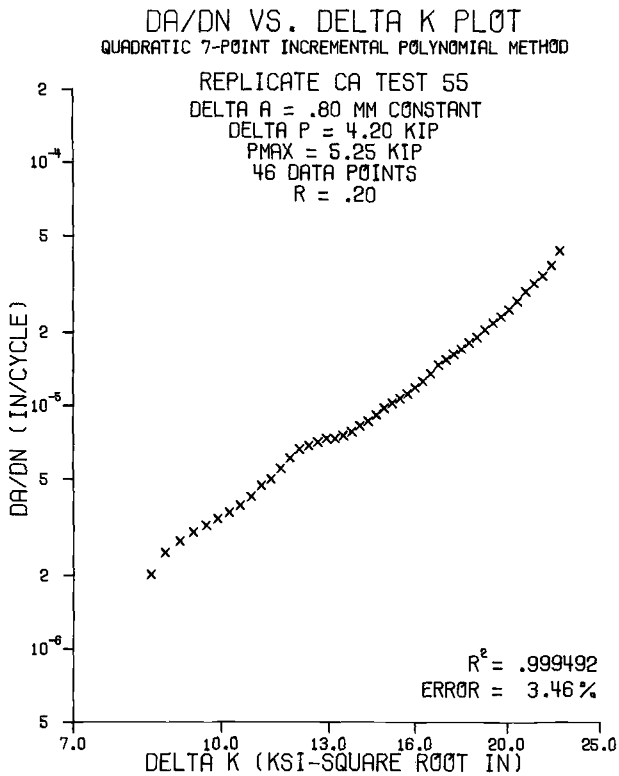

FIG. 4—da/dN *versus* ΔK *for quadratic seven-point incremental polynomial differentiation method with* Δa *equal to 0.8 mm.*

ticipated that experimental error which would have a normal distribution could be adding to the normal material variance. This could change the resulting distribution and make it difficult to identify the true distribution for crack growth rate data. Increasing the Δa-increment reduces the effect of the experimental error; therefore it was anticipated that a clearly definable distribution would be evident at larger Δa-increments.

In this investigation Virkler's distribution determination programs were used to evaluate the *da/dN* data for each Δa-increment considered previously and for each of the two differentiation methods. The goodness-of-fit criteria for each distribution were compared and the distributions ranked at each level.

The distribution determination programs computed the chi-square statistic, the Kolmogorov-Smirnov statistic [*6*], and a closeness parameter [*4*] for each distribution. For each Δa-increment the growth rate would be evaluated at each corresponding a-level for all 68 tests. Then at each a-level

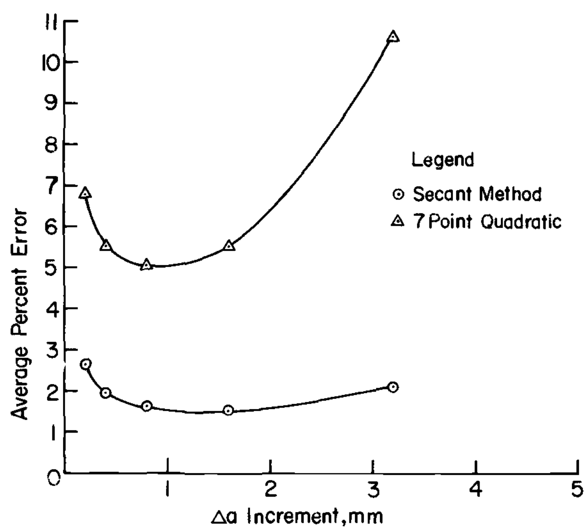

FIG. 5—*Average percent error in calculating* N *from* da/dN *versus the* Δa *increment size.*

TABLE 1—*Effect of* Δa-*increment on percent error.*

	Secant Method			Quadratic 7-point Polynomial Method		
Δa	% Error	Standard Deviation	No. of Times Minimum Error	% Error	Standard Deviation	No. of Times Minimum Error
0.2	2.70	0.33	...	6.83	0.98	...
0.4	1.94	0.24	2	5.53	1.08	15
0.8	1.62	0.31	22	5.21	1.35	32
1.6	1.51	0.42	43	5.51	1.87	21
3.2	2.05	0.75	...	10.67	3.11	...

TABLE 2—*Distribution rankings—secant method.*

	Number of Times Selected as Best Distribution				
Distribution	Δa, 0.2 mm	Δa, 0.4 mm	Δa, 0.8 mm	Δa, 1.6 mm	Δa, 3.2 mm
2-parameter normal	27	19	9	6	6
2-parameter lognormal	37	13	13	3	1
3-parameter lognormal	26	10	2	3	1
3-parameter Weibull	19	20	11	7	2
3-parameter gamma	27	26	6	3	1

the growth rates from each of the 68 tests would be used in the distribution determination programs. The aforementioned three statistics were determined for each distribution at each of the a-levels. Virkler found that the Kolomogorov-Smirnov statistic appeared to provide the best measure of goodness of fit. This statistic was used to rank the distribution in this study.

From these rankings the number of times each distribution was considered to be the best was determined. The rankings were made at each a-level using all 68 replicate tests. These results are given in Table 2 for the secant differentiation method, and in Table 3 for the quadratic seven-point incremental polynomial differentiation method. From these it is seen that increasing the Δa-increment did not lead to a single distribution among the five candidate distributions which best represents the crack growth rate data. In comparing the data it was observed that some of the da/dN data was skewed left, some symmetrical, and some skewed right. This resulted in different distributions being required to represent the data. Also, the Δa-increment did not seem to change this, and therefore it is not evident what the distribution is for da/dN. Furthermore, because of the types of distributions considered, it is not anticipated that some other type of distribution would be found that would better represent da/dN. It may be possible that since ΔN was the dependent variable in the experimental test, $\Delta N/\Delta a$ would show a consistent distribution.

Conclusions

A large data set was analyzed and it was found that there is a Δa measurement increment which produces a minimum error. For these data this Δa was between 0.8 and 1.6 mm. Also, the secant differentiation method showed considerably less error than the quadratic seven-point incremental polynomial method. Of the five candidate distributions considered there was no single distribution that would adequately represent the crack growth rate data. In addition, increasing the Δa-increment did not change this. It does

TABLE 3—*Distribution rankings—7-point incremental polynomial method.*

	Number of Times Selected as Best Distribution				
Distribution	Δa, 0.2 mm	Δa, 0.4 mm	Δa, 0.8 mm	Δa, 1.6 mm	Δa, 3.2 mm
2-parameter normal	22	20	9	7	5
2-parameter lognormal	34	14	13	3	1
3-parameter lognormal	24	13	3	3	1
3-parameter Weibull	29	19	9	6	2
3-parameter gamma	24	22	6	3	2

not appear that the distribution for the variation in *da/dN* is a single type, although this may be in part due to the fact that Δa was constant in these tests, with ΔN being the dependent variable in the experimental tests.

References

[1] Hudak, S. J., Jr., Saxena, A., Bucci, R. J., and Malcolm, R. C., "Development of Standard Methods of Testing and Analyzing Fatigue Crack Growth Rate Data," AFML-TR-78-40, Air Force Materials Laboratory, May 1978.

[2] Clark, W. G., Jr., and Hudak, S. J., Jr., "Variability in Fatigue Crack Growth Rate Testing," ASTM Task Group E24.04.01 report, Sept. 1974.

[3] Wei, R. P., Wei, W., and Miller, G. A., "Effect of Measurement Precision and Data-Processing Procedures on Variability in Fatigue-Crack Growth-Rate Data," *Journal of Testing and Evaluation*, Vol. 7, No. 2, March 1979.

[4] Virkler, D. A., Hillberry, B. M., and Goel, P. K., "The Stastical Nature of Fatigue Crack Propagation," AFFDL-TR-78-43, Air Force Flight Dynamics Laboratory, April 1978.

[5] Virkler, D. A., Hillberry, B. M., and Goel, P. K., *Journal of Engineering Materials and Technology, Transactions of the American Society of Mechanical Engineers*, Vol. 101, April 1979, p. 101.

[6] Massey, F. J., Jr., *Journal of the American Statistical Association*, Vol. 46, 1951, p. 68.

Discussion

L. P. Pook[1] *(written discussion)*—In the statistical analysis of any type of fatigue data serious problems can arise if the statistical model used is not physically realistic.[2] The difficulties which arose in the analysis of the effect of Δa-increment are very much those to be expected from consideration[3] of the analogies between fatigue crack growth and random process theory.[4,5]

The optical method used provides an estimate of crack length by sampling only one point on the crack front. A method, such as potential drop, which averages crack length over the whole crack front would be expected to show much less variability.[3] Physically this means that variability due to crack-front shape changes is reduced. Was there any evidence of crack-front shape changes in the vicinity of irregularities in the *a* versus *N* curves?

Once the precise method of obtaining estimates of crack length is settled it is in principle easy to obtain statistics of the variability in fatigue crack growth rates by sampling the crack length at appropriate intervals. Using the

[1] Senior principal scientific officer, National Engineering Laboratory, Glasgow, Scotland.

[2] Frost, N. E., Marsh, K. J., and Pook, L. P., *Metal Fatigue*, Clarendon Press, Oxford, 1974.

[3] Pook, L. P., *Journal of the Society of Environmental Engineering*, Vol. 15-4, No. 71, 1976, pp. 3-10.

[4] Papoulis, A., *Probability, Random Variables and Stochastic Processes*, McGraw-Hill, London, 1976.

[5] Bendat, J. S. and Piersol, A. G., *Random Data Analysis and Measurement Procedures*, Wiley-Interscience, New York, 1971.

analogy with random process theory it follows that measurements should be made at least once per cycle. That is Δa-increments three orders of magnitude smaller than those actually used and indicated; these would be much smaller than the precision of the measurement used. It is therefore not surprising that it was found difficult to find a satisfactory statistical description of variability in da/dN. It follows that at the present state of the art it is not possible to reconstruct variability in replicate a versus N curves from a knowledge of variability in da/dN versus ΔK curves. From a practical viewpoint it is encouraging that, by selecting appropriate Δa-values, empirical correlations can be found between variability in da/dN and variability in total life.[6]

The shift in the minimum shown in Fig. 5 confirms the prediction[3] that curve fitting increases the effective value of Δa. The bias introduced by the 7-point quadratic method appears to be because the fatigue crack growth process cannot be regarded as statistically stationary as a result of the increase in ΔK with crack length. In future work this could perhaps be avoided by using a "constant K" specimen. A recently proposed disk specimen[7] appears particularly appropriate for this type of work. Finally, some of the variability in the a versus N data could have been caused by lack of symmetry in crack growth about the specimen center line. Was the symmetry of the crack growth checked, or any correction made to ΔK to allow for asymmetry?

D. F. Ostergaard, J. R. Thomas, and B. M. Hillberry (authors' closure)—We want to thank Dr. Pook for his comments and suggestions concerning the difference between the surface crack length and the crack front. It is agreed that there may be a difference and that the potential method would probably show less variability due to its inherent averaging which in itself may reduce the sensitivity. The crack-front shape was not examined in these tests.

We agree with Dr. Pook that precise measurement of the crack length of each cycle would provide the necessary data to determine the actual distribution. The result of not being able to measure this results in effectively adding an averaging filter. In these data, possibly more importantly, the independent variable was Δa, and therefore $\Delta N/\Delta a$ would have probably been the better parameter to examine.

The symmetry of the crack length was monitored carefully in the initial tests. It was found that there was very little variation in the length of each end of the crack and its effect was negligible.

[6]Shaw, W. J. D. and Le May, I., "Fatigue Crack Growth Prediction and Intrinsic Material Scatter," Symposium on Statistical Analysis of Fatigue Data, American Society for Testing and Materials, Pittsburgh, October 1979.

[7]Yarema, S. Ya., *Soviet Materials Science*, Vol. 12, No. 4, 1976, pp. 361-374.

M. S. Miller[1] *and J. P. Gallagher*[1]

An Analysis of Several Fatigue Crack Growth Rate (FCGR) Descriptions

REFERENCE: Miller, M. S. and Gallagher, J. P., "**An Analysis of Several Fatigue Crack Growth Rate (FCGR) Descriptions,**" *Fatigue Crack Growth Measurement and Data Analysis, ASTM STP 738.* S. J. Hudak, Jr. and R. J. Bucci, Eds., American Society for Testing and Materials, 1981, pp. 205–251.

ABSTRACT: This report presents the results of a round-robin life-prediction effort conducted by ASTM Task Group E24.04.04 on FCGR Descriptions. The fatigue crack growth rate (FCGR) data supplied to the task group participants for description purposes are provided along with the definition of the life-prediction effort and results. It is shown that the majority of the participants could describe the FCGR data well enough that the resulting constant amplitude life predictions were within ±20 percent of the test lives for more than 80 percent of the tests.

KEY WORDS: stress ratio, fatigue crack propagation, fracture mechanics, aluminum alloys

Generally, fatigue crack growth rate (FCGR) behavior in metals follows the trend of the schematic (log-log) sigmoidal curve shown in Fig. 1, wherein the FCGR behavior (da/dN) is described as a function of the stress-intensity factor ΔK ($= K_{max} - K_{min}$ if $K_{min} > 0$, $= K_{max}$ otherwise). The behavior (of the FCGR curve) is frequently described as having three regions. Region I is associated with the very slow FCGR behavior in the vicinity of the threshold stress-intensity factor (ΔK_{th}). Region II (frequently referred to as the central region) describes stable, subcritical FCGR behavior which correlates ΔK with minimum scatter. This region of behavior has been extensively studied. Region III describes the behavior exhibited at very high FCGR where the mechanism of growth is influenced by the onset of material fracture.

[1] Engineering aide and group leader, respectively, Service Life Management, Aerospace Mechanics, University of Dayton Research Institute, Dayton, Ohio 45469. Appendixes have been contributed by J. Fitzgerald, F. K. Haake, J. M. Krafft, M. S. Miller, L. Mueller, J. C. Newman, A. Saxena, and M. L. Vanderglass.

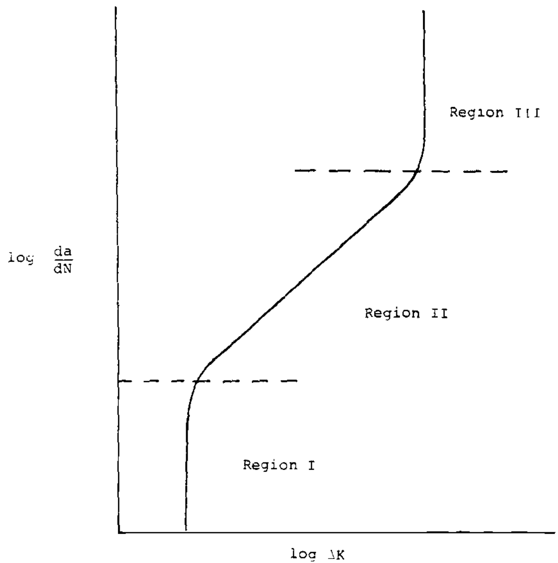

FIG. 1—*Schematic FCGR curve.*

An FCGR description that has been in use since 1960 is the "Paris" power law, which has the form

$$\frac{da}{dN} = C\Delta K^m \tag{1}$$

where C and m are empirically determined. This equation has been observed to describe the behavior in the central region of the FCGR curve. The data in the upper and lower FCGR regions, however, are asymptotic to vertical lines, and a power-law equation does not model the behavior in these regions.

There are currently many FCGR descriptions which account for stress ratio (R) or other effects under constant-amplitude loading conditions. In order to accumulate and evaluate the various descriptions, ASTM Task Group E24.04.04 on FCGR Descriptions was formed.

This report documents the results of an activity of the task group. In February 1979, each task group member received a set of baseline data containing specimen test parameters (load, stress ratio, crack length interval) and FCGR data for varying stress ratios. The material used for the tests was 2219-T851 aluminum. The FCGR data were to be described by an equation or model of the participants' choice. As a measure of the accuracy of the chosen description, each participant was asked to predict specimen lives for a set of specimens chosen by the task group chairman. The life predictions were to be made for both the entire crack growth interval reported and a shorter interval contained within the larger one. Table 1 lists the task group members who actively participated in the evaluation of FCGR descriptions.

Material and Data Descriptions

The data used for the task group activity were taken from the complete set of FCGR data collected by Westinghouse R&D and Alcoa under an Air Force Materials Laboratory (AFML) contract. For each of the five stress ratios used in the testing, specimens representative of the entire growth-rate curve from threshold to failure were selected for distribution to potential participants. Table 2 identifies the test specimen designation and the available test parameter information associated with the FCGR data distributed.

There were sixteen separate FCGR data sets distributed; six were not accompanied with test related information, hence the blanks in Table 2. All positive stress ratio ($R > 0$) tests were conducted using compact tension (CT) specimens; the negative stress ratio ($R = -1.0$) tests employed the center-crack panel (CCP) test geometry. Tables 3*a* to 3*e* give the distributed 2219-T851 aluminum FCGR data for stress ratios of 0.1, 0.3, 0.5, 0.8, and -1.0, respectively; these same data are presented graphically in Fig. 2.

Table 4 contains the fatigue crack growth (FCG) data [that is, crack length (a) versus cycle (N) data] for three specimens tested at a stress ratio of 0.1; these data were also given so that the participants could evaluate FCGR data-generation techniques or calibrate their predictive schemes to match the data supplied.

Tables 5 and 6 present the test control conditions and crack length intervals which were separately provided to the task group members for their use

TABLE 1—*Active participants and their organizations.*

Name	Affiliation
C. G. Annis	Pratt & Whitney Aircraft
F. K. Haake	
J. Fitzgerald	Northrop Corporation
J. P. Gallagher[a]	University of Dayton Research Institute
M. S. Miller	
S. J. Hudak, Jr.	Westinghouse R&D Center
A. Saxena	
J. M. Krafft	Naval Research Laboratory
D. E. Macha	Air Force Materials Laboratory
L. Mueller	Alcoa Laboratories
B. Mukherjee	Ontario Hydro
M. L. Vanderglas	
J. C. Newman	NASA Langley Research Center

[a]Chairman, ASTM Task Group E24.04.04 on FCGR Descriptions.

TABLE 2—*Test variables associated with FCGR data sets supplied for analysis.*[a]

R	Specimen No.	Specimen Type	B, in.	W, in.	P_{max}, kip	Frequency, Hz	Temperature, °F	Environment	a_o, in.	a_f, in.	a versus N, No. of Points	da/dN, No. of Points
0.1	2219-4	CT	0.25	2.0	0.33	5	75	air	0.609	1.409	45	39
0.1	2219-6	CT	0.25	2.0	0.170	50 to 100	75	air	0.710	1.615	48	42
0.1	2219-7											14
0.1	2219-11	CT	0.25	2.0	0.330	5	75	air	0.615	1.513	40	34
0.1	2219-20	CT	0.25	2.0	0.550	5	75	air	0.590	1.388	47	41
0.1	2219-28											25
0.3	2219-56	CT	0.25	2.0	0.357	30	75	air	0.588	1.540	49	43
0.3	2219-71	...	...	...	...	...	...	...	...	...	...	39
0.5	2219-12	...	...	...	...	...	...	...	...	...	...	49
0.5	2219-54	CT	0.25	2.0	0.70	30	75	air	0.597	1.290	35	29
0.5	2219-60	CT	0.25	2.0	1.2	30	75	air	0.580	1.036	24	18
0.8	2219-8	...	...	...	...	...	...	...	...	...	...	23
0.8	2219-27	CT	0.25	2.0	1.5	0.1	75	air	0.601	0.945	29	27
0.8	2219-37	CT	0.25	2.0	0.70	5	75	air	0.610	1.220	33	10
−1.0	2219-CCP-9	CCT	0.25	3.0	3.5	5	75	air	0.382	1.341	51	45
−1.0	2219-CCP-19	CCT	...	...	...	...	...	...	...	...	...	29

[a] 1 in. = 2.54 cm; 1 kip = 4448 N.

TABLE 3a—*FCGR data for 2219-T851 aluminum alloy for a stress ratio* (R) *of 0.1.*[a]

Specimen 2219-4		Specimen 2219-6		Specimen 2219-7	
$\frac{da}{dN}$, 10^{-6} in./cycle	ΔK, ksi $\sqrt{\text{in.}}$	$\frac{da}{dN}$, 10^{-6} in./cycle	ΔK, ksi $\sqrt{\text{in.}}$	$\frac{da}{dN}$, 10^{-6} in./cycle	ΔK, ksi $\sqrt{\text{in.}}$
0.625	5.28	0.0229	2.98	0.007	2.57
0.663	5.34	0.0290	3.05	0.016	2.67
0.758	5.46	0.0356	3.13	0.013	2.77
0.871	5.60	0.0401	3.17	0.031	2.87
0.938	5.71	0.0437	3.21	0.023	2.97
1.04	5.84	0.0550	3.27	0.039	3.08
1.03	5.97	0.0661	3.35	0.009	2.61
1.14	6.10	0.0710	3.38	0.009	2.68
1.27	6.24	0.0799	3.47	0.0044	2.55
1.48	6.35	0.0872	3.54	0.0053	2.66
1.62	6.54	0.0945	3.61	0.0043	2.61
1.80	6.73	0.105	3.71	0.0068	2.69
2.03	6.92	0.121	3.82	0.0076	2.80
2.18	7.15	0.150	3.93	0.011	2.93
2.53	7.36	0.166	4.04		
2.94	7.58	0.194	4.10		
3.46	7.80	0.233	4.26		
3.93	8.04	0.269	4.39		
4.53	8.29	0.352	4.66		
4.97	8.53	0.436	4.82		
5.37	8.80	0.490	4.99		
5.95	9.12	0.558	5.17		
6.53	9.38	0.696	5.37		
7.34	9.73	0.823	5.58		
8.12	10.0	0.965	5.80		
9.61	10.5	1.28	6.17		
10.6	10.9	1.44	6.30		
11.9	11.3	1.80	6.65		
13.6	11.8	2.01	6.88		
15.5	12.3	2.44	7.29		
17.7	12.8	2.88	7.73		
20.7	13.4	3.23	8.02		
23.7	13.8	3.64	8.42		
26.8	14.5	3.90	8.86		
31.9	15.4	4.15	9.42		
37.4	16.1	4.89	9.82		
42.4	16.7	6.07	10.4		
51.3	17.5	9.42	11.2		
67.3	18.6	13.6	12.5		
		17.5	13.4		
		22.5	14.3		
		28.7	15.1		

[a] 1 in./cycle = 2.54×10^4 μm/cycle; 1 ksi $\sqrt{\text{in.}}$ = 1.1 MPa $\sqrt{\text{m}}$.

TABLE 3b—*FCGR data for 2219-T851 aluminum alloy for a stress ratio* (R) *of 0.3.*[a]

Specimen 2219-56		Specimen 2219-71	
$\frac{da}{dN}$, 10^{-6} in./cycle	ΔK, ksi $\sqrt{\text{in.}}$	$\frac{da}{dN}$, 10^{-6} in./cycle	ΔK, ksi $\sqrt{\text{in.}}$
0.440	4.29	0.51	4.19
0.511	4.39	0.36	3.88
0.575	4.49	0.32	3.66
0.616	4.58	0.23	3.43
0.653	4.69	0.19	3.18
0.667	4.77	0.22	3.03
0.681	4.87	0.16	2.87
0.656	4.99	0.067	2.71
0.685	5.11	0.061	2.53
0.809	5.24	0.014	2.36
0.839	5.43	0.014	2.31
0.864	5.58	0.027	2.24
0.981	5.74	0.43	4.19
1.15	5.90	0.36	3.91
1.40	6.05	0.24	2.67
1.70	6.23	0.20	3.43
1.85	6.41	0.16	3.16
2.07	6.59	0.077	2.68
2.09	6.77	0.031	2.59
2.23	6.95	0.023	2.25
2.39	7.14	0.020	2.23
2.59	7.39	0.0044	2.11
2.89	7.57	0.0069	2.21
3.16	7.82	0.014	2.31
3.68	8.10	0.099	2.70
4.05	8.44	0.14	3.39
4.75	8.78	0.30	3.80
5.49	9.14	0.26	4.06
6.12	9.42	0.37	4.34
6.77	9.93	0.57	4.70
7.38	10.3	0.70	5.20
8.03	10.8	1.1	5.74
9.08	11.3	1.4	6.24
11.0	11.9	2.2	6.81
13.1	12.4	3.5	7.49
14.3	13.0	4.9	8.25
16.9	13.8	5.4	9.16
20.1	14.4	7.4	10.24
25.5	15.2	101	12.31
34.5	16.1		
43.9	17.1		
57.9	18.1		
70.0	19.3		

[a] 1 in./cycle = 2.54×10^4 μm/cycle; 1 ksi $\sqrt{\text{in.}}$ = 1.1 MPa $\sqrt{\text{m}}$.

TABLE 3c—*FCGR data for 2219-T851 aluminum alloy for a stress ratio* (R) *of 0.5.*[a]

Specimen 2219-12		Specimen 2219-54		Specimen 2219-60	
$\frac{da}{dN}$, 10^{-6} in./cycle	ΔK, ksi $\sqrt{\text{in.}}$	$\frac{da}{dN}$, 10^{-6} in./cycle	ΔK, ksi $\sqrt{\text{in.}}$	$\frac{da}{dN}$, 10^{-6} in./cycle	ΔK, ksi $\sqrt{\text{in.}}$
0.054	1.86	1.73	6.14	10.8	10.3
0.052	1.93	1.91	6.27	11.6	10.6
0.052	2.00	2.12	6.42	12.4	10.8
0.028	1.66	2.36	6.57	13.5	11.0
0.0029	1.38	2.62	6.72	14.9	11.2
0.0051	1.42	2.88	6.89	16.7	11.4
0.016	1.45	3.06	7.06	18.9	11.7
0.0062	1.50	3.34	7.23	22.7	12.0
0.0085	1.54	3.50	7.42	26.4	12.3
0.013	1.58	3.72	7.61	30.6	12.6
0.017	1.63	4.02	7.81	35.4	12.9
0.033	1.68	4.41	7.98	39.3	13.2
0.027	1.73	4.71	8.19	47.4	13.6
0.035	1.78	5.00	8.42	60.4	14.2
0.055	1.84	5.25	8.66	68.8	14.4
0.041	1.90	5.60	8.91	83.2	14.8
0.062	1.95	5.97	9.16	106	15.3
0.065	2.01	6.69	9.37	136	15.8
0.051	2.08	7.48	9.69		
0.060	2.14	8.38	10.0		
0.087	2.21	9.31	10.4		
0.083	2.29	10.6	10.7		
0.070	2.38	12.7	11.1		
0.091	2.47	16.2	11.5		
0.099	2.56	19.8	12.0		
0.10	2.65	25.7	12.4		
0.15	2.75	44.5	13.0		
0.12	2.86	79.4	13.4		
0.16	2.97	132.4	14.0		
0.13	3.09				
0.15	3.22				
0.26	3.36				
0.24	3.52				
0.23	3.68				
0.31	3.86				
0.35	4.05				
0.37	4.25				
0.41	4.48				
0.56	4.72				
0.67	4.99				
0.88	5.28				
1.0	5.61				
1.5	5.96				
1.8	6.36				
1.5	6.80				
5.3	7.29				
3.3	7.83				
4.8	8.45				
7.4	9.15				

[a] 1 in./cycle = 2.54×10^4 μm/cycle; 1 ksi $\sqrt{\text{in.}}$ = 1.1 MPa $\sqrt{\text{m}}$.

TABLE 3d—*FCGR data for 2219-T851 aluminum alloy for a stress ratio* (R) *of 0.8.*[a]

Specimen 2219-8		Specimen 2219-27		Specimen 2219-37	
$\frac{da}{dN}$, 10^{-6} in./cycle	ΔK, ksi $\sqrt{\text{in.}}$	$\frac{da}{dN}$, 10^{-6} in./cycle	ΔK, ksi $\sqrt{\text{in.}}$	$\frac{da}{dN}$, 10^{-6} in./cycle	ΔK, ksi $\sqrt{\text{in.}}$
0.060	2.07	2.27	5.00	0.144	2.45
0.080	2.14	2.35	5.06	0.111	2.47
0.040	1.74	2.39	5.07	0.122	2.55
0.037	1.62	3.15	5.16	0.147	2.62
0.033	1.67	3.17	5.17	0.165	2.67
0.040	1.72	3.58	5.26	0.182	2.73
0.013	1.44	3.54	5.28	0.204	2.79
0.015	1.52	3.54	5.32	0.223	2.85
0.0015	1.17	3.54	5.38	0.231	2.92
0.0016	1.21	3.47	5.40	0.231	3.01
		4.95	5.55	0.235	3.09
		4.68	5.55	0.280	3.17
		5.80	5.67	0.323	3.21
		7.15	5.81	0.383	3.30
		8.99	5.92	0.405	3.44
		8.63	5.99	0.447	3.49
		8.83	6.05	0.466	3.62
		10.0	6.19	0.501	3.72
		10.1	6.29	0.565	3.80
		13.2	6.45	0.708	3.95
		18.7	6.62	0.846	4.07
		29.3	6.78	1.06	4.21
		53.9	7.01	1.21	4.34
				1.47	4.49
				1.81	4.66
				2.32	4.83
				3.08	5.01

[a]1 in./cycle = 2.54×10^4 µm/cycle; 1 ksi $\sqrt{\text{in.}}$ = 1.1 MPa/ cycle.

in making life predictions. The participants were asked to complete the tables and return them along with a short description of the model used to fit the FCGR data. Note that the initial and final crack length values (a_o and a_f) in Table 6 are contained within the corresponding crack length intervals given in Table 5. This apparent duplication was justified by a desire to minimize initial and final crack length influences on the FCGR behavior. The life predictions associated with the Table 5 crack length interval will be subsequently referred to as the life predictions for the full crack growth interval; those from Table 6 will be referred to as the life predictions for the shortened crack growth interval.

The six specimens identified with an asterisk in Tables 5 and 6 are those for which test condition data are available. These replace six specimens that did not have test data reported (see Table 2). None of the FCGR data asso-

TABLE 3e—*FCGR data for 2219-T851 aluminum alloy for a stress ratio* (R) *of −1.0.*[a]

Specimen 2219-CCP-9		Specimen 2219-CCP-19	
$\frac{da}{dN}$, 10^{-6} in./cycle	ΔK, ksi $\sqrt{\text{in.}}$	$\frac{da}{dN}$, 10^{-6} in./cycle	ΔK, ksi $\sqrt{\text{in.}}$
1.07	5.84	0.75	4.08
1.11	5.98	0.49	3.84
1.18	6.10	0.46	3.59
1.31	6.38	0.32	3.35
1.36	6.45	0.23	3.14
1.45	6.67	0.20	2.93
1.46	6.76	0.14	2.73
1.62	6.93	0.11	2.49
1.68	7.08	0.098	2.56
1.85	7.25	0.087	2.36
1.94	7.51	0.031	1.52
2.02	7.64	0.028	1.40
2.23	7.83	0.0060	1.09
2.33	8.03	0.0080	1.14
2.50	8.23	0.014	1.18
2.61	8.42	0.011	1.21
2.79	8.70	0.014	1.27
2.86	8.72	0.024	1.33
3.05	9.02	0.022	1.37
3.41	9.21	0.028	1.44
3.76	9.33	0.037	1.50
4.34	9.57	0.036	1.56
4.50	9.81	0.030	1.64
4.58	10.1	0.049	1.69
5.07	10.5	0.047	1.78
5.13	10.7	0.056	1.87
5.43	10.9	0.059	1.94
5.86	11.4	0.061	2.07
5.84	11.6	0.079	2.20
5.87	12.1		
5.85	12.4		
6.63	12.8		
6.89	13.1		
8.09	13.6		
8.89	14.0		
10.4	14.5		
11.4	15.0		
12.0	15.7		
13.0	16.3		
14.5	17.0		
17.2	17.6		
22.7	18.6		
25.7	19.2		
30.0	19.9		
30.4	20.7		

[a] 1 in./cycle = 2.54 × 10^4 μm/cycle; 1 ksi $\sqrt{\text{in.}}$ = 1.1 MPa/cycle.

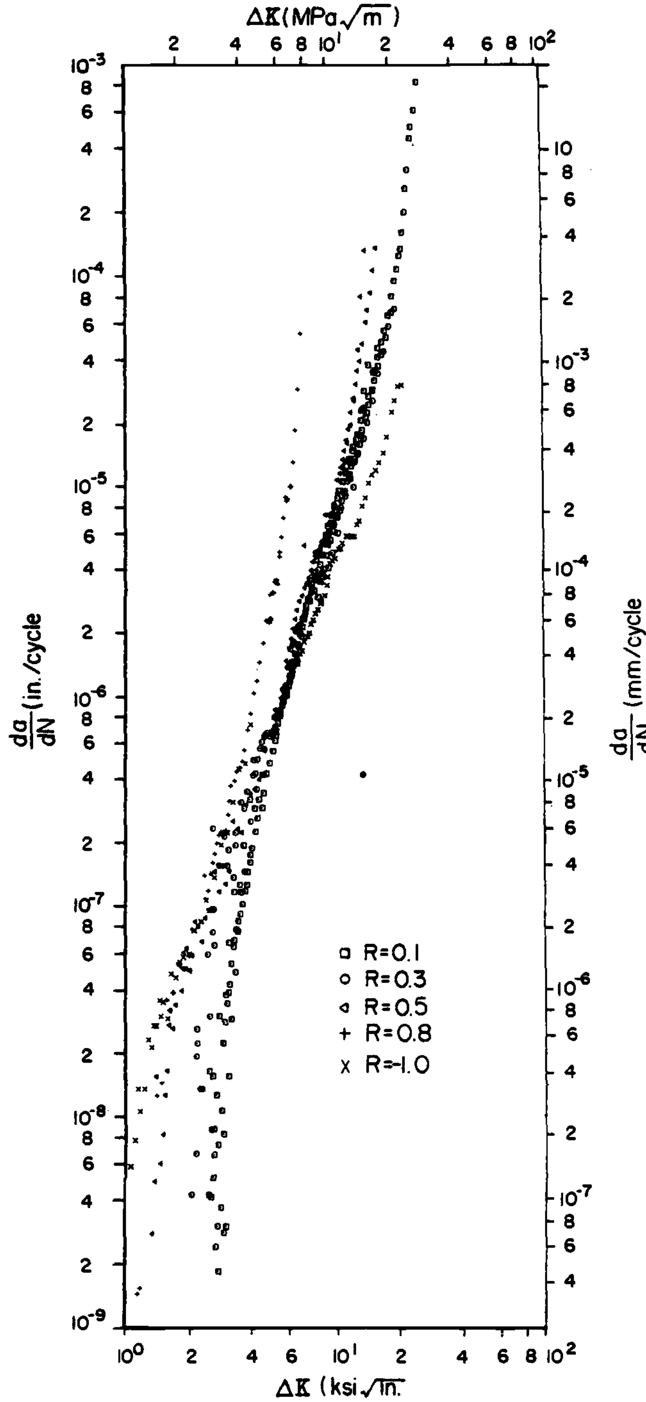

FIG. 2—*FCGR data described to Task Group members.*

TABLE 4—a *versus* N *data for a stress ratio* (R) *of 0.1.*

Specimen 2219-4		Specimen 2219-6		Specimen 2219-11	
a, in.	*N*	*a*, in.	*N*	*a*, in.	*N*
0.609	0	0.710	0	0.615	0
0.6275	56420	0.725	951100	0.627	18930
0.655	109160	0.745	1957700	0.648	49950
0.671	155880	0.765	3104099	0.668	76700
0.680	163360	0.785	4085500	0.685	109870
0.700	192190	0.805	4690399	0.705	126750
0.7225	217610	0.815	4828000	0.728	151350
0.7385	236630	0.825	5108199	0.748	175610
0.7575	257190	0.840	5536000	0.769	194300
0.776	274840	0.860	5804699	0.794	218430
0.7935	288710	0.865	5964299	0.814	234170
0.8115	303240	0.885	6139000	0.835	250700
0.825	322000	0.900	6347000	0.856	263700
0.8485	331590	0.915	6537000	0.877	277800
0.870	343890	0.835	6715000	0.895	286430
0.8905	355650	0.955	6908000	0.919	299320
0.915	367180	0.975	7110000	0.935	307240
0.936	377280	0.995	7190199	0.955	312570
0.957	385310	1.005	7268000	0.973	318460
0.9775	392780	1.030	7394000	1.005	327790
0.998	397670	1.048	7479000	1.013	329970
1.018	402750	1.085	7586000	1.038	335960
1.0365	406900	1.105	7663000	1.050	339670
1.056	410500	1.125	7702000	1.073	344230
1.0785	414260	1.145	7728000	1.090	346740
1.095	417350	1.165	7772000	1.108	349710
1.1165	420590	1.185	7804000	1.130	352950
1.134	422820	1.205	7833299	1.150	355750
1.1575	425700	1.235	7853000	1.190	359980
1.1775	427710	1.245	7861899	1.208	361280
1.195	429290	1.270	7878000	1.228	362800
1.2165	430900	1.285	7885000	1.248	364140
1.2365	432600	1.310	7898299	1.278	365800
1.257	433770	1.335	7907099	1.288	366330
1.278	434800	1.350	7911799	1.308	367240
1.2915	435630	1.370	7919099	1.330	367340
1.3125	436450	1.390	7923399	1.350	367990
1.3365	437250	1.410	7927899	1.373	368460
1.356	437850	1.425	7932099	1.420	369930
1.3705	438300	1.445	7936299	1.513	370150
1.389	438680	1.470	7941699		
1.409	439060	1.505	7944799		
1.42	439270	1.525	7945599		
1.44	439490	1.545	7947000		
1.46	439660	1.560	7947799		
		1.585	7943500		
		1.600	7948900		
		1.615	7949200		

TABLE 5—*Test conditions for the specimens and the full crack-length*

R	Specimen No.	Specimen Type	B, in.	W, in.	P_{max}, kip	Frequency, Hz
0.1	2219-3*	CT	0.25	2.0	0.240	50 to 100
0.1	2219-4	CT	0.25	2.0	0.33	5
0.1	2219-5*	CT	0.25	2.0	0.20	50 to 100
0.1	2219-6	CT	0.25	2.0	0.170	50 to 100
0.1	2219-11	CT	0.25	2.0	0.330	5
0.1	2219-20	CT	0.25	2.0	0.550	5
0.3	2219-56	CT	0.25	2.0	0.357	30
0.3	2219-50*	CT	0.25	2.0	0.571	30
0.5	2219-52*	CT	0.25	2.0	0.40	30
0.5	2219-54	CT	0.25	2.0	0.70	30
0.5	2219-60	CT	0.25	2.0	1.2	30
0.8	2219-19*	CT	0.25	2.0	1.5	5
0.8	2219-27	CT	0.25	2.0	1.5	0.1
0.8	2219-37	CT	0.25	2.0	0.70	5
−1.0	2219-CCP-9	CCT	0.25	3.0	3.5	5
−1.0	2219-CCP-11*	CCT	0.25	3.0	3.5	5

[a] 1 in. = 2.54 cm; 1 kip = 4448 N; 1 in./cycle = 2.54×10^4 μm/cycle.
[b] An asterisk indicates those specimens for which test condition data are available.

ciated with asterisked specimens in Tables 5 and 6 were distributed to the task group participants. Thus only ten of the sixteen life predictions requested for each table (5 and 6) would be based on the FCGR data derived from these ten tests.

Description of Models

The descriptions presented in this report attempt to model all three regions (low, central, and high) of the crack growth rate curve. Table 7 provides a summary of all descriptions utilized by the participants. This section briefly summarizes the parameters and coefficients employed in the descriptions given in Table 7, and refers the reader to specific appendixes for more details on each equation. The appendixes also provide information on (*1*) measures of accuracy of the FCGR fit, (*2*) methods used to establish the description's coefficients (or constants), and (*3*) methods of integrating $da/dN = f(\Delta K, R)$, for those cases where such information is available.

Description 1 in Table 7 is a modified Paris power-law equation where

$$\overline{\Delta K} = \frac{\Delta K_{eff} - \Delta K_o}{1 - \left(\frac{K_{max}}{K_c}\right)^2} \tag{2}$$

interval defined (material = 2219-T851 aluminum).[a,b]

Temperature, °F	Environment	a_o, in.	a_f, in.	N_f, cycles	$\frac{da}{dN}\vert$ low, 10^{-6} in./cycle	$\frac{da}{dN}\vert$ high, 10^{-6} in./cycle
75	air	0.700	1.283	...	0.2413	6.223
75	air	0.609	1.46	...	0.625	67.3
75	air	0.730	1.615	...	0.1189	45.3
75	air	0.710	1.615	...	0.0229	28.74
75	air	0.615	1.513	...	0.7301	45.5
75	air	0.590	1.388	...	2.999	819.5
75	air	0.588	1.540	...	0.4398	69.96
75	air	0.595	1.10	...	2.305	6.71
75	air	0.598	1.440	...	0.2308	21.06
75	air	0.597	1.290	...	1.728	132.4
75	air	0.580	1.036	...	10.77	135.9
75	air	0.603	0.903	...	5.67	43.95
75	air	0.601	0.945	...	2.273	53.
75	air	0.610	1.220	...	0.1112	3.077
75	air	0.382	1.341	...	1.065	30.36
75	air	0.433	0.887	...	1.742	5.193

and

$$K_{\text{eff}} = (1 - P_o/P_{\max}) \cdot K_{\max} \tag{3}$$

are utilized to define the independent variable. The ratio $P_o/P_{\max}$ is calculated from a crack closure model under plane-strain conditions. The coefficients C_1, C_2, K_c, and ΔK_o are derived by least-squares procedures. Further details can be found in Appendix I.

Description 2 is a five-parameter model. The relationship between crack growth rate and stress-intensity factor is

$$\frac{da}{dN} = P_1 \frac{(\Delta K - \Delta K_t)^{P_2}}{(\Delta K_c - \Delta K)^{P_3}} \tag{4}$$

The constants P_1, P_2, P_3, ΔK_t, and ΔK_c are derived from the FCGR data in the manner outlined in Appendix II.

In Description 3, n_1 and n_2 are graphically determined from FCGR data plots. The exponents n_1 and n_2 are the slopes of the data in lower and central FCGR regions, respectively. The term C' is calculated from the exponent n_2, the stress ratio R, and a constant, K_c, which characterizes the stress-intensity

TABLE 6—*Major test conditions and the shortened crack-length interval defined (material = 2219-T851 aluminum).*[a,b]

R	Specimen No.	Specimen Type	B, in.	W, in.	P_{max}, kip	a_o in.	a_f in.	N_f, cycles
0.1	2219-3*	CT	0.25	2.0	0.240	0.700	1.000	...
0.1	2219-4	CT	0.25	2.0	0.33	0.700	1.000	...
0.1	2219-5*	CT	0.25	2.0	0.20	0.730	1.000	...
0.1	2219-6	CT	0.25	2.0	0.170	0.710	1.000	...
0.1	2219-11	CT	0.25	2.0	0.330	0.700	1.000	...
0.1	2219-20	CT	0.25	2.0	0.550	0.700	1.000	...
0.3	2219-56	CT	0.25	2.0	0.357	0.700	1.000	...
0.3	2219-58*	CT	0.25	2.0	0.571	0.700	1.000	...
0.5	2219-52*	CT	0.25	2.0	0.40	0.700	1.000	...
0.5	2219-54	CT	0.25	2.0	0.70	0.700	1.000	...
0.5	2219-60	CT	0.25	2.0	1.2	0.700	1.000	...
0.8	2219-19*	CT	0.25	2.0	1.5	0.700	0.903	...
0.8	2219-27	CT	0.25	2.0	1.5	0.700	0.945	...
0.8	2219-37	CT	0.25	2.0	0.70	0.700	1.000	...
−1.0	2219-CCP-9	CCT	0.25	3.0	3.5	0.450	0.850	...
−1.0	2219-CCP-11*	CCT	0.25	3.0	3.5	0.450	0.850	...

TABLE 7—*FCGR descriptions.*

Participant/ FCGR Description No.	Form	Corresponding Appendix
(1)	$\frac{da}{dN} = C_1 \overline{\Delta K}^{C_2}$	I
(2)	$\frac{da}{dN} = P_1 \frac{(\Delta K - \Delta K_t)^{P_2}}{(\Delta K_c - \Delta K)^{P_3}}$	II
(3)	$\frac{1}{da/dN} = \frac{A_1}{(\Delta K)^{n_1}} + A_2 \left[\frac{1}{(\Delta K)^{n_2}} - C'\right]$	III
(4)	$\frac{da}{dN} = C(K_{max})^m \left[(K_{max} + K_e)(1 - R_{eff}) + {}^*K\right]^2$	IV
(5)	$\log_{10}\left(\frac{da}{dN}\right) = P_1 \exp(P_2 x) + P_3 \exp(P_4 x) + P_5$	V
(6)	$\frac{da}{dN} = {}_{10}\{C_1 \sinh[C_2(\log \Delta K + C_3)] + C_4\}$	VI
(7)	$\frac{da}{dN} = {}_{10}\{C_1 \sinh[C_2(\log \Delta K + C_3)] + C_4\}$	...
(8)	$\frac{da}{dN} = e + (v - e)\left[-\ln\left(1 - \frac{\Delta K}{K_b}\right)\right]^{1/k}$	VII
(9)	tensile ligament instability model	VIII
(10)	table lookup procedure	IX

factor at the onset of instability. The relationship between C' and n_2 is given by

$$C' = \frac{1}{K_c(1 - R)^{n_2}} \tag{5}$$

where K_c is also determined graphically from a plot of the data. The coefficients A_1 and A_2 are then determined using multiple linear regression analysis. A more extensive discussion of this description can be found in Appendix III.

Description 4 is another modified Paris power-law equation, the extra factor being used to account for environmental effects on crack growth rate. In the fitting process, C and m are calculated from the modulus of elasticity, with

$$C = E^2 \cdot (10^{-23}) \tag{6a}$$

and

$$m = 1.442 \cdot \ln [10^{7.5}/E] \tag{6b}$$

with E expressed in units of pounds per square inch. The environmental parameter is K_e, where

$$K_e = K_{e_{\text{const}}} \left[\frac{(K_{\text{max}} - K_{e_o})}{(K_{\text{plat}} - K_{e_o})} \right] \tag{7}$$

for $K_{\text{max}} < K_{\text{plat}}$, and $K_e = 0$ for $K_{\text{max}} \leq K_{e_o}$. The K_{plat} value is the point at which K_e becomes constant. The effective stress ratio is given by

$$R_{\text{eff}} = \frac{K_{\text{min}} + \Delta K_o}{K_{\text{max}}} \tag{8}$$

where ΔK_o is a threshold value of ΔK (which is identical for each stress ratio). The $*K$ term is used to fit the upper end of the growth rate data and is given by

$$*K = \alpha e^{\beta (K_{\text{max}})} \tag{9}$$

where α and β are fitted constants. A further explanation of the terminology is given in Appendix IV.

Description 5 is a five-parameter model where the values of P_1, P_2, P_3, P_4, and P_5 are determined by least-square procedures, and where x is related to the stress-intensity factor range by

$$x = \log_{10} (\Delta K) \tag{10}$$

This FCGR description is further discussed in Appendix V.

Descriptions 6 and 7 employ the hyperbolic sine equation which was separately applied by two participants. The parameters C_1, C_2, C_3, and C_4 are obtained by fitting the equation to the supplied FCGR data and using least-squares techniques. The hyperbolic sine equation is further described in Appendix VI.

Description 8 is based on a three-parameter Weibull-type distribution function with a fourth parameter added to normalize the range in stress-intensity factor. The four coefficients are

K_b = normalizing parameter for ΔK

k = shape parameter

e = threshold (location) parameter

v = characteristic value (shape parameter)

For determining the coefficients for this description, the sum of the squared perpendicular distances between the measured and predicted values was minimized by the participant rather than the squared residuals in the x or y direction, as is usually done. The Weibull FCGR description is covered in Appendix VII.

Description 9, the tensile ligament instability model, is described in Appendix VIII.

Description 10, a table lookup procedure, involves a table of da/dN versus ΔK values for each stress ratio. These tabulated values are obtained from a graphically smoothed curve evaluated at regular log da/dN intervals. The ΔK-values determined from the current crack length increment are used in conjunction with the tabular ΔK-values to linearly interpolate the tabular da/dN values, obtaining the corresponding crack growth rate for the current crack length increment. Further explanation of Description 10 can be found in Appendix IX.

Results

The sets of life-prediction results were tabulated according to the model used and the crack-length interval covered. These data were reduced to a corresponding set of life-prediction rates—the ratio of predicted specimen life (N_p) to actual measured specimen life (N_A). Tables 8 and 9 list these ratios. Table 8 gives ratios for the full crack length interval, and Table 9 for the shortened interval. The numbers at the top of both tables correspond to the participant/FCGR description numbers given in Table 7.

Due to trouble with the evaluation of the function, Participant 8 was unable to predict a life for several specimens. Participant 4 did not report any predictions for specimens with a stress ratio of -1.0.

As can be seen from the tables, Specimen 2219-19 resulted in life-prediction ratios substantially above 1.0 for every description except No. 4. This inconsistency can be traced to the difference between the FCGR behavior exhibited by Specimen 2219-19 and that of the other specimens tested at a stress ratio of 0.8. Figure 3 shows that the FCGR data for Specimen 2219-19 are substantially faster (nonrepresentative) than those exhibited by the other tests. Thus the participants making life predictions based on the data distributed would be expected to overpredict the life (FCG behavior) of Specimen 2219-19, and thus the corresponding life-prediction ratios would also be high. Consequently the life-prediction ratios for Specimen 2219-19 were neglected when comparisons of the participants' results were made.

The predictions for specimen 2219-20 were consistently low for the full crack growth interval, but not for the shorter interval. This phenomenon can be attributed to the fact that the upper end of the specimen's FCGR curve is in the unstable growth region of the FCGR curve for specimens with a stress

TABLE 8—*Life-prediction ratios for the full interval a_o to a_f.*

Specimen No.	Participant FCGR Description No.									
	1	2	3	4	5	6	7	8	9	10
2219-3	0.96	0.70	0.81	0.77	1.01	1.01	0.99	0.99	1.30	1.03
2219-4	1.04	0.73	0.77	0.82	0.85	0.86	0.89	1.00	1.31	0.94
2219-5	0.71	0.56	0.99	0.65	1.01	1.01	0.91	0.81	0.95	0.91
2219-6	0.40	0.41	1.77	0.74	1.09	1.10	0.83	...	0.55	0.91
2219-11	1.20	0.85	0.89	0.95	0.98	1.00	1.03	1.16	1.50	1.08
2219-20	0.84	0.66	0.70	0.64	0.65	0.66	0.67	...	1.29	0.64
2219-56	0.87	0.82	1.05	0.96	0.95	1.03	1.02	1.03	1.04	0.99
2219-58	0.68	0.69	0.97	0.68	0.97	0.80	0.88	0.96	1.01	0.88
2219-52	0.89	0.66	0.86	0.86	1.04	0.89	23.29	0.95	0.85	1.07
2219-54	0.83	0.70	0.84	0.67	1.11	0.92	0.96	...	1.01	1.00
2219-60	0.90	0.90	1.17	0.66	0.86	0.79	0.95	...	1.47	1.10
2219-19	2.48	1.47	2.22	0.74	1.60	2.61	1.59	...	2.06	1.71
2219-27	1.54	0.93	1.34	0.45	0.99	1.68	0.97	...	1.25	1.02
2219-37	1.13	0.48	0.94	0.98	0.94	0.91	1.00	...	0.54	0.92
2219-CCP-9	0.95	0.73	0.84	...	0.87	...	0.15	...	1.21	0.87
2219-CCP-11	1.26	0.96	1.10	...	1.14	...	0.24	...	0.55	1.14

TABLE 9—*Life-prediction ratios for the shortened crack length interval.*

Specimen No.	Participant FCGR Description No.									
	1	2	3	4	5	6	7	8	9	10
2219-3	0.93	0.68	0.80	0.72	1.01	1.02	0.99	0.98	1.33	1.05
2219-4	1.15	0.82	0.84	0.91	0.93	0.95	0.98	1.11	1.22	0.99
2219-5	0.67	0.54	1.04	0.62	1.04	1.03	0.92	0.80	0.83	0.91
2219-6	0.37	0.39	1.90	0.75	1.12	1.13	0.84	...	0.50	0.93
2219-11	1.16	0.83	0.85	0.92	0.94	0.96	0.99	1.12	1.24	1.00
2219-20	1.17	0.96	1.00	0.89	0.98	0.99	0.99	1.02	1.87	0.93
2219-56	0.79	0.75	0.72	0.86	0.91	0.92	0.96	0.95	0.88	0.92
2219-58	0.65	0.68	0.95	0.64	0.99	0.79	0.86	0.94	1.04	0.86
2219-52	0.86	0.65	0.85	0.80	1.09	0.87	6.52	0.95	0.89	1.16
2219-54	0.86	0.75	1.10	0.68	1.18	1.00	0.99	1.20	1.10	1.01
2219-60	0.95	1.04	1.18	0.67	0.87	0.73	0.95	...	1.41	0.92
2219-19	3.21	2.19	2.23	0.52	1.73	3.40	1.80	...	1.55	1.97
2219-27	1.77	1.21	1.14	0.27	0.93	1.85	0.95	...	0.79	1.04
2219-37	0.58	0.46	0.89	0.80	0.96	0.91	0.97	0.97	0.71	0.93
2219-CCP-9	1.04	0.80	0.91	...	0.95	0.95	0.17	2.79	0.30	0.95
2219-CCP-11	1.27	0.97	1.11	...	1.15	1.16	0.21	3.40	0.37	1.16

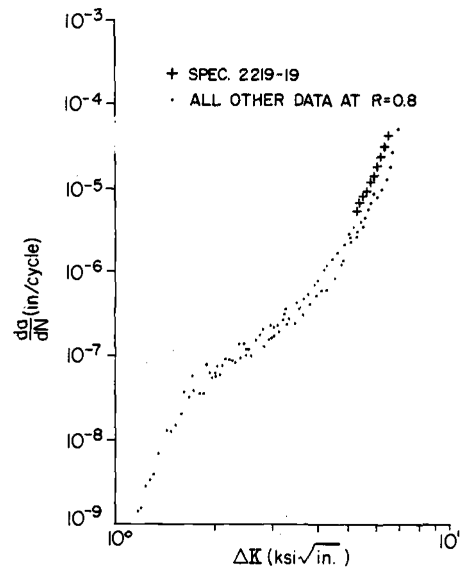

FIG. 3—*Comparison of FCGR data for Specimen 2219-19 and other specimens at the same stress ratio.*

ratio of 0.1. The extremely high *da/dN* values on this portion of the curve lead to low life projections.

As a method of comparing the different descriptions, the mean and standard deviation for each set of life predictions were calculated and then listed in Table 10 for both crack growth intervals. Since the shortened crack growth interval would exhibit a more stable crack growth pattern, it is used as the basis for comparing each of the descriptions. Table 10 shows that six of the descriptions resulted in a mean life-prediction ratio within 5 percent of the optimum value of 1.0 for the shortened interval. One of the four remaining descriptions was within 12 percent of 1.0; the rest fell between 22 and 27 percent of 1.0. The standard deviation was selected to represent a measure of scatter of the data about the mean of the sample. Those descriptions with the smallest overall standard deviation exhibited the smallest amount of scatter.

As a further method of comparison, the percentage of life-prediction ratios within 20 percent of 1.0 and within 10 percent of 1.0 was calculated for each FCGR description. The ratios for the shortened crack growth interval were used for these calculations. The results of using these methods of comparison are listed in Table 11. The ten FCGR descriptions were divided into four groups:

Group I—90 to 100 percent life-prediction ratios within 20 percent of 1. Descriptions 5 and 10 fell within this group.

TABLE 10—*Means and standard deviation of sets of life-prediction ratios.*

	Participant FCGR Description No.									
	1	2	3	4	5	6	7	8	9	10
Full crack growth interval										
Mean	0.95	0.72	1.00	0.76	0.96	0.97	2.32	0.99	1.05	0.96
Standard	0.27	0.16	0.27	0.15	0.12	0.24	5.81	0.10	0.32	0.12
Short crack growth interval										
Mean	0.95	0.77	1.02	0.73	1.00	1.02	1.22	1.35	0.96	0.98
Standard	0.34	0.22	0.28	0.17	0.09	0.26	1.49	0.83	0.41	0.09
Group number	IV	IV	II	IV	I	III	II	II	IV	I

TABLE 11—*A further comparison of FCGR descriptions.*

Participant FCGR Description No.	Percent of All Predictions Within: ±20 % of 1.0	±10 % of 1.0	Group Rank No.
1	53.3	20.0	IV
2	33.3	20.0	IV
3	86.7	26.7	II
4	38.5	15.4	IV
5	100.0	73.3	I
6	73.3	53.3	III
7	80.0	66.7	II[a]
8	89.5	57.9	II
9	31.3	18.8	IV
10	100.0	80.0	I

[a]Could downgrade ranking to III on the basis of results presented in Table 10.

Group II—80 to 90 percent life-prediction ratios within 20 percent of 1. Descriptions 3, 7, and 8 fell within this group.

Group III—70 to 80 percent life-prediction ratios within 20 percent of 1. Description 6 fell within this group at 73.3 percent.

Group IV—Less than 70 percent life-prediction ratios within 20 percent of 1. Descriptions 1, 2, 4, and 9 fell within this group.

While this evaluation identified the better fatigue crack growth rate prediction schemes, it also has identified that one of the task group's objectives was not truly met. It was realized after the evaluation that the better prediction schemes were providing individual data fits to each stress-ratio set of FCGR data prior to predicting the life for that stress-ratio set. Table 12 identifies the procedure for fitting the data (single stress-ratio sets or collective stress-ratio set) and the overall prediction group level (I, II, III, or IV).

On the basis of these observations, it would be fruitful to distribute the second set of FCGR data generated by Westinghouse and Alcoa (on 10Ni steel) and request that the task force predict the behavior of an intermediate stress-ratio data set that would not be supplied to them. By this new experiment, the participating task force members would determine the ability of the various FCGR descriptions to accurately interpolate stress-ratio effects.

Conclusions

This study has shown that there are several competitive fatigue crack growth rate (FCGR) descriptions which will adequately model FCGR be-

TABLE 12—*Stress-ratio fitting procedure and accuracy grouping.*

Participant FCGR Description No.	Description of Stress-Ratio Data Sets	Accuracy of Prediction Group No.
1	collective	IV
2	collective	IV
3	collective	II
4	collective	IV
5	individual	I
6	individual	III
7	collective	II
8	individual	II
9	collective	IV
10	individual	I

havior such that constant-amplitude fatigue crack growth (FCG) behavior can be accurately predicted. The reader will find that the paper has been written to give additional participants the opportunity to evaluate their FCGR descriptions using the same guidelines and data provided herein. For more information, contact the current chairman of ASTM Subcommittee E24.04 on Subcritical Crack Growth.

APPENDIX I

Participant/FCGR Description No. 1

The crack growth rate equation used for all stress ratios in the ASTM Task Group E24.04.04 predictions was

$$\frac{da}{dN} = C_1 \left[\frac{\Delta K_{\text{eff}} - \Delta K_o}{1 - \left(\dfrac{K_{\max}}{K_c}\right)^2} \right]^{C_2} \tag{11}$$

where

$C_1 = 2.68 \times 10^{-8}$,
$C_2 = 2.85$,
$\Delta K_o = 0.7 \text{ ksi} \sqrt{\text{in.}}$,
$K_c = 60 \text{ ksi} \sqrt{\text{in.}}$, and
$\Delta K_{\text{eff}} = (1 - P_o/P_{\max})K_{\max}$.

All stress-intensity factors are given in ksi/in.$^{1/2}$ (1.1 MPa $\sqrt{\text{m}}$).

The crack-opening load ratio ($P_o/P_{\max}$) was calculated from a crack-closure model under "simulated" plane-strain conditions. The values were

R	P_o/P_{max}
-1	0.318
0.1	0.365
0.3	0.428
0.5	0.585
0.8	0.818

The constants C_1 and C_2 in Eq 11 were obtained from a least-squares fit to all stress-ratio data except Specimen CCP-19. The constants ΔK_o and ΔK_c were selected to approximate the stress-intensity threshold (ΔK_o) and fracture toughness (K_c), respectively. The life predictions were obtained by numerically integrating Eq 11 from the initial crack length to the final crack length.

APPENDIX II

Participant/FCGR Description No. 2

The crack growth rate is given by

$$\frac{da}{dN} = \frac{P_1 (\Delta K - \Delta K_t)^{P_2}}{(\Delta K_c - \Delta K)^{P_3}} \tag{12}$$

where ΔK_t and ΔK_c are constants defining the asymptotes at low and high ΔK, respectively. P_1 shifts the (log-log) curve up or down, and P_2 and P_3 influence curvature.

The data were initially grouped for each stress ratio, and Eq 12 was separately fitted to these data giving five sets of constants. Both a commercial statistical package program (BMDP) and an "in-house" curve-fitting program were used (standard least-squares routines).

After the initial curve fits, and some trial and error, a refined version of Eq 12 was used to fit all the data for $R > 0$. From this fit the two equations obtained were

$$\text{For } R > 0 \; \frac{da}{dN} = \approx 275 \times 10^{-6} (1 - R) \frac{[\Delta K - 2.3\sqrt{1 - R}\,]^2}{[60 (1 - R - \Delta K]} \tag{13}$$

$$\text{For } R = -1 \; \frac{da}{dN} = \approx 37 \times 10^{-6} (1 - R) \frac{\left[\Delta K - \dfrac{2.3\sqrt{1 - R}}{2}\right]^2}{[60 (1 - R) - \Delta K]} \tag{14}$$

ΔK is defined as peak-to-peak value for all R including -1, ΔK in ksi $\sqrt{\text{in.}}$, and da/dN in inch/cycle.

The computer program employed to obtain Eqs 13 and 14 did not provide any statistical measure of goodness of fit.

The stress-intensity factors were calculated by using

$$\Delta K = \frac{\Delta P (a)^{1/2}}{BW} \frac{(1 - a/W)}{2 (a/W)^{1/2} (1 - a/W)^{3/2}} [7.0 - 7.05 (a/W) + 4.275 (a/W)^2] \tag{15}$$

For the compact tension (CT) specimens (those at positive stress ratios), and

$$\Delta K = \frac{\Delta P}{BW}(\pi a)^{1/2}\,[\sec(\pi a/W)]^{1/2} \tag{16}$$

For center-cracked panel (CCP) specimens (those at a stress ratio of −1.0), where

$\Delta P = p_{max} - p_{min}, R > 0,$
B = specimen thickness,
W = specimen width, and
a = crack length.

The growth law was integrated numerically using a central difference algorithm. Since, at constant load, the stress intensity is a monotonically increasing function of crack length, the error in ΔN can be determined as follows. For a growth law that is written in the form

$$\frac{da}{dN} = f(\Delta K) \tag{17}$$

the corresponding interval is

$$\int \frac{da}{f(\Delta K)} = \int dN = \Delta N \tag{18}$$

for growth from a_o to $a_o + \Delta a$, because $f(\Delta K)$ is a monotonically increasing function

$$\frac{\Delta a}{f(\Delta K[a_o])} > \Delta N > \frac{\Delta a}{f(\Delta K[a_o + \Delta a])} \tag{19}$$

A crack growth increment, Δa, was chosen such that the difference between the bounds was less than 1 percent of the total cycles.

APPENDIX III

Participant/FCGR Description No. 3 (Three-Component Model)

The equation describing the three-component model for a constant-load ratio is

$$\frac{1}{(da/dN)} = \frac{A_1}{(\Delta K)^{n_1}} + \frac{A_2}{(\Delta K)^{n_2}} - \frac{A_2}{[K_c(1-R)]^{n_2}} \tag{20a}$$

or alternatively

$$\frac{1}{(da/dN)} = \frac{A_1}{(\Delta K)^{n_1}} + A_2\left[\frac{1}{(\Delta K)^{n_2}} - C\right] \tag{20b}$$

where

$$C = \frac{1}{[K_c(1 - R)]^{n2}} \tag{20c}$$

A_1, A_2, n_1, n_2, and K_c are fitting constants, and R is the stress ratio.

This model is based upon combining the materials' resistance to fatigue crack growth in the three commonly observed regions of the sigmoidally shaped log (da/dN) versus log (ΔK) behavior. The three terms on the right-hand side of Eq 20*a* characterize the behavior in the three regions of crack growth rate, and the transition regions are characterized by a combination of two adjacent terms.

The exponents n_1 and n_2 characterize the slopes of the straight lines describing the log da/dN versus log ΔK behavior in Regions I and II, respectively. The constants A_1 and A_2 are the intercepts of the straight lines (that is, da/dN at $\Delta K = 1.0$). The parameter K_c characterizes the onset of instability. Although this term is related to the materials' fracture toughness, it is not necessarily a material property; for example, it may depend on crack length or specimen thickness. Thus it is more appropriate for the purposes here to think of K_c as a fitting parameter.

If wide-range fatigue crack growth rate data are available for several load ratios, the model can be written to account for complex effects of load ratio as

$$\frac{1}{(da/dN)} = \frac{A_1(R)}{(\Delta K)^{n_1}} + A_2(R)\left[\frac{1}{(\Delta K)^{n_2}} - \frac{1}{[K_c(1 - R)]^{n2}}\right] \tag{21}$$

It will be shown later that common values of n_1, n_2, and K_c can be determined so as to provide adequate fits to data obtained over a wide range of load ratios. Thus complex load ratio effects can be modeled by $A_1(R)$ and $A_2(R)$, which are simple functions of load ratio.

In the following discussion, the procedures for regression analysis to fit fatigue crack growth rate data to the three-component model and subsequent integration of the fitted equations to obtain the predicted life of CT and CCP geometries are described. The procedure for modeling the load ratio effects is also discussed.

Regression Analysis

The regression analysis procedure is as follows. Firstly, the slopes of straight lines that were graphically fitted through the data in Regions I and II were determined. These slopes are the n_1 and n_2 values, respectively, in Eq 20*a*. Next, the critical stress-intensity range at which specimen fracture occurred was estimated, also from the graphical plot of the data. This value is approximated by $(1 - R)K_c$.

Best estimates of A_1 and A_2, using a modified multiple-linear-regression analysis were obtained for n_1, n_2, and K_c values of 12.5, 3.0, and 34 ksi $\sqrt{\text{in.}}$ (37.4 MPa$\sqrt{\text{m}}$), respectively. The fits were obtained separately for the various load ratios, using n_1, n_2, and K_c for each load ratio.

Generally, when using a multiple-linear-regression analysis of the type required for obtaining best estimates of A_1 and A_2, the sum of squares of the residuals (SSR), as given by Eq 22, is minimized.[2]

[2] Walpole, R. W. and Myers, R. H., *Probability and Statistics for Engineers and Scientists*, Macmillan, New York, 1972.

$$\mathrm{SSR} = \sum_{i=1}^{\ell} (y_i - \hat{y}_i)^2 \tag{22}$$

where

y_i = i_{th} observed value of the dependent variable corresponding to the independent variable x_i,
$\hat{y}_i$ = predicted value of y at x_i, and
ℓ = number of data points.

Since $1/(da/dN)$ values range from 10^9 to 10^4 cycles/in. in a majority of the data sets analyzed, the contribution to SSR is much larger for the higher $1/(da/dN)$ values (low growth rate regime) in the data set. This in effect assigns high weights to the data in Region I and low weights to—and perhaps ignores—data in Regions II and III. This problem was resolved by minimizing the relative error instead of the absolute error. The relative error was defined by

$$(\mathrm{SSR})_{\text{rel.}} = \sum_{i=1}^{\ell} \left[\frac{y_i - \hat{y}_i}{\hat{y}_i}\right]^2 \tag{23}$$

Since the predicted value $\hat{y}_i$ was used in the weighting function, the regression analyses had to be conducted iteratively. Initial guesses for the values of A_1 and A_2 were graphically obtained from the intercepts of the straight lines describing the behavior in Regions I and II, respectively, with the $\Delta K = 1.0$ axis. These values were used to describe the weighting function in the first iteration while improved values of A_1 and A_2 were calculated. Subsequently these improved values of A_1 and A_2 were used to determine the weighting function, and new values of A_1 and A_2 were obtained. This was repeated until the $(\mathrm{SSR})_{\text{rel.}}$ did not change by more than 5.0 percent in two subsequent runs. This convergence was typically accomplished in 2 to 3 iterations.

Procedure Used for Life Prediction

Fatigue lives were predicted for several CT and CCP specimens under loading conditions identical to those used for generating the original data by integrating the various equations. The integration was performed numerically using Simpson's rule with the aid of a digital computer.

Modeling Load Ratio Effects

It was mentioned earlier while describing the model that the data for a wide range of load ratios may be mathematically represented by selecting common n_1, n_2 and K_c values for all load ratios, and representing A_1 and A_2 as simple functions of R. It was also shown that common n_1, n_2, and K_c values can in fact be defined for the data at all load ratios between -1.0 and 0.8. The Region I behavior for $R = -1.0$ is excluded from this discussion because it is not characterized by sufficient data.

The values of A_1 and A_2 are plotted as function of $(1 - R)$ in Figs. 4 and 5, respectively. Conducting a simple least-square regression analysis results in the simplified equations

$$\begin{aligned} A_1 &= 3.6 \times 10^{14} (1 - R)^{15} && \text{for } 0.1 \le R \le 0.5 \\ A_1 &= 1.1 \times 10^{10} && \text{for } 0.5 \le R \le 0.8 \end{aligned} \tag{24}$$

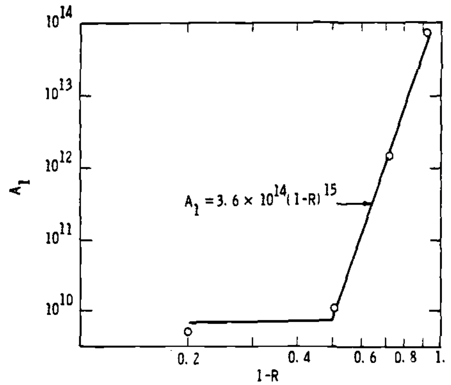

FIG. 4—*Value of the coefficient* A_I *(Eq 21) as a function of load ratio* R.

Similarly, the function describing the value of A_2 as a function of R is given by

$$A_2 = 1.74 \times 10^8 (1 - R)^{0.3} \text{ for } -1.0 \leq R \leq 0.8 \tag{25}$$

Equations 24 and 25 show that R-dependence is strong in Region I for $0.1 \leq R \leq 0.5$, and is weak in Region II for all load ratios. It is noted that the dependence of A_2 on R is consistent with the definition of $\Delta K_{\text{eff}} = (1 - R)^m \Delta K$ commonly used to normalize load ratio effects in Region II. Thus the wide-range fatigue crack growth rate data for $0.1 \leq R \leq 0.8$ can be represented by the equations

$$\frac{1}{(da/dN)} = \frac{3.6 \times 10^{14} (1 - R)^{15}}{(\Delta K)^{12.5}} + 1.74 \times 10^8 (1 - R)^{0.3} \left[\frac{1}{(\Delta K)^3} - \frac{1}{[34(1 - R)]^3}\right] \tag{26a}$$

for $0.1 \leq R \leq 0.5$ and

$$\frac{1}{(da/dN)} = \frac{1.1 \times 10^{10}}{(\Delta K)^{12.5}} + 1.74 \times 10^8 (1 - R)^{0.3} \left[\frac{1}{(\Delta K)^3} - \frac{1}{[34(1 - R)]^3}\right] \tag{26b}$$

for $0.5 \leq R \leq 0.8$

The predicted da/dN versus ΔK behavior for four load ratios between 0.1 and 0.8 are plotted in Fig. 6 along with the experimental data. Excellent agreement between the predicted lines and data are obvious. Thus it has been shown that the model has the necessary flexibility to model complex effects of load ratio on wide-range fatigue crack growth rate data. It is recognized that for other materials it may be necessary to

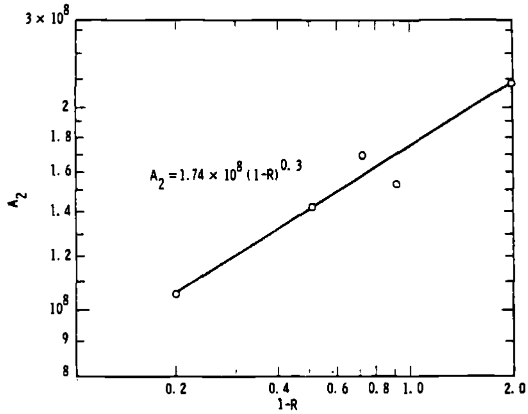

FIG. 5—*Value of the coefficient* A_2 *(Eq 21) as a function of load ratio* R.

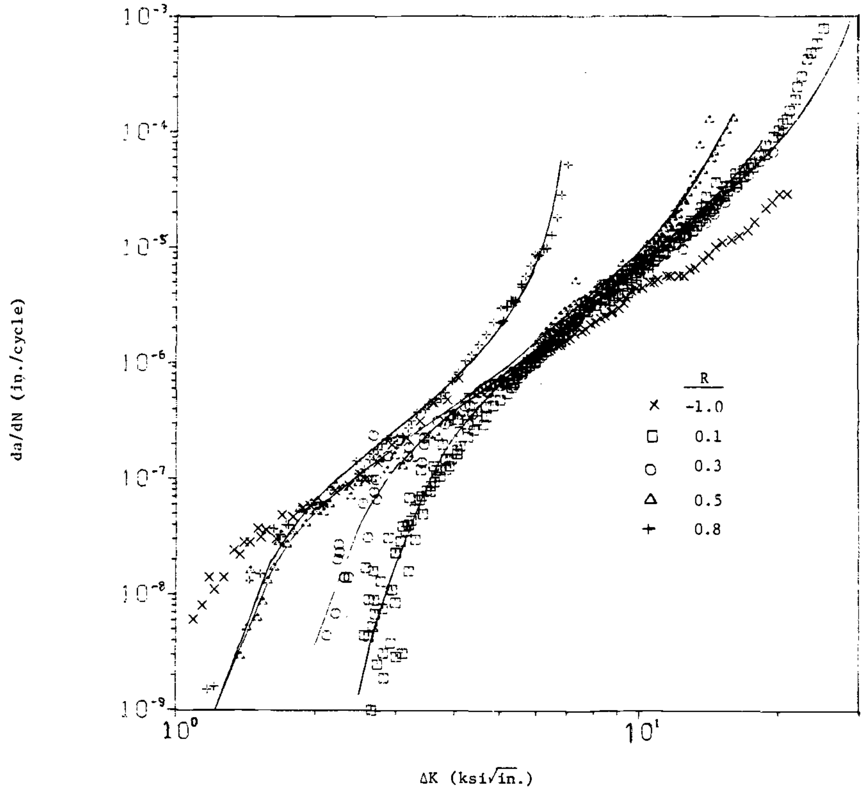

FIG. 6—*Comparison between the predicted FCGR behavior from Eqs* 26a *and* 26b *and the experimental data for 0.1* $\leq$ R $\leq$ *0.8.*

represent K_c as a function of R to get good fits. This change can be easily accommodated in the model.

By using search routines that are not available in a modern computer center or by using a multiple-nonlinear-regression analysis technique, it is possible to input available data for all load ratios and obtain best-fit parameters for all five constants in Eq 20*a* (that is, A_1, A_2, n_1, n_2, and K_c). This would replace the graphical determination of n_1, n_2, and K_c and subsequently choosing common values of these parameters for all load ratios which may result in judgment error.

APPENDIX IV

Participant/FCGR Description No. 4

The description considered is given in the form

$$da/dN = C\,(K_{max})^m\,[(K_{max} + K_e)(1 - R_{eff}) + {}^*K]^2 \tag{27a}$$

where the coefficients C and m are derived from Young's modulus by

$$C = E^2/1 \times 10^{23} \tag{27b}$$

$$m = 1.442 \times \ell n\,(10^{7.5}/E) \tag{27c}$$

with E expressed in units of pounds per square inch.

The threshold effect (ΔK_0 or ΔK_{th}) is accounted for by using an effective stress ratio defined by

$$R_{eff} = \frac{(K_{min} + \Delta K_0)}{K_{max}} \tag{28}$$

where ΔK_0 is a threshold value of ΔK that can be calculated directly if environmental effects are negligible ($K_e \cong 0$) by

$$\Delta K_0 = \Delta K - [da/dN/C\,(K_{max})^m]^{1/2} \tag{29}$$

When environmental effects are present, or suspect, the measured da/dN values from various stress ratios are projected and collapsed to a common curve (K_{max} versus projected da/dN) by

$$\text{measured } da/dN \left(\frac{1}{1 - R_{eff}}\right)^2 \tag{30}$$

Trial values of ΔK_0 are used to determine the best mesh. The so-determined value of ΔK_0 is then used in subsequent calculation and is constant.

To account for the influence that the environment has on the behavior, a stress-intensity factor parameter K_e is utilized; the parameter is given by

$$K_e = [\text{projected } da/dN/C\,(K_{max})^m]^{1/2} - K_{max} \tag{31}$$

which shows that K_e progresses in a linear fashion from 0 to a constant. The following terms apply to this behavior:

K_{e0} = K_{max} level where $K_e = 0$, and
K_{plat} = "plateau" K_{max} level where K_e becomes constant.

Then: For $K_{max} < K_{plat}$

$$K_e = K_{econst}\left[\frac{(K_{max} - K_{e0})}{(K_{plat} - K_{e0})}\right] \tag{32}$$

and $K_{e0} = 0$ for $K_{max} \leq K_{e0}$.

The material behavior in the upper region of FCGR is described through the use of a stress-intensity factor parameter $*K$. When $K_{max} > K_{fc}$, $*K$ is normally used. The parameter K_{fc} is defined as K "fatigue critical" and is determined during the extraction of ΔK_0 or K_e; that is, at K_{fc} the value of ΔK_0 will begin to decrease, while K_e will increase. K_{fc} is also quite obvious when the data are projected to a common base. (Values for ΔK_0 and K_e are ignored for K_{max} levels above K_{fc} when $*K$ is used; however, they do offer an alternative fit to the upper end of data.) The parameter $*K$ is given by

$$*K = \left[\frac{da/dN}{C\,(K_{max})^m}\right]^{1/2} - (K_{max} + K_e)(1 - R_{eff}) \tag{33}$$

Using Eq 33, a least-square fit of the form $*K = \alpha \exp\,[\beta \cdot K_{max}]$ is accomplished to determine α and β.

The set of parameters utilized to obtain the life predictions presented in Tables 8 and 9 are given in Table 13.

Method for Computing N_f

A simple computer program was written to determine the total number of cycles (N_f) required to propagate a crack from a specified initial to final length ($W = a_f - a_o$). The crack was "stepped" across this span in fixed increments using the relationship.

$$\text{increment} = W/X$$

where $X \geq 100$.

An expression for a mean stress-intensity ($\overline{K}$) was used in Eq 27*a* to calculate the crack growth rate.

$$\overline{K} = [(K_1 + K_2) \div 2 + 2K_3] \div 3 \tag{34}$$

K_1 is from a_1,
K_2 is from a_2 and $a_2 = a_1 + W/X$, and
K_3 is from a_3 and $a_3 = (a_1 + a_2/2$.

ΔN for an increment of crack growth is simply

$$\Delta N = \frac{W/X}{da/dN\ \text{predicted}} \tag{35}$$

ΔN is then predicted and if a_{final} has not been reached another pass begins where a_1 now equals a_2 etc.

TABLE 13—*Values of parameters for FCGR Description No. 4.*

Parameter	Value
ΔK_0 (ksi $\sqrt{\text{in.}}$)	1.55
K_0	3.0
$K_{e\text{const}}$	4.0
K_{plat}	4.43
K_{fe}	20.0
α	1.2×10^{-5}
β	0.4
E (psi)	10.3×10^{6}
C	1.06×10^{-9}
M	1.61754

APPENDIX V

Participant/FCGR Description No. 5

The FCGR description is given by the equation

$$\log_{10} (da/dN) = P_1 \exp (P_2 x) + P_3 \exp (P_4 x) + P_5 \tag{36}$$

This description is similar to the "SINH" models described in Appendix VI, except that different curvatures in the upper and lower regions are allowed through the choice of the pairs P_1, P_2, and P_3, P_4. The coefficient P_5 shifts the entire curve up or down.

The data were initially grouped by individual stress-ratio values and Eq 36 was fitted, giving five sets of constants. These were then plotted against R, but an attempt to correlate P_1, P_2, . . . , P_5 with R was unsuccessful.

A commercial statistical package program (BMDP) and an "in-house" curve-fitting program were used, both employing standard least-squares routines.

The constants for use with Eq 36 are

R	P_1	P_2	P_3	P_4	P_5
−1.0	0.01122	2.690	−5.250	−1.021	−4.381
0.1	0.00461	4.385	−13.720	−3.404	−5.083
0.3	0.7152	1.281	−25.300	−8.741	−7.792
0.5	1.096	1.240	−7.574	−14.43	−8.769
0.8	0.1156	3.780	−3.148	−8.100	−7.241

The statistical measures of goodness of fit are

R	RMS	Serial Correlation Coefficient
−1.0	0.004	0.383
0.1	0.029	0.778
0.3	0.015	0.117
0.5	0.012	0.106
0.8	0.006	0.176

where

$$\begin{aligned} \text{RMS} &= \text{residual mean square,} \\ \text{serial correlation coefficient} &= \Sigma r_i r_{i-1}/[\Sigma r_i^2\, \Sigma r_{i-1}^2]^{1/2} \\ r_i &= i\text{th residual.} \end{aligned} \tag{37}$$

For a description of the method used to integrate for a life prediction, see the appropriate section of Appendix II.

APPENDIX VI

Participant/FCGR Description No. 7 (Hyperbolic Sine Model)

The hyperbolic sine model is defined by

$$\log da/dN = C_1 \sinh [C_2(\log \Delta K + C_3)] + C_4 \tag{38}$$

where

$\log da/dN$ is plotted versus $\log \Delta K$,
C_1 = scale factor for vertical ($\log da/dN$) axis,
C_2 = scale factor for horizontal ($\log \Delta K$) axis,
C_3 = horizontal location of the hyperbolic sine point of inflection, and
C_4 = vertical location of the hyperbolic sine point of inflection.

Figures 7 to 10 illustrate the effect of varying each fitting parameter, C_1 to C_4, on the fatigue crack growth curve.

The fitting parameters, C_1 to C_4, are determined by minimizing the sum of the squared errors between the data and the regression line, as defined in Fig. 11. The minimum is determined by setting the partials of the error function equal to zero and solving the four resulting nonlinear equations simultaneously. The solutions are obtained by employing an iteration technique.

Two measures of fitting error are utilized. The standard error of the estimate (SEE), which is a measure of the true variability in $\log da/dN$ about the regression

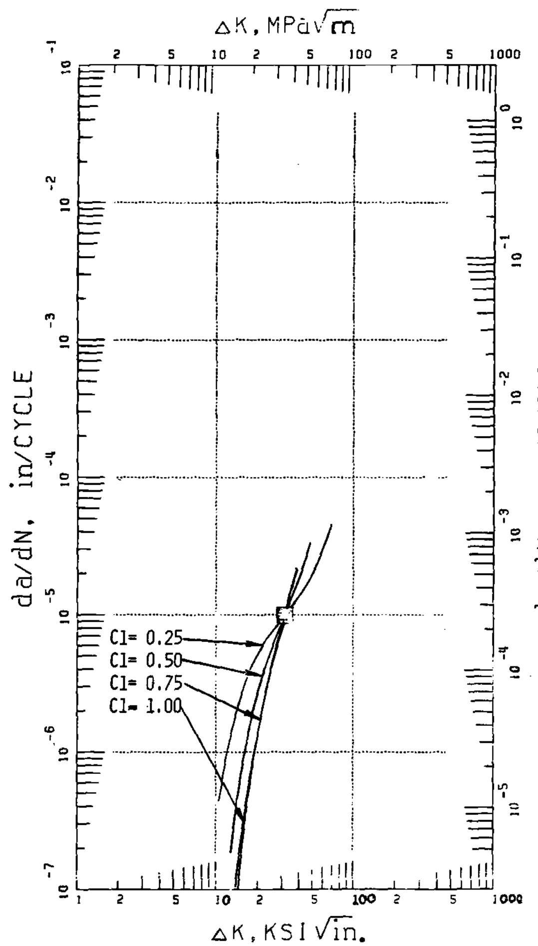

FIG. 7—*Effect of changing* C_l *on hyperbolic sine curve.*

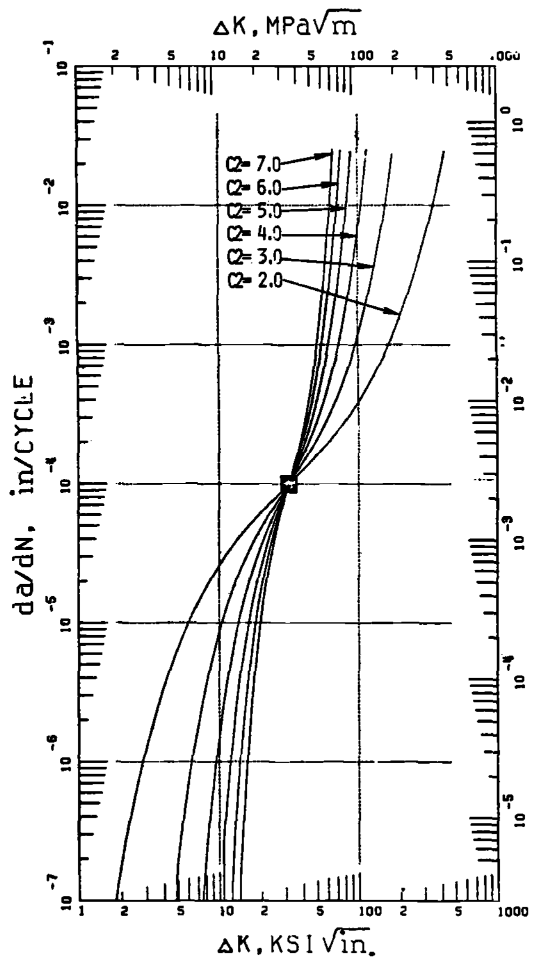

FIG. 8—*Effect of changing* C_2 *on hyperbolic sine curve.*

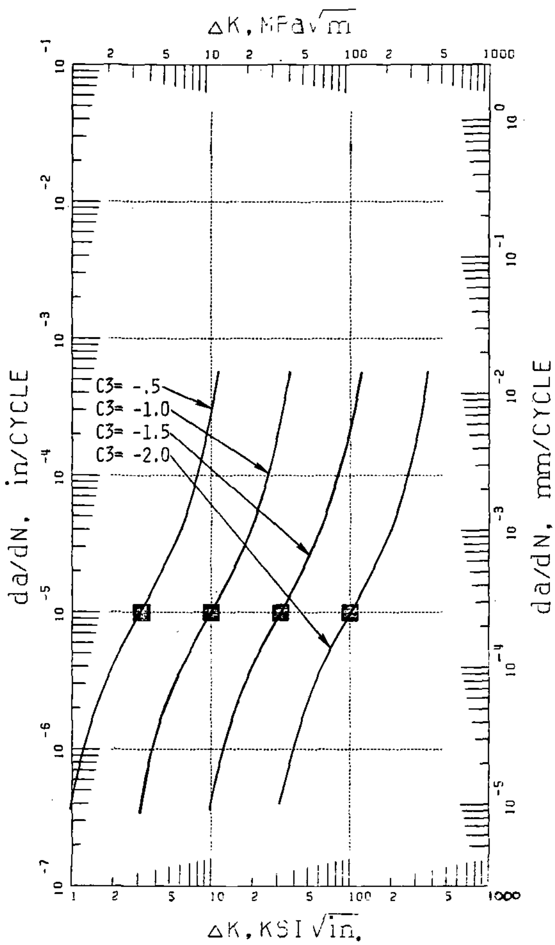

FIG. 9—*Effect of changing C_3 on hyperbolic sine curve.*

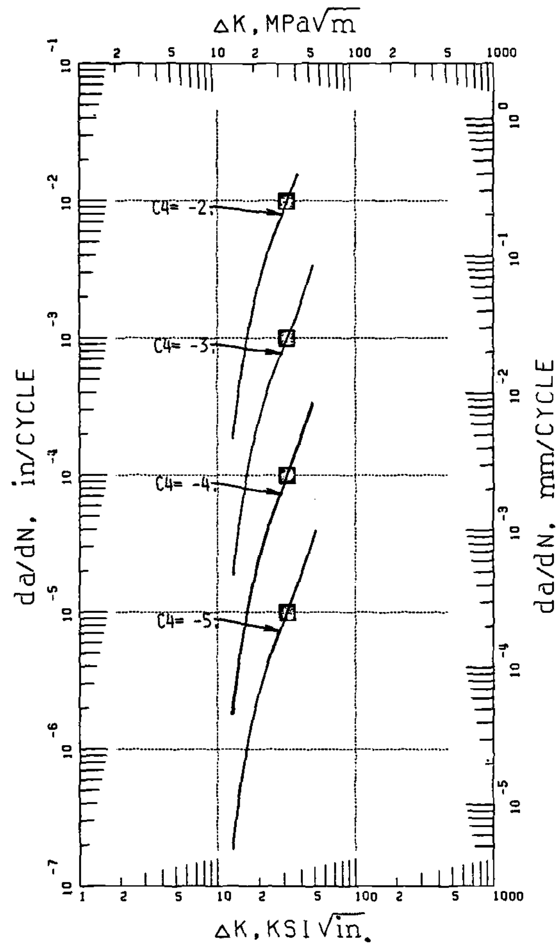

FIG. 10—*Effect of changing C_4 on hyperbolic sine curve.*

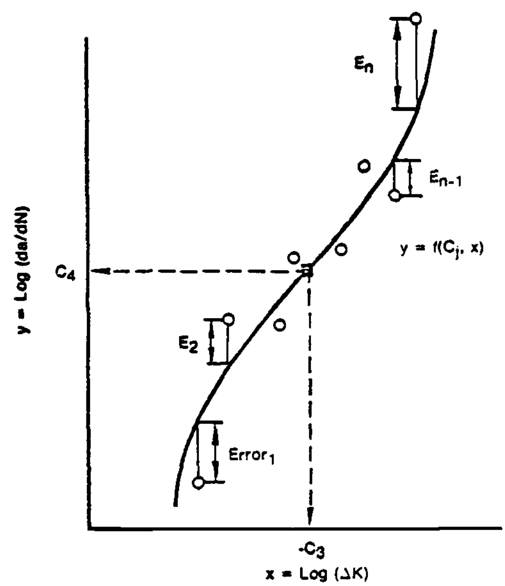

FIG. 11—*Method of least squares.*

line, and the sample coefficient of determination (R^2), which is the fraction of the total variation in log da/dN accounted for by the regression line. SEE and R^2 are defined as

$$\text{SEE} = \left(\frac{\Sigma\,(Y - \overline{Y_x})^2}{N - 2}\right)^{1/2} \tag{39}$$

and

$$R^2 = 1 - \frac{\Sigma\,(Y - Y_x)^2}{\Sigma\,(Y - \overline{Y})^2} \tag{40}$$

where

Y = log da/dN,
x = log ΔK,
$\overline{Y}$ = mean value of Y,
Y_x = mean value of Y from regression line, and
N = number of data points.

Table 14 gives values of R^2 and SEE for each stress ratio.

The life predictions (N_f) were obtained by numerically integrating, cycle by cycle, the expression

$$N_f = \int_{a_i}^{a_f} \frac{da}{da/dN} \tag{41}$$

where

$$da/dN = 10^{(C_1 \sinh[C_2(\log \Delta K + C_3)] + C_4)} \quad (42)$$

The FCGR data were fitted both individually for each stress ratio and collectively for all positive stress ratios. Table 15 lists the values of C_1, C_2, C_3, and C_4 for the individual stress-ratio fits. The collective models were generated using software specifically for producing FCGR models. This software has the capability of modeling FCGR data for varying stress ratio, temperature, frequency, dwell, overload ratio, and cycles between overload.

APPENDIX VII

Participant/FCGR Description No. 8

The description used was the four-parameter Weibull equation, which is actually a three-parameter Weibull cumulative distribution function with a fourth parameter added to normalize the stress-intensity variable.

The function is

$$\frac{da}{dN} = e + (v - e)\left[-\ln\left(1 - \frac{\Delta K}{Kb}\right)\right]^{1/k} \quad (43)$$

in terms of ΔK, this is

$$\Delta K = Kb^{*}\{1 - \exp\left[-\left(\left\{\frac{da/dN - e}{v - e}\right\}^{k}\right)\right] \quad (44)$$

The four coefficients (see Table 16) are

K_b = the normalizing parameter for ΔK (physically this represents the upper asymptote on the ΔK-axis),
k = shape parameter,
v = characteristic value (shape parameter), and
e = threshold (location parameter). This parameter can be thought of as Y (da/dN) axis intercept when it is positive. When it is negative it indicates

TABLE 14—*Values of* R^2 *and SEE for individual stress-ratio fits.*

Stress Ratio	R^2	SEE[a]
0.1	0.9820	0.1716
0.3	0.9797	0.1412
0.5	0.9781	0.2434
0.8	0.9933	0.0822
−1.0	0.9962	0.0652

[a] SEE = standard error of the estimate.

that there is a lower asymptote (threshold value) on the ΔK-axis. The threshold ΔK-value can then be solved by using Eq 44 and setting da/dN to zero.

The four coefficients in this equation were optimized to each data set by a rather unique procedure which utilizes nonlinear regression analysis and minimizes the sum of the squared normalized *perpendicular* distances between the predicted and actual da/dN, ΔK points. This optimization procedure is used rather than minimizing the sum of the squared residuals in the Y (dependent variable) or the X (independent variable) directions. If the residuals are minimized in the Y-direction, problems can be encountered due to the asymptotes and to the fact that the da/dN values can cover over five orders of magnitude. The residuals should not be minimized in the X (independent variable) direction for statistical reasons. Therefore, by minimizing the squared perpendiculars, these problems are eliminated.

Life-prediction determinations are obtained by numerical analysis with the fitted Weibull four-parameter function. For this investigation, life was predicted by calculating the integral

$$\int_{a_0}^{a_f} \frac{1}{f(\Delta K)} da = \int_{o}^{N_f} dN \tag{45}$$

The $f(\Delta K)$ was calculated from the optimized Weibull parameters and 200 equally spaced crack lengths between a_0 and a_f. Then an eight-knot spline function was fit to the $1/f(K_i)$ versus a_i data set to obtain the integral. A spline fit was used be-

TABLE 15—*Coefficients of the sinh equation for individual stress-ratio fits.*

Stress Ratio	Coefficients			
	C_1	C_2	C_3	C_4
0.1	0.8483	3.751	−0.948	−5.341
0.3	0.8173	3.350	−0.865	−5.561
0.5	1.2600	2.546	−0.754	−5.855
0.8	0.5930	5.236	−0.451	−6.656
−1.0	1.5386	1.524	−0.796	−5.884

TABLE 16—*Coefficients for the Weibull FCGR description.*

Stress Ratio	Coefficients				
	e	v	k	K_b	SSQ[a]
−1.0	−0.0142	277.469	0.4319	66.605	0.0024
0.1	−0.10355	82.3283	0.34296	28.77	0.0018
0.3	−0.08603	70.4906	0.3928	30.545	0.0028
0.5	−0.01919	9.17318	0.40443	15.736	0.0030
0.8	−0.01411	1.1506	0.3869	6.8466	0.0017

[a] A factor used to measure the sum of the squared residuals in the perpendicular direction.

cause it was already programmed, and the integration was done automatically. The fit always gave correlation coefficients equal to 1.0. The dependency of the life prediction on the Δa-increments was checked by dividing the crack interval into 500 equally spaced increments rather than 200. The life predictions were found to be identical for the cases checked.

This life-prediction procedure was not workable in all cases owing to the fact that the Weibull function is a mean curve fit. Therefore in the threshold regime there are some data points which are on both sides of the fitted mean curve. If at a given crack length the stress-intensity factor is determined to have a value below the threshold value obtained from the fitted Weibull function then the FCGR is undefined. By taking into account confidence bonds and probabilities, this problem can be alleviated.

The FCGR data sets were each fitted individually; the joined data sets for each R-ratio were also fit. Two of the joined data set fits are shown in Figs. 12 and 13 for stress ratios of 0.1 and 0.3, respectively.

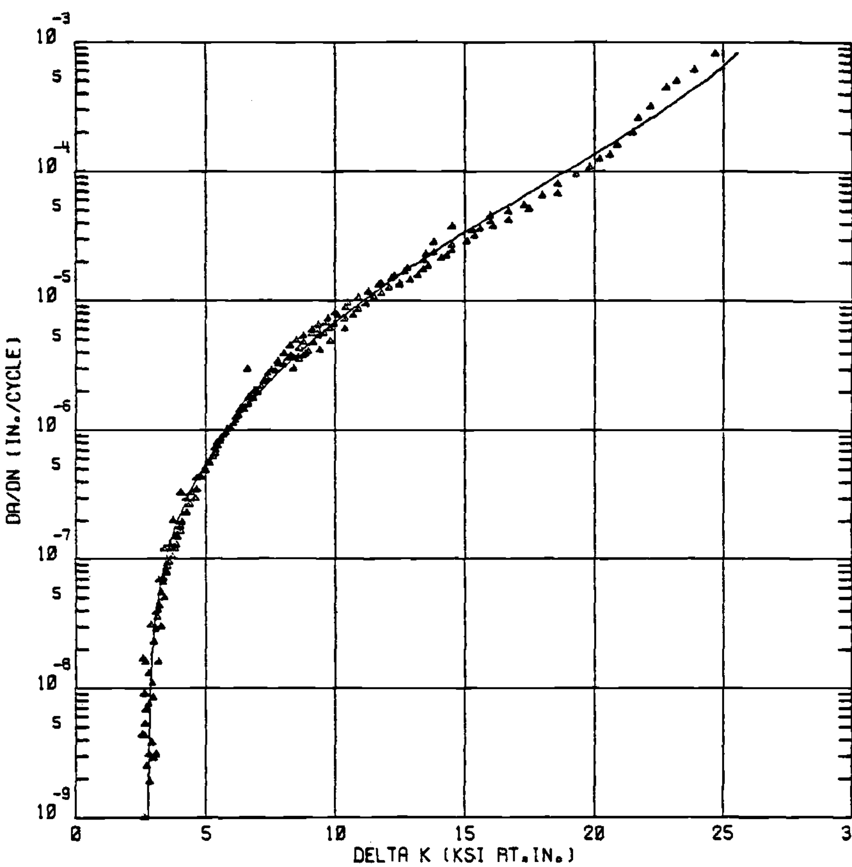

FIG. 12—*FCGR data and fitted curve for a stress ratio* (R) *of 0.1.*

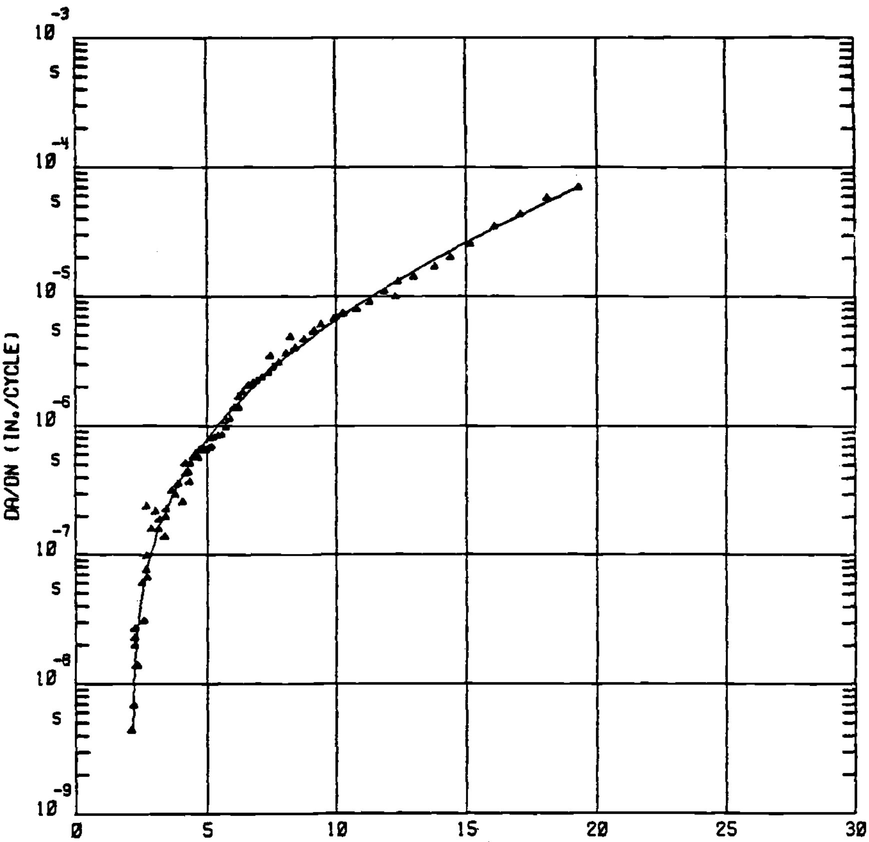

FIG. 13—*FCGR data and fitted curve for a stress ratio* (R) *of 0.3.*

APPENDIX VIII

Participant/FCGR Description No. 9 (Tensile Ligament Instability Model)

The tensile ligament instability model (TLIM) predicts crack growth behavior by assuming that instability mechanisms induce separation of microstructural tensile ligaments at the crack tip. The model associates properties of such microligaments with measurements of monotonic and full cyclic stress-strain curves of macrospecimens. Crack growth is taken as a means of strain-hardening microligaments along the crack tip to offset strength reductions, hence instability tendencies, from three effects: (*1*) Poisson contraction, (*2*) stress relaxation, and (*3*) environmental surface attack. The properties used are values of true stress σ and plastic-only strain hardening rate

θ_p ($= d\sigma/d\epsilon_p$) as a function of total elastic plus plastic strain ϵ. These define a dimensionless growth rate factor G for each condition (Fig. 14).

$$G = \left[\epsilon\left(\frac{\theta_p}{\sigma-} - \sqrt{3/2}\right)\right]^{-1} \tag{46}$$

The values of monotonic growth rate factors (G_1) are generally much greater than cyclic ones (G_2). The model associates all stress-relaxation-induced crack growth with G_2; all environmentally induced growth with G_1, yielding

$$\Delta a = 4 r_T m \ln(1 + t_N/t_L) G_2 + 8 \Delta r_T G_1 \tag{47}$$

for an overall growth rate factor (GRF), with typical loading wave form

$$\mathrm{GRF} = G_2 + [\Delta r_T/r_T] G_1/0.15m \tag{48}$$

where a is crack length, r_T is microligament radius and Δr_T its environmental surface attack depth in one cycle, m is the stress-relaxation exponent, and t_L and t_H are the loading time and hold duration of the fatigue wave form, respectively. Lacking knowledge of Δr_T and of r_T, their ratio is varied parametrically as 2^N, where N is varied from -21 to -6.

$$\overline{G}(N) = G_2 + [2^N] G_1/0.15m \tag{49}$$

The $G(N)$ family of curves generally fits threshold and Stage II corrosion fatigue growth, in which the amount of surface attack is limited by time or the saturation level of time-dependent processes. Another way to limit Δr_T is by the ligament-disturbing plastic strain $\Delta\epsilon$ due to loading and growth of the crack in the cycle

$$G(M) = G_2 + \Delta\epsilon\left[\frac{\Delta r_T/r_T}{\Delta\epsilon}\right] G_1/0.15m \tag{50}$$

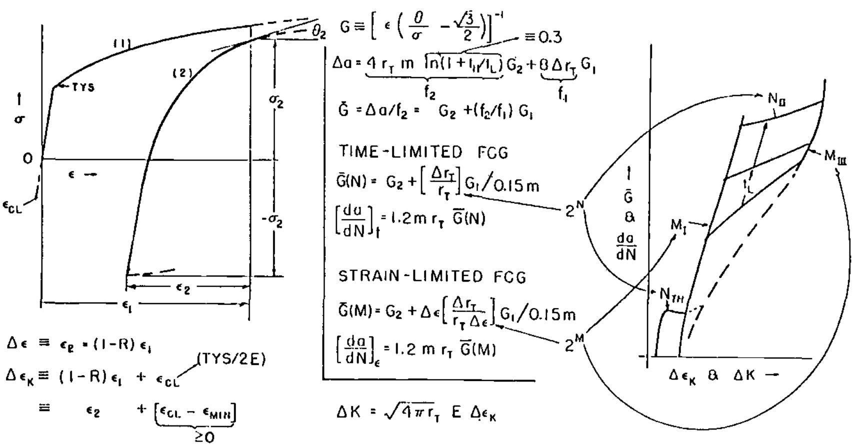

FIG. 14—*Tensile ligament instability model.*

where the strain-normalized surface attack is varied as a parameter, by giving it the value 2^M, where M is varied from -10 to $+6$. The strain excursion associated with these overall growth rate factors, and with ΔK as well, is

$$\Delta \epsilon_K = (1 - R)\epsilon_1 + \epsilon_{CL} = \epsilon_2 + [\epsilon_{CL} - \epsilon_{min}] \geq 0 \quad (51)$$

$$\Delta K = \sqrt{4\pi r_T}\ \Delta \epsilon_K \quad (52)$$

Here R is the stress ratio and ϵ_{CL} is a "closure strain" set equal to TYS/2E, where TYS is monotonic yield strength and E is Young's modulus.

The predictions are set up as parametric curve familes of $G(N)$ and $G(M)$ versus $\Delta\epsilon_K$, drawn to the same log scale as the FCGR data. A graphical overlay matching procedure fixes the value of r_T and values of M and N fitting the various stages of FCGR independently of R.

Virtues of this model include its basis in measured mechanical properties, and the fitting parameters are minimal in number and have some physical connotation.

APPENDIX IX

Participant/FCGR Description No. 10 (A Table Lookup Procedure)

A table lookup procedure obtains FCGR (da/dN) values from a table containing FCGR and corresponding stress-intensity factor range (ΔK) data. To build the table, the experimental FCGR data for each stress ratio were graphically described as a function of ΔK. The data at each stress ratio were then graphically fitted with a curve describing the mean FCGR behavior. Since the curve is visually fitted to the data, its ability to predict the FCGR behavior depends on the care with which it is drawn. Each stress ratio was fitted individually. A sample data set with its associated curve is shown in Fig. 15. The da/dN and ΔK points in the table were taken from points on the curve. Due to the shape of the curve and the scale of the plots, the da/dN axis was divided into equal log (da/dN) intervals. For the task group activity, five points were taken per decade [for example, 10^{-5}, 1.6×10^{-5}, 2.5×10^{-5}, 4.0×10^{-5}, 6.3×10^{-5}, and 10^{-4} in./cycle (2.54 μm/cycle)]. Division of the ΔK-axis into similar segments would have resulted in ten or fewer values being taken, causing a loss of accuracy in the prediction of the FCGR data. Obtaining an equal number of points by subdividing the ΔK-axis in a similar manner was impossible to accomplish with any accuracy with the scale and length of the ΔK-axis used.

The table used in the procedure is organized as shown in Table 17. In order to predict the experimental FCGR data, the values contained in the table were interpolated. Several methods of interpolation were tried: a seventh-order lagrangian interpolation, linear interpolation between the logs of two values, and linear interpolation between two values in the table. Life predictions for the specimens in Table 4 were made using each of the interpolation schemes. All three methods provided reasonably accurate life predictions for the specimens used. The third scheme was chosen to be used for the rest of the life predictions because of its simplicity. The coefficients of correlation for this FCGR prediction scheme are listed in Table 18 as a function of stress ratio.

To find predicted specimen lives, an incremental crack length (Δa) was first found

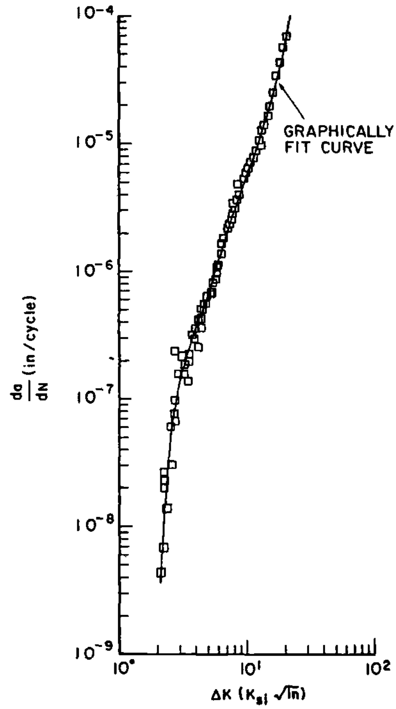

FIG. 15—*Curve fit to data set.*

TABLE 17—*Organization of FCGR versus ΔK table.*[a]

$\frac{da}{dN}$	ΔK ($R = 0.1$)	ΔK ($R = 0.3$)
0.004	2.76	2.10
0.0063	2.78	2.16
0.01	2.80	2.20
0.016	2.88	2.29
0.0255	2.98	2.37
0.04	3.16	2.48
...	...	...
...	...	...
...	...	...

[a] da/dN in inch/cycle and ΔK in ksi $\sqrt{\text{inch}}$.

TABLE 18—*Coefficients of correlation for the graphical/table lookup/interpolation scheme.*

Stress Ratio (R)	Coefficient of Correlation
0.1	0.957
0.3	0.996
0.5	0.951
0.8	0.993
−1.0	0.994

for each specimen so that the change in crack length just prior to the final crack length (a_f) kept the relative stress-intensity factor change below some level; that is

$$\frac{\Delta K|_{af} - \Delta K|_{af - \Delta a}}{\Delta K|_{af}} \approx k \tag{53}$$

Several values for k were tried in order to determine the one that gave the best predictions for the three specimens listed in Table 4. The value finally chosen for k was 0.001. Once the crack growth increment on the basis of Eq 53 is calculated, the predicted life is determined. A stress-intensity factor is calculated at the current crack length, and the table is interpolated to find the corresponding crack growth rate, using the interpolation scheme decided upon earlier. An increment of life (ΔN_i) is calculated by

$$\Delta N_i = \frac{\Delta a}{da/dN|_i} \tag{54}$$

The current crack length is then incremented by Δa and the procedure repeated. The final life is found by summing all the ΔN_i from a_o to a_f.

Bibliography

Chu, H. P., "Effect of Mean Stress Intensity on Fatigue Crack Growth in a 5456-H117 Aluminum Alloy," presented at the Seventh National Symposium on Fracture Mechanics, College Park, Md., Aug. 1973.

Collipriest, J. E. and Ehret, R. M., "A Generalized Relationship Representing the Sigmoidal Distribution of Fatigue Crack Growth Rates," Rockwell International Space Division, Paper No. SD 74-CE-0001, March 1979.

Elber, Wolf, "The Significance of Fatigue Crack Closure," *Damage Tolerance In Aircraft Structures, ASTM STP 486,* American Society for Testing and Materials, 1971, pp. 230-242.

Fitzgerald, J. H., "Empirical Formulations for the Analysis and Prediction of Trends for Steady-State Fatigue Crack Growth Rates," *Journal of Testing and Evaluation,* Vol. 5, No. 5, Sept. 1977, pp. 343-353.

Hall, L. R., Engstrom, W. L., and Shah, R. C., "Fatigue and Fatigue Crack Growth Behavior of Surface Flaws and Flaws Originating at Fastener Holes," AFFDL-TR-74-47, Vol. 1, Air Force Flight Dynamics Laboratory, Wright-Patterson AFB, Ohio, 1977.

Hudak, S. J., Jr., Saxena, A., Bucci, R. J., and Malcolm, R. C., "Development of Standard

Methods of Testing and Analyzing Fatigue Crack Growth Rate Data," AFML-TR-78-40, Air Force Materials Laboratory, Wright-Patterson AFB, Ohio, 1978.

Hudson, C. M., "Effect of Stress Ratio on Fatigue Crack Growth in 7075-T6 and 2024-T3 Aluminum Alloy Specimens," NASA TN D-5390, National Aeronautics and Space Administration, Aug. 1969.

Hudson, C. M. and Newman, J. C., Jr., "Effect of Specimen Thickness on Fatigue Crack Growth Behavior and Fracture Toughness of 7075-T6 and 7178-T6 Aluminum Alloys," NASA TW D-7173, National Aeronautics and Space Administration, April 1973.

James, L. A., "The Effect of Stress Ratio on Fatigue Crack Propagation of Type 304 Stainless Steel," *Nuclear Technology*, No. 14, 1972, p. 163.

Jaske, C. E., Fedderson, C. E., Davies, K. E., and Rice, R. C., "Analysis of Fatigue, Fatigue Crack Propagation, and Fracture Data," NASA CR 132332, National Aeronautics and Space Administration, Nov. 1973.

Katcher, M. and Kaplan, M., "Effects of *R*-Factor and Crack Closure on Fatigue Crack Growth for Aluminum and Titanium Alloys," *Fracture Toughness and Slow-Stable Cracking, ASTM STP 559*, American Society for Testing and Materials, 1974, pp. 264-282.

Krafft, J. M. and Smith, H. L., "Ligament Instability Model for Stress Corrosion and Fatigue Crack Propagation in a 4340 Steel," NRL Memo Report No. 2597, Naval Research Laboratory, Washington, D.C., April 1973.

Krause, D. J. and Crooker, T. W., "Effects of Constant Amplitude Loading Parameters on Low-Cycle Fatigue Crack Growth in 140- to 130-ksi Yield Strength Steel," Report of NRL Progress, Naval Research Laboratory, Washington, D.C., March 1973.

Mayle, R., "A Critical Study of Several Crack Growth Equations Which Model the Effect of Load Ratio," AFFDL-TM-FBR-73-154, Air Force Flight Dynamics Laboratory, Wright-Patterson AFB, Ohio, 1973.

Paris, P. C. and Erdogan, F., "A Critical Analysis of Crack Propagation Laws," *Journal of Basic Engineering, Series D of the Transactions of the American Society of Mechanical Engineers*, Vol. 85, No. 3, 1963, p. 528.

Reeves, R. K. and Hoeppner, D. W., "A Useful Analysis of Center Cracked Panel Crack Growth Data of a 0.40/0.50 Carbon Steel," *Engineering Fracture Mechanics*, Vol. 10, 1978, pp. 571-581.

Roberts, R. and Erdogan, F., "The Effect of Mean Stress on Fatigue Crack Propagation in Plates Under Extension and Bending," *Journal of Basic Engineering, Series D of the Transactions of the American Society of Mechanical Engineers*, Vol. 89, 1967, p. 885.

Walker, K., "The Effect of Stress Ratio During Crack Propagation and Fatigue for 2024-T3 and 7075-T6 Aluminum," *Effects of Environment and Complex Load History on Fatigue Life, ASTM STP 462*, American Society for Testing and Materials, 1970, pp. 1-14.

Engineering Applications

S. W. Hopkins[1] *and C. A. Rau, Jr.*[1]

Prediction of Structural Crack Growth Behavior under Fatigue Loading

REFERENCE: Hopkins, S. W. and Rau, C. A., Jr., "**Prediction of Structural Crack Growth Behavior under Fatigue Loading,**" *Fatigue Crack Growth Measurement and Data Analysis. ASTM STP 738.* S. J. Hudak, Jr., and R. J. Bucci, Eds., American Society for Testing and Materials, 1981, pp. 255-270.

ABSTRACT: Structural components which undergo operational fatigue cycles have historically been designed for fatigue resistance based upon crack initiation data generated on smooth and notched laboratory specimens. More recently, reliability has been improved by using linear elastic fracture mechanics (LEFM) to assure that flaws, even if present, cannot grow to a dangerous size during service. The methodology and input data utilized for LEFM evaluation are described, and the impact of variations in key input parameters are discussed in detail. Specifically, the paper describes the sensitivity to (*1*) loading parameters: applied cyclic stresses, mean stresses, residual stresses, load spectrum, and stress distributions, (*2*) local crack driving force: crack size, shape, orientation, growth, and growth mode, (*3*) materials properties: crack growth rate constants, crack growth threshold, and response to spectrum overloads, and (*4*) initial flaw size, with and without nondestructive inspection.

Presently, LEFM analyses are often deterministic and utilize conservative (worst-case) assumptions for all input parameters which are not known. The assumptions that all worst-case conditions occur simultaneously lead to extremely conservative designs which may be economically unacceptable. Probabilistic fracture mechanics methods have been developed which incorporate the statistical variations or uncertainties that actually exist and establish a more realistic quantitative basis for design allowables and accept/reject criteria, which optimize the cost/risk trade-offs that must be made.

KEY WORDS: crack propagation, fatigue (materials), crack growth threshold, fracture toughness, spectrum overloads, initial crack, final crack, nondestructive inspection, linear elastic fracture mechanics, probabilistic fracture mechanics, inspection reliability, pre-inspection material quality

The reliability of structural components which undergo various operational fatigue cycles has been of increasing concern during recent years. Historically, structural components have been designed for either infinite or

[1]Manager, Fracture Mechanics Group, and vice-president and general manager, respectively, Failure Analysis Associates, Palo Alto, Calif. 94304.

finite cyclic life based upon crack initiation data generated in the laboratory. To evaluate structural reliability when defects are possible or to extend the cyclic life of existing designs, linear elastic fracture mechanics (LEFM) has been used in conjunction with the various nondestructive inspection (NDI) techniques. The NDI technique and its reliability to detect defects of specified sizes is a major factor in implementing a fracture mechanics-based life prediction. This paper describes how specific NDI requirements and optimum accept/reject criteria can be defined by fracture mechanics analysis and evaluation of the cost/risk trade-offs.

Analysis Procedure

There are four major inputs to a fracture mechanics fatigue life prediction: (*1*) the loads and stresses, (*2*) the materials properties, (*3*) the crack driving force, and (*4*) the crack size after inspection. (Subsets to each major input item will be discussed later.) Utilizing these inputs, life-prediction computer codes can calculate crack growth progression as a function of cycles, as shown schematically in Fig. 1.

Loads and Stresses

The first items necessary to calculate the crack driving forces are the structural loadings, which consist of both applied and residual stresses. One important observation is that, unlike conventional crack initiation calculations, the stress distribution along potential crack paths needs to be known as well as the surface stresses. It is relatively straightforward, although at times expensive, to compute the stresses in an unflawed structure due to applied loadings. However, the residual fabrication stresses are unknown in a majority of the structures. It is important to at least identify the sign of any residual stresses and to make a reasonable estimate of their magnitudes. The sign of the residual stresses will identify whether the predicted crack growth rates are conservative. For example, if tensile residual stresses are present, then the predicted crack growth rates would be slower if those stresses were ignored than observed in the field. On the other hand, if compressive residual stresses are present, then the predicted crack growth rates would be faster than expected in the field. To put residual stresses and mean stress in perspective, it should be stated that the crack growth rates are much less affected by a change in mean stress than they would be by a similar change in the cyclic stress.

Crack Driving Force

Knowing the uncracked stress field, we must compute the crack driving force (that is, the crack-tip stress intensity factor K as the crack grows

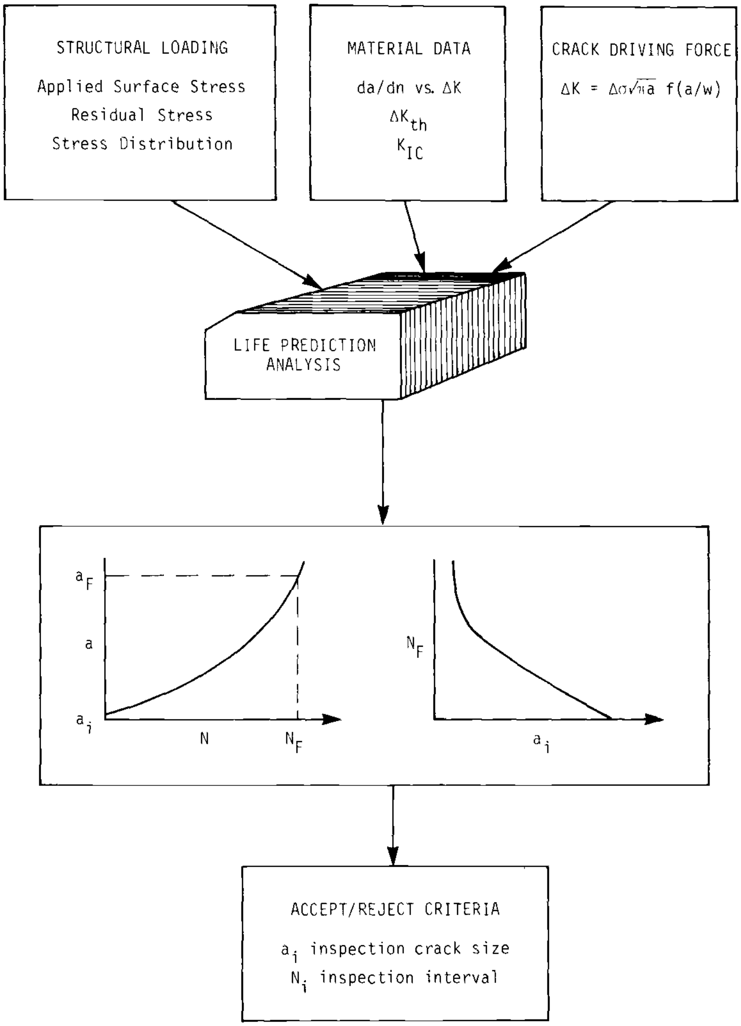

FIG. 1—*Deterministic linear elastic fracture mechanics (LEFM) life-prediction system.*

through the structure). There are various handbooks [*1,2*][2] available with *K*-solutions for most common crack shapes, simple structures, and loading types. There are also several general computer codes. One such computer code, called BIGIF [*3*], incorporates a substantial library of *K*-solutions, and also has the capability to both compute the rate of crack growth and to numerically integrate to compute total life from any specified initial crack.

[2]The italic numbers in brackets refer to the list of references appended to this paper.

Most codes have only a limited number of K-solutions, and these may not exactly represent the structure to be analyzed. Some engineering modeling will often be necessary to perform an appropriate K-calculation and life prediction. The extent of the engineering modeling will depend upon the complexity of the cracked structure and the accuracy required from the prediction.

Materials Properties

In general, for fatigue life predictions, three types of materials crack growth data are necessary, each for the environment and loading rates of concern in service. Firstly, we must obtain the crack growth rate as a function of the range (ΔK) of crack-tip stress intensity factor and mean (K_{mean}) value. That is

$$\frac{da}{dN} = f(\Delta K, K_{mean}, \text{loading rate, environment, etc.}) \qquad (1)$$

where ΔK must be defined in the prediction model in the same manner as was used to report the crack growth rate data. Specifically, when the structure undergoes tension-compression cycling ($R < 0$), whether or not the compression loading is used to calculate ΔK should be consistent with the manner in which ΔK was calculated in the reported crack growth rate data. Secondly, we must obtain the materials fracture toughness (K_c) where unstable crack growth occurs. Finally, the materials fatigue crack growth threshold (ΔK_{TH}) below which cracks will not grow at the specified mean stress levels should be obtained. Many structures experience a range of spectrum of cyclic loads rather than constant amplitude cyclic loading. In such cases when the cracks are small, only the highest loads produce ΔK that exceed the crack growth threshold and contribute to crack advancement. However, when the crack becomes larger, more of the cyclic loads contribute to crack advancement.

Typical crack growth rate data are shown in Fig. 2 for a Ti-6Al-4V alloy [*4*] at both 294 K (room temperature) and 616 K (650°F) in laboratory air environment, and for eight different R-ratios, where ($R \equiv \sigma_{min}/\sigma_{max} \equiv K_{min}/K_{max}$) is related to the mean stress or mean K. As can be seen from the data, a doubling of the cyclic stress (that is, doubling ΔK for a fixed crack length) increases the crack growth rate by a factor of ten (10). On the other hand, a five-fold increase in R from 0.1 to 0.5 has a somewhat lesser effect, increasing the crack growth rate by 2.5. This illustrates why small residual stresses only moderately affect the fatigue life of a structure.

The crack growth rate data in Fig. 2 were found to be independent of the cyclic loading rate at room temperature, and only slightly different at 616 K. However, in aggressive environments or at elevated temperatures, this is not generally true, and the crack growth rates may depend on both the cyclic

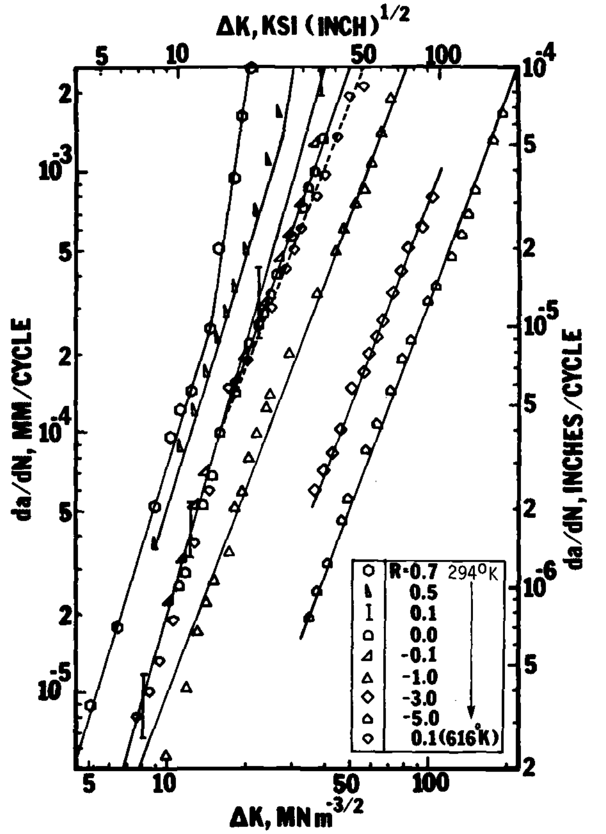

FIG. 2—*Crack growth rate as a function of stress intensity range for various* R*-ratios on Ti-6Al-4V material.*

loading rate as well as the materials yield strength. Rolfe and Barsom [5] have shown the effect of cyclic frequency and yield strength on the crack growth rate of steels in a 3 percent sodium chloride (NaCl) environment. The crack growth rate will usually increase with decreasing cyclic loading rates.

For most applications, specific crack growth rate data for the precise loading conditions experienced will not be available, and therefore some interpolation or extrapolation of the data will be necessary. To extend the crack growth rate data to other R-ratios, we have utilized [4] the following approach: (*1*) replace ΔK by ΔK_{eff} in the crack growth rate equation, and (*2*) estimate ΔK_{eff} by

$$\Delta K_{\text{eff}} = \frac{B}{A - R} \Delta K \tag{2}$$

where ΔK is calculated using the full range of $\Delta\sigma$ independent of R-ratio, A is a material and environment parameter, and B is determined so that $\Delta K_{eff} = \Delta K$ at the R-ratio where the data exist.

For the titanium data (Fig. 2) we determined that A ($=B$) $= 1.73$, which allows easy computation of ΔK_{eff} and the crack growth rates for both positive and negative R-ratios. Equation 2 is just one of many equations [4] that have been used to predict crack growth rate data where data for the specific R-ratio do not exist. Elber [6], for example, has presented an equation which predicts observed experimental data on aluminum at positive R; however, at large negative R-ratios, his equation calculates a negative ΔK_{eff} which is physically and computationally unreasonable.

The next materials input required is the materials fracture toughness (K_c) in the environment of concern. This parameter is more sensitive to thickness, yield strength, and environment than the fatigue crack growth rate data. Once the thickness exceeds a critical value, plane strain conditions are obtained and the fracture toughness is independent of thickness. However, below this critical thickness, there is an inverse relationship between the fracture toughness and thickness. There is also an inverse relationship between the materials yield strength and the fracture toughness of the material. For environments which cause time-dependent crack extension, the fracture toughness data should be replaced by some other material property in the cyclic life calculation. If elevated temperature is the environment, then K_{max} for some acceptable time-dependent crack extension (da/dt) should be used to establish the critical crack size. Or, if NaCL is the environment, then K_{ISCC} should be used to establish the critical crack size. In most applications which experience large numbers of cycles at low stress levels, a large variation in critical crack size will only moderately affect the cyclic life of the structure, as will be discussed in detail later. Therefore the exact fracture toughness value will not be critical.

The materials fatigue threshold (ΔK_{TH}) is the other materials input necessary for this analysis. ΔK_{TH} is defined as the ΔK-level below which a crack will not propagate. ΔK_{TH} can define the defect size which will grow under the fatigue loading, or it can also define the largest crack which can be tolerated before small vibratory stresses cause very rapid crack growth to failure. Hopkins et al [7] have shown a linear relationship between R-ratio and ΔK_{TH} for a titanium (Ti-6Al-4V) alloy (Fig. 3). Because ΔK_{TH}-data for most materials at various R-ratios are limited, this linear relationship is extremely useful to approximate behavior, where the exact material behavior is not available.

Life Prediction: Accept/Reject Criteria

Once all of the various material and structural inputs have been obtained, the life prediction can be performed through integration of Eq 1. This integration to predict crack length versus cycles in most cases needs to be done

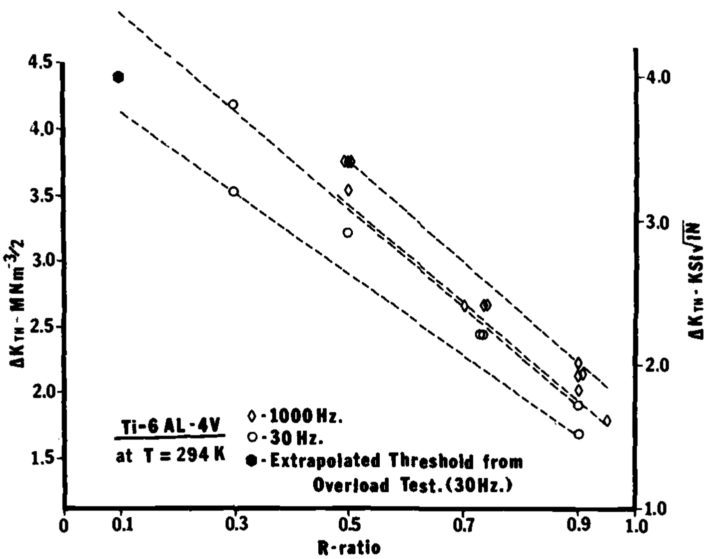

FIG. 3—*Basic threshold stress intensity factor as a function of stress ratio for Ti-6Al-4V at 294 K and 30 and 1000 Hz (Ref 7).*

numerically using a computer code. If, however, a large number of simplifying assumptions are made, then the calculation can be done in closed form. In general, the material's crack growth behavior is represented by Eq 1 as shown in Fig. 2. If the loading on the structure is assumed to be such that a constant relationship between ΔK and K_{mean} (R = constant) exists, and the material's crack growth rate can be represented by a simple power law, then Eq 1 becomes

$$\frac{da}{dN} = A\,\Delta K^n \tag{3}$$

where A and n are constants that depend on the mode of loading, the type of crack growth, operating environment, and material. By rearranging Eq 3 and integrating, we can obtain a simple closed-form equation (Eq 4) for the failure lifetime starting with an initial crack length (a_i) and failing where the crack driving force equals the fracture toughness of the material ($a = a_c$ at $K = K_c$). The critical crack size (a_c) is the upper limit of the integration.

$$N_f = \int_0^{N_f} dn = \int_{a_i}^{a_c} \frac{da}{A\,\Delta K^n} = \frac{1}{A(\Delta\sigma\sqrt{\pi\lambda}\,)^n} \int_{a_i}^{a_c} \frac{da}{a^{n/2}} \tag{4}$$

$$N_f = \frac{1}{A(\Delta\sigma\sqrt{\pi\lambda}\,)^n\left(\dfrac{n}{2} - 1\right)} \left[\left(\frac{1}{a_i}\right)^{n/2-1} - \left(\frac{1}{a_c}\right)^{n/2-1} \right]$$

where λ is a geometry/load factor that depends on the shape of the crack, the structure, and the loading type. For this integration, λ has been assumed to be a constant. For more complex geometries, where λ is not a constant or where the material's crack growth behavior can not be represented with Eq 3, the integration can not be done in closed form, but the same procedure is done numerically with a computer code.

At a constant R-ratio, the material's crack growth behavior will not be represented by the simple power law (Eq 3), where A and n are constants for the entire crack growth rate of concern. For low crack growth rates, A and n will have one set of values and will change as the crack growth rate increases. In general, these data can usually be represented from ΔK_{TH} ($da/dN <$ 10^{-10} in./cycle) to K_c ($da/dN > 10^{-3}$ in./cycle) with four sets of A and n. By using this segmented power law relationship, numerical integration of Eq 3 is simplified, and the limits of integration are established by the ΔK-levels over which that specific set of A and n are valid. If four sets of constants are required to represent the crack growth rate data, then four integrations of Eq 3 will be required to calculate the total cyclic crack growth of the structure.

The output of this analysis is a table or a curve (Fig. 1) of crack length versus cycles under service conditions. The total crack propagation lifetime will depend on the initial crack size input into the analysis. To avoid having to repeat the analysis unnecessarily, an initial crack size smaller than anticipated to be of concern is usually input. The results can eventually be replotted for different initial crack sizes and cycles remaining (Fig. 1). This allows an easy evaluation of cyclic life for different initial crack sizes. When acceptable cyclic life is defined, the maximum acceptable initial crack size (or defect) that needs to be found with NDI can be determined. Alternatively, if the NDI capability is known, then the number of acceptable cycles between inspections can be determined.

To illustrate the aforementioned fracture mechanics fatigue analysis procedure, we will describe an example which includes a predominant low cycle fatigue (LCF) loading, with periodic overloads and high-frequency vibrations of low amplitude (Fig. 4). The stress indicated in Fig. 4 is the maximum surface stress on the structure. The low frequency loading in this example is very simple, typical of the start-up/shutdown cycle of most rotating machinery. The fatigue cycle could also be much more complex without any change in the procedure, except that a block of cycles representing the smallest repeatable increment of loading would be utilized instead of individual LCF cycles.

The material data used in this hypothetical analysis are (*1*) Fig. 2, fatigue crack growth rate behavior, (*2*) Fig. 3, threshold data, and (*3*) the assumption that this material has a plane strain fracture toughness of $K_{\mathrm{Ic}} = 65$ MN m$^{-3/2}$. The stress distribution along the crack path has a stress gradient slightly larger than that associated with a stress concentration factor of three (3). A semicircular crack with an aspect ratio ($a/2c$) equal to 0.5 was mod-

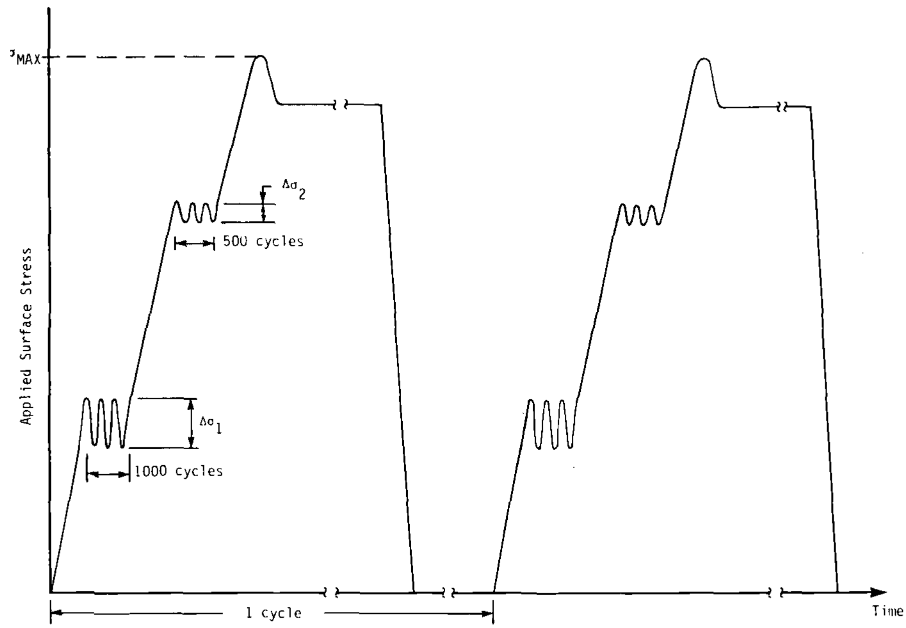

FIG. 4—*Typical surface stresses for most rotating machinery which operates at speeds above its natural resonant frequency. In this example the operating speed is above the second resonant frequency.*

eled to obtain the appropriate stress intensity solution, and the BIGIF computer code was used to perform a fracture mechanics fatigue life prediction.

The life-prediction analysis is performed on a block-loading basis, in which one block consists of three different loadings: one (1) cycle from 0 to σ_{max}, 1000 cycles of $\Delta\sigma_1$, and 500 cycles of $\Delta\sigma_2$. The residual stresses within the structure have been assumed to be negligible. The analysis predicts a crack length versus cycles curve as shown in Fig. 5, Curve A. The life curve for this example is unusual, but was selected to point up the importance of considering all cyclic stresses within a structure. The initial part of the curve shows the crack growth rate decreasing with increasing crack length because of the large stress gradient in the critical location. The latter part of the curve shows a dramatic increase in the crack growth rate with increasing crack length, because both $\Delta\sigma_1$ and $\Delta\sigma_2$ contribute to crack growth. This curve shows the common observation that the exact value of K_{Ic} does not significantly affect the fatigue life of the structure. When the crack is small, the start-up/shut-down (LCF) cycle is driving the crack, and the high-frequency cyclic stresses, $\Delta\sigma_1$ or $\Delta\sigma_2$ or both, produce ΔK below threshold values which do not contribute to crack advancement. However, as the crack grows, the high-frequency cycles cause crack growth and actually dominate

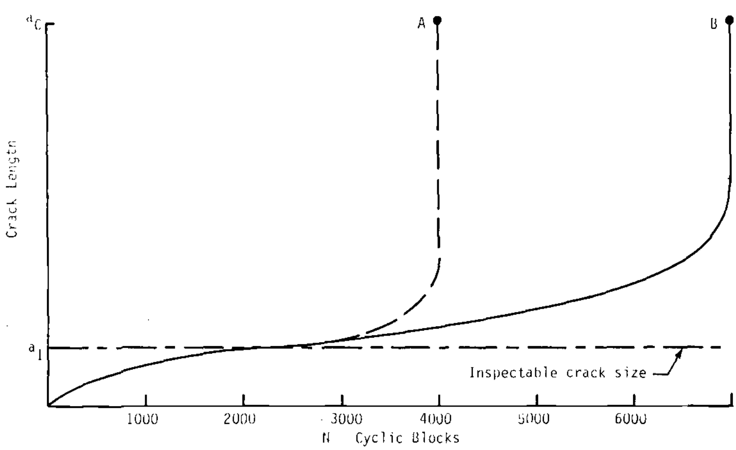

FIG. 5—*Predicted crack length versus operational cycles for service stresses shown in Fig. 4. Curve A ignores the beneficial effects of overloads; Curve B includes these effects.*

crack advancement, and cause the structure to fail in a couple of LCF cycles. Therefore, for this example, ΔK_{TH} (not K_c) is the material property which effectively truncates the low cycle fatigue (LCF) crack growth in the structure. For most structures, it may not be as dramatic as in this example, but the exact value of K_{Ic} only slightly affects the cyclic life, because most of the fatigue life occurs when the cracks are small. The number of loading blocks remaining for various initial crack sizes (a_i) to grow to failure (a_c) is shown in Fig. 6, Curve A, for this example.

Having seen that the predicted cyclic life was dependent upon the high-frequency fatigue threshold, the effects of overloads which increase the effective threshold ΔK_{TH} were then included in the analysis. These effects have been reported previously [7], and are illustrated in Fig. 7. When the overload effects are included, the predicted cyclic life is extended as shown with Curve B of Figs. 5 and 6. The largest stress (σ_{max}) from the previous LCF cycle acts as a major overload for $\Delta\sigma_1$, and acts as a slight overload for $\Delta\sigma_2$. The overloads affect the life predicted in this example by increasing ΔK_{TH} and thereby eliminating any crack extension due $\Delta\sigma_1$, until after σ_{max} and $\Delta\sigma_2$ have propagated the crack. The predicted cyclic life of the structure is also extended because $\Delta\sigma_2$ does not contribute to crack propagation until a larger crack size.

Nondestructive Inspection

Once the life-prediction analysis is available (Figs. 5 and 6), an appropriate nondestructive inspection (NDI) technique can be chosen. It is im-

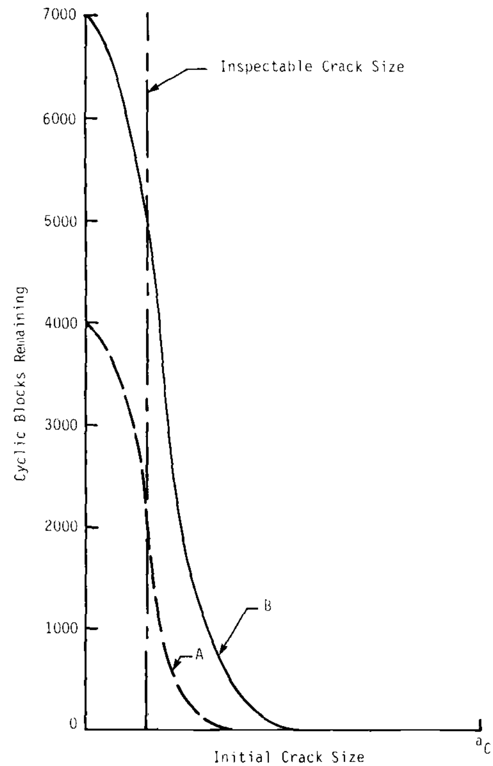

FIG. 6—*Predicted operational cycles remaining for various initial crack sizes. Curve A ignores the beneficial effects of overloads; Curve B includes these effects.*

portant to have performed the life-prediction analysis before the inspection technique is selected and the inspection performed. The life-prediction analysis will determine the size of cracks that the NDI inspector must be capable of detecting. For example, if the NDI inspector was looking for 10-cm crack lengths, and the analysis indicated that the remaining life from 1-mm crack length was too short, then the inspection was a waste of time. On the other hand, a large amount of money might be spent inspecting a structure for very small defects, only to find out that the crack of concern is so large that a much less expensive inspection could have been conducted to assure sufficient reliability.

The crack size which the NDI technique must be able to detect and size can be determined from Fig. 6, which contains the same data as in Fig. 5 replotted as initial crack size versus remaining cyclic blocks. Typically, the way in which the accept/reject criteria are determined is to pick an allowable crack size and corresponding inspection interval so that the inspector will

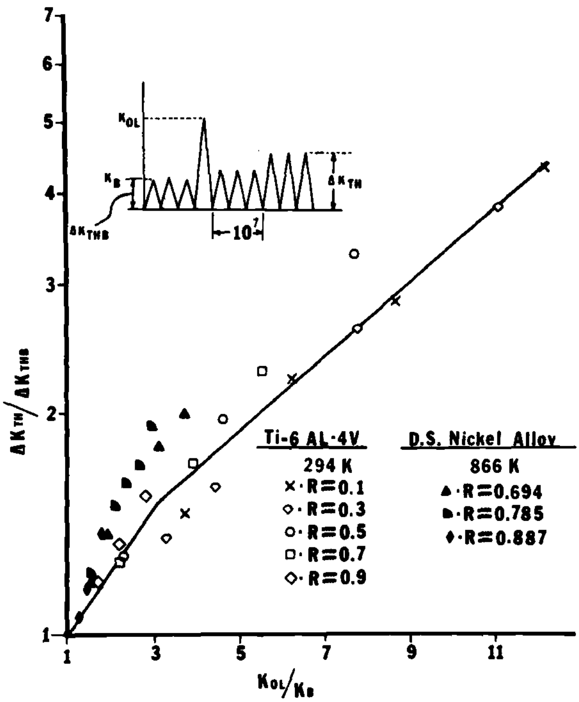

FIG. 7—*Relative change in fatigue threshold after single-cycle overloads as a function of the relative overload for two alloys at various* R*-ratios (Ref 7).*

have multiple (for example, three) chances to find a crack before it grows to a critical size. For example, in Figs. 5 and 6, the cycles to failure are plotted for a specified maximum initial flaw a_i. If every inspection were perfect, the inspection interval could be selected without a safety factor (that is, 2000 blocks for Case A, which ignores overload effects, or 5000 blocks for Case B, which includes overload effects). However, since the inspections are not perfect, and a crack of size a_i may be missed, the inspection interval will be set so that the inspector will still have multiple chances to find the crack and retire the structure before failure. The interval between inspections (or number of inspections) during crack growth will vary with application and manufacturer, and be dependent upon the reliability of the inspection and the costs of inspection, replacement, repair, and failure should it occur.

Retirement for Cause

If the design allowable for this hypothetical structure had been established to permit 10 percent of the structures to be cracked, but require that less than 0.01 percent fail in one design life time, then Figure 8 might represent this structure. Figure 8 shows the probability of the crack initiating, the probability of the crack propagating from a_i to a_c, and the probability of the structure failing for various design lives. Without any NDI evaluation of the structure, 90 percent of the structures would have no cracks when they are retired at one design life. With the use of a Retirement-For-Cause approach based upon fracture mechanics life prediction and NDI, the useful life of at least 90 percent of the structures can be extended without reduction in structural reliability. In fact, the reliability of life-extended parts may actually exceed that of new parts designed conventionally for crack initiation, which results in a 0.01 percent failure rate.

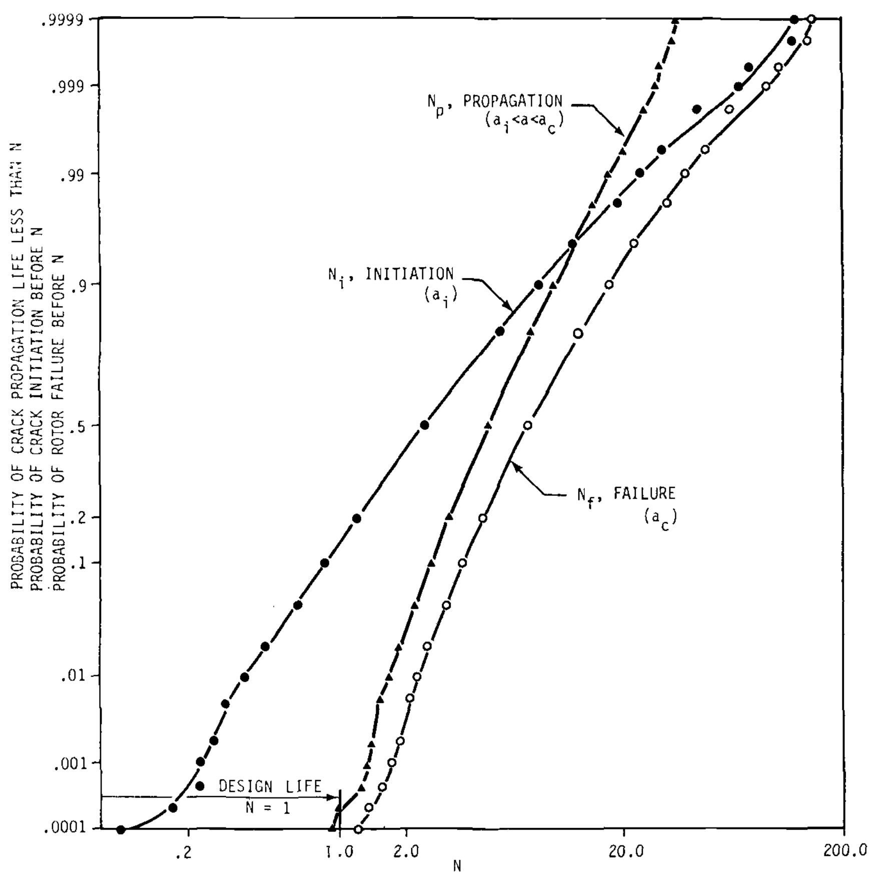

FIG. 8—*Cumulative probability distributions of lives required for simulated crack initiation, crack propagation, and failure for 10 000 simulated rotors.*

Probabilistic Fracture Mechanics: The Impact of Uncertainty

If each of the input parameters (Fig. 1) and the detectable crack size are known exactly, we get an exact calculation of remaining life (N_f) (Figs. 5 and 6). In practice, however, the input parameters are not known exactly; in fact, the uncertainties vary considerably from one input to another. The probabilistic fracture mechanics approach [*8,9*] accepts uncertainties in the various input parameters, quantifies them, and calculates a failure probability as a function of continued operating cycles, rather than a precise remaining lifetime. The engineering community has generally accepted the fact that various input parameters are uncertain and that the probabilistic approach is more realistic than deterministic life predictions. However, to quantify the specific uncertainties for each piece of input data is not an easy task. Therefore the general fracture mechanics practice is to assume "worst-case" conditions. The initial crack size used in design computation is based on laboratory evaluation of the maximum crack size that might go undetected by the NDI equipment, or the maximum size that an NDI operator might miss. Furthermore, no account is taken of the pre-inspection material quality and its effect on the probability that the critical, highly stressed locations actually contain a defect that could be missed by the inspection. Likewise, the fracture toughness is usually assumed to be the lowest possible value in the particular environment, and the peak tensile stress is assumed simultaneously present along with all other worst-case conditions. Under these unrealistically conservative constraints, fracture mechanics predictions offer a conservative bound which may be far from the optimum design or life extension strategy. In fact, in some cases, incorporation of a conservative, deterministic fracture mechanics approach to design supercedes a phenemonological design approach which more correctly incorporates, in a qualitative way, the actual statistical variations by a heavier reliance on laboratory and field experience.

Probabilistic Fracture Mechanics (PFM)

Many satisfactory components, which might be rejected, can be saved by removing the arbitrary and unrealistic constraints imposed by worst-case assumptions and allowing the model to account probabilistically for actual variation in critical parameters based on test or field experience. Various probabilistic structural analyses [*10*] and probabilistic fracture mechanics [*8,9*] representations are possible, which calculate the probability of failure $P(F)$, rather than an exact life or strength, by quantifying the variability of key engineering, materials, and inspection parameters. One convenient representation [*11*] is to write the component failure probability $P(F)$ in terms of several key conditional failure probabilities. That is

$P(F)$ = probability of a component acceptance times
probability of a nonreject defect causing failure

Mathematically

$$P(F) = \exp(-PN_R)[1 - \exp(-PN_F)] \quad (5)$$

where PN_F is the probable number of component failure sites or indications in a component not rejected and causing failure, and PN_R is the probable number of rejection sites in a component. These probable numbers are calculated from

$$PN_R = \int_0^{\infty} pn(a)P(R\backslash a, S)\,da \quad (6)$$

and

$$PN_F = \int_0^{\infty} pn(a)[1 - P(R\backslash a, S)P(F\backslash a)]\,da \quad (7)$$

where $pn(a)\,da$ represents the pre-inspection material quality or the probable number[3] of defects of size $a \pm da/2$, $P(R\backslash a, S)$ represents the rejection probability of a component given that an actual defect of size a exists and that inspection rejection level is set at size S, and $P(F\backslash a)$ represents the probability of a component failure from an existing defect of size a.

Note that failure probability depends strongly on three distributions. $P(F\backslash a)$ is generally understood when discussing *PFM*. However, most design engineers do not fully comprehend the impact of inspection uncertainties and pre-inspection flaw size distribution, or the need and procedures for evaluating them quantitatively.

Because of inspection uncertainty, there is a definite probability of rejecting components with actual imperfections smaller than S, and a finite probability of not rejecting components with actual imperfections larger than S. Furthermore, deterministic fracture mechanics approaches have very conservatively assumed that (*1*) $pn(a) = 1$, and (*2*) the probability of a flaw remaining in the part after inspection is exactly equal to the probability of the inspection missing a flaw of size a, if it exists. More realistically, the probability distribution of imperfections present after inspection depends upon both the pre-inspection flaw size distribution and inspection reliability. The actual failure probability, given by Eq 5, depends on all three probabilities: the conditional failure probability $P(F\backslash a)$, the pre-inspection materials quality, and the inspection reliability.

Whether a design is based upon deterministic or probabilistic fracture mechanics, selection of the specific accept/reject criteria should be based upon optimization of the relative costs and risks associated with various options [*8,11–15*]. Specifically, the effects of realistic inspection, analysis, or usage uncertainties must be quantified and used to predict the probable cost[4] of inspection, analysis, repair replacement, and failure. The optimum strategy can then be selected on a quantitative basis, like minimum total cost, if all costs including indirect ones are included.

[3]The "probable number" function is simply the probability density function [$pd(a)$] times the probable or expected number of defects of all sizes in the component.

[4]Probable cost is the cost if it occurs times the probability that it will occur.

Summary and Conclusions

Fracture mechanics methods which accurately evaluate the effect of actual or potential defects are now utilized in conjunction with traditional design analyses. The accuracy and applicable range of the fracture mechanics calculations continue to improve, and more extensive materials data become available each day. Nevertheless, uncertainties and errors remain in our input data and analyses, and there is a need to utilize probabilistic analysis techniques to realistically assess fatigue failure probability. Worst-case assumptions regarding initial flaws, inspection uncertainty, and crack progression are unrealistically conservative and economically unacceptable. The probabilistic fracture mechanics approach can be used to quantify the impact of uncertainties that actually exist and to establish a quantitative basis for accept/reject criteria which optimize the cost/risk tradeoffs that must be made.

References

[1] Tada, H., Paris, P. C., and Irwin, G. R., "The Stress Analysis of Cracks Handbook," Del Research Corporation, St. Louis, Mo., 1973.

[2] Rooke, D. P. and Cartwright, D. J., "Stress Intensity Factors," Her Majesty's Stationary Office, London, 1976.

[3] Besuner, P. M. et al, "BIGIF Fracture Mechanics Code for Structures," EPRI Report NP-838, Environmental Protection Research Institute, July 1978.

[4] Yuen, A., Hopkins, S. W., Leverant, G. R., and Rau, C. A., Jr., *Metallurgical Transactions*, Vol. 5, 1974, p. 1833.

[5] Rolfe, S. T. and Barsom, J. M., *Fracture and Fatigue Control in Structures*, Prentice-Hall, Englewood Cliffs, N.J., 1977.

[6] Elber, W., *Engineering Fracture Mechanics*, Vol. 4, 1970, p. 543.

[7] Hopkins, S. W., Rau, C. A., Jr., Leverant, G. R., and Yuen, A. in *Fatigue Crack Growth Under Spectrum Loads, ASTM STP 595*, American Society for Testing and Materials, 1976, pp. 125-141.

[8] Rau, C. A., Jr., et al, *Nuclear Engineering and Design*, Vol. 43, 1977, p. 1.

[9] Besuner, P. M. and Tetelman, A. S., *Nuclear Engineering and Design*, Vol. 43, 1977, p. 99.

[10] Freudenthal, A. M., Garrelts, J. M., and Shinozuka, M., "The Analysis of Structural Safety," *Structural Division Journal*, American Society of Civil Engineers, Vol. 92, No. ST 1, February 1966.

[11] Johnson, D. P., *Nuclear Engineering and Design*, Vol. 43, 1977, p. 207.

[12] Rau, C. A., Jr., "The Impact of Inspection and Analysis Uncertainty on Reliability Prediction and Life Extension Strategy," ARPA/AFML Review of Progress in Quantitative NDE, Advanced Research Projects Agency/Air Force Materials Laboratory, San Diego, Calif., July 1978.

[13] Starr, C., "Benefit-Cost Studies in Socio-Technical Systems," Colloquium on Benefit-Risk Relationships for Decision-Making, Washington, D.C., April 1971.

[14] Thomas, J. M., Hanagud, S., and Hawk, J. D. in *1975 Reliability and Maintainability Symposium Proceedings*, pp. 255-262.

[15] Rau, C. A., Jr., and Besuner, P. M., *Journal of Engineering Materials and Technology*, Vol. 102, 1980, pp. 56-63.

J. R. Gebman[1] *and P. C. Paris*[2]

A Practical Probabilistic Method for Evaluating the Fail-Safeness of Structures that May Fail Due to Fatigue

REFERENCE: Gebman, J. R. and Paris, P. C., "**A Practical Probabilistic Method for Evaluating the Fail-Safeness of Structures that May Fail Due to Fatigue,**" *Fatigue Crack Growth Measurement and Data Analysis, ASTM STP 738,* S. J. Hudak, Jr., and R. J. Bucci, Eds., American Society for Testing and Materials, 1981, pp. 271-280.

ABSTRACT: The undetected propagation of a fatigue crack constitutes a significant cause of aircraft and other structural failures. To raise the structural failure load to a relatively high level, the manufacturer can divide the structure into many small elements, which significantly increases the ability of a structure to tolerate an element failure. This paper presents a procedure for calculating the probability that the structure has not failed, as the function of the crack propagation history for an undetected fatigue crack. The form of the procedure is so simple that computations with a desk calculator can yield reasonably accurate results. Moreover, the necessary input data are often readily available. By adopting such a procedure, aircraft manufacturers and operators can better identify those elements that pose the greatest threat to structural integrity.

KEY WORDS: fatigue (mechanics), fatigue life, damage, cracking (fracturing), crack propagation, life expectancy, requirements, faults, tolerance, failure (mechanics), loads (forces), failure, probability, mechanics, structural properties, structures

Consider a multiple-element structure that carries a time-varying load that can cause a fatigue crack to propagate through a particular element of interest. For the special case where detection of the crack does not occur until after the cracked element has failed, this paper proposes a method for estimating the likelihood that such undetected crack propagation will *not* cause the structure to collapse. By applying the method to each of the fatigue-prone elements in a structure, one can help identify elements that deserve special attention by the structure's manufacturers and operators.

[1]Senior engineer, Engineering and Applied Sciences Department, The Rand Corporation, Santa Monica, Calif. 90406.

[2]Professor of Mechanics, Washington University, St. Louis, Mo. 63130.

For aircraft structures, designers and maintainers currently use two different philosophies to guard against the possibility of a fatigue failure causing a catastrophic structural failure:

1. The *fail-safe* philosophy holds that an aircraft structure should have enough independent elements to provide assurance that for a specified applied load, the failure of any single element will not lead to a catastrophic structural failure.
2. The *safe-life* philosophy holds that the specified operating life for an aircraft structure should not exceed the time required for a specified initial crack to propagate to a length (referred to as the *critical length*) at which a specified applied load would cause the element containing the crack to fail.[3,4]

Both philosophies require the specification of a design load. But no matter how large a design load the operator specifies, there is still the possibility that an even larger load may occur. Also, no matter how large an initial crack size the operator specifies for a safe-life approach, an even more severe condition may arise.

Aircraft manufacturers and operators currently use fixed extreme values for the design load and the initial crack size. Although such values may reflect the best judgment of the most knowledgeable individuals, neither the manufacturer's nor the operator's management can relate the subjective basis for such assessments to an understanding of the likelihood that a postulated fatigue crack may cause a catastrophic structural failure. Thus, managers have difficulty finding a consistent basis for allocating resources to reduce uniformly the chances that a catastrophic structural failure will result from an element failure in an aircraft structure.

A Probabilistic Approach

This report proposes a probabilistic approach that avoids the extreme value judgments mentioned previously and supplements the information provided by the safe-life and fail-safe approaches. This probabilistic approach, which accepts the existence of the crack as a given and uses a distribution to represent the applied loads, has the following unique features:

1. The approach requires no knowledge of what causes a crack to start or of how fast the crack propagates during its initial phase of development.
2. Once the crack has reached a size where it begins to contribute to the calculated probabilities, the approach accurately represents the crack propagation history calculated by fracture mechanics methods.

[3]Coffin, M. D. and Tiffany, C. F., *Journal of Aircraft*, Vol. 13, No. 2, February 1976, pp. 93–98.

[4]Kaplan, M. P. and Reiman, J. A., *Journal of Aircraft*, Vol. 13, No. 2, pp. 99–103.

When this probabilistic approach has been applied to various elements, they can then be ranked according to the likelihood that their failure would lead to a structural failure. The most failure-critical elements constitute candidates for either redesign or special maintenance attention, such as more frequent inspections. In some cases a special rework or even replacement of the element may be warranted.

Such a procedure for consistently quantifying a structure's ability to tolerate undetected fatigue cracks may help manufacturers and operators to apply their available resources more effectively. For example, during the design and manufacturing phase, such a procedure can (*1*) help identify the most failure-critical elements in a given design, (*2*) provide a basis for design and manufacturing standards, and (*3*) give managers an opportunity to see how design trade-offs may influence the chances of structural failure. During the operating phase, such a procedure can (*1*) help reassess the most failure-critical elements based on actual operating conditions, (*2*) provide a basis for an inspection and modification standard, and (*3*) give managers/regulators an opportunity to see how inspection and modification trade-offs may influence the chances of structural failure.

Although the approach can be applied to structures other than aircraft, it does not apply to situations where (*1*) a large number of fatigue cracks may have weakened a structure over a broad general area, (*2*) prompt detection of a failed element would not occur, or (*3*) the nature of the structure or its operating environment makes the preparation of inputs impractical.

Model of the Failure Process

An element will fail when the intensity of the internal structural loads (referred to here as simply *load intensity*, σ) exceeds the element's remaining strength.[5] But such a failure will not extend to adjoining elements as long as the load intensity does not exceed the remaining strength of the elements adjoining the failure site.

Once a fatigue crack enlarges to a size where it first begins to weaken the element, any additional enlargement reduces the remaining strength of that element. As the remaining strength of an element decreases, the minimum load intensity that can cause the element to fail (σ_{ef}) decreases (for example, see Fig. 1). Thus, in some situations, an element may not fail until the crack is large enough to cause an appreciable degradation in the element's remaining strength. In that case, the load intensity level that causes the element to fail may not exceed the level required to also cause the adjoining elements to fail. In such an event, the element fails (ef) but no structural failure (nsf) occurs. For such a "safe" (or "noncatastrophic") element failure to occur dur-

[5]For aircraft structures, the gross area stress is used as the measure of the intensity of the internal structural loads.

ing a specific operating interval (for example, during one flight of an aircraft):

1. The element must not have failed during a prior operating interval, and
2. During the designated operating interval,
   a. At some time the load intensity must exceed the minimum level required to fail the cracked element, and
   b. At no time following the element failure can the load intensity exceed the minimum level required to fail the remaining structure once the element of interest has failed.

The remaining or residual strength of the structure, once the element has failed (σ_{rs}), depends on the failure mode postulated for the structure, as well as the condition of adjoining elements.

Because the crack of interest will enlarge and the remaining strength of the element containing the crack will decrease during successive operating intervals, our probabilistic approach must explicitly represent the process whereby the crack enlarges as the structure accumulates operating time. It must also account for the process whereby crack enlargement reduces the element's remaining strength. Our approach represents both of these processes with deterministic relationships. It also uses a deterministic input to represent the load intensity level at which structural failure can occur, once the

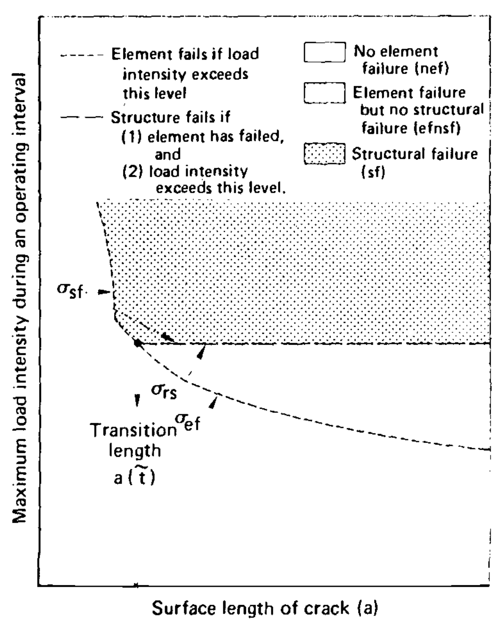

FIG. 1—*Illustration of how crack length and load intensity influence failure events.*

element containing the crack has failed. Because load intensity levels vary widely during the operation of such structures—especially aircraft structures—this approach uses a distribution to represent the load intensity.

Underlying Assumptions

To keep the calculation procedure simple and straightforward, a few limitations are imposed so that calculations can be made by hand, and the basic phenomena influencing the results can be better understood. The first two assumptions help to narrow the scope of the necessary calculations:

Assumption 1—Detection of the cracked element does not occur before the crack fails the element.

Assumption 2—Once the cracked element fails, a completely effective repair/replacement of that element occurs before the structure begins the next operating interval.

The approximations introduced by the remaining assumptions justify certain simplifications that significantly reduce the complexity of the necessary calculations.

Assumption 3—All operating intervals have the same duration.

Assumption 4—When each operating interval starts, a single step increase in the crack length provides an adequate representation for the total crack extension that occurs during the operating interval.

Assumption 5—The operations during each operating interval occur independently of the operations during all previous operating intervals.

Assumption 6—If the load intensity exceeds the level required to fail the element more than once during a given operating interval, the highest load intensity level occurs first.

The reader should see Appendix F to Gebman and Paris[6] for a discussion of the implications of these assumptions.

General Equations

For a designated element, postulate that a crack exists at a specified location. According to Assumption 1, detection of the cracked element does not occur before the crack fails the element. Let $a(t)$ represent the crack's surface length as a function of cumulative operating time (t). Define the origin for t such that $a(0)$ represents the initial crack length considered by this approach. Assumption 3 provides that each operating interval has a constant length (say, Δt). After i such intervals, the crack will have a surface length

[6]Gebman, J. R. and Paris, P. C., "Probability That the Propagation of an Undetected Fatigue Crack Will Not Cause a Structural Failure," Report R-2238-RC, June 1978, The Rand Corporation, Santa Monica, Calif. 90406.

$a(t_i)$, where $t_i \triangleq i\,\Delta t$. Because $a(t)$ varies slowly in an operating interval (except for the interval where element failure occurs), simplify the problem by assuming that the crack size has a constant value of $a(t_i)$ throughout the ith interval (Assumption 4).

For the postulated crack site, let $\sigma(t)$ represent the time-varying intensity of the internal structure loads that the applied loads would cause in an idealized structure without any holes or cracks. Let $\hat{\sigma}_i$ represent the maximum value of $\sigma(t)$ that occurs during the ith operating interval. If $\hat{\sigma}_i \geq \sigma_{\text{ef}}$, the crack will instantaneously fail the element. If $\hat{\sigma}_i \geq \sigma_{\text{sf}}$, the structure will immediately collapse. Because both σ_{ef} and σ_{sf} depend on the crack's size (see Fig. 1), let $\sigma_{\text{ef}} = \sigma_{\text{ef}}(a)$ and $\sigma_{\text{sf}} = \sigma_{\text{sf}}(a)$ represent these relationships.

The postulated crack can lead to an element failure during the jth interval only if it has not failed the element during a prior interval. Similarly, because Assumption 2 stipulates that the structure does not start an operating interval with a failed element, the postulated crack can lead to a structural failure during the jth interval only if it has not led to the element's failure during a prior interval. Thus, for $x = e$ and $x = s$

$$\begin{aligned} P_{xf}(t_{j-1}, t_j) &= 1 - P_{nxf}(t_{j-1}, t_j) \\ &= \text{Prob}\,\{\hat{\sigma}_i < \sigma_{\text{ef}}[a(t_i)];\ i = 1, 2, \ldots, j-1)\} \\ &\quad\ \text{Prob}\,\{\hat{\sigma}_j \geq \sigma_{xf}[a(t_j)]\} \end{aligned} \tag{1}$$

denotes the probability that the postulated crack leads to a type x failure during the jth interval, where $x = e$ for an element failure and $x = s$ for a structural failure. Justification for the product contained in the right-hand side of Eq 1 comes from the fact that $\hat{\sigma}_j$ must not depend on $\hat{\sigma}_i$ $(i = 1, 2, \ldots, j-1)$, because Assumption 5 stipulates that the operating conditions during the jth interval occur independently of the operating conditions during prior intervals; note that the operating conditions govern $\sigma(t)$ and hence $\hat{\sigma}_j$.

For k consecutive operating intervals, k different outcomes may occur for failure type x. Thus

$$P_{nxf}(0, t_k) = 1 - \sum_{j=1}^{k} P_{xf}(t_{j-1}, t_j) \qquad (x = e, s) \tag{2}$$

denotes the probability that during the time $(0, t_k)$ the postulated crack condition will not lead to a type x failure.[7] When $x = e$, and as long as Prob $\{\hat{\sigma}_j \geq \sigma_{\text{ef}}[a(t_j)]\} \ll 1$, the mathematical approximation

$$P_{\text{nef}}(0, t_k) = \prod_{j=1}^{k} [1 - \text{Prob}\,\{\hat{\sigma}_j \geq \sigma_{\text{ef}}[a(t_j)]\}] \tag{3}$$

provides a useful replacement for Eqs 1 and 2.

[7]The time $t = 0$ is selected so that the length of the postulated crack is so small that one can safely ignore the probability that a failure (induced by that crack) may have occurred prior to time $t = 0$.

For convenience, define

$$r_{xf}(t_i) \triangleq n\{\sigma_{xf}[a(t_i)]\}/t_d \qquad (x = e, s) \tag{4}$$

where $n(\sigma_{xf})$ represents the expected number of times that the load intensity would exceed σ_{xf} during one design lifetime of operation. The design lifetime (t_d) must have the same units as Δt. For the jth operating interval, $r_{xf}(t_j)\,\Delta t$ represents the expected number of times that the load intensity would exceed $\sigma_{xf}[a(t_j)]$ during one operating interval. Because all operating intervals have the same fixed duration (Assumption 3), these intervals must be uniformly distributed over the cumulative operating time. Thus, given Assumption 6, the uniform distribution and independence properties that stem from Assumptions 3 and 5 and the restriction that $r_{xf}(t_j)\,\Delta t \ll 1$, the relation

$$\text{Prob}\,\{\hat{\sigma}_j \geq \sigma_{xf}[a(t_j)]\} = r_{xf}(t_j)\,\Delta t \tag{5}$$

provides a reasonable approximation for our purposes.

If $\hat{\sigma}_j \geq \sigma_{ef}[a(t_j)]$, the element of interest will fail; the structure will also fail if $\hat{\sigma}_j \geq \sigma_{rs}$ (see the dashed line in Fig. 1). Define $\tilde{t}$ as the time when $\sigma_{ef}[a(\tilde{t})] = \sigma_{rs}$ (Fig. 1). Prior to time $\tilde{t}$, $\sigma_{ef}[a(t_j)] > \sigma_{rs}$, and thus $\sigma_{sf}[a(t_j)] = \sigma_{ef}[a(t_j)]$. After time $\tilde{t}$, $\sigma_{ef}[a(t_j)] < \sigma_{rs}$, and thus $\sigma_{sf}[a(t_j)] = \sigma_{rs}$. Incorporate these results in Eq 4 and recognize that $n(\sigma_{xf})$ decreases as σ_{xf} increases, whence

$$r_{sf}(t_j) = \min\{r_{ef}(t_j), n(\sigma_{rs})/t_d\} \tag{6}$$

Thus, from Eqs 3, 4, and 5

$$P_{nef}(0, t_k) = \prod_{j=1}^{k}\{1 - r_{ef}(t_j)\,\Delta t\} \tag{7a}$$

and from Eqs 1, 2, and 5

$$P_{nsf}(0, t_k) = 1 - \sum_{j=1}^{k} P_{nef}(0, t_{j-1})\, r_{sf}(t_j)\,\Delta t \tag{7b}$$

Equations 4, 6, and 7 present the general procedure. Appendix G to Gebman and Paris[6] gives an alternative formulation that uses integrals. One might use that form along with simple expressions for $n(\sigma)$, $\sigma_{ef}(a)$, and $a(t)$ to obtain an approximate analytical solution.

An Approximate Procedure for Hand Calculations

The values for r_{ef} and r_{sf} vary in a sufficiently slow manner that one can make a useful approximate calculation by hand if he assumes that the values for r_{ef} and r_{sf} remain constant over a sequence of consecutive operating intervals. Let such a sequence define a calculation interval; assign a value to the index α to represent each calculation interval ($\alpha = 1, 2, 3, \ldots$). Assume that each calculation interval contains an even number of operating intervals; let $2k_\alpha$ represent that number. Thus the midpoints for successive calculation intervals (for example, $\bar{t}_\alpha$) are given by

$$\bar{t}_\alpha = \bar{t}_{\alpha-1} + (k_{\alpha-1} + k_\alpha)\,\Delta t \tag{8}$$

where $k_0 \triangleq 0$ and $\bar{t}_0 \triangleq 0$.

Let the last operating interval that occurs prior to time $\bar{t}_\alpha$ have an index L_α. From Eq 8

$$L_\alpha = k_\alpha + \sum_{\beta=0}^{\alpha-1} 2k_\beta$$

Assume that r_{ef} and r_{sf} have constant values equal to $r_{ef}(\bar{t}_\alpha)$ and $r_{sf}(\bar{t}_\alpha)$ during calculation interval α. Thus, for the last half of interval $\alpha - 1$

$$\prod_{j=L_{\alpha-1}+1}^{L_{\alpha-1}+k_{\alpha-1}} \{1 - r_{ef}(t_j)\,\Delta t\} = \{1 - r_{ef}(\bar{t}_{\alpha-1})\,\Delta t\}^{k_{\alpha-1}} \tag{9a}$$

and

$$\sum_{j=L_{\alpha-1}+1}^{L_{\alpha-1}+k_{\alpha-1}} \frac{P_{nef}(0, t_j)}{1 - r_{ef}(t_j)\,\Delta t}\, r_{sf}(t_j)\,\Delta t = k_{\alpha-1} \times \frac{P_{nef}(0, \bar{t}_{\alpha-1})}{1 - r_{ef}(\bar{t}_{\alpha-1})\,\Delta t}\, r_{sf}(\bar{t}_{\alpha-1})\,\Delta t \tag{9b}$$

Similarly, for the first half of interval α

$$\prod_{j=L_\alpha-k_\alpha+1}^{L_\alpha} \{1 - r_{ef}(t_j)\,\Delta t\} = \{1 - r_{ef}(\bar{t}_\alpha)\,\Delta t\}^{k_\alpha} \tag{9c}$$

and

$$\sum_{j=L_\alpha-k_\alpha+1}^{L_\alpha} \frac{P_{nef}(0, t_j)}{1 - r_{ef}(t_j)\,\Delta t}\, r_{sf}(t_j)\,\Delta t = k_\alpha \frac{P_{nef}(0, \bar{t}_\alpha)}{1 - r_{ef}(\bar{t}_\alpha)\,\Delta t}\, r_{sf}(\bar{t}_\alpha)\,\Delta t \tag{9d}$$

Thus, from Eqs 7 and 9

$$P_{nef}(0, \bar{t}_\alpha) = P_{nef}(0, \bar{t}_{\alpha-1})\,\{1 - r_{ef}(\bar{t}_{\alpha-1})\,\Delta t\}^{k_{\alpha-1}}\,\{1 - r_{ef}(\bar{t}_\alpha)\,\Delta t\}^{k_\alpha} \tag{10a}$$

and

$$P_{nsf}(0, \bar{t}_\alpha) = P_{nsf}(0, \bar{t}_{\alpha-1}) - k_{\alpha-1} \frac{P_{nef}(0, \bar{t}_{\alpha-1})}{1 - r_{ef}(\bar{t}_{\alpha-1})\,\Delta t}\, r_{sf}(\bar{t}_{\alpha-1})\,\Delta t - k_\alpha \frac{P_{nef}(0, \bar{t}_\alpha)}{1 - r_{ef}(\bar{t}_\alpha)\,\Delta t}\, r_{sf}(\bar{t}_\alpha)\,\Delta t \tag{10b}$$

A calculation should start (that is, $t = 0$) with a sufficiently small crack size $a(0)$ that $P_{\text{nef}}(-\infty, 0) \cong 1.0$, and $P_{\text{nsf}}(-\infty, 0) \cong 1.0$.[8] In such a case, one can prudently commence the calculation with the initial conditions $P_{\text{nef}}(0, \bar{t}_0) = 1.0$ and $P_{\text{nsf}}(0, \bar{t}_0) = 1.0$. With such initial conditions, Eqs 4, 6, and 10 prescribe all of the necessary calculations. Inspection of these equations shows that the input information needed for the calculations consists of a crack propagation history $[a(t)]$, the load intensity distribution $[n(\sigma)]$, the remaining strength for the cracked element $[\sigma_{\text{ef}}(a)]$, and the remaining strength for the structure when the cracked element fails (σ_{sf}). All of these inputs are readily available for any fatigue-prone part that is already subjected to both a safe-life and a fail-safe analysis. Consequently, the proposed approach poses a very small computational burden relative to the resources already devoted to the safe-life and fail-safe analyses.

Illustration of Utility

To illustrate the utility of these kinds of calculations, the authors have applied the method to a service-limiting element in an aircraft structure. The element of interest is a pair of skin panels that are joined in a lap joint. The element failure mode is defined as the simultaneous failure of both panels due to the simultaneous propagation of a crack in each panel. The crack in each panel is assumed to originate at the same fastener location along the lap joint. Table 1 presents the results of the authors' computations.[9] For the particular element considered (subject to the previously noted assumption), the table shows all of the element failures occurring after the crack reaches a length of 20 mm (0.8 in.). For the case where the element failure leads to a structural failure, the table shows the element's crack length between 20 and 90 mm (0.8 and 3.5 in.) just prior to the failure. For this element, therefore, the table shows that the most threatening element cracks are in the range of 20 to 90 mm. If such cracks go undetected until after element failure occurs, the table shows that 2.6 percent $[(1 - 0.974) \times 100]$ of the element failures would lead to a structural failure.

The foregoing results have identified the most threatening crack lengths and the probable consequences of undetected fatigue crack propagation for the selected element. Similar results for other elements could help the operator of this aircraft to better tailor his inspection and maintenance procedures according to the nature of the threat that faces each element.

[8]One must heuristically determine how small is small enough. The authors have found that $a(0)$ is sufficiently small as long $\{1 - P_{nsf}(0, \Delta t)\}/\Delta t < 10^{-6}$.

[9]See Section IV of Gebman and Paris (Footnote 6) for the actual calculations. Their report is published by The Rand Corporation and archived at over 300 libraries—mostly at universities. To order a copy, write to Publications Department, The Rand Corporation, 1700 Main Street, Santa Monica, Calif. 90406.

TABLE 1—*Summary of results for a sample calculation.*

Cumulative Flight Time, h			Probability that the Dual Panel Crack Condition Does Not Lead to	
From a 1.3-mm Crack	From the Start of the Calculation (t)	Crack Length in mm (a)	Element Failure by Time t, $P_{ncf}(0,t)$	Structural Failure by Time t, $P_{nsf}(0,t)$
7900	300	20	1.000	1.000
8500	900	30	0.995	0.995
8800	1200	41	0.98	0.989
9050	1450	51	0.95	0.985
9600	2000	89	0.50	0.976
9875	2275	124	0.05	0.974
9925	2325	135	0.01	0.974

SOURCE: Gebman, J. R. and Paris, P. C., "Probability That the Propagation of an Undetected Fatigue Crack Will Not Cause a Structural Failure," Report R-2238-RC, June 1978, The Rand Corporation, Santa Monica, Calif., p. 26.

Discussion

The approach proposed here provides a capability to help assess the risk incurred when an undetected fatigue propagates through an element. The approach could also help assess the risk of continuing to operate aircraft even after they reach their original design life. For example, the safe-life approach to establishing a design life attempts to assess when a crack with a limit load critical crack length might develop in the structure. As a consequence of the necessarily conservative assumptions incorporated in the assessment process, an aircraft might arrive at the specified design life without exhibiting any significant evidence of service-limiting fatigue cracks in the structure. In such an event, the operator may want to use the aircraft beyond the original limit. In such a case, the proposed probabilistic approach could be used to assess the consequences of undetected fatigue crack propagation in the fatigue-prone elements. Selective maintenance/replacement of the most critical elements might help to provide sufficient assurance for the operator to continue the use of the aircraft beyond its originally intended design life.

The calculation of a safe service limit, based on an assumed initial flaw size, provides a reasonable and useful procedure for controlling the design stress levels and materials used in future aircraft. It also provides a preliminary estimate for a design life or service limit. The proposed probabilistic approach provides a procedure for assessing the structure's ability to tolerate element failures resulting from undetected fatigue crack propagation. Thus, operators and manufacturers could augment their service limit assessment procedures with a probabilistic approach such as the one presented here, to provide a superior approach for managing the risk presented by unexpected and undetected fatigue cracks.

W. H. Bamford[1] *and D. P. Jones*[2]

The Use of Fatigue Crack Growth Technology in Fracture Control Plans for Nuclear Components

REFERENCE: Bamford, W. H. and Jones, D. P., **"The Use of Fatigue Crack Growth Technology in Fracture Control Plans for Nuclear Components,"** *Fatigue Crack Growth Measurement and Data Analysis, ASTM STP 738,* S. J. Hudak, Jr., and R. J. Bucci, Eds., American Society for Testing and Materials, 1981, pp. 281-299.

ABSTRACT: The American Society of Mechanical Engineers (ASME) Boiler and Pressure Vessel Code now suggests the use of fatigue crack growth analysis in the evaluation of indications found during in-service inspection of nuclear components. In this paper the role of crack growth analysis in the evaluation process is reviewed in some detail, and the background and philosophy of its implementation is discussed.

Each of the steps in the crack growth analysis process is discussed in order to point out the assumptions possible and their implications. A detailed consideration of crack shape change during growth is presented, as well as a statement of guidelines for choosing a reference crack growth law.

The ASME approach is compared with the approaches taken in other industries and, finally, a number of areas in need of further work are highlighted.

KEY WORDS: fatigue crack growth, ASME Code, analysis methods, integrity analysis

The American Society of Mechanical Engineers (ASME) Boiler and Pressure Vessel Code (hereafter referred to as the Code) has contained requirements for in-service inspection of nuclear components since the 1970 edition. These requirements are found in Section XI [*1*].[3] The first edition of Section XI contained only inspection requirements, with no guidelines on how to judge the acceptability of flaws detected. As luck would have it, one of the first vessels to be inspected was found to have a flaw, and an immediate dilemma arose as to what basis should be used to determine if it should be

[1]Senior engineer, Strategic Operations Division, Westinghouse Electric Corporation, Pittsburgh, Pa. 15230.

[2]Fellow engineer, Westinghouse Bettis Atomic Power Laboratory, West Mifflin, Pa. 15122.

[3]The italic numbers in brackets refer to the list of references appended to this paper.

repaired. As a result, even though the flaw was shown to be acceptable by a fracture analysis, repair was required because of the lack of a consensus criterion.

As a result of this incident, standing committees were set up to develop acceptance standards and a standard methodology for evaluating defects which exceeded the standards. These rules were inserted into Section XI of the 1974 edition of the Code. The evaluation methods have since been used on at least two operating plants to justify continued operation without repair.

Fatigue crack growth analysis plays a very important part in the evaluation of flaws or indications detected during periodic in-service inspection. Section XI now contains recommended practices for performing in-service inspections and tabular standards for determining the acceptability of indications found. These standards are conservative by design to allow a quick assessment. If an indication does not meet the standards, the owner has the option of performing a fracture evaluation of the component or repairing it.

The evaluation consists of two basic parts, and in each the indication is assumed to be a sharp crack. The first is a prediction of the growth of the flaw during future service (for example, until the next inspection). The second part of the evaluation involves determination of the critical flaw size for a flaw located in the area of the detected indication. The size of the flaw after crack growth is then compared with the critical flaw size, and the margins required for acceptability are specified. These are

$$a_f < 0.1\, a_c \tag{1}$$

$$a_f < 0.5\, a_i \tag{2}$$

where

a_f = crack depth after fatigue crack growth analysis,
a_c = critical crack depth for normal, upset conditions, and
a_i = critical crack depth for emergency and faulted conditions.

These dimensions are further explained in Fig. 1.

Since these margins are specified in the Code, the decision as to acceptability for further service without repair rests on the determination of the critical flaw sizes and on the fatigue crack growth analysis. This decision has immense implications in terms of both safety and cost, so it is not to be taken lightly. This makes the methodology used and the assumptions made in the crack growth analysis very important. The aim of this paper is to review the entire analysis process by providing a detailed assessment of the critical assumptions. The intent is to provide a view of the philosophy behind such an analysis procedure and some guidelines for performing future analysis.

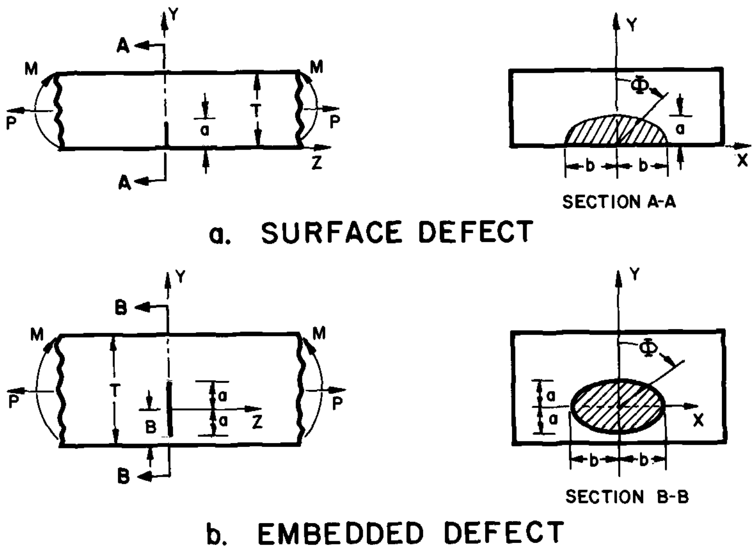

FIG. 1—*Defect characterization.*

Analysis Methodology

A crack growth analysis procedure is quite simple at first glance, perhaps deceptively so. All procedures are dependent to some extent on all of the following factors: (*1*) geometry of component, (*2*) crack size and shape, (*3*) crack orientation, (*4*) service conditions, (*5*) environment, and (*6*) crack-growth law.

The crack growth relationships specified at present in the Code are of the form originally suggested by Paris and Erdogan [*2*], which relates the crack growth per cycle da/dN to the range of applied stress-intensity factor ΔK:

$$\frac{da}{dN} = C\,\Delta K^n \tag{3}$$

This relationship is the most widely accepted at present, and is also used, for example, in the U.S. Air Force Damage Tolerant Design Handbook [*3*]. The parameters C and n in Eq 3 are considered material properties for inert environments; their determination and use will be discussed in some detail in the next section. Fatigue crack growth of many structural materials is also influenced by the level of mean stress. This can be accounted for by adjusting the value of ΔK or the values of C and n by a function of the ratio of minimum to maximum applied stress intensity factor (called the R-ratio). This will be further discussed later.

The simplest calculation of fatigue crack growth is possible when C and n are material constants and there is a single value of applied ΔK at the tip of the crack. In this case Eq 3 can be integrated, and the relationship between cyclic stress and ΔK of Eq 4 can be used to obtain the final crack length a_f in terms of the initial crack length a_o and the number of times (N) the single stress range cycles are repeated. Accordingly

$$\Delta K = C_1 \, \Delta\sigma \sqrt{a} \tag{4}$$

$$a_f = a_o \left\{ 1 + \left(\frac{2-n}{2} \right) C \, [C_1 \Delta\sigma]^n N \, [a_o]^{(n-2)/2} \right\}^{2/(2-n)} \tag{5}$$

where

C_1 = shape factor for the geometry,
$\Delta\sigma$ = applied stress range (far field), and
a = crack depth.

If there are a number of different stress range blocks in a given stress history spectrum, then for any block, the crack growth equation can be integrated to give the final crack size as a result of that block. Therefore, for the k^{th} stress cycle where the initial crack length is a_k, the crack length at the beginning of the $k + 1$ stress block is

$$a_{k+1} = a_k \left\{ 1 + \left(\frac{2-n}{2} \right) C \, [C_1 \Delta\sigma_k]^n \, [N_{k+1} - N_k] \, a^{(n-2)/2} \right\}^{2/(2-n)} \tag{6}$$

In practice, Eq 6 can be used to accumulate the crack growth for any number of blocks of constant amplitude stress ranges. In doing so, the order of consideration of the blocks is unimportant, as long as C and n are constants. The small and large amplitude stress ranges can be applied in any order and the same final length will be obtained, since for a given value of ΔK, the same value of crack growth per cycle will always be obtained from Eq 3.

There are a number of difficulties associated with the implementation of the simple procedure just outlined. The problems for the most part are directly related to the degree of conservatism acceptable for the calculations. If one is willing to live with a degree of conservatism in return for the simplicity of calculation, this procedure can be used. This conservatism results from two assumptions which must be made to use the method:

1. The crack shape remains constant, and growth is governed by ΔK at a single point on the crack (maximum value).
2. The crack growth rate law parameters C and n are material constants, and growth is governed by the highest R-ratio available.

These two assumptions can prove prohibitively conservative for cracks in geometric discontinuity areas and for many materials and environments where the growth rate law is bilinear in a logarithmic plot. For example, crack growth behavior of pressure vessel steels in water environments is typically bilinear when plotted as the logarithm of da/dN versus the logarithm of ΔK [4]. At elevated temperatures, many austenitic steels display multilinear regions on the log-log plot of da/dN versus ΔK [5]. In these cases Eq 3 is valid only over the particular segment of the piece-wise linear portion of the da/dN curve which is associated with the value of ΔK, and a cycle-by-cycle integration of Eq 3 is required. As a result of the multilinear crack growth curves, the final crack size a_f is a function of the order that the stress-cycle blocks are applied. Further, it may be necessary to break the stress-cycle blocks up into smaller divisions to ensure that the correct portion of the crack growth curve is being integrated.

A standard approach to integrate numerically a piece-wise linear da/dN versus ΔK curve cycle-by-cycle is given in the following algorithm:

1. Select stress-cycle block.
2. Set a_1 to initial crack length a_o.
3. Sum on $N = 1$ to the total number of repetitions of cycle block:
   a. Compute C_1, $K_{\min}$, $K_{\max}$, ΔK, R-ratio for a_i crack length.
   b. From table of C and n versus ΔK determine C and n.
   c. Setting $\Delta N = 1$, update crack length using

$$a_{i+1} = a_i \left\{ 1 + \left(\frac{2-n}{2} \right) C \, [C_1 \Delta\sigma]^n [a_i]^{(n-2)/2} \right\}^{2/(2-n)}$$

   d. Continue Steps 3a to 3c until the total number of stress cycles are considered.
4. Select new stress-cycle block.
5. Set a_1 to last crack length calculated in Step 3.
6. Repeat Steps 3 to 5 until all stress blocks are accounted for.

This algorithm should be repeated considering all possible ordering of the stress blocks until the largest final crack length is obtained. If a specific order of stress blocks is known, then advantage should be taken of this knowledge. One possible way to approximate the ordering effect is to break the spectrum up so that each stress-cycle block is subdivided equally. Then the spectrum is repeated sequentially until the total number of cycles is accounted for. Although this procedure is approximate and cannot be guaranteed to give conservative results, sufficient refinement of the loading spectrum will lead to reasonably conservative results. It should be pointed up here that both the magnitude and number of design cycles used in these calculations are extremely conservative relative to actual occurrences.

Because of this conservatism in design cycles, it is essential not to be overly conservative in counting cycles for an analysis using these cycles. It is therefore recommended that the design cycles be assumed to occur independently, and the range of applied stress be determined in this manner. On the other hand, for failure analyses or other applications where the cycles are more or less random, the well-known rain-flow technique should be used.

All of the aforementioned procedures are derived considering that the shape of the crack does not change during the cyclic growth. This simplifies the integration of Eq 3, since under these circumstances C_1 is only a function of the depth of the crack. Usually, however, design and in-service inspection results require the determination of crack growth of semi-elliptical surface flaws or elliptical embedded flaws or both. For these situations ΔK is not a constant on the periphery of the crack and is strongly affected by the aspect ratio of the crack (ratio of crack depth to half length a/b).

In most fatigue crack growth situations, such cracks do not maintain a constant shape (or a/b ratio) throughout life. As discussed by Corn [*6*] and others, this phenomenon has been observed experimentally for a variety of materials and applied stress fields. In the remainder of this paper, an evaluation is made of the importance of accounting for this shape change in fatigue crack growth calculations in power generation pressurized components.

To evaluate the impact of the change of crack shape, a series of calculations were carried out using two different assumptions. In one case the original aspect ratio was held constant during the entire analysis; in the second case the crack was allowed to grow both in length and depth according to the value of ΔK calculated at the semimajor and semiminor axes, respectively.

For the growth of the depth of the crack, Eq 3 is used with

$$\Delta K_a = g_{Ma}\,\Delta\sigma_M\sqrt{a} + g_{Ba}\,\Delta\sigma_B\sqrt{a} \tag{7}$$

where g_{Ma} and g_{Ba} are the magnification factors determined for the depth of the crack, $\Delta\sigma_M$ is the range of the membrane stress, and $\Delta\sigma_B$ is the range of the bending stress on the uncracked cross section. g_{Ma} and g_{Ba} are obtained directly from the results of Raju and Newman [*7*]. These factors are a function of the a/b and a/T ratios, where T is the section thickness.

The stress-intensity factor expressions of Raju and Newman were used in the examples here because they are believed to be the most accurate results available and because they are applicable over a wider range of geometries. An extensive study of the available expressions was carried out by Raju and Newman, wherein they compared their results with earlier expressions and with results from tests performed on epoxy models. Although they did not specifically compare their results with those available in Appendix A of Section XI of the ASME Code [*1*], they did compare their results with the original references upon which the Code curves are based. A comparison of the Raju-Newman results with the Code curves for both membrane and bending magnification factors is provided in Figs. 2 and 3 for surface flaws.

Consider the case of the membrane magnification factors (Fig. 2). The Code stress-intensity factors are more conservative for virtually every crack shape and size, with the most conservatism appearing for the long narrow cracks and the least for semicircular cracks where the expressions are nearly equal. There are no expressions available in Section XI for the magnification factor at the intersection of the crack plane and the surface of the component. Raju and Newman do provide such a result, which is a major advantage in the study of crack shape change. The bending magnification factors shown in Fig. 3 are more complicated to compare, since solutions are available at both the surface and deepest point (denoted as $\beta = 0$ deg). Comparing solutions at the deepest point, the Section XI solutions are more conservative for very narrow cracks, but as a/ℓ[4] increases to 0.2 the two solutions are about equal, and at a/ℓ greater than 0.2 the Raju-Newman solutions are the largest. Again the Raju-Newman work provides more expressions at the surface than does the Code, but only a few are plotted for comparison to keep the figure readable. For most cases compared, the Code curves are more conservative.

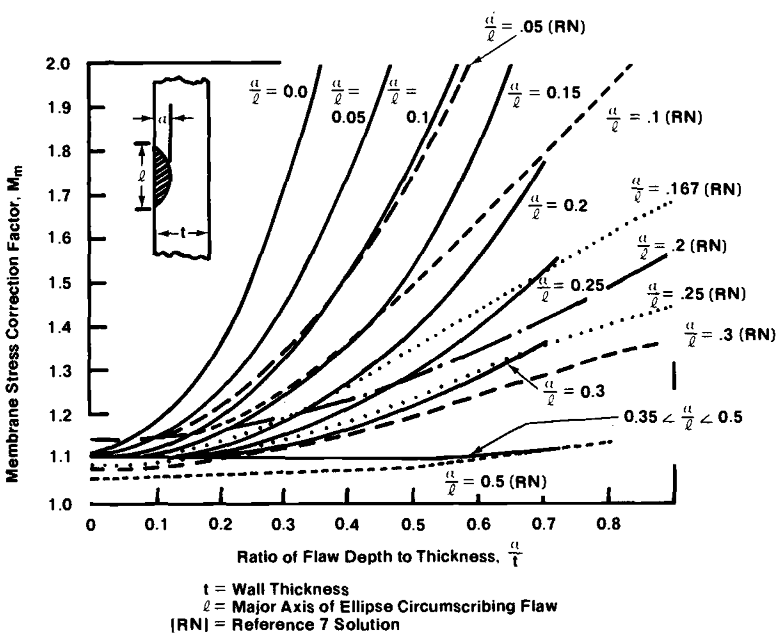

FIG. 2—*Comparison of correction factors for surface flaws.*

[4]"ℓ" is the Code terminology for "$2b$" as used in this paper and defined in Fig. 1.

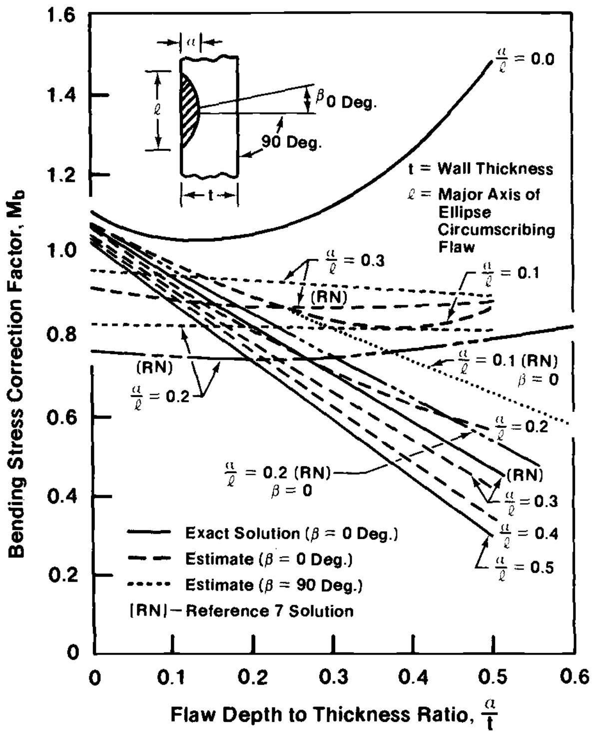

FIG. 3—*Comparison of bending correction factors for surface flaws.*

It can be concluded then that the Code curves are nearly always more conservative than those of Raju and Newman, but it appears from their work that the Raju-Newman curves are more accurate. Another advantage of the Raju-Newman solutions is that they are available for more crack depths and, particularly, are more useful for the calculation of K at the crack-surface intersection.

To compute the effect of the change in shape of the cracks, the crack growth at the surface must also be computed. Analogous to Eq 3, assume that the rate of change of the surface length can be obtained as

$$\frac{db}{dN} = C\,\Delta K^n \tag{8}$$

The stress intensity at the intersection of the surface of the plate and the defect is [7]

$$\Delta K_b = g_{Mb}\sqrt{\frac{a}{b}}\,\Delta\sigma_M\sqrt{b} + g_{Bb}\sqrt{\frac{a}{b}}\,\Delta\sigma_B\sqrt{b} \tag{9}$$

where g_{mb} and g_{Bb} are the magnification factors for the stress-intensity factor at the intersection of the crack and the surface.

The calculation of crack growth for the case of two dimensional growth requires a cycle-by-cycle integration of the crack growth law where the magnification factors are updated each cycle to account for the change in aspect ratio and crack depth. The crack growth cycle-by-cycle integration algorithm used to account for crack shape change is as follows:

1. Select a stress-cycle block.
2. Set a_1 and b_1 to their initial values and computer a_1/b_1 (or a_i/b_i).
3. Sum crack length and depth cycle-by-cycle with a_i/b_i fixed during each cycle:
   a. Compute g_{ij}, ΔK_a, ΔK_b.
   b. From ΔK_a and ΔK_b determine the appropriate C and n.
   c. For $\Delta N = 1$, update crack depth using Eq 6.
   d. For $\Delta N = 1$, update crack surface length using Eq 6, substituting b for a.
   e. Compute a_{i+1}/b_{i+1} and a_{i+1}/T and continue Steps 3a to 3d until the total number of cycles has been accounted for.
4. Select new stress-cycle block.
5. Set a_1 and b_1 and a_1/b_1 to last values computed in Step 3e.
6. Repeat Steps 3 to 5 until all stress-cycle blocks are accounted for.

Obviously this simple procedure neglects many of the phenomena that affect the shape of fatigue cracks, but the effects of crack shape and subsequent changes in shape on the computational aspects of fatigue crack growth can be studied.

Figure 4 shows the results of the calculations for the case of membrane loads only. Three curves are shown: the length of the crack at the surface, the depth of the crack, and the crack depth considering growth constant on the periphery of the crack using ΔK equal to the maximum of ΔK_a or ΔK_b. From this plot it can be seen that the a/b ratio slowly changes from the initial value of ⅓ to about ⅔. The figure also shows that a conservative design evaluation is possible if a/b is considered fixed throughout the cyclic history to the ratio of ⅓.

Figure 5 shows similar results for pure bending. In this case, however, the initial a/b ratio of ⅓ changes greatly as a/T approaches one half. Again, conservative results are obtained if a/b is fixed at ⅓ throughout the cyclic loading history.

Figure 6 shows a mixed bending plus tension case. In this case a/b changes from the initial ⅓ to about ½, but because the ratio of $\Delta\sigma_m$ to $\Delta\sigma_b$ was unity, the crack continued to grow past the a/T value of ½. As before, fixing a/b to ⅓ throughout the cycles is conservative.

The results of these sample problems were obtained with the use of a sim-

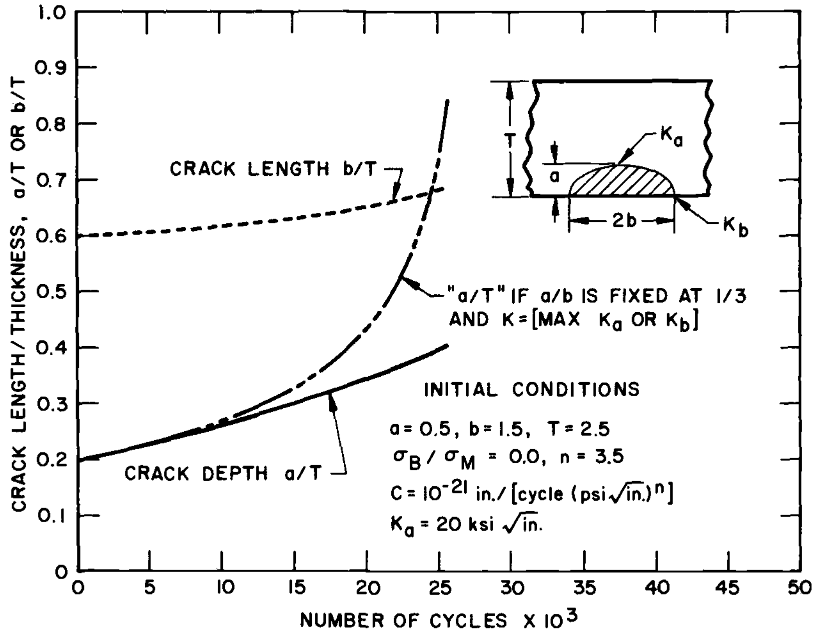

FIG. 4—*Crack growth behavior for membrane loading.*

ple fatigue crack growth law, with $C = 10^{-21}$ [in./cycle-(psi$\sqrt{\text{in.}}$)^n] and n = 3.5. Further calculations show that the comparative results of the assumptions on crack shape change are not affected by the values of C and n chosen.

A second series of examples was carried out for the case of a bilinear (logarithmic portrayal) fatigue crack growth rate curve shown in Ref *4* to be applicable to growth of cracks in carbon and low-alloy steels in a water environment. The examples used were specifically formulated so that both parts of the crack growth rate law would be used. Results of these calculations, although different in magnitude to those of Figs. 4 to 6, showed the same relative behavior. In each case, the constant shape assumption is conservative, provided the maximum applied ΔK along the crack front is used to govern growth. As before, there is no difference between the growth obtained by using ΔK at the deepest point of the crack and that obtained using the maximum ΔK until the amount of growth becomes significant, thus shifting the point of maximum ΔK to the surface.

These sample problems show that crack shape change can be significant in crack growth calculations, but only under conditions where significant growth is experienced. It is always conservative to assume that the crack has a constant shape of a/b = ⅓, and that its growth is governed by the maximum value of ΔK along the entire crack. The assumption that growth is

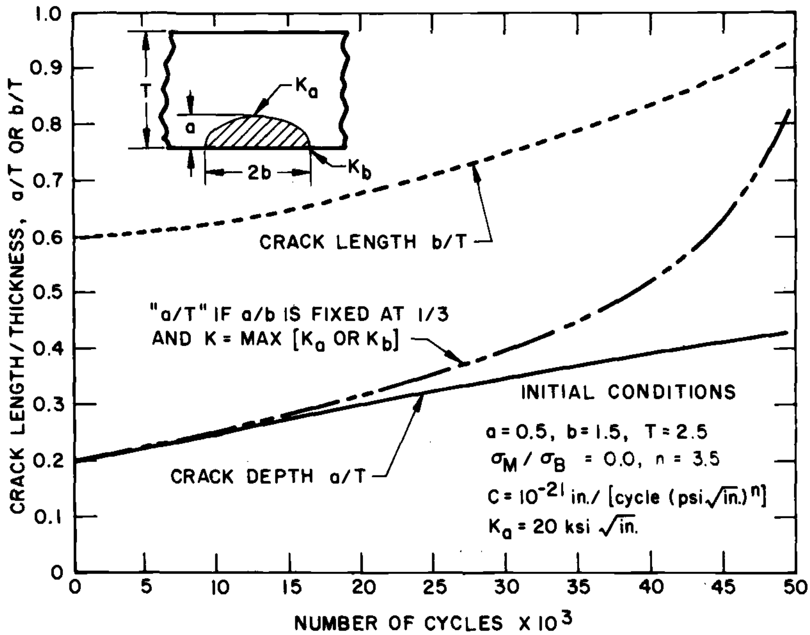

FIG. 5—*Crack growth behavior for bending loading.*

governed by the applied ΔK at the deepest point of the crack is also adequate for 50 to 60 percent of the crack propagation life of the structure (Figs. 4 to 6).

For accurate calculation of crack growth, a cycle-to-cycle numerical integration scheme is necessary. This type of analysis tool requires fewer restrictive assumptions regarding stress-cycle ordering. Also, other important considerations, such as a bilinear crack growth rate law, can easily be included in the analysis. The results obtained from these examples are qualitatively consistent with experimental results (given, for example, in Ref *6*).

Another most important consideration worthy of some discussion is which approach should be taken when very high loads are present, resulting in part or all of the structure becoming plastic. This type of situation occurs relatively often in failure analysis, but no universally accepted procedure has yet been developed. One of the more promising methods now available for such treatment is the J-integral approach pioneered for crack growth by Dowling and Begley [*8*] in 1975. Since that time it has been demonstrated that fatigue crack growth rate data presented in terms of applied ΔJ remain linear much further than would have been expected, up to an equivalent ΔK of over 220 MPa$\sqrt{\text{m}}$ (200 ksi$\sqrt{\text{in.}}$) for low-alloy pressure vessel steel [*9*] and up to an equivalent ΔK of over 165 MPa$\sqrt{\text{m}}$ (150 ksi$\sqrt{\text{in.}}$) for Type 304 stainless steel [*10*].

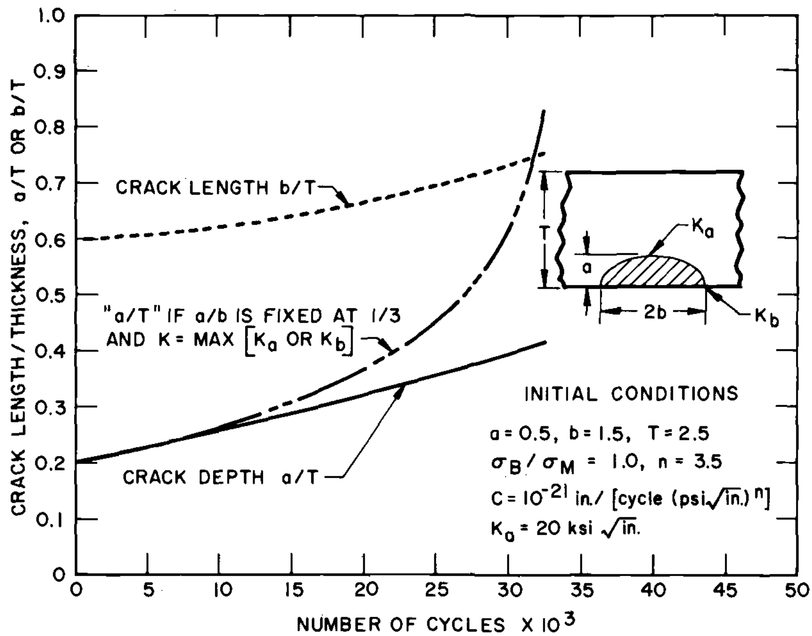

FIG. 6—*Crack growth behavior for combined membrane and bending loading.*

When performing a crack growth analysis for a structure in the plastic range great care must be taken because of the yielded zone and its progression during transients. A crack growing in a structure loaded well into the plastic range could result in considerable crack extension for each plastic cycle. As an example, considering only the stable crack extension due to high values of applied J, significant crack growth can be obtained by referring to a plastic R-curve for the material. However, for more moderate levels of cyclic loading, it is usually found that the extension of the crack is significant only for a few cycles, after which the structure shakes down to elastic behavior. Further cycling is then elastic and hence the simpler elastic analysis is again accurate.

To accomplish a crack growth analysis in the plastic range, usually the total strain fluctuation for the far field is required, as well as the cyclic plastic properties of the material at the temperature of interest. Cycling past the first cycle is then complicated by residual stresses and the cyclic hardening found in most nuclear construction steels. This type of analysis is generally needed only for failure analysis because the ASME Code precludes normal operation with materials loaded into the range of full cross-section yielding. Local plasticity is allowed in the normal operation of a plant, and the procedures of

Section XI of the Code are corrected for the plastic zone at the crack tip by adjusting the factor g_{Ma} and g_{Ba} of Eq 7.

This correction is incorporated into the Code procedure by adjustment of the magnification factors so that the crack length is effectively increased as the remote stress approaches the yield stress. The plastic-zone size expression used is

$$r_y = \frac{1}{5.66\pi}\left(\frac{K_I}{\sigma_y}\right)^2 \tag{10}$$

where

r_y = plastic-zone radius,
K_I = stress-intensity factor, and
σ_y = yield stress.

This correction is presently incorporated in the crack shape factor Q, and its impact is to increase K_I. This correction can add considerable conservatism to the calculation of crack growth, since the range of applied stress-intensity factor is raised to a power of 3 to 8 in the expression for crack growth per cycle. Over a large number of cycles overestimates of crack growth can be significant, since generally no plasticity correction is used in the calculation of ΔK from crack growth rate test results. Thus another conservatism is inherent in the present Code procedure.

Crack Growth Rate Law Considerations

The reference fatigue crack growth rate laws presently contained in the ASME Code are for only one class of materials: carbon and low-alloy pressure vessel steels with minimum specified yield strengths less than 345 MPa (50 ksi). The air environment and the reactor water environment are considered.

These laws were provided at the inception of the Section XI evaluation procedure, which was originally intended for application to the nuclear reactor vessel. Since the original adoption of Section XI in the 1974 edition of the Code, inspection requirements have been extended to other components and acceptance standards have been developed. These developments have led to the need for reference fatigue crack growth rate laws for other materials (for example, stainless steels and Inconel alloys). The operation of other reactor systems than the light water reactor in the United States has also resulted in the need to consider other materials; some examples are listed in Table 1.

There are a number of variables that need to be considered when specifying a reference fatigue crack growth rate law for a given material, but not all of these variables must be treated explicitly. The application of the reference

TABLE 1—*Examples of nuclear materials.*

Vessels	Piping/Tubing
SA 302 GR B	SA 106 GR B, C
SA 515 GR 70	SA 155 GR KCF
SA 516 GR 60, 70	SA 304
SA 517 GR B, F	SA 316
SA 533 CL 1 GR A, B	A511 TYPE 403
SA 542	ALLOY 600
SA 105 GR 2	...
SA 181	...
SA 182 GR H, F6	...
SA 508 CL 1, 2	...
SA 350 LF 2	...
SA 216 GR WCB, WCC	...

laws is the most important information to be kept in mind in their formulation. The philosophy used must also consider generalization of the reference law as much as can be justified based on the current state of the art. Clearly some variables will be important for some applications but not others, so efforts must be made to achieve the desired generality without sacrificing important information.

For example, in assessing the acceptability of a detected flaw, growth rate data in the low ΔK range are important. On the other hand, in making a design assessment, using a relatively large postulated flaw, growth rate data in the intermediate-to-high range of applied ΔK are necessary.

Among the variables that need not be accounted for separately in a reference law are differences between weld, base metal, and heat-affected zone behavior. Small differences do exist, but based on present knowledge [*4,5*] they are not of sufficient magnitude to be worth the extra effort required. Variables such as ramp and hold time can be classified as testing variables, and as such should only be considered in light of the intended application. This is important in situations where creep-fatigue interactions are important, but these situations are deserving of special treatment. Effects of damage processes such as thermal aging and irradiation are still under investigation, but based on present knowledge these effects would not have an impact on reference laws [*11*].

Although they might not be necessary in every application, the three variables that must be accounted for specifically in a reference law are temperature, R-ratio, and environment. Temperature effects are generally considered by choosing the temperature range of steady-state operation, although several temperatures may be required to account for the range of operation of a high-temperature reactor system. James [*12*] has suggested a simple method for making such an adjustment for austenitic stainless steels, which also includes frequency effects.

The effect of R-ratio is extremely important for some applications (for example, carbon and low-alloy steels in water, and austenitic stainless steels in any environment). A number of models are available to account for R-ratio in the fatigue growth rate characterization through a modification of the crack growth rate parameter [13-15]. For example, Walker [13] proposed that the parameter ΔK be replaced with $K_{eff} = K_{max} (1 - R)^m$. This portrayal is fairly adequate to account for the R-ratio effects in most test results now available, which tend to be between $R = 0$ and $R = 0.7$.

The major difficulty in applying the Walker model to crack growth analysis in a reactor component is that the model predicts great increases in the crack growth rate with increasing R-ratio. This can be seen in Table 2, where several examples are presented for various R-ratios and values of m. The Walker model provides for no saturation effect with R-ratio, and the predicted crack growth becomes very conservative for high R-ratios. In fact, the correction for R-ratio increases exponentially as R-ratio approaches the value of one. This behavior is not consistent with much of the observed experimental data [4].

It is easily seen from Table 2 that crack growth per cycle at high R-ratio is very high for the models which correct for R in a continuous manner, even at low ΔK-values. Since there are often millions of such cycles in transient specifications, these laws would predict extreme amounts of crack growth. However, experience has shown that very large crack growth has not occurred in service, and some experimental results [4] are available which do not show extreme crack growth for high R-ratios. It is thus concluded that a model to continuously account for R-ratio should not be employed at present, and not until sufficient data are available at high R-values to cover the range of applications.

Perhaps the most obvious variable in need of direct treatment is the environment. It is now well known that corrosion fatigue processes are very different in different environments. This is particularly true with regard to carbon and low-alloy steels in water environments.

Since it is likely that reference fatigue crack growth rate laws will soon be formulated for a number of other steels and alloys to accompany the present two, some thoughts on the philosophy of such determinations are offered here. As stated earlier, the application of the laws must be kept in mind in their determination. From the point of view of Section XI of the Code, it appears that the desired results of such a calculation is a "best estimate" of how much a known crack will grow during a service period. Therefore no margins of safety should be built into such a calculation; this is because these margins will be brought in specifically when the criteria are evaluated to determine suitability for further service, as in Eqs 1 and 2.

Keeping consistent with this philosophy would indicate that a mean of the crack growth rate behavior should be used for design. A statistically determined mean of future data, called a global confidence limit, is well suited for

TABLE 2—*Comparison of* R-*ratio corrections.*

Model	ΔK[a]	Crack Growth per Cycle[b] At R-ratio Equal to 0.2	0.7	0.95
1. Section XI [1] $\frac{da}{dn} = 3.7 \times 10^{-10}\, \Delta K^{3.726}$	5	1.4879×10^{-7}	1.4879×10^{-7}	1.4879×10^{-7}
	10	1.9688×10^{-6}	1.9688×10^{-6}	1.9688×10^{-6}
	15	8.919×10^{-6}	8.919×10^{-6}	...
2. $\frac{da}{dn} = 3.7 \times 10^{-10}\, K_{eff}^{3.726}$	5	2.6627×10^{-7}	3.4382×10^{-6}	3.6805×10^{-4}
	10	3.5234×10^{-6}	4.5496×10^{-5}	4.87×10^{-3}
$K_{eff} = K_{max}\,(1 - R)^{0.3}$	15	1.5962×10^{-5}	2.0611×10^{-4}	...
3. $\frac{da}{dn} = 3.7 \times 10^{-10}\, K_{eff}^{3.726}$	5	7.8476×10^{-7}	1.1723×10^{-3}	$7.3763 \times 10^{+2}$
	10	1.0384×10^{-5}	1.5513×10^{-2}	$9.7606 \times 10^{+3}$
$K_{eff} = K_{max}/(1 - R)$	15	4.7043×10^{-5}	7.0277×10^{-2}	...
4. $\frac{da}{dn} = \frac{3.7 \times 10^{10}\, K_{eff}^{3.726}}{(1 - R)^{1.863}}$	5	3.417×10^{-7}	1.3207×10^{-5}	1.0476×10^{-2}
	10	4.5216×10^{-6}	1.7476×10^{-4}	1.3862×10^{-1}
$K_{eff} = K_{max}\,(1 - R)^{0.5}$	15	2.0484×10^{-5}	7.9171×10^{-5}	...

[a] $\Delta K = K_{max}\,(1 - R)$.
[b] Growth per cycle in inches; to obtain centimetres, multiply by 2.54.

this purpose. The decision to use the mean of the crack rate data could also be reached from a consideration of the mechanics of fatigue crack growth, which is a process by which a crack extends slowly due to many cycles of loading. As such, an averaging process is built in. The crack growth may be higher than average for one cycle and lower than average for later cycles, with the net resulting crack growth adequately predicted by using the mean growth rate.

Whenever possible the determination of reference laws should be aided by the use of information on the mechanisms of the crack growth process. A temptation in such endeavors is to make use of processes which tend to reduce the growth rate, such as overload effects which influence nearly all materials, and interruptions in loading that appear to retard crack growth in tests involving enhancement due to water environments. This is a dangerous step to take without thorough knowledge of the mechanisms involved and the reliability of such interruptions or overloads. This is not recommended for conservative application of fatigue crack growth technology in the design of power-generation components.

Comparison of Techniques with Those of Other Industries

The procedures of fatigue crack growth analysis described previously are very similar to those used in other industries. The number of the simplifying assumptions and the simplification in computational approach may be somewhat different depending on the degree of conservatism that can be tolerated in the design stages of the product development.

The aerospace industry, and particularly the U.S. Air Force, has incorporated fatigue crack growth analysis as a primary consideration in the design and maintenance of aircraft [*16*]. The geometries of interest here are generally thin shell and narrow structural members rather than the thick sections generally analyzed in the power industry. The loadings are much more predictable in this industry, if not in absolute magnitude then in order of loading, so overload retardation effects can be used. This subject is covered in some depth by Wood [*17*].

Civil engineering design codes do not at present explicitly require fatigue crack growth analysis procedures, but in many instances failure analyses of bridges do take advantage of crack growth technology. An example is the analysis of the Lafayette Street Bridge girder fracture [*18*]. The analysis showed that fatigue crack growth led to the final brittle fracture. The cracks were found to originate at lack-of-fusion areas in the lateral bracing stiffening details. More detailed consideration of crack growth analysis methodology for these structures is provided by Barsom.[5]

The automotive industry also utilizes fatigue crack growth calculations

[5]This publication, pp. 300-318.

[19]. The automotive and civil engineering designers are concerned with very long-lived structures subjected to random vibratory loadings producing rather low stress levels. Under these types of loadings the basic design philosophy has been the prevention of crack initiation rather than the control of crack growth. This philosophy is apparently adequate for the design of redundant structures as long as the fabrication flaws are controlled.

Much progress has recently been made to bridge the gap between crack initiation and crack growth [20]. It is still a debatable question, however, as to what constitutes the initiation of a crack of engineering significance and at what stage the propagation phase takes over.

Suggested Future Work

Although fatigue crack growth analysis has been a part of the ASME Code since the 1974 edition of Section XI, many steps can be taken to improve on the present treatment. Perhaps the most significant improvement would be to provide reference crack growth laws for a range of materials and environments more representative of those covered by inspection standards. More work is also needed to better understand the mechanisms of fatigue (especially corrosion fatigue), so that the reference laws can be more reliably constructed.

The transition between crack initiation and growth needs to be further studied; when this is successfully characterized, both crack initiation and growth can be accounted for in design considerations and failure assessment. More information is also needed concerning the size and location of defects which could be present as a result of the fabrication process, and which would not be detected by preservice and nondestructive examination. The entire integrity assessment process will be aided by improvements now being studied in the area of nondestructive examination.

Another area in need of considerable development is the characterization of crack growth under elastic-plastic conditions. This area has been the subject of studies by Dowling and Begley [8] and others, but much remains to be done. The major use of such technology is expected to be in best-estimate failure analyses rather than the prediction of crack growth during service.

References

[1] American Society of Mechanical Engineers Boiler and Pressure Vessel Code, 1978 edition, Section XI.

[2] Paris, P. C. and Erdogan, F., *Journal of Basic Engineering, Transactions of the American Society of Mechanical Engineers*, December 1963, pp. 528-34.

[3] *Damage Tolerant Design Handbook*, MCIC HBol, Materials and Ceramics Information Center, Columbus, Ohio, January 1975.

[4] Bamford, W. H., "Application of Corrosion Fatigue Crack Growth Rate Data to Integrity

Analyses of Nuclear Reactor Vessels," *Journal of Materials Technology, Transactions of the American Society of Mechanical Engineers,* July 1979.
[*5*] James, L. A., *Atomic Energy Review,* Vol. 14, 1976, pp. 37-86.
[*6*] Corn, D. L., *Engineering Fracture Mechanics,* Vol. 3, 1971, pp. 45-52.
[*7*] Raju, I. S. and Newman, J. C., Jr., "Improved Stress Intensity Factors for Semi-elliptical Surface Cracks in Finite-Thickness Plates," NASA TM-X-72825, National Aeronautics and Space Administration, 1977.
[*8*] Dowling, N. E. and Begley, J. A. in *Mechanics of Crack Growth, ASTM STP 590,* American Society for Testing and Materials, 1976, pp. 82-103.
[*9*] Dowling, N. E. in *Cracks and Fracture, ASTM STP 601,* American Society for Testing and Materials, 1976, pp. 19-32.
[*10*] Brose, W. R. and Dowling, N. E. in *Elastic-Plastic Fracture, ASTM STP 668,* American Society for Testing and Materials, 1979, pp. 720-735.
[*11*] James, L. A., "Effects of Irradiation and Thermal Aging Upon Fatigue Crack Growth Behavior of Reactor Pressure Boundary Materials," *Proceedings,* Meeting on Time and Load Dependent Degradation of Engineering Materials, International Atomic Energy Agency, 1978.
[*12*] James, L. A., "Frequency Effects in the Elevated Temperature Crack Growth Behavior of Austenitic Stainless Steel—A Design Approach," ASME Paper 78-PVP-92, American Society of Mechanical Engineers, 1978.
[*13*] Walker, K. in *Effects of Environment and Complex Load History on Fatigue Life, ASTM STP 462,* American Society for Testing and Materials, 1970, pp. 1-14.
[*14*] Forman, R. G., Kearney, V. E., and Engle, R. M., *Journal of Basic Engineering, Transactions of the American Society of Mechanical Engineers,* Vol. 89, Series D, September 1967, p. 459.
[*15*] Krafft, J. M. and Smith, H. L., "Ligament Instability Model for Stress Corrosion and Fatigue Crack Propagation in a 4340 Steel," NRL Memo Report No. 2598, Naval Research Laboratory, Washington, D.C., April 1973.
[*16*] Pinckert, R. E., "Damage Tolerance Assessment of F-4 Aircraft," MCAIR 76-015 Revision A, McDonnell Douglas Corporation, 1976.
[*17*] Wood, H. A., "USAF Experiences with Fatigue Crack Propagation Data in the Evaluation of Aircraft Structures," ASTM Symposium on Fatigue Crack Growth Evaluation and Data Analysis, 29-30 Oct. 1979, Pittsburgh, Pa.
[*18*] Fisher, J. W., Pense, A. W., and Roberts, R., *Journal of the Structural Division, American Society of Civil Engineers Transactions,* Vol. 103, No. ST7, Paper 13059, July 1977, pp. 1339-57.
[*19*] Downing, S., Galliart, D., and Berenyi, T., "A Neuber's Rule Fatigue Analysis Procedure for Use with a Mobile Computer," Society of Automotive Engineers, Paper 700317, Automotive Engineering Congress and Exposition, February 1976, Detroit, Mich.
[*20*] Dowling, N. E., "Notched Member Fatigue Life Predictions Combining Crack Initiation and Propagation," Westinghouse R&D Report 79-1D3-PALFA-P1, January 1979.

J. M. Barsom[1]

Fatigue Considerations for Steel Bridges

REFERENCE: Barsom, J. M., "**Fatigue Considerations for Steel Bridges,**" *Fatigue Crack Growth Measurement and Data Analysis, ASTM STP 738,* S. J. Hudak, Jr., and R. J. Bucci, Eds., American Society for Testing and Materials, 1981, pp. 300–318.

ABSTRACT: This paper discusses the characteristics of the discontinuities that are the origins of fatigue cracks in various welded details, and presents the American Association of State Highway and Transportation Officials (AASHTO) fatigue-design curves for those details. The paper also presents a summary of the fatigue-crack-propagation data that have been obtained for bridge steels and weldments, and discusses some of the problems that need to be resolved to better predict the fatigue life of welded bridge details by using fracture-mechanics technology. It is suggested that until these problems are rectified the AASHTO fatigue-design curves present an excellent alternative to fracture-mechanics technology to ensure the structural integrity of welded details subjected to cyclic loadings.

KEY WORDS: fatigue crack growth, bridge steels and weldments, fatigue design curves

It is estimated that there are more than 350 000 steel highway and railroad bridges in the United States. With only a few exceptions, these structures have performed safely and reliably despite the fact that many of them have carried cyclic loads far in excess of the number for which they were designed. Field experience has indicated that the relatively few failures of bridge components have been caused primarily by fatigue. The knowledge gained from studying these failures and the extensive research that has been conducted on fatigue behavior of bridge steels and weldments have resulted in a substantial change in the fatigue provisions of bridge-design specifications. This paper presents the American Association of State Highway and Transportation Officials (AASHTO) fatigue design curves for steel bridge components and some problems in the use of fracture mechanics to predict the fatigue life of welded bridge components.

[1]Chief, Materials Technology Division, U.S. Steel Corporation, Monroeville, Pa. 15146.

AASHTO Fatigue-Design Curves for Welded Bridge Components

Bridge engineers have recognized for a long time the effect of cyclic loading on the structural integrity of welded bridge components. The American Welding Society (AWS) *Specifications for Welded Highway and Railway Bridges* [*1*][2] was based on fatigue tests of welded details that were conducted in the 1940's. In the late 1950's, the observation of fatigue cracks at welded details in the American Association of State Highway Officials (AASHO) Road Test [*2*] bridges indicated the need for further study of the fatigue behavior of welded details and for modifications of the existing specifications. The present AASHTO fatigue-design specifications [*3,4*] are based on extensive fatigue-test results and field experience that have been accumulated since the early 1960's.

The present AASHTO fatigue design specifications are based on experimental curves that relate the fatigue life, N, of a welded detail to the total (tension plus compression) applied nominal stress range $\Delta\sigma$ [*5*]. A large number of tests for a given detail have been conducted to generate a statistically significant stress-range—fatigue-life relationship. The design curves represent the 95 percent confidence limit for 95 percent survival for a given detail.

Figures 1 and 2 present fatigue-test results for welded beams and cover-plated beams, respectively, fabricated from bridge steels having yield strengths between 248 and 690 MPa (36 and 100 ksi) and subjected to various minimum loads. Statistical analysis of the available data indicates that the minimum stress, the maximum stress, and the grade of steel have a secondary influence on the fatigue behavior of welded components [*5,6*].

Other fatigue tests were conducted on beams and girders with welded attachments and with transverse stiffeners [*7*]. Figure 3 presents the fatigue life of 101-mm (4-in.)-long welded attachments superimposed on those for welded cover plate and plain welded beams. The data presented in Figure 3 show the fatigue strength of a girder with welded attachments having a length less than 50 mm (2 in.). The available fatigue data for various attachments show that the fatigue strength of a girder with welded attachments is strongly governed by the length of the attachment [*4,7*]. The longer the attachment, the higher the stress concentration at the toe of the weld and the lower the fatigue strength. Welded attachments longer than 203 mm (8 in.) have fatigue strengths equivalent to welded partial length cover plates. Transverse stiffeners are similar to very short attachments and have fatigue strengths equivalent to those of welded attachments that are 50 mm (2 in.) long or shorter.

The extensive fatigue data that have been obtained by testing welded bridge details have been used to establish allowable stress ranges for various

[2]The italic numbers in brackets refer to the list of references appended to this paper.

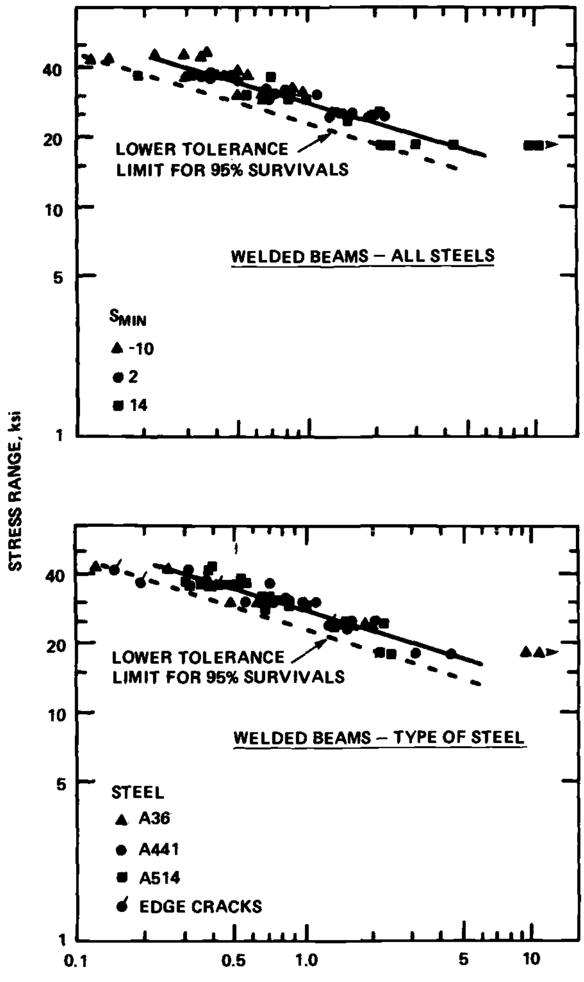

FIG. 1—*Effects of minimum stress and steel grade on the fatigue strength of welded beams.*

categories of steel bridge details (Fig. 4). Each category represents welded-bridge details that have equivalent fatigue strengths. The curve for each category corresponds to the 95 percent confidence limit for 95 percent survival of the details in a given category. Categories A, B, C, D, and E correspond to plain plate and rolled beams, plain welds and welded beams and plate girders, stiffeners and short attachments [less than 50 mm (2 in.) long], 101-mm (4-in.)-long attachments, and cover-plated beams, respectively. Category E′ corresponds to thick flanges and thick cover plate, and suggests

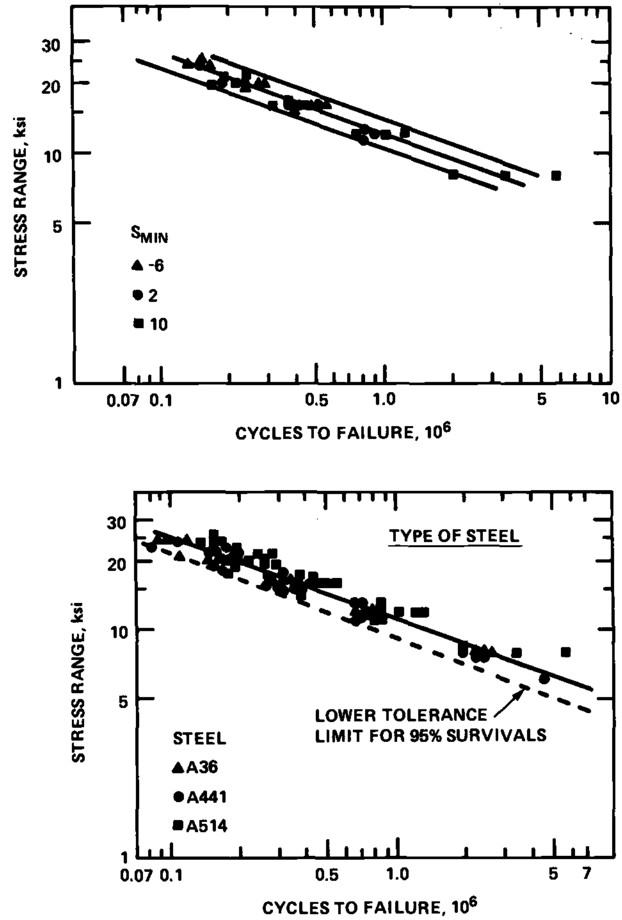

FIG. 2—*Effects of minimum stress and steel grade on the fatigue strength of beams with transverse end-welded cover plates.*

that thickness may also affect the fatigue strength of welded girders, as has been observed from highway bridges [*8*] and laboratory tests [*9*]. The horizontal lines for each category represent the applied nominal stress range corresponding to the fatigue strength (over 2×10^6 cycles) and are extremely important for highway bridges located on heavily traveled roads. The stress-range threshold corresponding to long life for a given category must be related to either fatigue-crack-initiation threshold or fatigue-crack-propagation threshold. Further research is necessary to better define the magnitude of the threshold stress range for each category and to establish the effects of infrequent excursions above these thresholds during variable-amplitude loading of welded-bridge details [*6*].

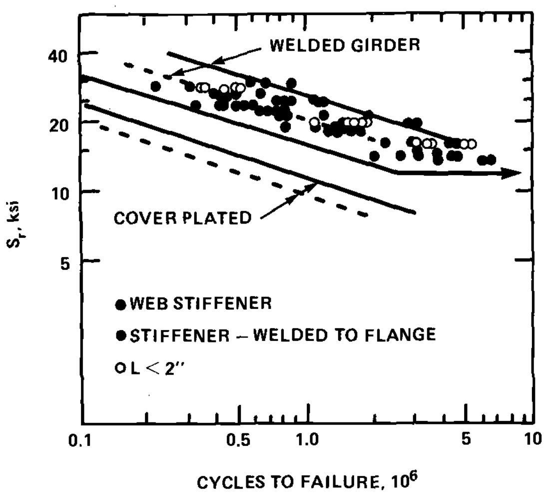

FIG. 3—*Summary plot for various types of transverse stiffeners. Types 1 and 2 welded to web alone; Type 3 welded to web and flange.*

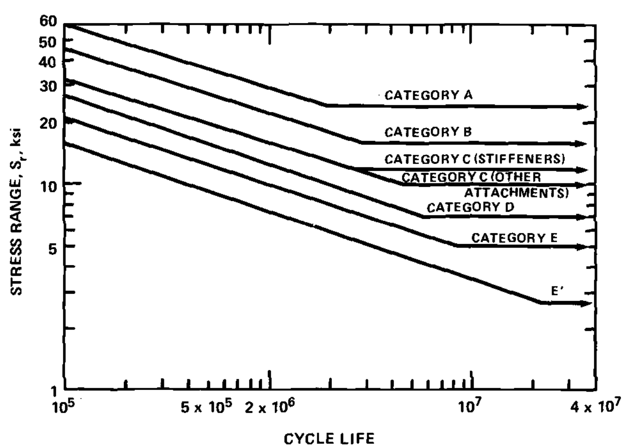

FIG. 4—*Design stress range curves for Categories A to E'.*

Fatigue Behavior of Weldments

General Discussion

Bridges, like most engineering structures, are built in accordance with well-defined rules and specifications. The specifications for bridges have been established by AASHTO and are closely related to specifications for materials, fabrication, and inspection that are specified by the American Society for Testing and Materials (ASTM), the American Welding Society (AWS), and others. These codes recognize the possible existence of tolerable discontinuities that should not adversely affect the performance of the structure for the intended application. In many instances, attempts to remove allowable discontinuities may result in conditions worse than the original condition. It is also recognized that significant deviations from the appropriate specification may adversely affect the performance of the structure. Consequently the present discussion relates to the fatigue behavior of welded bridge components that have been designed, fabricated, and inspected in accordance with AASHTO specifications.

Origins of Fatigue Cracks

Fatigue cracks in weldments originate either at internal discontinuities such as porosity, lack of fusion, and trapped slag [*10*] or at weld toes and weld terminations usually from slag intrusion [*5,10,11*]. The majority of fatigue cracks in welded bridge girders originate at a weld toe or at a weld termination rather than from internal discontinuities. This behavior is attributed to the fact that for a given fatigue life a much larger embedded discontinuity can be tolerated than a surface discontinuity. Furthermore, unlike embedded discontinuities, surface discontinuities that cause fatigue-crack initiation occur in regions of weld toes and weld terminations that are invariably regions of stress concentrations as a result of the physical shape of the joint.

Fatigue cracks that initiate at the root of web-to-flange fillet welds are a good example of fatigue cracks that originate from internal discontinuities (Fig. 5). The crack shown in Fig. 5 initiated at a gas pocket and propagated as an embedded crack that continually changed its shape until it intersected the fillet-weld surface as a penny-shaped crack (Fig. 5*a*). These types of fatigue cracks continue to propagate in all directions in a plane perpendicular to the direction of maximum tensile stress until they become three-corner cracks (Fig. 5*b*). Figure 6 shows that over 90 percent of the fatigue life of the component was exhausted prior to crack penetration through the back surface of the tension flange.

The majority of fatigue cracks in bridge girders initiate at a weld toe or at a weld termination near a stiffener, or other attachments such as a gusset plate, or end of a cover plate. These are regions of high stress concentration and high residual stresses that may contain small [less than 0.4-mm (0.016-in.)] [*10,11*] weld discontinuities such as slag intrusion. Moreover, because the surface of the deposited weld metal is invariably rippled, the toe angle between the weld metal and the base metal can vary significantly at neighboring points along the weld toe, resulting in variation in the stress concentration. Figure 7 shows crack formation at the toe of a longitudinal fillet weld (Fig. 7*a*), and at the toe of a transverse fillet weld (Fig. 7*b*), in cover-

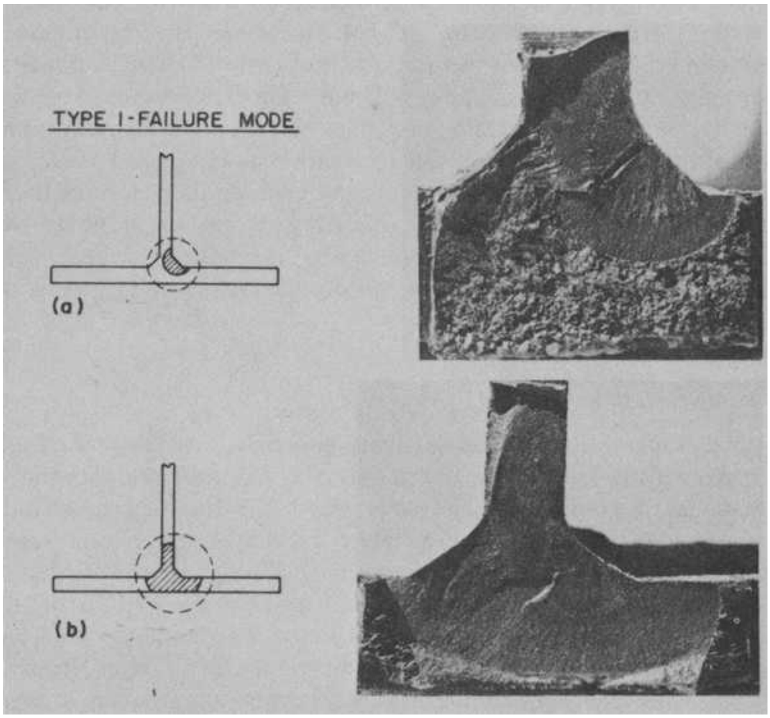

FIG. 5—*Fatigue cracks in web-to-flange fillet welds.*

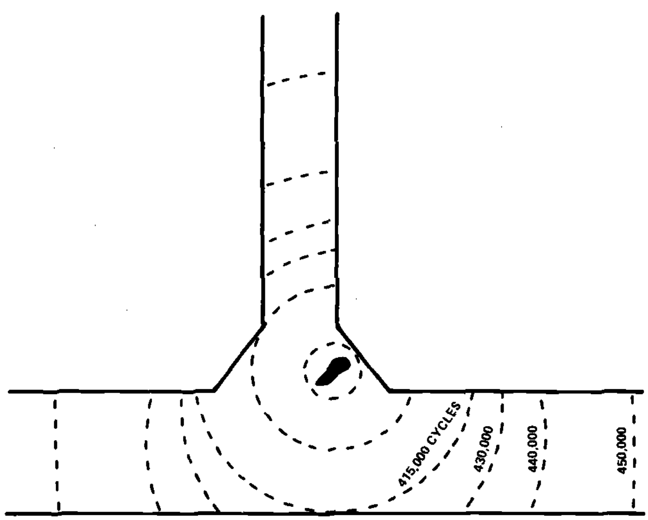

FIG. 6—*Stages of crack propagation for a web-to-flange fillet weld.*

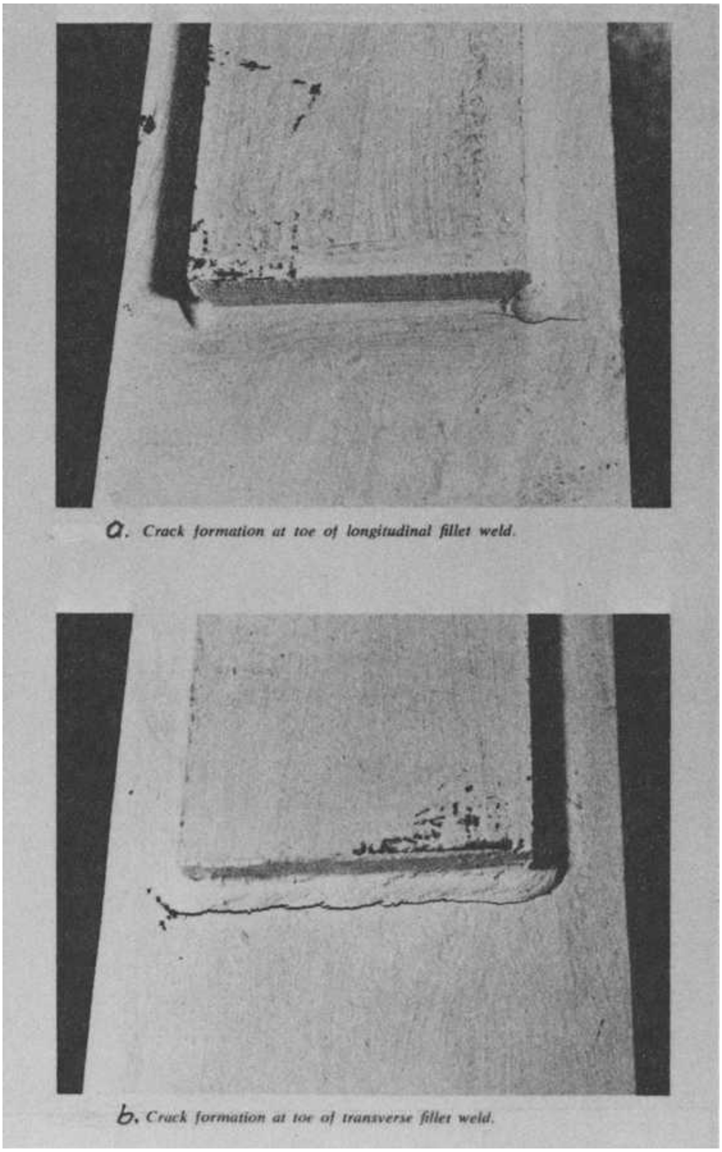

FIG. 7—*Fatigue crack at ends of cover plates.*

plate details. For the cover plate with longitudinal fillet welds, the fatigue crack initiates at the termination of the weld and propagates as a part-through crack (Fig. 8), until it penetrates the opposite surface of the tension flange. The crack then continues to propagate first as a through-thickness

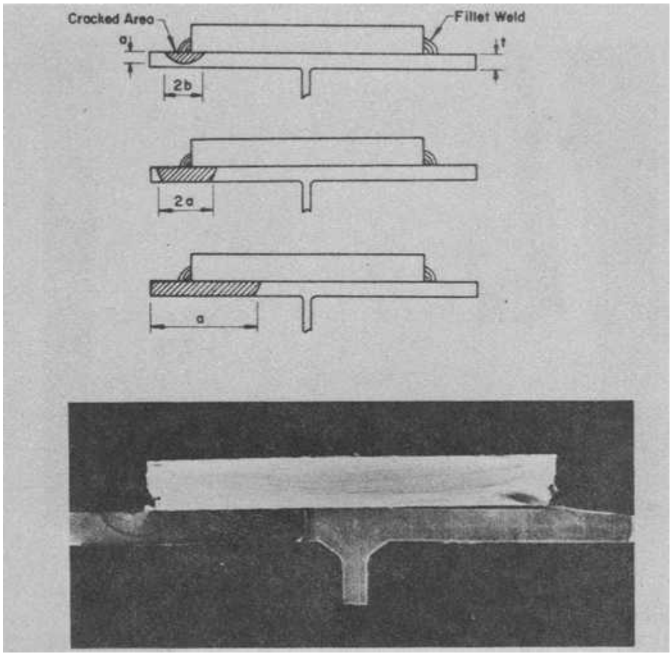

FIG. 8—*Stages of crack propagation at the end of longitudinally welded cover-plate detail.*

crack and then as an edge crack. For the cover plate with transverse fillet welds (Fig. 7*b*) multiple fatigue cracks initiate at the toe of the weld. These cracks propagate as part-through cracks that continually change in shape as their size increases and as they approach adjacent propagating cracks. Subsequently these cracks link up to form a single part-through crack (Fig. 9). This part-through crack continues to change its shape as it propagates through the thickness of the flange into the web and then penetrates the back surface of the flange to form a three-corner crack. Over 90 percent of the fatigue life is exhausted prior to the crack penetrating the back surface of the flange. Because the rate of fatigue-crack propagation increase exponentially with increased crack length, most of the fatigue life of welded bridge components is expended when the fatigue crack is small. Consequently a significant increase in the fracture toughness would have a secondary effect on the fatigue life of the weldment.

Another pertinent observation is that cracks can initiate in compression flanges as well as in tension flanges of welded girders. Fatigue-crack initiation and propagation in compression flanges occur in regions of tensile residual stresses. These cracks propagate out of the residual tensile-stress field and stop. The magnitude of the tensile residual stresses depends on welding sequence, weldment geometry, and welding process, and can be

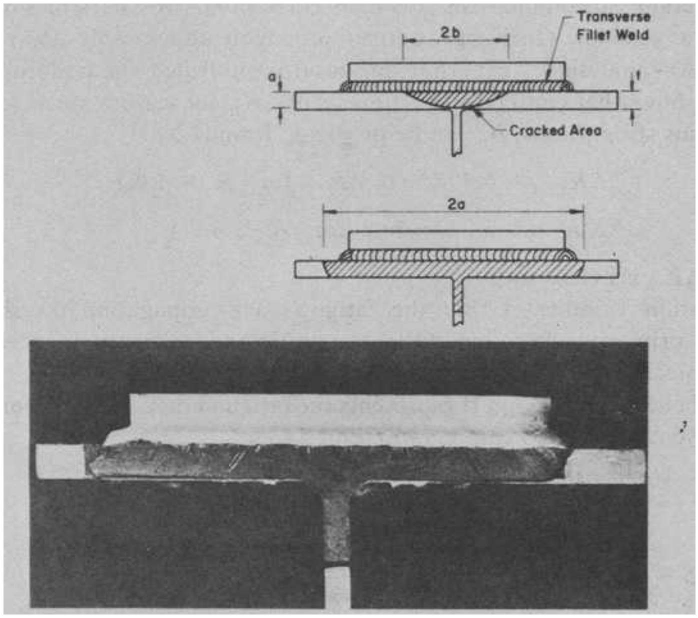

FIG. 9—*Stages of crack propagation at the end of a transverse welded cover-plate detail.*

equal to the yield point of the steel [5]. These residual stresses become redistributed under the influence of cyclic loading [5].

The preceding brief discussion shows that fatigue cracks in welded bridge girders, like other weldments, can (*1*) initiate from small discontinuities that are either embedded or on the surface, (*2*) be located in regions of high stress concentration where the level of stress concentration may vary appreciably in small neighboring locations along the weld toe, and (*3*) reside in regions of high residual stress that become redistributed under cyclic loading. The discontinuities from which fatigue cracks initiate have different characteristics, sizes, and shapes, and in most cases are very difficult and costly to locate and define nondestructively. Moreover, the fatigue crack changes its shape throughout most of its propagation life. The magnitude of the change depends on the shape and location of the fatigue-crack initiating discontinuity, the stress field distribution, and the physical shape of the weld and joint configuration.

Fatigue-Crack Propagation

General Discussion

The fatigue-crack-propagation behavior for metals can be divided into three regions (Fig. 10). The behavior in Region I exhibits a fatigue-crack-propagation threshhold, ΔK_{th}, which corresponds to the stress-intensity-factor range below which cracks do not propagate under cyclic-stress fluctuations. An analysis of experimental results published on nonpropagating cracks shows that conservative estimates of ΔK_{th} for various steels subjected to various stress ratios, R, can be predicted from [12,13]

$$\begin{aligned} \Delta K_{th} &= 6.4(1 - 0.85R) \quad \text{for} \quad R > +0.1 \\ \Delta K_{th} &= 5.5\ \text{ksi}\sqrt{\text{in.}} \quad \text{for} \quad R < +0.1 \end{aligned} \tag{1}$$

where ΔK_{th} is in ksi$\sqrt{\text{in.}}$

Equation 1 indicates that the fatigue-crack-propagation threshold for steels is primarily a function of the stress ratio and is essentially independent of chemical composition or mechanical properties.

The behavior in Region II represents the fatigue-crack-propagation behavior above ΔK_{th}, which can be represented by

$$\frac{da}{dN} = A(\Delta K)^n \tag{2}$$

where

a = crack length,
N = number of cycles,
ΔK = stress-intensity-factor range, and
A and n are constants.

This behavior is discussed further in the following sections.

In Region III the fatigue-crack propagation per cycle is higher than predicted in Region II. Acceleration of fatigue-crack-propagation rates that determines the transition from Region II to Region III appears to be caused by the superposition of ductile-tear or brittle mechanisms onto the mechanism of cyclic subcritical-crack extension, which leaves fatigue striations on the fracture surface [12].

Fatigue-Crack-Propagation Data for Bridge Steels

Extensive fatigue-crack propagation-rate data have been obtained for various constructional steels including ASTM A36, A572, A588, A514, and A517 steels used for bridge applications [12,14,15]. Most of the data are in Region II and show that the primary parameter affecting the rate of propagation is the range of the stress-intensity factor, and that the mechanical and metallurgical properties of the steels have little effect on the fatigue-crack-propagation rate in a room-temperature air environment. The data also show that the stress ratio, mean stress, frequency of cyclic loading, and wave form (sinusoidal, triangular, square, and trapezoidal) have negligible effects on the rate of fatigue-crack propagation in Region II [12]. Moreover, fatigue-

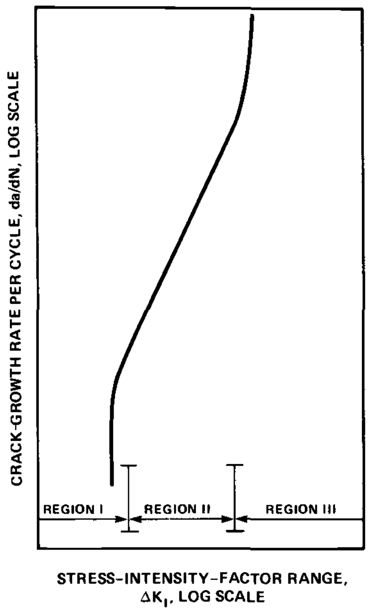

FIG. 10—*Schematic presentation of fatigue-crack propagation in metals.*

crack-propagation rates under variable-amplitude cyclic loadings that simulate actual bridge loadings can be predicted from constant-amplitude cyclic loading by using the root-mean-square (RMS) model [*12,14*].

Fatigue-crack-propagation rates for weld metals and heat-affected zones of constructional steel weldments fabricated in accordance with existing welding specifications (for example, AWS) are equal to or less than the rate of propagation for the base metal [*12,16*]. This behavior can be caused by compressive residual stresses and/or asymmetry of the plastic-zone shape relative to the plane of the crack caused by localized variations in microstructure and mechanical properties of the deposited weld metal.

Extensive corrosion fatigue-crack-propagation data and stress-corrosion-cracking data for bridge steels are available [*14*] and more research is in progress [*17*]. However, a discussion of environmental effects on fatigue behavior of bridge steels and weldments is beyond the scope of this document.

Difficulties in Application of Fracture Mechanics to Fatigue of Welded Steel Bridges

Fracture-mechanics technology has had a significant impact on the ability to design safe and reliable structures. The application of fracture-mechanics concepts has identified and quantified some primary parameters that affect structural integrity. These parameters include material toughness, applied stress, and crack size, shape, orientation, and rate of propagation.

Several investigations have been conducted to establish the fracture toughness, stress-corrosion cracking, and subcritical crack-propagation behavior of bridge steels [*12*]. The results of this research and the application of fracture-mechanics methodology have been used to establish fracture-toughness requirements for bridge steels and to modify the AASHTO fatigue-design specifications for fracture-critical members. Research is under way to determine the threshold stress-intensity-factor range, ΔK_{th}, in room-temperature air and in various environments.

Because fracture-mechanics technology is a relatively new and rapidly developing engineering discipline, some problems remain in its application to engineering structures [*18*]. Therefore, to better predict the fatigue life of welded bridge components by the use of fracture mechanics, further research is necessary (*1*) to characterize nondestructively the size, shape, and orientation of the fatigue-crack initiating discontinuities, (*2*) to establish the initiation and propagation behavior of these discontinuities, and (*3*) to analyze the interaction between the fatigue cracks emanating from them.

Nondestructive Characterization of Initial Discontinuities

The fatigue-crack-propagation life of a component that contains a discontinuity can be estimated best by using fracture-mechanics technology. Accurate prediction of the crack-propagation life requires a knowledge of the rate of propagation under conditions similar to those for the particular application, the stress magnitude and fluctuation, and the size, shape, and orientation of the initial discontinuity and the propagating crack. Because the rate of fatigue-crack propagation increases exponentially with increased crack length, most of the fatigue life is expended when the crack is small. Thus accurate prediction of the characteristics, especially size, of the initial discontinuity is of paramount importance for accurate estimate of the fatigue-crack-propagation life of the component.

Metallographic investigations of welded steel components indicate that the maximum depth of the fatigue-crack-initiating discontinuities at the toe of welds is less than about 0.4 mm (0.016 in.) with an average depth of about 0.075 mm (0.003 in.) (Fig. 11) [*11*]. The maximum radius for embedded discontinuities, such as gas pockets, in fillet welds is about 2 mm (0.08 in.) with an average radius of about 1 mm (0.04 in.). These discontinuities reside in regions of complex geometries that make their detection by nondestructive testing (NDT) very difficult and extremely costly. A survey of the available literature shows that the probability of nondestructive detection and characterization of such small discontinuities is very low, even in demonstration programs which often have simple geometries that can be inspected easily.

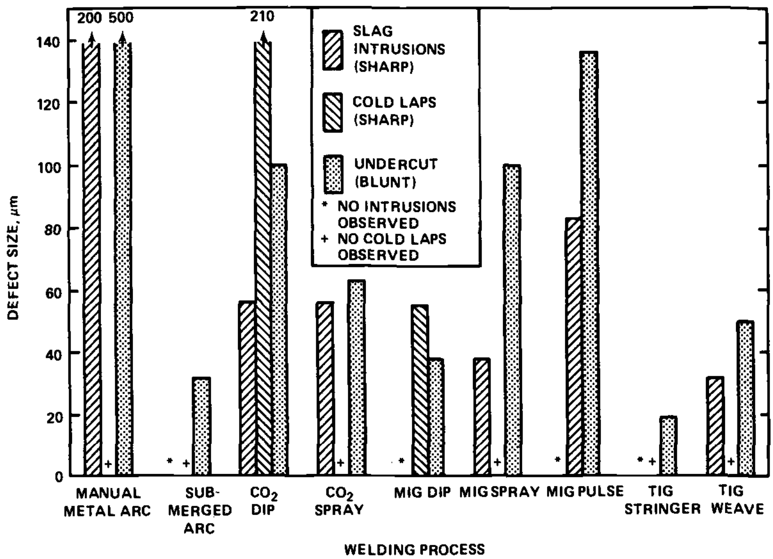

FIG. 11—*Depth of different types of toe discontinuities observed in fillet welds made by various processes.*

The probability of detecting these small discontinuities in complex weldments is extremely low.

One of the assumptions frequently used in the application of fracture-mechanics technology to predict the fatigue life of components is to set the size of the initial discontinuity equal to the largest crack size that can escape detection for the particular nondestructive technique used. Unfortunately the size of the nondetectable crack can be relatively large and depends not only on the nondestructive procedure (Fig. 12) [*18,19*], but also on the operator who uses the instrumentation [*20*]. The use of this assumption can result in overly conservative estimates of the fatigue life of components, and is difficult to justify for building safe and reliable engineering structures that are also economical. Consequently significant progress in the detection, characterization, and prediction of initial discontinuities is required if fracture mechanics concepts are to be used to better predict the fatigue life of complex welded structures (such as bridges, ships, and offshore platforms).

Analysis of Fatigue-Crack-Propagation Behavior for Small Discontinuities

Extensive research has been conducted to predict the fatigue life of various weldments by using linear-elastic fracture-mechanics concepts [*6,7,21-25*]. This effort is based on many assumptions, including the following:

1. Fatigue cracks in welded components initiate from pre-existing discontinuities that behave like pre-existing fatigue cracks. Consequently the fatigue life of a weldment is governed by the rate of fatigue-crack propagation.

2. The stress-intensity factor, K_I, and the stress-intensity-factor range, ΔK_I, for the pre-existing discontinuities can be calculated by using linear-elastic fracture-mechanics concepts.

3. The fatigue-crack-propagation rate for the pre-existing discontinuities is equal to the rate of propagation obtained by testing specimens that satisfy ASTM requirements and can be represented by a power-law relationship (Eq 2).

Fatigue cracks for plain welded beams usually initiate from a gas pocket in the web-to-flange fillet weld. These gas pockets are usually ellipsoidal, with the major axis oriented at about 45 deg to the plane of the web and the plane of the flange (Fig. 5). Fracture-mechanics prediction of the fatigue life for these discontinuities, which is based on the assumption of a pre-existing fatigue crack having the same shape and size as the ellipsoidal discontinuity, results in a conservative fatigue life that could be significantly less than the true fatigue life of the weldment because the analysis eliminates the fatigue-crack-initiation life from the total life.

Fatigue cracks at a weld toe or weld termination initiate from slag intrusions and undercuts. The geometries of these discontinuities are usually more

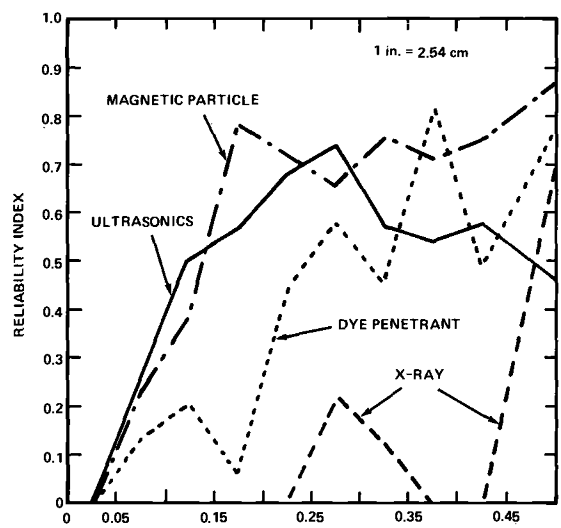

FIG. 12—*Comparison of four NDT techniques on reliability of flaw detection in steel cylinders.*

irregular than those of gas pockets in fillet welds. However, the plane of these discontinuities, especially that for undercuts, is usually curved and on an angle that is less than 45 deg to the direction of the primary stress. Moreover, available data indicate that even for cover-plate details the initiation life is an important part of the total fatigue life [*6*]. Consequently fracture-mechanics calculations of the total fatigue life of welded details, which are based on pre-existing fatigue crack-like discontinuity and neglect the initiation life, can result in conservative predictions for these details.

Clark [*26*] investigated the behavior of small cracks and concluded that linear-elastic fracture-mechanics concepts are directly applicable to small crack-tip plastic zone size, r_p, if the crack length is at least 25 times larger than the associated crack-tip plastic zone size where

$$r_p = \frac{1}{6\pi}\left(\frac{K_I}{\sigma_{ys}}\right)^2$$

The discontinuities with an average size of 0.075 mm (0.003 in.) that may exist at the toe of a weld reside in a residual tensile-stress zone that can be equal to the yield point of the steel. Moreover, based on a maximum design stress of more than one half the yield strength that is used for bridges and with a stress concentration that approaches 4 at the end of a cover plate, it is reasonable to assume that the 0.075 mm (0.003 in.) discontinuity resides in a plastically deformed region where the local stresses are equal to the yield point of the steel. Under these conditions the plastic-zone size, if it can be calculated by using linear-elastic fracture mechanics, is too large to satisfy Clark's observation even for the case of cyclic loading in which the plastic zone may be smaller than under equivalent static loading. Consequently the applicability of linear-elastic fracture mechanics to the small discontinuities observed in welded bridge components is questionable. Further research is needed to establish the limits of applicability of fracture-mechanics technology to small defects and to develop concepts that could be used to analyze their behavior.

Fracture-mechanics analysis of the fatigue-crack-propagation life of welded components is based on the assumption that the rate of propagation for the small weld discontinuities can be represented by Eq 2. The use of Eq 2 implies the applicability of linear-elastic fracture mechanics to small weld discontinuities which, from the preceding discussion, appears to be questionable. Moreover, Eq 2 is based on experimental data obtained by testing fracture-mechanics-type specimens that contain cracks significantly larger than the weld discontinuities under consideration. The applicability of the relationship between the fatigue-crack-propagation rate, da/dN, and the stress-intensity-factor range, ΔK_I, and the correlating constants in Eq 2 must be established for the small discontinuities that are observed in welded bridge components.

Finally, the application of fracture mechanics to predict the fatigue life of welded components is based on a postulation by Maddox [27] that K_I (or ΔK_I) at the toe of a welded joint can be derived from that for the corresponding crack in a flat plate multiplied by a factor M_k, which takes into account the stress-concentration effect of the weld shape and joint configuration. Several finite-element analyses have been made to establish the value of M_k for joints involving transverse non-load-carrying fillet welds and for transverse butt welds [21-24,28]. Unfortunately these results differ significantly. Moreover, the available analyses, which are for weldments having idealized geometries, show that the value of M_k depends on joint configuration, weld geometry, weld toe angle, ratio of crack length, and plate thickness, as well as other parameters that are usually very difficult to establish for welded components in actual structures.

The preceding discussion of the various problems that need to be resolved to better predict the fatigue life of welded bridge components by using fracture-mechanics technology indicates that at the present time the AASHTO fatigue-design curves present an excellent alternative to ensure the structural integrity of welded details subjected to cyclic loadings.

Summary

This paper discusses the characteristics of the discontinuities that are the origins of fatigue cracks in various welded details and presents the AASHTO fatigue-design curves for those details. The paper also presents a summary of the fatigue-crack-propagation data that have been obtained for bridge steels and weldments, and discusses some of the problems that need to be resolved to better predict the fatigue life of welded bridge details by using fracture-mechanics technology. It is suggested that until these problems are rectified the AASHTO fatigue-design curves present an excellent alternative to fracture-mechanics technology to ensure the structural integrity of welded details subjected to cyclic loadings.

Note

It is understood that the material in this paper is intended for general information only and should not be used in relation to any specific application without independent examination and verification of its applicability and suitability by professionally qualified personnel. Those making use thereof or relying thereon assume all risk and liability arising from such use or reliance.

References

[1] *Specifications for Welded Highway and Railway Bridges*, American Welding Society, 1941.
[2] Fisher, J. W. and Viest, I. M. "Fatigue Life of Bridge Beams Subjected to Controlled

Truck Traffic," preliminary publication, 7th Congress, International Association for Bridge and Structural Engineering, 1964.
[3] *Standard Specifications for Highway Bridges,* American Association of State Highway and Transportation Officials, 1977.
[4] Fisher, J. W., *Bridge Fatigue Guide—Design and Details,* American Institute of Steel Construction, 1977.
[5] Fisher, J. W. et al, "Effect of Weldments on the Fatigue Strength of Steel Beams," NCHRP Report 102, National Cooperative Highway Research Program, Transportation Research Board, 1970.
[6] Shilling, C. G. et al, "Fatigue of Welded Steel Bridge Members Under Variable-Amplitude Loadings," NCHRP Report 188, Transportation Research Board, 1978.
[7] Fisher, J. W. et al, "Fatigue Strength of Steel Beams with Transverse Stiffness and Attachments", NCHRP Report 147, National Cooperative Highway Research Program, Transportation Research Board, 1974.
[8] Bower, D. G., "Loading History—Span No. 10, Yellow Mill Pond Bridge I-95, Bridgeport, Conn.," Highway Research Record 428, Transportation Research Board, 1973.
[9] Slockbower, R. E. and Fisher, J. W., "Fatigue Resistance of Full Scale Cover-Plated Beams," Fritz Engineering Laboratory Report No. 386-9(78), Lehigh University, June 1978.
[10] Signes, E. G. et al, "Factors Affecting the Fatigue Strength of Welded High Strength Steels," *British Welding Journal,* Vol. 14, No. 3, 1967.
[11] Watkinson, F. et al, "The Fatigue Strength of Welded Joints in High Strength Steels and Methods for its Improvement," in *Proceedings: Conference on Fatigue of Welded Structures,* The Welding Institute, Brighton, England, July 1970.
[12] Rolfe, S. T. and Barsom, J. M., *Fracture and Fatigue Control in Structures.* Prentice-Hall, Inc., Englewood Cliffs, N.J., 1977.
[13] Garwood, S. J., "Fatigue Crack Growth Threshold Determination—A Simple Estimation Technique," *Research Bulletin of the Welding Institute,* Vol. 20, No. 9, September 1979.
[14] Barsom, J. M. and Novak, S. R., "Subscritical Crack Growth and Fracture of Bridge Steels," NCHRP Report 181, National Cooperative Highway Research Program, Transportation Research Board, 1977.
[15] Hertzberg R. W. and Nordberg, H., "Fatigue Crack Propagation in A514 Steel," Fritz Engineering Laboratory Report No. 358.7, Lehigh University, 1969.
[16] Maddox, S. J., "Assessing the Significance of Flaws in Welds Subjected to Fatigue," *Welding Journal,* Vol. 53, No. 9, September 1974.
[17] "Corrosion Fatigue Characteristics of Bridge Steels," DOT Project FH-11-9448, Department of Transportation, 1979.
[18] Clark, W. G., Jr., "Some Problems in the Application of Fracture Mechanics," Scientific Paper 79-1D3-SRIDS-P1. Westinghouse Research and Development Center, 1979.
[19] Packman, P. F. et al, "The Applicability of a Fracture Mechanics Nondestructive Testing Design Criterion," U.S. Air Force Report AFML-TR-68-32, May 1968.
[20] Lewis, W. H. et al, "Quantitative Measurement of the Reliability of Nondestructive Inspection on Aircraft Structures," *Prevention of Structural Failures,* American Society for Metals, 1978.
[21] Gurney, T. R., "Theoretical Analysis of the Influence of Toe Defects on the Fatigue Strength of Fillet Welded Joints," Report No. 32/1977/E, The Welding Institute, Abington, England, March 1977.
[22] Gurney, T. R. and Johnston, G. O., "A Revised Analysis on the Influence of Toe Defects on the Fatigue Strength of Transverse Non-Load-Carrying Fillet Welds," Report No. 62/1978/E, The Welding Institute, Abington, England, April 1978.
[23] Gurney, T. R., "Theoretical Analysis of the Invluence of Attachment Size on the Fatigue Strength of Transverse Non-Load-Carrying Fillet Welds," Report No. 91/1979, The Welding Institute, Abington, England, May 1979.
[24] Frank, K. H., "The Fatigue Strength of Fillet Welded Connections," Ph.D. thesis, Lehigh University, 1971.
[25] Fisher, J. W. et al, "Minimizing Fatigue and Fracture in Steel Bridges," *Structural Integrity Technology,* American Society of Mechanical Engineers, 1979.
[26] Clark, W. G., Jr., in *Cracks and Fracture, ASTM STP 601,* American Society for Testing and Materials, 1976, pp. 138–153.

[27] Maddox, S. J., "An Analysis of Fatigue Cracks in Fillet Welded Joints," Research No. E/49/72, The Welding Institute, Abington, England, 1972.

[28] Gurney, T. R., "Stress Intensity Factors for Cracks at the Toes of Transverse Butt Welds," Report No. 88/1979, The Welding Institute, Abington, England, 1979.

Appendixes

APPENDIX I

Designation: E 647 - 78 T

Tentative Test Method for CONSTANT-LOAD-AMPLITUDE FATIGUE CRACK GROWTH RATES ABOVE 10^{-8} m/CYCLE[1]

This tentative method has been approved by the sponsoring committee and accepted by the Society in accordance with established procedures, for use pending adoption as standard. Suggestions for revisions should be addressed to the Society at 1916 Race St., Philadelphia, Pa. 19103.

1. Scope

1.1 This method[2] covers the determination of constant-load-amplitude fatigue crack growth rate above 10^{-8} m/cycle, using either compact type (CT) or center-cracked-tension (CCT) specimens.[3] Results are expressed in terms of the crack-tip stress intensity range, defined by the theory of linear elasticity.

1.2 Materials that can be tested by this method are not limited by thicknesses or by strength so long as specimens are of sufficient thickness to preclude buckling and of sufficient planar size to remain predominantly elastic during testing.

1.3 A range of specimen sizes with proportional planar dimensions is provided, but size is variable to be adjusted for yield strength and applied load. Specimen thickness may be varied independent of planar size.

1.4 Specimen configurations other than those contained in this method may be used provided that well-established stress intensity calibrations are available and that specimens are of sufficient size to remain predominantly elastic during testing.

2. Applicable Documents

2.1 *ASTM Standards:*

E 4 Load Verification of Testing Machines[4]

E 8 Tension Testing of Metallic Materials[5]

E 337 Test for Relative Humidity by Wet- and Dry-Bulb Psychrometer[6]

E 338 Sharp-Notch Tension Testing of High-Strength Sheet Materials[7]

E 399 Test for Plane-Strain Fracture Toughness of Metallic Materials[7]

E 467 Recommended Practice for Verification of Constant Amplitude Dynamic Loads in an Axial Load Fatigue Testing Machine[7]

E 561 Recommended Practice for *R*-Curve Determination[7]

3. Summary of Method

3.1 The method involves constant-load-amplitude cyclic loading of notched specimens that have been acceptably precracked in fatigue. Crack length is measured, either visually or by an equivalent method, as a function of elapsed cycles and these data are subjected to numerical analysis to establish the rate of crack growth. Crack growth rates are expressed as a function of the stress intensity factor range, ΔK, which is calculated from expressions based on linear elastic stress analysis.

4. Significance

4.1 Fatigue crack growth rate expressed as a function of crack-tip stress intensity range,

---

[1] This method is under the jurisdiction of ASTM Committee E-24 on Fracture Testing, and is the direct responsibility of Subcommittee E24.04 on Subcritical Crack Growth.

Current edition approved March 31, 1978. Published May 1978.

[2] For additional information on this method, see RR: E 24 - 1001. Available from ASTM Headquarters, 1916 Race St., Philadelphia, Pa. 19103.

[3] Determination of fatigue crack growth rates below 10^{-8} m/cycle requires specialized testing considerations. Test procedures for this growth rate regime are being formulated within by ASTM Subcommittee E24.04 on Subcritical Crack Growth.

[4] *Annual Book of ASTM Standards*, Parts 10, 14, 32, 35, and 41.

[5] *Annual Book of ASTM Standards*, Parts 6, 7, and 10.

[6] *Annual Book of ASTM Standards*, Parts 20, 26, 32, and 41.

[7] *Annual Book of ASTM Standards*, Part 10.

da/dN versus ΔK, characterizes a material's resistance to stable crack extension under cyclic loading. Background information on the rationale for employing linear elastic fracture mechanics to analyze fatigue crack growth rate data is given in Refs **(1)** and **(2)**.[8]

4.1.1 In innocuous (inert) environments, constant-amplitude fatigue crack growth rates above 10^{-8} m/cycle are primarily a function of ΔK and the load ratio, R, or K_{max} and R (Note 1). Temperature and aggressive environments can significantly affect da/dN versus ΔK, and in many cases accentuate R-effects and also introduce effects of other loading variables, such as cyclic frequency and waveform. Attention needs to be given to the proper selection and control of these variables in research studies and in the generation of design data.

NOTE 1—ΔK, K_{max}, and R are not independent of each other. Specification of any two of these variables is sufficient to define the loading condition. It is customary to specify one of the stress intensity parameters (ΔK or K_{max}) along with the load ratio, R.

4.1.2 Expressing da/dN as a function of ΔK provides results that are independent of planar geometry, thus enabling the exchange and comparison of data obtained from a variety of specimen configurations and loading conditions. Moreover, this feature enables da/dN versus ΔK data to be utilized in the design and evaluation of engineering structures.

4.1.3 Fatigue crack growth rate data are not always geometry-independent in the strict sense since thickness effects sometimes occur. However, data on the influence of thickness on fatigue crack growth rate is mixed. Fatigue crack growth rates over a wide range of ΔK have been reported to either increase, decrease, or remain unaffected as specimen thickness is increased. Thickness effects can also interact with other variables such as environment and heat treatment. In addition, materials may exhibit thickness effects only over the terminal range of da/dN versus ΔK, which is associated with either nominal yielding (Note 2) or a K_{max}-controlled instability. The potential influence of specimen thickness should be considered when generating data for research or design.

NOTE 2—This condition will be avoided in tests that confrom to the specimen size requirements of 7.2.

4.2 This method can serve the following purposes:

4.2.1 To establish the influence of fatigue crack growth on the life of components subjected to cyclic loading, provided data are generated under representative conditions and combined with appropriate fracture toughness data (for example, see Method E 399), defect characterization data, and stress analysis information (for example, see Refs **(3)** and **(4)**).

NOTE 3—Fatigue crack growth can be significantly influenced by load history. During variable amplitude loading, crack growth rates can be either enhanced or retarded (relative to steady-state, constant-amplitude growth rates at a given ΔK) depending on the specific loading sequence. This complicating factor needs to be considered in using constant-amplitude growth rate data to analyze variable amplitude fatigue problems (for example, see Ref **(5)**).

4.2.2 To establish material selection criteria and nondestructive inspection requirements for quality assurance.

4.2.3 To establish, in quantitative terms, the individual and combined effects of metallurgical, fabrication, environmental, and loading variables on fatigue crack growth.

5. Definitions

5.1 *crack length, a* [L]—in fatigue, the physical crack size used to determine the crack growth rate and the stress-intensity factor. For the CT specimen, a is measured from the line connecting the bearing points of load application, for the CCT specimen, a is measured from the perpendicular bisector of the central crack.

5.2 *cycle—in fatigue*, one complete sequence of values of applied load that is repeated periodically in fatigue. The symbol N represents the number of cycles.

5.2.1 *maximum load, P_{max}* [F]—*in fatigue*, the greatest algebraic value of applied load in a fatigue cycle. Tensile loads are considered positive and compressive loads negative.

5.2.2 *minimum load, P_{min}* [F]—*in fatigue*, the least algebraic value of applied load in a fatigue cycle.

5.2.3 *load range, ΔP* [F]—*in fatigue*, the algebraic difference between the maximum and minimum loads in a fatigue cycle.

5.2.4 *load ratio* (also called *stress ratio*), *R*—

[8] The boldface numbers in parentheses refer to the list of references appended to this method.

E 647

in fatigue, the algebraic ratio of the minimum to maximum load in a fatigue cycle, that is, $R = P_{min}/P_{max}$.

5.3 *fatigue crack growth rate*, da/dN, [L]—the rate of crack extension caused by constant-amplitude fatigue loading, expressed in terms of crack extension per cycle of fatigue.

5.4 *stress-intensity calibration, K calibration*—a mathematical expression, based on pirical or analytical results, that relates the stress intensity factor to load and crack length for a specific specimen planar geometry.

5.5 *stress-intensity factor, K* $[FL^{-3/2}]$—the magnitude of the ideal crack-tip stress field in a linear-elastic body. In this method, mode I is assumed. Mode I corresponds to loading such that the crack surfaces are displaced apart, normal to the crack plane.

5.5.1 *maximun stress-intensity factor*, K_{max} $[FL^{-3/2}]$—the maximum value of the stress-intensity factor in a fatigue cycle. This value corresponds to P_{max}.

5.5.2 *minimum stress-intensity factor*, K_{min} $[FL^{-3/2}]$—*in fatigue*, the minimum value of the stress-intensity factor in a cycle. This value corresponds to P_{min} when $R > 0$ and is taken to be zero when $R \leq 0$.

5.6 *stress-intensity factor range*, ΔK $[FL^{-3/2}]$—*in fatigue*, the variation in the stress-intensity factor in a cycle, that is, $K_{max} - K_{min}$.

NOTE 4—The loading variables R, ΔK, and K_{max} are related such that specifying any two uniquely defines the third according to the following relationship: $\Delta K = (1 - R)K_{max}$ for $R \geq 0$ and $\Delta K = K_{max}$ for $R \leq 0$.

NOTE 5—These operational stress-intensity factor definitions do not include local crack-tip effects; for example, crack closure, residual stress, and blunting.

6. Apparatus

6.1 *Grips and Fixtures for CT Specimen*—A clevis and pin assembly (Fig. 3) is used at both the top and bottom of the specimen to allow in-plane rotation as the specimen is loaded. This specimen and loading arrangement is to be used for tension-tension loading only.

6.1.1 Suggested proportions and critical tolerances of the clevis and pin are given (Fig. 3) in terms of either the specimen width, W, or the specimen thickness, B, since these dimensions may be varied independently within certain limits.

6.1.2 The pin-to-hole clearances are designed to minimize friction, thereby eliminating unacceptable end-movements that would invalidate the specimen K-calibration provided herein. The use of a lubricant (for example, MoS_2) on the loading pins is also recommended to minimize friction.

6.1.3 Using a 1000-MPa (~ 150 ksi) yield-strength alloy (for example, AISI 4340 steel) for the clevis and pins provides adequate strength and resistance to galling and fatigue.

6.2 *Grips and Fixtures for CCT Specimens*—The type of grips and fixtures to be used with the CCT specimens will depend on the specimen width, W (defined in Fig. 2), and the loading conditions (that is, either tension-tension or tension-compression loading). The minimum required specimen gage length varies with the type of gripping and is specified so that a uniform stress distribution is developed in the specimen gage length during testing. For testing of thin sheets, constraining plates may be necessary to minimize specimen buckling (see Recommended Practice E 561 for recommendations on buckling constraints).

6.2.1 For tension-tension loading of specimens with $W \leq 75$ mm (3 in.), a clevis and single pin arrangement is suitable for gripping provided that the specimen gage length (that is, the distance between loading pins) is at least $2W$ (Fig. 2). For this arrangement it is also helpful to either use brass shims between the pin and specimen or to lubricate the pin to prevent fretting-fatigue cracks from initiating at the specimen loading hole. Additional measures that may be taken to prevent cracking at the pinhole include attaching reinforcement plates to the specimen (for example, see Method E 338) or employing a "dog-bone" type specimen design. In either case, the gage length shall be defined as the uniform section and shall be at least $1.7W$.

6.2.2 For tension-tension loading of specimens with $W \geq 75$ mm (3 in.), a clevis with multiple bolts is recommended (for example, see Recommended Practice E 561). In this arrangement, the loads are applied more uniformly; thus, the minimum specimen gage length (that is, the distance between the innermost rows of bolt holes) is relaxed to $1.5W$.

6.2.3 The CCT specimen may also be gripped using a clamping device instead of the above arrangements. This type of gripping is necessary for tension-compression loading. An example of a specific bolt and keyway design for clamping CCT specimens is given in Fig. 4. In addition, various hydraulic and mechanical-wedge systems that supply adequate clamping forces are commercially available and may be used. The minimum gage length requirement for clamped specimens is relaxed to $1.2W$.

6.3 *Alignment of Grips*—It is important that attention be given to achieving good alignment in the load train through careful machining of all gripping fixtures. For tension-tension loading, pin or gimbal connections between the grips and the load frame are recommended to achieve loading symmetry. For tension-compression loading, the length of the load train (including the hydraulic actuator) should be minimized and rigid, non-rotating joints should be employed to reduce lateral motion in the load train.

7. Specimen Configuration, Size, and Preparation

7.1 *Standard Specimens*—The geometry of standard CT and CCT specimens is given in Figs. 1 and 2, respectively. The specific geometry of CCT specimens depends on the method of gripping as specified in 6.2. Notch and precracking details for both specimens are given in Fig. 5. The CT specimen is not recommended for tension-compression testing because of uncertainties introduced into the K-calibration.

7.1.1 It is required that the machined notch, a_n, in the CT specimen be at least $0.2W$ in length so that the K-calibration is not influenced by small variations in the location and dimensions of the loading-pin holes.

7.1.2 The machined notch, $2a_n$, in the CCT specimen shall be centered with respect to the specimen centerline to within $\pm 0.001W$. The length of the machine notch in the CCT specimen will be determined by practical machining considerations and is not restricted by limitations in the K-calibration.

NOTE 6—It is recommended that $2a_n$ be at least $0.2W$ when using the compliance method to monitor crack extension in the CCT specimen so that accurate crack length determinations can be obtained.

7.1.3 For both specimens, the thickness, B, and width, W, may be varied independently within the following limits, which are based on specimen buckling and through-thickness-crack-curvature considerations:

7.1.3.1 For CT specimens it is recommended that thickness be within the range $W/20 \leq B \leq W/4$. Specimens having thicknesses up to and including $W/2$ may also be employed; however, data from these specimens will often require through-thickness crack-curvature corrections (9.1). In addition, difficulties may be encountered in meeting the through-thickness crack straightness requirements of 8.3.2 and 8.6.4.

7.1.3.2 Using the above rationale, the recommended upper limit on thickness in CCT specimens is $W/8$, although $W/4$ may also be employed. The minimum thickness necessary to avoid excessive lateral deflections or buckling in CCT specimens is sensitive to specimen gage length, grip alignment, and load ratio, R. It is recommended that strain gage information be obtained for the particular specimen geometry and loading condition of interest and that bending strains not exceed 5 % of the nominal strain.

7.2 *Specimen Size*—In order for results to be valid according to this method, it is required that the specimen be predominantly elastic at all values of applied load. The minimum in-plane specimen sizes to meet this requirement are based primarily on empirical results and are specific to specimen configuration **(6)**.

7.2.1 For the CT specimen it is required that the uncracked ligament, $W - a$, be equal to or greater than $(4/\pi)(K_{max}/\sigma_{YS})^2$, where σ_{YS} is the 0.2 % offset yield strength of the test material (measured by Methods E 8) at the temperature for which fatigue crack growth rate data are to be obtained.

7.2.2 For the CCT specimen it is required that the nominal stress in the uncracked ligament, given by the following:

$$\sigma_N = \frac{P_{max}}{BW\left(1 - \frac{2a}{W}\right)}$$

be less than σ_{YS}.

NOTE 7—The above criteria are likely to be restrictive, that is, they may require overly large specimen sizes for materials that exhibit a high degree of strain hardening (for example, annealed low-alloy ferritic steels, annealed austenitic stainless

E 647

steels, etc.). Currently, there are insufficient data on these materials to formulate easily calculable size requirements that are analogous to those given above. However, data from specimens smaller than those allowed by 7.2 may be validated by demonstrating that da/dN versus ΔK results are equivalent to results from larger specimens that meet the requirements of 7.2. Supplementary information on the extent of plastic deformation encountered in any given test specimen can be obtained by measuring specimen deflections as described in Appendix X2.

7.2.3 Figure 6 gives the limiting K_{max} values, designated K_{maxL}, which are defined by the above specimen size criteria. This information is expressed in dimensionless form so that the curves can be used to calculate either: (*1*) the value of K_{maxL} for a given combination of specimen size, W, and material yield strength, σ_{YS}, or (*2*) the minimum specimen size required to obtain valid data up to a desired K_{max} value for a given material strength level. (However, it should be noted that the desired K_{max} value cannot be achieved if it is greater than the K value for unstable fracture.) All values of $K_{max}/(\sigma_{YS}\sqrt{W})$ that fall below the respective curves for the two specimens satisfy the specimen size requirements of this method.

7.3 *Notch Preparaton*—The machined notch for either of the standard specimens may be made by electrical-discharge machining (EDM), milling, broaching, or sawcutting. The following notch preparation procedures are suggested to facilitate fatigue precracking in various materials:

7.3.1 *EDM*—ρ < 0.010 in. (ρ = notch root radius), high-strength steels ($\sigma_{ys} \geq 170$ ksi), titanium and aluminum alloys.

7.3.2 *Mill or Broach*—$\rho \leq 0.003$ in., low or medium-strength steels ($\sigma_{ys} \leq 170$ ksi), aluminum alloys.

7.3.3 *Grind*—$\rho \leq 0.010$ in., low or medium-strength steels.

7.3.4 *Mill or Broach*—$\rho \leq 0.010$ in., aluminum alloys.

7.3.5 *Sawcut*—Aluminum alloys.

7.3.6 Examples of various machined-notch geometries and associated precracking requirements are given in Fig. 5 (see 8.3).

8. Procedure

8.1 *Number of Tests*—Variability in da/dN data at a given ΔK may vary by a factor of 2 (**7**). It is a good practice to conduct replicate tests; when this is impractical, tests should be planned such that regions of overlapping da/dN versus ΔK data are obtained. Since confidence in inferences drawn from the data increases with the number of tests, the desired number of tests will depend on the end use of the data.

8.2 *Specimen Measurements*—The specimen dimensions shall be within the tolerances given in Figs. 1 and 2.

8.3 *Fatigue Precracking*—Conduct fatigue precracking with the specimen fully heat treated to the condition in which it is to be tested. The precracking equipment shall be such that the load distribution is symmetrical with respect to the machine notch and K_{max} during precracking is controlled to within ± 5 %. Any convenient loading frequency that enables the required load accuracy to be achieved can be used for precracking. The machined notch plus the precrack must lie within the envelope, shown in Fig. 5, that has as its apex the end of the fatigue precrack. In addition, the fatigue precrack shall be not less than $0.1B$ or h, whichever is greater (Fig. 5).

8.3.1 The final K_{max} during precracking shall not exceed the initial K_{max} for which test data are to be obtained. If necessary, loads corresponding to higher K_{max} values may be used to initiate cracking at the machined notch. In this event, the load range shall be stepped-down to meet the above requirement. Furthermore, it is suggested that the reduction in P_{max} for any of these steps be no greater than 20 % and that measurable crack extension occur before proceeding to the next step. To avert transient effects in the test data, apply the load range in each step over a crack length increment of at least $(3/\pi)(K'_{max}/\sigma_{YS})^2$, where K'_{max} is the terminal value of K_{max} from the previous load-step. If P_{min}/P_{max} during precracking differs from that used during testing, see the precautions described in 8.5.1.

8.3.2 Measure the fatigue precrack length from the tip of the machined notch to the crack tip on the front and back surfaces of the specimen to within 0.10 mm (0.004 in.) or $0.002W$, whichever is greater. Measure both cracks, front and back, in the CCT specimens. If any two crack length measurements vary by more than $0.025W$ or by more than $0.25B$, whichever is less, the precracking operation is not suitable and subsequent testing would be invalid under this method. If a fatigue crack departs more than ± 5 deg from the plane of symmetry the specimen is not suitable for subsequent testing. In either case, check for potential problems in alignment of the loading system or details of the machined notch, or both, before continuing to precrack to satisfy the above requirements.

8.4 *Test Equipment*—The equipment for fatigue testing shall be such that the load distribution is symmetrical to the specimen notch.

8.4.1 Verify the load cell in the test machine in accordance with Method E 4 and Recommended Practice E 467. Conduct testing such that ΔP and P_{max} are controlled to within ± 2 % throughout the test.

8.4.2 An accurate digital device is required for counting elapsed cycles. A timer is a desirable supplement to the counter and provides a check on the counter. Multiplication factors (for example, ×10 or ×100) should not be used on counting devices when obtaining data at growth rates above 10^{-5} m/cycle since they can introduce significant errors in the growth rate determination.

8.5 *General Test Procedure*—It is preferred that each specimen be tested at a constant ΔP and a fixed set of loading variables. However, this may not be feasible when it is necessary to generate a wide range of information with a limited number of specimens. When loading variables are changed during a test, potential problems arise from several types of transient phenomenon. The following test procedures should be followed to minimize or eliminate transient effects.

8.5.1 If load range is to be incrementally varied it should be done such that P_{max} is increased rather than decreased to preclude retardation of growth rates caused by overload effects; retardation being a more pronounced effect than accelerated crack growth associated with incremental increase in P_{max}. Transient growth rates are also known to result from changes in P_{min} or R. Sufficient crack extension should be allowed following changes in load to enable the growth rate to establish a steady-state value. The amount of crack growth that is required depends on the magnitude of load change and on the material.

8.5.2 When environmental effects are present, changes in load level, test frequency, or waveform can result in transient growth rates. Sufficient crack extension should be allowed between changes in these loading variables to enable the growth rate to achieve a steady-state value.

8.5.3 Transient growth rates can also occur, in the absence of loading variable changes, due to long-duration test interruptions, for example, during work stoppages. In this case, data should be discarded if the growth rates following an interruption are less than those before the interruption.

8.6 *Measurement of Crack Length*—Make fatigue crack length measurements as a function of elapsed cycles by means of a visual, or equivalent, technique capable of resolving crack extensions of 0.10 mm (0.004 in.), or $0.002W$, whichever is greater. For visual measurements, polishing the test area of the specimen and using indirect lighting aid in the resolution of the crack tip. It is recommended that, prior to testing, reference marks be applied to the test specimen at predetermined locations along the direction of cracking. Crack length can then be measured using a low power (20 to 50×) traveling microscope. Using the reference marks eliminates potential errors due to accidental movement of the traveling microscope. If precision photographic grids or polyester scales are attached to the specimen, crack length can be determined directly with any magnifying device that gives the required resolution. It is preferred that measurements be made without interrupting the test.

8.6.1 When tests are interrupted to make crack length measurements, the interruption time should be minimized (for example, less than 10 min) since transient growth rates can result from interruptions of long duration. A static load not exceeding the maximum load applied during the fatigue test, may be applied during measurement interruptions in order to enhance the resolution of the crack-tip provided that it does not cause static-load crack extension or creep deformation.

8.6.2 Make crack length measurements at intervals such that da/dN data are nearly evenly distributed with respect to ΔK. The following measurement intervals are recommended according to specimen type:

8.6.2.1 *CT Specimen:*

$$\Delta a \leq 0.02W \text{ for } 0.25 \leq a/W \leq 0.60$$
$$\Delta a \leq 0.01W \text{ for } a/W \geq 0.60$$

8.6.2.2 *CCT Specimen:*

$$\Delta a \leq 0.03W \text{ for } 2a/W < 0.60$$
$$\Delta a \leq 0.02W \text{ for } 2a/W > 0.60$$

8.6.2.3 In any case, the minimum Δa shall be 0.25 mm (0.01 in.) or ten times the crack length measurement precision, whichever is greater.

NOTE 8—The crack length measurement precision is herein defined as the standard deviation on the mean value of crack length determined for a set of replicate measurements.

8.6.3 If crack length is monitored visually the following procedure applies. For specimens with $B/W \leq 0.15$, the crack length measurements need only be made on one side of the specimen. For specimens with $B/W \geq 0.15$, make measurements on both the front and back sides of the specimen and use the average value of these measurements (two values for the CT specimen; four values for the CCT specimen) in subsequent calculations.

8.6.4 If at any point in the test the average through-thickness fatigue crack departs more than ± 5 deg from the plane of symmetry of the specimen, the data are invalid according to the method. In addition, data are invalid where any two crack lengths at a given number of cycles differ by more than $0.025W$ or $0.25B$, whichever is less.

9. Calculations and Interpretation of Results

9.1 *Crack Curvature Correction*—After completion of testing, examine the fracture surfaces, preferably at two locations (for example, at the precrack and terminal fatigue crack lengths), to determine the extent of through-thickness crack curvature (commonly termed "crack tunneling"). If a crack contour is visible, calculate a five point, through-thickness average crack length in accordance with paragraph 8.2.3 of Method E 399. The difference between the average through-thickness crack length and the corresponding crack length recorded during the test (for example, if visual measurements were obtained this might be the average of the surface crack length measurements) is the crack curvature correction.

9.1.1 If the crack curvature correction results in a greater than 5 % difference in calculated stress intensity factor at any crack length, then employ this correction when analyzing the recorded test data.

9.1.2 If the magnitude of the crack curvature correction either increases or decreases with crack length, use a linear interpolation to correct intermediate data points. Determine this linear correction from two distinct crack contours separated by a minimum spacing of $0.25W$ or B, whichever is greater. When there is no systematic variation of crack curvature with crack length, employ a uniform correction determined from an average of the crack contour measurements.

9.1.3 When employing a crack length monitoring technique other than visual, a crack curvature correction is generally incorporated in the calibration of the technique. However, since the magnitude of the correction will probably depend on specimen thickness, the above correction procedures may also be necessary.

9.2 *Determination of Crack Growth Rate*—Determine the rate of fatigue crack growth from the crack length versus elapsed cycles data (a versus N). Recommended methods are provided in Appendix X1.

NOTE 9—Both recommended methods for processing a versus N data are known to give the same average da/dN response. However, the secant method often results in increased scatter in da/dN relative to the incremental polynomial method, since the latter numerically "smooths" the data **(7, 8)**. This apparent difference in variability introduced by the two methods needs to be considered, especially in utilizing da/dN versus ΔK data in design.

9.3 *Determination of Stress Intensity Range, ΔK*—Use the crack length values of 9.1 and Appendix X1 to calculate the stress intensity range corresponding to a given crack growth rate from the following expressions:

9.3.1 For the CT specimen calculate ΔK as follows:

$$\Delta K = \frac{\Delta P}{B\sqrt{W}}\frac{(2+\alpha)}{(1-\alpha)^{3/2}}(0.886 + 4.64\alpha - 13.32\alpha^2 + 14.72\alpha^3 - 5.6\alpha^4)$$

where $\alpha = a/W$; expression valid for $a/W \geq 0.2$ **(9, 10)**.

9.3.2 For the CCT specimen calculate ΔK consistent with the definitions of 5.5; that is:

$$\Delta P = P_{max} - P_{min} \quad \text{for} \quad R > 0$$
$$\Delta P = P_{max} \quad \text{for} \quad R \leq 0$$

in the following expression **(11)**:

$$\Delta K = \frac{\Delta P}{B}\sqrt{\frac{\pi\alpha}{2W}\sec\frac{\pi\alpha}{2}}$$

where $\alpha = 2a/W$; expression valid for $2a/W < 0.95$.

NOTE 10—Implicit in the above expressions are the assumptions that the test material is linear-elastic, isotropic, and homogeneous.

9.3.3 Check for violation of the specimen size requirement by calculating K_{maxL} (see 7.2 and Fig. 6). Data are considered invalid according to this method when $K_{max} > K_{maxL}$.

10. Report

10.1 The report shall include the following information:

10.1.1 Specimen type, including thickness, B, and width, W. Figures of the specific CCT specimen design and grips used, and a figure if a specimen type not described in this method is used shall be provided.

10.1.2 Description of the test machine and equipment used to measure crack length and the precision with which crack length measurements were made.

10.1.3 Test material characterization in terms of heat treatment, chemical composition, and mechanical properties (include at least the 0.2 % offset yield strength and either elongation or reduction in area measured in accordance with Methods E 8). Product size and form (for example, sheet, plate, forging, etc.) shall also be identified.

10.1.4 The crack plane orientation according to the code given in Method E 399. In addition, if the specimen is removed from a large product form, its location with respect to the parent product shall be given.

10.1.5 The terminal values of ΔK, R, and crack length from fatigue precracking. If precrack loads were stepped-down, the procedure employed shall be stated and the amount of crack extension at the final load level shall be given.

10.1.6 Test loading variables, including ΔP, R, cyclic frequency, and cyclic waveform.

10.1.7 Environmental variables, including temperature, chemical composition, pH (for liquids), and pressure (for gases and vacuum). For tests in air, the relative humidity as determined by Method E 337 shall be reported. For tests in "inert" reference environments, such as dry argon, estimates of residual levels of water and oxygen in the test environment (generally this differs from the analysis of residual impurities in the gas supply cylinder) shall be given. Nominal values for all of the above environmental variables, as well as maximum deviations throughout the duration of testing, shall be reported. Also, the material employed in the chamber used to contain the environment and steps taken to eliminate chemical/electrochemical reactions between the specimen-environment system and the chamber shall be described.

10.1.8 Analysis methods applied to the data, including the technique used to convert a versus N to da/dN, specific procedure used to correct for crack curvature, and magnitude of crack curvature correction.

10.1.9 The specimen K-calibration and size criterion to ensure predominantly elastic behavior (for specimens not described in this method).

10.1.10 da/dN as a function of ΔK shall be plotted. (It is recommended that the independent variable, ΔK, be plotted on the abscissa and the dependent variable, da/dN, on the ordinate. Log-log coordinates are commonly used. For optimum data comparisons, the size of the ΔK-log cycles should be two to three times larger than da/dN-log cycles.) All data that violate the size requirements of 7.2 and Appendix X2 shall be identified.

10.1.11 Description of any occurrences that appear to be related to anomalous data (for example, transients following test interruptions or changes in loading variables).

10.1.12 It is desirable, but not required, to tabulate test results. When using this method of presentation, the following information shall be tabulated for each test: a, N, ΔK, da/dN, and, where applicable, the test variables of 10.1.3, 10.1.6, and 10.1.7. Also, all data determined from tests on specimens that violate the size requirements of 7.2 and Appendix X2 shall be identified.

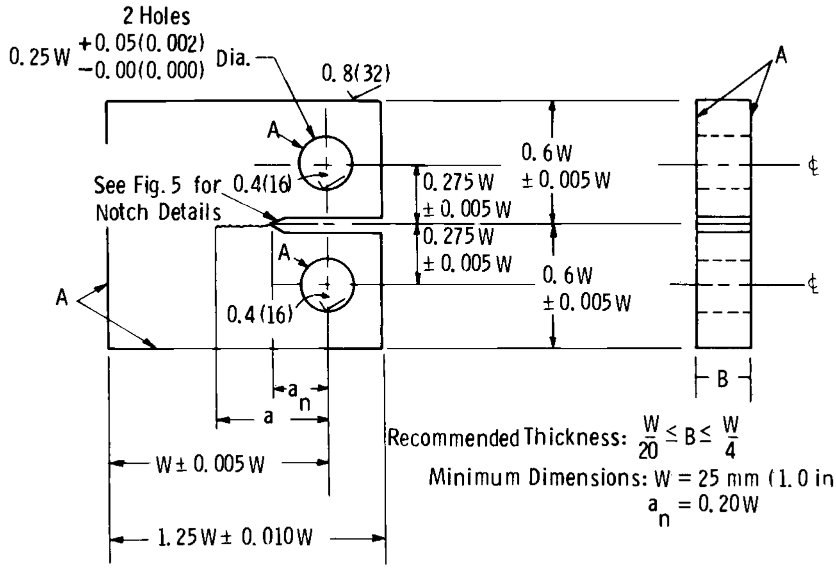

NOTE 1—Dimensions are in millimetres (inches).

NOTE 2—*A*-surfaces shall be perpendicular and parallel as applicable to within 0.002 *W*, TIR.

NOTE 3—The intersection of the tips of the machined notch (a_n) with the specimen faces shall be equally distant from the top and bottom edges of the specimen to within 0.0005 *W*

FIG. 1 Standard Compact-Type (CT) Specimen for Fatigue Crack Growth Rate Testing.

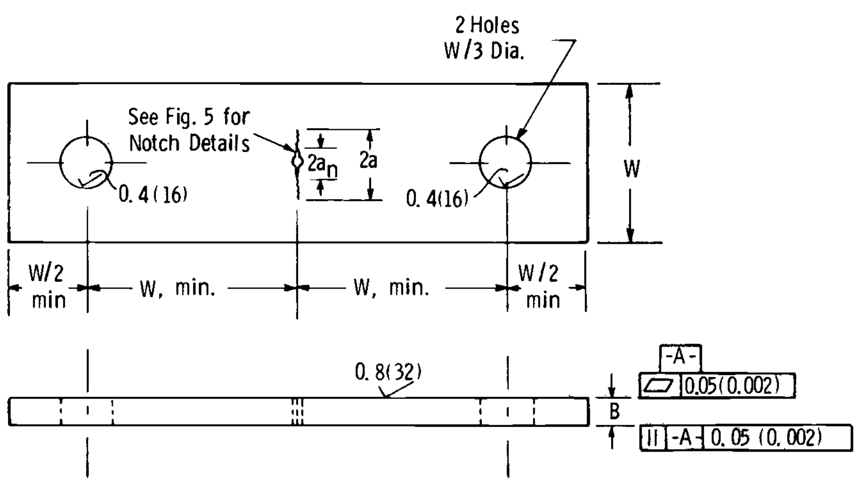

NOTE 1—Dimensions are in millimetres (inches).

NOTE 2—The machined notch ($2a_n$) shall be centered to within ±0.001 *W*.

FIG. 2 Standard Center-Cracked-Tension (CCT) Specimen for Fatigue Crack Growth Rate Testing when $W \leq 75$ mm (3 in.).

E 647

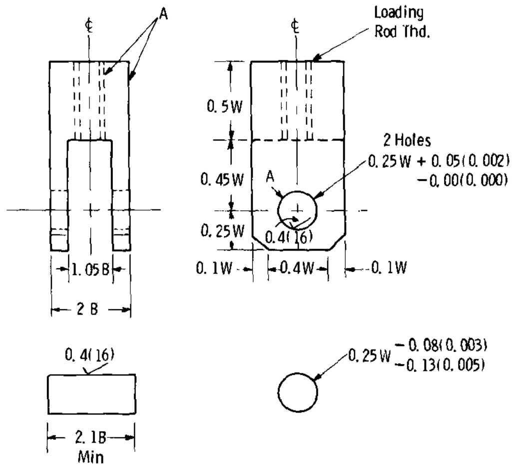

NOTE 1—Dimensions are in millimetres (inches).
NOTE 2—*A*-surfaces shall be perpendicular and parallel as applicable to within 0.05 mm (0.002 in.), TIR.

FIG. 3 Clevis and Pin Assembly for Gripping CT Specimens.

E 647

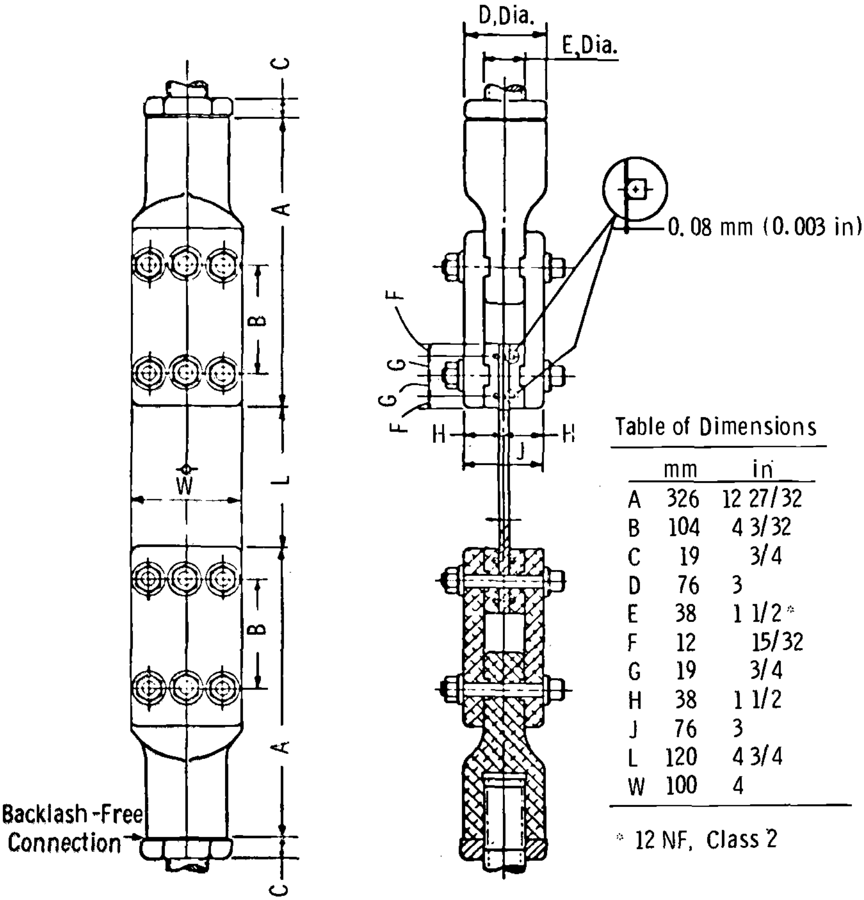

Table of Dimensions

	mm	in
A	326	12 27/32
B	104	4 3/32
C	19	3/4
D	76	3
E	38	1 1/2*
F	12	15/32
G	19	3/4
H	38	1 1/2
J	76	3
L	120	4 3/4
W	100	4

* 12 NF, Class 2

FIG. 4 Example of Bolt and Keyway Assembly for Gripping 100-mm (4-in.) wide CCT Specimen.

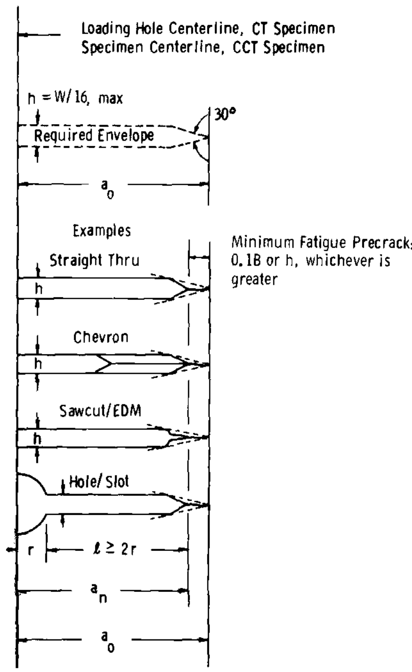

FIG. 5 Notch Details and Minimum Fatigue Pre-cracking Requirements.

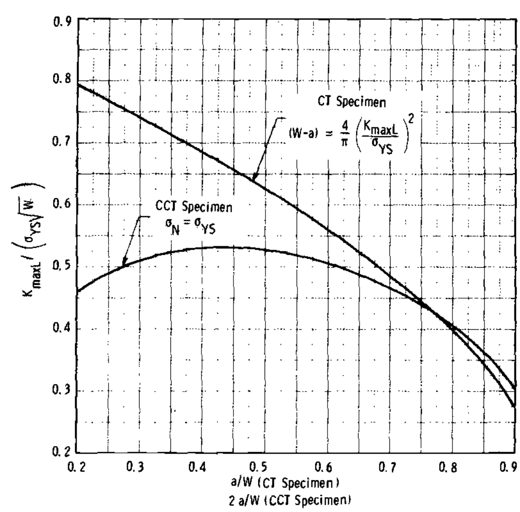

FIG. 6 Normalized Size Requirements for Standard Fatigue Crack Growth Specimens.

APPENDIXES

X1. RECOMMENDED DATA REDUCTION TECHNIQUES

X1.1 Secant Method

X1.1.1 The secant or point-to-point technique for computing the crack growth rate simply involves calculating the slope of the straight line connecting two adjacent data points on the a versus N curve. It is more formally expressed as follows:

$$(da/dN)_{\bar{a}} = \frac{a_{i+1} - a_i}{N_{i+1} - N_i} \qquad \text{(X1)}$$

Since the computed da/dN is an average rate over the $(a_{i+1} - a_i)$ increment, the average crack length, $\bar{a} = {}^1\!/_2(a_{i+1} + a_i)$, is normally used to calculate ΔK.

X1.2 Incremental Polynomial Method

X1.2.1 This method for computing da/dN involves fitting a second-order polynomial (parabola) to sets of $(2n + 1)$ successive data points, where n is usually 1, 2, 3, or 4. The form of the equation for the local fit is as follows:

$$\hat{a}_i = b_0 + b_1\left(\frac{N_i - C_1}{C_2}\right) + b_2\left(\frac{N_i - C_1}{C_2}\right)^2 \qquad \text{(X2)}$$

where:

$$-1 \leq \left(\frac{N_i - C_1}{C_2}\right) \leq +1$$

and b_0, b_1, and b_2 are the regression parameters that are determined by the least squares method (that is, minimization of the square of the deviations between observed and fitted values of crack length) over the range $a_{i-n} \leq a \leq a_{i+n}$. The value $\hat{a}_i$ is the fitted value of crack length at N_i. The parameters $C_1 = {}^1\!/_2(N_{i-n} + N_{i+n})$ and $C_2 = {}^1\!/_2(N_{i+n} - N_{i-n})$ are used to scale the input data, thus avoiding numerical difficulties in determining the regression parameters. The rate of crack growth at N_i is obtained from the derivative of the above parabola, which is given by the following expression:

$$(da/dN)_{\hat{a}_i} = \frac{b_1}{C_2} + 2b_2(N_i - C_1)/C_2^2 \qquad \text{(X3)}$$

The value of ΔK associated with this da/dN value is computed using the fitted crack length, $\hat{a}_i$, corresponding to N_i.

X1.2.2 A Fortran computer program that utilizes the above scheme for $n = 3$, that is, 7 successive data points, is given in Table X1.1 (see Note X1.1). This program uses the specimen K-calibrations given in 9.3 and also checks the data against the size requirements given in 7.2.

NOTE X1.1 It should be noted that the basic regression equations that are used to calculate da/dN can also be solved on a programmable calculator; thus large electronic computer facilities are not required to use this technique.

X1.2.3 An example of the output from the program is given in Table X1.2. Information on the specimen, loading variables, and environment are listed in the output along with tabulated values of the raw data and processed data. A(MEAS.) and A(REG.) are values of total crack length obtained from measurement and from the regression equation (Eq X2), respectively. The goodness of fit of this equation is given by the multiple correlation coefficient, MCC (note that MCC = 1 represents a perfect fit). Values of DELK (ΔK) and DA/DN (da/dN) are given in the same units as the input variables (for the example problem these are ksi$\sqrt{\text{in.}}$ and in./cycle, respectively). Values of da/dN that violate the specimen size requirement appear with an asterisk and note as shown in Table X1.2 for the final nine data points.

X1.2.4 The definition of input variables for the program and formats for these inputs are given in Table X1.3.

```
      DIMENSION A(200),N(200),EE(3),DADN(200),DELK(200),ID(7)
      DIMENSION AA(10),NN(10)
      REAL N
      REAL NN
      INTEGER GG
      INTEGER TYPE
   10 FORMAT(/A6, 9H SPECIMEN,5X,2HB=,F6.3,5H IN. ,5X,2HW=,F6.3,5H IN.
     * ,5X,3HAN=,F6.3,5H IN. )
   15 FORMAT(1H1,' SEVEN POINT INCREMENTAL POLYNOMIAL METHOD FOR DETERMI
     *NING DA/DN ')
   17 FORMAT(/)
   20 FORMAT(/6H PMIN=,F6.3,4HKIPS,5X,5HPMAX=,F6.3,4HKIPS,5X,2HR=,F6.3,5
     *X,10HTEST FREQ=,F6.3,3HHZ.)
   22 FORMAT(/7H TEMP.=,F4.0,1HF,5X,12HENVIRONMENT=,A15)
   25 FORMAT (A6,9X,F5.1,F8.3,A6,9X)
   30 FORMAT(6A6,A4,2I6)
   35 FORMAT (////11H SPEC. NO.    , 6A6,A4,10X,14H NO.POINTS  = ,I3)
   40 FORMAT(4 (F6.4, F9.0))
   55 FORMAT(/8H OBS.NO., 5X,6HCYCLES,11X,8HA(MEAS.),8X,7HA(REG.),9X,6HM
     *.C.C.,14X,4HDELK,14X,5HDA/DN)
   92 FORMAT(I4,9X,F8.0,7X,F8.3,8X,F8.3,8X,F8.6,11X,F8.2,12X,E8.3)
   95 FORMAT(I4,9X,F8.0,7X,F6.3)
   98 FORMAT(I4,9X,F8.0,7X,F8.3,8X,F8.3,8X,F8.6,11X,F8.2,12X,E8.3,2H *)
   99 FORMAT(F6.3,F6.3,F6.1,F6.3,F6.3,F6.3)
  200 FORMAT(////10H          )
  300 FORMAT(/45H * - DATA VIOLATE SPECIMEN SIZE REQUIREMENTS )
C     TYPE=1 FOR CT AND 2 FOR A CCP
  500 READ(5,30,END=1000) (ID(I),I=1,7),NPTS,TYPE
      READ(5,99) PMIN,PMAX,F,B,W,AM
C     KIND=CT,CCP,ETC.
      READ (5,25) ENV,TEM,YS,KIND
      READ(5,40)(A(I),N(I),I=1,NPTS)
      PRINT 15
      PRINT 35,(ID(II),II=1,7),NPTS
      PRINT 10,KIND,B,W,AM
      R=PMIN/PMAX
      PRINT 20 ,PMIN,PMAX,R,F
      PRINT 22 , TEM , ENV
      PRINT 55
      PRINT 200
      DO 31 I=1,NPTS
      A(I)=A(I) + AM
   31 CONTINUE
      K=0
      PI=3.1416
      PP=PMAX-PMIN
      DO 110 I=1,3
      PRINT 95,I,N(I),A(I)
  110 CONTINUE
      NPTS=NPTS-6
      DO 100 I=1,NPTS
      L=0
      K=K+1
      K1=K+6
      DO 60 J= K,K1
      L=L+1
      AA(L) = A(J)
      NN(L) = N(J)
   60 CONTINUE
      C1 = 0.5*(NN(1)+NN(7))
      C2 = 0.5*(NN(7)-NN(1))
      SX=0
      SX2=0
      SX3=0
      SX4=0
      SY=0
      SYX=0
      SYX2=0
```

TABLE X1.1 Fortran Computer Program for Data Reduction by the Seven Point Incremental Polynomial Technique

```
      DO 70 J=1,7
      X = (NN(J)-C1)/C2
      YY = AA(J)
      SX = SX + X
      SX2 = SX2 + X**2
      SX3 = SX3 + X**3
      SX4 = SX4 + X**4
      SY = SY + YY
      SYX = SYX + X*YY
      SYX2 = SYX2 + YY*X**2
   70 CONTINUE
      DEN=7.0*(SX2*SX4-SX3**2)-SX*(SX*SX4-SX2*SX3)+SX2*(SX*SX3-SX2**2)
      T2=SY*(SX2*SX4-SX3**2)-SYX*(SX*SX4-SX2*SX3)+SYX2*(SX*SX3-SX2**2)
      BB(1) = T2/DEN
      T3=7.0*(SYX*SX4-SYX2*SX3)-SX*(SY*SX4-SYX2*SX2)+SX2*(SY*SX3-SYX*SX2
     *)
      BB(2) = T3/DEN
      T4=7.0*(SX2*SYX2-SX3*SYX)-SX*(SX*SYX2-SX3*SY)+SX2*(SX*SYX-SX2*SY)
      BB(3) = T4/DEN
      YB = SY/7.0
      RSS = 0
      TSS = 0
      DO 75 J=1,7
      X = (NN(J)-C1)/C2
      YHAT = BB(1)+BB(2)*X+BB(3)*X**2
      RSS = RSS+(AA(J)-YHAT)**2
      TSS = TSS+(AA(J)-YB)**2
   75 CONTINUE
      R2 = 1.0-RSS/TSS
      DADN(I)= BB(2)/C2 + 2.0*BB(3)*(NN(4)-C1)/C2**2
      X=(NN(4)-C1)/C2
      AR=BB(1)+BB(2)*X+BB(3)*X**2
      S=1E+10
      SNET=0
      QQ=I+3
      GO TO(1,2) ,TYPE
    1 CONTINUE
      T = AR/W
      FT=((2+T)*(0.886+4.64*T-13.32*T**2+14.72*T**3-5.6*T**4))/(1-T)**1.
     *5
      S = YS*SQRT(PI*W*(1-T))/2
      GO TO 190
    2 CONTINUE
      T= 2*AR/W
      SEC = 1.0/(COS(PI*T/2))
      FT = SQRT((PI*T*SEC)/2.0)
      SNET=PMAX/(B*W*(1-T))
  190 DELK(I)=(FT*FF)/(B*SQRT(W))
      AX=DELK(I)/(1-R)
      IF(AX.GE.S) GO TO 97
      IF(SNET.GE.YS)GO TO 97
   91 PRINT 92,QQ,N(QQ),A(QQ),AR,R2,DELK(I),DADN(I)
      GO TO 100
   97 PRINT 98,QQ,N(QQ),A(QQ),AR,R2,DELK(I),DADN(I)
  100 CONTINUE
      J=NPTS+4
      K=NPTS+6
      DO 120 I=J,K
      PRINT 95,I,N(I),A(I)
  120 CONTINUE
      PRINT 17
      PRINT 17
      PRINT 300
      GO TO 500
 1000 CALL EXIT
      END
```

TABLE X1.1 *Continued*

SEVEN POINT INCREMENTAL POLYNOMIAL METHOD FOR DETERMINING DA/DN

SPEC. NO. 10N-9 NO.POINTS = 37

CT SPECIMEN B= .250 IN. W= 2.000 IN. AN= .500 IN.

PMIN= 4.000KIPS PMAX= 5.000KIPS R= .800 TEST FREQ= .100HZ.

TEMP.= 75.F ENVIRONMENT= AIR

OBS.NO.	CYCLES	A(MEAS.)	A(REG.)	M.C.C.	DELK	DA/DN
1	0.	.539				
2	15480.	.631				
3	22070.	.656				
4	30240.	.674	.677	.996911	17.56	.323-05
5	36090.	.698	.698	.996347	18.03	.337-05
6	41370.	.718	.715	.995268	18.44	.337-05
7	46850.	.735	.736	.998739	18.93	.344-05
8	50090.	.746	.746	.998733	19.17	.345-05
9	54380.	.759	.760	.999740	19.53	.350-05
10	60320.	.781	.781	.999713	20.08	.382-05
11	65160.	.801	.801	.999411	20.60	.403-05
12	70240.	.821	.822	.999473	21.19	.433-05
13	74690.	.843	.842	.999461	21.76	.453-05
14	80070.	.865	.866	.999436	22.51	.480-05
15	83860.	.886	.885	.999299	23.11	.493-05
16	88080.	.906	.906	.999176	23.79	.517-05
17	91460.	.925	.924	.999120	24.41	.545-05
18	95620.	.945	.946	.999483	25.21	.583-05
19	99000.	.967	.967	.999173	25.99	.611-05
20	102360.	.988	.988	.998500	26.84	.623-05
21	105110.	1.008	1.006	.997105	27.58	.668-05
22	108440.	1.028	1.028	.997266	28.55	.693-05
23	111660.	1.047	1.051	.997266	29.60	.741-05
24	113410.	1.067	1.064	.997552	30.23	.759-05
25	116810.	1.090	1.091	.996303	31.65	.843-05
26	118730.	1.108	1.108	.995912	32.59	.898-05 *
27	121220.	1.128	1.130	.998627	33.91	.105-04 *
28	121860.	1.138	1.137	.998593	34.32	.111-04 *
29	122830.	1.148	1.148	.998087	35.00	.114-04 *
30	124280.	1.166	1.166	.999287	36.20	.127-04 *
31	125820.	1.187	1.185	.999156	37.54	.134-04 *
32	127460.	1.207	1.208	.992990	39.20	.165-04 *
33	128700.	1.226	1.227	.994644	40.79	.201-04 *
34	129760.	1.245	1.249	.977629	42.69	.279-04 *
35	130790.	1.277				
36	131480.	1.298				
37	131550.	1.323				

* - DATA VIOLATE SPECIMEN SIZE REQUIREMENTS

TABLE X1.2 Example Output from Incremental Polynomial Computer Program

TABLE X1.3 Definition of Input Variables for Fortran Program

Input Card	Program Line	Fortran Code	Variable Definition	Card Columns
1	28	ID(I)	Specimen identification, for example specimen number, heat number, material	1-40+
	28	NPTS	Number of paired (a, N) data points	40-46*
	26	TYPE	TYPE = 1 for CT specimen TYPE = 2 for CCT specimen	47-52*
2	29	PMIN	Minimum load, P_{min}, in kips	1-6°
	29	PMAX	Maximum load, P_{max}, in kips	7-12°
	29	F	Test frequency	13-18°
	29	B	Specimen thickness, B	19-24°
	29	W	Specimen width, W	25-30°
	29	AM	Machine notch length, a_n	31-36°
3	31	ENV	Test environment	1-6+
	31	TEM	Test temperature, °F	7-11°
	31	YS	0.2 % yield stress of specimen	12-19°
	31	KIND	Specimen type, that is, CT or CCT	20-25+
4, 5, 6, etc.	32	A(I)	Crack length, a, measured from machine notch, a_n	A(1) 1-6° N(1) 7-15°
	32	N(I)	Elapsed cycles, N	A(2) 16-21° N(2) 22-30° A(3) 31-36° N(3) 37-45° A(4) 46-51° N(4) 52-60° } 4 paired (a, N) data points per card A(5) 1-6° N(5) 7-15° etc. } next card

Key
+ alphanumeric
* integer, entered to far right of available columns
° use decimal point

X2. RECOMMENDED PROCEDURE FOR SPECIMENS VIOLATING SECTION 7.2

X2.1 This appendix presents a recommended empirical procedure for use when test specimens do not meet the size requirements of 7.2 (Note X2.1). This procedure is of the greatest utility for low-strength materials, especially those exhibiting much monotonic strain-hardening. Currently, there are insufficient data on these materials to formulate an easily calculable size requirement that would be analogous to those specified in 7.2. For this reason, it is recommended that specimen deflections be measured during testing in order to provide quantitative information on the extent of plastic deformation in the specimen.

NOTE X2.1—*The purpose of the size requirements of 7.2 is to limit the extent of plastic deformation during testing so that results can be analyzed using linear-elastic theory.

X2.2 During a constant-load-amplitude fatigue crack growth test with commonly used specimen geometries, the specimen load-deflection behavior is influenced by plastic deformation as illustrated in Fig. X2.1. As the fatigue crack grows from length a_1 to a_3, the mean specimen deflection, as well as the compliance (that is, the inverse slope of the curves in Fig. X2.1), increase in a manner predictable from linear-elastic theory. However, as the fatigue crack continues to grow, the mean specimen deflection can eventually become larger than the elastically calculated mean deflection. This difference is due to a plastic deflection, $V_{plastic}$, which is depicted for crack length a_4 in Fig. X2.1.

X2.3 The plasticity phenomenon described above develops and increases continuously as the fatigue crack grows. This development is illustrated in Fig. X2.2 where both the measured and elastically calculated deflections, corresponding to minimum and maximum load are given. The increasingly larger plastic deflection causes the measured deflections, V_{min} and V_{max}, to become increasingly larger than the elastically calculated deflections, $V_{min}{}^e$ and $V_{max}{}^e$. However, for any given crack length the measured and elastically calculated deflection ranges remain approximately equal (Fig. X2.2) since the cyclic plasticity remains small (Fig. X2.1).

X2.4 Although the cyclic plasticity remains small, it would appear necessary to limit $V_{plastic}$. Limited data on A533-B steel **(12)** indicate that crack growth rates can be properly analyzed using linear elastic theory provided:

$$V_{plastic} \leq V^e_{max} \quad \text{(X4)}$$

This condition can be more conveniently expressed in terms of directly measurable quantities by using the following relationships, which are consistent with Fig. X2.2. Equation X4 is equivalent to

$$V_{max} \leq 2V^e_{max} \quad \text{(X5)}$$

and

$$\Delta V = V_{max} - V_{min} = V^e_{max} - V^e_{max} \quad \text{(X6)}$$

thus

$$V^e_{max} = \frac{\Delta V}{1 - R} \quad \text{(X7)}$$

combining Eqs X5 and X7 yields:

$$V_{max} \leq \frac{2\,\Delta V}{1 - R} \quad \text{(X8)}$$

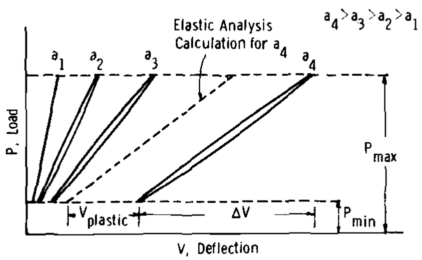

FIG. X2.1 Effect of Plastic Deformation on Specimen Load-Deflection Behavior During Fatigue Crack Growth Rate Testing at Constant-Load-Amplitude.

X2.5 When it is necessary to generate data using specimens that do not meet the size criteria of *Section* 7.2, *it is suggested that* specimen deflections be measured and that data that violate Eq X8 be so labeled. Information of this type will provide data to further test Eq X8 and will hopefully lead to the formulation of an easily calculable size requirement that would be appropriate for all materials.

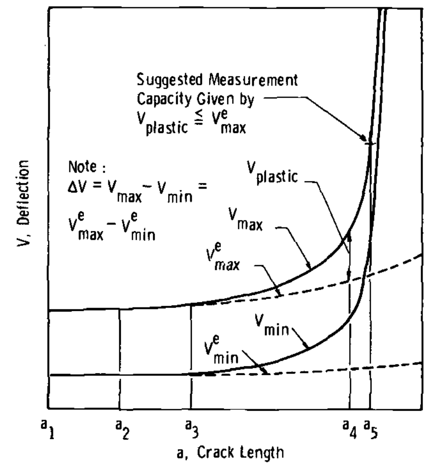

FIG. X2.2 Suggested Specimen Measurement Capacity Based on Comparison of Measured (Elastic Plus Plastic) and Elastic Deflections During a Constant-Load-Amplitude Fatigue Crack Growth Rate Test.

REFERENCES

(1) Paris, P., and Erdogan, F., "A Critical Analysis of Crack Propagation Laws," *Journal of Basic Engineering*, Series D of the Transactions of the ASME, JBAEA, December 1963, pp. 528–534.

(2) Paris, P. C., "The Fracture Mechanics Approach to Fatigue," *Proceedings of the Tenth Sagamore Army Materials Research Conference*, Syracuse University Press, 1964, pp. 107–132.

(3) Clark, Jr., W. G., "Fracture Mechanics in Fatigue," *Experimental Mechanics*, EXMCA, September 1971, pp. 1–8.

(4) Hoeppner, D. W., and Krupp, W. E., "Prediction of Component Life by Application of Fatigue Crack Growth Knowledge," *Engineering Fracture Mechanics*, EFMEA, Vol 6, 1974, pp. 47–70.

(5) *Fatigue Crack Growth Under Spectrum Loads, ASTM STP 595*, Am. Soc. Testing Mats., 1976.

(6) Hudak, Jr., S. J., Saxena, A., Bucci, R. J., and Malcolm, R. C., "Development of Standard Methods of Testing and Analyzing Fatigue Crack Growth Rate Data—Final Report," *AFML TR 78-40*.

(7) Clark, Jr., W. G., and Hudak, Jr., S. J., "Variability in Fatigue Crack Growth Rate Testing," *Journal of Testing and Evaluation*, JTEVA, Vol 3, No. 6, 1975, pp. 454–476.

(8) Clark, Jr., W. G., and Hudak, Jr., S. J., "The Analysis of Fatigue Crack Growth Rate Data," to be published in *Proceedings of the 22nd Sagamore Army Materials Research Conference on Application of Fracture Mechanics to Design*.

(9) Newman, Jr., J. C., "Stress Analysis of the Compact Specimen Including the Effects of Pin Loading," *Fracture Analysis, ASTM STP 560*, Am. Soc. Testing Mats., 1974, pp. 105–121.

(10) Srawley, J. E., "Wide Range Stress Intensity Factor Expressions for ASTM Method E 399 Standard Fracture Toughness Specimens," *International Journal of Fracture*, Vol 12, June 1976, pp. 475–476.

(11) Feddersen, C. E., "Discussion in Plane-Strain

Crack Toughness Testing of Metallic Materials," *ASTM STP 410*, Am. Soc. Testing Mats., 1976, pp. 77-79.
(12) Dowling, N. E., "Fatigue Crack Growth Rate Testing at High Stress Intensities," *ASTM STP 631*, Am. Soc. Testing Mats., 1977, pp. 139-158.

STP738-EB/Jul. 1981

APPENDIX II

PROPOSED ASTM TEST METHOD FOR MEASUREMENT OF FATIGUE CRACK GROWTH RATES[1]

1. Scope

1.1 This method covers the determination of steady-state fatigue crack growth rates using either compact type (CT) or center-cracked-tension (CCT) specimens. Results are expressed in terms of the crack-tip stress-intensity range, defined by the theory of linear elasticity.

1.2 Several different test procedures are provided, the optimum test procedure being primarily dependent on the magnitude of the fatigue crack growth rate to be measured.

1.3 Materials that can be tested by this method are not limited by thickness or strength so long as specimens are of sufficient thickness to preclude buckling and of sufficient planar size to remain predominantly elastic during testing.

1.4 A range of specimen sizes with proportional planar dimensions is provided, but size is variable to be adjusted for yield strength and applied load. Specimen thickness may be varied independent of planar size.

1.5 Specimen configurations other than those contained in this method may be used provided that well-established stress-intensity calibrations are available and that specimens are of sufficient size to remain predominantly elastic during testing.

2. Applicable Documents

2.1 *ASTM Standards*:

E 4 Load Verification of Testing Machines[2]

E 8 Tension Testing of Metallic Materials[3]

E 337 Relative Humidity by Wet- and Dry-Bulb Psychrometer[4]

E 338 Sharp-Notch Tension Testing of High-Strength Sheet Materials[5]

E 399 Plane-Strain Fracture Toughness of Metallic Materials[5]

E 467 Recommended Practice for Verification of Constant Amplitude Dynamic Loads in an Axial Load Fatigue Testing Machine[5]

E 561-75 T Recommended Practice for R-Curve Determination[5]

E 647-78 T Constant-Load-Amplitude Fatigue Crack Growth Rates Above 10^{-8} m/Cycle[5]

2.2 *ASTM Data File*:

Research Report E24-1001[6]

[1]This document, developed under the jurisdiction of ASTM Committee E-24 on Fracture Testing, expands ASTM Method E 647-78 T to include procedures for near-threshold fatigue crack growth rate measurements. Although changes are likely to occur before final adoption of near-threshold test procedures into an ASTM standard, this document serves as a useful testing guideline in the interim. **This document is published as information only.**

[2]*Annual Book of ASTM Standards*, Parts 10, 14, 32, 35, and 41.

[3]*Annual Book of ASTM Standards*, Parts 6, 7, and 10.

[4]*Annual Book of ASTM Standards*, Parts 20, 26, 32, and 41.

[5]*Annual Book of ASTM Standards*, Part 10.

[6]Available from ASTM Information Center, 1916 Race Street, Philadelphia, Pa. 19103.

3. Summary of Method

The method involves cyclic loading of notched specimens which have been acceptably precracked in fatigue. Crack length is measured, either visually or by an equivalent method, as a function of elapsed fatigue cycles, and these data are subjected to numerical analysis to establish the rate of crack growth. Crack growth rates are expressed as a function of the stress-intensity factor range (ΔK) which is calculated from expressions based on linear elastic stress analysis.

4. Significance

4.1 Fatigue crack growth rate expressed as a function of crack-tip stress-intensity factor range (da/dN versus ΔK) characterizes a material's resistance to stable crack extension under cyclic loading. Background information on the rationale for employing linear elastic fracture mechanics to analyze fatigue crack growth rate data is given in Refs *1* and *2*.[7]

4.1.1 In innocuous (inert) environments fatigue crack growth rates are primarily a function of ΔK and load ratio (R), or K_{max} and R.

NOTE 1—ΔK, K_{max}, and R are not independent of each other. Specification of any two of these variables is sufficient to define the loading condition. It is customary to specify one of the stress-intensity parameters (ΔK or K_{max}) along with the load ratio (R). Temperature and aggressive environments can significantly affect da/dN versus ΔK, and in many cases accentuate R-effects and also introduce effects of other loading variables such as cyclic frequency and waveform. Attention needs to be given to the proper selection and control of these variables in research studies and in generation of design data.

4.1.2 Expressing da/dN as a function of ΔK provides results which are independent of planar geometry, thus enabling exchange and comparison of data obtained from a variety of specimen configurations and loading conditions. Moreover, this feature enables da/dN versus ΔK data to be utilized in the design and evaluation of engineering structures.

4.1.3 Fatigue crack growth rate data are not always geometry-independent in the strict sense, since thickness effects sometimes occur. However, data on the influence of thickness on fatigue crack growth rate are mixed. Fatigue crack growth rates over a wide range of ΔK have been reported to either increase, decrease, or remain unaffected as specimen thickness is increased. Thickness effects can also interact with other variables such as environment and heat treatment. In addition, materials may exhibit thickness effects only over the terminal range of da/dN versus ΔK which are associated with either nominal yielding[8] or a K_{max}-controlled instability. The potential influence of specimen thickness should be considered when generating data for research or design.

4.2 This method can serve the following purposes:

4.2.1 To establish the influence of fatigue crack growth on the life of components subjected to cyclic loading, provided data are generated under representative conditions, and combined with appropriate fracture toughness data (for example, see Method E 399), defect characterization data, and stress-analysis information (for example, see Refs *3* and *4*).

NOTE 2—Fatigue crack growth can be significantly influenced by load history. During variable amplitude loading, crack growth rates can be either enhanced or retarded

[7]The italic numbers in brackets refer to the list of references appended to this paper.

[8]This condition will be avoided in tests which conform to the specimen size requirements of this method.

(relative to steady-state, constant-amplitude growth rates at a given ΔK), depending on the specific loading sequence. This complicating factor needs to be considered in using constant-amplitude growth rate data to analyze variable amplitude fatigue problems (for example, see Ref 5).

4.2.2 To establish material selection criteria, design allowables, and nondestructive inspection requirements for quality assurance.

4.2.3 To analyze failures and formulate appropriate remedial measures.

4.2.4 To establish in quantitative terms, the individual and combined effects of metallurgical, fabrication, environmental, and loading variables on fatigue crack growth.

5. Definitions

5.1 *cycle*—one complete sequence of values of applied load that is repeated periodically in fatigue. The symbol N represents the number of cycles.

5.1.1 *maximum load*, P_{max}[F]—the greatest algebraic value of applied load in a fatigue cycle. Tensile loads are considered positive and compressive loads negative.

5.1.2 *minimum load*, P_{min}[F]—the least algebraic value of applied load in a fatigue cycle.

5.1.3 *load range*, ΔP[F]—the algebraic difference between the maximum and minimum loads in a fatigue cycle.

5.1.4 *load ratio* (also called "stress ratio"), R—the algebraic ratio of the minimum to maximum load in a fatigue cycle (that is, $R = P_{min}/P_{max}$).

5.2 *stress-intensity-factor*, $K[FL^{-3/2}]$—the magnitude of the ideal-crack-tip stress field in a linear-elastic body. In this method, Mode 1 is assumed. Mode 1 corresponds to loading such that the crack surfaces are displaced apart, normal to the crack plane.

5.2.1 $K_{max}[FL^{-3/2}]$—the maximum value of stress-intensity factor in a fatigue cycle. This value corresponds to P_{max}.

5.2.2 $K_{min}[FL^{-3/2}]$—the minimum value of stress-intensity factor in a fatigue cycle. This value corresponds to P_{min} when $R > 0$, and is taken to be zero when $R \leq 0$.

5.2.3 $\Delta K[FL^{-3/2}]$—the variation in stress-intensity factor in a fatigue cycle (that is, $K_{max} - K_{min}$).

NOTE 3—The loading variables R, ΔK, and K_{max} are related such that specifying any two uniquely defines the third according to the following relationship: $\Delta K = (1 - R)K_{max}$ for $R \geq 0$, and $\Delta K = K_{max}$ for $R \leq 0$.

NOTE 4—These operational stress-intensity factor definitions do not include local crack-tip effects (for example, crack closure, residual stress, and blunting).

5.3 *normalized* K-*gradient*, $C = 1/K \cdot dK/da[L^{-1}]$—the fractional rate of change of K with increasing crack length.

NOTE 5—When C is held constant the percentage change in K is constant for equal increments of crack length. The following identity is true for the normalized K-gradient in a constant-load ratio test:

$$\frac{1}{K}\cdot\frac{dK}{da} \equiv \frac{1}{K_{max}}\cdot\frac{dK_{max}}{da} \equiv \frac{1}{K_{min}}\cdot\frac{dK_{min}}{da} \equiv \frac{1}{\Delta K}\cdot\frac{d\Delta K}{da}$$

5.3.1 K-*increasing test*—a test in which the value of C is nominally positive. For the standard specimens in this method, the constant-load-amplitude test will result in a K-increasing test where the C-value changes but is always positive.

5.3.2 K-*decreasing test*—a test in which the value of C is nominally negative. In this method K-decreasing tests are conducted by shedding load, either continuously or by a series of decremental steps, as the crack grows.

5.4 *stress-intensity calibration, K*-calibration—a mathematical expression, based on empirical or analytical results, which relates stress-intensity factor to load and crack length for a specific specimen planar geometry.

5.5 *crack length, $a(L)$*—the physical crack size used to determine crack growth rate and stress-intensity factor in fatigue. For the CT specimen, a is measured from the line connecting the bearing points of load application (Fig. 1); for the CCT specimen, a is measured from the perpendicular bisector of the central crack (Fig. 2).

5.6 *fatigue crack growth rate, da/dN* or $\Delta a/\Delta N$, (LT^{-1})—crack extension caused by fatigue loading and expressed in terms of crack extension per cycle of fatigue.

5.7 *fatigue crack growth threshold,* $\Delta K_{th}(FL^{3/2})$—that value of ΔK at which da/dN approaches zero. For most materials it is practical to define ΔK_{th} as ΔK which corresponds to a fatigue crack growth rate of 10^{-10} m/cycle. The procedure for determining this ΔK_{th} is given in Section 9.4.

6. Apparatus

6.1 *Grips and Fixtures for CT Specimen*—a clevis and pin assembly (Fig. 3) is used at both the top and bottom of the specimen to allow in-plane rotation as the specimen is loaded. This specimen and loading arrangement is to be used for tension-tension loading only.

6.1.1 Suggested proportions and critical tolerances of the clevis and pin are given (Fig. 3) in terms of either the specimen width (W) or the specimen thickness (B), since these dimensions may be varied independently within certain limits.

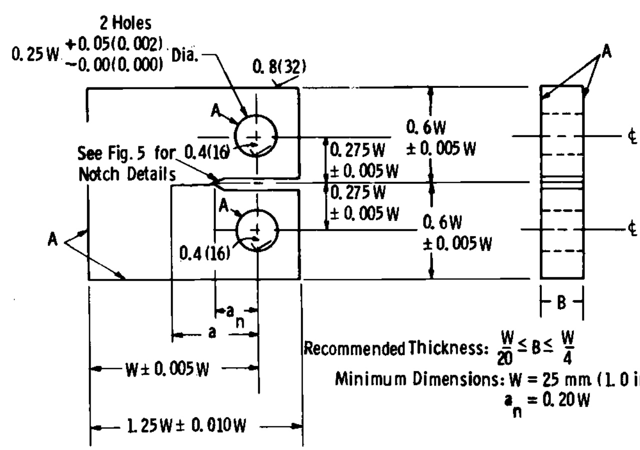

Notes: 1 - Dimensions are in millimeters (inches)
2 - A - surfaces shall be perpendicular and parallel as applicable to within 0.002 W, TIR.
3 - The intersection of the tips of the machined notch (a_n) with the specimen faces shall be equally distant from the top and bottom edges of the specimen to within 0.0005 W

FIG. 1—*Standard compact-type (CT) specimen for fatigue crack growth rate testing.*

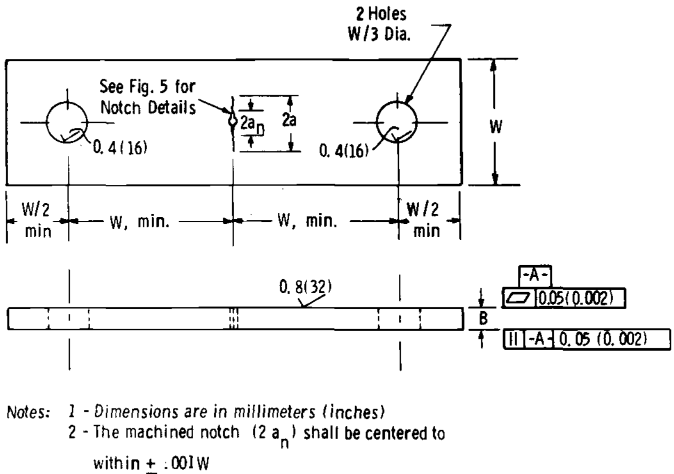

FIG. 2—*Standard center-cracked-tension (CCT) specimen for fatigue crack growth rate testing when* W ≤ *75 mm (3 in.).*

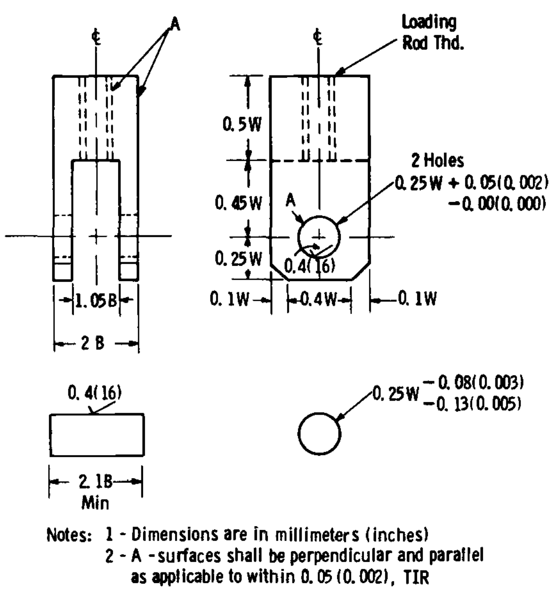

FIG. 3—*Clevis and pin assembly for gripping CT specimens.*

6.1.2 The pin-to-hole clearances are designed to minimize friction, thereby eliminating unacceptable end-movements which would invalidate the specimen K-calibrations provided herein. The use of a lubricant (for example, MoS_2) on the loading pins is also recommended to minimize friction.

6.1.3 Using a 1000 MN/m^2($\sim$ 150 ksi) yield strength alloy (for example, AISI 4340 steel) for the clevis and pins provided adequate strength and resistance to galling and fatigue.

6.2 *Grips and Fixtures for CCT Specimens*—the type of grips and fixtures to be used with the CCT specimens will depend on the specimen width (W) (defined in Fig. 2) and the loading conditions (that is, either tension-tension or tension-compression loading). The minimum required specimen gage length varies with the type of gripping, and is specified so that a uniform stress distribution is developed in the specimen gage length during testing. For testing of thin sheets, constraining plates may be necessary to minimize specimen buckling (see Recommended Practice E 561 for recommendations on buckling constraints).

6.2.1 For tension-tension loading of specimens with $W \leq 75$ mm (3 in.) a clevis and single pin arrangement is suitable for gripping, provided that the specimen gage length (that is, the distance between loading pins) is at least $2W$ (Fig. 2). For this arrangement it is also helpful either to use brass shims between the pin and specimen or to lubricate the pin to prevent fretting-fatigue cracks from initiating at the specimen loading hole. Additional measures which may be taken to prevent cracking at the pinhole include attaching reinforcement plates to the specimen (for example, see Method E 338) or employing a "dog-bone"-type specimen design. In either case, the gage length is defined as the uniform section and shall be at least $1.7W$. This gage length requirement is for all dog-bone designs regardless of methods of gripping.

6.2.2 For tension-tension loading of specimens of uniform width $W \geq 75$ mm (3 in.) a clevis with multiple bolts is recommended (for example, see Recommended Practice E 561). In this arrangement the loads are applied more uniformly; thus the minimum specimen gage length (that is, the distance between the innermost rows of bolt holes) is relaxed to $1.5W$.

6.2.3 The CCT specimen of uniform width may also be gripped using a clamping device instead of the above arrangements. This type of gripping is necessary for tension-compression loading. An example of a specific bolt and keyway design for clamping CCT specimens is given in Fig. 4. In addition, various hydraulic and mechanical-wedge systems which supply adequate clamping forces are commercially available and may be used. The minimum gage length requirement for clamped specimens is relaxed to $1.2W$.

6.3 *Alignment of Grips*—It is important that attention be given to achieving good alignment in the load train through careful machining of all gripping fixtures. For tension-tension loading, pin or gimbal connections between the grips and load frame are recommended to achieve loading symmetry. For tension-compression loading, the length of the load train (including the hydraulic actuator) should be minimized, and rigid nonrotating joints should be employed to reduce lateral motion in the load train.

7. Specimen Configuration, Size, and Preparation

7.1 *Standard Specimens*—The geometry of standard compact type (CT) and center-cracked-tension (CCT) specimens is given in Figs. 1 and 2, respectively. The specific geometry of center-cracked-tension (CCT) specimens depends on the method of gripping as specified in Section 6.2. Notch and precracking details for both specimens are given in Fig. 5. The CT specimen is not recommended for tension-compression testing, because of uncertainties introduced into the K-calibration.

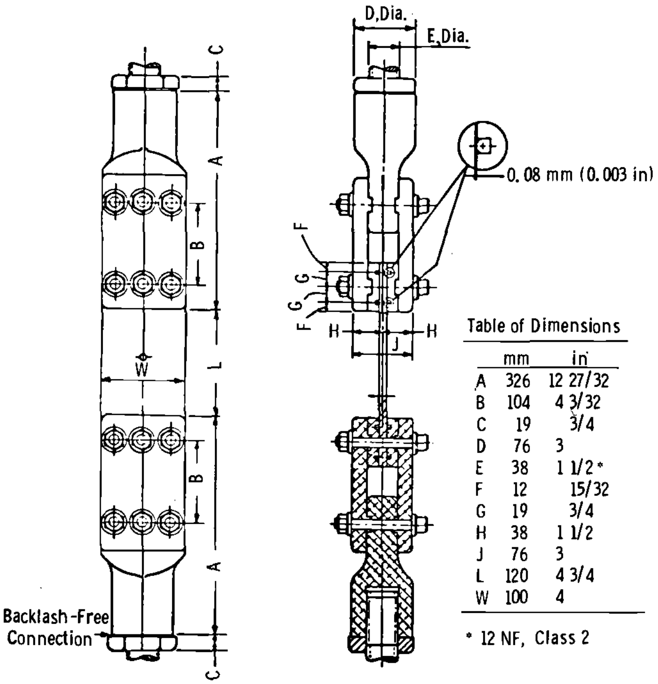

Table of Dimensions

	mm	in
A	326	12 27/32
B	104	4 3/32
C	19	3/4
D	76	3
E	38	1 1/2*
F	12	15/32
G	19	3/4
H	38	1 1/2
J	76	3
L	120	4 3/4
W	100	4

* 12 NF, Class 2

FIG. 4—*Example of bolt and keyway assembly for gripping 100-mm (4-in.)-wide CCT specimen.*

7.1.1 It is required that the machined notch (a_n) in the CT specimen be at least $0.2W$ in length so that the K-calibration is not influenced by small variations in the location and dimensions of the loading-pin holes.

7.1.2 The machined notch ($2a_n$) in the CCT specimen shall be centered with respect to the specimen centerline to within $\pm 0.001W$. The length of the machine notch in the CCT specimen will be determined by practical machining considerations and is not restricted by limitations in the K-calibration.

NOTE 6—It is recommended that $2a_n$ be at least $0.2W$ when using the compliance method to monitor crack extension in the CCT specimen so that accurate crack length determinations can be obtained.

7.1.3 For both specimens the thickness (B) and width (W) may be varied independently within the following limits which are based on specimen buckling and crack-front-curvature considerations:

7.1.3.1 For CT specimens it is recommended that thickness be within the range $W/20 \leq B \leq W/4$. Specimens having thicknesses up to and including $W/2$ may also be employed; however, data from these specimens will often require through-thickness crack curvature corrections (Section 9.1). In addition, difficulties may be encountered in meeting the through-thickness crack straightness requirements of Sections 8.3.3 and 8.7.4.

7.1.3.2 Using the above rationale, the recommended upper limit on thickness in CCT specimens is $W/8$, although $W/4$ may also be employed. The minimum thickness necessary to avoid excessive lateral deflections or buckling in CCT specimens is sensitive to specimen gage length, grip alignment, and load ratio (R). It is recommended that strain gage information be obtained for the particular specimen geometry and loading condition of interest, and that bending strains not exceed 5 percent of the nominal strain.

7.2 *Specimen Size*—In order for results to be valid according to this method it is required that the specimen be predominantly elastic at all values of applied load. The minimum in-plane specimen sizes that meet this requirement are based primarily on empirical results and are specific to specimen configuration [*6*].

7.2.1 For the CT specimen it is required that the uncracked ligament, $(W - a)$, be equal to or greater than $(4/\pi)(K_{max}/\sigma_{YS})^2$, where σ_{YS} is the 0.2 percent offset yield strength of the test material (measured by Methods E 8) at the temperature for which fatigue crack growth rate data are to be obtained.

7.2.2 For the CCT specimen it is required that the nominal stress in the uncracked ligament given by

$$\sigma_N = \frac{P_{max}}{BW(1 - \frac{2a}{W})}$$

be less than σ_{YS}.

NOTE 7—The above criteria are likely to be restrictive; that is, they may require overly large specimen sizes for materials which exhibit a high degree of strain hardening (for example, annealed low-alloy ferritic steels, annealed austenitic stainless steels, etc.). Currently there are insufficient data on these materials to formulate easily calculable size requirements which are analogous to those given above. However, data from specimens smaller than those allowed by Section 7.2 may be validated by demonstrating that da/dN versus ΔK results are equivalent to results from larger specimens which meet the requirements of Section 7.2. Supplementary information on the extent of plastic deformation encountered in any given test specimen can be obtained by measuring specimen deflections as described in Appendix X2 of Method E 647.

7.2.3 Figure 6 gives the limiting K_{max}-values, designated K_{maxL}, which are defined by the above specimen size criteria. This information is expressed in dimensionless form so that the curves can be used to calculate either (*1*) the value of K_{maxL} for a given combination of specimen size (W) and material yield strength (σ_{YS}), or (*2*) the minimum specimen size required to obtain valid data up to a desired K_{max}-value for a given material strength level. (However, it should be noted that the desired K_{max}-value cannot be achieved if it is greater than the K-value for unstable fracture.) All values of $K_{max}/(\sigma_{YS}\sqrt{W})$ which fall below the respective curves for the two specimens satisfy the specimen size requirements of this method.

7.3 *Notch Preparation*—The machined notch for either of the standard specimens may be made by electrical-discharge machining (EDM), milling, broaching, or sawcutting. The following notch preparation procedures are suggested to facilitate precracking in various materials:

7.3.1 *EDM*, $\rho <$ 0.25 mm (0.010 in.) (ρ = notch root radius)—high-strength steels, $\sigma_{YS} \geq$ 1172 MPa (170 ksi), titanium and aluminum alloys.

7.3.2 *Mill or broach*, $\rho \leq$ 0.08 mm (0.003 in.)—low/medium strength steels, $\sigma_{YS} \leq$ 1172 MPa (170 ksi), aluminum alloys.

7.3.3 *Grind*, $\rho \leq$ 0.25 mm (0.010 in.)—low/medium strength steels.

7.3.4 *Mill or broach*, $\rho \leq$ 0.25 mm (0.010 in.)—aluminum alloys.

7.3.5 *Sawcut*—aluminum alloys.

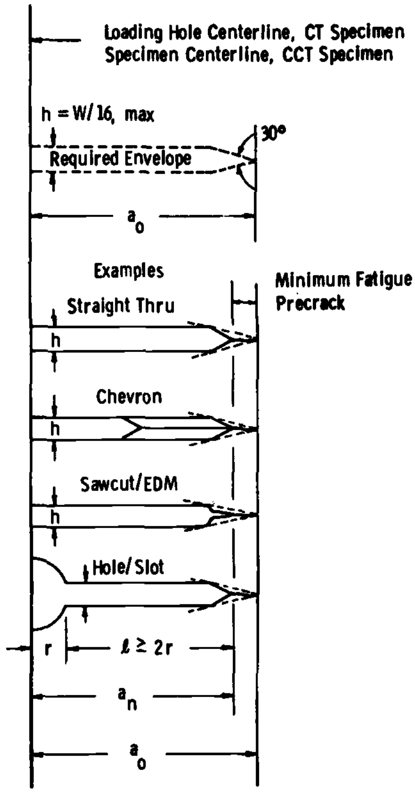

FIG. 5—*Notch details and minimum fatigue precracking requirements.*

7.3.6 Examples of various machined notch geometries and associated precracking requirements are given in Fig. 5 and Section 8.3.

8. Procedure

8.1 *Number of Tests*—At crack growth rates greater than 10^{-8} m/cycle, the range in da/dN at a given ΔK may vary by about a factor of two [7]. At rates below 10^{-8} m/cycle, the variability in da/dN may increase to a value of about five due to increased sensitivity of da/dN on small variations in ΔK. This scatter may be further increased by variables such as material differences, residual stresses, load precision, and data processing techniques, which take on added significance in the low crack growth rate regime. It is good practice to conduct replicate tests; when this is impractical, tests should be planned such that regions of overlapping da/dN versus ΔK data are obtained. Since confidence in inferences drawn from the data increases with number of tests, the desired number of tests will depend on the end use of the data.

8.2 *Specimen Measurements*—The specimen dimensions shall be within the tolerances given in Figs. 1 and 2.

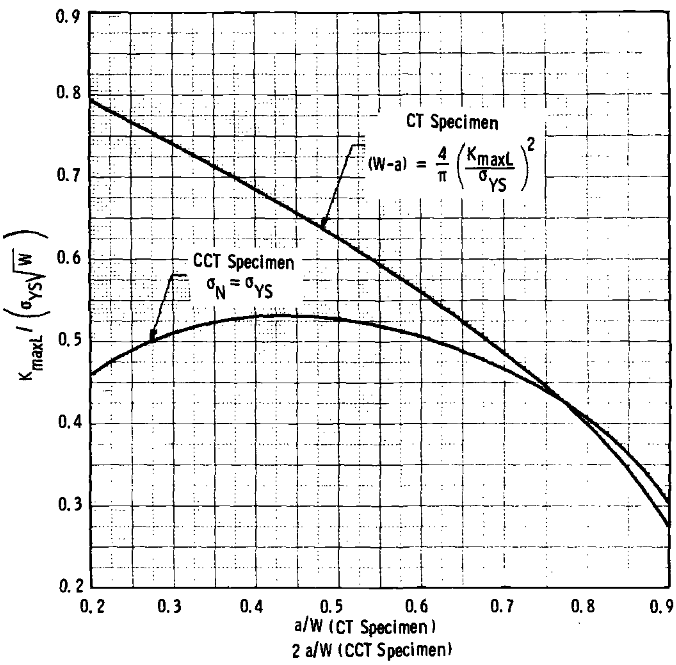

FIG. 6—*Normalized size requirements for standard fatigue crack growth specimens.*

8.3 *Fatigue Precracking*—The importance of precracking is to provide a sharpened fatigue crack of adequate size and straightness (also symmetry for the CCT specimen) which ensures (*1*) the effect of the machined starter notch is removed from the specimen K-calibration, and (*2*) elimination of effects on subsequent crack growth rate data caused by changing crack front shape or precrack load history.

8.3.1 Fatigue precracking shall be conducted with the specimen in the same metallurgical condition in which it is to be tested. The precracking equipment shall be such that the load distribution is symmetrical with respect to the machine notch, and K_{max} during precracking is controlled to within ± 5 percent. Any convenient loading frequency that enables the required load accuracy to be achieved can be used for precracking. The machined notch plus fatigue precrack must lie within the envelope, shown in Fig. 5, that has as its apex the end of the fatigue precrack. In addition, the fatigue precrack length shall not be shorter than 2.5 mm (0.10 in.), $0.10B$ or h, whichever is greater (Fig. 5).

8.3.2 The final K_{max} during precracking shall not exceed the initial K_{max} for which test data are to be obtained. If necessary, loads corresponding to K_{max}-values higher than initial test values may be used to initiate cracking at the machined notch. In this event the load range shall be stepped-down to meet the above requirement. It is suggested that reduction in P_{max} for any step be no greater than 20 percent, and that measurable crack extension occur before proceeding to the next step. To avoid transient effects in the test data, the load range in each step shall be applied over a crack length increment of at least $(3/\pi)(K_{max_i}/\sigma_{YS})^2$, where K_{max_i} is the terminal value of

K_{max} from the previous load step. If P_{min}/P_{max} during precracking differs from that used during testing, see the precautions of Section 8.5.1.

8.3.3 Measure the fatigue precrack length from the tip of the machined notch to the crack tip on the front and back surfaces of the specimen to within 0.10 mm (0.004 in.) or $0.002W$, whichever is greater. Measure both cracks, front and back, in the CCT specimens. If any two crack length measurements differ by more than $0.025W$ or by more than $0.25B$, whichever is less, the precracking operation is not suitable, and subsequent testing would be invalid under this method. If a fatigue crack departs more than ±5 deg from the plane of symmetry, the specimen is not suitable for subsequent testing. In either case, check for potential problems in alignment of the loading system or details of the machined notch, or both, before continuing to precrack to satisfy the above requirements.

8.4 *Test Equipment*—The equipment for fatigue testing shall be such that the load distribution is symmetrical to the specimen notch.

8.4.1 The load cell in the test machine shall be verified in accordance with Methods E 4 and Recommended Practice E 467. Testing shall be conducted such that both ΔP and P_{max} are controlled to within ±2 percent throughout the test.

8.4.2 An accurate digital device is required for counting elapsed cycles. A timer is a desirable supplement to the counter and provides a check on the counter. Multiplication factors (for example, ×10 or ×100) should not be used on counting devices when obtaining data at growth rates above 10^{-5} m/cycle, since they can introduce significant errors in the growth rate determination.

8.5 K-*Increasing Test Procedure for* da/dN > 10^{-8} *m/Cycle*—This test procedure is well suited for fatigue crack growth rates above 10^{-8} m/cycle; however, it becomes increasingly difficult to use as growth rates decrease below 10^{-8} m/cycle because of precracking considerations (Section 8.3.3). (A K-decreasing test procedure which is better suited for rates below 10^{-8} m/cycle is provided in Section 8.6). When using the K-increasing procedure it is preferred that each specimen be tested at a constant ΔP and a fixed set of loading variables. However, this may not always be feasible when it is necessary to generate a wide range of information with a limited number of specimens. When loading variables are changed during a test, potential problems arise from several types of transient phenomena. The following procedures should be followed to minimize or eliminate transient effects while using this K-increasing test procedure:

8.5.1 If load range (ΔP) is to be incrementally varied, it should be done such that P_{max} is increased rather than decreased. This is to preclude retardation of growth rates caused by overload effects, retardation being a more pronounced effect than accelerated crack growth associated with incremental increase in P_{max}. Transient growth rates are also known to result from changes in P_{min} or R. Sufficient crack extension should be allowed following changes in load to enable the growth rate to establish a steady-state value. The amount of crack growth that is required depends on the magnitude of load change and on the material.

8.5.2 When environmental effects are present, changes in load level, test frequency, or waveform can result in transient growth rates. Sufficient crack extension should be allowed between changes in these loading variables to enable the growth rate to achieve a steady-stage value.

8.5.3 Transient growth rates can also occur, in the absence of loading variable changes, due to long-duration test interruptions (for example, during work stoppages). In this case data should be discarded if the growth rates following an interruption are less than those before the interruption.

8.6 K-*Decreasing Procedure for* da/dN < 10^{-8} *m/Cycle*—This procedure is started by cycling at a ΔK and K_{max} level equal to or greater than the terminal precracking values. Subsequently, loads are shed (decreased) as the crack grows, and test data are recorded until the lowest ΔK or crack growth rate of interest is achieved. The test may then be continued at constant load limits to obtain comparison data under K-increasing conditions.

8.6.1 Load shedding during the K-decreasing test may be conducted as decreasing load steps at selected crack length intervals, as shown in Fig. 7. Alternatively, the load may be shed in a continuous manner by an automated technique (for example, by use of an analog computer or digital computer or both) [8].

8.6.2 The rate of load shedding with increasing crack length shall be gradual enough to (1) preclude anomalous data resulting from reductions in the stress-intensity factor and concomitant transient growth rates, and (2) allow the establishment of about five (da/dN, ΔK) data points of approximately equal spacing per decade of crack growth rate. The above requirements can be met by limiting the normalized K-gradient, $C = 1/K \cdot dK/da$, to a negative value having a magnitude equal to or less than 0.08 mm^{-1} (2 in.$^{-1}$). That is

$$|C| = \left| \frac{1}{K} \cdot \frac{dK}{da} \right| \leq 0.08\,\text{mm}^{-1}\,(2\,\text{in.}^{-1})$$

When loads are incrementally shed, the requirements on C correspond to the nominal K-gradient depicted in Fig. 7.

NOTE 8—Acceptable values of C may depend on load ratio, alloy type, and environment. Negative values of C less than the magnitude indicated above have been dem-

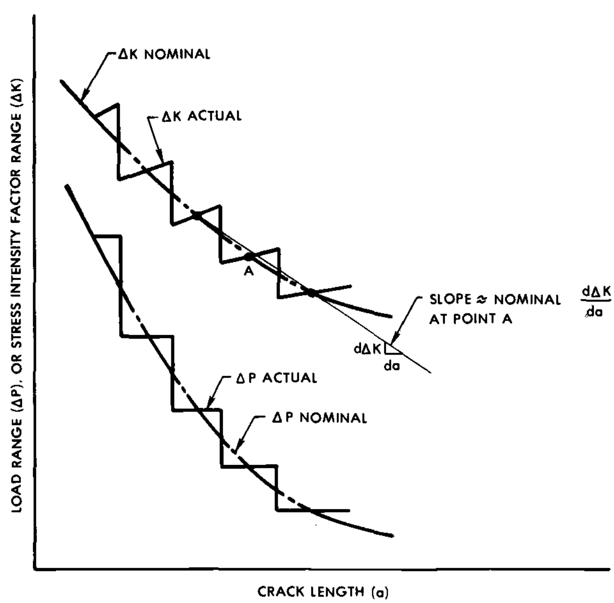

FIG. 7—*Typical* K-*decreasing test by stepped-load shedding.*

onstrated as acceptable for several steel alloys and aluminum alloys tested in laboratory air over a wide range of load ratios [6,8].

8.6.3 If the magnitude of a negative value C exceeds that prescribed in Section 8.6.2, the procedure shall consist of decreasing K to the lowest growth rate of interest followed by a K-increasing test at a constant ΔP (conducted in accordance with Section 8.5). Upon demonstrating that data obtained using K-increasing and K-decreasing procedures are equivalent for a given set of test conditions, the K-increasing testing may be eliminated from all replicate testing under these same test conditions.

8.6.4 It is recommended that the load ratio (R) and C be maintained constant during K-decreasing testing.

8.6.5 The K-history and load history for a constant C-test is given as follows:

8.6.5.1 $\Delta K = \Delta K_o \exp[C(a - a_o)]$, where ΔK_o is the initial ΔK at the start of the test, and a_o is the corresponding crack length. Because of the identity given in Section 5.3, the above relationship is also true for K_{max} and K_{min}.

8.6.5.2 The load histories for the standard specimens of this method are obtained by substituting the appropriate K-calibrations given in Section 9.3 into the above expression.

8.6.6 When employing step shedding of load, as in Fig. 7, the reduction in P_{max} of adjacent load steps shall not exceed 10 percent of the previous P_{max}. Upon adjustment of maximum load from P_{max1} to a lower value, P_{max2}, a minimum crack extension of 0.50 mm (0.02 in.) is recommended.

8.6.7 When employing continuous shedding of load, the requirement of Section 8.6.6 is waived. Continuous load shedding is defined as $(P_{max1} - P_{max2})/P_{max1} \leq 0.02$.

8.7 *Measurement of Crack Length*—Fatigue crack length measurements are to be made as a function of elapsed cycles by means of a visual, or equivalent, technique capable of resolving crack extensions of 0.10 mm (0.004 in.) or $0.002W$, whichever is greater. For visual measurements, polishing the test area of the specimen and using indirect lighting aid in the resolution of the crack tip. It is recommended that, prior to testing, reference marks be applied to the test specimen at predetermined locations along the direction of cracking. Crack length can then be measured using a low power (20 to 50×) traveling microscope. Using the reference marks eliminates potential errors due to accidental movement of the traveling microscope. If precision photographic grids or Mylar scales are attached to the specimen, crack length can be determined directly with any magnifying device which gives the required resolution.

8.7.1 It is preferred that measurements be made without interrupting the test. When tests are interrupted to make crack length measurements, the interruption time should be minimized (for example, less than 10 min), since transient growth rates can result from interruptions of long duration. To enhance resolution of the crack tip, a static load not exceeding the maximum load of the previously applied load cycle may be applied during measurement interruptions. This procedure is permissible provided that it does not cause static-load crack extension or creep deformation.

8.7.2 Crack length measurements shall be made at intervals such that da/dN data are nearly evenly distributed with respect to ΔK. The following measurement intervals are recommended according to specimen type:

8.7.2.1 *CT Specimen:*

$$\Delta a \leq 0.02W \text{ for } 0.25 \leq a/W \leq 0.60$$
$$\Delta a \leq 0.01W \text{ for } a/W > 0.60$$

8.7.2.2 *CCT Specimen*:

$$\Delta a \leq 0.03W \text{ for } 2a/W < 0.60$$
$$\Delta a \leq 0.02W \text{ for } 2a/W > 0.60$$

8.7.2.3 In any case, the minimum Δa shall be 0.25 mm (0.01 in.) or ten times the crack length measurement precision,[9] whichever is greater.

8.7.3 If crack length is monitored visually the following procedure applies. For specimens with $B/W \leq 0.15$, the length measurements need only be made on one side of the specimen. For specimens with $B/W \geq 0.15$, measurements are to be made on both front and back sides of the specimen, and the average value of these measurements (2 values for the CT specimen, 4 values for the CCT specimen) used in subsequent calculations.

8.7.4 If at any point in the test the average through-thickness fatigue crack departs more than ± 5 deg from the plane of symmetry of the specimen, the data are invalid according to the method. In addition, data are invalid where any two surface crack lengths at a given number of cycles differ by more than $0.025W$ or by more than $0.25B$, whichever is less.

9. Calculations and Interpretation of Results

9.1 *Crack Curvature Correction*—After completion of testing the fracture surfaces shall be examined, preferably at two locations (for example, at the precrack and terminal fatigue crack lengths), to determine the extent of through-thickness crack curvature. If a crack contour is visible, calculate a five-point, through-thickness average crack length in accordance with Method E 399, Section 8.2.3. The difference between the average through-thickness crack length and the corresponding crack length recorded during the test (for example, if visual measurements were obtained this might be the average of the surface crack length measurements) is the crack curvature correction.

9.1.1 If the crack curvature correction results in a greater than 5 percent difference in calculated stress intensity at any crack length, then the correction shall be employed when analyzing the recorded test data.

9.1.2 If the magnitude of the crack curvature correction either increases or decreases with crack length, a linear interpolation shall be used to correct intermediate data points. This linear correction shall be determined from two distinct crack contours separated by minimum spacing of $0.25W$ or B, whichever is greater. When there is no systematic variation of crack curvature with crack length, a uniform correction determined from an average of the crack contour measurements shall be employed.

9.1.3 When employing a crack length monitoring technique other than visual, a crack curvature correction is generally incorporated in the calibration of the technique. However, since the magnitude of the correction will probably depend on specimen thickness, the above correction procedures may also be necessary.

9.2 *Determination of Crack Growth Rate*—The rate of fatigue crack growth is to be determined from the crack length versus elapsed cycles data (a versus N). Recommended approaches which utilize the secant or incremental polynomial methods are given in Appendix X1 of Method E 647. Either method is suitable for the K-increasing, constant ΔP test. For the K-decreasing tests where load is shed in decremental steps, as in Fig. 7, the secant method is recommended. Where shedding of K is per-

[9]The crack length measurement precision is herein defined as the standard deviation on the mean value of crack length determined for a set of replicate measurements.

formed continuously with each cycle by automation, the incremental polynomial technique is applicable. A crack growth rate determination shall not be made over any increment of crack extension which includes a load step.

NOTE 9—Both recommended methods for processing a versus N data are known to give the same average da/dN response. However, the secant method often results in increased scatter in da/dN relative to the incremental polynomial method, since the latter numerically "smooths" the data [*7,9*]. This apparent difference in variability introduced by the two methods needs to be considered, especially in utilizing da/dN versus ΔK data in design.

9.3 *Determination of Stress-Intensity Range* ΔK—Use the crack length values of Section 9.1 and Appendix X1 of Method E 647 to calculate the stress-intensity range corresponding to a given crack growth rate from the following expressions:

9.3.1 For the CT specimen calculate ΔK as

$$\Delta K = \frac{\Delta P}{B\sqrt{W}} \frac{(2 + \alpha)}{(1 - \alpha)^{3/2}} (0.886 + 4.64\alpha - 13.32\alpha^2 + 14.72\alpha^3 - 5.60\alpha^4)$$

where $\alpha = a/W$; expression valid for $a/W > 0.2$ [*10,11*].

9.3.2 For the CCT specimen calculate ΔK consistent with the definitions of Section 5.2; that is

$$\Delta P = P_{max} - P_{min} \text{ for } R > 0$$

$$\Delta P = P_{max} \qquad \text{for } R \leq 0$$

in the following expression [*12*]

$$\Delta K = \frac{\Delta P}{B} \sqrt{\frac{\pi\alpha}{2W} \cdot \sec\left(\frac{\pi\alpha}{2}\right)}$$

where $\alpha = 2a/W$; expression valid for $2a/W < 0.95$.

NOTE 10—Implicit in the above expressions are the assumptions that the test material is linear-elastic isotropic and homogeneous.

9.3.3 Check for violation of the specimen size requirement by calculating K_{maxL} (see Section 7.2 and Fig. 6). Data are considered invalid according to this method when $K_{max} > K_{maxL}$.

9.4 *Determination of a Fatigue Crack Growth Threshold*—The following procedure provides an operational definition of the threshold stress-intensity factor range for fatigue crack growth, ΔK_{th}, which is consistent with the general definition of Section 5.8:

9.4.1 Determine the best-fit straight line from a linear regression of log da/dN versus log ΔK using a minimum of five (da/dN, ΔK) data points of approximately equal spacing between growth rates of 10^{-9} and 10^{-10} m/cycle.

NOTE 11—Limitations of the linear regression approach of Section 9.4.1 are described in Ref *13*. Alternative nonlinear approaches and their advantages are also given in Ref *13*.

9.4.2 Calculate the ΔK-value which corresponds to a growth rate of 10^{-10} m/cycle using the above fitted line; this value of ΔK is defined as ΔK_{th} according to the operational definition of this method.

10. Report

10.1 The report shall include the following information:

10.1.1 Specimen type, including thickness (B) and width (W). Provide figures of the specific CCT specimen design and grips used; also, provide a figure if a specimen type not described in this method is used.

10.1.2 Description of the test machine and equipment used to measure crack length. State the precision with which crack length measurements were made.

10.1.3 Test material characterization in terms of heat treatment, chemical composition, and mechanical properties (include at least the 0.2 percent offset yield strength and either elongation or reduction in area measured in accordance with Methods E 8). Identify product size and form (for example, sheet, plate, forging, etc.).

10.1.4 The crack plane orientation in accordance with the code given in Method E 399. In addition, if the specimen is removed from a large product form give its location with respect to the parent product.

10.1.5 The terminal values of ΔK, R, and crack length from fatigue precracking. If precrack loads were stepped-down, state the procedure employed and give the amount of crack extension at the final load level.

10.1.6 Test loading variables, including ΔP, R, cyclic frequency, and cyclic waveform.

10.1.7 Environmental variables, including temperature, chemical composition, pH (for liquids), and pressure (for gases and vacuum). For tests in air, report the relative humidity as determined by Method E 337. For tests in "inert" reference environments, such as dry argon, give estimates of residual levels of H_2O and O_2 of the test environment (generally this differs from the analysis of residual impurities in the gas supply cylinder). Report nominal values for all of the above environmental variables, as well as maximum deviations throughout the duration of testing. Describe the material employed in the chamber used to contain the environment, and steps taken to eliminate chemical/electrochemical reactions between the specimen-environment system and the chamber.

10.1.8 Analysis methods applied to the data, including technique used to convert a versus N to da/dN, specific procedure used to correct for crack curvature, and magnitude of crack curvature correction.

10.1.9 The specimen K-calibration and size criterion to ensure predominantly elastic behavior (for specimens not described in this method).

10.1.10 Plot da/dN as a function of ΔK. (It is recommended that the independent variable, ΔK, be plotted on the abscissa and the dependent variable, da/dN, on the ordinate. Log-log coordinates are commonly used. For optimum data comparisons, the size of the ΔK-log cycles should be two-to-four times larger than the da/dN-log cycles.) Identify all data which violate the size requirements of Section 7.2 and Appendix X2 of Method E 647.

10.1.11 Description of any occurrences which appear to be related to anomalous data (for example, transients following rest interruptions or changes in loading variables).

10.1.12 For K-decreasing tests, report C and also initial values of K and α. Indicate whether or not the K-decreasing data were verified by K-increasing data. Report ΔK_{th}, the equation of the fitted line (Section 9.4) used to establish ΔK_{th}, and any procedures used to establish ΔK_{th} which differ from those of Section 9.4

10.1.13 It is desirable, but not required, to tabulate test results. When using this method of presentation, tabulate the following information for each test: a, N, ΔK, da/dN, and where applicable, the test variables of Sections 10.1.3, 10.1.6, 10.1.7, and 10.1.12. Identify all data determined from tests on specimens which violate the size requirements of Section 7.2 and Appendix X2 of Method E 647.

References

[1] Paris, P. C. and Erdogan, F., *Journal of Basic Engineering, Transactions of the ASME, Series D,* December 1963, pp. 528-534.
[2] Paris, P. C. in *Proceedings,* 10th Sagamore Army Materials Research Conference, Syracuse University Press, 1964, pp. 107-132.
[3] Clark, W. G., Jr., *Experimental Mechanics,* September 1971, pp. 1-8.
[4] Hoeppner, D. W. and Krupp, W. E., *Engineering Fracture Mechanics,* Vol. 6, 1974, pp. 47-70.
[5] *Fatigue Crack Growth Under Spectrum Loads, ASTM STP 595,* American Society for Testing and Materials, 1976.
[6] Hudak, S. J., Jr., Bucci, R. J., Saxenda, A., and Malcolm, R. C., "Development of Standard Methods of Testing and Analyzing Fatigue Crack Growth Rate Data — Third Semi-Annual Report," Westinghouse Research Report 77-9E7-AFCGR-R1, Westinghouse Research Laboratories, Pittsburgh, Pa., AFML Contract F33615-75-C-5064, March 1977.
[7] Clark, W. G., Jr., and Hudak, S. J., Jr., *Journal of Testing and Evaluation,* Vol. 3, No. 6, 1975, pp. 454-476.
[8] Saxena, A., Hudak, S. J., Jr., Donald, J. K., and Schmidt, D. W., *Journal of Testing and Evaluation,* Vol. 6, No. 3, 1978, pp. 167-174.
[9] Clark, W. G., Jr., and Hudak, S. J., Jr., "The Analysis of Fatigue Crack Growth Rate Data," Westinghouse Scientific Paper 75-9E7-AFCGR-P1, Westinghouse Research Laboratories, Pittsburgh, Pa.; to be published in *Proceedings,* 22nd Sagamore Army Materials Research Conference on Application of Fracture Mechanics to Design.
[10] Newman, J. C., Jr. in *Fracture Analysis, ASTM STP 560,* American Society for Testing and Materials, 1974, pp. 105-121.
[11] Srawley, J. E., *International Journal of Fracture,* Vol. 12, June 1976, pp. 475-476.
[12] Feddersen, C. E. in *Plane Strain Crack Toughness Testing of High-Strength Metallic Materials, ASTM STP 410,* American Society for Testing and Materials, 1967, pp. 77-79.
[13] Bucci, R. J. in *Fatigue Crack Growth Measurement and Data Analysis, ASTM STP 738,* American Society for Testing and Materials, 1981, pp. 5-28.

Summary

Summary

The papers contained in this publication inherently fall into four groups: (*1*) *General Test Procedures*—information on optimum test procedures for measuring near-threshold fatigue crack growth rates, problem areas in near-threshold testing, specimen size requirements for testing low-strength materials at high growth rates, and alternative specimens for fatigue crack growth rate (FCGR) testing; (*2*) *Remote Crack Monitoring Techniques*—descriptions of equipment and discussions of procedures to measure crack extension using elastic compliance (or COD), a-c and d-c electrical potential, and acoustic emission; (*3*) *Statistical Analysis and Representation of Data*—application of regression analysis to FCGR data, analysis of variance for reproducibility within a laboratory and repeatability between laboratories, and a summary of mathematical representations of wide-range FCGR data including effects of load ratio; and (*4*) *Engineering Applications*—utilization of FCGR data in probabilistic design and reliability analyses, fatigue crack growth considerations in the Boiler and Pressure Vessel Code of the American Society of Mechanical Engineers, and problem areas in the use of fracture mechanics to predict the fatigue life of welded structures.

Papers in the first two groups are closely tied to two ASTM methods for FCGR testing. The first of these is ASTM Method for Constant-Load-Amplitude Fatigue Crack Growth Rates Above 10^{-8} m/Cycle (E 647-78 T), which was developed by ASTM Task Group E24.04.01 on Fatigue Crack Growth. The second is a working document of ASTM Task Group E24.04.03 on Near-Threshold Fatigue Crack Growth. This document, a modification of ASTM E 647, contains specialized techniques for near-threshold testing. In order to provide for convenient reference, these documents are respectively provided in Appendixes I and II of this publication.

Papers in the last two groups provide much needed information to bridge the gap between generation of materials' FCGR properties in the laboratory and application of this information to the design and reliability assurance of structures.

The following sections summarize the papers from each of the four groups.

General Test Procedures

Information which provided the basis for the proposed test procedures for fatigue crack growth rates below 10^{-8} m/cycle is summarized by Bucci. The key feature of these procedures is a K-decreasing technique which involves generating data while the applied load, and therefore stress-intensity factor, is decreased, either continuously or in step-wise fashion. The advantage of this procedure is that it eliminates the tedious and costly precracking period. The importance of controlling the nominal rate at which K is decreased is demonstrated by comparing FCGR data obtained under K-decreasing and K-increasing (constant-load-amplitude) conditions. Decreasing K at too fast a rate causes anomalously high growth rates and, consequently, low values of the threshold stress intensity (ΔK_{th}). Testing under conditions of nominally constant $1/K\ (dK/da)$ appears to be an optimum, since it corresponds to a constant nominal rate of change of the crack-tip plastic zone. Data on several materials show that comparable K-decreasing and K-increasing results are obtained provided $1/K\ (dK/da) > -0.08\ \text{mm}^{-1}$. This limiting value of the normalized K-gradient appears to be appropriate for tests at low load ratios, although it may be unnecessarily restrictive for tests at high load ratios; that is, it may be acceptable to decrease K and the plastic-zone size more rapidly in high load ratio tests. Additional tests are needed on a larger variety of materials to better define this limit, particularly for high load ratios and in the presence of various aggressive environments. Bucci also discusses problems associated with transient growth rates which can cause FCGR data to be dependent on crack size, load history, and environment. Although these effects are generally not well understood, guidelines are presented for their control or elimination, or both, during testing.

The second paper (Amzallag et al) which addresses near-threshold crack growth testing summarizes results from a cooperative interlaboratory test program conducted by the Fatigue Commission of the French Metallurgical Society. Ten laboratories participated in the program which involved near-threshold FCGR testing on a 2618-T651 aluminum alloy and a 316 stainless steel. The results demonstrate the marked differences in near-threshold FCGR behavior which can occur for different materials. A clearly definable ΔK_{th}-value was observed in the aluminum alloy but not in the steel. These results also provide a useful documentation of the difficulties which can be encountered in interpreting results due to crack "tunneling" in specimens having too large a thickness-to-width ratio (B/W). The significant "tunneling" encountered in compact-type (CT) specimens having $B/W = 1/2$ supports the need for the current ASTM recommendation of $B/W \leq 1/4$. In fact, this ratio may need to be decreased for near-threshold testing where "tunneling" problems are often accentuated. Post-test corrections for this phenomenon are often ineffective, since adequate data on crack front profiles are difficult to acquire because tunneling often changes throughout the course of a test and, in addition, can vary from material to material and specimen to specimen. "Tunneling" problems, in combination with the variable K-gradients used during the tests, are likely to have contributed to the overall variability in FCGR, which was about a factor of ten in the 316 stainless steel. Within this data scatter, it was concluded that specimen type, specimen thickness, crack length, test frequency, and waveform had no measurable effect on ΔK_{th} or the near-threshold FCGR. However, in agreement with other studies, increasing the load ratio caused an increase in growth rates and a decrease in ΔK_{th}.

As indicated in the previous two papers, two factors are of primary importance in measuring near-threshold FCGR using K-decreasing tests: (*1*) the K-gradient, or more specifically the normalized K-gradient, and (*2*) the step-loading history—that is, the magnitude of the load decrement as well as the crack growth increment at a given load. Thus procedures which enable the load to be decreased in a preselected, continuous, and automatic fashion are desirable. Systems for accomplishing this using digital computer control of the test machine have been developed. Brown and Dowling present a low-cost alternative procedure using simple electronic circuitry. The circuitry is readily combined with elastic compliance methods and interfaced with closed-loop, electrohydraulic test machines. This system then enables tests to be conducted under various combinations of load-deflection control, thereby allowing tests to be performed automatically at preselected constant values of $1/K\ (dK/da)$. The utility of this approach is demonstrated by showing agreement between near-threshold FCGR data obtained under K-decreasing and K-increasing conditions. This approach has the advantage of being simple to implement and requiring little initial cost. These advantages need to be compared with those of digital computerization. In the latter, the high initial cost is balanced by lower long-term operating costs since data can also be gathered automatically.

Regarding FCGR testing at high growth rates, a fundamental issue has been the definition of adequate specimen sizes such that data could be properly analyzed using linear elastic fracture mechanics. James addresses this issue using FCGR tests on 304 stainless steel at 288°C. The equivalence of results from different sized specimens indicates that the current requirement on specimen size in ASTM E 647 is, under certain conditions, conservative for low-strength, high strain hardening materials. Therefore it is proposed that the flow strength, instead of the 0.2 percent yield strength, be used to compute the allowable uncracked ligament size. Physically this change corresponds to accounting for the materials' strain hardening capacity in an approximate sense by employing a higher effective yield strength. Although James' data support such a change, conflicting data for other temperatures and materials are available in the literature. Until the conditions for K-controlled crack growth under cyclic loading are better delineated and understood, it would appear advisable to discriminate between data which comply with size requirements based on both yield strength and flow strength.

Currently ASTM E 647 contains detailed information on the use of CT specimens and center-cracked tension (CCT) specimens in FCGR testing. However, the use of alternative specimens is allowed, provided adequate

K-calibrations are available. James and Mills evaluate one such alternative specimen, the so-called round compact specimen (RCS). Existing K-calibrations are compared and found to be in reasonable agreement; nevertheless, the expression developed by Newman is recommended since it has the advantage of being applicable over the widest range of relative crack lengths. The utility of the RCS specimen is demonstrated by showing that equivalent FCGR data are obtained from RCS and CT specimens. This specimen geometry offers a saving in both preparation cost and material, and is ideally suited for generating FCGR data with cracks in the circumferential-radial (C-R) orientation in bar stock.

Remote Crack Monitoring Techniques

Raw data in the form of crack length versus the number of elapsed cycles (a versus N) is fundamental to the establishment of FCGR data.

For acquisition of the basic a versus N information, visual crack monitoring techniques are convenient and are widely used. When visual access to the crack is limited, as when testing in severe corrosive or thermal environments, alternative forms of crack monitoring are often required. Several remote crack monitoring methods have gained acceptance as reliable, accurate, and cost-effective methods for measuring crack length in fracture mechanics-type specimens. These measures can be readily integrated into many data acquisition systems, and thus afford opportunity for automation of data handling and test machine control. Continuous monitoring of crack growth experiments by automated techniques implies tremendous cost-saving potential, particularly where large quantities of crack growth data are sought, or where measurement of very slow growth rates is of interest.

A primary source of variability in fatigue crack growth measurement is the scatter encountered in establishing the raw a versus N data. Successful remote crack monitoring for this purpose, therefore, requires understanding of causes of variability associated with the measurement technique and its instrumentation package. The minimization of experimental error in crack length measurement is dependent upon experience, as experimental objectives, technique, and the instrumentation package generally vary from user to user. Yoder et al and Wei and Brazill describe crack opening displacement (COD) and electrical potential methods of monitoring fatigue crack growth, respectively. The authors' laboratories pioneered the developments of these two techniques, which have been in existence for over 15 years. This experience, shared by the authors, should be of considerable benefit to users of both approaches. Detailed guidelines on the COD technique, addressed by Yoder et al, form the basis of a recently proposed modification to ASTM E 647 for measurement of FCGR in marine environments. Wei and Brazill fully describe a-c and d-c electrical-potential systems for FCGR measurements. Calibration techniques and trade-offs between the two electrical-potential systems are described, and many useful operating hints are given.

Gangloff describes an extension of the electrical-potential method developed to monitor the formation and propagation of small surface cracks. Accurate, quantitative, and reproducible growth rates were obtained, thereby validating use of the procedure for future studies on influences of metallurgical, mechanical, and environmental variables on the formation and growth of small surface cracks. Gangloff used this approach to examine crack growth kinetics of physically "short" cracks in a 10Ni steel alloy. The da/dN versus ΔK information extracted from the small crack specimens was in good agreement with data obtained from more conventional long crack specimens. Accelerated growth often reported to be associated with "short" cracks was not operative for the applied stress, crack sizes, and material condition(s) investigated. The experimental technique described represents a useful tool for assessing and developing refinements to present fracture mechanics methodology for analyzing growth of very small cracks.

Nakajima et al demonstrate the feasibility of acoustic emission methods for the detection and monitoring of growing fatigue cracks exposed to high-temperature water environment typical of coolant used in nuclear reactors. If experimental difficulties associated with estimating crack growth rate can be resolved, the technique described represents a promising nondestructive approach for surveillance of structural integrity of plants under operating conditions.

Statistical Analysis and Representation of Data

Understanding and quantifying the variability associated with FCGR data is attracting increasing attention. The impetus for this work is primarily due to the increased emphasis on probabilistic prediction of structural life. Several papers in this section address key issues related to the application of statistical methods to the characterization of FCGR variability—an important input to probabilistic life prediction.

Fong and Dowling present a relatively simple, quantitative approach to assessing the variability in FCGR data. This is accomplished by re-analyzing a portion of the FCGR data from a previous cooperative interlaboratory test program sponsored by the Society of Automotive Engineers. Firstly, a useful review of the nomenclature and formulas of conventional regression analysis is given. The authors proceed to point out that the precision of any test method consists of both reproducibility within a laboratory and repeatability between laboratories. The necessity of conducting replicate tests in order to estimate these two sources of variability is emphasized. A new *ad hoc* procedure consisting of an "agreement matrix" is proposed to quantify the process of deciding how well two sets of data are in agreement. The use of this procedure should prove to be useful in planning cooperative test programs, characterizing interlaboratory data, and formulating more rational engineering safety factors.

Bastenaire et al address a basic problem often overlooked when regression analysis is used to establish a mathematical representation of FCGR data. One of the implicit assumptions of conventional regression techniques is that the individually measured responses—in this case, da/dN_i—are independent random variates. However, the physics of the crack growth process, as well as subsequent data processing, causes neighboring da/dN_i values to be related, or correlated, to some degree. This situation is often accounted for by introducing an autocorrelation function into the analysis. The authors present an alternative approach based on reformulating the statistical model in terms of crack length differences which, unlike absolute crack lengths, are likely to be independent random variates. A power law relation between da/dN and ΔK is used; thus a random error having lognormal distribution is assumed, as in conventional regression analyses. This hypothesis is shown to be valid by examining the residuals of an example analysis. The application of statistical tests to examine the degree of correlation in the random error would be an interesting next step in assessing the success of this overall approach.

It is important to recognize that the variability associated with a given set of FCGR data contains contributions from two sources, specifically (*1*) inherent material scatter, and (*2*) measurement error. The former is of primary interest; however, it is obscured to some degree by the latter. The latter is linked to the details of the test technique; thus it is to some extent under the control of the test engineer. For example, the measurement error can be minimized by selecting an optimum crack length measurement interval. The optimum interval depends on both the precision of the crack length measurement technique and the K-gradient of the specimen—the interval should be large compared with the measurement precision, but small compared with the K-gradient.

Ostergaard et al demonstrate the existence of an optimum crack length measurement interval and provide a detailed analysis of the combined effect of measurement interval and data processing procedures on the bias, or "error", associated with converting a versus N to da/dN versus ΔK. This "error" is determined by numerically integratng da/dN versus ΔK and comparing the resulting a versus N data with those which were originally measured. For these experiments, the optimum crack length measurement interval was found to be between 0.8 and 1.6 mm. Even at the optimum measurement interval the "errors" produced by a seven-point incremental polynomial data processing method were about three times greater than those associated with a secant method. However, the absolute values of these "errors"—less than 6 percent on cyclic life—are likely to be of little practical significance considering the uncertainties associated with material variability, as well as those associated with determining the initial crack sizes, load history, damage accumulation, and K-analyses for engineering structures.

Previous papers in this section were able to employ a simple power law to relate the "driving force" (ΔK) and the material response (da/dN), since they considered only a limited range of growth rates—about two to three orders of magnitude. More complex mathematical expressions are needed to describe the complete range of growth rates from ΔK_{th} to final instability, including the effects of load ratio.

Miller and Gallagher present the results of an analytical round-robin program to evaluate methods of describing wide-range FCGR behavior; this program was conducted by ASTM Task Group E24.04.04 on FCGR Descriptions. Nine mathematical expressions and one tabular/graphical method, representing varying degrees of complexity, were included in the program. These methods were evaluated by comparing cyclic life predictions from the different methods with empirical results covering a wide range of growth rates. On this basis, the descriptions exhibited varying degrees of accuracies and were classified into four groups accordingly. It is encouraging for the designer that several methods exist which can provide predictions within ± 20 percent better than 80 percent of the time. These statistics are likely to represent the best that can be achieved considering the inherent variability in FCGR data. Of course, the additional problems associated with predicting lives under variable amplitude loading add substantially more uncertainty to the design procedure.

Engineering Applications

Technological demands for higher performance and more efficient engineering structures, availability of increased strength materials, and improved analytical methods have produced a trend toward higher operating stresses in engineering components. However, these same factors enhance the prospect of failure by rapid fracture at some fatal flaw size, which evolves through propagation of a fatigue crack originating from a small initial defect. New requirements in which designs must guarantee safe crack growth have established the need for experimental and analytical evaluation of FCGR in materials and engineering structure. The first and perhaps most notable of these requirements is the U.S. Air Force structural integrity requirement (MIL-STD-1530). Section IX of the Boiler and Pressure Vessel Code of the American Society of Mechanical Engineers now suggests the use of FCGR analysis for the evaluation of indications found during in-service inspection of nuclear components. Bamford and Jones describe the use of FCGR technology in fracture control plans for nuclear components. The standard procedures employed are known to be conservative to allow quick assessment of a situation. If an indication does not meet the standards, the owner then has the option of performing a more extensive fracture evaluation of the component or repairing it. Since their incorporation into the ASME code, FCGR analyses have been used on several operating plants to justify continued operation without repair.

Barsom discusses the characteristics of discontinuities that are origins of fatigue cracks in various details of welded bridge structure, and presents the AASHTO (American Association of State Highway and Transportation Officials) fatigue design curves for these details. The paper also summarizes FCGR data that have been obtained for bridge steels and weldments. Civil engineering codes do not at present explicitly require FCGR analyses, but in many instances failure analysis can take advantage of crack growth technology. Because of the complexity of crack initiation and growth processes in welded structures, Barsom states reasons why bridge design based on present crack growth technology would result in costly overdesign of certain structural details. He discusses some of the critical problems that need to be resolved to better predict the fatigue life of welded bridge details using fracture mechanics concepts. In particular, one important question raised by Barsom and other symposium authors (Bucci, Gangloff, and Bamford and Jones) relates to the uncertainty of prediction of early stages of crack formation and growth of small crack-like defects. Until this issue is resolved, the AASHTO fatigue-design curves presented by Barsom offer an alternative means of ensuring structural integrity of welded bridge details subjected to cyclic loading.

Hopkins and Rau discuss the utility of probabilistic fracture mechanics methods for crack growth analyses. The approach accepts uncertainties in the various input parameters (namely, initial flaw sizes, loads, uncertainty of inspection, etc.), quantifies them, and calculates a failure probability which provides a basis for assessing cost/risk trade-offs. The common fracture mechanics practice which assumes "worst case" conditions is thereby avoided. As a consequence, satisfactory components, which might be rejected, can be saved by removing the constraints imposed by worst-case assumptions and allowing the analysis to account probabilistically for actual variation in critical parameters based on test or field experience.

Gebman and Paris present a simple procedure for calculating the probability that a structure has not failed, assuming an undetected fatigue crack is present. This procedure is shown to be applicable to the complex, redundant structure of an aircraft. A major advantage of the procedure is that computations can be made on a desk calculator using readily available input data. The procedure is useful for identifying components, or structural elements, which pose the greatest threat to structural integrity, and as a supplement to conventional decision making processes regarding continued operation of structures beyond their original design lives.

S. J. Hudak, Jr.

Southwest Research Institute
San Antonio, Tex. 78284; symposium co-chairman and co-editor

R. J. Bucci

Alcoa Laboratories
Alcoa Center, Pa. 15069; symposium co-chairman and co-editor

Index

K

L

M

N

O

P

R

S